Université d'Ottawa · University of Ottawa

Extent of Magma Mixing as Determined from Pumice Fragments Tenerife, Canary Islands: An electron microprobe and Nomarski Interference study of feldspar and host glass

by

Craig Russell Scott

A thesis submitted to the School of Graduate Studies and Research
in partial fulfillment of the requirements
for the degree of M.Sc. in Earth Science

OTTAWA-CARLETON GEOSCIENCE CENTRE
AND
UNIVERSITY OF OTTAWA
OTTAWA, CANADA

0-612-28458-1

Abstract

Feldspar and glass from two ignimbrite deposits from pre-calderan rocks of the Diego Hernández Formation, Tenerife, Canary Islands are studied in detail using electron microprobe (EMP) and Nomarski Differential Interference Contrast (NDIC) to better understand magma mixing events. Banded pumice fragments contain contrasting magma compositions from basaltic trachyandesite (mafic) to phonolite (felsic) recognized by their black to green color, respectively. Both physical and chemical magma mixing are identified in banded pumice based on EMP and NDIC. Phonolitic magma is homogenous with a distinctive feldspar population ($\approx Or_{40}$), whereas the mafic member ranges from basaltic trachyandesite to trachyandesite, with two feldspar populations (An_{40} and An_{70}). A chemical mixing event is proposed between an alkali basalt (with feldspar An_{70}) and a trachyandesite (feldspar An_{40}) to form a hybrid melt of trachyandesite. Physical mixing between the hybrid and phonolite melts occurs just prior to or during the eruptive event forming banded pumice fragments.

Both ignimbrites studied show evidence of injection of mafic magma with the presence of calcic plagioclase ($\approx An_{70}$) and other mafic minerals, but only one is associated with caldera collapse of Diego Hernández. Incomplete reaction textures and wider range in glass chemistry indicate incomplete mixing between pre-existing trachyandesite and injected alkali basalt for the collapse event suggesting a more violent injection and subsequent eruption of this ignimbrite leading to collapse of the magma chamber. Distal deposits of collapse event are more widespread as compared to the ignimbrite not associated with collapse which also indicates the larger scale related to caldera collapse.

Acknowledgements

As with any thesis outside help was plentiful and greatly appreciated over the past several years. Financial support came in the form of Natural Sciences and Engineering Research Council grants to Drs. Tony Fowler and Karen St. Seymour, along with grants from the European Community to Dr. Karen St. Seymour. Numerous teaching assistantships from the University of Ottawa were also received.

Numerous discussions with fellow graduate students not only increased my overall knowledge of geology but also provided encouragement. I would like to particularly thank Matthew Leybourne for advice, use of reference material and introducing me to the world of Mac and to Marianne Molgat and Natalie Ham, both of whom provided mental breaks during stressful times. Glen Poirer from McGill was of invaluable help in microprobe work and Scott Bryan from Australia helped with some geology questions from the south coast of Tenerife.

A special thank you goes out to Elizabeth Armitage who put up with me for several years and helped relieve stress with those magicai hands, without which my shoulders would permanently be attached to by ears.

I am particularly grateful to my advisors, Drs. Tony Fowler and Karen St. Seymour, who took a huge chance on giving me this project. For this I am eternally thankful. To Tony I would really like to express my gratitude for his support over and above a thesis supervisor, without his encouragement and confidence this thesis would not have been possible. Simple words are not enough. Thank you.

Finally I would like to thank my new found sister, Tracy. Her love and support enable me to continue when my goals seemed out of reach. She made me believe in myself and pushed me to finish. Thanks sis.

Table of Contents

List of Tables

List of Figures

List of Plates

1 Introduction

1.1 Purpose & Approach

This thesis project examines evidence of magma mixing found in pumice fragments from several pyroclastic deposits located on Tenerife, Canary Islands. The pumiceous pyroclastic deposits are defined as *ignimbrites* (Cas and Wright 1987) and will be used throughout the remainder of the text. The term " magma mixing" has been used in recent literature to mean different degrees of mixing. To clear up any misconceptions whenever mixing is mentioned it refers to the complete homogenization of two or more distinct magmas to form a hybrid melt, whereas commingling is the physical/mechanical incomplete mixing of two distinct magmas without the formation of a homogeneous hybrid melt (Bardintzeff 1992; Blake and Koyaguchi 1991). Commingled magmas are distinctive in that they exist as streaks or bands of one magma in the other.

Pumice fragments allow an estimation of the magma composition that existed in the magma chamber just prior to eruption and pyroclastic deposits have an added feature of preserving a 'snapshot' of a magma chamber at this time. Such deposits have an inverse relationship with the magma chamber, with the top portion of the deposit related to the bottom of the magma chamber (if the chamber is completed erupted). Any heterogeneities in the chamber, if present, will be observed in a vertical section of the pyroclastic deposit. Glassy juvenile fragments have long been recognized as more dependable recorders of heterogeneities in magmatic systems than analogous crystalline igneous rocks (Anderson 1976; Wolff and Storey 1984). Sampled properly, juvenile fragments will provide a reliable guide to pre-eruptive magmatic processes (Wolff and Storey 1984).

Minerals commonly preserve the complex and diverse history of magmatic liquids. Through careful study of textures and mineral compositions the petrologist can discriminate the role of magma mixing in a particular deposit (Stimac and Pearce 1992). Feldspars are particularly effective in the preservation of changing magmatic conditions, by providing a record through zoning and reaction textures (Singer et al. 1995; Singer et al. 1993). A major reason for the preservation of zoning is due to sluggish NaSi - CaAl interdiffusion rates (Smith and Brown 1988; St. Seymour et al. 1990) which will be discussed in more detail in a later section.

Two ignimbrites, related to the last caldera forming event, are chosen in this study due to their accessibility and abundance of 'mixed' pumice fragments. In the field, banded pumice is recognized by the physically mingled appearance of distinct phases. The pumices vary from black, green, or white in color, depending on silica content. Three samples were collected from each ignimbrite of the mafic and felsic end-members, as well as banded specimens. Evidence of mixing will be pursued both petrographically and chemically. Petrographically, mixing will be apparent by disequilibrium assemblages and mineral textures. Feldspar morphology is used extensively in determining whether mixing has occurred. Textures such as skeletal, resorbed, sieved or fritted crystals all point to the possible mixing of compositionally distinct magmas. Nomarski differential interference contrast (NDIC) is applied to help in observing minute textural details of phenocryts (Pearce and Clark 1989), plus it aides in detecting glass that has been devitrified.

1.2 Regional Geology & Previous Work

The island of Tenerife is the largest (2,053 km^2) of the seven islands comprising the Canary archipelago located off the southern coast of Morocco (Fig. 1.1). The island's name stems from the guanche word meaning snow-capped mountain. Teide is the highest peak (3718 m) not only in the Canary Islands, but all of Spain and is usually covered by a veneer of snow.

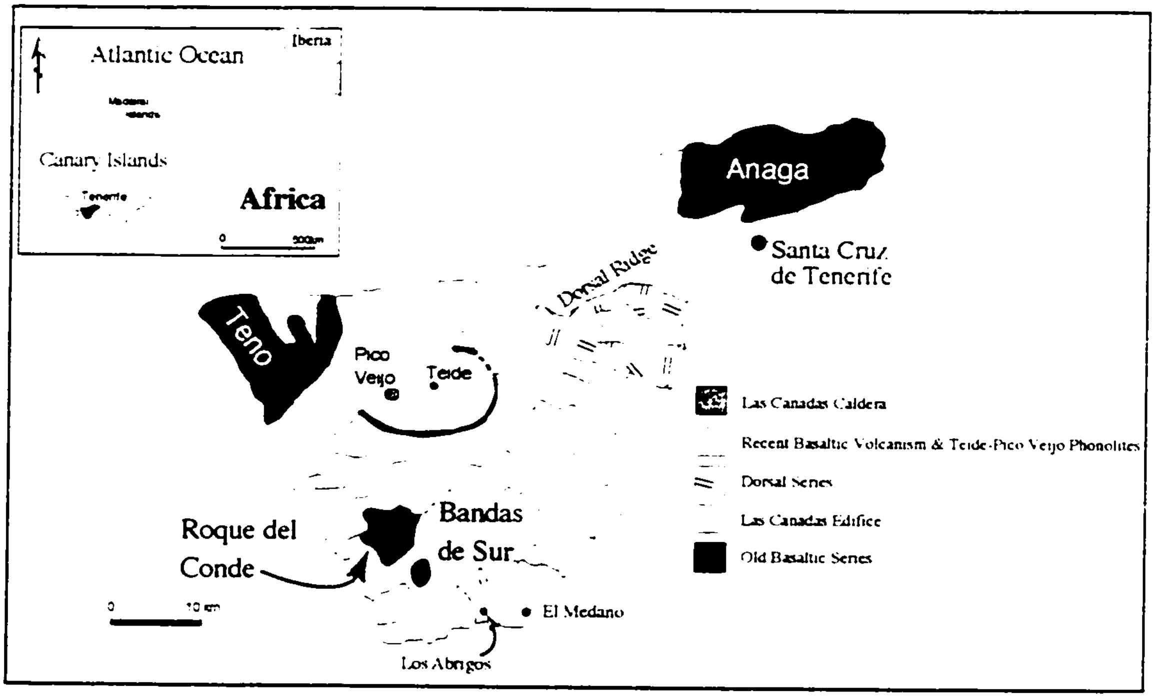

Figure 1.1: Simplified geology map of Tenerife. Canary Islands. Modified from Marti et al. (1994).

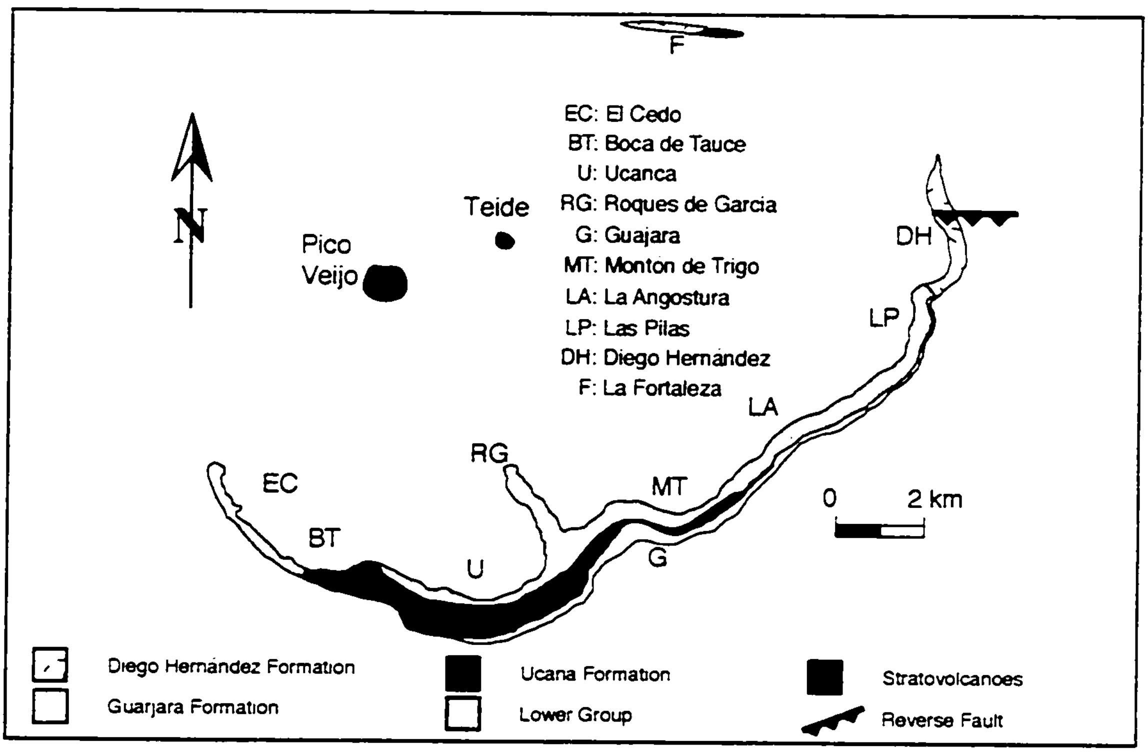

Figure 1.2: Simplified sketch of Las Cañadas Caldera wall showing the distribution of Upper and Lower Groups (modified from Marti et al. (1994)).

In combination with the stratovolcano Pico-Veijo, they make up the dominant physical feature on the island, the so called central system. Both are built in a large caldera known as Las Cañadas Caldera (Valentin et al. 1990). Las Cañadas Caldera is an elliptical depression situated 2000 m above sea level measuring 17 X 21 km, with a maximum depth of 600 m (Martí et al. 1990). As noted in the ship's log, Teide's last major eruption was observed by Christopher Columbus as he set sail for the Americas (Marti per. com). There have been eight historic eruptions outside the central system, with three from 1420-1430 (Arenas, Frailes and Gañanias volcanoes), one in 1704 (Sieta Fuentas volcano), two in 1705 (Fasnia and Arafo volcanoes), one in 1706 (Montaña Negra) and the most recent in 1909 (Chinyero volcano) (Valentin et al. 1990).

Rocks from Tenerife are part of the alkali basalt-trachybasalt-trachyandesite-phonolite evolutionary trend (Borley 1974). Tenerife is constructed from two major periods of sub-aerial volcanic activity. The first, the Old Basaltic Series, ranges in age from 12 to 3.3 Ma ago. Fissure eruptions of ankaramites, basanites and alkali-basalts, form this series and make up the three massifs of Teno, Anaga and Roque del Conde (Fig. 1.1) (Arana et al. 1994; Martí et al. 1994b). From 3 Ma to the present, differentiated volcanic rocks (ie phonolites and trachyandesites) and basalts have dominated, resulting in the formation of the central volcanic complex, Las Cañadas Edifice. Erupted products range from highly differentiated peralkaline phonolitic magmas, along with parental basalts and magmas of intermediate compositions. The evolved phonolitic magmas indicate the existence of a high level magma chamber under the complex (Martí et al. 1994b). The last major event of this period culminated with the formation of Las Cañadas Caldera. The last 0.2 Ma has seen the construction of the twin stratovolcanoes Teide and Pico Veijo within the caldera (Arana et al. 1994).

Las Cañadas Caldera

Las Cañadas Caldera is considered to be a nested caldera, in that it is the result of three separate collapse events. The caldera has an overall horseshoe shape, open to the north (Fig. 1.1 & 1.2.). It can be subdivided into western and eastern sections by a large spur known as Roques de García. The western sector is 150 m deeper than the eastern one (Martí and Mitijavila 1995; Martí et al. 1994b).

The caldera wall exposed at Las Cañadas provides geologists with almost continuous outcrop of pre-caldera rocks making up the Las Cañadas Edifice. Previous models attempted on the edifice, were based only on its outcropping portions. These models are of limited utility because the base of the edifice is not accessible in either the caldera wall or on the flanks of the shield (Martí and Mitijavila 1995). One such model has the caldera elongated in a NNE-SSW direction and less than 3000m deep. The volcanic edifice was defined by sets of volcanic vents arranged parallel to the main tectonic trends of NW-SE and NE-SW (Martí et al. 1994b).

Martí *et al.*. (1995) concentrate on just the upper exposed part to explain the evolutionary history of the edifice. From the exposed stratigraphy two main groups are recognized, namely a Lower Group and an Upper Group. The ages obtained help to constrain the timing of construction along with the duration of volcanic activity and periods of quiescene.

Radiometric dates indicated (Table 1.1) in the text are from two detailed studies performed in Las Cañadas Caldera by Ancochea *et al.* (1990) and Martí *et al.* (1994), carried out on both phonolitic and basaltic rocks. Age determinations of phonolitic rocks were obtained on mineral separates of alkali feldspar phenocrysts, mainly from the sanidine-high albite series. Dating of basaltic rocks involved whole rock and/or groundmass analysis. Atomic absorption spectrometry was used for K analyses and Ar analyses used mass spectrometry. Martí *et al.* (1994) performed a single $^{40}Ar/^{39}Ar$ age determination on sanidine crystals, from Diego

Table 1.1. K-Ar ages for Las Cañadas Caldera & Bandas del Sur rocks

Sample	% K	$^{40}Ar^{*}/^{40}Ar_T$	Age ± 1σ
Bandas del Sur			
Abrigo**			179 ka
Abrigo (T.26.A)*	5.32		130 ± 20 ka
Arico (T.25.A)*	3.79		650 ± 30 ka
Guaza (T.6.F)*	4.12		670 ± 30 ka
Upper Group			
Diego Hernández Formation			
F11	4.42	0.557	170 ± 8 ka
DH76/1H	5.16	0.045	173 ± 31 ka
DH76/1	5.35	0.102	178 ± 20 ka
DH76/5	5.23	0.088	176 ± 35 ka
DH58	5.18	0.064	255 ± 26 ka
T.13.CH*	4.61	0.048	370 ± 35 ka
T.2.CH*	1.3	0.084	542 ± 30 ka
Guajara Formation			
93720	3.04	0.142	650 ± 20 ka
PA3	4.89	0.096	712 ± 41 ka
9377	4.11	0.141	800 ± 50 ka
AD32	1.25	0.140	850 ± 12 ka
Ucanca Formation			
T.12.A*	3.01	0.223	1.14 ± 0.05 Ma
T.1.C.*	4.27	0.339	1.29 ± 0.01 Ma
ES5	4.62	0.146	1.18 ± 0.07 Ma
ES6	4.67	0.120	1.48 ± 0.04 Ma
T.14.A*	4.35	0.294	1.39 ± 0.04 Ma
R7	3.42	0.244	1.19 ± 0.01 Ma
LP20	3.54	0.035	1.54 ± 0.26 Ma
Lower Group			
Las Pilas			
9372	1.11	0.014	2.09 ± 0.21 Ma
El Cedro			
C90	2.03	0.132	2.20 ± 0.06 Ma
9374	2.13	0.513	3.05 ± 0.09 Ma

Data from Martí *et al.* (1994), * Ancochea *et al.* (1990), ** per comm Scott Bryan 1996 - no errors cited. For sample locations see Martí *et al.* (1994), figure 3.

Hernández Wall, to corroborate their K-Ar ages. The age of 179 ± 9 ka agreed with their K-Ar age (179 ± 11 ka - weighted average) indicating neither excess Ar nor xenolith crystals were present in phonolitic pyroclastic deposits. Excess Ar was observed in basaltic rocks (Mitjavila and Villa 1993). Thus age data determined from basaltic rocks are questionable.

Lower Group

Due to discontinuous exposure at the base of the caldera, the stratigraphy of the Lower Group has not been studied in any great detail and only three radiometric ages have been determined (Table 1.1). The stratigraphy is only on informal sequences and based on the presence of palaeosols and erosional discontinuities. The oldest exposed deposits are the Roques de García-Los Azulejos sequences and the basaltic sequences of Boca de Tauce, El Cabez6n and Mont6n de Trigo (Fig. 1.2). Deposition of the Los Angostura sequence was preceded by an erosional period. An angular unconformity separates this formation from the Las Pilas formation, which combined with the El Cedro formation are the youngest Lower Group rocks (Martí and Mitijavila 1995; Martí et al. 1994b).

The three radiometric ages determined are 3.05 ± 0.09 Ma and 2.20 ± 0.06 Ma in the lower and middle part of the El Cedro sequence, respectively, and 2.09 ± 0.21 Ma from the lowest phonolitic lavas of the Las Pilas sequence (Table 1.1). These samples are located at high stratigraphic positions indicating that earlier lavas and pyroclastics are older than 3 Ma. A major erosional disconformity separates the Lower Group from the Upper Group rocks, indicating a significant period of quiesence before Upper Group volcanism. The oldest age from the Upper group is 1.54 ± 0.26 Ma, thus the unconformity represents up to 0.4 Ma of missing geological history (Martí and Mitijavila 1995; Martí et al. 1994b).

Upper Group

The Upper Group forms most of the exposed caldera wall, compsed mostly of phonolitic pyroclastic deposits with associated basaltic rocks. A noticeable difference between the Lower and Upper Group rocks is their distribution within the caldera. Lower Group rocks tend to be more irregular and discontinuous, suggesting the existence of several partially overlapping volcanic vents. Upper Group rocks are widely distributed and are observed mantling, covering and infilling the palaeotopography of the Lower Group (Martí and Mitjavila 1995; Martí et al. 1994b). Based on age, stratigraphic relationships and petrology, Martí *et al.* (1995) divided the Upper Group into three formations, namely the Ucanca, Guarjara and Diego Hernández Formations, each representing a separate volcanic cycle and collapse episode.

The Ucanca Formation ranges in age from 1.54 Ma (± 0.26) to 1.14 Ma (± 0.05), largely composed of sparsely porphyritic, peralkaline phonolitic lavas and pyroclastics. Common minerals include anorthoclase, amphibole, Na-augite, Fe-Ti oxides, nepheline with occasional biotite. The formation is capped by basaltic rocks. Different eruptive sequences are interpreted based on evidence of palaesols and minor erosion surfaces in several members. Different eruptive phases of single eruptions are inferred from the observed internal discontinuities shown by sharp contacts, changes in grain-size and/or color changes within flow units. Several welded units can be traced outside of the caldera to the south, but only for a limited distance (< 4 km). Correlation with coastal pyroclastic sequences is extremely difficult due to erosion of the intermediate facies (Martí and Mitjavila 1995).

The Guajara and Ucanca Formations are separated by discontinuous basaltic scorias and lavas. The age of the Guajara ranges from 850 ± 12 to 650 ± 20 Ka (Martí et al. 1994b), but recent work dates the top of the Guajara at 300 Ka (Scott Bryan per. comm. 1996). Mineral assemblages are similar to those in the Ucanca and the rocks typically are peralkaline phonolites. Guajara rocks are more porphyritic than Ucanca lavas and contain haüyne rather than nepheline (Martí and Mitijavila 1995).

Guajara phonolitic pyroclastic deposits have a wide range of lithofacies with both welded and non-welded components. While most deposits dip gently to the south, some dip towards the interior of the caldera, mantling the wall. Again, erosion of intermediate facies makes correlation with the southern pyroclastic deposits difficult (Martí and Mitjavilla 1995). On-going work by Scott Bryan (per. comm. 1996) may prove the non-welded Granadilla Ignimbrite and Fall units in the south to be correlated with welded rocks from Guajara Formation.

The Diego Hernández Formationhas a relatively restricted distribution resulting from its deposition in a valley excavated on the eastern side of the Las Cañadas edifice, bounded to the south by the Lower Group rocks of the Las Pilas sector and to the north by several basaltic strombolian cones formed contemporaneously with the phonolitic deposits. Diego Hernández Formation is the uppermost (i.e. youngest) portion of the Upper Group making up Las Cañadas Caldera, ranging from 266 ± 17 to 170 ± 8 Ka in age (Martí and Mitijavila 1995; Martí et al. 1994b).

Diego Hernández is sub-divided into two stages separated by a period of erosion and non-deposition. A date of 542 ± 30 ka was obtained from a basalt from the first stage, but it has since been shown to contained excess Ar (Mitjavila and Villa 1993). The main part of the formation is represented in the second stage. The second stage is well constrained, dated between 266 and 179 ka. This stage is composed of non-welded peralkaline phonolitic pyroclastics with interbedded lapilli deposits and basaltic lavas. The upper portion is dominantly non-welded ignimbrites with variable contents of lithic and pumice fragments, occasionally associated with intraformational breccias. Mineralogically these deposits contain potassium feldspar, aegirine-augite, hornblende, magnetite, haüyne and accessory biotite. Black and white pumice are common due to mixing of phonolitic and basaltic magmas. Clasts rich in lithic fragments, comprise the intraformational co-ignimbrite lag breccia found in the uppermost part of the formation, laterally grading into a widespread non-welded ignimbrite known as the El Abrigo Ignimbrite in the south (Martí and Mitjavila 1995; Martí et al. 1994b).

Bandas del Sur

The Bandas del Sur pyroclastics rocks (Fig. 1.1), on the southern coast of Tenerife, are composed of peralkaline phonolitic pyroclastic deposits. The stratigraphy is extremely complex due to extensive erosion and dissection. As with Las Cañadas Caldera, these pyroclastic rocks can be subdivided into two sequences, a Lower Sequence and an Upper Sequence. The Lower Sequence correlates with the Guajara Formation whereas the Upper Sequence correlates with the Diego Hernández Formation, both of which are pre-caldera rocks of the Upper Group of Las Cañadas Caldera. Correlation is based on overlaps in radiometric dates and stratigraphic relations (Bryan 1995).

The Lower Sequence is composed of peralkaline phonolitic pyroclastic deposits of fall and flow origin, debris-flow/lahar deposits and minor basaltic lava flows. Most pyroclastic units are biotite- and alkali feldspar-phyric and some have compositional zoning. Evidence of "magma mixing" is uncommon, but banded pumice is observed in the Arico Ignimbrite and in the "banded pumice" ignimbrite located around El Médano (Bryan 1995). Ancochea *et al.* (1990) dated the base of the Arico Ignimbrite at 650 $\pm$ 0.03 Ka by the K/Ar method and showed it to be time equivalent to the end of the Guajara Formation. The Arico ignimbrite is distinctive it that it is the only welded pyroclastic unit in the south. The Granadilla Fall and Ignimbrite, having an air fall facies over 8 m thick and ignimbrite facies 24 m thick (valley-ponded facies), has been dated at 495 Ka by K/Ar. The Granadilla is one of the most voluminous deposits in the south. From the combination of its extent and physical characteristics it is considered to have resulted from the second caldera collapse event of the Las Cañadas edifice (Bryan 1995).

The Upper Sequence is distinctive due to the presence of banded pumice, accretionary lapilli and syenite lithic fragments. The banded pumice is evidence of possible magma commingling, whereas the accretionary lapilli are evidence of water interaction with ash in the eruptive column (rain flushing). Pyroclastic deposits dominate along the coastline from Los Abrigos to Poris de Abona. Fall deposits are common further to the east and higher up the slope towards the caldera. The Abrigo Ignimbrite is the youngest unit in the Upper Sequence (Bryan 1995). This ignimbrite is characterized by abundant lithic clasts and has been dated at 130 ± 0.02 Ka by Ancochea *et al.* (1990). A co-ignimbrite lag breccia from the top of the Diego Hernández Formation, dated at 180 Ka, is interpreted to grade laterally into the Abrigo Ignimbrite (Martí *et al.* 1994). This ignimbrite, like the Granadilla of the Lower Sequence, is the most voluminous deposit within the Upper Sequence suggesting that it records the third and final caldera collapse event of the Las Cañadas edifice (Bryan 1995).

The two sequences are separated by flank emissions that form extensive alkali basaltic lava flows originating from numerous stromboli cones. Activity is concentrated in the southwestern portion of the island and to the east of Poris de Abona. Further to the east there is overlap with basaltic lavas from the Cordillera Dorsal (Bryan 1995).

Two eruptions centres contemporaneous with the Lower and Upper Sequences are located outside the Las Cañadas Caldera in the southwestern portion of the islands near Los Cristianos. To the west of Los Cristianos there is the 670 ± 30 Ka Montaña Guaza trachyte flow/dome complex that is contemporaneous with the Guajara Formation/Lower Sequence. To the north of Los Cristianos is Caldera de Rei, a pyroclastic deposit from fall, flow and surge mechanisms, interbedded with the Upper Sequence, and correlating with the Diego Hernández Formation (Bryan 1995). The Caldera de Rei deposits mantle some of the stromboli cones associated with flank emissions separating the two sequences (Scott Bryan per. comm. 1995).

Sedimentary deposits are observed in the south as well, separating many pyroclastic sequences. These palaeosol horizons are significant since they indicate hiatus periods in volcanic activity. It should be noted that palaeosol horizons are poorly developed or non-existent in the caldera wall. Fluvial gravel deposits from barrancos (valleys) make up most sedimentary deposits, but reworked pumice (mainly from fall deposits) and shallow marine sediments are also observed (Bryan 1995).

1.3 Analytical Techniques

Nomarski differential interference contrast (NDIC) is a method commonly used in metallurgy and ore microscopy. Anderson (1983) introduced this technique to study internal zoning in calcic plagioclase crystals. Polished sections, from Deigo Hernández and El Abrigo ignimbrites, representing the mafic, felsic and banded pumice members were etched in fluoroboric acid, HBF_4, for 30 - 360 s. This results in Ca-rich zones in feldspar crystals being etched preferentially to Na-rich zones resulting in a microtopographic relief . Under reflected light, NDIC enhances this microtopographic relief (Plate 1.1) thereby improving the visibility of observable internal zonations such as sieve textures, truncated zoning, along with other minute features that are normally unnoticed during routine petrographic work (Pearce and Clark 1989; Singer et al. 1993). Note that NDIC cannot resolve absolute chemical composition but rather indicate chemical variations.

Another use of NDIC is that it enhances crystal boundaries and internal features in the

Plate 1.1: NDIC of sieved feldspar illustrating the enhanced microtopographic relief created by etching section with fluoroboric acid.

Plate 1.1

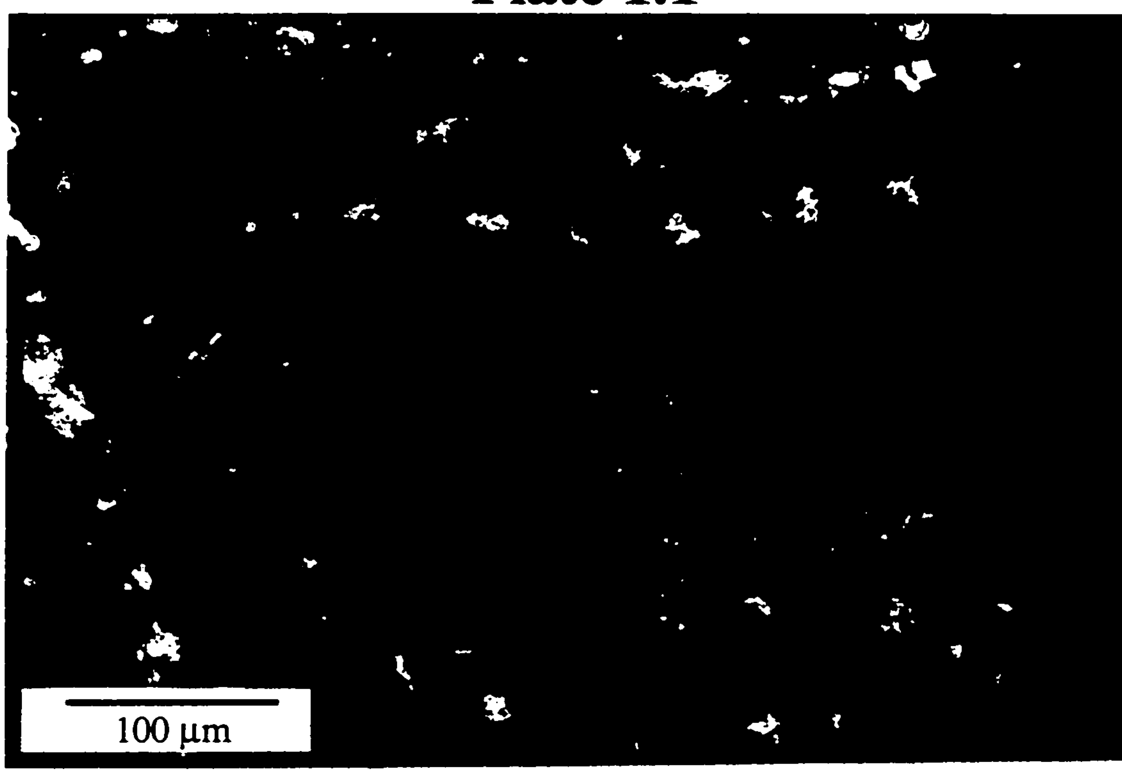

surrounding glass in comparison to standard microscopic techniques. Glass devitrification, not observable under standard conditions, was easily recognized by NDIC (Plate 1.2). This helped in selection of glass points to analyze during microprobe sessions.

Electron microprobe work was done at McGill University, Montreal using a JEOL Superprobe 8600-L wavelength-dispersive spectrometer (WDS) microprobe. Numerous sessions were completed, with each session concentrating on a particular ignimbrite and/or mineral. More detailed work was performed on feldspar crystals based on optical and NDIC observations as well as on its overall abundance.

Electron microprobe work on minerals were performed at an accelerated voltage of 15.0 kV at a beam diameter of 5 μm. Glass analyses were done with an accelerated voltage of 15.0 kV with beam diameter varying from 5 to 15 μm. Extensive electron microprobe work was performed on feldspar crystals in all samples to determine not only compositional variations within samples but within the crystals themselves. Two techniques employed were: (1) various points on the crystals from the core to the rim; and (2) line traverses from core to rim with a 10 μm spacing.

1.4 Aside

This thesis makes use of geochemical techniques, but it also applies the lost art of petrographic observations. By combining classical petrographic techniques with Nomarski Differential Interference Contrast (NDIC) it is possible to observe very fine details in crystal morphology. With the advancement of geochemical analysis the emphasis or importance of petrographic observations have taken a back seat in geological research. It is the hope of this thesis that researchers will realize that a careful combination of both techniques can lead to a better understanding of geological processes.

Plate 1.2A: Unetched section in reflected light with contact between mafic (top) and felsic (bottom) glass. Note feldspar in upper part of photo as reference point to Plate 1.2B.

Plate 1.2B: Etched section in NDIC showing contact between mafic (top) and felsic (bottom) glass. Feldspar in mafic glass (upper part of photo) used for reference.

Plate 1.2A

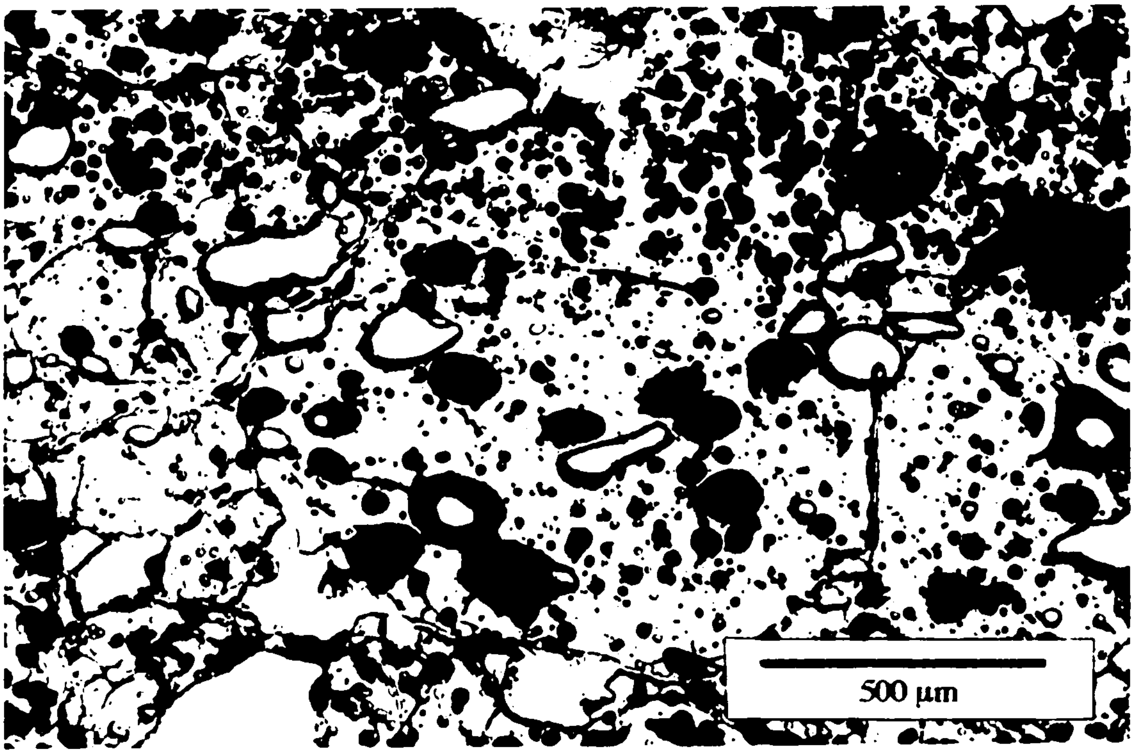

Plate 1.2B

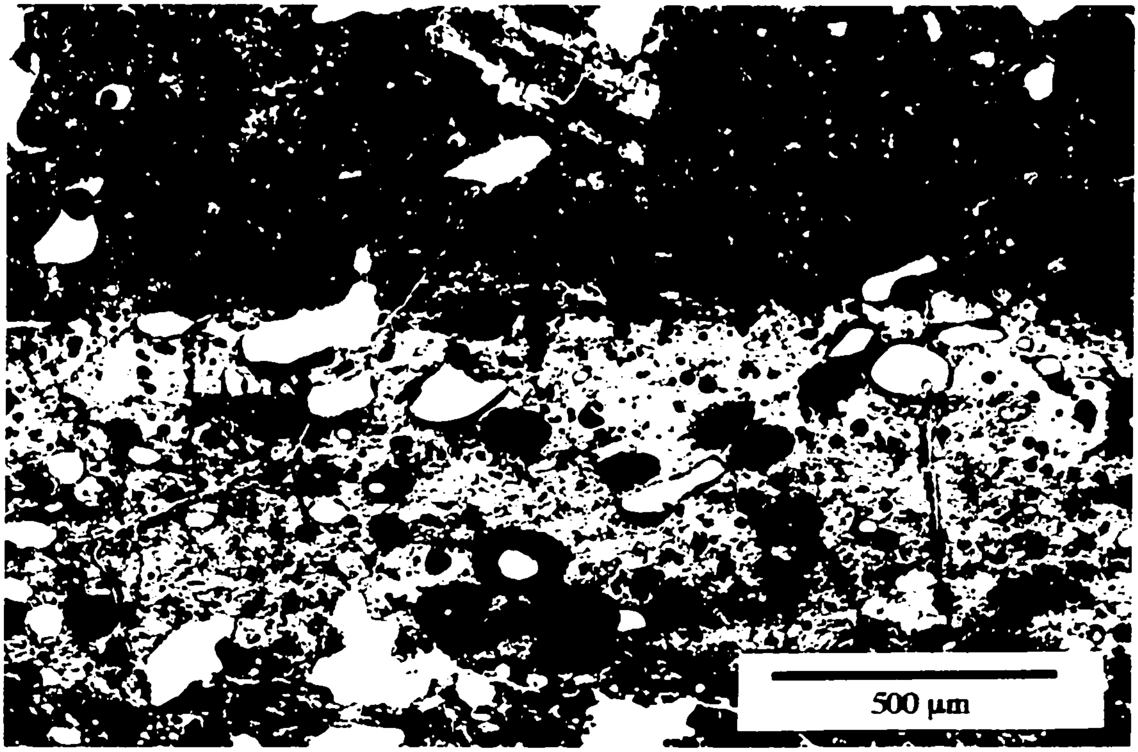

2 Background Information

2.1 Pyroclastic Rocks

The following section is intended to give the reader some background information on pyroclastic processes, particularly pyroclastic flows. The term pyroclastic describes clastic material originating from a volcanic event, typically from an explosive event. Pyroclastic ejecta are subdivided into three types according to their origin, namely juvenile, cognate and accidental. Juvenile (or essential) pyroclasts are clastic material derived directly from the disintegration of fresh magma. Clasts can consist of dense or inflated particles of chilled melt, or crystals that are entrained in the magma prior to eruption (pyrogenic crystals). Cognate (or accessory) pyroclasts are fragmented co-magmatic volcanic rocks from previous eruptions from the same volcano. Accidental clasts are fragments derived from the subvolcanic basement and can be of any rock composition (Fisher and Schmincke 1984).

Pyroclastic deposits are composed of three types of components, namely juvenile fragments (glass shards and pumice), crystals and lithic fragments. It is possible for a large proportion of crystal and lithic components to be xenoliths. Phenocrysts in ignimbrites contrast to those in lava flows in that they are commonly broken. This fragmentation results from eruption and transportation mechanisms, since the crystals within comagmatic pumice lapilli or blocks are relatively unbroken. Post-emplacement fragmentation is also possible due to compaction, indicated by slight separation in crystal fragments that are infilled with glass and feldspar laths that are boudinaged. Crystals are typically enriched in the matrix rather than in pumice lapilli and bombs due to preferential concentration in the matrix relative to glass shards during emplacement (Fisher and Schmincke 1984).

The main transport mechanisms for pyroclastic material are falls, flows and surges.

Typically pyroclastic transport originate from eruption columns. Eruption columns can be subdivided into two components, a gas-thrust and convective thrust phase, controlled by decompression and buoyancy, respectively. Convection is not possible when the effective density of the eruptive column is greater than the atmosphere. Where insufficient absorption and heating of atmospheric air occurs, or large clasts remain in the column then convection will be inhibited, thereby initiating gravitional column collapse and lateral movement of the gas/solid dispersion down the volcanoes flanks (Sparks and Wilson 1976). Another mechanism for the formation of pyroclastics is by a direct lateral blast similar to Mount St. Helens in 1980, where slope failure resulted in sudden pressure release. Pyroclastics can also originate from collapse of lava domes due to disintegration or at the head of lava flows, where internal pressure (from volatile exsolution) and gravity (on slope) can cause fragmentation.

Pyroclastic falls involve pyroclastic material falling through air or water from the eruptive column. Movement is laterally from the vent by a combination of wind drifting, lateral expansion in the ash column and initial lateral movement imparted at the vent. Fall deposits mantle the pre-existing topography, draping all but the steepest slopes (Fig. 2.1A). Sorting is generally well developed and are characterized by internal stratification (although very faint) due to variations in eruptive column conditions (Walker 1981; Wright et al. 1980).

Movement in pyroclastic surges is also lateral. Here, pyroclastic particles are entrained in turbulent gas in a ground-hugging dilute particle flow having a low particle:gas ratio. Manlting of topography is possible, but deposits tend to accumulate in depressions (Fig. 2.1B). Surge deposits have sedimentary bedforms typical of unidirectional flow, such as cross-stratification, dunes, antidunes, planar lamination, pinch and swell structures and chute and pool structures, with generally well sorted individual laminae (Walker 1981; Wright et al. 1980).

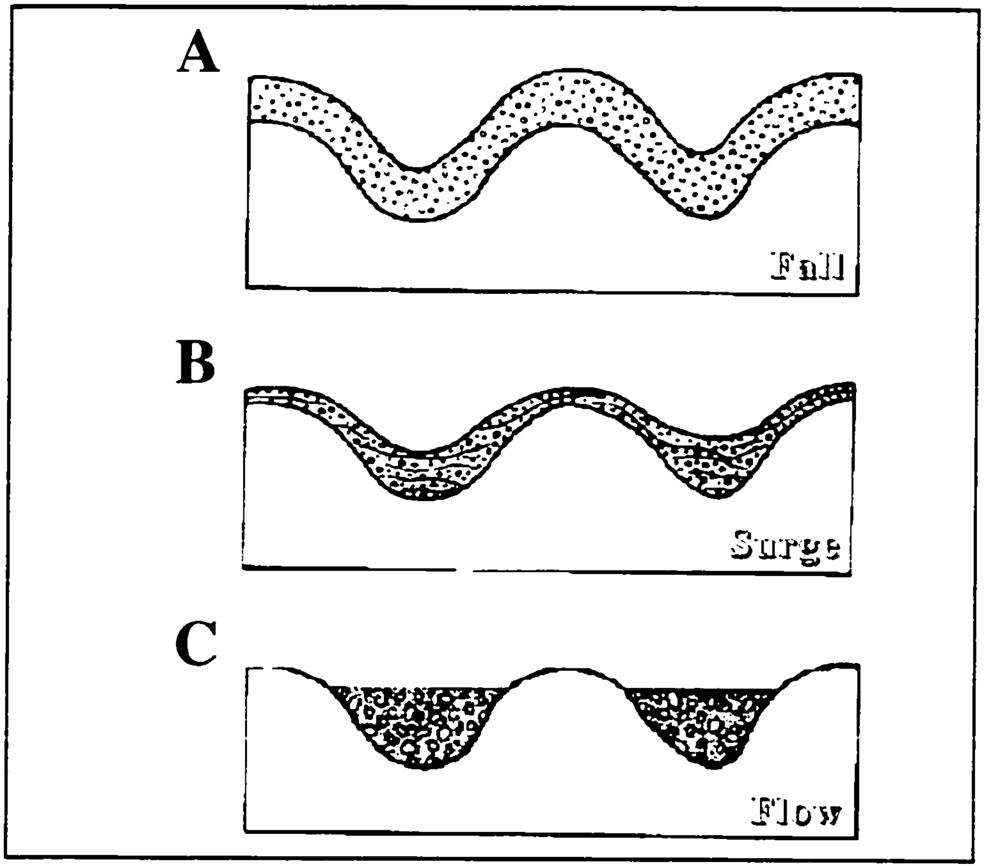

Figure 2.1: Different types of pyroclastic transport mechanisms: (A) Fall; (B) Surge; and (C) Flow. (Modified from Cas & Wright 1987).

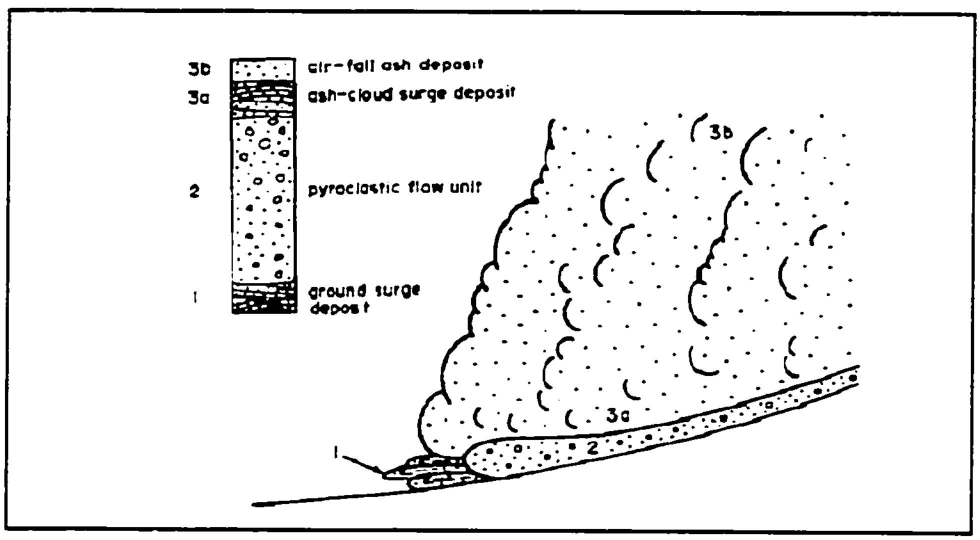

Figure 2.2: Deposition facies and their location from pyroclastic body (From Sparks et al. 1973).

Pyroclastic flows are a type of sediment gravity flow. Such flows are unique fluids due to intrinsic properties, such as density and viscosity, consistently change during movement, unlike fluids of water and air, where these properties are constant. The main driving force of any sediment gravity flow is the action of gravity on the particles entrained in the moving flow (Cas and Wright 1987).

Pyroclastic flows are denser than air, gas-particle currents that travel along the ground at velocities up to 300 m/sec, with temperatures exceeding 1000°C (Cas and Wright 1987). Pyroclastic flows move over the ground as a hot, concentrated particle flow with a high particle:gas ratio. Deposits are topographically controlled, infilling valleys and depressions (Fig. 2.1C). Sorting is normally poor but sometimes pyroclastic flows have coarse tails. Poor sorting is attributed to high particle concentrations and not turbulence, with the dominant flow mechanism being *laminar* and/or plug flow (Walker 1981; Wright et al. 1980).

A pyroclastic flow can be divided into three regions, a tail, body and head, each with different fluidization states. This in turn controls the development of separate layers and facies within deposits (Cas and Wright 1987). The different facies were first described by Sparks et al. (1973), with each facies reflecting a different depositional regime that existed within the flow during transport (Fig. 2.2). The lowest layer, Layer 1, is thought to be the result of a dilute pyroclastic surge, envisioned to occur at the head of the flow. Layer 2, comprises the main body of the flow, while Layer 3 represents the overriding ash cloud. Note that much controversy still surrounds the method of emplacement of pyroclastic flows and this is an ideal and simple case.

Rocks deposited from of pyroclastic flows can be described in physical terms by their degree of welding and their aspect ratios. Welding is defined as the sintering together of hot pumice fragments and glass shards under compactional load. The most important controls are:

(1) emplacement temperature; and (2) lithostatic load, which depends on the thickness of the deposit. When welding nears completion three zones can be identified, a densely welded, partially welded, and non-welded zone. Flattened glassy juvenile clasts, commonly observed in these welded zones, are termed *fiamme*. When these glass shards define a planar foliation it is called *eutaxitic* texture. Welding may be associated with distinctive color changes due to different oxidation states of iron. Columnar cooling joints can develop in densely welded zones (Cas and Wright 1987).

Grades of ignimbrites describe the development of welding. In high-grade ignimbrites the amount of welding is high over large zones. Low-grade ignimbrites usually are not welded or only have a very small welded zones.

The emplacement temperature of ignimbrites is highly variable. Whether an ignimbrite welds or not may be related to flow parameters, such as the height of the eruptive column. High eruptive columns will have a higher heat loss, than low eruptive columns. Another parameter is that lower eruptive columns have smaller volumes of vitric ash, which in turn will not expand to the same degree. Welding tends to increase in stratigraphic height of an ignimbrite deposit (i.e. duration of eruption). This results from the expansion of the volcanic vent and decrease in gas content over time, thereby favoring higher emplacement temperatures (Cas and Wright 1987).

2.2 Magma Chamber Processes

2.2.1 Magma Mixing

Before discussing magma mixing it is first necessary to review magma dynamics. If two magmas of contrasting composition come into contact in a sub-volcanic or deep crustal environment will they immediately mix? If not, what conditions need to be overcome to initiate mixing? These are just some of the questions concerning magma mixing.

Magma mixing was envisaged by early workers in the 19^{th} century (Bunsen 1851), but encountered much criticism due to new physicochemical methods and models. Over the past couple of decades the concept of magma mixing has enjoyed a resurgance (Anderson 1976) and seems to be a more prominent process than first imagined.

Many workers have reported the occurrence of magma mixing from plutonic rocks (e.g. Vogel et al. 1987; Wiede 1987) in extrusive domes and lava flows (e.g. Arana et al. 1994; Stimac and Pearce 1992; Thompson and Dungan 1985) and in pyroclastic fall and flow deposits (e.g. Freundt and Schmincke 1992; Gardner et al. 1995; Sigurdsson and Sparks 1981; Swanson et al. 1994; Vogel et al. 1987; Wolff 1985).

Mixed magmas can take many forms. Several workers have described texturally homogeneous volcanic rocks containing complex mineral assemblages inherited from the homogenization of two phenocrystic magmas (Eichelberger 1978). Interfingered association of silicic and mafic magmas in pumice are described from the Valley of Ten Thousand Smokes Ignimbrite, Alaska (Blake and Koyaguchi 1991). These streaky pumice fragments are formed by the simultaneous eruption of different magmatic liquids (Gardner et al. 1995; Hildreth 1984; Swanson et al. 1994). Felsic lavas have been described to contain globular enclaves of chilled mafic magma that result from simultaneous eruption of different magmas (see Blake and Koyaguchi 1991). Numerous examples exist of homogeneous volcanic rocks containing a disequilibrium phenocryst assemblage (Bacon 1986; Sparks and Sigurdsson 1977).

Mixing intensity is variable as shown by the above examples. Unfortunately with numerous independent studies done on mixed magmas it is of no surprise that descriptive chaos exists in the literature. The terminology used throughout the text is outline by Sparks and

Marshall (1986) and Blake and Koyaguchi (1991). *Mixed magmas* are any magmas that originate by the mixing of two or more magmas. This types is subdivided into *commingled magmas*, where streaks of one magma are observed in another magma, and *hybrid magmas* that are compositionally intermediate between end-member magmas involved, depending on initial proportions. The scale of heterogeneity for a magma to be termed commingled is such that an uncontaminated end member can be recognized. Normally the size range of distinct compositional domains is between 0.3 to 3 cm, but is proportional to the size and abundance of the largest phencryst (Blake and Koyaguchi 1991).

Interaction between mafic and felsic melts is controlled by thermal, compositional and volume contrasts. Where thermal and compositional contrasts are large (mafic/felsic << 1), extensive crystallization of mafic melt will result, with little to no hybrid formation (Bacon 1986; Sparks and Marshall 1986; Stimac and Pearce 1992). Conversely, when the mafic:felsic ratio is larger (> 0.4) or compositional differences are minor (< 10 wt% SiO_2) chemical mixing is more significant (Nixon and Pearce 1987; Stimac and Pearce 1992).

When two or more contrasting magmas come into contact, thermal equilibrium will be attained before any appreciable chemical exchange is possible since thermal diffusion is faster than chemical diffusion. Characteristic times of thermal diffusion is expressed as:

$$\tau_T = a^2 / k \qquad (1)$$

where a is the radius of a spherical body of mafic magma and k is the diffusivity of heat. Whereas chemical diffusion time scales are expressed as:

$$\tau_C = a^2 / D \qquad (2)$$

where D is the chemical diffusivity (Blake and Koyaguchi 1991). At magmatic temperatures D ranges from 10^{-5} to 10^{-11} cm^2s^{-1} (Hofmann 1980), while $k = 8 \times 10^{-3}$ cm^2s^{-1}. Hence thermal equilibrium will be attained quicker than chemical equilibrium.

The following is an ideal situation involving the interaction of two static magma bodies of varying composition. Static implies no vigorous convection, or rapid injection of melt phase, etc. Given favorable mixing proportions of mafic and felsic magmas, the rate of mixing is controlled by the intensity of mechanical stirring, the rheological contrasts between the magmas (Blake and Koyaguchi 1991; Sparks and Marshall 1986) along with time of interaction (Δt). With mechanical mixing, both magmas involved maintain their physical and compositional characterisitcs and will thermally equilibrate to some intermediate temperature given enough time. This intermediate temperature is dependant on proportions of the magmas, their initial temperatures and the heats of fusion of crystalline phases (Blake and Koyaguchi 1991). The lower temperature melt will remain a liquid at the new temperature with a corresponding reduction in viscosity. The higher temperature magma will now be in one of three physical states: (1) a solid (glass if quenched); (2) a melt approaching 60% crystallinity, with a viscosity greater than the felsic magma; or (3) a melt with a viscosity lower than the other magma (Sparks and Marshall 1986). After thermal equilibrium, contrasting magmas will commingle or hybridize, depending on the rheologies of the end members at the equilibrium temperature (Blake and Koyaguchi 1991; Sparks and Marshall 1986). If both magmas are still liquids with the mafic magma retaining a lower viscosity than the felsic magma then hybridization is possible.

Following a *general case* outlined by Sparks and Marshall (1986), we consider two magmas, denoted M and S, for mafic and felsic melts, respectively. The felsic magma has a high viscosity and low temperature as compared to the mafic magma that has a high temperature and low viscosity. On initial mingling both M and S melts maintain their chemical and physical attributes. Heat exchange between the end members results in an equilibrium temperature that is intermediate between their initial temperatures. Shape need not be maintained at this stage, with deformation or flow common during heat exchange.

Heat gained (H_s) and heat lost (H_m) from felsic and mafic magmas, respectively, are given as:

$$H_s = \{C_s(\theta - T_s) + X_s L_s\}(1 - x) \tag{3}$$

$$H_m = \{C_m(T_m - \theta) + X_m L_m\}x \tag{4}$$

where $C_{m,s}$ are heat capacities of both solid and liquid phases (assumed to be equal), $T_{m,s}$ are initial melt temperatures, $L_{m,s}$ are heats of fusion or crystallization of solid phases, X_m is mass fraction of new crystals in mafic magma, X_S is mass fraction of dissolved crystals in felsic magma, θ is equilibrium temperature and x is mafic magma fraction of mixture. Again, the above equations represent a simple ideal case.

Magma S undergoes heating to reach the equilibrium temperature, resulting in a viscosity decrease and dissolution of any pre-existing crystals. In magma M there is a cooling effect, resulting in a viscosity increase and crystallization. Sparks and Marshall (1986) examine viscosity in magmas S and M after thermal equilibrium as a function of proportion of magma M involved in the mixture (Fig. 2.3A). With large mafic:felsic ratios the viscosity of magma M is lower than S (regime I) even though magma S has been superheated and its viscosity is lower than its original value. As the ratio decreases (proportion of S increases), the viscosity of M increases. At a critical point the viscosity of M will be greater than that of S (regime II). This critical point is where the viscosity curves cross-over. With further decrease in the mafic:felsic ratio the viscosity of M will increase to the point where the magma is essential a solid (regime III). The transition from liquid to solid is defined when the crystallinity of the liquid reaches

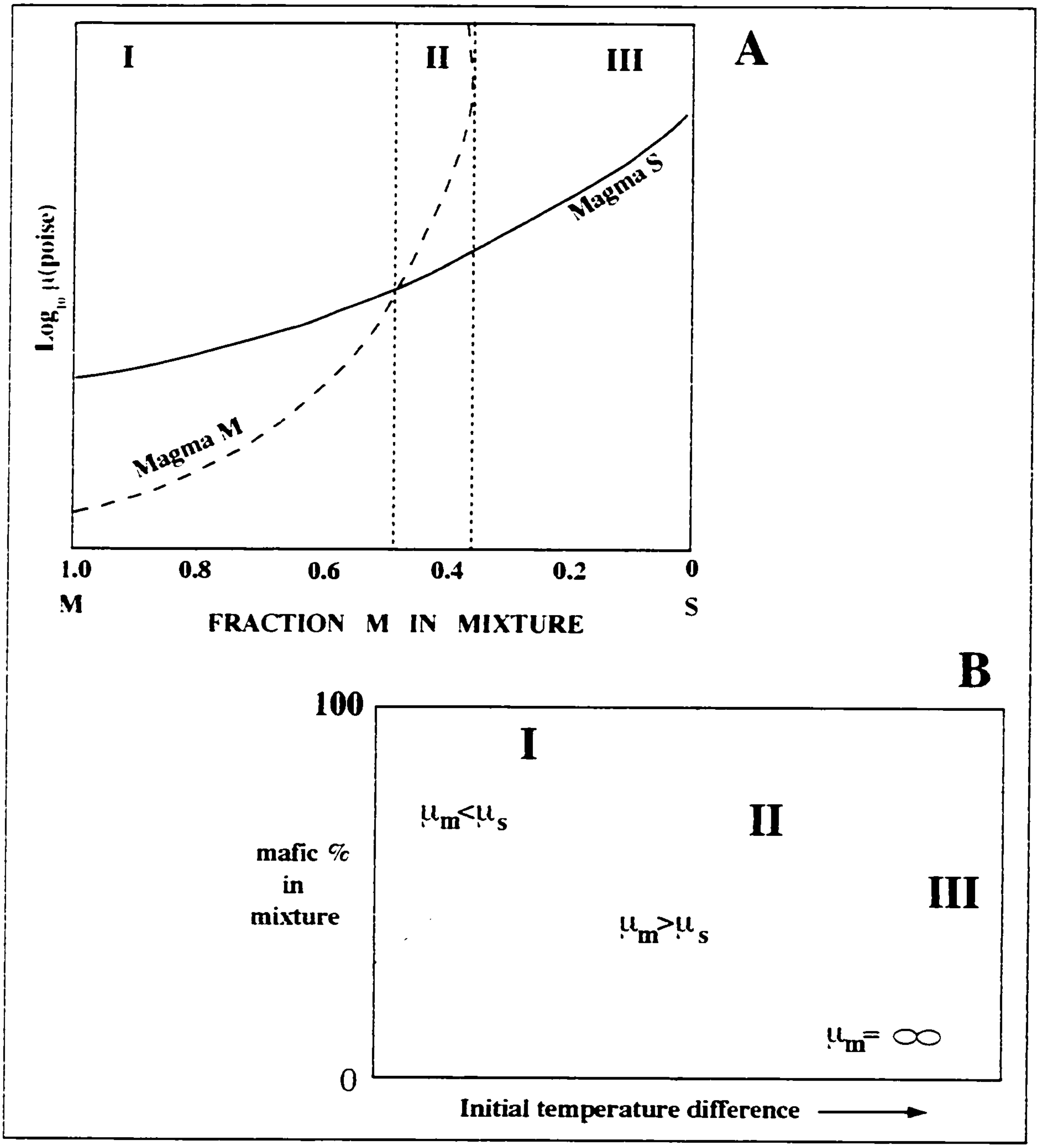

Figure 2.3: Composition-mixing diagrams in a two component system of mafic (M) and felsic (S). (A): Mixing states for variations of viscosity with fraction of mafic magma. Cross-over point of curves M & S separates where magma M has lower viscosity (regime I) from where it has a higher viscosity (regime II). Regime III is where magma M is a solid (Modified from Sparks & Marshall 1986). (B): Mixing states for variations in % mafic magma and inital temperature contrast. Viscosity (μ) of end members included in each regime (From Blake & Koyaguchi 1991).

about 60% (Marsh 1988; Marsh 1996).

Sparks and Marshall (1986) calculated numerous mixing diagrams varying such parameters as viscosity, mafic magma composition, water content of magmas, crystal content and temperature contrasts. While parameters such as water content will affect the viscosity and liquidus temperature of magmas, from all their figures and diagrams it is obvious that the temperature contrast plays a very important role. Blake and Koyaguchi (1991) summarize all the calculations performed by Sparks and Marshall (1986) to derive their own composition-mixing diagram (Fig. 2.3B). The three conditions are based on viscosity as is the diagram by Sparks and Marshall. It is observed that the larger the initial temperature contrast between end members the less likely mixing will be complete. Temperature difference is related to compositional contrast in that the smaller the initial temperatures the similar the end members are chemically.

Hybrid formation is possible in regimes I and II given enough time (Sparks and Marshall 1986). Other workers (Frost and Mahood 1987) regard the boundary between regimes I and II (where $\mu_m \cong \mu_s$), the cross-over point in figure 2.3A, as the best conditions for hybrid formation. It is here that viscosity contrasts are at a minimum. Under conditions in regime III mafic melt will form solid enclaves in their felsic host. All these results indicate that hybrid mixtures between basaltic and rhyolitic magmas is unlikely unless the proportion of basalt is large in the mixture. Silicic hybrids are more probable when mixing andesitic and rhyolitic melts (Blake and Koyaguchi 1991), whereas mafic hybrids are more likely between basalts and andesites.

Blake and Koyaguchi (1991) describe three potential situations for the interaction of a mafic and felsic magmas. Mixing is possible during development of thermal and chemical equilibrium. On approach to thermal equilibrium mixing is limited to physical mixing with end member magmas retaining their original compositions. During chemical equilibrium a wide spectrum can exist from a heterogeneous to homogeneous mixture. Volcanic eruptions (at t_e) will interrupt the mixing process at any stage of its development, whether it is before or after either τ_T or τ_C.

In the situation where eruption occurs simultaneously (Fig. 2.4A) with initial interaction ($t_e < \tau_T$) mixing results from dynamic instabilities. These instabilities occur during magma ascent producing banded pumice in pyroclastic eruptions (e.g. Mount St. Helens: Gardner et al. 1995). Many workers believe that mixing in this case is likely to develop in the volcanic conduit (Blake and Campbell 1986; Koyaguchi 1985). Both host and mixed 'enclave' retain their original composition since $t_e \ll \tau_C$, with sharp contacts between intermingled glasses (microprobe scale), indicating quenching soon after mixing (Sparks and Sigurdsson 1977).

After thermal equilibrium, when the equilibrium temperature (θ) is less than the solidification temperature (T_{ST}) of the mafic magma (Fig. 2.4B), type III conditions of **figure 2.3** persist. Large temperature differences between end members or small mafic:felsic mixing ratios lead to this type of situation. What results are mafic-rich enclaves hosted in a more felsic magma due to incomplete mixing.

In the final scenario, mixing takes place between two magmas that are similar in composition and temperature, thereby preventing the more mafic melt to behave as a solid, type I and II conditions in figure 2.3. Here the equilibrium temperature (θ) is greater that the solidification temperature (T_{ST}) of mafic magma. These conditions favor complete mixing to form a hybrid magma after thermal equilibrium. Figure 2.4C illustrates this scenario. On initial

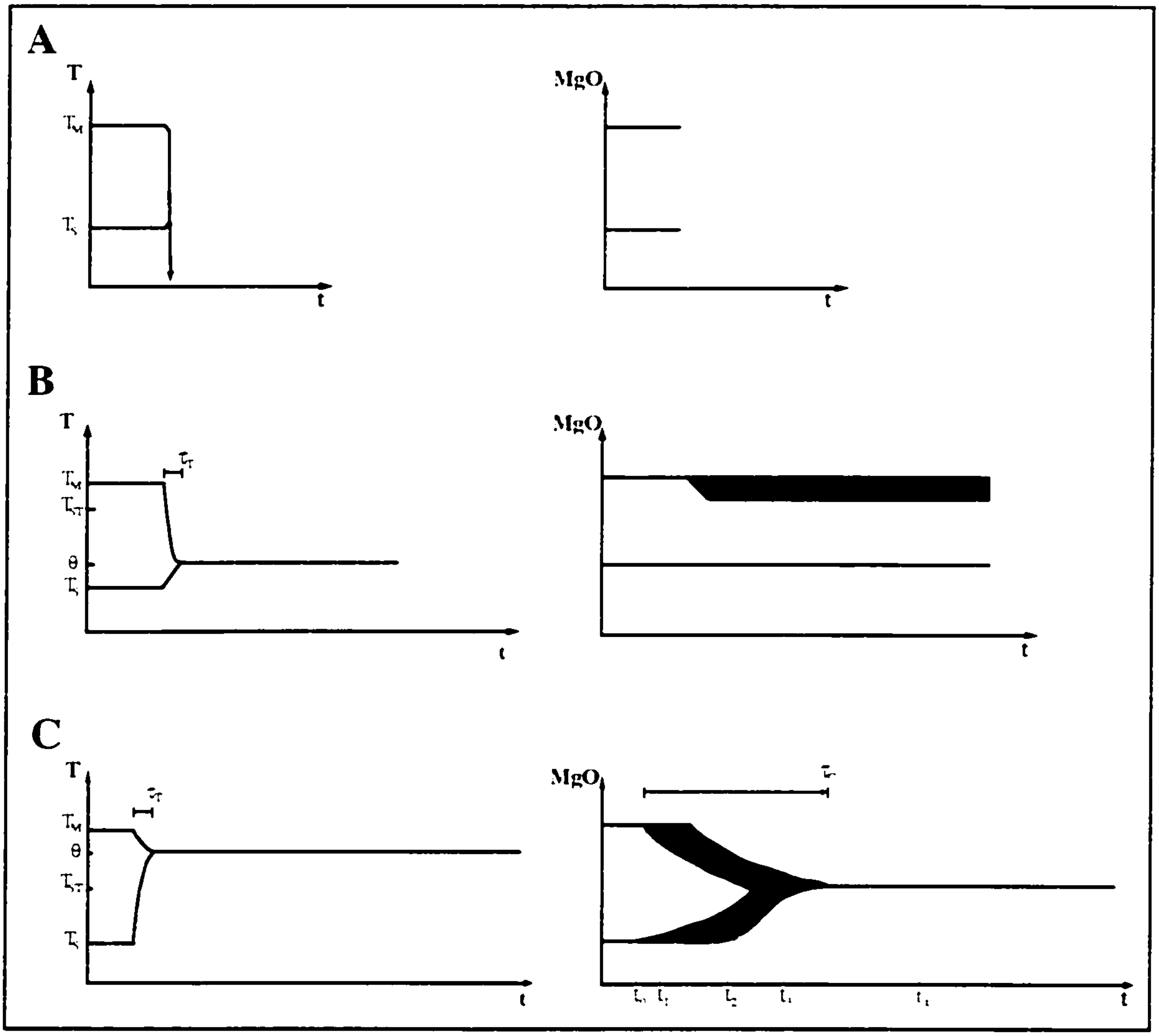

Figure 2.4: Diagrams of temperature (T) and composition (MgO) in magmas before and during magma mixing as a function of time (t). (A) Simultaneous mixing and eruption resulting in physical commingling, with each magma retaining its original composition. (B) Thermal equilibrium (t_T) attained, producing rigid mafic enclaves in felsic magma since the equilibrium temperature (θ) is less than the solidification temperature (T_{ST}). (C) Thermal (t_T) and chemical (t_C) equilibrium reached ($\theta > T_{ST}$) allowing hybridization. See text for further explanation (From Blake & Koyaguchi 1991).

mixing (t_0) both end members are homogeneous. At time t_1 mixing as begun but is incomplete with large compositional gap. Time t_2 mixing is almost complete but a compositional gap still exists. At time t_3 homogenization is almost complete but their is still a slight variation in composition. Time t_4 mixing is complete with the formation of a single homogeneous magma (Blake and Koyaguchi 1991).

2.2.2 Diffusion

Before proceeding further it necessary to discuss information on chemical diffusion since it will be mentioned throughout the following text. Chemical diffusion is a mass transport phenomenon possible in solids, liquids and gases. This chemical transport is controlled by non-equilibrium thermodynamics. Transport of chemical components results from a gradient in chemical potential such as concentration, temperature, or some other operative gradient (Smith and Brown 1988). As a result of this element migration, a net flux of that element is transported which may cause simultaneous transport of charge-balancing species in the opposite direction (Watson and Baker 1990). Liquids are limited to surface and volume diffusion, while diffusion within solids can occur either through the crystal (volume diffusion) or along surfaces, grain boundaries and through dislocations (non-volume diffusion). Non-volume (extrinsic) diffusion is important under low temperature conditions and in deformed or fine-grained rocks, whereas volume (intrinsic) diffusion is important at high temperatures. Volume diffusion mainly requires point defects, which are more prevalent at elevated temperatures. When an atom migrates from one site into a defect it in turn creates a defect, allowing further diffusion. At low temperatures new defects are limited, thus diffusion occurs by migration of defects to sinks. Non-volume diffusion may be important between a solid (crystal) and a liquid, with exchange involving solution/precipitation mechanism (Smith and Brown 1988). This will be demonstrated to be important later for explaining plagioclase textures.

Equilibrium conditions, in igneous systems, have been recognized by both petrologists and geochemists to be hindered by slow diffusion of certain elements in magma. Consequently there is a need for experimental work on natural and synthetic melts to determine chemical diffusion rates. Objectives of these studies have been two-fold: (1) to constrain rates at which natural processes can occur; and (2) to retrieve details about the thermal history experienced in a given system preserving disequilibrium conditions (Watson and Baker 1990).

Feldspar

In natural feldspars, diffusion may occur through a variety of processes with different diffusion coefficients (D), where D relates to the flux (J) of particles to the gradient in chemical potential (μ) by:

$$J = D \frac{d\mu}{dx} \tag{5}$$

which describes Ficks 1^{st} law. To understand these processes it is first necessary to distinguish between varying kinds of diffusion mechanisms or types. Mass transport done on a species found only in trace amounts in a system is defined as *tracer diffusion*. The diffusion coefficient is now the tracer diffusion coefficient (D*). Where D* depends on the composition of the host material, but not dependant on the concentration of the tracer if the tracer is very dilute. *Self-diffusion* describes atomic migration under conditions of *no* potential gradient, thus resulting in no net flux. Composition of the host is important, but has only been determined for end-member feldspars. *Interdiffusion* coefficients are dependant on the composition and are referenced to a specific pair of species in a given material (Smith and Brown 1988). For a more detailed description of the various types if diffusion mechanisms the reader is directed to reviews by Crank (1975) and Hofmann (1980).

Interdiffusion is not limited to high temperatures, especially in alkali feldspars. Observations of exsolution formation at low temperatures in perthites illustrate the efficiency of alkali interdiffusion. Plagioclase feldspar interdiffusion is not as straight forward due to coupled NaSi ⌡ CaAl diffusion. Both Si and Al atoms have high activation energies for movement, which is responsible for common preservation of chemical zoning in plagioclase crystals. While no direct measurements have been made on self-diffusion of Al or Si in feldspar, the diffusivities are on the order of 10^{-4} to 10^{-10}, smaller than for any other atom (Smith and Brown 1988).

Interdiffusion is possible between a feldspar and another mineral, liquid or fluid of different cation ratio, between two feldspars of different composition or when exsolution or homogenization occurs. Plagioclase interdiffusion must deal with coupled diffusion of NaSi and CaAl in order to maintan electrostatic neutrality. Through numerous experiments in interdiffusion on plagioclase feldspar, workers have come to the conclusion that the presence of water will increase values of the diffusion constant on the order of 10^3. It was noted that in all cases interdiffusion values in plagioclase were lower than alkali interdiffusion in alkali feldspar by a factor of 10^{-6} to 10^{-8} (Smith and Brown 1988).

Diffusion in Melts

It is now widely accepted that during ascent and final emplacement magmas are modified by interaction with other magmas or country rock. One such interaction considered is diffusion in the melt phase. Diffusion through melts has the potential to affect various igneous processes. One such process is crystal growth. Diffusion of raw materials to and from the crystal/melt interface can control the growth rate of that mineral phase (Baker 1990).

Diffusivities of elements other than alkalies are thought to be controlled by the diffusivity of Si during interdiffusion of mafic and felsic magmas, as Si^{4+} is the rate controlling factor. This hypothesis is based on experimental work demonstrating that as SiO_2 content in the melt increases, melt becomes more polymerized and diffusivities of other elements decrease (Baker 1990).

Alkali diffusivity (K and Na) is measured to be 5 orders of magnitude greater than the diffusivities measured for other major elements (Baker 1990). Typical range of diffusivities for alkalies are 10^{-5} to 10^{-7} cm^2/sec at temperatures of 1200 to 1500°C. Diffusivity of large alkalies are generally lower than smaller alkalies with which they diffuse. Therefore, transport of another cation (normally Ca^{2+}) is required to maintain charge balance (Hofmann 1980; Watson and Baker 1990).

Alkali to alumina ratios can affect the chemical diffusivity in a melt by influencing the melt viscosity, where melt viscosity is inversely related to chemical diffusivity. Alkalies can serve as network-modifiers (acids) breaking bonds of $(Si,Al)O_4$ tetrahedra and resulting in depolymerization causing a decrease in melt viscosity (Baker 1990).

Experimental work on liquid/liquid interdiffusion done by Watson (1982) involved mafic magma interaction with felsic melts. Basaltic magma was placed in a diffusion couple with molten feldspar or granite to simulate mafic magma intruding into continental crust. Detailed work revealed the phenomenon of non-linear or selective interdiffusion. In all experimental runs (0.001 and 6 kbar; 1200 and 1300°C) the following conditions apply: (1) with respect to SiO_2, mafic and felsic diffusional mixing is low, with interdiffusion profiles giving Boltzmann-Matand diffusivities on the order of 10^{-9} to 10^{-10} cm^2/sec; (2) alkali interdiffusion up to 10^{-5} cm^2/sec, resulting in net fluxes either down or up the initial concentration gradient (uphill diffusion - diffusion from low SiO_2 melt to high SiO_2 melt), whichever tends to establish a felsic/basaltic liquid concentration ratio of ≈ 2:1 - 3:1; and (3) where diffusion reservoirs are finite, initial rapid transfer of alkalies ceases and concentration gradients for all elements become equal to that of SiO_2. It is concluded that interdiffusion of magmatic constituents is rate controlled by the diffusion of SiO_2, since the activation energy for Si diffusion is very high. In melts of high silica content certain melt components, particularly alkalies, have lower activation energies (at given concentrations), whereas other elements such as CaO, MgO and FeO the opposite is true. This results in all components responding such as to establish *transient partitioning* equilibrium between high and low silica melts. As long as the two melts remain separated structurally due to slow SiO_2 diffusion equilibrium will be maintained (Watson and Baker 1990).

Other chemical diffusion experiments performed with intermediate and silicic melts (along with peralkaline and peraluminous melts) demonstrate that diffusivity of non-alkali cations is controlled by the diffusivity of network formers Si and Al. Again, alkalies diffuse much more quickly than other elements (Baker 1990). In comparing diffusivities to SiO_2 content of the melt it is observed that there is only a moderate affect. Their observations are problematic since chemical diffusivities are dependant upon the chemical potential gradient during diffusion. A larger gradient is to be expected between a mafic/felsic interdiffusion experiment as compared to a dacite/rhyolite. However, at 65 wt% SiO_2 the Si diffusivity measured between the mafic/felsic melt of Watson (1982) and the dacite/rhyolite melt of Baker (1990) only vary by a factor of 3 at 1300°C. Pressure differences are considered insignificant as the Si diffusivity decreases only 1.5 orders of magnitude over the range of 56 to 75 wt% SiO_2 at the pressures studied (Watson and Baker 1990).

Diffusion in Glass

Diffusion in glass is considerably faster than in crystals by a factor of about 10^5 to 10^6. From experimental work, diffusion coefficients of elements in a glass were noted to decrease with increasing ionic radius. Glass of albitic composition, at 973K (700°C), has diffusion coefficients for Na (10^{-10}), K (10^{-12}), Rb (10^{-14}) and Cs (10^{-17}). Overall, divalent cations (ie Ca^{2+}) diffuse slower then univalent cations (ie Na^+) in melts of feldspar composition. Diffusivity of both Ca^{2+} and Sr^{2+} were found to decrease slightly with pressure and increase slightly with H_2O content (up to 4 wt%) (Smith and Brown 1988).

Crystal Dissolution

Introduction of a mineral phase into a melt undersaturated with respect to that phase results in dissolution leading to chemical heterogeneity as well as chemical diffusion. Under natural melting conditions dissolution processes are assumed to be rate limited by diffusion within the melt, not by crystal/liquid interface kinetics. Experimental work has shown that diffusion gradients next to dissolving minerals agree very well with ideal diffusion models. This would not be the case if interface kinetics regulated the release of diffusant at the crystal surface (Watson and Baker 1990).

Crystal Growth

Crystal growth can lead to chemical diffusion effects in the surrounding melt. Diffusion gradients are expected near rapidly growing crystals of composition different from that of the host melt. Consequently, incompatible elements are enriched at the crystal/melt interface while compatible elements are deleted if diffusion within the melt cannot keep pace with crystal growth. A boundary condition is established around the growing crystal as compatible and incompatible elements diffuse to and from the crystal/melt interface. This boundary is a chemical gradient which can be up to 50 μm thick (Watson and Baker 1990).

Pressure Effects

There is a lack of experimental work done on the effects of pressure on diffusion. While various pressures have been used in experiments, the effect of varying pressure in diffusivities has not been investigated. From the few studies that have performed it is noted that a positive correlation does exist between pressure and diffusion. Baker (1990) observed that the pressure effect is minimal, with a factor of 4 at 1300°C from a pressure variation from 1 atm to 10 kbars (Watson and Baker 1990).

Diffusivity Calculations

Early workers believed that it was possible to calculate chemical coefficients from the bulk gain or loss of a component or tracer in a substance if both initial and boundary conditions are known. This approach gave no information about the transport process and was not reliable for processes other than volume diffusion (Hofmann 1980). The problem with calculating chemical diffusivities is that they vary with chemical composition. However, Baker (1990) demonstrated that *transition state theory* (TST) has some promise in allowing chemical diffusivities to be calculated without diffusion measurements for interdiffusion of silicate melts. The relative insensitivity of alkali diffusion to melt composition make them particular good candidates for application of TST to compute diffusivities. However, non-alkalies require detailed structural and thermodynamic data for the melts in question before TST can be applied to compute diffusivities. Fortunately, TST can also yield diffusivities indirectly from melt viscosity through the Eyring equation:

$$D = \frac{k_B T}{\lambda \eta} \tag{6}$$

where k_B is Boltzmann's constant, T is temperature in degree Kelvin, λ is the jump distance for the diffusing species during each diffusive step and η is the melt viscosity.

In comparison studies, the relationship between measured and calculated diffusivities is very good. Over a range of 10^{-11} to 10^{-7} cm^2/sec the Eyring equation can predict to within a factor of 3 of the measured diffusivities of non-alkalies during interdiffusion (Watson and Baker 1990).

By comparing Shaw's (1972) method of calculation of melt viscosities and the Eyring equation, it is possible to calculate the rates of diffuse interaction between juxtaposed melts of different composition (Watson and Baker 1990).

2.3 Feldspars

The most abundant crystal phase in all pumice samples collected from Tenerife is feldspar, making up 15 vol % of the rock. In the rocks studied there exists a wide range in the morphological habits of feldspar, from euhedral phenocrysts to dendritic microphenocrysts. Typically all these forms are found within the same pumice sample, indicating quite different crystallization histories.

Feldspar crystals are studied in detail, not only due to their abundance, but also for the substantial amount of literature on them and their related magmatic processes. However, the most important reason is that feldspars are one of the best group of minerals in recording the history of a crystallizing magmatic body, especially in terms of *magmatic growth*, *subsolidus transformation* and *deuteric alteration* (Brown and Parsons 1994).

The magmatic growth stage operates in all but completely glassy rocks. This stage involves nucleation and growth of feldspars with high Si, Al disorder. Both growth and partial dissolution are possible during this stage if different liquids are in contact during crystallization (ie magma mixing). Very slow Si, Al diffusion in plagioclase and CaAl and NaSi coupling result in crystal zonation, with zoning paths well preserved and approaching ideal fractionation. Water contents in crystallizing magma will dramatically lower the liquidus temperatures (Brown and Parsons 1994).

Depending on the cooling rate, the subsolidus transformation stage affects the intracrystalline relations by phase-transformation and exsolution microtextures. The scale and extent of the microtextures depend inversely on cooling rate, since they involve Si, Al ordering or interdiffusion or both. However, these microtextures are often sub-microscopic in scale and are normally not given adequate attention by petrologists and geochemists. Due to lattice coherency and misfit feldspars, especially alkali feldspars (due to ionic size difference between

Na and K), may store very large amounts of elastic energy (Brown and Parsons 1994).

Once feldspar crystals have been nucleated they may initially undergo continued growth or partly dissolve before cooling causes increases undercooling. Cooling rates control whether nucleation is homogeneous (formation of new crystals within the liquid) or heterogeneous (overgrowth on pre-existing crystals), followed by overgrowth. Rapid cooling will increase undercooling to the point where homogeneous nucleation and overgrowth are possible. This results in two size generations of feldspar, large phenocrysts and small groundmass (quenched) crystals. Where cooling is slow, undercooling will not be sufficient for homogeneous nucleation to operate in the liquid. Entrained crystals will just be overgrown (heterogeneous nucleation) *in situ* , unless diffusion is very slow as in felsic magmas (Brown and Parsons 1994).

Extremely rapid cooling conditions result in strong disequilibrium growth. Both compositions and zoning paths are, for the most part, unpredictable in detail with crystals approaching non-fractional or partitionless crystallization. Crystal compositions are closer to bulk composition of the liquid than expected. Crystal morphology is strongly skeletal to spherulitic. Under slow cooling conditions crystallization will approach equilibrium, with euhedral crystals. Complete equilibrium crystallization requires continuous interdiffusion within the crystal and exchange with the liquid at the interface such that the growing crystal remains homogeneous and of the correct composition. Note that complete equilibrium crystallization involving plagioclase is not probable because Si, Al interdiffusion is extremely slow relative to growth rates. Growth of plagioclase can approach ideal fractionation crystallization, with equilibrium being maintained at the interface only and not within the crystal, which becomes compositionally zoned. Where crystallizing plagioclase is in contact with different liquids, or the same liquid but under different pressure conditions or activity of some components, developing textures may be quite complex along with zoning paths. Under these conditions crystals may have experienced periods of dissolution (Brown and Parsons 1994).

3 Diego Hernández Wall

3.1 Formation and History

Diego Hernández wall is a distinctive section of Las Cañadas Caldera, composed of pre-caldera rocks exposed in the eastern and northeastern section of the caldera (Fig. 1.2). Its vertical exposure of 250 m is the maximum exposed thickness of the Diego Hernández Formation. Diego Hernández wall is probably the best exposed and accessible group of pyroclastic rocks found in Las Cañadas Caldera making it ideal for intensive study. The northern section of the wall is dominanted by a large dyke that runs perpendicular to flow bedding. This dyke serves not only as a marker, but also as a natural staircase for climbing to various sections of the wall (Fig. 3.1A). The dyke is oriented in a NE-SW direction corresponding to one of the proposed regional tectonic trends (Martí et al. 1994b). A reverse fault, radial with respect to the caldera, is located just north of dyke (Fig. 3.1B) and is related to caldera collapse (Martí et al. 1994a).

The Diego Hernández Formation results from several eruptive events that produced mainly nonwelded pyroclastic deposits. Different events are recognized by the presence of erosional surfaces and intercalated basaltic rocks that signify intervals between pyroclastic episodes. Phonolitic pyroclastics dominate the stratigraphic sequences, with several minor intraformational breccias. Both welded tuffs and clastogenic lavas are conspicuous by their absence from the Diego Hernández Formation as compared to the underlying Ucanca and Guajara formations (Martí and Mitijavila 1995). This may indicate a lower emplacement temperature or that the eruptive event was not as large as the former two collapse events.

Martí et al. (1995) identify two main ignimbrite types in the Diego Hernández wall. The first type is a lithic fragment-rich ignimbrite, where pumice fragments are angular and are less

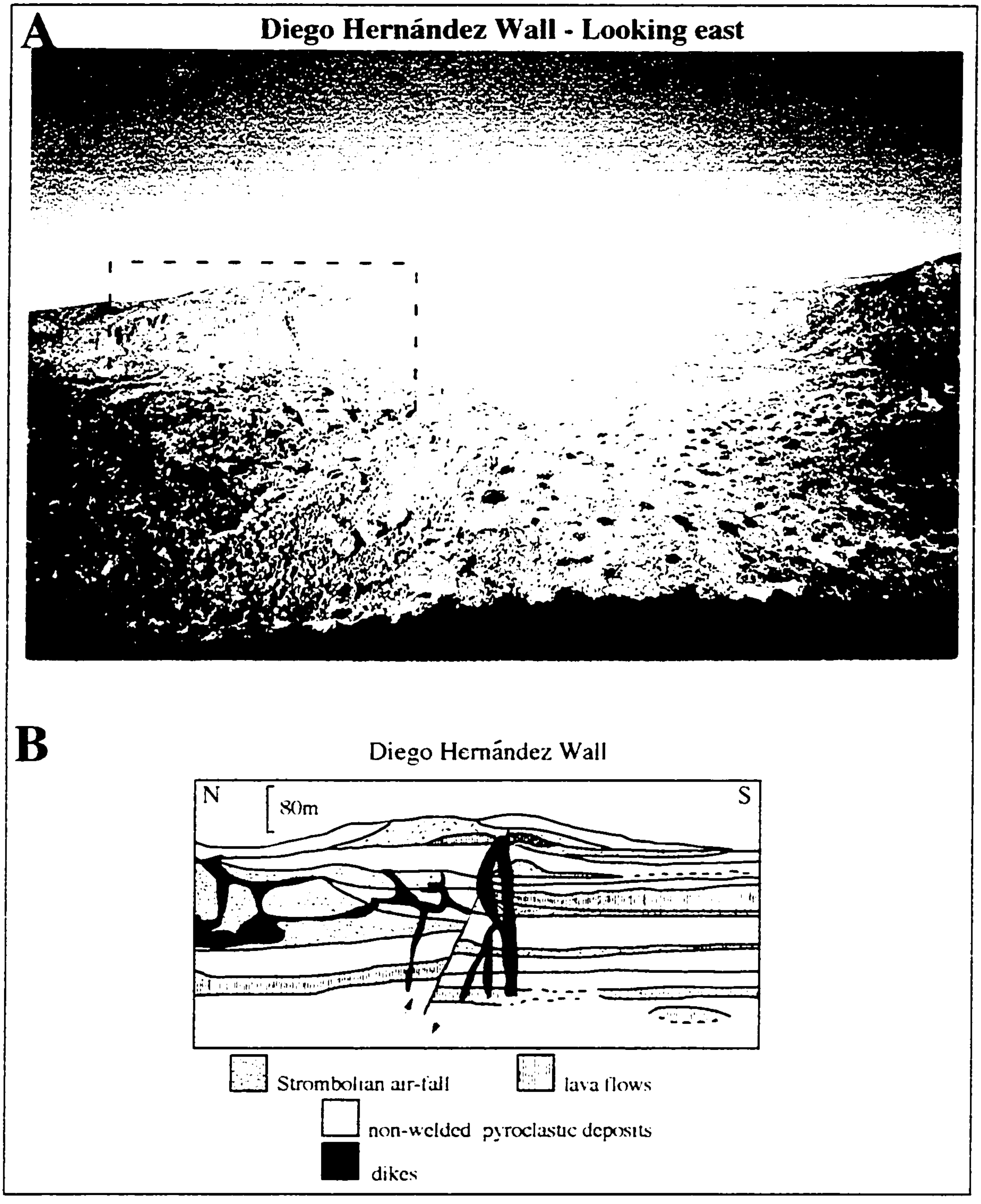

Figure 3.1.: Diego Hernández Wall. (A) Plate of Diego Hernández Wall looking east showing location of samples. (B) Sketch of Diego Hernández Wall looking east. Sketch location is shown in plate (A). Sketch is after Marti et al. 1994.

than a few centimeters in size. Intraformational breccias are sometimes associated with fragmental lithic-rich ignimbrites. The second type is pumice-rich ignimbrites, characterized by a veneer and valley-ponded lateral facies. Pumice fragments are typically rounded, ranging from less than one centimeter up to several decimeters. Lithic fragments are normally graded and concentrated towards the base of the ignimbrite whereas pumice fragments are reversely graded. Both types of ignimbrites include banded black and green pumice (Plate 3.1).

Polygenetic lithic clasts are commonly hydrothermally altered and may indicate that the eruption had a phreatomagmatic component. Hydrothermal alteration of lithic fragments prior to incorporation into these lithic-rich ignimbrites is implied from an inferred low temperature emplacement and that both altered and non-altered lithic clasts are found together in the deposit. Hydrothermally altered lithic fragments are observed to increase in abundance up the stratigraphic section (Martí and Mitjavila 1995).

In the uppermost section of the Diego Hernández Formation there is a polygenetic intra-formational breccia containing abundant co-magmatic syenite clasts. Also present are gabbro fragments and K-feldspar phenocrysts. This breccia coincides with the last pre-caldera deposit, dated at 178 ± 20 Ka (Table 1.1). Evidence for a lag origin associated with a major pyroclastic flow is supported by the presence of subordinate rounded pumice fragments and the deposits widespread distribution. No massive pyroclastic deposit can be traced laterally back to the caldera from the coast due to erosion. Correlation of the nature and abundance of lithic fragments, composition of juvenile fragments, crystals and their stratigraphic relationships, along with geochronological data indicate that this breccia may be a proximal facies of the El Abrigo Ignimbrite (Martí and Mitjavila 1995).

Samples for this project were taken from lower portions of the Diego Hernández Formation, located between 40 and 50 m from the base of the Diego Hernández wall (Joesph

Plate 3.1: Banded pumice from Diego Hernández Wall with distinctive green and black commingled appearance. Several hydrothermally altered lithic fragments also in field of view. Portion of pen in photo is 11 cm long.

Plate 3.2: Surge layer seperating two pumice flow deposits from Diego Hernández Wall. Several green and black banded pumice fragments in field of view. Lens cap is 6 cm wide.

Plate 3.1

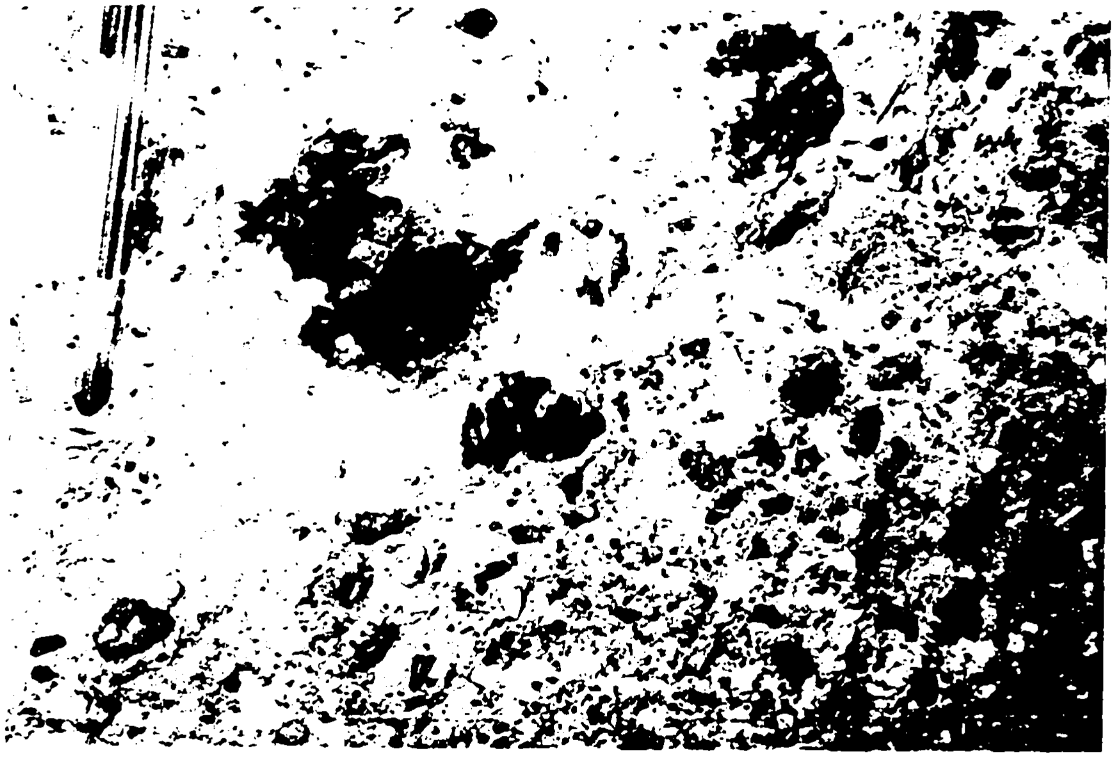

Plate 3.2

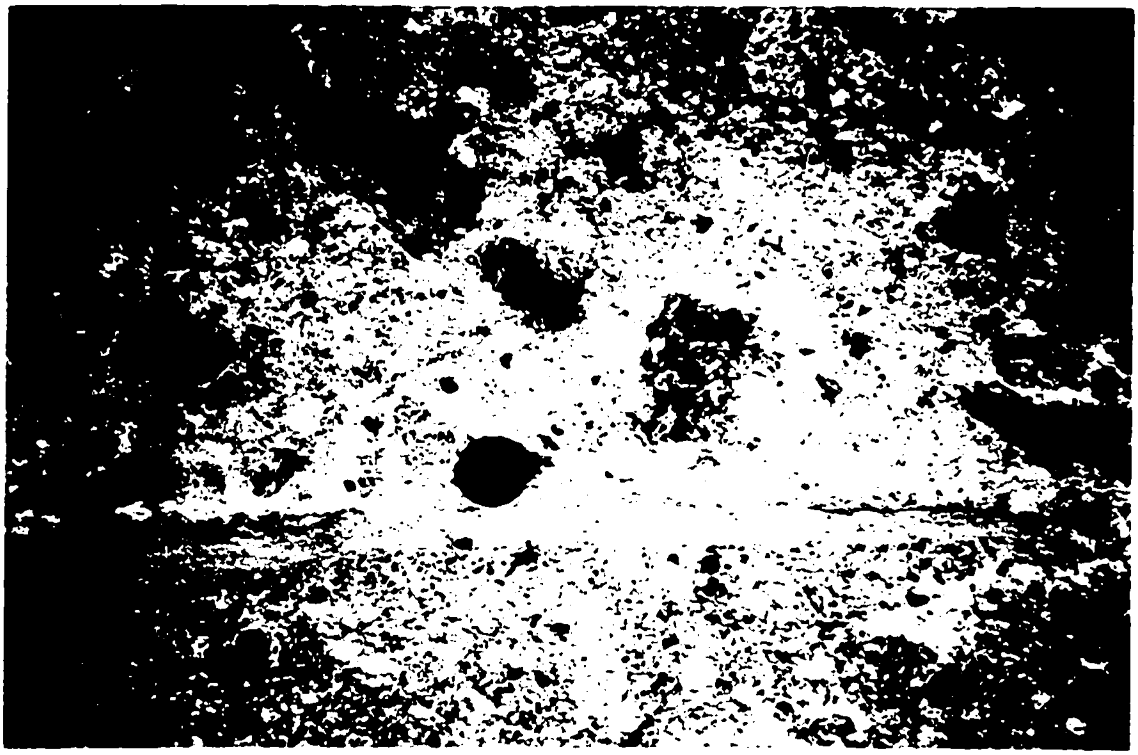

Mitjavila pers. comm. 1995) according to simplified stratigraphic section (Fig. 3.2). Two sample series were taken from the wall, both from pumice-rich ignimbrites. The first series was aquired in the Spring of 1994 by Drs. Tony Fowler and Karen St. Seymour while attending a field trip led by Dr. Joan Martí. The second series was collected by the author in the Spring of 1995 while attending the "Workshop on Explosive Eruptions in Phonolitic Magmas" given on the island of Tenerife. The two series are separated by a thin surge deposit (Plate 3.2) with no more than 5 m separating the two. The surge layer maybe part of the underlying or overlying ignimbrite, depending on whether it was an ash cloud surge or preceding surge of a flow, respectively, or it may even contain portions of both surges. The surge represents a time gap between the two ignimbrites. However, no significant time gap exists between these pumice-rich flows, since there is no evidence of an associated airfall, lava flow or paleosol. The lower ignimbrite sampled has been dated to be 266 ± 17 Ka (DH23B in Table 1.1) (Alvarez 1990; Martí and Mitijavila 1995)

3.2 Petrography & Chemistry

A suite of samples were collected from two ignimbrite sections of the lower portion of Diego Hernández wall. Care was taken to obtain representative samples of a mafic, felsic and banded pumice. After careful examination of the units two samples from the lower ignimbrite (LI) were examined, namely a mafic and felsic pumice. From the upper ignimbrite (UI) two banded and a mafic pumice are examined. Polished thin sections were made from each of these samples. All pumice fragments had to be flooded with epoxy prior to thin section preparation due to their friable nature.

It should be noted that whereas mafic pumice hand samples appear homogenous, on the microscopic scale trace amounts of felsic glass occurs within them. Felsic glass occurs as small

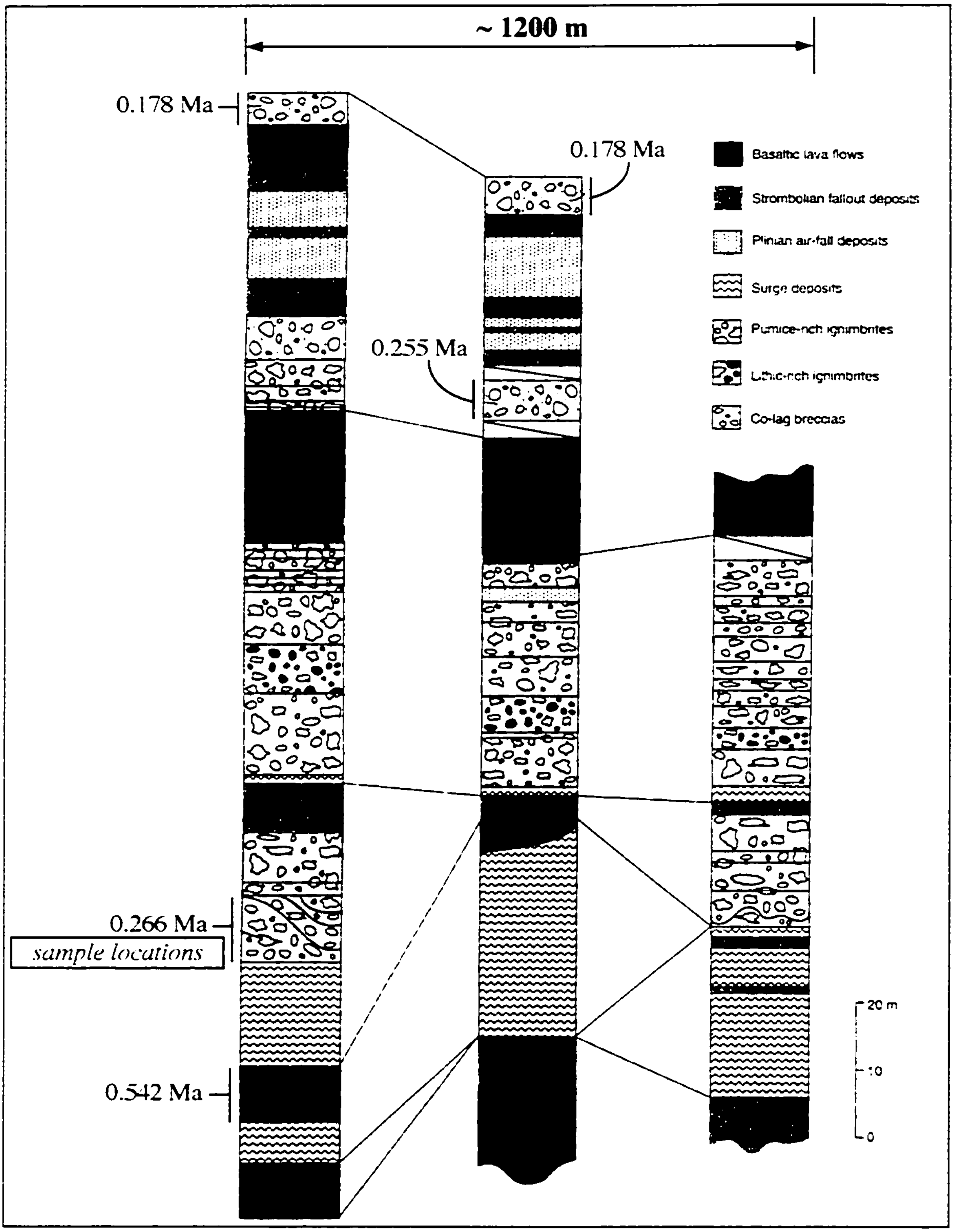

Figure 3.2.: Simplified stratigraphic sections from Diego Hernandez Formation showing age relationships (see Table 1.1) and sample locations. From Marti & Mitjavilla (1995).

blebs or discontinuous streaks (Plate 3.3) rather than stretched out, continuous bands found in banded pumice samples (Plate 3.4).

From LI the mafic (TK-9C) and felsic samples (TK-9D) were collected by Drs. Fowler and Seymour. Mafic (CS-010A) and banded (CS-010 and CS-011) samples are from UI, collected by the author. See figure 3.3 for sample locations. From a selection of 35 thin sections, detailed petrography and mineral chemistry were carried out on five sections. These five sections were selected, after thorough examination of the sample suite, due to their glass associations and presence of all phenocryst phases.

Mafic and felsic pumice are defined by color intensity. Mafic pumice are identified in the field by their dark color, typically black, with trace millimeter-sized feldspar crystals. Felsic pumice are recognized in the field by their lighter color, ranging from white to lime green, with rare millimeter-sized feldspar crystals.

3.2.1 Glass

Glass was analyzed by electron microprobe from all polished thin sections in an attempt to quantify different end member compositions and to assess whether any diffusion occurred in mingled pumice samples. Glass end members are identified microscopically by color, with pale green to clear glass being the felsic end member and dark brown to black glass the mafic end member. Unless stated otherwise the terms mafic and felsic are used to distinguish the more Si-rich glass (felsic) from the Si-poor glass (mafic) and does not imply any chemical composition. Mafic and felsic glasses are intimately associated, from continuous to discontinuous bands or streaks (Plate 3.3 & 3.4) in all but felsic pumice samples. Contacts are extremely sharp with little to no interaction evident optically, even in NDIC (See Plate 1.2). Color variation is apparent in the mafic member, as exhibited by different shades of brown,

Plate 3.3: Dissolution streak/band of clear to pale green felsic glass in black to dark brown mafic glass. Photo is from mafic pumice sample CS-010A. Diego Hernández Wall.

Plate 3.4: Continuous streaks of interwoven dark brown mafic glass with clear to pale green felsic glass. Sodalite crystal seen in upper portion of photo. Photo from mixed pumice sample CS-010.

Plate 3.3

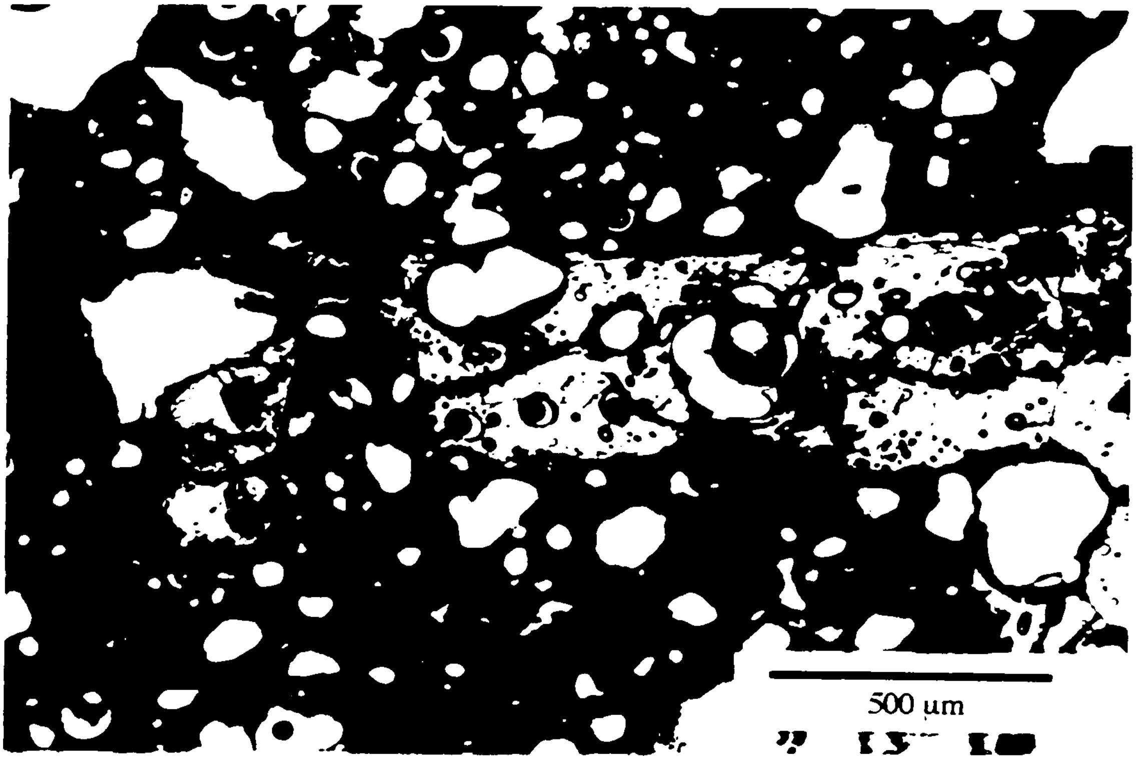

Plate 3.4

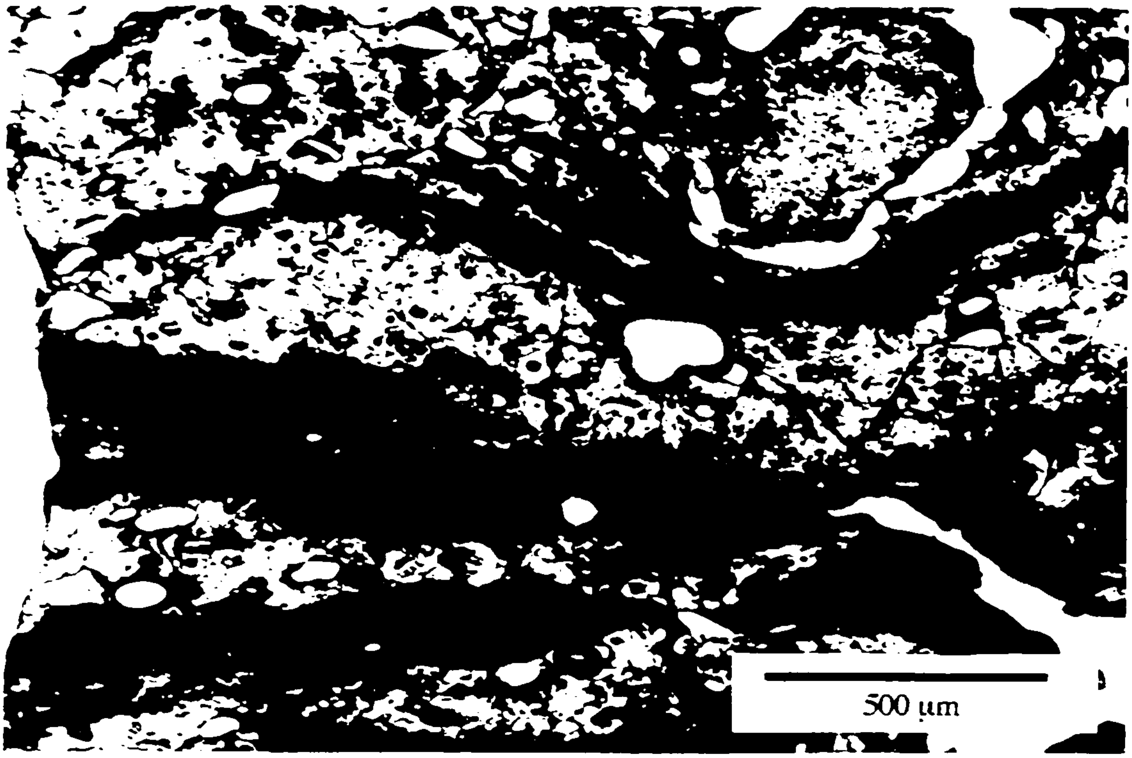

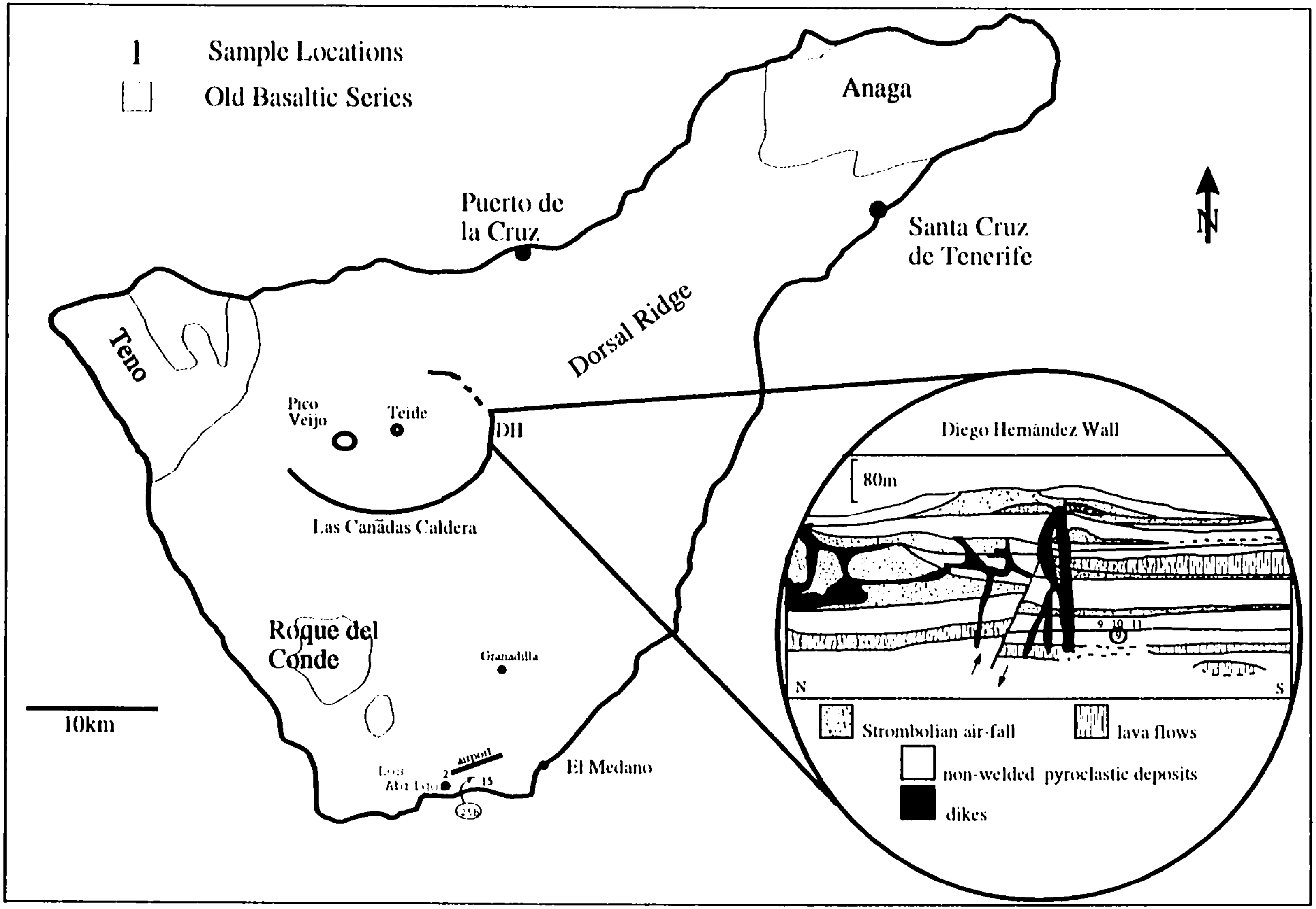

Figure 3.3: Sample location map. Circled sample number is from Drs. Fowler & Seymour. Deigo Hernández wall sketch from Marti et al (1994).

from dark brown to light brown, whereas felsic glass is more uniform. When mafic glass was etched with fluoroboric acid, in that it was found to be very rich in microlites and highly vesicular (Plate 1.2). These microphenocrysts are all euhedral and are considered to represent near-equilibrium growth from the liquid just prior to solidification, hence after expulsion from the magma chamber. By increasing the beam size during EMP analysis, it is assumed that if these microlites are part of the beam spot that their near-equilibrium composition will not affect the data collected, which overall seems to be the case (ie. we have a "whole-rock" analysis) (Table 3.1). Felsic glass analysis did not suffer from this problem, as all analyses were done in microlitic and vesicular free zones. Another result from the EMP analyses was that basing the end members on color was a correct assumption as the pale green glass was more acidic than the dark brown/black glass.

Pumice glass from Diego Hernández is conspicuous by its fairly homogenous major element composition given the diverse phenocryst assemblages, with compositions only ranging from trachyandesite to trachyte/phonolite on a total alkali silica diagram (Fig. 3.4). The basic melt, interpreted to have crystallized Ca-rich plagioclases (labradorite and bytownite) and titanaugites, is missing from the rock record. This may be the result of complete homogenization with a more intermediate melt (trachyandesite) that pre-existed in the sub-volcanic magma chamber prior to injection of the more mafic phase. This trachyandesite is the probable host that crystallized the andesitic plagioclase phenocrysts and salite pyroxenes.

Harker variation diagrams for all individual glass points (excluding line traverse points) exemplify the difference between mafic and felsic glass. Mafic glass define a clear trend with negative slopes of Ti, Ca, Fe, and Mg with SiO_2 (Fig. 3.5) which may indicate a mixing or fractionation trend. Felsic glass is more heterogeneous, with a particular disparity between felsic glass analyzed in mafic and banded samples (TK-9C, CS-010A & CS-010) and those

Table 3.1: Representative EMP analysis of glass. See Appendix A.1 for complete data.

	Felsic glass						
	G003-002	G007-002	G011-005	G015-003	G024-004	G025-021	G037-002
SiO_2	10.836	9.853	9.466	7.927	8.663	8.14	9.309
TiO_2	20.665	20.961	19.282	18.88	20.157	19.002	19.078
Al_2O_3	57.239	57.749	58.031	59.617	59.288	59.734	59.172
FeO_T	0.181	0.146	0.547	0.555	0.401	0.438	0.331
MnO	0.334	0.32	0.854	0.805	0.674	0.752	0.651
MgO	5.565	5.901	5.577	5.954	5.859	5.908	5.541
CaO	0.639	0.803	1.412	1.333	1.085	1.212	0.753
Na_2O	2.815	2.632	3.175	2.88	3.013	2.873	3.065
K_2O	0.223	0.198	0.19	0.114	0.154	0.167	0.235
Total	98.497	98.563	98.534	98.065	99.294	98.226	98.135

Table 3.1: Con't

	Mafic Glass						
	G004-003	G005-004	G010-004	G013-005	G014-004	G020-012	G023-009
SiO_2	6.932	7.228	6.625	6.887	6.825	6.943	6.581
TiO_2	18.581	18.594	17.987	18.424	18.803	18.223	18.607
Al_2O_3	54.769	55.194	54.076	55.423	55.332	54.515	55.961
FeO_T	1.582	1.29	1.88	1.84	1.325	1.555	1.48
MnO	1.528	1.482	1.736	1.743	1.626	1.635	1.404
MgO	5.324	4.859	5.168	4.675	4.884	4.764	4.784
CaO	2.923	3.086	3.512	3.83	3.176	3.363	3.567
Na_2O	4.442	4.516	4.923	4.887	4.869	4.91	4.514
K_2O	0.116	0.116	0.129	0.158	0.16	0.167	0.136
Total	96.197	96.365	96.036	97.867	97	96.075	97.034

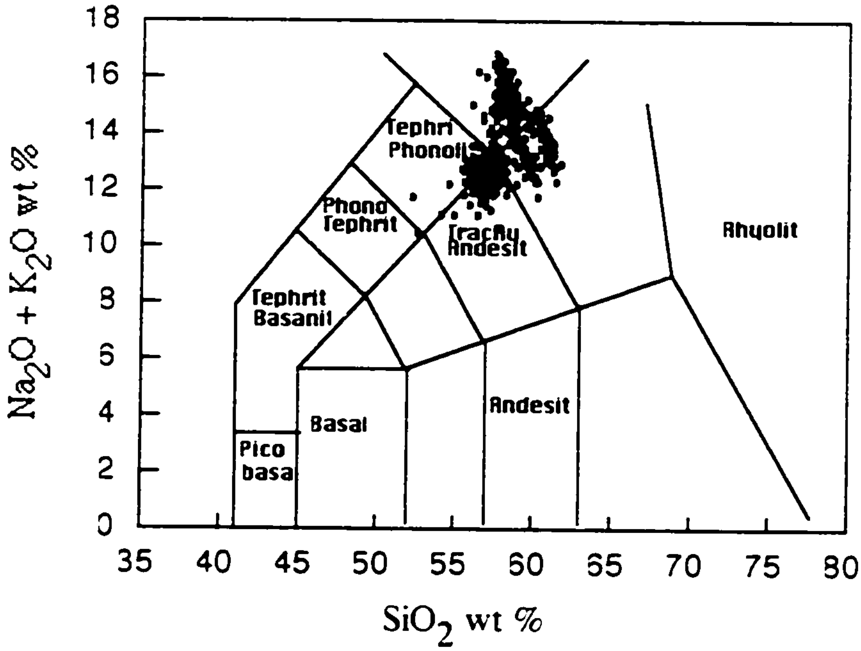

Figure 3.4: Total alkali-silica diagram for all glass from DH Wall. Glass is normalized.

from the felsic sample (TK-9D). Felsic pumice (TK-9D) is especially enriched in Al and notably depleted in Ti, Ca and Mg, some depletion in Fe, and shows little variation with increasing SiO_2 content (Fig. 3.5).

Along with the spot analyses of mafic and felsic glass, 23 traverse lines were done across intermingled glass contacts. The goal was to identify any interaction between the contrasting glass compositions, in terms of a diffusion profile, before quenching. It was then hoped that these profiles could be used to calculate "co-habitation" times. Several line traverses are examined in more detail, all crossing one or more mafic/felsic contacts. From careful examination of all line traverses it appears that little to no chemical interaction took place between individual glasses. In banded pumice (CS-010), line traverse LT045 was completed across two felsic/mafic contacts. Here the mafic glass is a continuous streak sandwiched

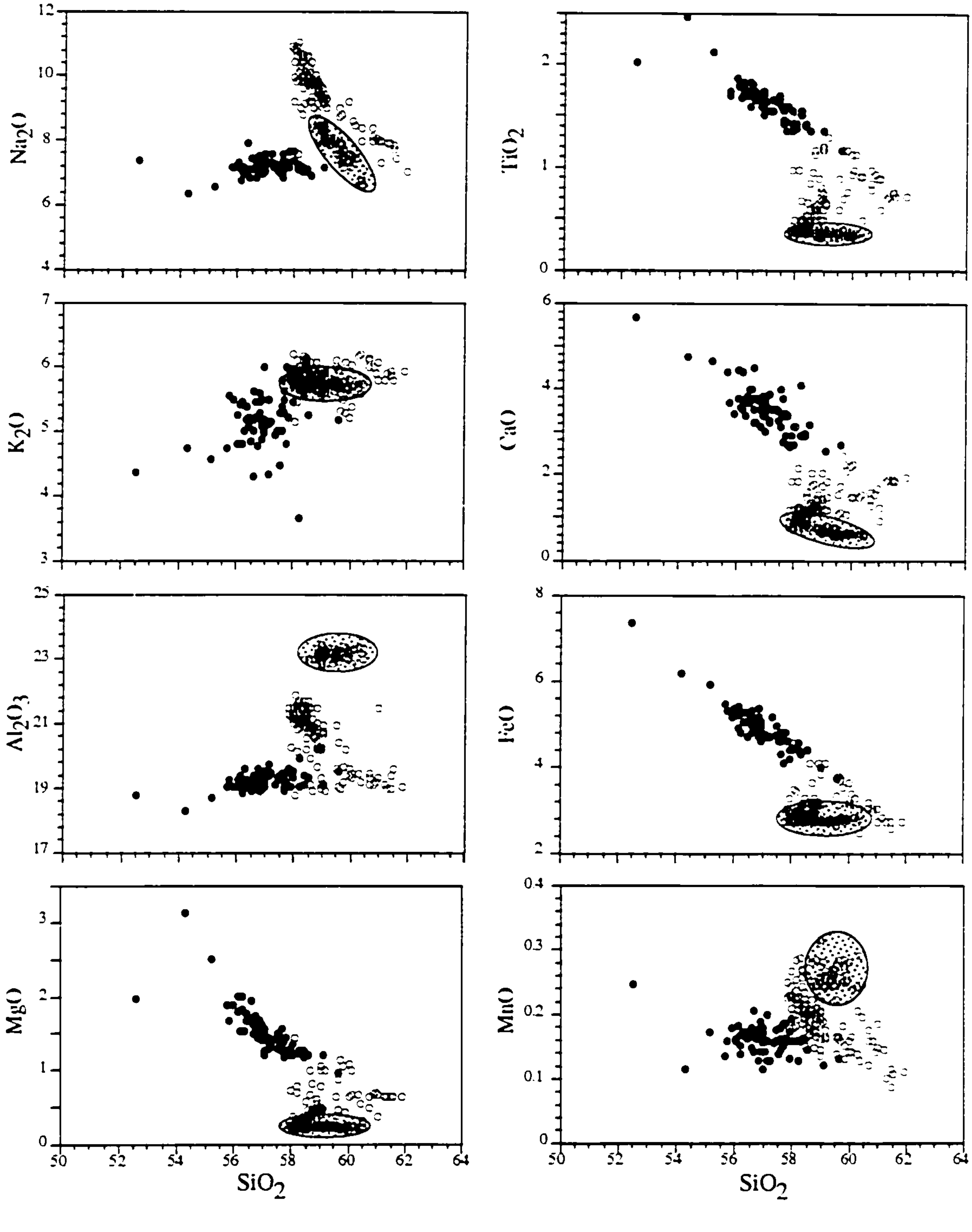

Figure 3.5: Harker diagrams for mafic (●) and felsic (○) glasses from Diego Hernández Wall pumice. Shaded regions are felsic glass from felsic pumice (TK-9D).

between two continuous felsic streaks. The mafic streak is a maximum of 200 μm wide and is has abundant crystals (microlites), whereas the felsic streak is > 400 μm with various degrees of flow-like textures. On the line traverse the mafic streak is obvious by the decrease in Si values over 50 μm to 140 μm (Fig. 3.6). The decrease in Si is accompanied by an analogous decrease in Na and K oxides over the same interval. Another traverse line examined is from mafic pumice, CS-010A. Line traverse LT053 commences at the mafic/felsic contact and moves into the felsic glass. The felsic glass represents a discontinuous streak measuring ≈ 850 μm at its maximum width hosted in recrystallized mafic glass.

3.2.2 Feldspar

Feldspars are the most dominant mineral in all pumice samples collected from Diego Hernández wall, making up approximately 75% of the total phenocryst population. They exhibit a continuous range in composition from bytownite through anorthoclase (Fig. 3.7). Detailed examination of feldspars allows for their classification into three distinct types based on crystal morphology, chemical composition and zoning. These three types are recognized in pre-calderan pumices, two containing phenocrysts and one containing microphenocrysts. The main divisions are *resorbed* (Type I), *non-resorbed* (Type II) and *microphenocrysts* (Type III). Use of NDIC further allows discrimination in several sub-types (Fig. 3.7 & 3.14) as discussed in following sections.

Feldspar - Type I

Type I feldspars are by far the most abundant, accounting for an estimated 60% of all observed feldspars, 9 vol % of the overall phenocryst population. The salient characteristic of Type I feldspars is that they are rounded and embayed, typical features of resorption.

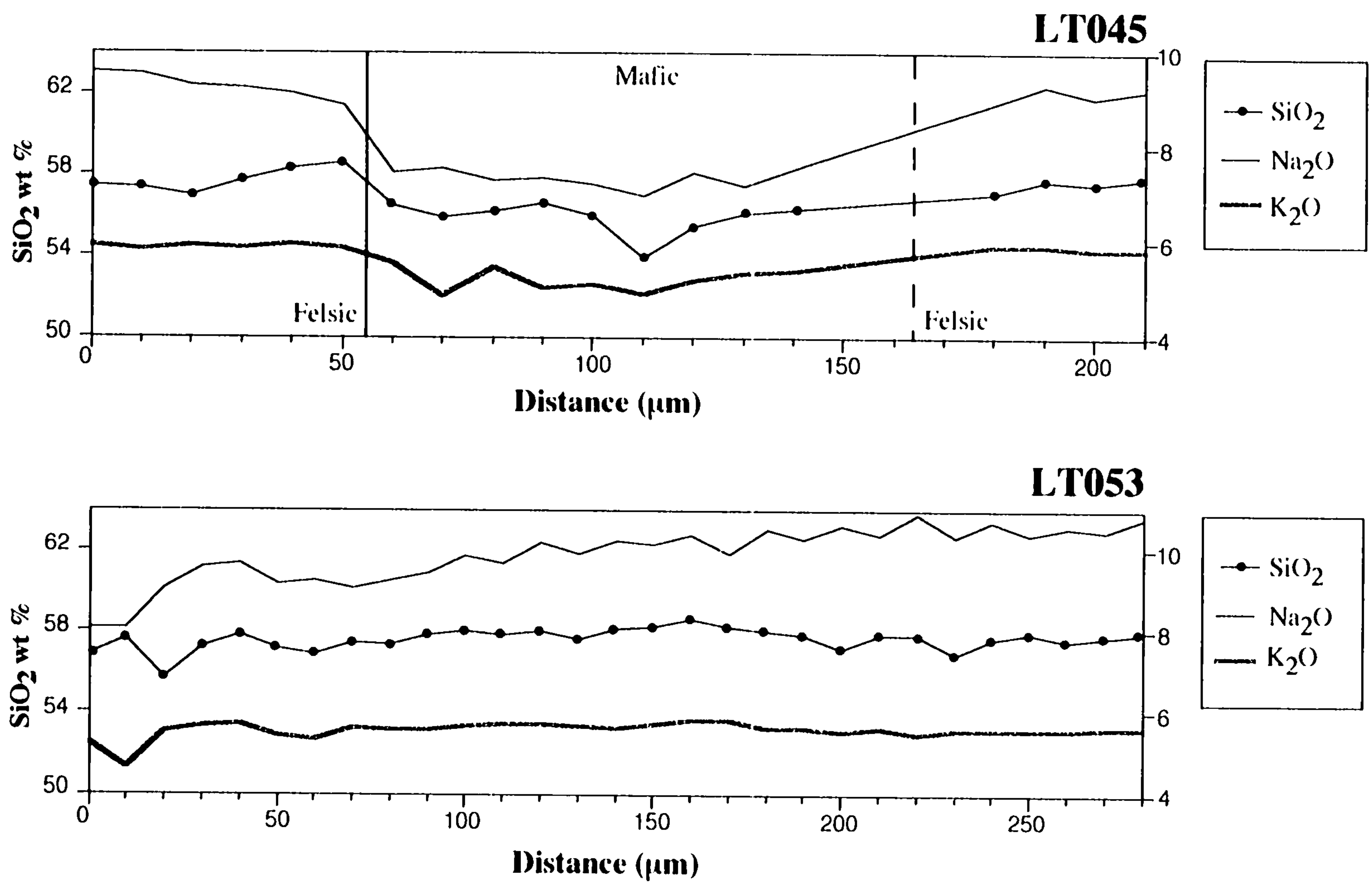

Figure 3.6: Glass line traverses from DH wall. LT045 from mixed pumice CS-010 and LT053 from mafic pumice CS-010A (•) represent EMP points, gaps are points that are not plotted due to "bad" totals. Mafic and felsic transitions indicated.

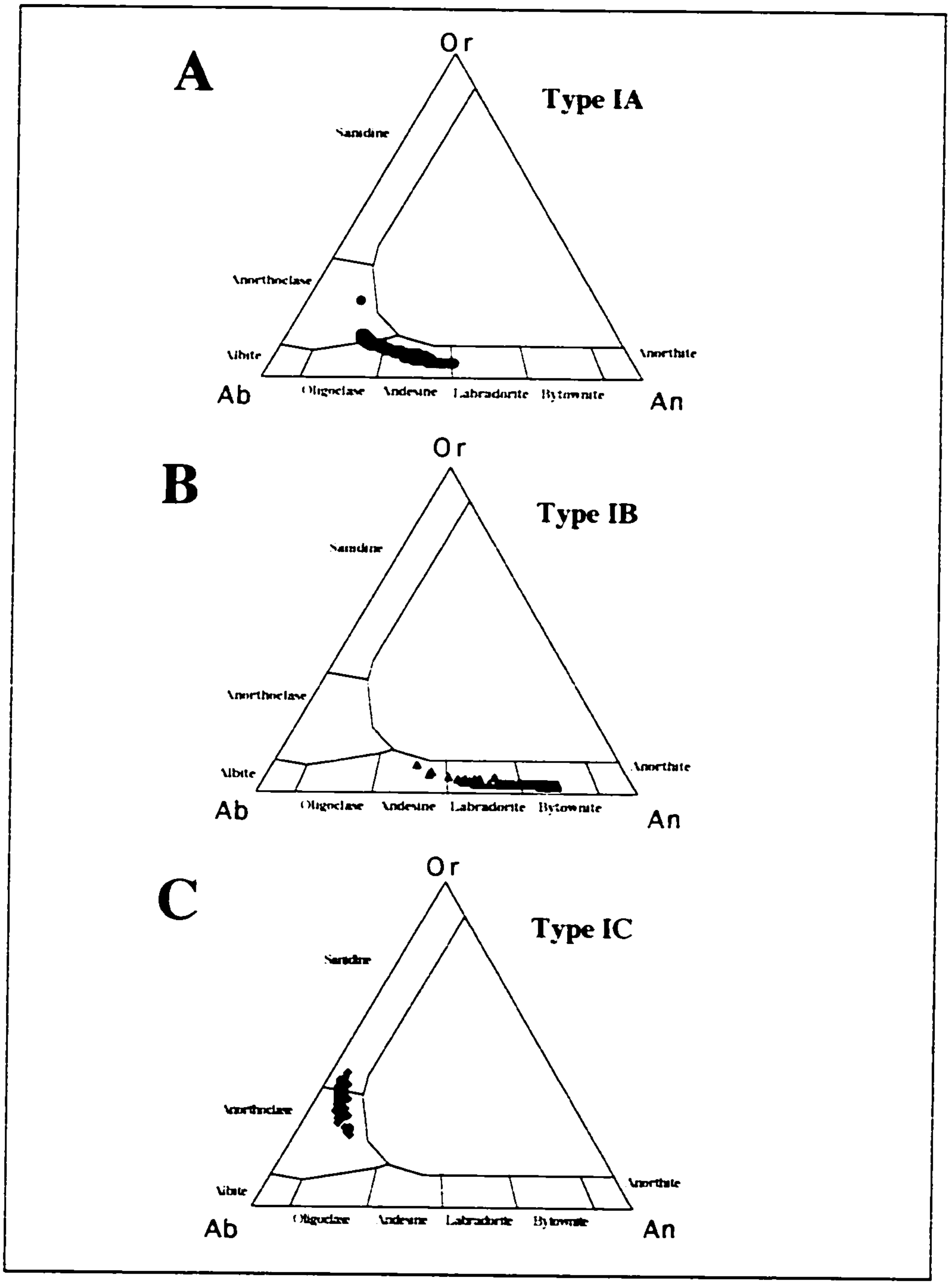

Figure 3.7 : An-Ab-Or plots for different feldspar types from Diego Hernandez Wall. (A) Type IA; (B) Type IB; (C) Type IC.

Resorption is not restricted to exterior crystal faces, but can be penetrative, resulting in a sieve-like texture (Plate 3.5). The largest feldspar phenocryst observed (4.0 mm) and largest phenocrysts overall are found within this group. Crystal facets range from euhedral to anhedral, depending on resorption style. Various recognized morphologies of resorption, interpreted to result from simple dissolution to a possible solution/reprecipitation mechanism (Johannes et al. 1993), are described below. Compositionally, these resorbed feldspar crystals range from alkali feldspar (Or_{40}) to calcic plagioclase (An_{78}) (Table 3.2). Zoning patterns are also variable with patchy zoning being dominant.

Recognition of resorbed crystals is based on rounded, lobate forms, embayments in exterior crystal structure and truncation and cross-cutting relationships (observed in NDIC). Type I feldspars are found in both mafic and banded pumice samples. While these feldspars are absent from felsic pumice, they are found in bands of felsic glass within banded samples, or felsic blebs in mafic samples. Both the degree and style of resorption, as well as composition and crystal size allow Type I feldspars to be divided into three sub-units.

Feldspar - Type IA

Type IA feldspars are very recognizable due to their distinctive morphology. They make up about 5 vol % of the overall crystal content. Crystals range in size from 0.8 to 4.0 mm and have a blocky to rectangular habit. Resorption is weakly to moderately developed, but limited to the core regions. Nomarski (DIC) reveals a complex zoning pattern throughout the crystal body (Plate 3.6, 3.7 & 3.8). Type IA feldspars are dominantly found in a medium to light brown glass and only rarely in dark brown/black or clear glass. Unfortunately, glass inclusions rarely survive thin section preparation. When preserved glass inclusions are medium brown to light brown, as is the matrix glass feldspar compositions are typically andesines

Plate 3.5: X-Nicols photomicrograph of sieved feldspar (Type IB). An_{78}. Sieve texture is crystallographically controlled as the resorbed regions are elongated parallel to polysynthethic twin planes.

Plate 3.6: NDIC photomicrograph of skeletal core region of Type IA feldspar. An_{35}. Core has complex NDIC zoning pattern with several dissolution surfaces situated in mantle.

Plate 3.5

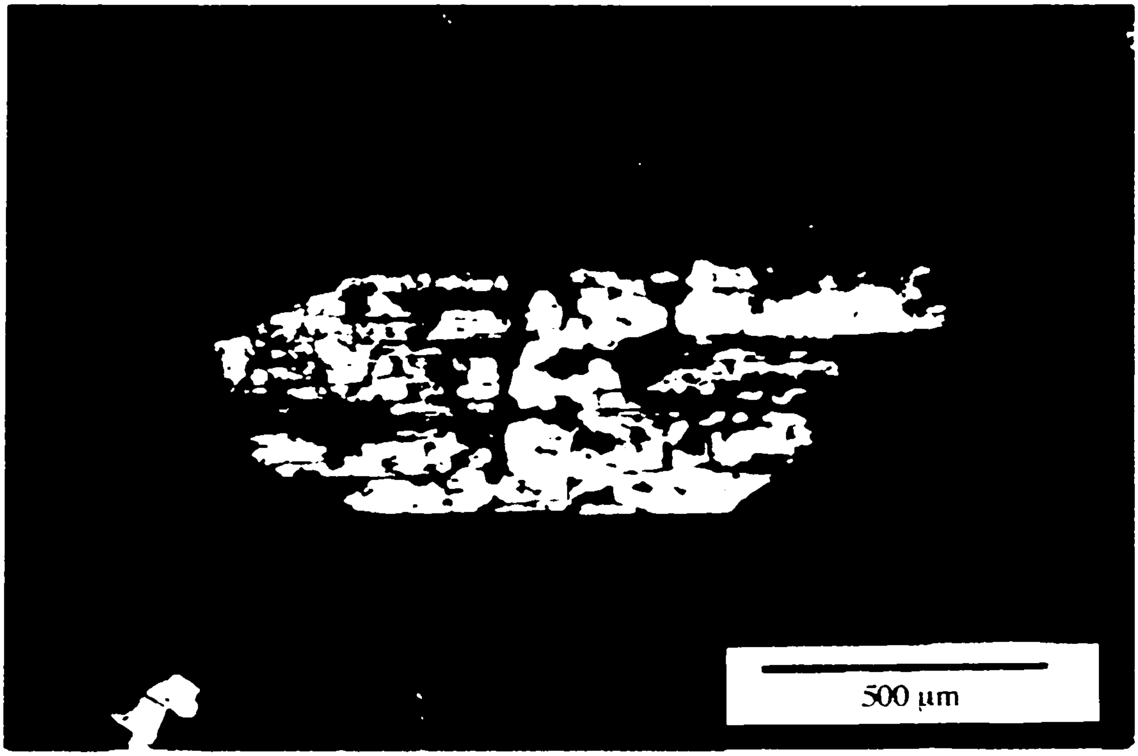

Plate 3.6

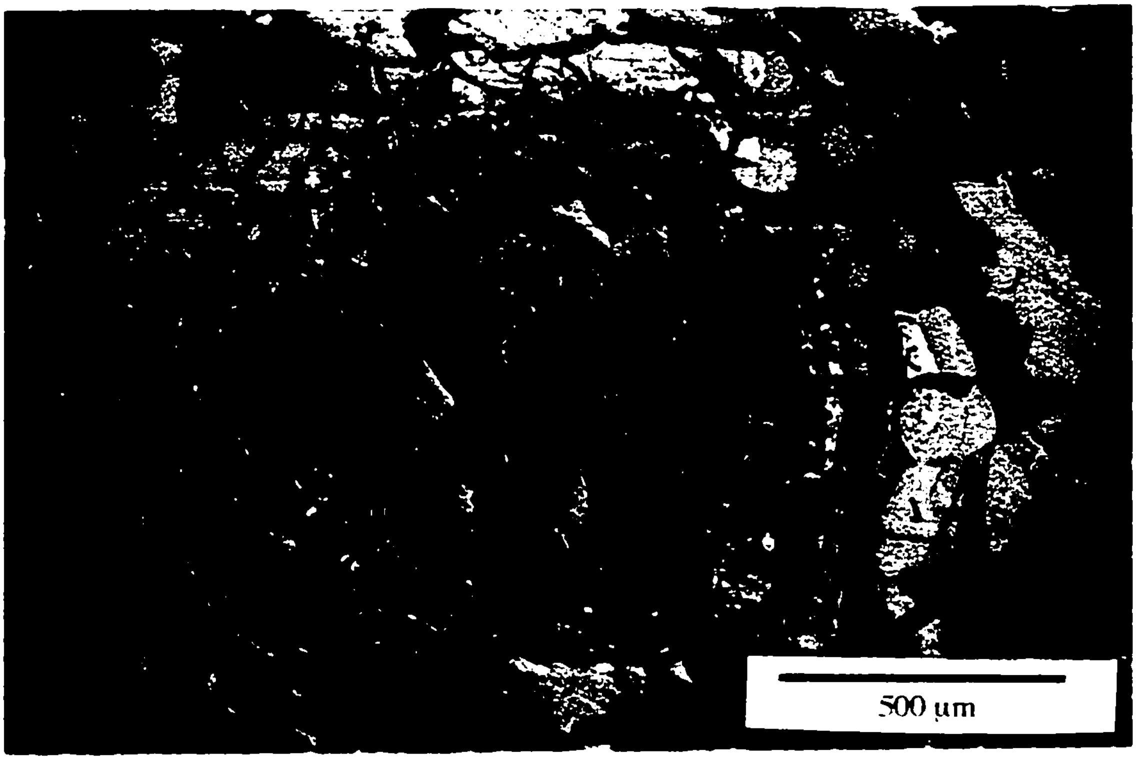

Table 3.2: Representative EMP analyses of feldspar from DH Wall. See Appendix A.2 for complete data.

	Type IA		Type IB				Type IC	
	008-010	008-001	LT007-040	LT007-074	003-016	003-004	LT070-001	LT070-027
	core	rim	core	rim	core	rim	core	rim
SiO_2	59.393	60.027	48.694	53.733	48.333	56.008	65.751	65.227
Al_2O_3	24.553	24.389	32.408	28.124	32.029	25.752	19.538	19.687
FeOT	0.374	0.385	0.586	0.653	0.559	1.017	0.246	0.261
MgO	0.009	0.028	0.056	0.1	0.064	0.293	0.011	0.012
BaO							0.248	0.187
SrO							0	0
CaO	6.504	6.336	15.852	11.187	15.832	8.859	1.305	1.464
Na_2O	6.646	6.77	2.311	4.489	2.23	5.457	6.675	6.919
K_2O	1.186	1.197	0.164	0.477	0.143	0.815	6.714	6.373
Total	98.66	99.13	100.07	98.76	99.19	98.2	100.49	100.13
				Oxygen = 32.000				
Si	10.756	10.812	8.925	9.852	8.936	10.292	11.786	11.732
Al	5.237	5.173	6.995	6.072	6.974	5.573	4.124	4.17
Fe*	0.057	0.058	0.09	0.1	0.086	0.156	0.037	0.039
Mg	0.002	0.008	0.015	0.027	0.018	0.08	0.003	0.003
Ba							0.017	0.013
Ca	1.262	1.223	3.113	2.198	3.136	1.744	0.251	0.282
Na	2.334	2.364	0.821	1.596	0.799	1.944	2.32	2.413
K	0.274	0.275	0.038	0.112	0.034	0.191	1.535	1.462
Ab	60.3	61.2	20.7	40.9	20.1	50.1	56.5	58
An	32.6	31.7	78.4	56.3	79	45	6.1	6.8
Or	7.1	7.1	1	2.9	0.9	4.9	37.4	35.2

Table 3.2: Con't

	Type IIA				Type IIB		Type III	
	LT004-026	LT004-002	LT060-001	LT060-014	LT010-005	LT010-001	015-007	038-001
	core	rim	core	rim	core	rim	skeletal	swallow-tail
SiO_2	57.656	59.253	64.782	66.397	55.074	54.192	50.311	61.238
Al_2O_3	25.37	24.433	18.697	18.746	27.299	28.336	30.562	20.992
FeOт	0.405	0.387	0.205	0.232	0.541	0.576	0.597	2.748
MgO	0.023	0.031	0	0	0.048	0.076	0.079	0.56
BaO			0	0.057				0.049
SiO			0	0				0
CaO	7.768	6.547	0.207	0.117	10.294	11.039	14.22	1.508
Na_2O	6.249	6.597	5.662	5.757	5.212	4.785	3.059	6.708
K_2O	0.768	1.098	9.258	9.522	0.452	0.409	0.189	6.564
Total	98.24	98.35	98.81	100.83	98.92	99.41	99.02	100.37
				Oxygen = 32.000				
Si	10.518	10.762	11.886	11.941	10.053	9.864	9.274	11.194
Al	5.45	5.226	4.04	3.97	5.868	6.074	6.634	4.519
Fe*	0.062	0.059	0.031	0.035	0.083	0.088	0.092	0.42
Mg	0.006	0.008	0	0	0.013	0.021	0.022	0.153
Ba			0	0.004				0.004
Ca	1.518	1.274	0.041	0.023	2.013	2.153	2.808	0.295
Na	2.21	2.323	2.014	2.008	1.845	1.689	1.093	2.378
K	0.179	0.254	2.167	2.185	0.105	0.095	0.044	1.531
Ab	56.6	60.3	47.7	47.6	46.6	42.9	27.7	56.6
An	38.9	33.1	1	0.5	50.8	54.7	71.2	7
Or	4.6	6.6	51.3	51.8	2.6	2.4	1.1	36.4

(Table 3.2), with some rim compositions extending into the oligoclase field (Table 3.3 & Fig. 3.7). In general zoning shows a normal trend of decreasing An content from core to rim, with core compositions averaging $\approx An_{38}$ to rim compositions of $\approx An_{28}$ (Fig. 3.8 & Table 3.3), however departures are evident in mantle with isolated sectors having reverse zoning (See Fig. 3.8) . Extinction patterns are slightly patchy in the core region and normal in mantle/rim.

Crystal faces enclose the core, the outer margins of which are generally euhedral to subhedral (Plate 3.6). Connection from core to crystal exterior, when evident, occurs along small fractures. These fractures are commonly filled with a dark material that unfortunately is extremely hard to identify due to high reflectance and small size. It is quite possible that it represents melt that expanded due to pressure release during the eruptive event. The crystal interface with host melt is typically sharp and smooth. In rare cases, where a dark brown glass is in contact with Type IA crystals, a thin overgrowth is present on the crystals (Plate 3.7 & 3.8). These overgrowths have rough interfaces with host melt due to skeletal growth patterns that extend into melt (Plate 3.8). Skeletal growth patterns are also observed mantling relic, lobate pieces of feldspar within resorbed cores.

All Type IA crystals larger than 2.0 mm are broken into two sub-equal fragments, exposing the core to host melt. These sub-equal fragments generally preserve two crystal faces each, giving the fragments a triangle shape (Plate 3.9). Smaller phenocrysts (< 2.0 mm) can also have this morphology, depending on the extent of core resorption. A heavily resorbed core will have a weaker structure thereby being more susceptible to breakage.

No Type IA feldspars are identified in the felsic pumice sample (TK-9D). Type IA feldspar are observed in equal numbers in both mafic and banded pumice, but the majority of feldspars analyzed by EMP are from the mafic pumice. It is observed that cores have an asymmetric zoning pattern in NDIC that are similar to topographic contours. This pattern is

Plate 3.7: Close up of transition from core to mantle in Type IA feldspar. Core (C) has complex zoning pattern in NDIC while mantle (M) has a regular to convoluted growth pattern. Boundary between core and mantle marked by dissolution surface (R). Second dissolution surface midway in mantle has truncated underlying growth surfaces. Very thin overgrowth (O) evident on outer crystal surface.

Plate 3.8: Close up of overgrowth (O) on outer crystal surface of Type IA feldspar in NDIC. Overgrowth has a distinctive dendritic pattern, made up of angular crystallographically controlled edges, indicating growth during undercooling.

Plate 3.7

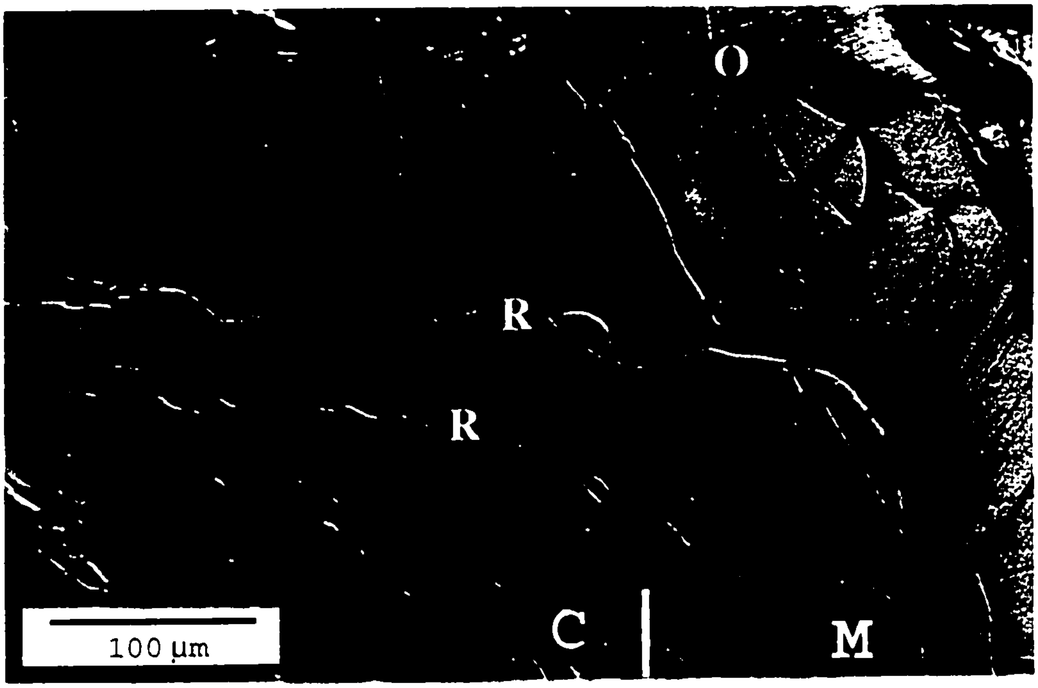

Plate 3.8

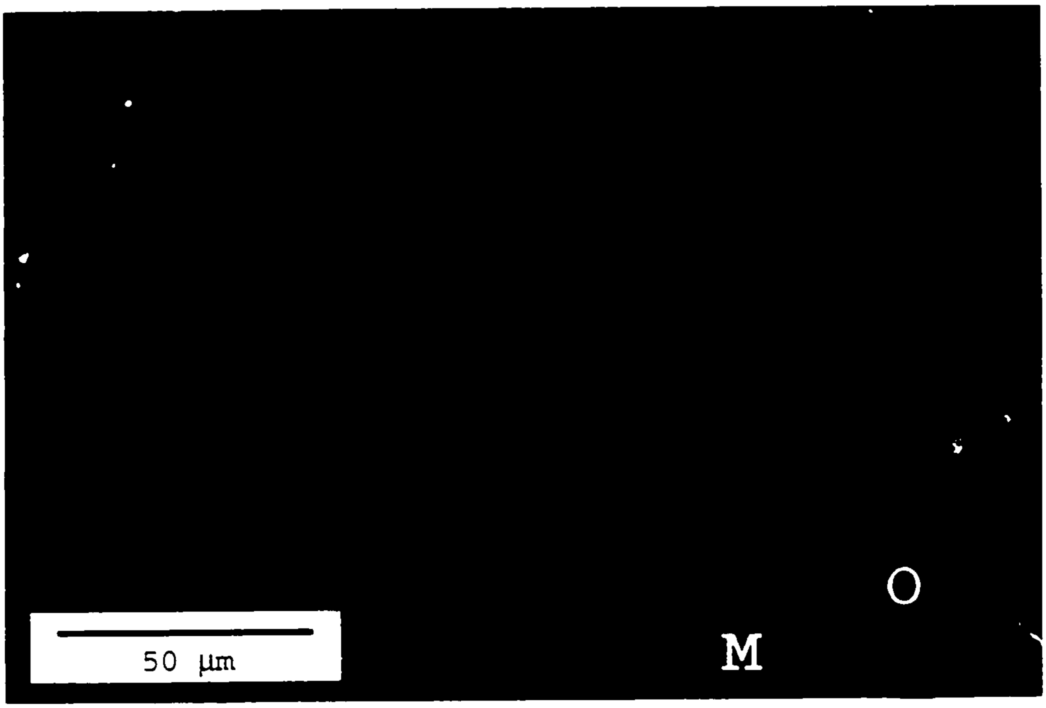

Table 3.3: Core and rim analyses of feldspar types from Diego Hernández wall.

Sample	Thin Section	Core	Rim
Type IA			
LT002	TK-9C (MP)	An_{34}	An_{33}
LT064	TK-9C (MP)	An_{44}	------
*LT065/066**	TK-9C (MP)	------	$An_{35.7}/An_{27.2}$
LT067	CS95-010 (XP)	An_{25}	$An_{15.5}$
001E	TK-9C (MP)	An_{34}	$An_{32.7}$
001F	TK-9C (MP)	An_{41}	An_{32}
008	TK-9C (MP)	An_{33}	An_{32}
009	TK-9C (MP)	An_{40}	An_{33}
013	CS95-010A (MP)	An_{24}	An_{24}
Type IB			
LT007	TK-9C (MP)	An_{78}	An_{56}
LT009	CS95-010A (MP)	An_{72}	An_{54}
LT016	CS95-010A (MP)	An_{78}	An_{60}
LT017	CS95-010A (MP)	An_{83}	An_{79}
003	TK-9C (MP)	An_{79}	$An_{57.5\text{--->}45}$
004	TK-9C (MP)	An_{74}	$An_{50\text{--->}40}$
005	TK-9C (MP)	An_{65}	An_{61}
006	TK-9C (MP)	An_{77}	------
007	TK-9C (MP)	An_{79}	------
010	TK-9C (MP)	An_{75}	An_{70}
012	CS95-010A (MP)	An_{79}	------
014	CS95-010A (MP)	An_{74}	An_{75}
017	CS95-010 (XP)	An_{77}	------
018	CS95-011 (XP)	An_{70}	An_{45}
Type IC			
LT006	TK-9C (MP)	Or_{36}	Or_{34}
LT069	CS95-010 (XP)	Or_{25}	Or_{29}
LT070	CS95-010 (XP)	Or_{37}	Or_{35}
001G	TK-9C (MP)	Or_{39}	Or_{30}
Type IIA			
LT001	TK-9C (MP)	An_{28}	An_{22}
LT004	TK-9C (MP)	An_{39}	An_{33}
LT008	TK-9C (MP)	Or_{51}	Or_{51}

Table 3.3: Con't

Type IIA			
LT058	TK-19D (FP)	Or_{50}	Or_{51}
LT059	TK-19D (FP)	Or_{46}	Or_{51}
LT060	TK-19D (FP)	Or_{52}	Or_{52}
LT061	TK-19D (FP)	Or_{48}	Or_{51}
LT068	CS95-010 (XP)	Or_{20}	Or_{20}
Type IIB			
LT003	TK-9C (MP)	An_{38}	An_{40}
LT010	CS95-010A (MP)	An_{51}	An_{54}
Type III			
015	CS95-010A (MP)	An_{70}	$An_{62--->52}$
038	CS95-010 (XP)	Or_{36}	------

MP, XP and FP are mafic, mixed and felsic pumice samples, respectively. LT064/065/066 are all done on the same crystal, with LT064 one core and LT065/066 on rim.

A

B

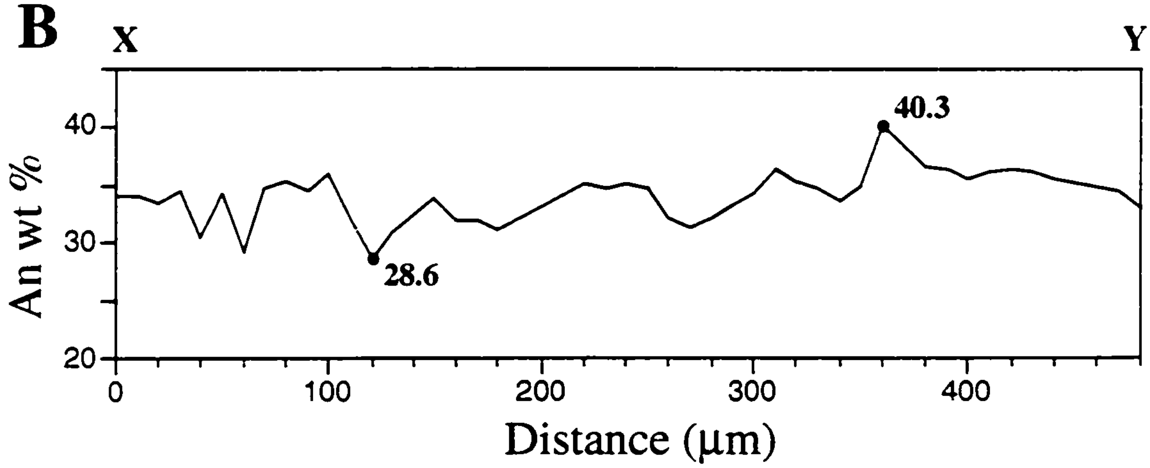

Figure 3.8.: Core to rim line traverse of Type IA feldspar (id # LT002) from Diego Hernandez Wall. X-Nicols microphotograph of feldspar LT002.

Plate 3.9: NDIC microphotograph of Type IA feldspar that has fragmented exposing core to host melt. Core has complex zoning pattern in NDIC.

Plate 3.10: Dissolution surface (R) in mantle of Type IA feldspar. Dissolution surface has truncated underlying crystal faces. EMP line traverse LT066 (See Appendix A.X) on photo. Direction to core (C) is indicated.

Plate 3.9

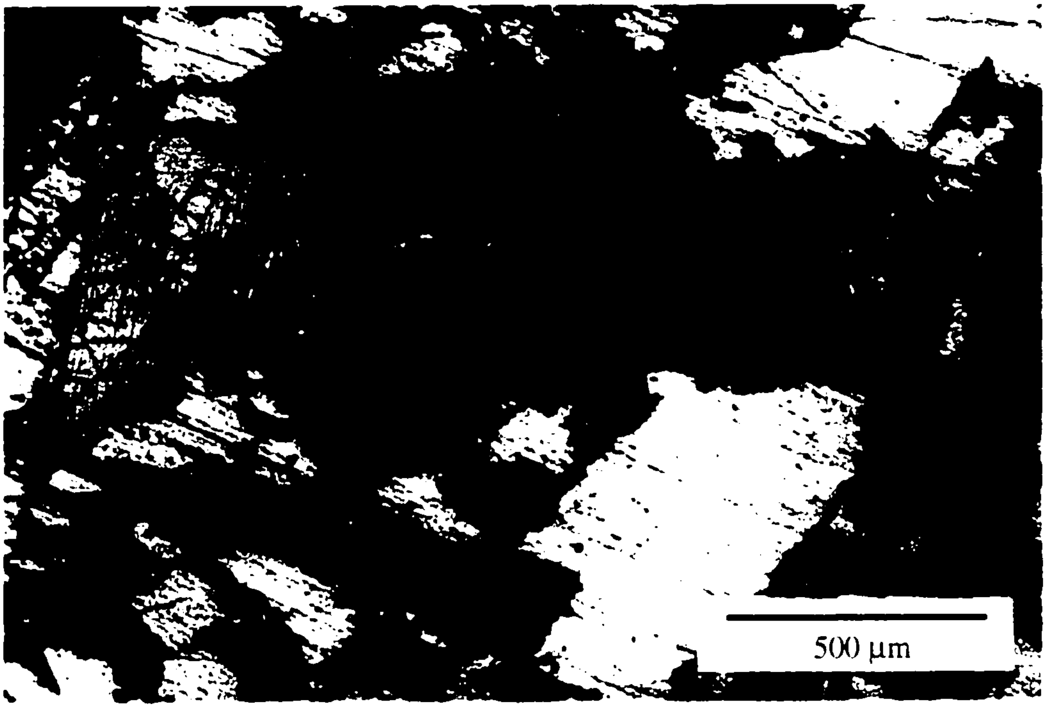

Plate 3.10

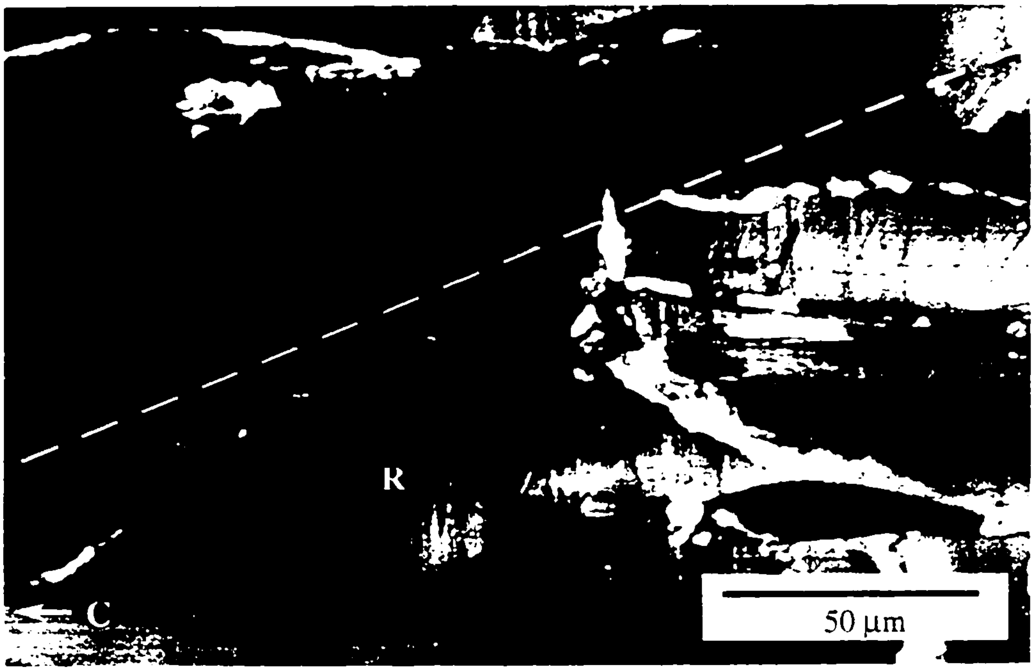

very similar to those observed in Type IB feldspars (discussed below). Both resorption textures and asymmetric patterns abruptly terminate at the core/mantle boundary. Immediately following this termination there is at least one major dissolution surface observed in NDIC (Plate 3.7). The mantle region commonly has convoluted conformable zoning (Plate 3.7) that is attributed to growth (Pearce 1993).

Interpretation of Type IA Feldspar

Textures apparently consistent with resorption are evident in the core region of Type IA feldspars, but their exact origin is more complicated. Two possible origins of the textures are examined: (1) resorption; and (2) growth.

Numerous physio-chemical mechanisms can result in resorption. A basic principle is that the magma hosting the entrained crystals must experience changes in its intensive variables or undergo a compositional change. Compositional changes are possible through fractionation crystallization, assimilation or mixing with one or more magmas. Magma fractionation crystallization will result in near-equilibrium growth of crystals that originate from this melt, rather being resorbed. Assimilation can change the composition of the host magma, but due to thermal constaints, the change is usually to higher Si values (ie. more evolved composition). Thus plagioclase crystals in equilibrium with new liquid host are lower in An content than pre-existing crystals (oversaturated), resulting in An-poor overgrowths on crystals **not** resorption (Tsuchiyama 1985). Magma mixing, where a hybrid magma is formed (see chapter 2), may lead to favorable conditions for resorption. However, resorption is restricted to those feldspars initially in equilibrium with the more evolved magma (felsic). In the hybrid magma, the 'felsic' plagioclase crystal will be undersaturated, in that the plagioclase in equilibrium with the hybrid is more An-rich than the felsic magma. Chemical resorption of felsic plagioclase crystals will in general start from the outer crystal surface and propagate inwards. High energy sites such as crystal defects and dislocations (ie. twin planes) will enhance resorption. After this initial period of resorption, growth will be renewed, but at higher An values, giving a noticeable jump in An content at the contact between the original crystal and the overgrowth. On the other hand, plagioclase crystals from the mafic magma will form an overgrowth of more sodic plagioclase (Tsuchiyama 1985).

Changes in intensive variables are linked, for the most part, to changes in composition. Temperature decreases are associated with a fractionation crystallization, assimilation of felsic material and magma mixing (undercooling of mafic end-member). With a decrease in temperature, crystallization will be enhanced in the mafic liquid, forming sodic-rich overgrowths without resorption. The felsic end-member involved in magma mixing will experience an increase in temperature and therefore resorption, as discussed above for magma mixing. Note that regardless of melt composition, if the melt temperature exceeds the plagioclase liquidus that plagioclase crystal will undergo resorption, termed *simple dissolution* by Tsuchiyama (1985), where in the resorbed crystal becomes progressively smaller, rounded and embayed.

Pressure changes are probably an important process for crystal growth/dissolution in rapidly ascending magmas. A rapid drop in pressure will lower the liquidus temperature of plagioclase, such that plagioclase which was in equilibrium will now undergo resorption (Nelson and Montana 1992; Pearce et al. 1987).

A possible explanation for Type IA plagioclase crystals is that the core region represents crystal relics that were in equilibrium with an early, more basic magma that contained calcic plagioclase phenocrysts of composition similar to Type IB (see below). Upon ascent to the shallow sub-volcanic environment these crystals underwent decompression resulting in resorption (Nelson and Montana 1992; Pearce et al. 1987). Following resorption, renewed growth of more Na-rich plagioclase (≈ An_{40}) is expected, mantling these relic crystals (Tsuchiyama 1985). This is where this hypothesis runs into difficulties. Two possibilities for chemical evolution exist after ascent of this basic magma, either it evolved to some intermediate composition or it was injected and banded with a pre-existing intermediate magma. If it is assumed that the original composition of these feldspars was similar to those of Type IB feldspars (≈ An_{75}), then a compositional gap is expected between the sieved core and mantle (Dungan and Rhodes 1978; Pearce and Kolisnik 1990). However, this is not observed in any EMP traverse done on Type IA feldspar. Since there is no compositional gap then the formerly calcic plagioclase crystals must have re-equilibrated to an intermediate composition of ≈ An_{45} (Table 3.3). Core fragments are on average 200 μm X 150 μm, which based on Grove et al. (1984) calculations of plagioclase interdiffusion, would take > 250,000 years to homogenize. This time seems unreasonable for this system, with an average of 100,000 years between major events (see Table 1.1). Therefore a resorption origin of early An-rich crystal (similar to Type IB) can be dismissed.

Another possible explanation is that the core regions may represent early skeletal growth from an undercooled intermediate host magma (ie. An ≈ 40). The intermediate melt may have initially gone through a period of undercooling followed closely by by slower cooling. Skeletal features are obscured by a dissolution event that occurred just before renewed growth giving these cores a "spongy" appearance (e.g. Pearce et al. 1987). Of note is that this dissolution event is not accompanied by a major change in An content. The skeletal crystals serve as nucleation sites for crystallizing feldspar in equilibrium with host melt.

The transition from the core to the mantle is normally marked by a dissolution surface

(Plate 3.7). This surface is distinguished from observed convoluted zoning by the truncation of underlying zones. Typically there is one more dissolution surface located in the midpoint of the mantle (Plate 3.10). Again convoluted zoning is evident leading up to this dissolution surface. These dissolution surfaces possibly represent local heterogeneities in the evolving melt, where there is a local phenomenon of increased temperature, since these surfaces are not associated with a fluctuation in composition (Fig. 3.8). Renewed growth forms an euhedral mantle on these skeletal cores.

Larger crystals may have been fragmented due to expansion of trapped melt. During eruption the magma trapped in these cores (especially those with no connection to surface) expands due to pressure release, resulting in the shattering of the phenocryst (Pearce et al. 1987; Shelley 1993). Another possible mechanism not to be overlooked is fragmentation during transport in the pyroclastic flow or the eruption itself, however the fragmentation appears to be restricted to Type IA feldspars.

Feldspar - Type IB

Type IB feldspars, like Type IA, make up about 3 vol % of the total crystal population and are identified by their distinctive morphology, characterized by their highly resorbed nature throughout. In general these feldspars are anhedral, but all have a relic, tabular outline (**Plate 3.5**). Crystal sizes range from 0.4 to 1.5 mm, with most being about 0.7 mm. These phenocrysts are found in both banded and mafic pumice, hosted by medium to dark brown glass. There are a few rare observations of Type IB feldspars in light brown glass, and only one example of a crystal being hosted in clear glass. No Type IB feldspars were identified in felsic pumice samples. Compositionally they are the most calcic plagioclase crystals observed, ranging from bytownite (An_{83}) to andesine (An_{40}) (Fig. 3.7 & 3.9 & Table 3.2). Overall zoning is normal with some small oscillations ending in more sodic rims (Fig. 3.10). Extinction patterns are patchy. Vance (1965) envisaged this type of pattern as being due to the infilling of resorption channelways formed in calcic plagioclase. The X-ray plot (Fig. 3.11) of the ratio of Ca/Na exhibits this channelway pattern clearly. These sodic channels typically coincide with drops of 15% An. Line traverses performed on Type IB feldspar crystals routinely have fluctuations of 10-15% in An content, with rebounds back to the original An content of An_{78} (see line traverse). These drops are abrupt over 10 μm indicating **NO** extensive diffusion profile. This pattern is similar to the one expected by a dissolution/reprecipitation mechanism described by Johannes et al. (1993).

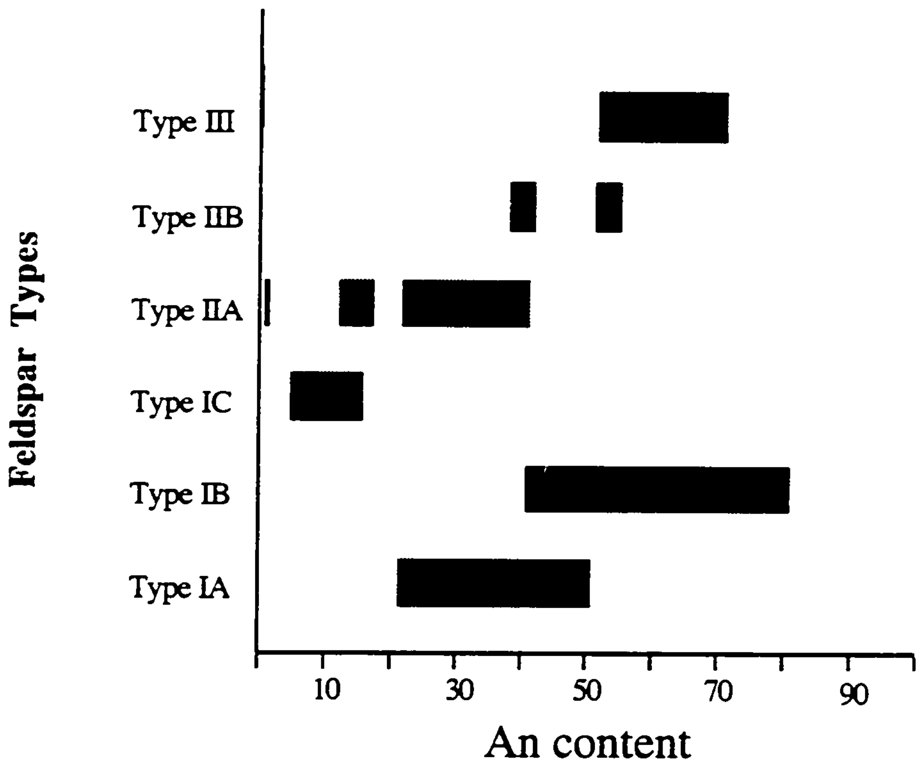

Figure 3.9: An Content with feldspar types showing overlap between different types. All from Diego Hernandez Wall.

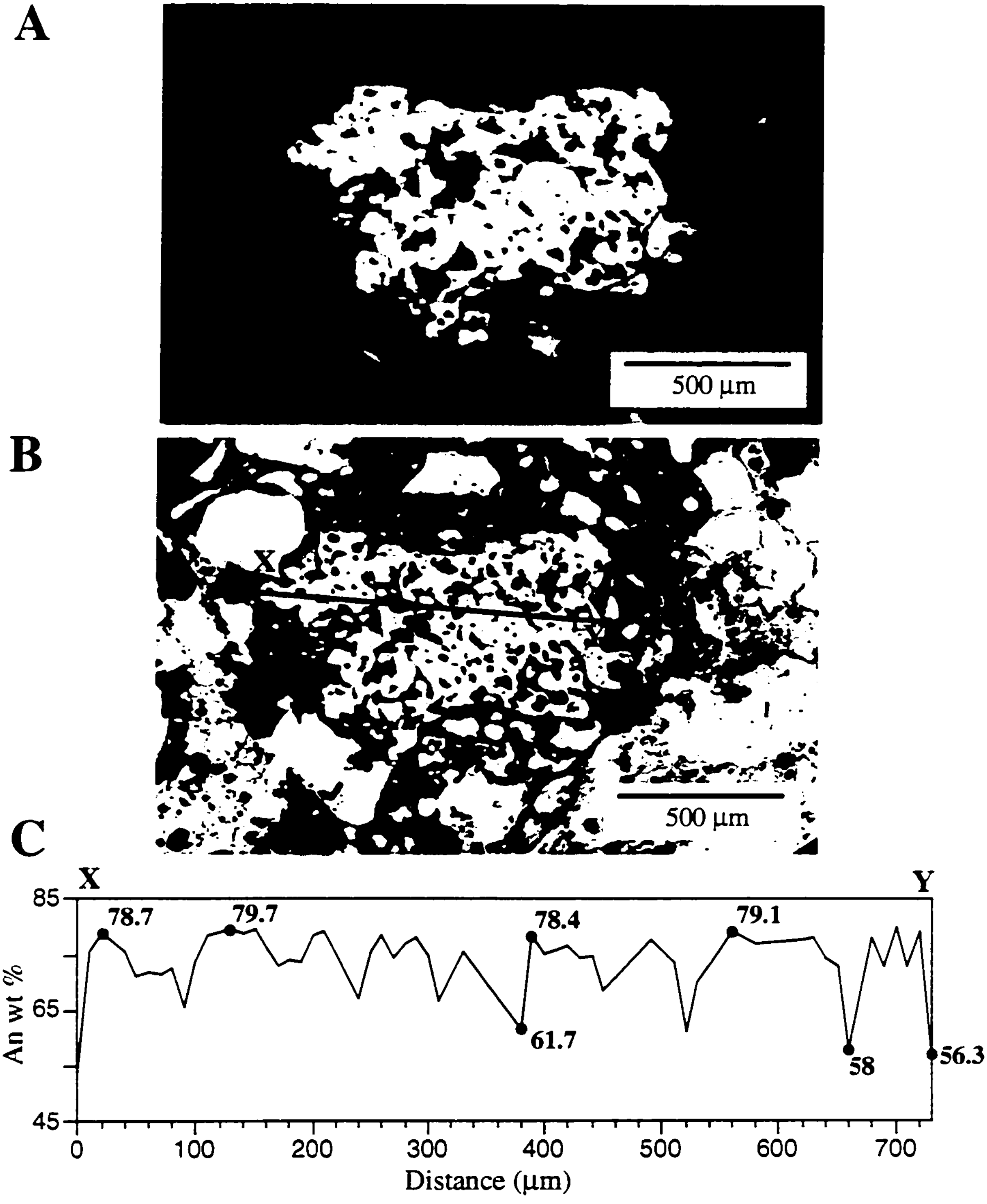

Figure 3.10.: Line traverse of Type IB feldspar LT007. (A) Plate in transmitted light, X-Nicols. (B) Plate in reflected light, EMP line along X-Y. (C) EMP analyses of An content across crystal.

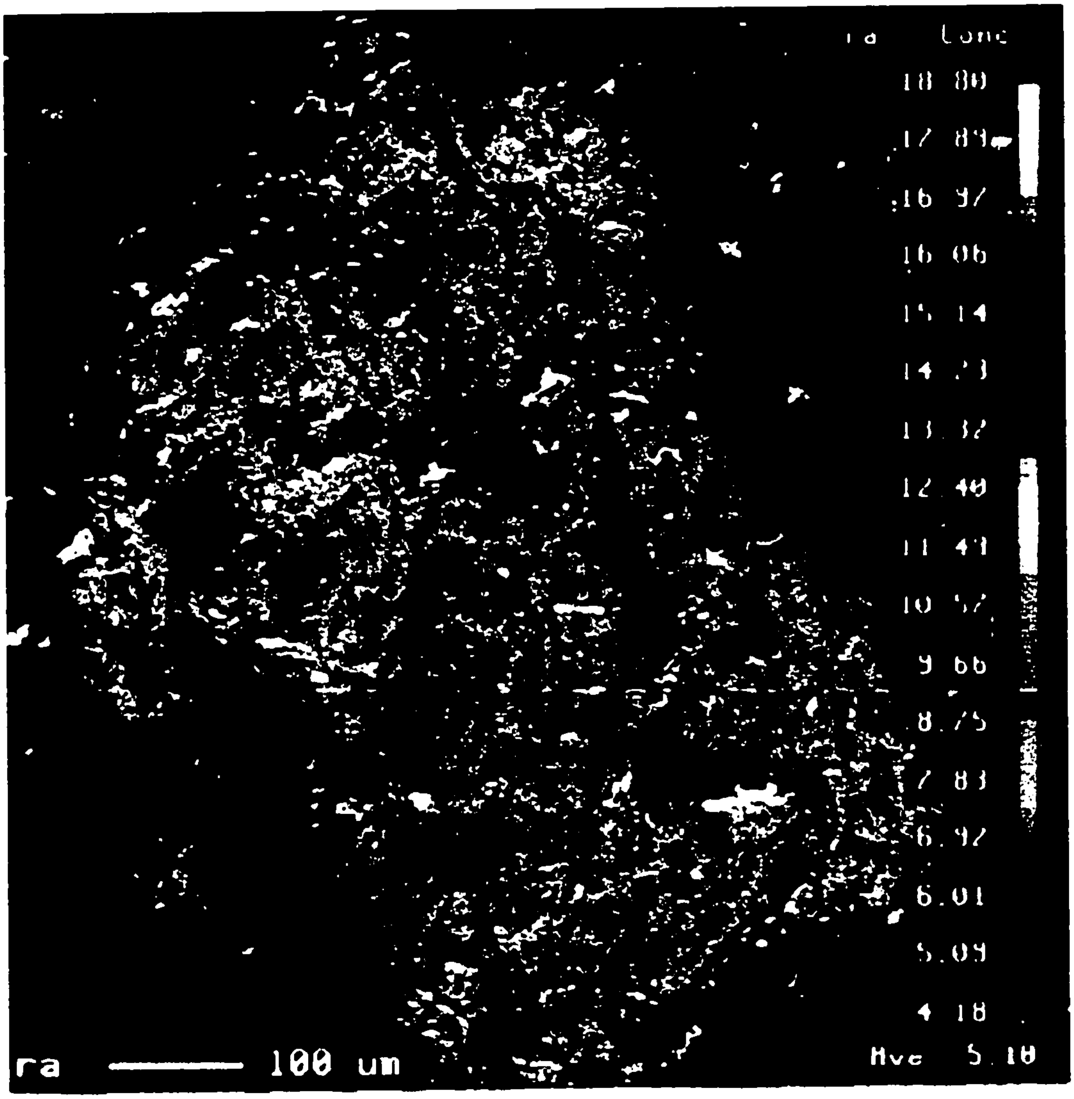

Figure 3.11: X-ray plot of Type IB feldspar. Ca/Na ratio is plotted in X-ray image. bar to the left shows scale. with lighter colored areas having high Ca/Na ratio. Image gives an impression of melting along channelways within crystal structure.

Type IB crystal textures can be described as sieved. Sieve-like patterns are normally parallel to lattice defects and other energetically favorable surfaces (polysynthetic twins), indicating a crystallographic control. This is evidence of a resorption origin as this process take advantage of defects that arise maybe within the crystal structure during growth. Hence the sieve textures post-date crystal growth (Anderson 1984; Dungan and Rhodes 1978; Pearce and Kolisnik 1990; Singer et al. 1993). Type IB feldspars are invariably enveloped by a veneer of black material. This material is not restricted to the exterior and is found coating the interior resorbed sections within the crystal. As with the black material found in fractures in Type IA feldspar, this material is unidentifiable due to its high reflectance and small size. In one case this opaque material forms an intricate dendritic growth patterns similar to Cr-spinel (Shore 1996, unpublished Ph.D. Thesis) (Plate 3.11).

In NDIC, the zoning patterns are asymmetric resembling topographic contours (Plate 3.12 & 3.13) similar to those observed in Type IA feldspar cores (Plate 3.14). It is not uncommon to have a thin overgrowth mantling these crystals. Overgrowths are more sodic with An ranging from 60-40% (20-40% lower than core) (Fig. 3.10).

Interpretation of Type IB Feldspars

Based on their high An contents, Type IB phenocrysts most likely originate from a basic melt that has not been identified in any glass analyses (see below). A possible explanation for Type IB feldspars and the lack of evidence for its initial basic host may be explained by injection into and subsequent mixing with an intermediate magma, hypothesized to be the same intermediate melt that hosts Type IA feldspar. In this case the injected basic melt would likely mix rather readily with this intermediate melt due a small difference both chemically and in temperature. Another possible mechanism for resorption is by decompression. It is envisioned

Plate 3.11A: Transmitted light close up of dendritic growth of opaque material within Type IB feldspar. Material has a distinctive christmas tree growth pattern.

Plate 3.11B: Transmitted light close up of intricate dendritic growth within Type IB feldspar crystal.

Plate 3.11A

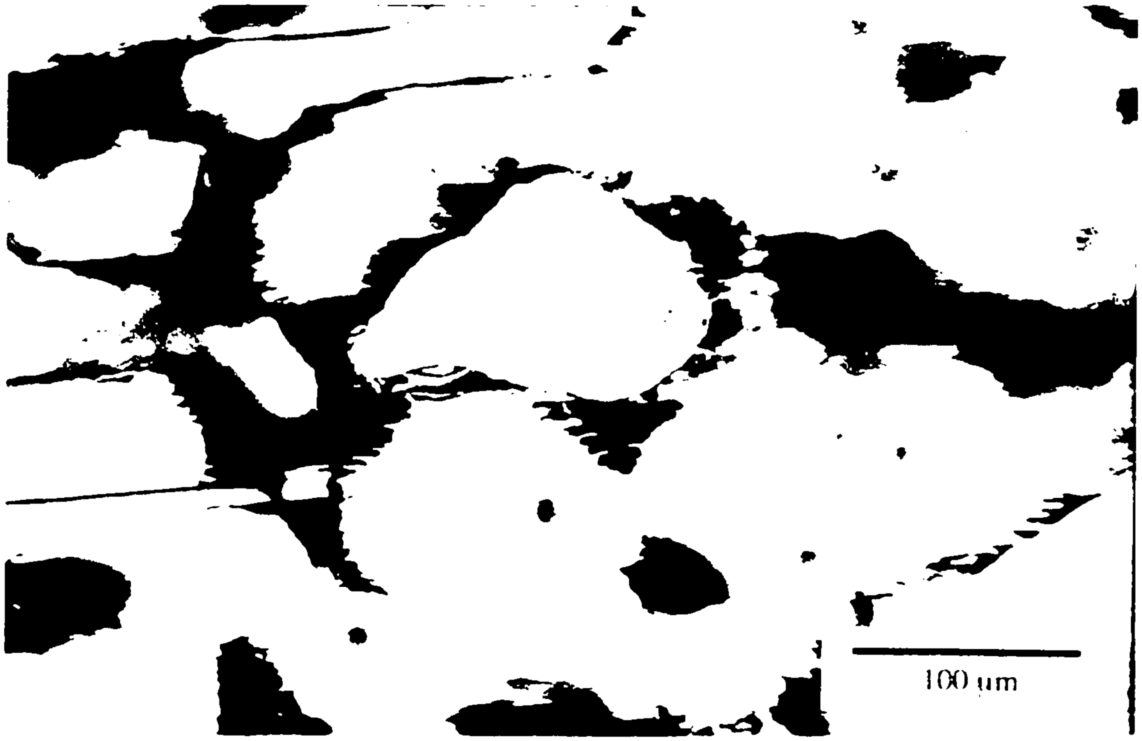

Plate 3.11B

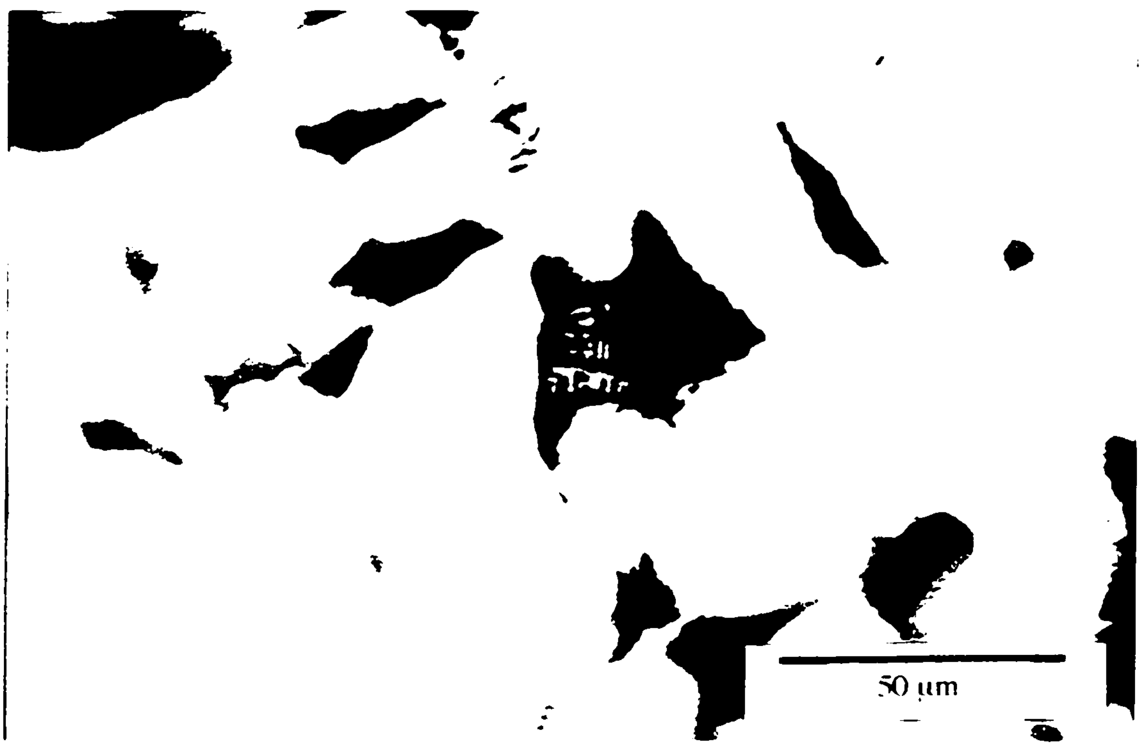

Plate 3.12: NDIC microphotograph of complex zoning pattern of Type IB feldspar (LT007). Zoning pattern is asymmetric resembling topographic contours in many cases.

Plate 3.13: NDIC Microphotograph close up of complex zoning of Type IB feldspar (LT007). Zoning pattern is asymmetric resembling topographic contours in many cases. Thin overgrowth (O) is shown in lower right hand portion of photo. Overgrowth is sodic-rich compared to the crystal as a whole.

Plate 3.12

Plate 3.13

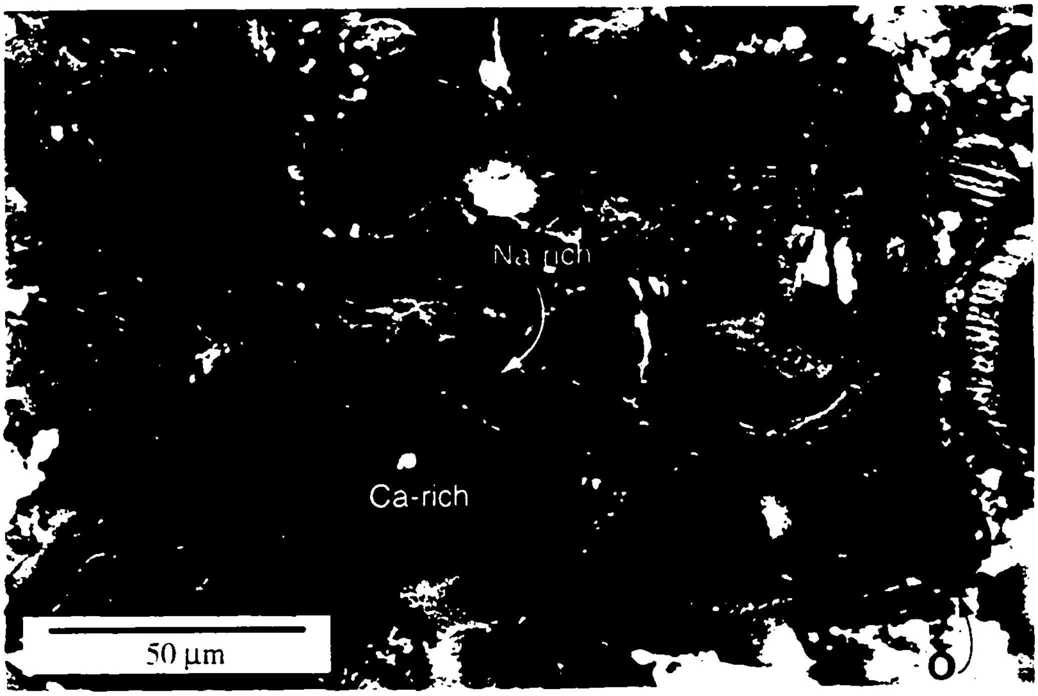

Plate 3.14: NDIC microphotograph of zoning pattern in Type IA feldspar crystal. Core (C) has complex zoning pattern in NDIC whereas mantle (M) has more laminar to convoluted growth.

Plate 3.15: NDIC microphotograph of two Type IC feldspars from mixed pumice CS-010. NDIC helps resolve the two glass types, with "mafic" glass being mostly crystalline and felsic glass is homogenous. Both Type IC feldspars are hosted in small bleb of felsic glass juxtaposed by mafic glass.

Plate 3.14

Plate 3.15

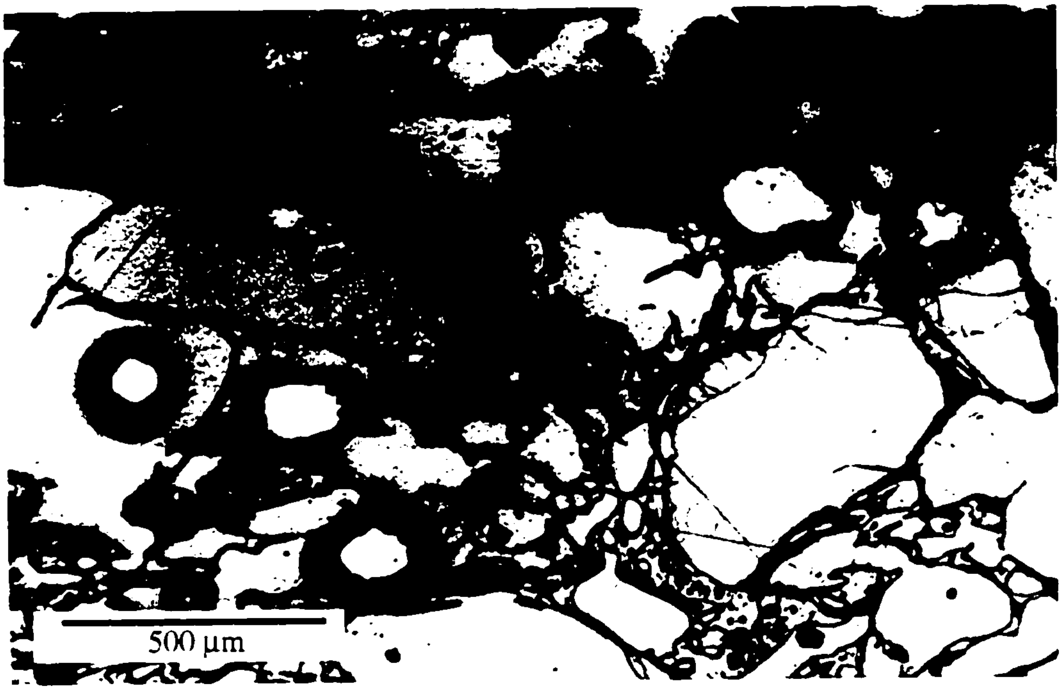

that as a basic magma is emplaced in a subvolcanic magma chamber from depth, the sudden change in pressure would lower the plagioclase liquidus invoking melting (Nelson and Montana 1992; Pearce et al. 1987).

The channelway pattern of sodic and calcic-rich plagioclase (Fig 3.11) can result from either infilling of sieved textured plagioclase by sodic-rich plagioclase (Vance 1965) or by dissolution/reprecipitation (Johannes et al. 1993). Sodic infilling requires the plagioclase liquidus to be lowered such that calcic plagioclase will undergo dissolution. This is possible by rapid decompression when the basic melt is emplaced from depth into the shallow sub-volcanic environment, resulting in depressing the plagioclase liquidus to below its melting temperature (Nelson and Montana 1992). Johannes et al. (1993) dissolution/reprecipitation mechanism describes the melting of a sodic plagioclase and reprecipitation of more calcic plagioclase epitaxially on the original sodic plagioclase. Thus the more sodic plagioclase analyzed within the feldspar structure represents relic fragments of the original feldspar crystal. This more sodic plagioclase averages about An_{62} as compared to the "reprecipitated" calcic plagioclase of An_{78} with a sodic overgrowth of An_{56}. Again, this mechanism requires that the plagioclase liquidus be lowered to below the temperature of the magma.

Due to the discrepancy between the 'sodic' plagioclase (An_{62}) within the feldspar crystal as compared to sodic plagioclase overgrowths (An_{56}) the Johannes et al (1993) mechanism of dissolution/reprecipitation is favored over the infilling mechanism of Vance (1965). The dissolution/reprecipitation mechanism has only been described under controlled conditions for experimental work on feldspars. To date this method has not been related to any natural feldspars. This is probably due to the lack of explanation for why sodic plagioclase melts to a more calcic plagioclase.

Feldspar - Type IC

The study of Type IC feldspars is more enigmatic than the other two sub-types, in part because they comprise just 1 vol % of the crystal population. Of the three sub-types, Type IC is the only alkali feldspar. Resorption has affected the outer crystal faces giving them a rounded appearance, anhedral morphology (Plate 3.15). Core regions are intact and unaffected by resorption. Crystal size ranges from 450 to 700 μm. Compositions extend from anorthoclase to sanidine (Fig 3.7) and core analyses range from Or_{29} to Or_{35} with rim values of Or_{39} to Or_{25}. Overall zoning is normal, with only a 8 % range in Or values (Fig 3.12). One discrepancy identified is Type IC feldspars hosted in mafic samples have a slightly higher range in Or (16%). NDIC does not reveal any distinguishing features.

Type IC feldspar are rare in mafic pumice samples, but when observed occurred only in small felsic blebs surrounded by mafic glass. Type IC crystals were seldom in banded pumice samples as well, but when present are found only within felsic glass (pale green glass). Felsic pumice sample (TK-9D) has no Type IC feldspars.

Interpretation of Type IC Feldspars

The abundance, locality and composition of this type of feldspar signifies its position in the pre-eruptive magma chamber. The only other K-rich feldspar type identified are Type IIA (described below). Besides the obvious morphological difference (anhedral vs euhedral), there is a slight compositional discrepancy between Type IC and Type IIA as well. Type IC feldspars are richer in Na than Type IIA, having average values of Ab_{60} and Ab_{50}, respectively. Both feldspar types originate from a phonolitic melt, but Type IIA feldspars have a more evolved composition that may indicate a higher stratigraphic level in the magma chamber. Interdiffusion of alkali feldspars is high enough (see section on diffusion) such that

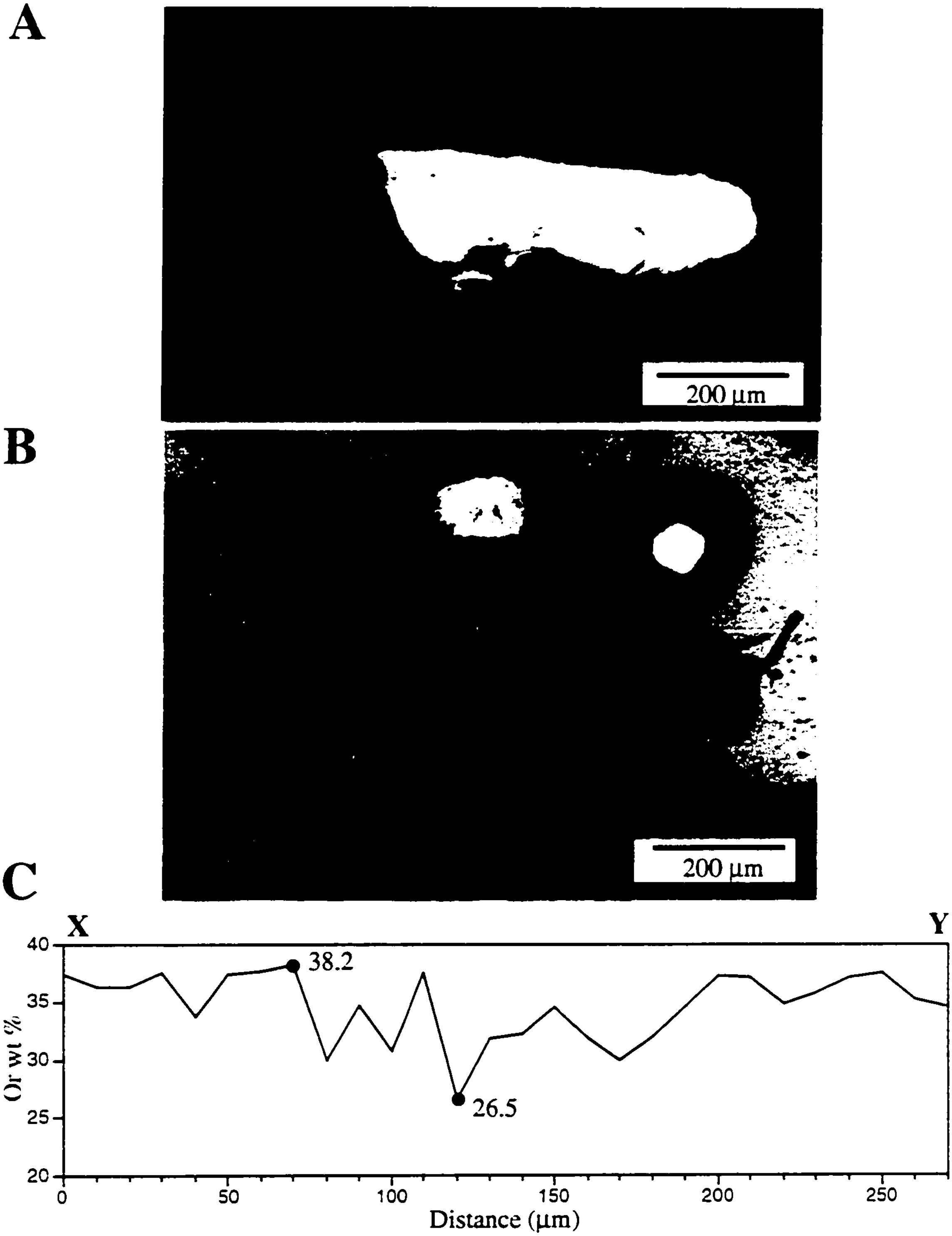

Figure 3.12.: Core to rim line traverse for Type IC feldspar, LT070. (A) Transmitted light (X-Nicols); (B) NDIC with traverse line; and (C) Or wt % plotted from core to rim.

these crystals could re-equilibrate to a more Na-rich alkali feldspar (Or_{26}). This high interdiffusion rate also explains the lack of a diffusional profile (range of≈ Or_8). Type IC feldspars are envisaged to exist close to the boundary between the phonolitic magma and the underlying intermediate magma. The few Type IC feldspars associated with mafic samples represent rare instances where alkali feldspar are incorporated into the intermediate magma. The association in banded samples is due to physical commingling between the phonolitic and intermediate magmas during the eruptive event.

The rounding of Type IC feldspars can be attributed to resorption (ie. simple dissolution). Tsuchiyama (1985) defined simple dissolution as the dissolution of a crystal in a melt that is undersaturated with respect to the equilibrium composition. In this situation the crystal is normally exposed to an increase in temperature as well. Thus, it is proposed that Type IC alkali feldspars were in an undersaturated intermediate melt and subjected to temperatures above their liquidus, causing them to melt (ie. went from phonolite to intermediate melt).

Feldspar - Type II

All feldspars of this type have very little or no resorption features. All such crystals are euhedral to subhedral with blocky, rectangular or lath-shaped morphology (Plate 3.16 & 3.17). Type II feldspars make up an estimated 5 vol % of the total crystal population. As with Type I, feldspar composition varies from plagioclase (An_{54}) to alkali feldspar (Or_{52}). The alkali feldspars from this group are the most K-rich analyzed. These K-rich feldspars are located dominantly in the felsic pumice sample (TK-9D) with only one being found in mafic pumice, TK-9C.

Type II feldspars are found in all samples. However, these feldspars are conspicuous due to their sparse numbers in banded pumice samples. There are a large number of crystal fragments that might be part of this group, but their size and morphology make it difficult to place in any particular group. Within individual crystals, major element composition is fairly homogenous. The largest variation shown by the plagioclase feldspars is 9% An (LT004). The K-rich feldspars typically have a 5% range in Or (LT059). Based on crystal shape and zoning it is possible to subdivide this type.

Feldspar - Type IIA

Feldspar crystals in this sub-type are euhedral to subhedral. They are usually blocky to equant with no resorption (Plate 3.16). This sub-type is the more dominant, making up approximately 3 vol %. Type IIA feldspars are observed in all samples, but are primarily found in mafic and felsic pumice. Three populations are evident from the An-Ab-Or ternary diagram (Fig. 3.13) and An histogram (Fig. 3.9), having compositions ranging from andesine through sanidine.

Two of the populations are alkali feldspars, plotting in the sanidine and anorthoclase field on the An-Ab-Or ternary diagram, and will be treated together. These alkali feldspars range in size from 0.45 to 1.2 mm. Only one feldspar (LT068) is characterized as Type IIA from banded pumice sample (CS-010), with the remaining crystals hosted in felsic pumice (TK-9D). Not only is this crystal the largest of this group but, it also represents the anorthoclase population. Core to rim traverses are fairly homogenous, with less than a 5% range in Or values, all with normal zoning. The sanidine population represents the most K-rich feldspars (Or_{52}) analyzed from Diego Hernández wall.

The plagioclase population extends from andesine (An_{42}) to oligoclase (An_{22}), forming

Plate 3.16: NDIC microphotograph of euhedral Type IIA feldspar crystal. EMP line traverse (LT004) is visible on crystal surface.

Plate 3.17: Euhedral lath Type IIB feldspar crystal in NDIC. Feldspar is hosted in highly recrystallized mafic glass.

Plate 3.16

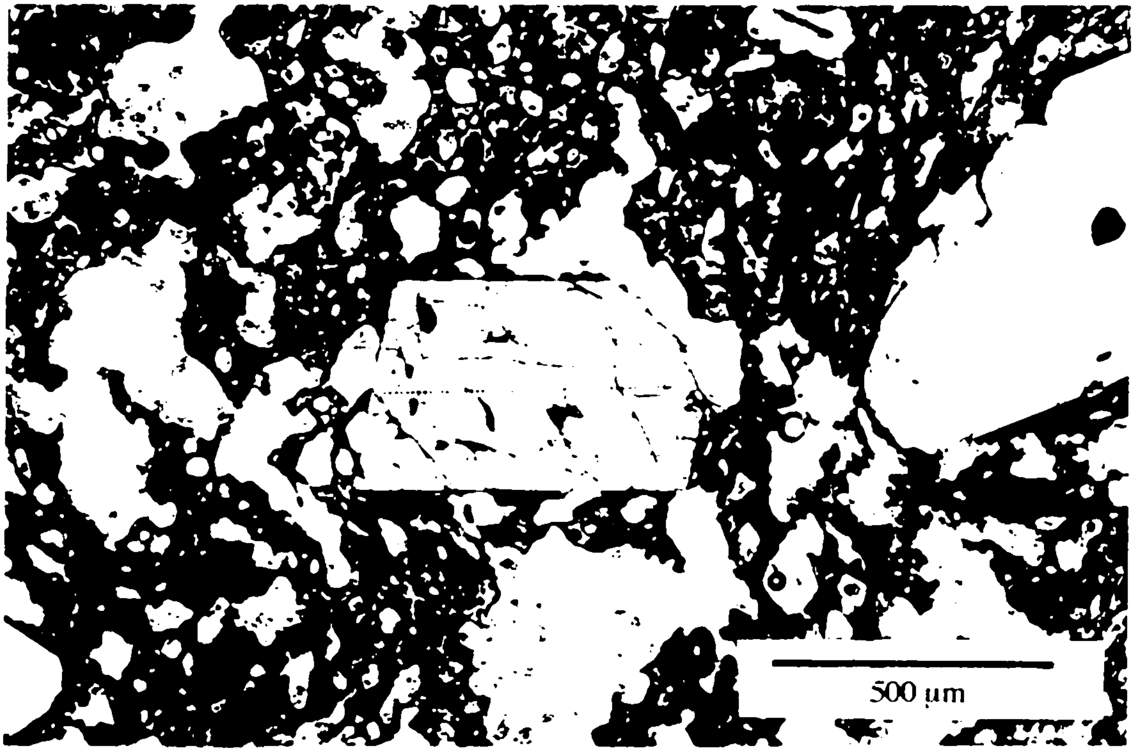

Plate 3.17

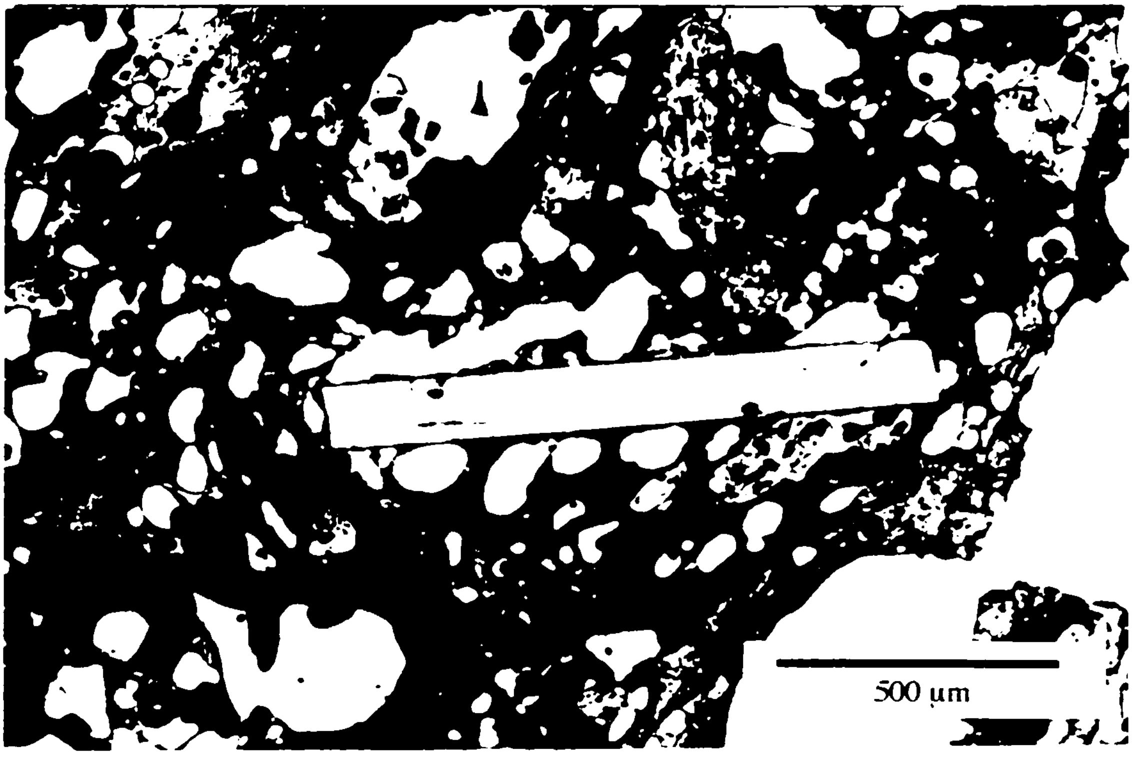

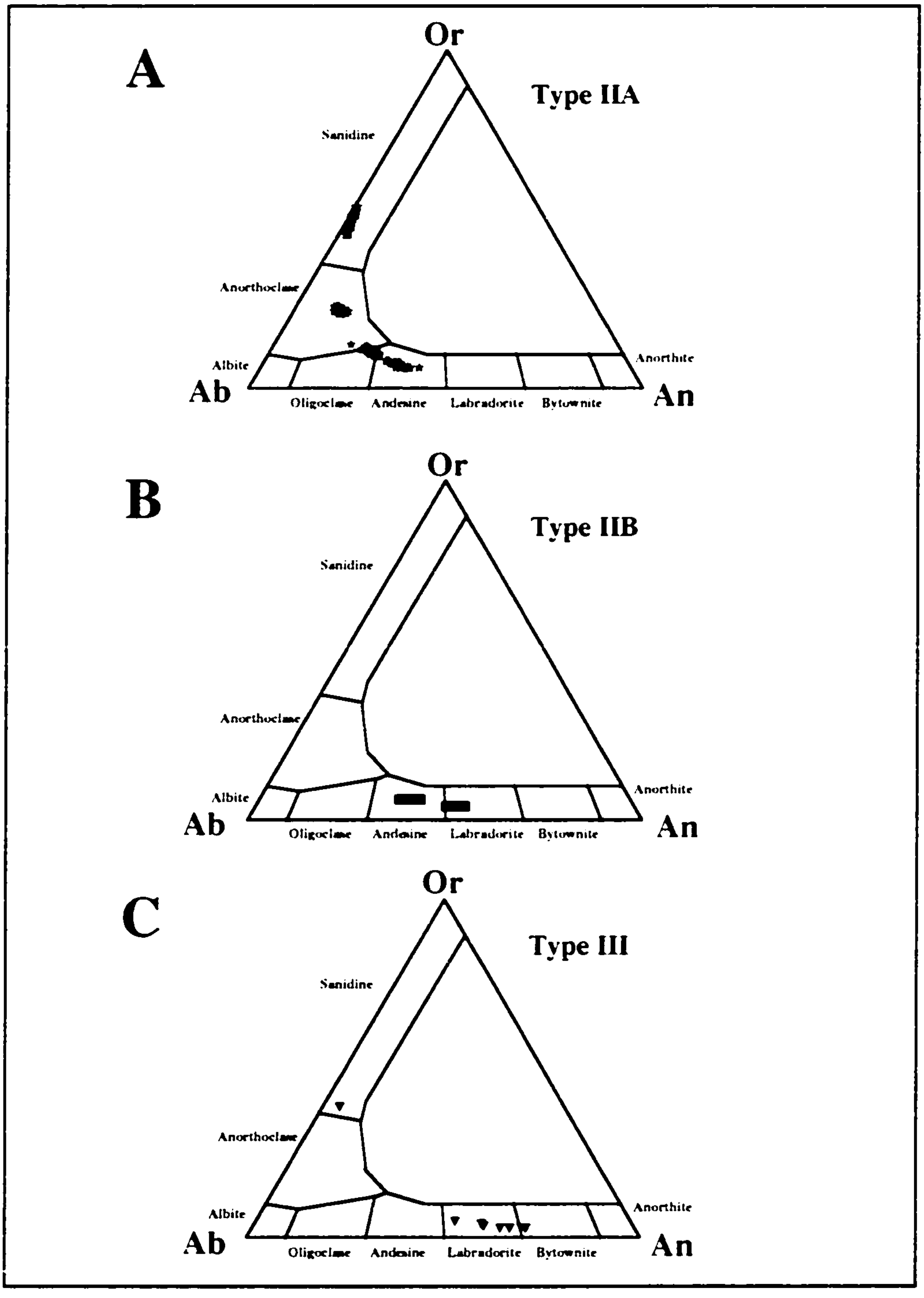

Figure 3.13.: An-Ab-Or plot for different feldspar types from Diego Hernandez Wall. (A) Type IIA; (B) Type IIB; (C) Type III.

a nearly continuous trend on An-Ab-Or ternary diagram (Fig. 3.13). Core to rim traverses of individual crystals have a range of less than 9% An, all with normal zoning (Table 3.3 & Fig. 3.14). Crystal sizes range from 500 to 850 µm. These crystals are only identified in mafic pumice. In comparing Type IA to this population (Fig. 3.9) there is a significant overlap in compositions (see interpretation below).

Feldspar - Type IIB

All Type IIB crystals are plagioclase feldspars that are euhedral and lath-shaped, having little to no resorption features. This sub-type is subordinate, much like Type IC, with only few crystals identified in mafic pumice samples. These crystals are hosted in dark brown to black glass. Again, Type IIB feldspars may be found in banded samples, but may not be recognized due to fragmentation. Crystals range in size from 700 to 900 µm.

These feldspars are characterized by having a simple Carlsbad twin. Another charactistic is that both ends of the crystal lath usually exhibit evidence of slight corrosion, otherwise their crystal structure is intact. Individual crystals have little variation in An content (< 5% An), however zoning in this case is reverse (Fig. 3.15). Overall compositions varyfrom labradorite (An_{55}) to andesine (An_{38}) (Fig. 3.13).

Interpretation of Type II Feldspars

Type II feldspar crystals are characterized by an euhedral morphology especially when compared to those of Type I feldspar. Nomarski (DIC) does not reveal any dissolution or zoning within either sub-type. Combined with the lack of compositional variation, as documented by EMP analyses, it is obvious that these crystals are the result of near-equilibrium

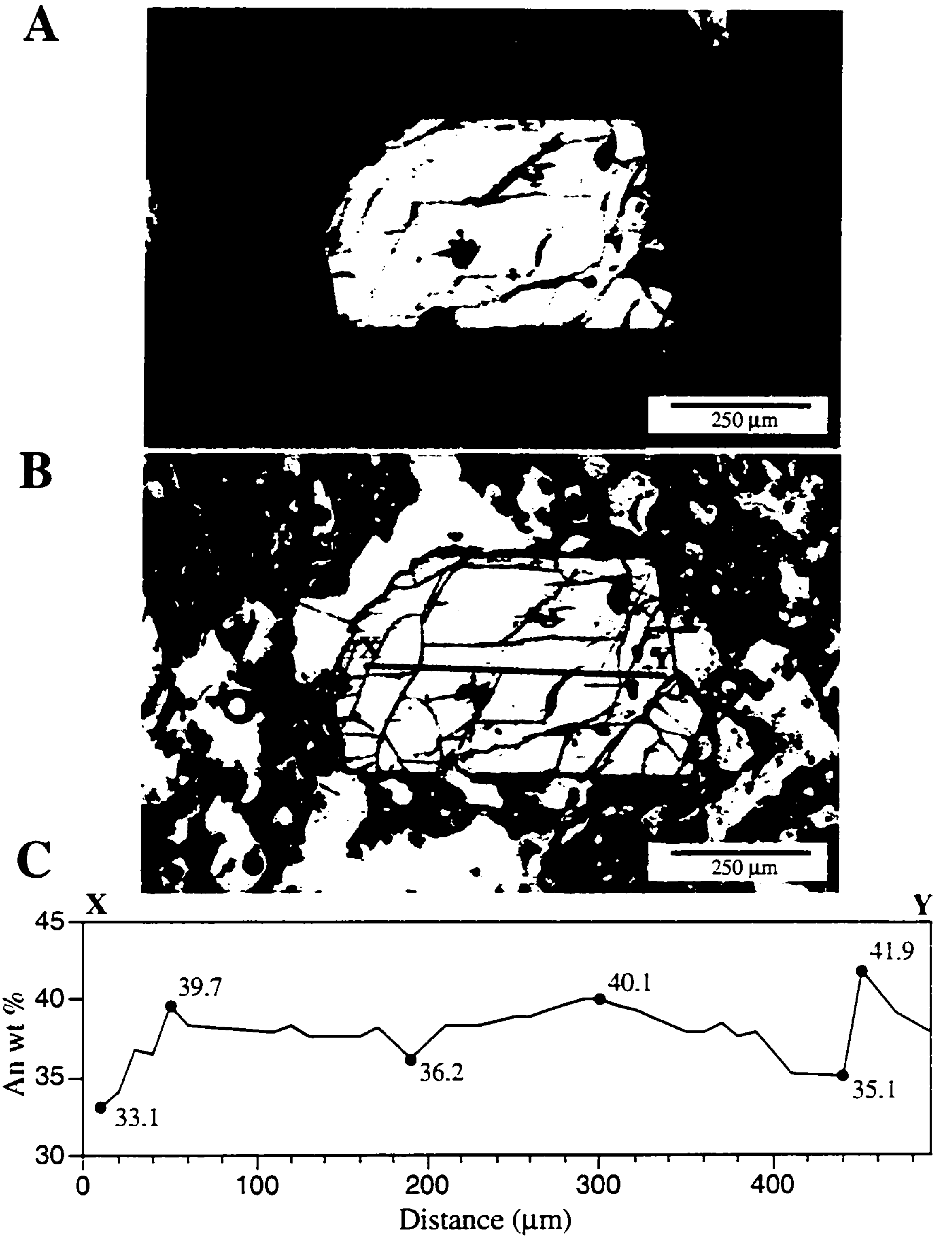

Figure 3.14.: Line traverse for Type IIA feldspar, LT004. (A) Transmitted light (X-Nicols) (B) NDIC with traverse line; and (C) An wt % plotted from rim to rim.

growth.

The three compositional populations identified in Type IIA along with Type IIB compositions demonstrate that there likely were discrete zones of isolated magma that underwent crystallization with limited, to no interaction with the bulk of its host liquid. The K-rich feldspars (the most K-rich feldspars analyzed) are interpreted to represent near-equilibrium crystallization from the more evolved felsic melt, a phonolite (see glass section). There is only one feldspar composition that plots in the anorthoclase field. It is distinctive not only due to its chemistry but also because it is from the banded pumice. This feldspar shows no signs of resorption, on the contrary it has euhedral crystal faces. It is possible that this crystal crystallized close to the boundary layer separating the phonolite and intermediate melt, where the phonolitic melt likely was not as potassic. The crystal overall shows no signs of resorption that may be attributed to the short time interval between mixing and eruption.

There are two observed plagioclase compositions. One belonging to Type IIA, the other to Type IIB. Type IIB feldspars are slightly more Ca-rich than the former feldspars. These feldspars represent near-equilibrium crystallization from a more mafic melt, either lower in the magma chamber or from isolated patches of melt that were dominated by the basic end member. There is one minor dissolution surface observed in NDIC, but there is only a 5% variation in An content the crystal. Their distinctive reverse zoning may be due to renewed growth from mafic melt. The more sodic plagioclase from Type IIA are blocky to equant and again represent an "equilibrium" composition. Compositionally, these plagioclase crystals overlap with Type IA feldspars (Fig. 3.9).

The maximum size of Type IIA plagioclase crystals can be related to the size of the mantle overgrowths observed in Type IA feldspars. The maximum size of any mantle overgrowth from Type IA is 285 μm, which is in the larger, broken crystals, whereas the

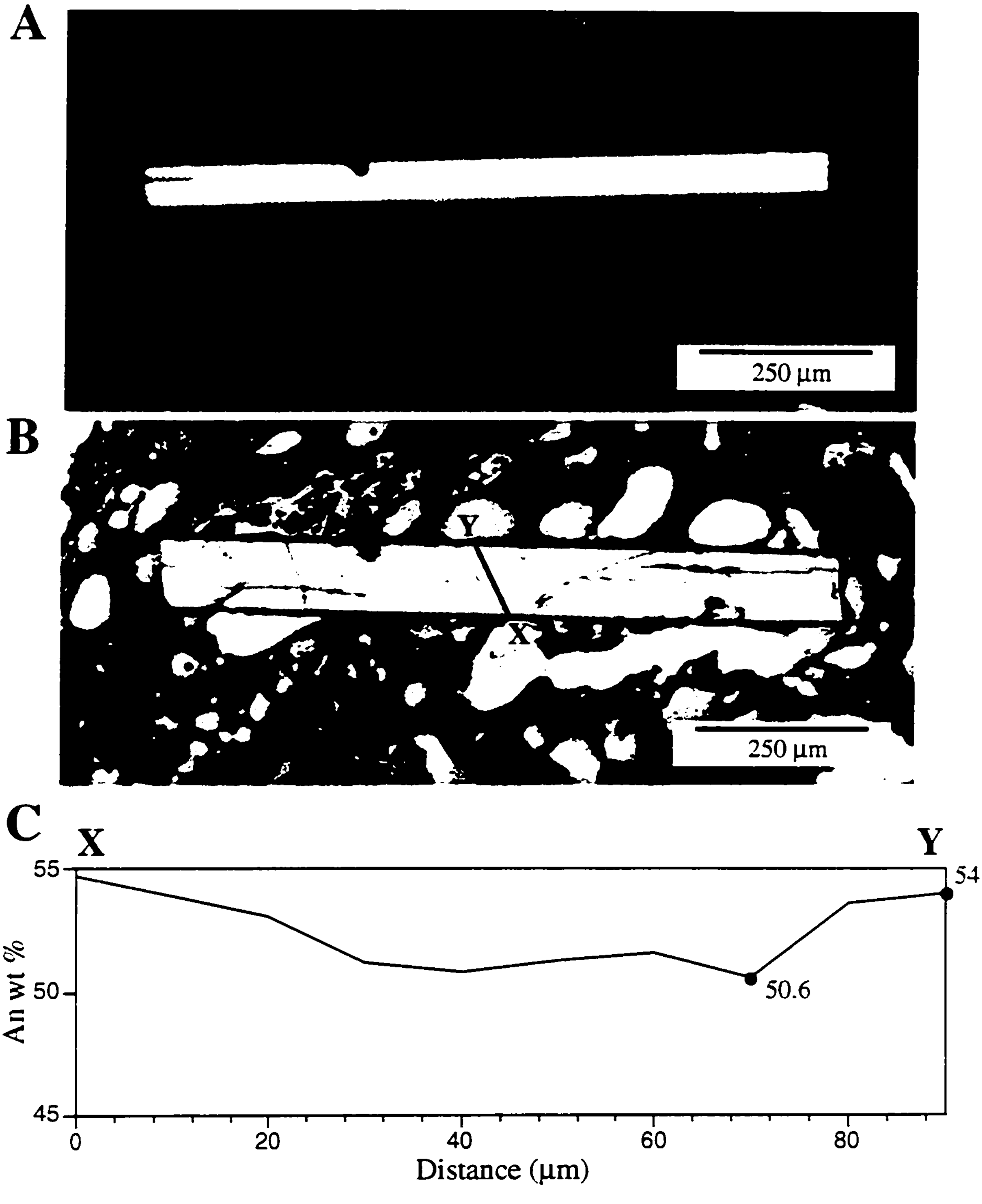

Figure 3.15.: Line traverse for Type IIB feldspar, LT010. (A) Transmitted light (X-Nicols): (B) NDIC with traverse line; and (C) An wt % plotted from rim to rim.

smaller intact feldspar crystals typically have a mantle of 50-80 μm. This mantle represents near-equilibrium growth from the intermediate magma as do Type IIA plagioclase crystals. The doubling of the maximum mantle size should roughly equal the maximum size of Type IIA feldspar crystals if mantle growth and new euhedral feldspar started at the same time. Overall the crystal size of Type II plagioclase crystals are fairly close to this doubled mantle value of 570 μm, with the maximum size observed being 850 μm. This discrepancy may be due to unobserved mantle that is larger or a slight time lag in mantle growth on older crystals.

The reader should note that the above concept is a very rough estimate of growth. Mechanisms regarding nucleation (Type II feldspar) versus growth (Type IA feldspar) are not considered. Diffusion restrictions concerning supply to a small nucleating crystal versus a large crystal are also ignored.

Feldspar - Type III

Type III feldspar crystals are crystals that for the most part can be described as microphenocrysts. The crystal size of the microphenocrysts presents a problem for analysis by EMP. Three possible microphenocrysts populations exist based on three hypothesized magma end-members (see glass discussion). Two are identified by EMP, namely the phonolitic (Or_{36}) and basic (An_{71}) feldspars (Table 3.2)

Microphenocrystic feldspars from the basic end-member are larger than those from the felsic (phonolitic) end-member. The largest observed feldspar is 300 μm long (Plate 3.18). These feldspars are distinctive due to their skeletal growth habit. These skeletal feldspars are located in mafic pumice samples (CS-010A), hosted in dark brown glass that is partially crystallized. EMP analyses reveal that inner zones around An_{70} (bytownite) with overgrowth regions having varying An content from An_{62} to An_{52} (labradorite) (Fig. 3.13). The skeletal crystal probably originates from rapid growth due to injection of the basic (last) melt into the intermediate melt. The resulting undercooling induces the rapid growth. The overgrowth represents near-equilibrium growth after the skeletal crystal is mixed into the intermediate host melt.

Microphenocrysts are observed throughout the felsic and mafic glass from banded pumice samples (CS-010). All are acicular crystals with most having swallow-tail texture (Plate 3.19). Unfortunately, due to their size EMP analyis was only successfully on one crystal, yielding Or_{36} (Fig. 3.13 & 3.9), hosted in phonolitic glass. Swallow-tailed feldspars are observed in all glass types. These crystals were probably growing in their respective melts just prior to eruption. The eruptive event undercooled the phonolitic melt inducing rapid growth on these preexisting microphenocrysts. The swallow-tailed texture is the end result of this undercooling and indicates diffusion controlled growth because crystal corners are exposed to a greater volume of melt relative to crystal faces and therefore preferentially grow. Microlties from both glasses probably represent near-equilibrium composition for their respective melts.

The EMP analysis within the body of swallow-tailed feldspar, Or_{36}, is interpreted to characterize the feldspar in equilibrium with the phonolite close to the compositional boundary with theintermediate melt. This is concluded because their existence in banded pumice samples. Type IC feldspars are also interpreted to have crystallized close to this boundary. Type IC compositions (Fig. 3.13 & 3.9) do overlap with this one Type III feldspar crystal, lending further evidence for their location close to the phonolite-intermediate magma boundary.

Plate 3.18: NDIC microphotograph of Type III skeletal feldspar crystal. Thin overgrowth is more sodic than rest of crystal.

Plate 3.19: Microphotograph in NDIC of Type III swallow-tailed feldspar crystal, hosted in felsic glass that is almost free of recrystallization.

Plate 3.18

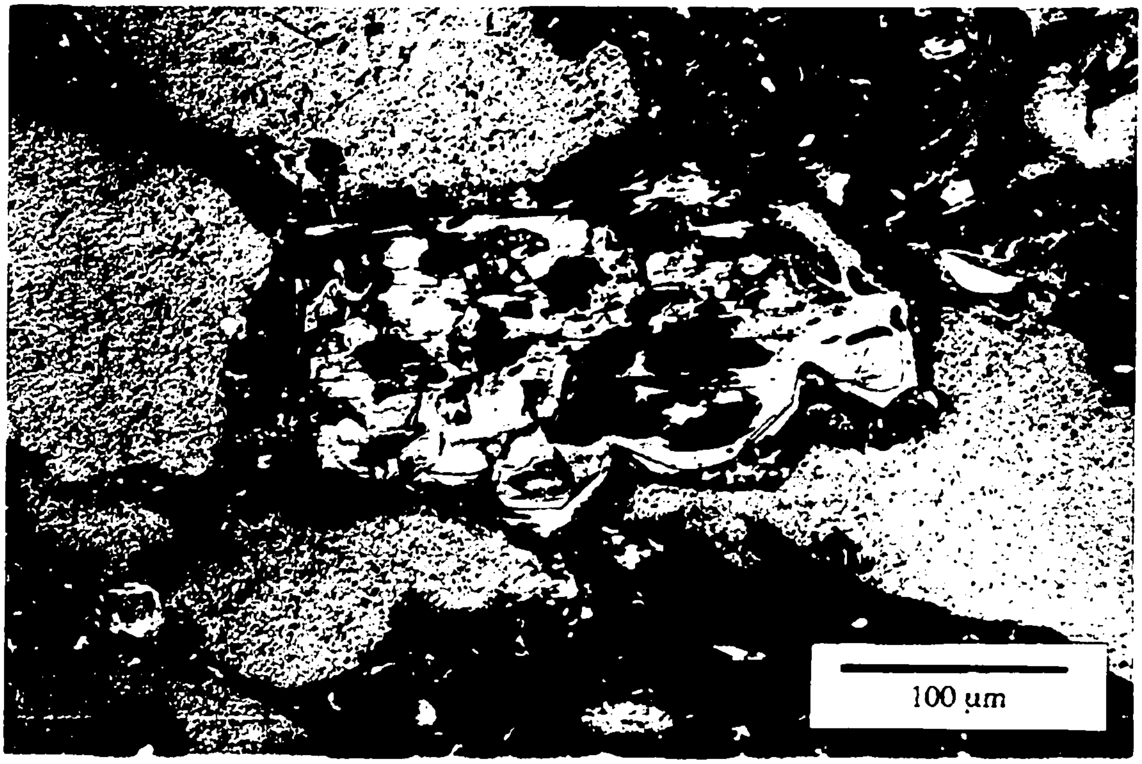

Plate 3.19

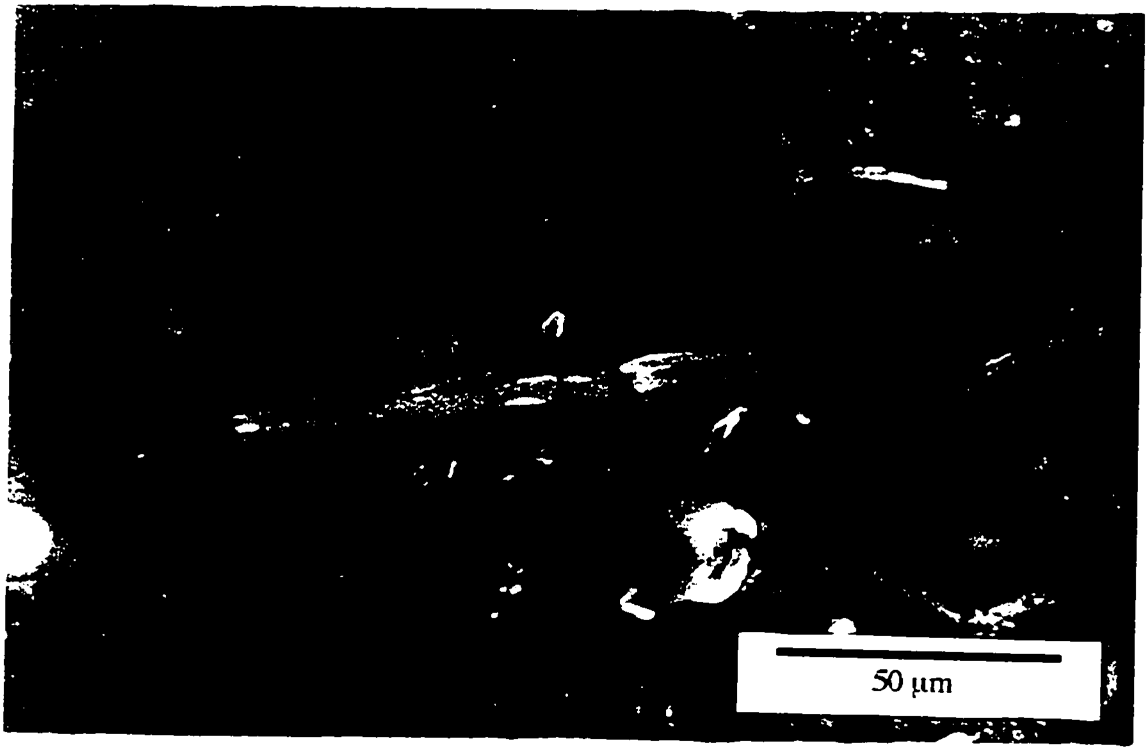

3.2.3 Pyroxene

The most abundant ferromagnesium mineral is the pyroxenes. Pyroxenes make up 2% by volume of the phenocryst population in mafic samples, 2 % in banded pumice, and traceamounts in felsic pumice. Three different pyroxenes are identified based on crystal habit and pleochroism. EMP analysis of pyroxenes allowed further subdivision based on pyroxene major element chemistry (see below).

The most abundant pyroxenes are blocky to tabular crystals that are for the most part euhedral (Plate 3.20), with crystals ranging from 0.4 to 1.0 mm in size. EMP analyses of these pyroxenes reveal that they have high Ti contents (up to 3.7 wt %), identifying them as titanaugites. Pleochroism varies from greenish blue, yellowish brown to a distinctive bleached pink. Zoning is typically normal, but several crystals exhibit hourglass zoning and simple twins along with oscillatory zones (Plate 3.21). Anhedral inclusions of Fe-Ti oxides are frequently associated with these pyroxenes. Titanaugites are hosted in dark brown to black glass with some rare cases of medium brown glass. None are observed in clear to pale green glass. Thus titanaugites are restricted to mafic pumice and mafic glass bands in banded pumice samples.

Lath-shaped crystals having a subhedral habit and define the other sub-type of pyroxene. These pyroxene phenocrysts range from 0.3 to 2.2 mm in size. Pleochroism varies from bright green, brownish green, yellowish green and bluish green. Compositionally theyare lower in Ti and Al and higher in Si, Mn and Na (Table 3.4) as compared to the titanaugites. Based on their EMP analyses these pyroxenes can be classified as salites. Fe-Ti oxide inclusions are common as are acicular microphenocrysts of apatite (Plate 3.22). The presence of apatite inclusions separates salites from titanaugites and may indicate different magma sources. As with titanaugites, salites are hosted in dark brown to black glass, but are also

Plate 3.20: Transmitted light microphotograph of euhedral, equant pyroxene phenocryst. This pyroxene has distinctive bleached pink pleochroism. Hosted in dark brown glass.

Plate 3.21: X-Nicols microphotograph of simple twin in euhedral pyroxene phenocryst.

Plate 3.20

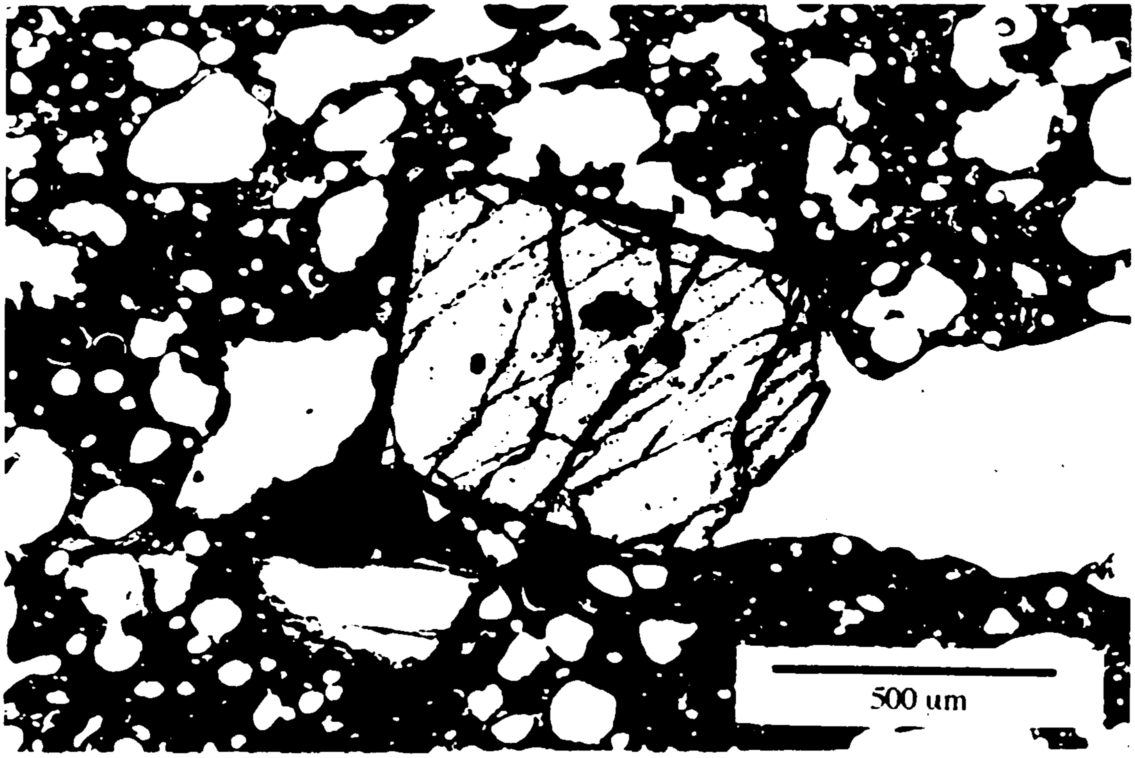

Plate 3.21

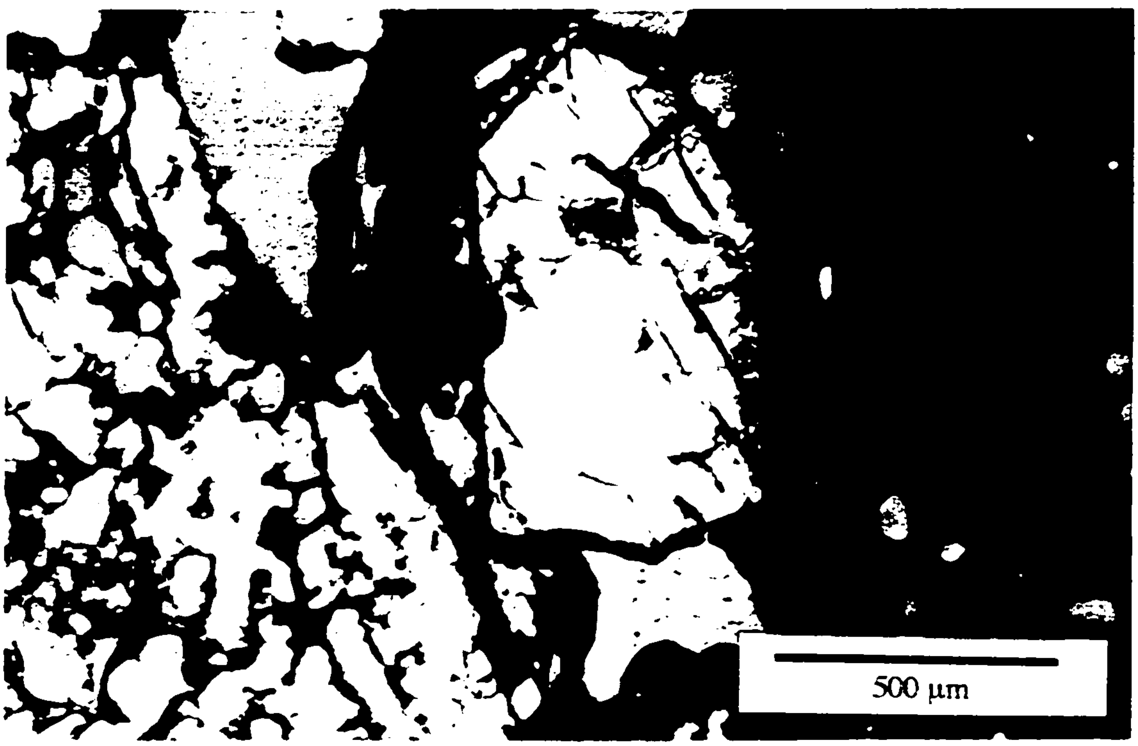

commonly hosted in medium brown glass. A few salite crystals are observed in light brown glass, but none are observed in clear to pale green glass. One such pyroxene hosted in light to medium brown glass is rounded and embayed indicating possible post-crystallization reactionwith the melt.

There are pyroxene crystals identified in the felsic pumice (TK-9D) sample, but they only occur as rare microphenocrysts, with a maximum size of 100 μm. These pyroxenes are euhedral with a characteristic deep green pleochroism. No other pyroxene observed in any of the other samples has this pleochroic color. Unfortunately these felsic pyroxenes have not been analyzed by EMP, but based on their strong pleochroism and felsic host they are tentatively identified as aegirine-augite (Deer et al. 1989). Of the two pyroxenes examined, one has mantled a titanite crystal (Plate 3.23). Both pyroxenes are hosted in transparent glass that has a stretched out and stringy appearance.

There are several pyroxene crystals distinct from the above three groups. Overall these pyroxenes have a subhedral, lath-like shape, with a maximum crystal size of 1.6 mm. Cores are green with one crystal's core being "dusty" (Fig. 3.16A). Rims are a buff pink, similar to the titanaugite phenocrysts suggesting that at least latter growth was from the more basic melt. Consistent with the pleochroism, the rim compositions are very similar compositionally to titanaugites as there is a noticeable jump to higher Al and Ti along with associated decreases in Na and Mn at the rim (Fig. 3.16). Core compositions cannot be correlated to any analyzedpyroxene due to its high Fe and low Mg content in comparison to other pyroxenes analyzed (Table 3.4). Inclusions of apatite are limited to core, and do not extend into those areas having the pink pleochroism, whereas Fe-Ti oxides are found throughout. These pyroxenes are normally hosted in black to dark brown glass with rare instances of hosting in a medium brown glass.

Table 3.4.: Representative EMP analyses of pyroxene. See Appendix A.3 for complete data set.

	Salite		Titanaugite				Green-cored Pyx	
	C001-001	C002-004	C003-002	C005-005	LT049-001 core	LT049-043 rim	LT050-003 core	LT050-024 rim
SiO_2	48.087	49.47	46.413	44.662	44.743	45.452	47.355	45.839
TiO_2	1.442	1.114	2.559	3.132	3.579	3.158	1.767	3.161
Al_2O_3	3.382	2.58	6.189	7.83	8.449	8.306	4.222	7.358
FeO_T	8.399	8.412	7.242	7.724	7.322	7.427	10.105	7.581
Cr_2O_3	0	0	0	0.004				
MnO	0.52	0.595	0.146	0.123	0.144	0.131	0.593	0.203
MgO	13.183	13.088	13.485	12.922	12.599	12.929	11.814	12.918
CaO	21.869	21.813	22.282	23.118	23.208	22.967	22.464	23.006
Na_2O	1.119	1.084	0.587	0.482	0.519	0.521	0.821	0.664
K_2O	0.017	0.019	0.029	0.025	0.027	0.014	0.025	0.023
Total	98.02	98.18	98.93	100.022	100.59	100.905	99.166	100.753
				Oxygen = 6.000				
Si	1.816	1.869	1.736	1.657	1.652	1.67	1.788	1.688
Al	0.15	0.115	0.272	0.342	0.368	0.36	0.188	0.319
Ti	0.041	0.032	0.072	0.087	0.099	0.087	0.05	0.088
Fe*	0.266	0.266	0.227	0.24	0.227	0.229	0.32	0.233
Cr	0	0	0	0	0	0	0	0
Mg	0.742	0.737	0.752	0.715	0.694	0.708	0.665	0.709
Mn	0.017	0.019	0.005	0.004	0.005	0.004	0.019	0.006
Ca	0.885	0.883	0.893	0.919	0.918	0.904	0.909	0.908
Na	0.082	0.079	0.043	0.035	0.037	0.037	0.06	0.047
K	0.001	0.001	0.001	0.001	0.001	0.001	0.001	0.001
WO	46	46	48	49	50	49	48	49
EN	39	39	40	38	38	38	35	38
FS	15	15	12	13	13	13	18	13

Plate 3.22: Transmitted light photomicrograph of lath-shaped subhedral pyroxene phenocryst. Morphology defines second pyroxene type. Pleochroism is light to pale green. Apatite (Ap) inclusions are found throughout this pyroxene type.

Plate 3.23: Small euhedral crystal of pyroxene from felsic pumice sample (TK-9D). This pyroxene is thought to be the third pyroxene type and is a possible aegirine-augite.

Plate 3.22

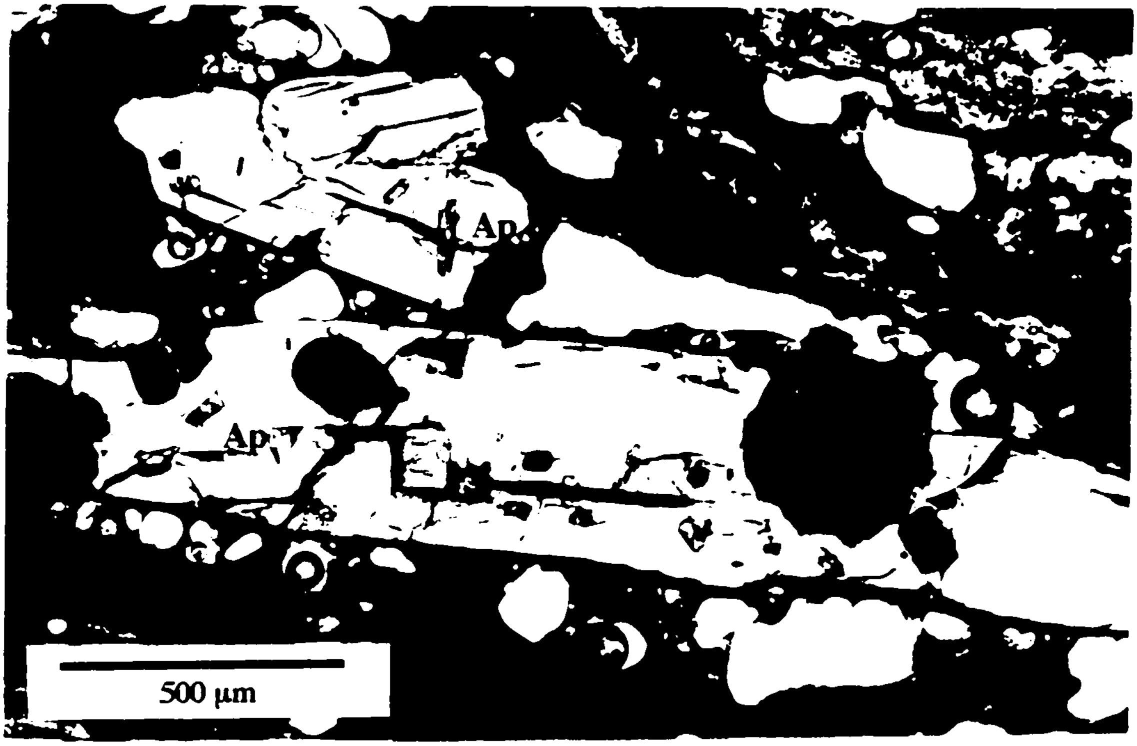

Plate 3.23

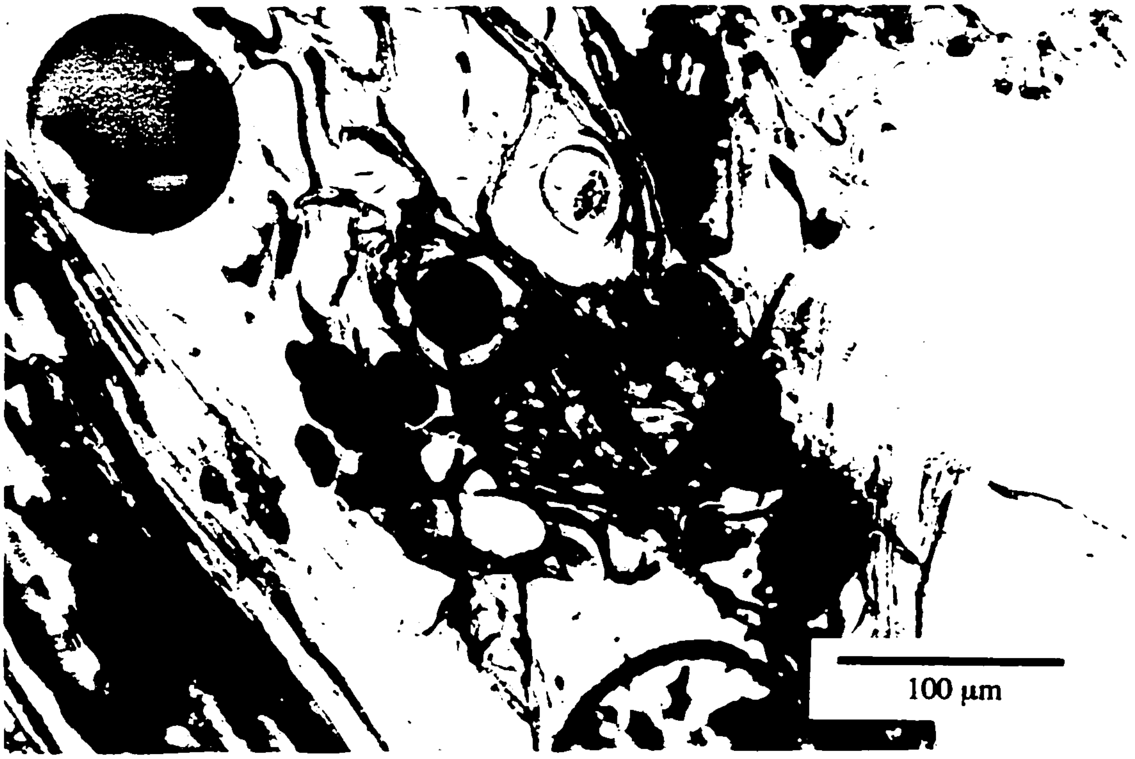

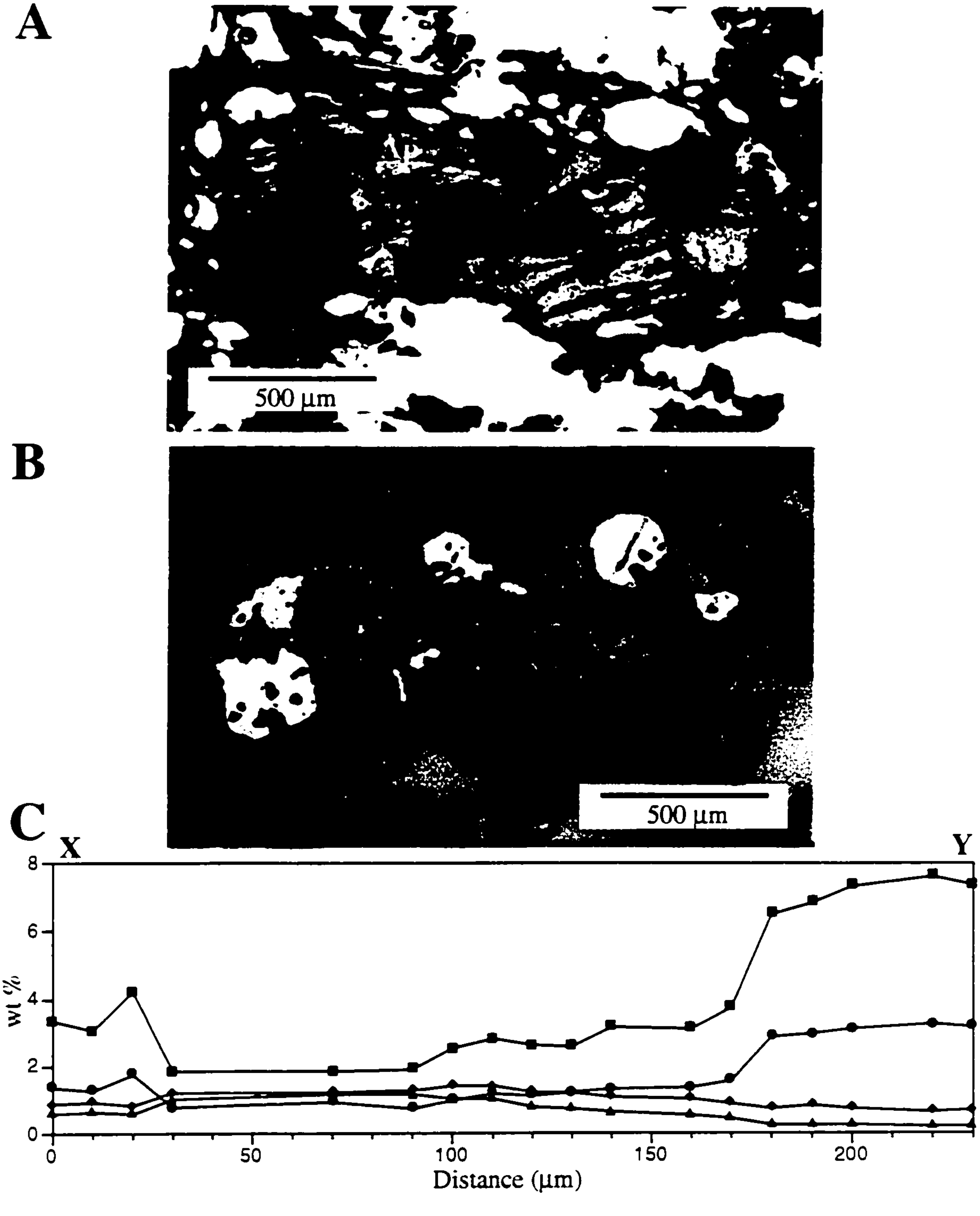

Figure 3.16.: Line traverse of dusty cored pyroxene phenocryst LT050. (A) Transmitted light (X-Nicols); (B) NDIC with line traverse; and (C) line traverse of Al (■), Ti (●), Mn (▲) and Na (◆) oxides. Ap is apatite.

3.2.4 Amphibole

Amphiboles are the second most abundant ferromagnesium mineral observed in DiegoHernández pumice samples. Amphibole phenocrysts are typically blocky and equant (Plate 3.24), with euhedral to subhedral crystal habits. Crystal sizes range from 0.2 to 1.3 mm. They are identified in mafic and banded pumice samples with approximately 2 vol % in each, with no amphiboles observed in felsic pumice. Morphologically, two amphibole populations are recognized; resorbed and non-resorbed. However, EMP analyses only distinguish one compositional population, kaersutite (Table 3.5). Resorbed amphiboles (Plate 3.25) are by far the more dominant variety, making up about 95% of observed crystals. Pleochroism varies from light to dark brown with some sections having a deep reddish brown. A few sections have a greenish yellow pleochroism and are only hosted in medium brown glass from banded pumice sample (CS-010), whereas most amphiboles are hosted in dark brown to black glass.

3.2.5 Biotite

Biotite is a minor mineral as only a few of crystals were observed. All crystals are rectangular in shape and have an euhedral habit. Crystal sizes are restricted to 0.4 to 0.9 mm. Biotite is observed in both mafic and banded pumice samples, but while they are hosted in medium brown glass they are typically mantled by a thin veneer of pale green glass. Unlike kaersutite, biotite crystals have a slight variation in Ti, Fe and to a lesser extent Mg contents (Table 3.6) between individual crystals. All crystals have the characteristic bird's eye extinction of biotite.

3.2.6 Feldspathoids

Crystals of nepheline and sodalite are found in trace amounts in collected pumice

Plate 3.24: Transmitted light microphotograph of euhedral amphibole phenocryst. Some resorption is evident in core region of crystal. Hosted in dark to medium brown glass.

Plate 3.25: Transmitted light microphotograph of highly resorbed anhedral amphibole phenocryst. Two large embayments have almost split these crystal into two sub-equal portions. Hosted in medium brown glass.

Plate 3.24

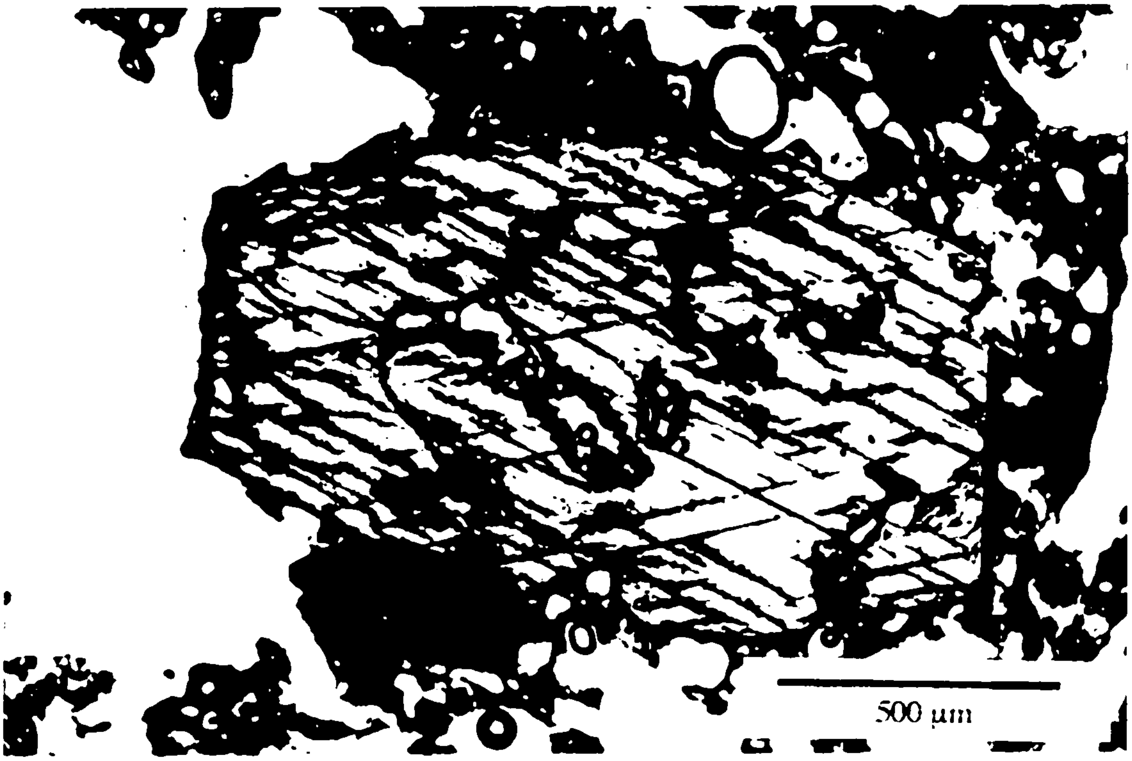

Plate 3.25

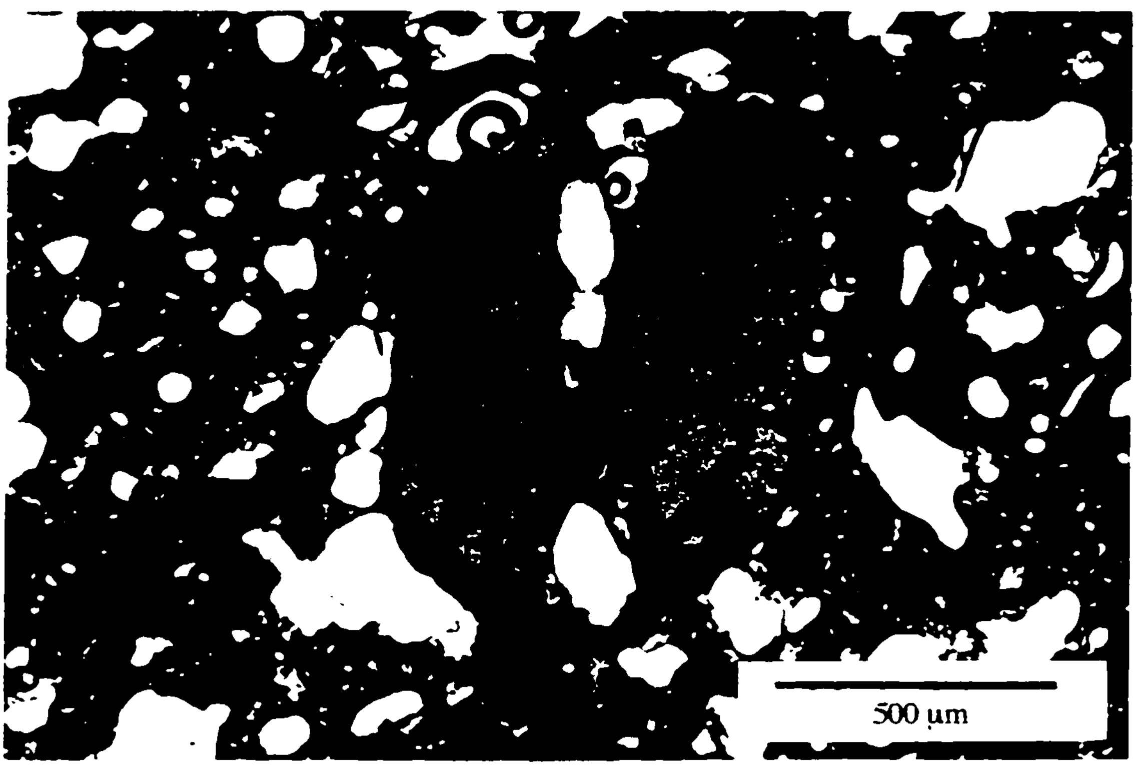

Table 3.5.: Representative EMP analyses for amphibole. See Appendix A.4 for complete data set.

	AM001-006	AM002-007	AM004-006	AM005-003	AM006-004	LT051-001 core	LT051-049 rim
SiO_2	39.557	39.767	39.245	39.228	39.776	39.769	38.297
TiO_2	5.97	5.874	5.99	6.458	6.439	6.346	6.534
Al_2O_3	11.755	11.531	12.537	13.057	12.693	12.855	13.145
FeO_T	12.248	12.321	13.717	12.012	11.063	11.194	10.09
Cr_2O_3	0.005	0	0	0.015	0	0.014	0.013
MnO	0.325	0.313	0.321	0.199	0.15	0.192	0.1
MgO	12.729	12.776	11.639	12.446	13.344	13.479	13.333
CaO	11.636	11.607	11.722	11.902	11.918	12.083	12.316
Na_2O	2.827	2.741	2.716	2.836	2.771	2.741	2.428
K_2O	1.268	1.275	1.195	1.117	1.071	1.039	1.086
F	0.051	0.142	0.047	0.069	0.048	0.086	0.083
Cl	0.017	0.028	0.022	0.008	0.014	0.014	0.018
Total	98.38	98.38	99.15	99.33	99.29	99.8	97.43
				Oxygen = 23.000			
Si	6.045	6.327	5.987	5.941	5.958	6.018	5.93
Al	2.116	2.16	2.253	2.329	2.239	2.29	2.396
Cr	0.001	0	0	0.002	0	0.002	0.002
Ti	0.686	0.703	0.687	0.736	0.726	0.722	0.761
Mg	2.9	3.03	2.647	2.81	2.98	3.04	3.077
Fe*	1.565	1.639	1.75	1.522	1.386	1.416	1.307
Mn	0.042	0.042	0.041	0.026	0.019	0.025	0.013
Ca	1.905	1.979	1.916	1.932	1.912	1.959	2.043
Na	0.838	0.846	0.803	0.833	0.805	0.804	0.729
K	0.247	0.259	0.233	0.216	0.205	0.201	0.215
Cl	0.004	0.008	0.006	0.002	0.004	0.004	0.005
F	0.025	0.071	0.023	0.033	0.023	0.041	0.041

samples. Nepheline occurs as euhedral, equant phenocrysts in all pumice samples, with crystal sizes ranging from 0.2 to 1.6 mm. The largest phenocryst observed is from a discontinuous felsic streak in a mafic pumice sample (TK-9C), where it is part of a nepheline glomerocryst. The smallest is hosted in felsic glass from the felsic pumice sample (TK-9D). All nepheline crystals have oscillatory zoning (Plate 3.26), which has been enhanced as a direct result of etching with fluoroboric acid. The only nepheline crystal hosted in dark brown glass (LT014 from CS95-011) shows evidence of resorption with rounding of all corners. Further evidence of an early dissolution event in this crystal is the truncation of zoning evident in NDIC. EMP analyses show that nepheline crystals are very homogenous (Table 3.7), even across the truncated zones.

Sodalite crystals all show signs of resorption and possible re-crystallization or reaction textures as all crystals have a mottled appearance. Overall, due to their resorbed nature, sodalite is typically anhedral. Their crystal sizes range from 0.2 to 1 mm. Surprisingly sodalite crystals are concentrated in dark brown to black glass, which may explain their resorbed nature. Of the few crystals that are observed in pale green glass their crystal habit is more euhedral, with several crystal faces preserved.

3.2.7 Fe-Ti Oxides

Almost all oxides are rounded to some degree, with the only exceptions being a few inclusions in silicate phases. Overall oxides are blocky and equant (Plate 3.27) with crystal sizes ranging from 0.2 to 0.7 mm. Two oxide phases are identified optically; namely magnetite and ilmenite. EMP analyses of magnetite have high enough Ti values (Table 3.8) such that these oxides can be classified as titanomagnetites. Careful examination of EMP data reveal three titanomagnetite and two ilmenite populations based on variations of Ti, Al, Fe, Mn and

Table 3.6.: Representative EMP analyses for biotite See Appendix A.5 for complete data set.

	BT001-001	BT001-003 rim	BT001-007 core	BT002-001	BT002-004	BT003-001 rim	BT003-003
SiO_2	36.012	36.313	36.008	37.15	36.95	36.803	37.269
TiO_2	8.184	8.006	8.099	4.896	4.263	7.569	7.13
Al_2O_3	14.383	14.181	14.249	13.292	13.211	13.996	13.852
Cr_2O_3	0.011	0	0	0	0	0	0
FeO_T	13.891	13.503	13.66	17.505	17.451	14.09	14.125
MnO	0.274	0.245	0.25	0.759	0.744	0.324	0.328
MgO	14.73	14.902	14.588	14.005	14.4	15.129	15.239
CaO	0.018	0	0.023	0.005	0	0.025	0.026
Na_2O	0.961	1.021	0.966	0.808	0.809	1.012	0.92
K_2O	8.708	9.013	8.885	9.648	9.717	9.454	9.627
F	0.211	0.158	0.158	0.272	0.302	0.229	0.208
Cl	0.024	0.021	0.023	0.019	0.012	0.02	0.024
Total	97.41	97.36	96.91	98.36	97.86	98.65	98.75
				Oxygen = 22.000			
Si	5.278	5.319	5.302	5.512	5.517	5.348	5.407
Al	2.483	2.446	2.471	2.323	2.323	2.395	2.367
Ti	0.902	0.882	0.897	0.546	0.479	0.827	0.778
Fe*	1.703	1.654	1.682	2.172	2.179	1.712	1.714
Cr	0.001	0	0	0	0	0	0
Mn	0.034	0.03	0.031	0.095	0.094	0.04	0.04
Mg	3.219	3.254	3.202	3.098	3.205	3.277	3.296
Ca	0.003	0	0.004	0.001	0	0.004	0.004
Na	0.273	0.29	0.276	0.232	0.234	0.285	0.259
K	1.628	1.684	1.669	1.826	1.851	1.753	1.782
F	0.196	0.146	0.147	0.255	0.285	0.21	0.191
Cl	0.012	0.01	0.011	0.01	0.006	0.01	0.012

Plate 3.26: Transmitted light microphotograph of euhedral nepheline phenocryst. Etching has enhanced the oscillatory zoning in core. Nepheline is acting as a stirring rod here, breaking up the contrasting melt phases.

Plate 3.27: Reflected light microphotograph of anhedral but equant Fe-Ti oxide. Oxide here is an ilmenite that has undergone moderate resorption.

Plate 3.26

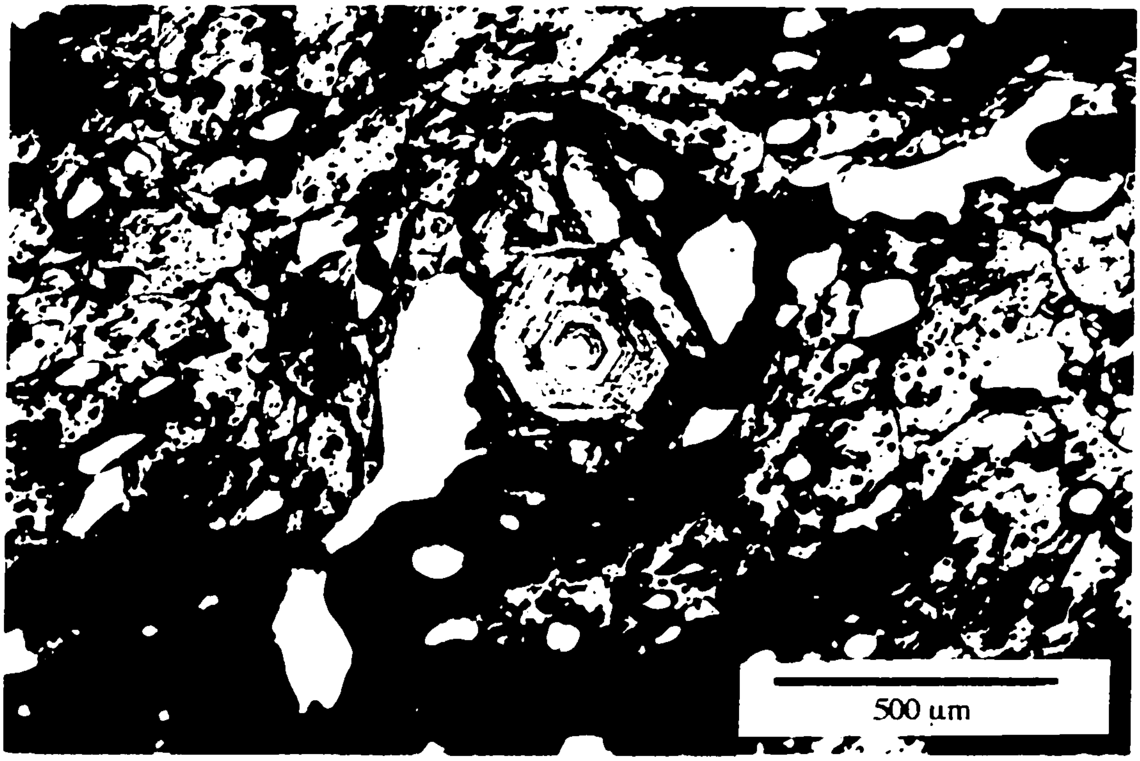

Plate 3.27

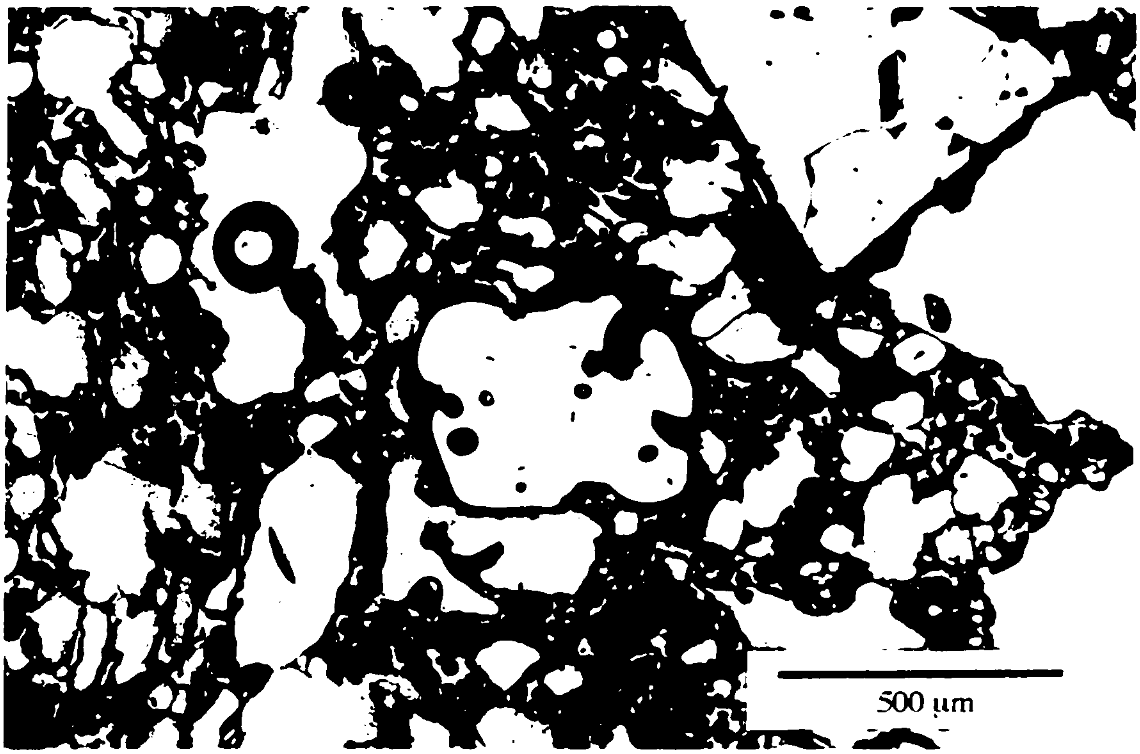

Table 3.7.: Representative EMP analyses of Nepheline. See Appendix A.6 for all data.

	LT012-001 core	LT012-082 rim	LT013-001 rim	LT013-050 core	LT014-001 rim	LT014-036 core	LT015-001 rim
SiO_2	45.741	45.887	45.002	45.905	45.54	46.652	45.838
Al_2O_3	32.383	32.276	32.183	32.261	32.286	32.27	32.414
FeO_T	0.548	0.587	0.606	0.643	0.63	0.66	0.584
MgO	0.004	0.014	0.005	0.004	0.007	0.009	0.004
CaO	0.769	0.764	0.808	0.736	0.819	0.794	0.794
Na_2O	16.499	16.125	16.399	16.457	16.357	16.799	16.507
K_2O	3.868	4.254	3.894	3.803	4.118	3.801	4.052
Total	99.81	99.91	98.9	99.81	99.76	100.99	100.19
			Oxygen = 32.000				
Si	8.687	8.713	8.64	8.714	8.671	8.756	8.683
Al	7.243	7.218	7.277	7.212	7.239	7.133	7.231
Mg	0.001	0.004	0.001	0.001	0.002	0.003	0.001
Fe*	0.087	0.093	0.097	0.102	0.1	0.104	0.093
Na	6.076	5.937	6.105	6.058	6.039	6.114	6.063
Ca	0.156	0.155	0.166	0.15	0.167	0.16	0.161
K	0.937	1.031	0.954	0.921	1.00	0.91	0.979

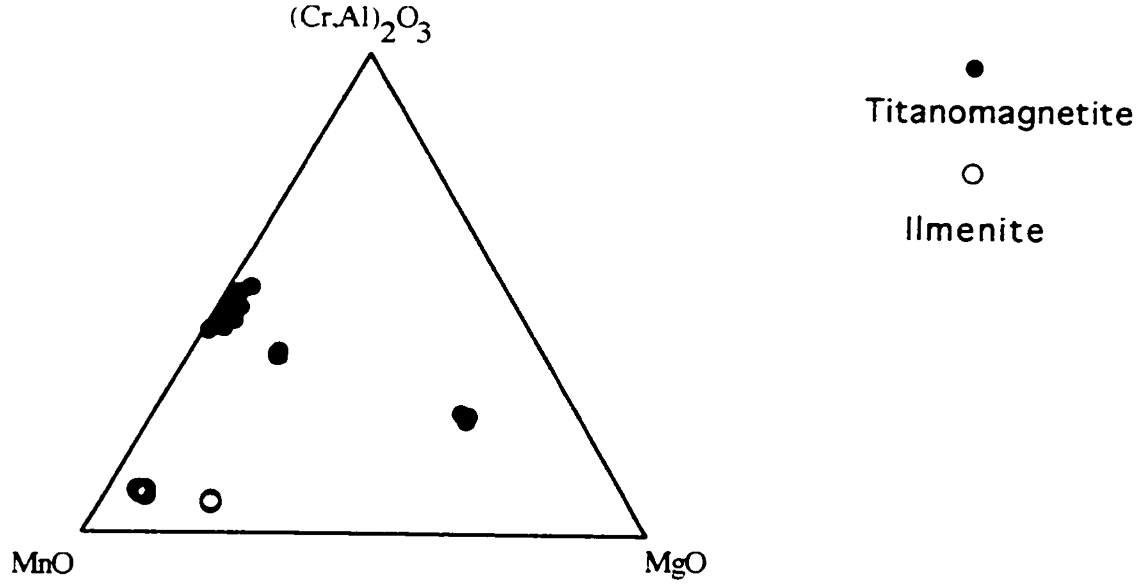

Figure 3.17: Oxide ternary diagram showing Titanomagnetite and Ilmenite populations.

Mg for titanomagnetite and Ti, Fe, Mn and Mg for ilmenite. These oxide populations are illustrated on a ternary plot of minor oxides (Fig. 3.17). Also of note are the opague dendrites identified in a Type IB feldspar (Plate 3.11). As mentioned previously these opagues are not resolvable in reflected light or even backscatter making their identification difficult, not to mention their actual size.

3.2.8 Accessory Phases

Accessory phases observed in pumice samples include apatite, titanite and pyrrhotite. All are rare phases with apatite and pyrrhotite normally occurring as inclusions in various silicate minerals. Several acicular apatite crystals are identified in backscatter images, but are

Table 3.8: Representative EMP analysis of Fe-Ti Oxides. See Appendix A.7 for all data.

	Titanomagnetite				Ilmenite		Titanite
	026-002	030-001	031-007	037-006	025-008	040-006	044-002
SiO_2	0.044	0.047	0.038	0.041	0.026	0.016	29.841
TiO_2	17.339	18.217	17.594	18.322	49.35	46.592	35.345
Al_2O_3	6.742	7.018	5.74	7.367	0.657	0.382	0.984
FeO_T	66.583	65.937	68.37	65.1	42.645	46.494	2.259
Cr_2O_3	0.646	0.029	0.035	0.017	0	0	0
MnO	0.469	0.448	0.542	0.421	0.586	1.356	0.145
MgO	7.224	7.486	6.628	7.91	7.379	4.917	0.023
NiO	0.031	0.024	0	0	0.015	0.004	0.021
CaO	0	0	0	0.005	0.033	0.378	27.473
Total	99.08	99.21	98.95	99.18	100.69	100.14	96.09
Si	0.002	0.002	0.001	0.002	0.001	0	4.085
Al	0.3	0.31	0.259	0.323	0.019	0.011	0.159
Ti	0.493	0.514	0.508	0.514	0.908	0.887	3.64
Fe*	2.107	2.068	2.194	2.03	0.872	0.984	0.259
Cr	0.019	0.001	0.001	0.001	0	0	0
Mn	0.015	0.014	0.018	0.013	0.012	0.029	0.017
Mg	0.407	0.419	0.379	0.44	0.269	0.185	0.005
Ni	0	0	0	0	0	0	0
Ca	0	0	0	0	0.001	0.01	4.03

Ions calculated based on 4, 3 and 20 oxygens for Titanomagnetite, Ilmenite and Titanite, respectively.

not resolvable under normal optical conditions. Only a few of pale-yellow brown titanite crystals are observed, all hosted in felsic glass. Titanite occurs as euhedral wedges (Plate 3.28) in felsic glass streaks from banded pumice sample (CS-010) and is intergrown with aegirine-augite in felsic pumice (TK-9D). None are identified in mafic pumice samples.

3.3 Discussion

Based on the mineral chemistry, zoning, textures and hosts it is possible to place all minerals observed from these pumice samples into three mineral assemblages (Table 3.9). Assemblage one contains crystals of calcic plagioclase (Type IB & Type III), titanaugite, high Mg-titanomagnetite and high Mg ilmenite, representing the basic melt, probably an alkali basalt. Assemblage two is an intermediate group with a crystal population of sodic plagioclase (Type IA & Type II), salite, medium Mg-titanomagnetite, medium ilmenite, kaersutite and possible biotite. Assemblage three has crystals of alkali feldspar (Type IC, Type IIA & Type III), nepheline, sodalite, aegirine-augite, low Mg-titanomagneite, titanite and possibly biotite, originating from a phonolitic host. Each of the three assemblages have a distinct feldspar, Fe-Ti oxide, and pyroxene population, as seen by major and/or minor oxides (Fig. 3.18). Further, the chemical composition of these mineral assemblages indicates the basic to acidic transition from assemblage one to assemblage three. Assemblage three pyroxene is identified in felsic pumice (TK-9D), but is not analyzed. Assemblage three ilmenite is missing, but is probably replaced by titanite, which is associated with the felsic (phonolite) glass host.

The alkali mafic magma that injected the intermediate magma has a complex history prior to injection. This is evident from the dusty cored pyroxenes identified above. Several workers (Brooks and Printzlau 1978) suggest that such pyroxenes result from rapid changes in the compositions of the precipitating magma (ie magma mixing). Line traverse, LT050, done

Plate 3.28: NDIC microphotograph of wedge-shaped titanite crystal. Hosted in felsic glass from mixed pumice (CS-010).

Plate 3.29: Transmitted light (PPL) microphotograph of feldspar crystal that is disrupting host melt, thereby breaking melt into smaller portions. Contacts between melts where there are disrupted by phenocrysts are not as sharp, but more diffuse.

Plate 3.28

Plate 3.29

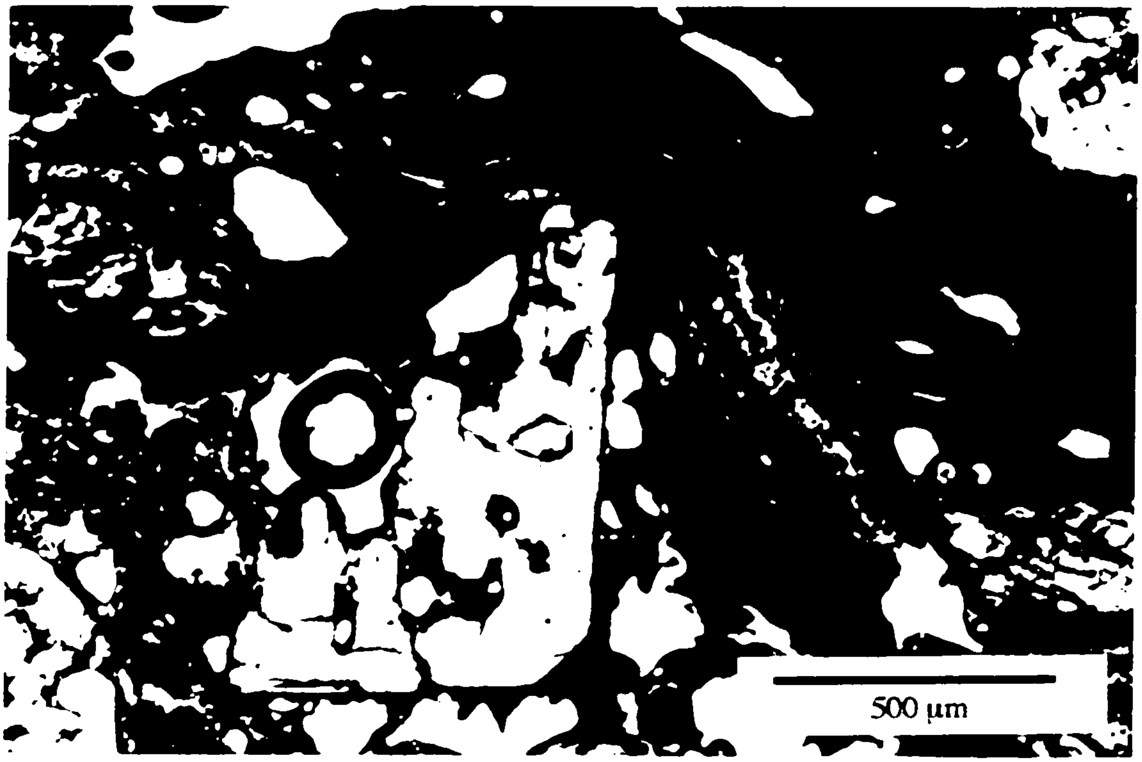

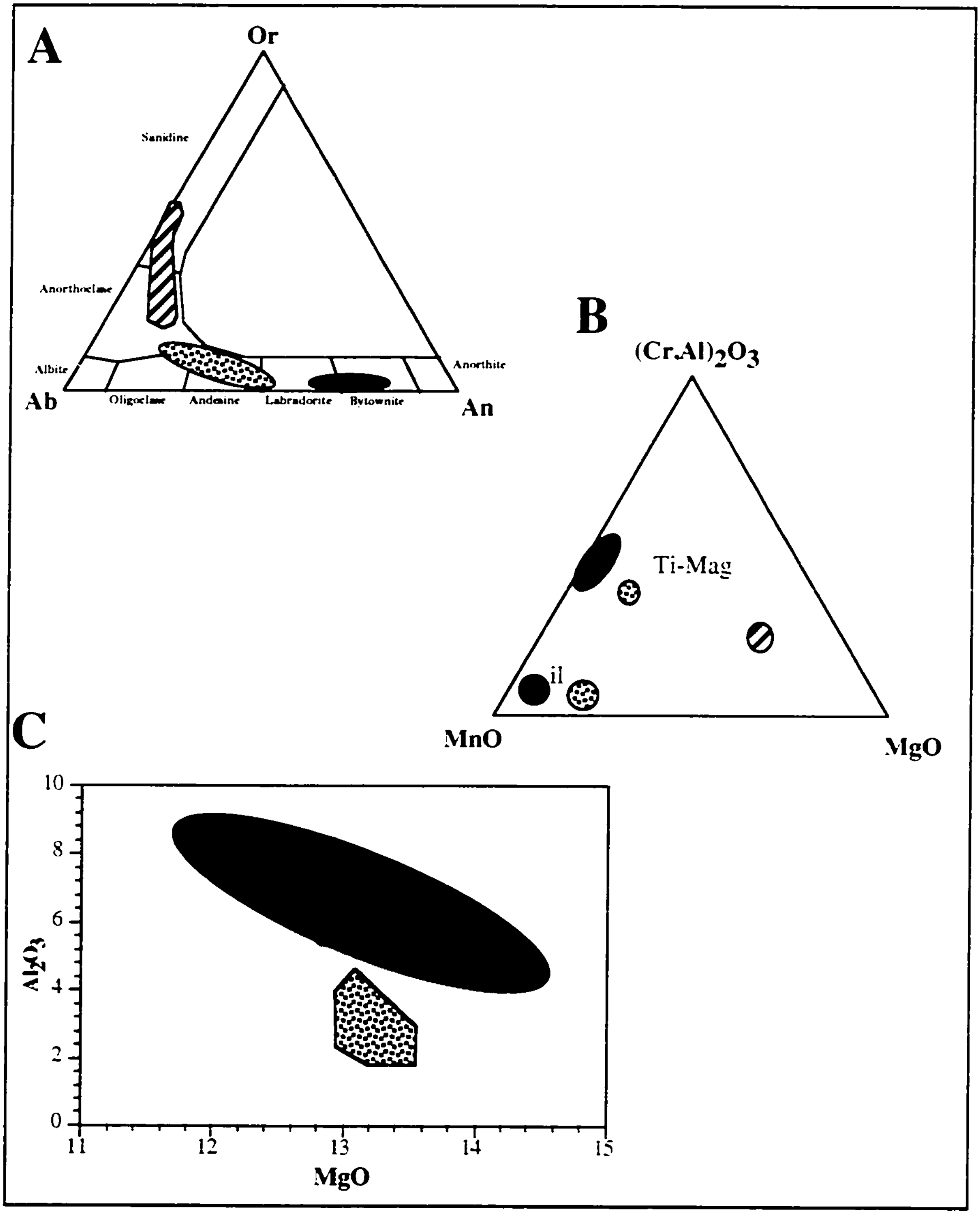

Figure 3.18: Three seperate figures demonstrating the three mineral assemablages based on major and minor oxides. Dark shaded area is assemblage one; stippled area is assemblage two; and stripped area is assemblage three. (A) Feldspar assemblages. (B) Fe-Ti oxide assemblages: ilmenite (il) & Ti-magnetite (Ti-Mag). (C) Pyroxene assemblages.

Table 3.9: Mineral Assemblages from Diego Hernández Wall.

Assemblage # 1	Assemblage # 2	Assemblage # 3
Calcic plagioclase Titanaugite High-Mg Titanomagnetite High-Mg Ilmenite	Sodic plagioclase Salite Medium-Mg Titanomagnetite Medium-Mg Ilmenite Kaersutite	Alkali feldspar Nepheline Sodalite Aegirine-augite Low-Mg Titanomagnetite Titanite Biotite

on such a phenocryst reveals a core region that is enriched in Na as compared to all other examples (maximum Na_2O of 1.42 wt %) and a mantle that fits with assemblage three titanaugites. This may indicate that the alkali mafic magma may have had a previous mixing event with a more evolved melt. However there is no other observed evidence to support this.

From detailed petrographic observations and chemical compositions, a model for feldspar generation during the first stage in the development of Diego Hernández Formation can be theorized.

Type IA feldspars, being the largest feldspar type, probably originate from a magma that resided the longest in the sub-volcanic chamber. The possibility that these feldspars are pre-existing, entrained crystals from the source region can be ruled out since Type IA feldspars are thought to result from initial skeletal growth, plus there is no compositional gap recognized from core to mantle that would represent a change from basic melt to an intermediate melt. On emplacement in the sub-volcanic environment the host magma endures undercooling from a combination of decreased temperature and pressure, forming skeletal plagioclase feldspars

(Fig. 3.19A). An intermediate composition (eg. trachyandesite) is assumed for the host for Type IA feldspars based on their predominantly andesine composition (Fig. 3.7) and glass compositions of trachyandesite to trachyte on total alkali-silica diagram (Fig. 3.4).

Crystal differentiation of the intermediate host results in an evolved melt phase. This evolve magma segregates from its parent melt due to a density contrast forming a capping layer of phonolite. Crystallization from the phonolitic magma forms euhedral Type IIA alkali feldspars during this stage (Fig. 3.19B). Also during this stage a basic magma is injected into the base of the intermediate magma. On route from its source region to injection into the sub-volcanic chamber, the basic melt undergoes rapid decompression. Such rapid decompression results in the lowering of the plagioclase liquidus (Nelson and Montana 1992), and entrained phenocrysts of An-rich plagioclase, Type IB, will resorb (Fig. 3.19B). Type IA feldspars experience weak to moderate resorption due to a slight increase in temperature from the influence of the injected basic magma. This is followed by renewed crystallization, under near-equilibrium conditions, within the intermediate melt forming euhedral mantles on resorbed, skeletal feldspars (Type IA) and new euhedral feldspars of Type IIA and IIB (Fig. 3.19B).

Before chemical mixing can proceed the intermediate and basic magmas must reach thermal equilibrium (τ_T). During this stage basic magma is undercooled (Fig. 3.19) such that Type III, An-rich skeletal plagioclase feldspars crystallize (Fig. 3.19C). Upon reaching thermal equilibrium (t_1 - Fig. 3.20) the intermediate and basic magmas begin to chemically mix. At time (t_2) a hybrid is formed between the intermediate and basic magmas (Fig. 3.20) that appears to be dominated by the intermediate end-member due to the lack of basic glass analysis, whereas the phonolitic end-member remains segregated from this underlying hybrid melt. However,

Figure 3.19:

A: Initial injection or filling of the sub-volcanic magma chamber beneath the Las Cañadas Edifice. The original magma was probably an intermediate magma such as a trachyandesite. Initial undercooling of this intermediate magma resulted in andesine skeletal feldspar crystals (Type IA). Grey represents initially homogenous magma.

B: Differentiation of intermediate magma leads to formation of phonolitic magma (clear layer). Due to density contrasts this magma forms a capping layer and is effectively isolated from underlying intermediate magma. Below the phonolite is a homogenous intermediate magma (stipple). Injection of mafic magma phase (black pattern) into the base of volcanic chamber occurs at this stage. The initial onset of mixing between the mafic and intermediate melts cause an increase in temperature in latter melt. This temperature increase causes weak to moderate resorption of Type IA skeletal feldspar crystal. As more steady state conditions are reached growth is renewed on Type IA, forming euhedral mantles of near-equilibrium feldspar. Euhedral Type IIA alkali and plagioclase feldspars begin to nucleate at this time in the phonolite and intermediate magmas, respectively. Euhedral Type IIB feldspars also begin crystallizing at this time. Mafic magma is rapid decompressed as it is injected into the sub-volcanic environment. This results in its entrained An-rich plagioclase crystals to be resorbed as the decrease in pressure lowers the plagioclase liquidus (Nelson and Montana 1992).

C: Exsolution of volatiles in injected magma results in overturn and convection. This mixes the intermediate and mafic magmas after thermal equilibrium. During this time the phonolitic magma is still segregated from the other magmas due to the density barrier. However, there is some exchange with a few alkali feldspar finding their way into the intermediate mixture. This results in simple dissolution forming Type IC feldspars. Rapid cooling of the mafic magma leads to nucleation and rapid growth forming skeletal Type III feldspars. Type III feldspars reside in the intermediate mixture for a short time, but long enough to have a thin overgrowth of a more equilibrium (sodic) composition. Type IB feldspars also experience renewed growth with a thin overgrowth that is in equilibrium with a more intermediate magma. No mafic magma has been identified in any EMP analyses. This may be due to the small size of the injection or the small size of segregated pockets.

D: Eruption stage. Continued vesiculation due to the injection of a mafic magma into the intermediate magma leads to the eruption. Some possible causes of the eruption are convective overturn and overpressure due to volume increase. Supercooling of the phonolitic member during the eruption forms swallow-tail growth forms on microphenocrysts, identified as Type III sanidines.

Fig 3.19: Feldspar Generation Model

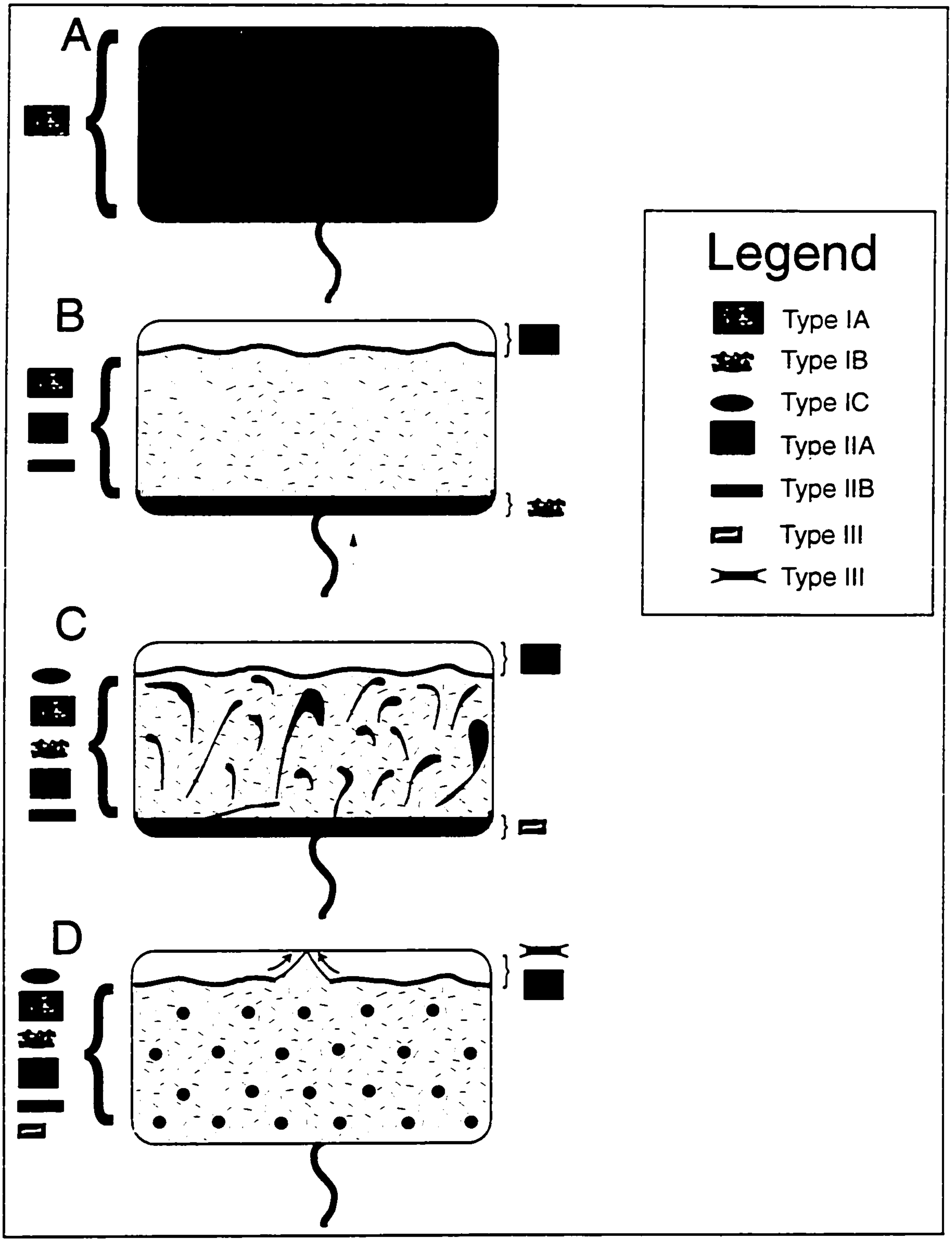

there is evidence of very limited interaction, with Type IC alkali feldspars hosted by a thin veneer of felsic glass in an intermediate to mafic magma (Plate 3.17). These small blebs of phonolitic material are envisioned to exist close to the boundary layer (Fig. 3.19C) between the hybrid and phonolite magmas where the temperature influence of the underlying hybrid is enough to induce simple dissolution.

Between the hybridization (t_2) and eruption stages (t_3) (Fig. 3.20), Type IB and Type III plagioclase feldspars, both originating from the basic magma, undergo near-equilibrium growth from the intermediate melt, resulting in thin, sodic-rich overgrowths (eg. Fig. 3.10). During the eruptive event (t_3) the phonolitic melt is undercooled causing dendritic growth on pre-exisiting feldspar microphenocrysts forming Type III swallow-tailed feldspars (Fig. 3.19D). As the eruption proceeds the hybrid magma is drawn up with the phonolitic magma to physically mingle in the volcanic conduit on route to the surface. The end result is streaky intermingled magma that is disrupted at the surface forming abundant pumice as the roof over the magma chamber collapses (Fig. 3.19D).

Unfortunately EMP analyses did not allow for the determination of the possible host for assemblage one, as shown from the total alkali silica diagram (Fig. 3.4). Two possibilities exist for the absence of the basic component: (1) complete homogenization on mixing with intermediate magma; or (2) the basic magma was not tapped during the eruption.

From experimental work and observations on natural samples Kouchi and Sunagawa (1985) concluded that complete homogenization of mafic and felsic end-members requires a large mafic:felsic ratio. When ratios are small, mixing is normally incomplete resulting in a banded texture. From their experimental work on the mixing of basalt and dacite, Kouchi and Sunagawa (1985) noted that basalt was readily transformed to an andesite, whereas the dacite barely changed. This indicates at least a 5 % increase in SiO_2 for a basalt to andesite

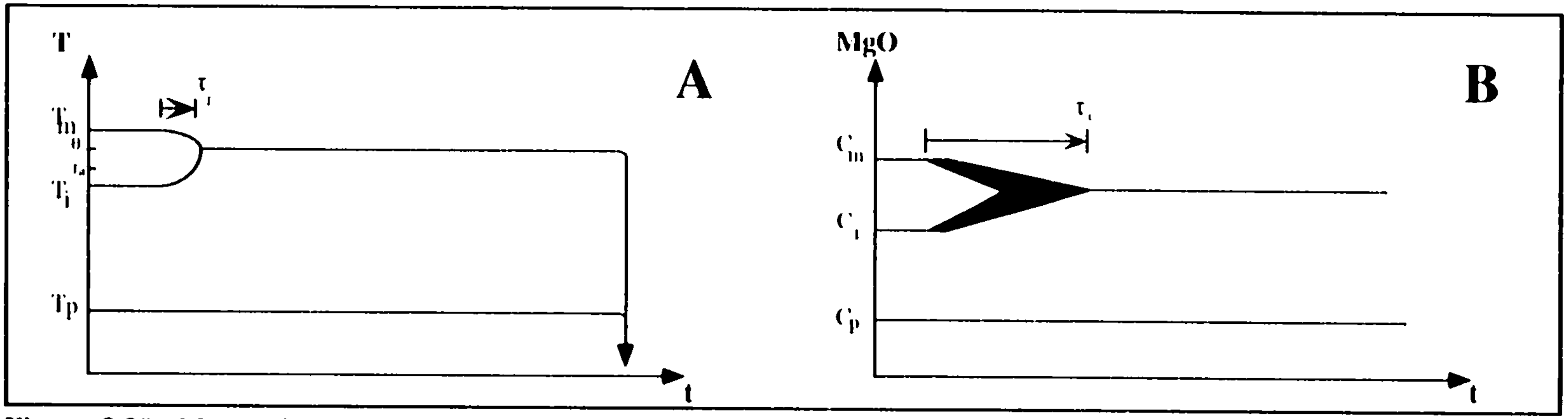

Figure 3.20.: Magmatic system of Diego Hernandez as a function of temperature (T) and composition (MgO) during magma mixing as a function of time (t). (A) Temperature diagram showing mafic and intermediate magmas thermal equilibriating (τ_T), then this hybrid erupting simultaneously with phonolitic magma. (B) Composition diagram where mafic and intermediate magmas reach compositional equilibrium (τ_c) and form a hybrid. Phonolitic magma retains it composition. T_m, T_i and T_p are original temperatures of mafic, intermediate and phonolitic magmas, respectively, wheres C_m, C_i and C_p are original compositions of mafic, intermediate and phonolitic magmas, respectively. Other symbols same as figure 2.4. (After Blake & Koyaguichi 1991).

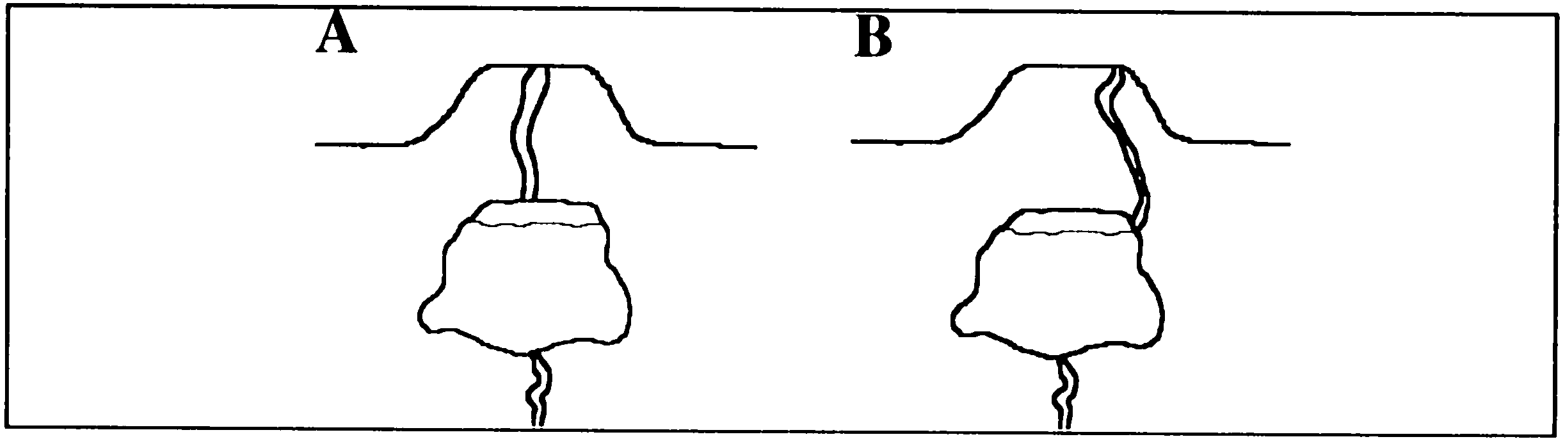

Figure 3.21.: Simplified sketches of two possible volcanic conduits exiting magma chamber beneath Diego Hernandez that lead to physically mixed pumice. (A) Conduit is located directly over phonolitic melt. (B) Conduit is situated closer to actual boundary of phonolite and hybrid magma.

compositional change. Applying the concept of basalt to andesite change from Kouchi and Sunagawa (1985) to EMP glass analyses from Diego Hernández, then the alkali basalt (assemblage one) changes anywhere from 10 wt % (SiO_2 of 46 wt %) to just 4 wt % (SiO_2 of 52 wt %), depending on the original SiO_2 of alkali basalt (46 wt % and 52 wt % SiO_2 being the approximate lower and upper limits of basalt). So it is quite feasible that the injected alkali basalt completed mixed with the intermediate melt to form a hybrid liquid. The wide spread in mafic glass analyses over the whole range of trachyandesite compositions (Fig. 3.4) along with the trends on Harker diagrams (Fig. 3.5) indicate a possible mixing origin. Another argument for possible mixing is by taking feldspar crystal populations as an indicator of melt composition. Near-equilibrium feldspar from the intermediate melt was roughly An_{40}, whereas the basic melt had a near-equilibrium composition of roughly An_{62}. Plagioclase composition of An_{40} is taken from Type IA and An_{62} is taken from relic plagioclase fragments not melted to form the more calcic plagioclase of An_{78}. This interpretation hinges on the assumption that the dissolution/reprecipitation mechanism of Johannes et al. (1993) is correct.

The other possibility is that alkali basalt was not tapped during the eruption. Other workers have noted that the least evolved magma will only be tapped or erupted from large eruptions from small chambers. It has been documented that a mafic mineral can infiltrate a more intermediate magma with no evidence of its basaltic host (Hildreth 1981). This mechanism does not seem viable with the amount of "basic" phenocrysts observed throughout sections.

The phonolitic magma did not interact with this hybrid magma to any large extent because it was separated from this lower intermediate melt by a boundary layer. There is evidence of limited interaction in the form of rounded alkali feldspars (Type IC). These feldspars probably became trapped along the boundary front and experienced some heating effects from the hotter intermediate magma below. The time frame for this heating event probable occurs from the time the capping layer formed and the alkali feldspars formed. Otherwise there is no evidence of mixing between these two units. This boundary layer may be explained by phenocryst content. In comparing felsic and mafic pumice there is an obvious discrepancy in the total crystal content. Felsic pumice (TK-9D) is aphyric with only a handful of observed crystals. In mafic pumice (TK-9C & CS-010A) samples, crystals make up 20% of total volume, while crystals in banded pumice (CS-010) make up 20% of total volume with felsic bands accounting for about 5-8% and mafic bands 12-15%. Thus, the Diego Hernández magma chamber has a downward increase in total crystal content. Some workers envisage a crystal mush boundary zone closing in from all sides during crystallization (Marsh 1989; Marsh 1996) within the magma chamber. Why then are the phonolitic magmas aphyric? Hildreth (1981) explains this aphyric nature in roof melts through the use of gradients within the magma chamber. The downward increase in crystallization is explained by the roofward depression of mineral liquidi due to the upward enrichment of dissolved volatiles. Another possible explaination is simply due to injection of 'hot' mafic magma that maintains the temperature of the magma chamber at temperatures just above crystallization for the phonolitic magma.

This rapid transition from an aphyric magma (TK-9D) to crystal-rich magma (CS-010, CS-010A & TK-9C) indicates the possible existence of a volatile-rich boundary layer (Hildreth 1981). This boundary layer may have effectively separated the felsic capping layer from the more intermediate magma below. Alternatively, the boundary layer simply reflects a density difference between the two magmas.

Sharp continuous contacts and very little to no diffusional profiles between the underlying hybrid and capping phonolitic glass mean that physical mixing was a late stage event. This physical mixing is envisioned as part of the final stage in the development of the Diego Hernández system, the actual eruption, where the underlying hybrid and the overlying phonolitic capping layer mechanically mixed. This interaction resulted in the observed intermingling of the hybrid and phonolite in banded pumice (CS-010A). The mingling is envisioned to have occurred within the volcanic feeder were the magmas are simultaneously withdrawn. Various workers (Blake and Campbell 1986; Blake and Ivey 1986; Freundt and Tait 1986; Koyaguchi 1985) have done experimental work on magma mingling within a conduit during the eruptive event, looking at viscous fingering of various fluids. Blake and Ivey (1986) studied the problem from the point of view of a draw up mechanism where the denser, underlying magma is drawn up through the overlying magma. If the conduit is not located direct above the phonolitic melt, but close to the actual boundary between melts, then chances are greater for both magmas to be withdrawn simultaneously (Fig. 3.21). Blake and Campbell (1986) conducted experiments on simultaneous withdrawal with a high viscosity fluid encasing a low viscosity fluid. By varying the flow rate of the central, low viscosity fluid they were able to get various degrees of flow behaviour. As the flow rate increases the central fluid segregates into streaks that become entrained in the moreviscous fluid. Of note is that these low viscosity streaks are aligned parallel to pipe walls that indicate that mixing is occurring due to shearing forces rather than by turbulent eddies.

Another mechanism may operate to stir the contrasting magmas once they enter the conduit, particularly the silicic magmas which tend to flow laminarly even under high eruptive rates (Wilson et al. 1980). Phenocrysts can serve as stirring rods, mechanically breaking the host melt into smaller portions and creating swirls or streaks in the melt (Plate 3.29) (Kouchi and Sunagawa 1985). This behaviour is evident in banded pumice (CS-010) where large phenocrysts (≈ 1 mm) have disrupted the hybrid melt into thin bands dispersed in the phonolitic melt. When phenocrysts are not present bands are thicker and contacts sharp (sharp color change), whereas contacts are more diffuse looking when associated with phenocrysts. Phenocrysts also create flow-like patterns in the phonolitic melt.

4 El Abrigo Ignimbrite

4.1 Formation and History

The El Abrigo Ignimbrite is an extensive pyroclastic deposit covering most of the south coast of Tenerife, so named for the town of Los Abrigos located about 3 km from the southern airport of Reina Sofia (Fig. 1.1). This ignimbrite, along with the Granadilla Ignimbrite and Pumice, are the only two identified flows to extend across the south coast of Tenerife (Fig. 4.1). As discussed in the preceding chapter, the El Abrigo Ignimbrite is thought to be the distal equivalent to the co-lag breccia found at the top the Diego Hernández wall (Martí and Mitijavila 1995). Examination of Table 1.1 shows an apparent age discrepancy for the correlation of the upper section of the Diego Hernández (170 ± 8 ka) with the El Abrigo Ignimbrite (130 ± 20 ka). However, Marti et al (1994) have averaged the Diego Hernández to 179 ka and have new age data for the El Abrigo Ignimbrite of 179 ka (K/Ar, no errors cited) (Scott Bryan Per. Comm. 1996). Other evidence used for the correlation is based on their common stratigraphic position, similarity of composition of alkali feldspars and lithic fragments (Martí et al. 1994b; Martí et al. 1995).

The ignimbrite is described as a sheet-like deposit composed of numerous flow units , three of which are observed near Los Abrigos. The basal flow comprises a well developed flow body with reverse graded pumice fragments. The middle unit is discontinuous, occurring as isolated pumice dunes, or as a thin pumiceous flow unit, while the upper flow unit exemplifies the El Abrigo Ignimbrite as a lithic fragment rich flow (Plate 4.1) with reverse grading at several localities. Due to the high-concentration of lithic fragments many clast supported textures are observed. A prominent lithic clast is syenite, believed to originate from the caldera as mentioned in the previous chapter (Martí and Mitijavila 1995). The amount of

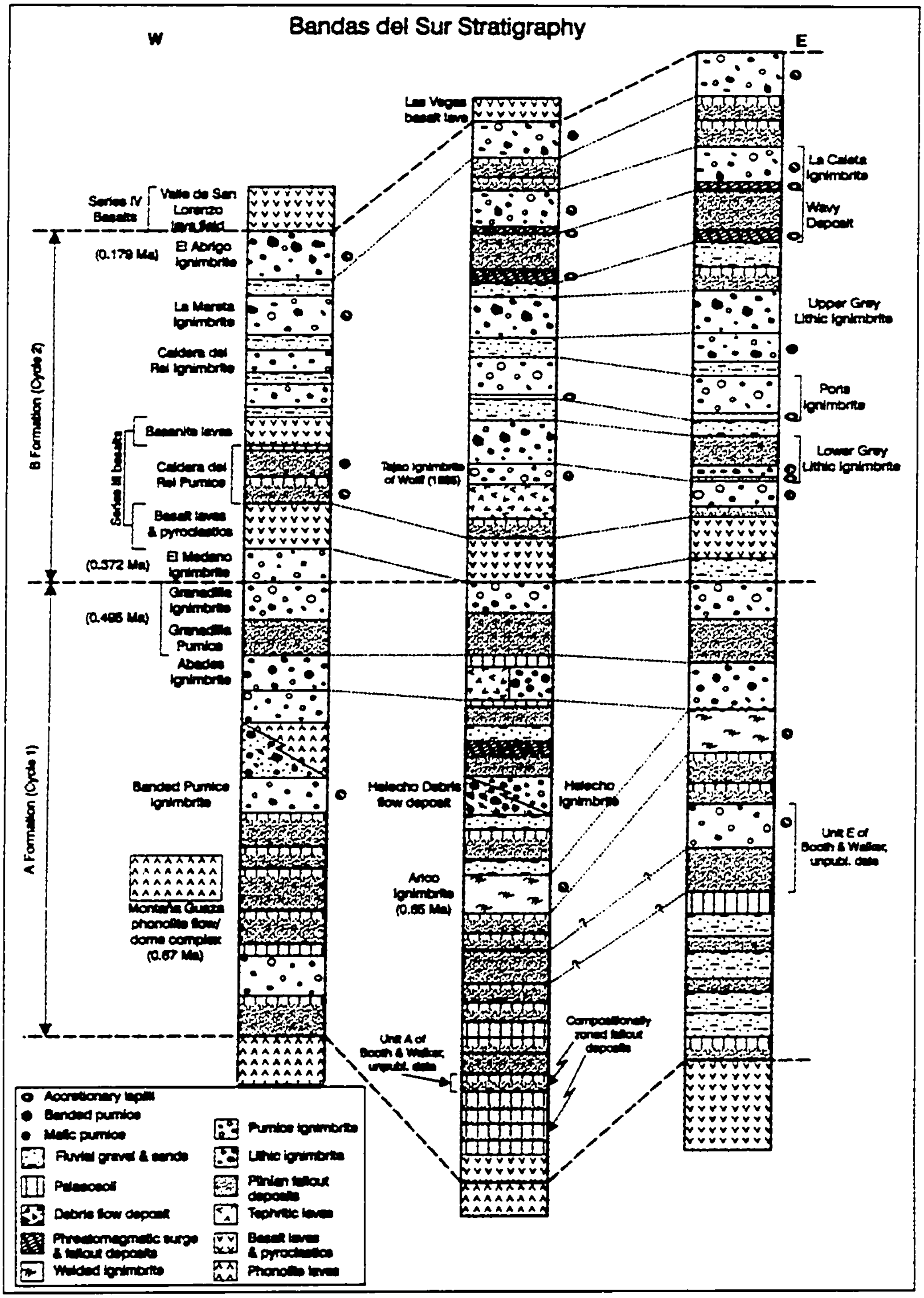

Figure 4.1: Stratigraphy of Bandas del Sur Showing some of the more extensive ignimbrite deposits, especially Granadilla and El Abrigo ignimbrites. From Bryan et al (submitted).

Plate 4.1: Lithic-rich portion of Ell Abrigo Ignimbrite. Numerous phases of lithic fragments present along with cm-sized banded pumice fragments. Field of view is ≈ 100 cm.

Plate 4.2: Banded pumice fragments from El Abrigo Ignimbrite. Pen is 14.5 cm long.

Plate 4.1

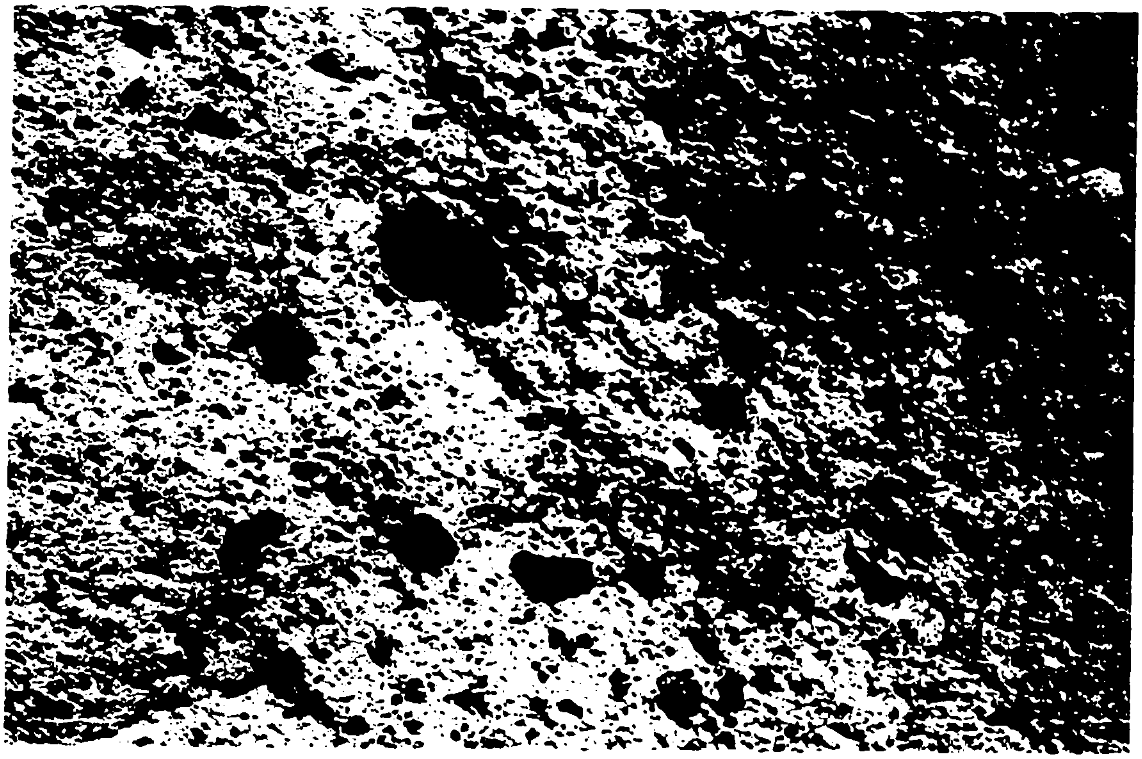

Plate 4.2

pyroclastic material within the El Abrigo Ignimbrite is estimated to be a minimum of 13 km^3 (dense rock equivalent; Martí et al. 1995). Another feature of this ignimbrite is the presence of banded pumice (Plate 4.2) having intricate mingling of green and black glasses, thought to correspond to contrasting magma compositions.

Samples were taken during two separate field seasons. A felsic pumice sample was collected in the Spring of 1994 by Drs. Tony Fowler and Karen St. Seymour while attending a field trip led by Dr. Joan Martí. Three banded pumice fragments and one green pumice were sampled by the author while attending the "*Workshop on Explosive Eruptions in Phonolitic Magmas*" in the Spring of 1995. Individual black pumice fragments are very rare and when observed are small and sunk into the flow matrix such that sampling is impossible. Both banded pumice samples are dominated by the green glass, with one having > 80 % of green glass component.

4.2 Petrography

As mentioned in the above section four samples were collected from the El Abrigo Ignimbrite (Fig. 3.3), three banded and one green pumice fragment. Black glass represents more mafic compositions while green glass is felsic, probably of phonolite composition. The felsic component of this eruption was dominant, with green glass being the principle component in banded pumice (> 80 % in some cases) whereas the black pumice is sparse (<15 %). Due to their friable nature all pumice samples had to be flooded with epoxy prior to thin section preparation. Banded pumice samples consist of samples CS-015A, CS-015B and CS-002, and the felsic pumice sample is TK-25B.

EMP analyses for the El Abrigo Ignimbrite are not as detailed as those of the Diego Hernández Formation. Analysis were only done on the major minerals (feldspar, pyroxene and amphibole) and glass. The main purpose of the work on El Abrigo is to document any variation between this ignimbrite and the lower ignimbrite of Diego Hernández through major minerals and glass compositions.

4.2.1 Glass

Analysis of glass from El Abrigo pumice was done on mafic and felsic glass, identified optically by color with shades of black to brown and pale green to clear with increasing silica content. The intention is to quantify each member and to ascertain whether diffusion occurred between mingled glasses from banded pumice samples. The terms mafic and felsic are used in a similar fashion to the previous chapter, where mafic describes Si-poor glass in comparison to felsic, or Si-rich glass, and does not imply any precise chemical composition. Consistent with Diego Hernández, EMP analysis confirmed that basing mafic and felsic glass on color variation was a correction assumption (Table 4.1). In banded pumice, mafic and felsic glasses are intermingled forming continuous and discontinuous streaks of brown and pale green glass (Plate 4.3). Contacts between pale green and brown glass are extremely sharp, however the mafic glass commonly has a color variation from light brown all the way to dark brown/black. Mafic glass has a large population of microlites, but unlike Diego Hernández mafic glass, it is possible to analyze microlitic-free glass.

Glass data from El Abrigo form an array on total alkali-silica (TAS) diagram increasing steadily in silica with a corresponding increase in Na and K oxides (Fig. 4.2), ranging from basaltic trachyandesite through trachyandesite to trachyte.

Harker variation diagrams for glass data illustrate the difference between mafic and felsic glass. Trends shown between mafic and felsic glass for Mg, Ti, Ca and Fe oxides, all having negative slopes, indicating a possible mixing or fractionation trend (Fig. 4.3). Oxides

Plate 4.3A: Transmitted light microphotograph in plane polarized of discontinuous black (mafic) glass streak surrounded by pale green (felsic) glass.

Plate 4.3B: NDIC microphotograph showing sharp contact between mafic (recrystallized) glass and homogeneous felsic glass.

Plate 4.3A

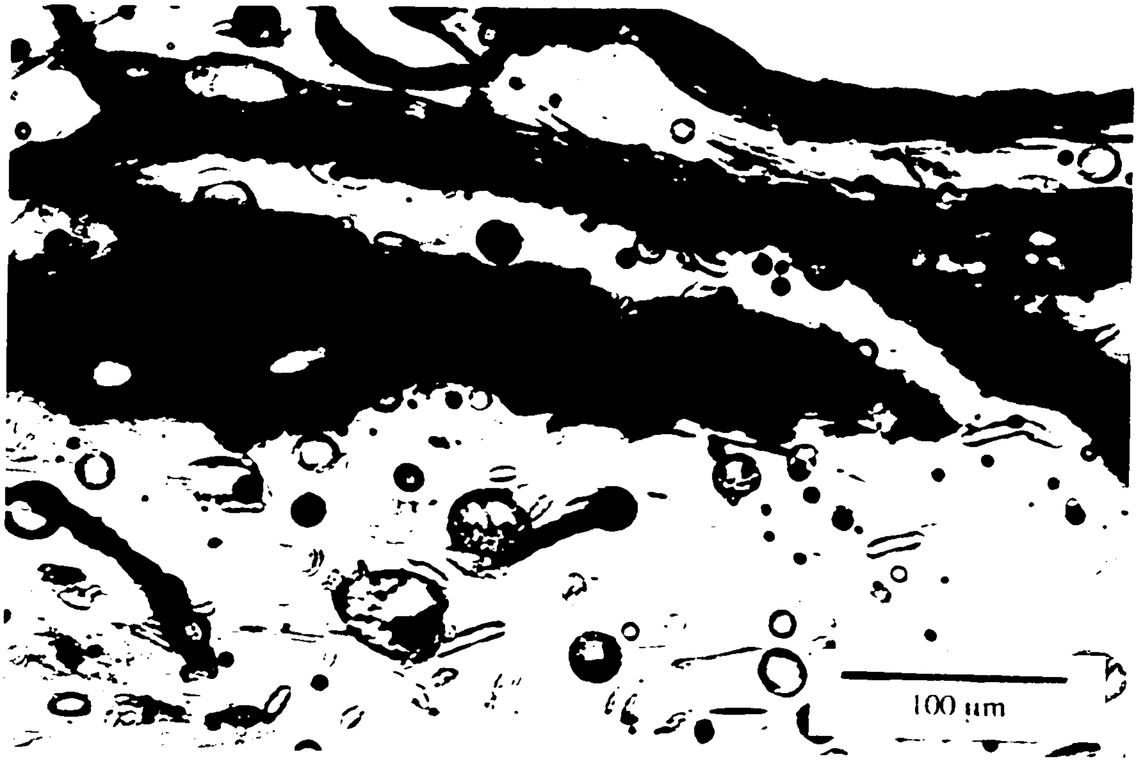

Plate 4.3B

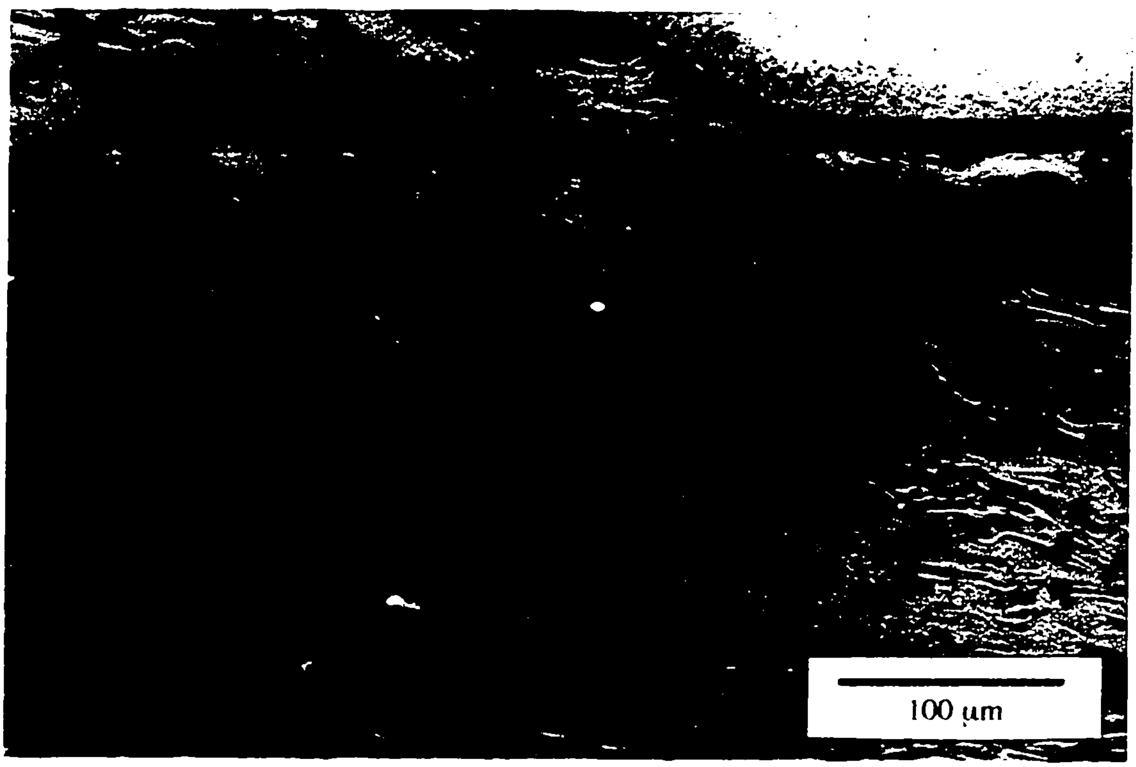

Table 4.1: Representative EMP analysis of glass. See appendix B.1 for complete data.

	Felsic Glass						
	G027-012	G032-001	G032-005	G034-006	G037-002	G049-012	G050-038
SiO_2	8.039	7.233	7.441	8.129	9.309	6.549	6.718
TiO_2	18.998	17.88	18.401	18.382	19.078	19.955	19.654
Al_2O_3	60.477	58.196	61.541	60.369	59.172	60.433	61.039
MnO	0.404	1.135	0.674	0.439	0.331	0.412	0.378
MgO	0.763	1.208	0.885	0.759	0.651	0.741	0.703
FeO	5.576	4.426	5.018	5.155	5.541	5.845	5.722
CaO	1.565	2.755	1.543	0.787	0.753	0.801	0.708
Na_2O	2.648	4.03	2.966	2.788	3.065	2.917	2.876
K_2O	0.14	0.195	0.127	0.169	0.235	0.217	0.262
Total	98.61	97.058	98.596	96.977	98.135	97.87	98.06

Table 4.1: Con't

	Mafic Glass						
	G027-003	G028-002	G029-016	G031-002	G033-002	G035-001	G035-006
SiO_2	7.814	6.594	7.063	5.617	6.351	6.403	6.77
TiO_2	18.742	18.067	18.213	16.567	16.791	16.873	17.436
Al_2O_3	55.314	52.451	53.396	50.206	52.999	50.89	52.657
MnO	1.297	1.598	1.643	2.882	2.395	2.7	2.296
MgO	1.413	2.149	1.844	2.991	2.341	2.424	2.283
FeO	4.683	4.496	4.138	4.276	2.943	2.136	3.563
CaO	3.632	4.684	5.369	5.79	5.206	5.801	5.598
Na_2O	4.545	5.964	5.027	8.941	7.121	8.116	6.735
K_2O	0.198	0.243	0.184	0.279	0.192	0.244	0.243
Total	97.638	96.246	96.877	97.549	96.339	95.587	97.581

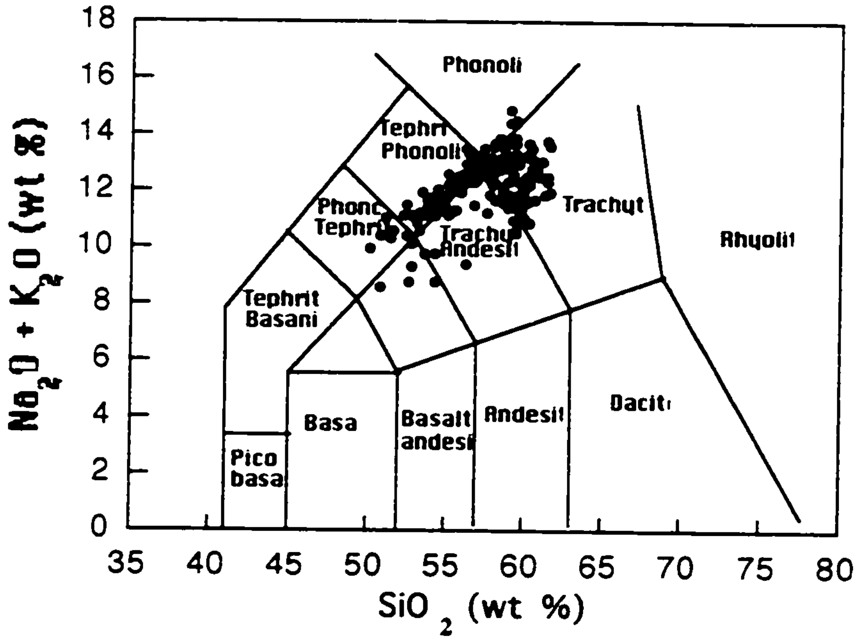

Figure 4.2: Total alkali-silica diagram for all glass from El Abrigo Ignimbrite. Glass is normalized.

of Na, K and Al are more widely scattered, particularly for felsic glass and especially felsic pumice (TK-25B). Felsic glass from felsic pumice is noticeably depleted in Na and enriched in Al oxides and has flat profiles for Mg, Ti, Ca and Fe oxides.

Several line traverses were done across contacts of mafic and felsic glass in order to determine the extent of interaction between the melts. It is hoped that such line traverses will reveal a diffusion profile defining probable liquid-liquid interaction before quenching. Two line traverses are plotted in figure 4.4 in order to test such interaction. Silica content is plotted to give a rough guide of mafic and felsic components, against the most diffuse oxides Na and K, to indicate possible diffusion. Line traverse LT057 was done across a mafic streak sandwiched by bands of felsic glass. From the profile, K follows silica content, whereas Na has a more flat profile across contacts (Fig. 4.4). This is interpreted as a possible diffusion profile, with Na

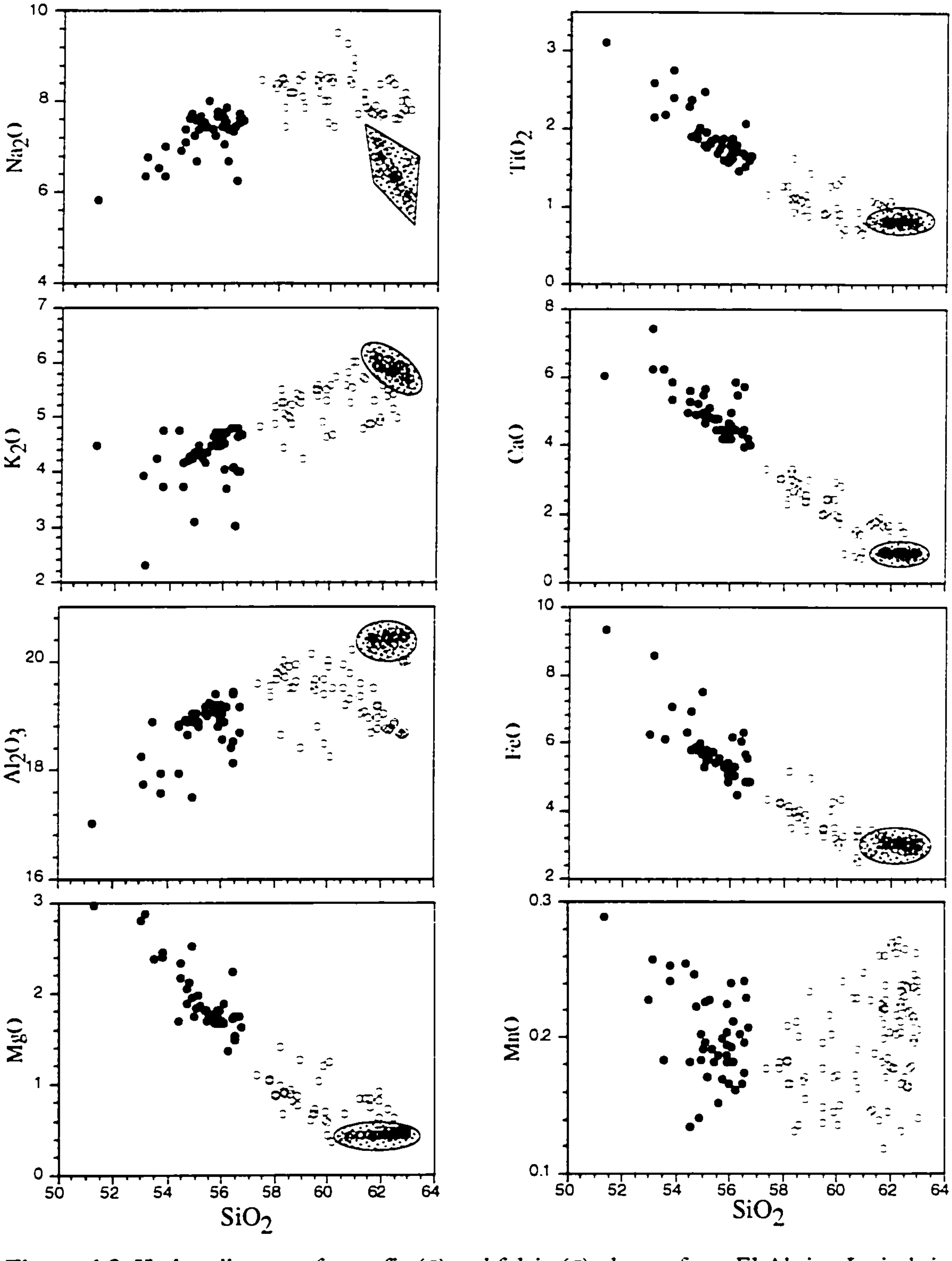

Figure 4.3: Harker diagrams for mafic (●) and felsic (○) glasses from El Abrigo Ignimbrite. Shaded regions are felsic glass from felsic pumice (TK-25B).

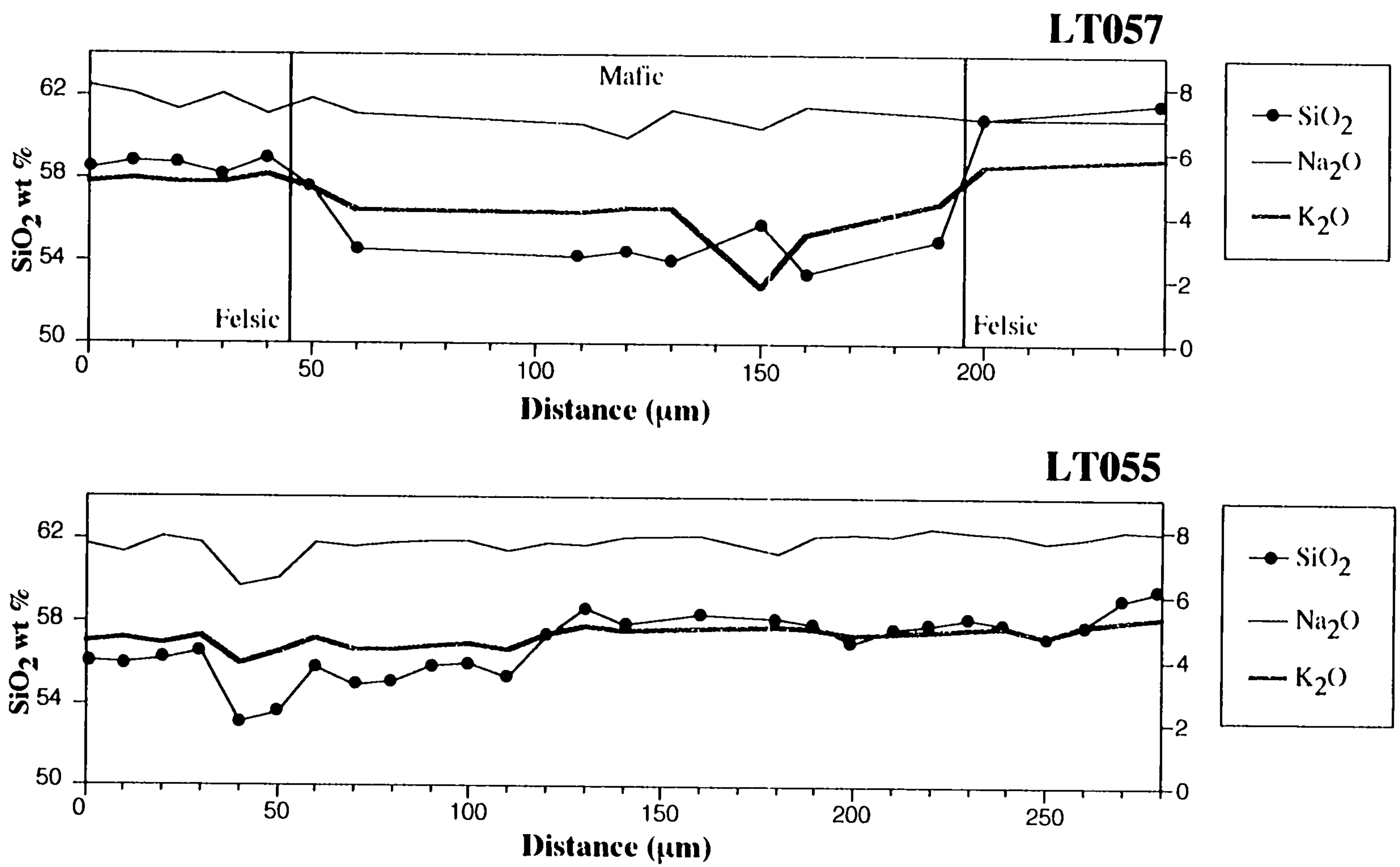

Figure 4.4: Glass line traverses from El Abrigo. Both LT057 & LT055 from banded pumice CS-002. (•) represent EMP points, gaps are points that are not plotted due to 'bad' totals. Mafic and felsic zones seen opitically indicated.

being slight homogenized across this mafic streak while K has been unaffected. The second line traverse (LT055) starts in a mafic glass and crosses into a felsic glass as indicated by the increase in silica at about 120 μm. Both K and Na oxides mimic a drop in silica at 40 μm, but overall both oxides have a slight decrease towards to the mafic/felsic contact (Fig. 4.4). This slight decrease is probably a diffusion profile of Na and K diffusing towards the mafic glass.

4.2.2 Feldspar

Overall the pumice samples examined are aphyric having a maximum of about 16 vol % phenocrysts identified in banded pumice (CS-015A) and a mere 4 vol % in felsic pumice (TK-25B). In both banded and felsic pumice, feldspar remains the dominant phenocryst, composing 95 % of the total phenocryst population. El Abrigo feldspars, like Diego Hernández, can be separated into three distinct types based on crystal morphology, chemical composition (Fig. 4.5) and zoning. The three divisions are the same used for Diego Hernández, with resorbed (Type I), non-resorbed (Type II) and skeletal/microlitic (Type III).

Feldspar - Type I

Type I resorbed feldspars are the most abundant feldspar type, comprising an estimated 6 vol % of the total phenocryst population. Optically these feldspars are recognized by rounded and embayed crystal forms, commonly associated with a resorption origin. Resorption is penetrative in many cases giving the crystal a sieve-like texture (Plate 4.4). Resorption style controls whether crystal facets are anhedral or subhedral. Morphology styles of resorption result from various mechanisms ranging from simple dissolution (Tsuchiyama 1985) to dissolution/reprecipitation (Johannes et al. 1993). From limited EMP analysis, compositions vary from calcic plagioclase (An_{75}) to alkali feldspar (Or_{21}) (Table 4.2).

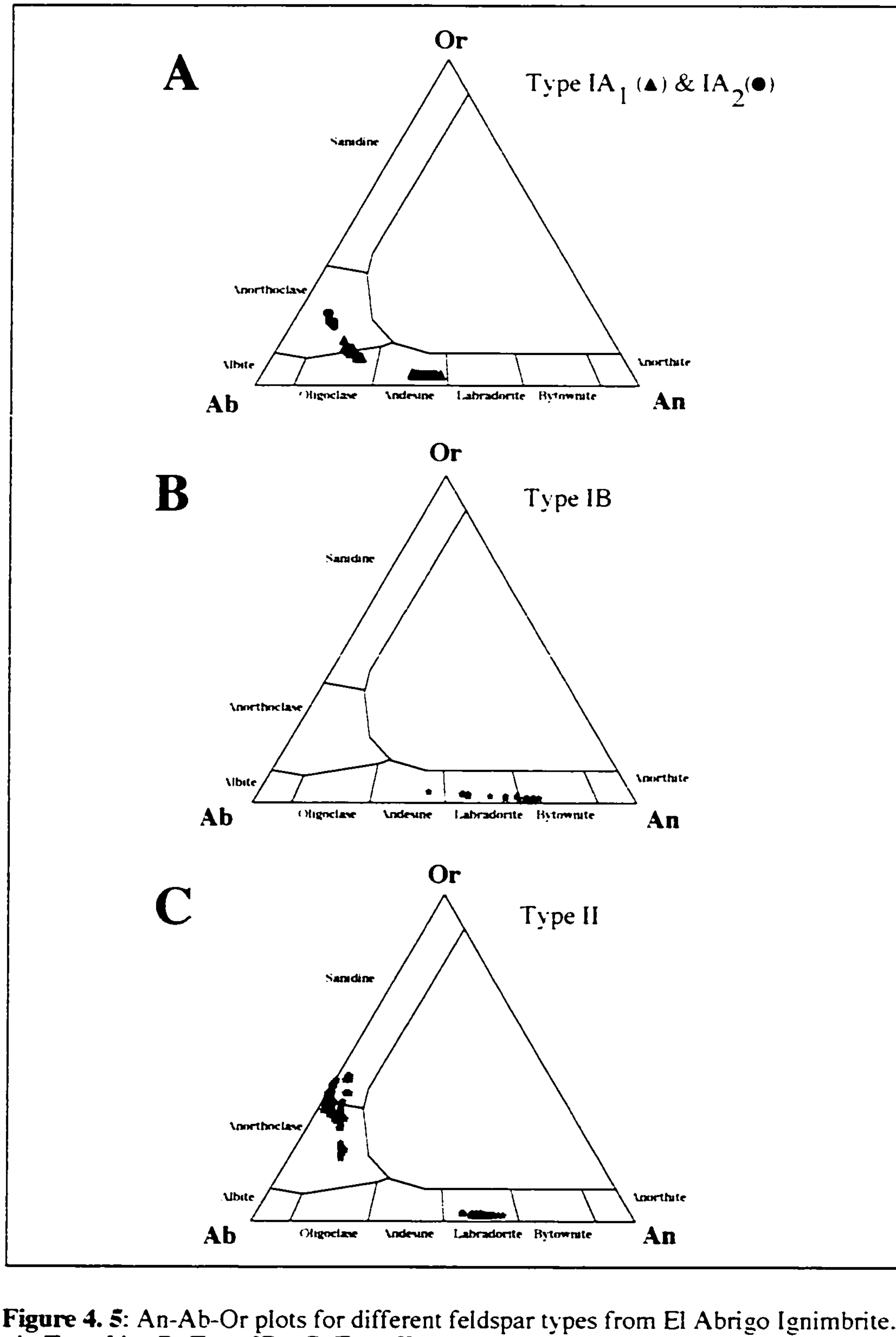

Figure 4. 5: An-Ab-Or plots for different feldspar types from El Abrigo Ignimbrite. (A) Type IA; (B) Type IB; (C) Type II.

Plate 4.4: NDIC microphotograph of three sieved feldspar phenocrysts hosted in black glass. Sieved texture is parallel to twin planes.

Plate 4.5: Transmitted light (X-Nicols) microphotograph of heavily resorbed feldspar phenocryst. Feldspar has enhanced cleavage pattern with large voids that extend from exterior of crystal surface to core.

Plate 4.4

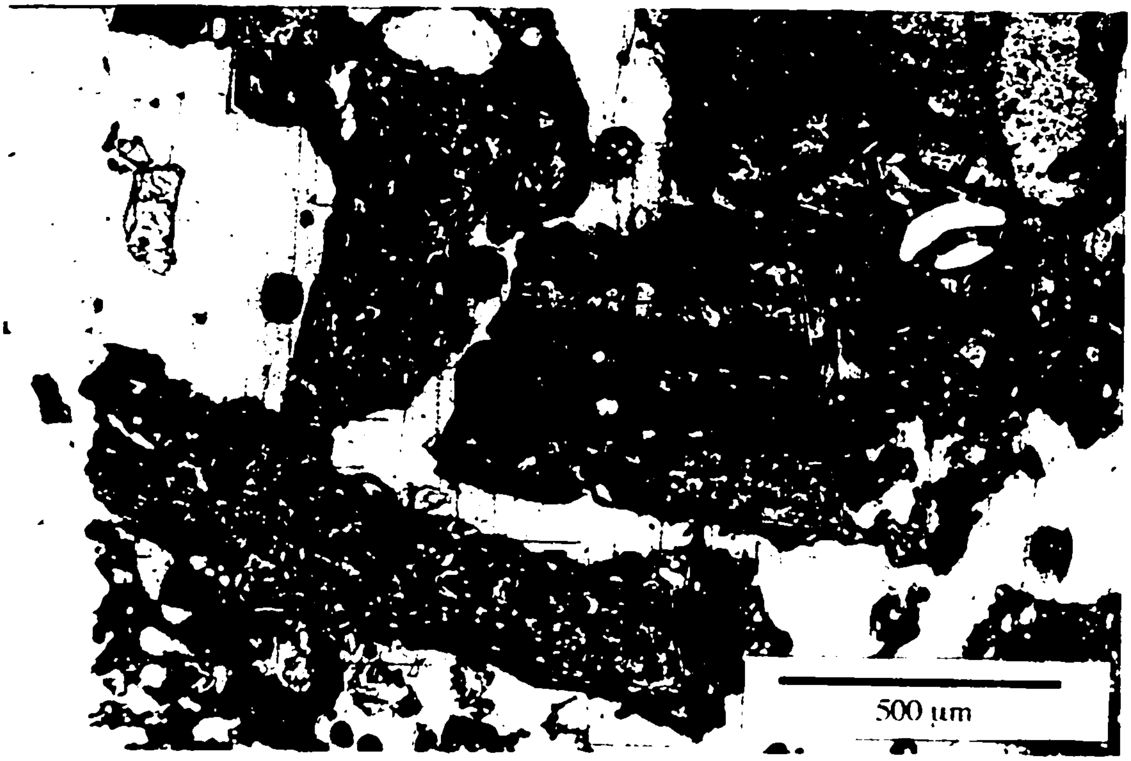

Plate 4.5

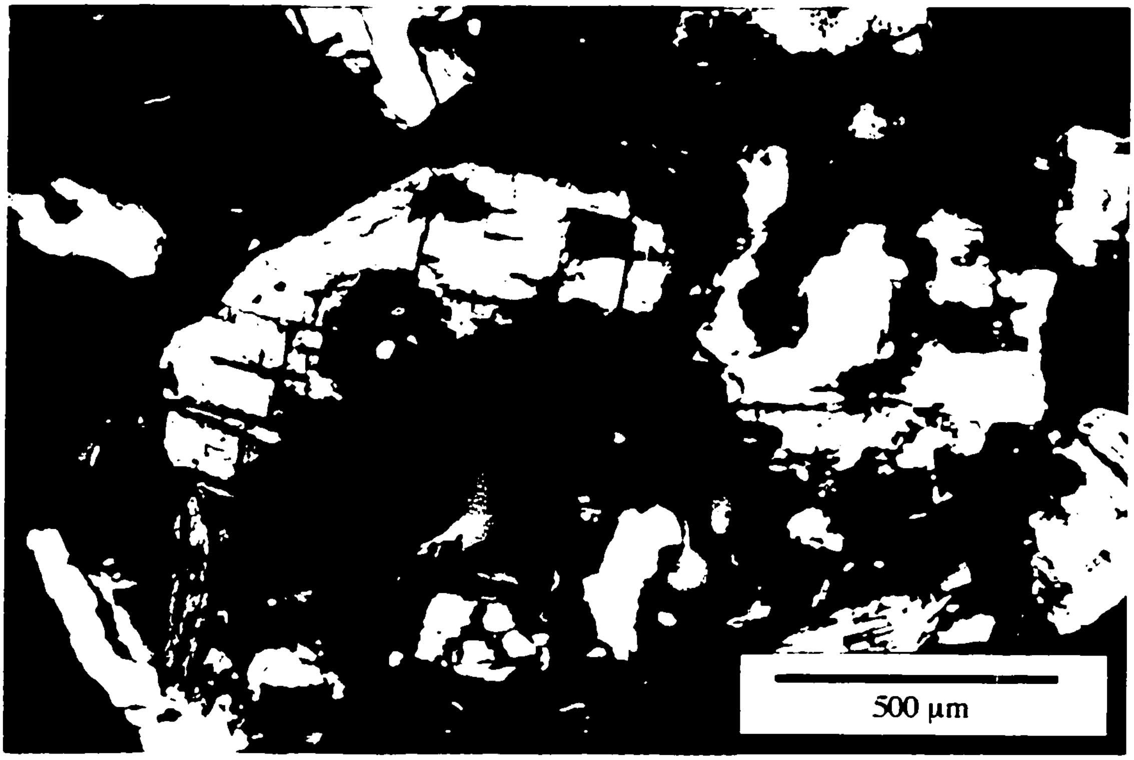

Table 4.2: Representative EMP analyses of feldspar from El Abrigo. See Appendix B.2 for complete data.

	Type IA$_1$				Type IA$_2$		Type IB			
	LT026.001	LT026.033	024.013	024.013	LT025.001	LT025.024	021.004	021.001	020.016	020.014
	core	rim	core	rim	core	rim	core	rim	core	overgrowth
SiO_2	56.981	56.033	61.846	61.846	64.674	64.312	49.909	50.517	49.706	55.601
Al_2O_3	27.155	26.712	23.18	23.18	20.788	20.859	31.299	30.393	30.259	26.146
FeO_t	0.492	0.567	0.412	0.412	0.309	0.356	0.606	0.511	0.576	0.614
MgO	0.045	0.037	0.016	0.016	0.008	0.002	0.051	0.062	0.061	0.042
BaO	0.2	0.214	1.196	1.196	0.888	1.066	0.059	0.045	0.047	0.261
SrO	0.57	0.603	0.373	0.373	0.06	0.14	0.512	0.536	0.46	0.706
CaO	9.324	9.493	4.631	4.631	2.097	2.19	14.877	14.111	14.294	8.99
Na_2O	5.785	5.524	7.74	7.74	8.048	7.933	2.87	3.211	2.923	5.717
K_2O	0.442	0.418	1.497	1.497	3.386	3.356	0.181	0.17	0.188	0.55
Total	100.99	99.6	100.89	100.89	100.26	100.21	100.36	99.56	98.51	98.63
					Oxygen = 32.000					
Si	10.201	10.185	11.047	11.047	11.564	11.53	9.131	9.292	9.245	10.223
Al	5.725	5.718	4.876	4.876	4.377	4.404	6.744	6.584	6.628	5.661
Fe*	0.074	0.086	0.062	0.062	0.046	0.053	0.093	0.079	0.09	0.094
Mg	0.012	0.01	0.004	0.004	0.002	0.001	0.014	0.017	0.017	0.012
Ba	0.014	0.015	0.084	0.084	0.062	0.075	0.004	0.003	0.003	0.019
Ca	1.788	1.849	0.886	0.886	0.402	0.421	2.916	2.781	2.849	1.771
Na	2.008	1.947	2.681	2.681	2.79	2.758	1.018	1.145	1.054	2.038
K	0.101	0.097	0.341	0.341	0.772	0.768	0.042	0.04	0.045	0.129
Ab	51.5	50	68.6	68.6	70.4	69.9	25.6	28.9	26.7	51.8
An	45.9	47.5	22.7	22.7	10.1	10.7	73.3	70.1	72.2	45
Or	2.6	2.5	8.7	8.7	19.5	19.5	1.1	1	1.1	3.3

Table 4.2: Con't

	Type II				Transitional (II & IB)		
	LT062-001 core	LT062 038 rim	LT022 001 core	LT022 013 rim	LT021 001 core	LT021 059 rim	019 012 resorbed
SiO_2	65.169	65.779	53.534	53.409	53.751	54.733	50.949
Al_2O_3	18.651	18.786	29.355	29.213	28.988	28.157	30.598
FeO_t	0.305	0.355	0.548	0.545	0.558	0.635	0.693
MgO	0.004	0.001	0.065	0.064	0.044	0.07	0.073
BaO	0.045	0.087	0.078	0.054	0.069	0.088	
SrO	0	0	0.491	0.534	0.591	0.484	0.366
CaO	0.425	0.462	12.084	12.053	11.782	11.064	14.129
Na_2O	7.22	7.037	4.402	4.351	4.499	4.884	3.328
K_2O	6.742	7.116	0.268	0.284	0.346	0.379	0.278
Total	98.56	99.62	100.83	100.51	100.63	100.49	100.41
				Oxygen = 32.000			
Si	11.893	11.895	9.666	9.674	9.725	9.893	9.293
Al	4.008	4.001	6.242	6.231	6.176	5.994	6.572
Fe*	0.047	0.054	0.083	0.083	0.084	0.096	0.106
Mg	0.001	0	0.017	0.017	0.012	0.019	0.02
Ba	0.003	0.006	0.006	0.004	0.005	0.006	0
Ca	0.083	0.09	2.338	2.339	2.284	2.143	2.761
Na	2.555	2.467	1.541	1.528	1.578	1.712	1.177
K	1.57	1.642	0.062	0.066	0.08	0.087	0.065
Ab	60.7	58.8	39.1	38.9	40	43.4	29.4
An	2	2.1	59.3	59.5	57.9	54.4	69
Or	37.3	39.1	1.6	1.7	2	2.2	1.6

Resorbed feldspars are recognized in thin section by rounded, lobate forms, exterior crystal embayments and truncation and cross-cutting relationships of zoning and polysynthetic twinning. Type I feldspars are observed in banded and felsic pumice samples. This differs from Diego Hermández, where no Type I feldspars were observed in felsic samples. Resorption styles and intensity and to a certain extent composition enable Type I feldspars to be divided into three sub-units.

Feldspar - Type IA

Type IA feldspars are recognized in thin section by resorption that is on a large scale and restricted, for the most part, to the core. Resorption is described as large scale in that there is no intricate interfingering of 'voids', instead voids are large (up to 600 μm) and more embayment-like (Plate 4.5). Resorption intensity varies from moderate to strong based on number and size of voids. These feldspars are the most abundant comprising about 4 vol % of the overall phenocryst population. Crystals range in size from 0.6 to 1.7 mm and have a rectangular to lath-shape habit.

After careful examination of Type IA feldspars, it is concluded that this type can be further subdivided based on internal crystal patterns, NDIC zoning, glass host and composition. The first sub-type will be identified as Type IA_1 and the second as Type IA_2.

Type IA_1 feldspars are on average smaller than Type IA_2 feldspars, ranging from 0.6 to 1.2 mm and are subordinate, making up about 1 vol % of crystal population. Nomarski (DIC) zoning is complex in cores, forming a complex topographic-like pattern, whereas both mantle and rims have more conformable zoning patterns (Plate 4.6). Type IA_1 feldspars are dominantly found in medium to light brown glass, and in a few rare mixtures of dark

Plate 4.6: NDIC microphotograph of Type IA_1 feldspar crystal fragment. Core has complex zoning pattern in NDIC with mantle having more conformable zoning.

Plate 4.7: NDIC microphotograph close up of Type IA_1 feldspar showing rough interface with black glass. Indicating possible simple dissolution due to contact with mafic melt.

Plate 4.6

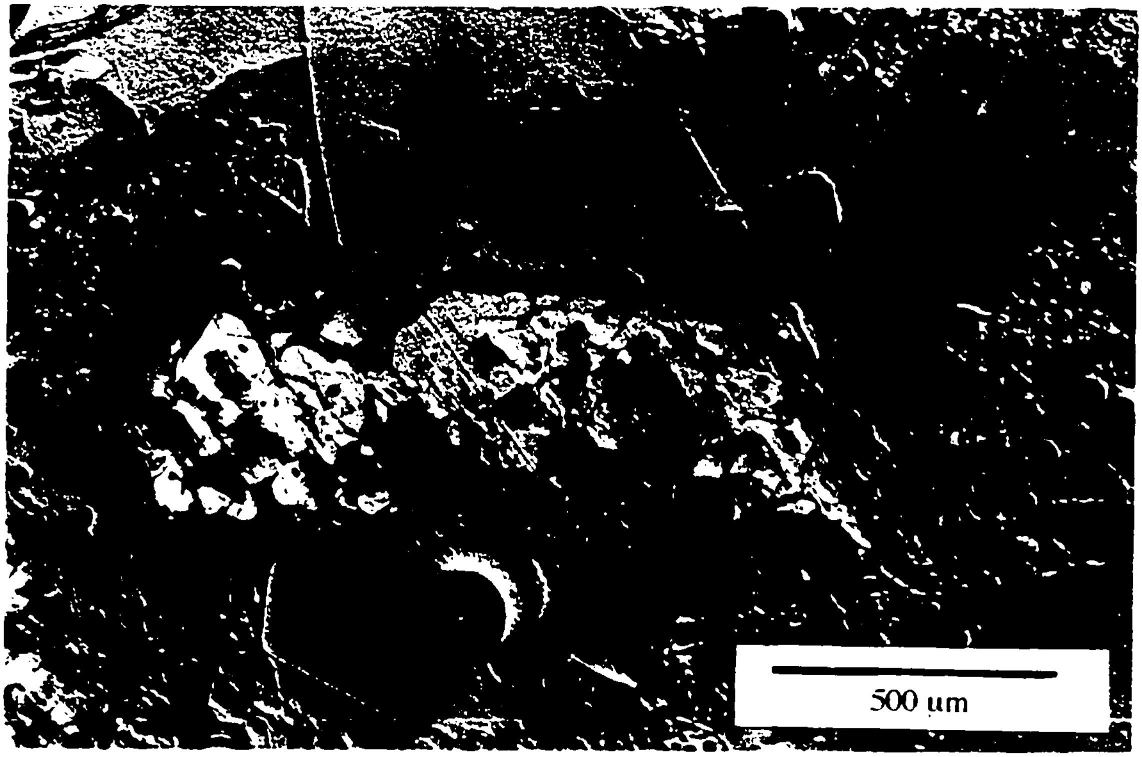

Plate 4.7

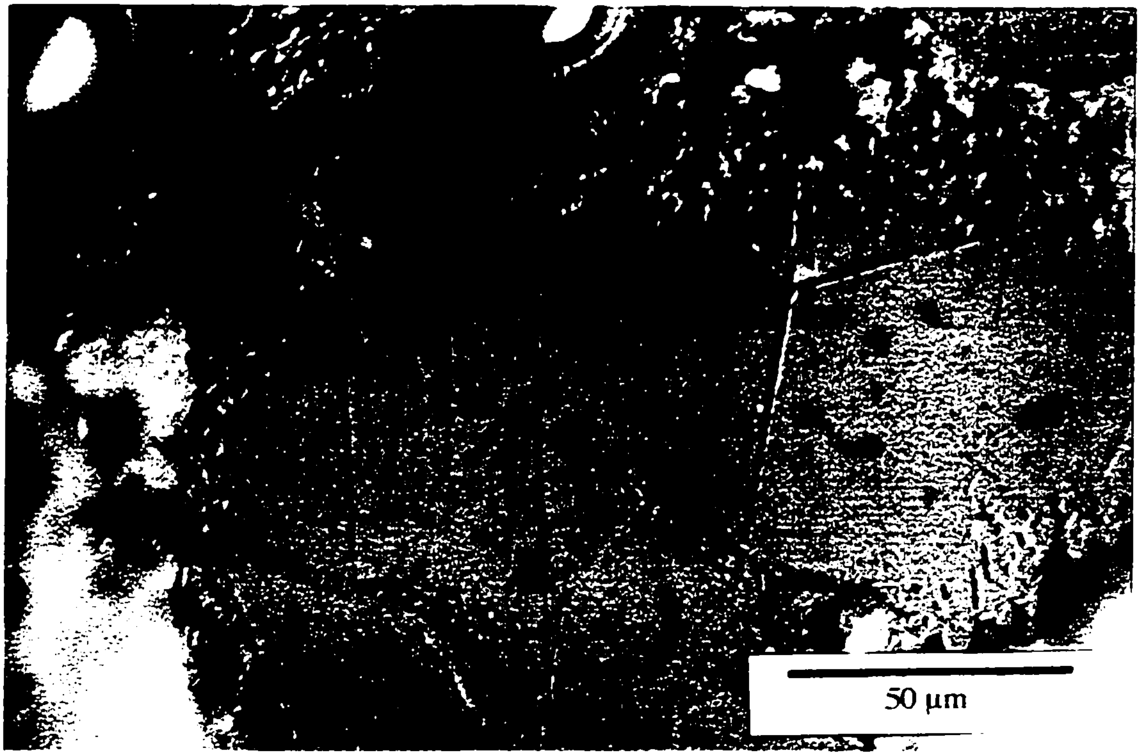

brown/black glass. Glass found throughout cores is the same as the host glass. In crystals hosted in dark brown/black glass, exterior crystal faces have rough interfaces indicating possible dissolution with the melt (Plate 4.7) (Tsuchiyama 1985). A rough interface is also observed where skeletal growth patterns are extended into the host melt. The skeletal patterns are present not only on exterior crystal faces, but mantle relic, lobate feldspar fragments within their resorbed core as well. Extinction patterns mimic NDIC zoning, with patchy zoning in core and normal zoning in mantle. Only one Type IA_1 feldspar was analyzed giving an andesine composition (An_{45}). Zoning is normal, with a core of An_{46} and rim of An_{44}.

No full, intact Type IA_1 feldspar crystals are observed, with all crystals having been fragmented into two sub-equal portions. Outer crystal margins are in general euhedral, except when the crystal is hosted in black glass, where it is subhedral due to slight rounding. No Type IA_1 feldspars are identified in felsic pumice (TK-25B).

Type IA_2 feldspars are larger than Type IA_1 and make up about 3 vol % of phenocryst population. Nomarski (DIC) reveals no etching pattern in these feldspars as compared to Type IA_1 feldspars. Type IA_2 feldspars are typically characterized by a mottled appearance having pronounced cleavage (Plate 4.5). This sub-type is dominantly hosted in pale green to clear glass, but rarely in light brown to medium brown glass. All Type IA_2 feldspar found in banded pumice (CS-015 & CS-002) are hosted in felsic glass blebs. Extinction patterns are normal overall with rare cases of patchy zoning. Compositionally these feldspars are transitional from alkali feldspar to Na-rich plagioclase (Fig. 4.5), ranging from Or_{20} to An_{23}, respectively. Na-rich Type IA_2 feldspars normally do not have the familiar mottled appearance of the alkali-feldspars, appearing more optically homogeneous. Outer crystal margins are subhedral, with slight rounding of crystal corners. Most Type IA_2 feldspars are fragmented, but a few rare intact crystals are observed, which probably survived due to their small size (700 μm). Interfaces with host melt are smooth in all cases observed.

Interpretation of Type IA Feldspars

Resorption textures are evident in both sub-types, but their exact origins are interpreted to be different. Based on NDIC zoning and composition Type IA_1 feldspar is interpreted to have had a more complicated history than Type IA_2 feldspar.

Compositions, morphologies, textures and zoning patterns (in NDIC) of Type IA_1 are exactly the same as Type IA from Diego Hernández wall (referred to as TIA-DH here after) (chapter 3). Remember that the section studied in chapter 3 represents the first eruptive episode from Diego Hernández whereas El Abrigo Ignimbrite is correlated to the second eruptive episode from Diego Hernández. TIA-DH feldspars were very abundant in the first eruptive episode (≈ 5 vol %) from Diego Hernández while in the second event they are very scarce (≈ 1 vol %). To refrain from repetition, the origin of Type IA_1 feldspars will only be summarized and refer to the previous chapter for a more detailed description.

Cores of Type IA_1 feldspars are thought to be remnants of an earlier skeletal growth phase resulting from the undercooling of an intermediate magma (≈ An_{40}). These skeletal feldspar crystals underwent a minor resorption event that rounded the skeletal features. This resorption event is probably due to the injection of a basic melt that raised the temperature of the intermediate end member causing simple dissolution (Tsuchiyama 1985). Once temperatures became stable the resorbed skeletal relics served as growth sites for crystallizing feldspar in equilibrium with intermediate host melt.

Type IA_2 feldspars are more abundant than Type IA_1 by a 3 to 1 ratio, are characterized by large voids in cores (Plate 4.5). Also diagnostic are their enhanced cleavage patterns that give the crystal a mottled appearance (Plate 4.5). Chemical composition of the host melt for these feldspars indicate that they probably originate from the felsic end member. Their resorption history is interpreted to stem from their having been in close proximity to the intermediate melt, either in the sub-volcanic environment, during the eruptive event, or a combination of both. Both situations result in heating Type IA_2 to just above their liquidus, thereby causing partial melting (Tsuchiyama 1985). The anorthoclase composition of Type IA_2 feldspars is further evidence of these crystals crystallizing in the lower portion of the felsic capping layer where compositions were probably not as evolved as compared to Type II feldspars from felsic pumice (TK-25B).

Feldspar - Type IB

Type IB feldspars comprise about 1 vol % of the total phenocryst population and are identified by their highly resorbed nature. Crystals range in size from 0.3 to 2.1 mm and are typically anhedral, although all have a relic tabular outline (Plate 4.4). This tabular habit is enhanced by at least one thin overgrowth ($\approx$ 5 µm) located along the long axis of the tabular outline. All Type IB feldspars are hosted in black to dark brown glass found in banded pumice samples. There is one exception to the last statement, where the tabular ends of an euhedral feldspar has complex zoning pattern in NDIC, with a sieved texture (analogous to Type IB). This crystal is hosted in a pale green glass, but is only 100 µm from dark brown glass and the crystal itself has a veneer of black material. Compositionally these feldspars are the most calcic plagioclases analyzed, ranging from An_{70} to An_{45}. (Fig. 4.5 & Table 4.2). Zoning is normal, with the most sodic compositions (An_{45}) located in rim overgrowths.

The texture of Type IB can be described as sieved. These sieve-like patterns are typically elongated parallel to lattice defects and other energetically favorable surfaces (ie. polysynthetic twins), indicating a crystallographic control. This is good evidence of resorption rather than growth origin for these textures as resorption processes make use of defects formed with the crystal during growth, thereby indicating a post crystal growth process for such textures (Anderson 1984; Dungan and Rhodes 1978; Pearce and Kolisnik 1990; Singer et al. 1993). In plane polarized light it appears that the host melt has penetrated the sieved areas to infill most of the voids. However, in reflected light the black material thought to be glass is highly reflective and is unidentifiable.

Zoning in NDIC is asymmetrical and quite complex, resembling topographic contours in certain cases (Plate 4.8). Wherever these complex zones are in contact with glass they are enveloped by non-zoned feldspar. Commonly this envelop of 'homogeneous' feldspar has sharp boundaries, giving the fragments an euhedral habit (Plate 4.9). These euhedral overgrowths are more sodic than the host feldspar, with one point found to be An_{45}, a full 30 % lower in An content than complexly zoned feldspar.

Interpretation of Type IB Feldspar

Type IB feldspars from El Abrigo Ignimbrite are directly comparable to Diego Hernández. El Abrigo Type IB feldspars, as with Diego Hernández Type IB (TIB-DH here after) feldspars, are the most calcic feldspars identified (by 30 % An) in their respective deposits. In both deposits the basic end member that must have crystallized these calcic

Plate 4.8: NDIC microphotograph of complex zoning in Type IB feldspar. Hosted in mafic, microlitic-rich glass. Glass has penetrated crystal structure with renewed growth both on outer and inner crystal surfaces (see plate 4.9).

Plate 4.9: NDIC microphotograph of Type IB feldspar hosted in mafic, microlitic-rich glass. Close up of feldspars in plate 4.8. Renewed crystal growth from hybrid melt has grown epitaxially on outer (OG) and inner (IG) crystal surfaces. New growth is more sodic than underlying plagioclase.

Plate 4.8

Plate 4.9

feldspars has not been identified by EMP analysis, thereby leading to the conclusion that this basic host for Type IB feldspar has probably been hybridized to a more intermediate composition.

El Abrigo Type IB feldspar, like TIB-DH feldspars, are envisioned to result from rapid decompression as its basic host was emplaced in the sub-volcanic magma chamber from its source. The sudden change in pressure will lower the plagioclase liquidus enough to allow these calcic plagioclase crystals to partially melt (Nelson and Montana 1992; Pearce et al. 1987).

One plagioclase feldspar is worthy of further investigation. Overall this feldspar crystal is euhedral with no sign of resorption, except that on either end of its tabular shape there is strong resorption (Plate 4.10). What makes the style of resorption particularly interesting is that it appears exactly the same as sieved Type IB feldspars in terms of zoning in NDIC (Plate 4.11), structure and composition. This feldspar crystal is anomalous in that it is hosted in pale green, felsic glass, but it has a veneer of black material that is highly reflective under reflected light and not identifiable. It appears that this crystal was preferentially resorbed at either end by a dissolution/reprecipitation mechanism where the newly precipitated feldspar is higher in An content than the origin crystal. The original crystal has a core composition of An_{58} and a resorbed region up to An_{69} (Fig. 4.6). This process of melting then reprecipitating, with the new plagioclase being more An-rich than the starting material is exactly the same process described by Johannes et al. (1994). The complex zoning observed in NDIC represents sharp contacts between old, sodic plagioclase and new, Ca-rich plagioclase, with the highly reflective, black material probably being left over melt (Plate 4.12). This particular feldspar crystal depicts a 'sodic' plagioclase crystal that was heated such that it began to melt, however

Plate 4.10A: Transmitted light (PPL) microphotograph of feldspar that is transitional between Type II and Type IB. Both ends of this feldspars tabular morphology are resorbed giving a sieved texture similar to those described for Type IB. Crystal has veneer of black material which is hosted in pale green glass.

Plate 4.10B: Transmitted light (X-Nicols) microphotograph of feldspar that is transitional between Type II and Type IB. Resorbed crystal ends are shown along with slightly zoning in core/mantle area.

Plate 4.10A

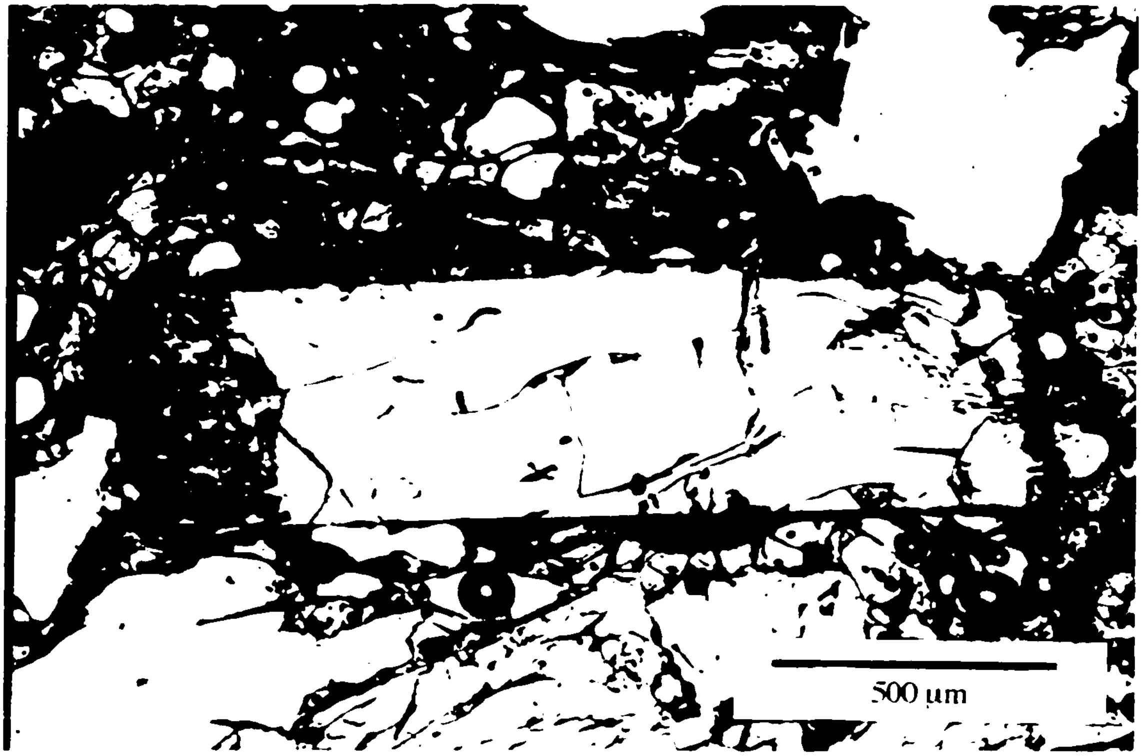

Plate 4.10B

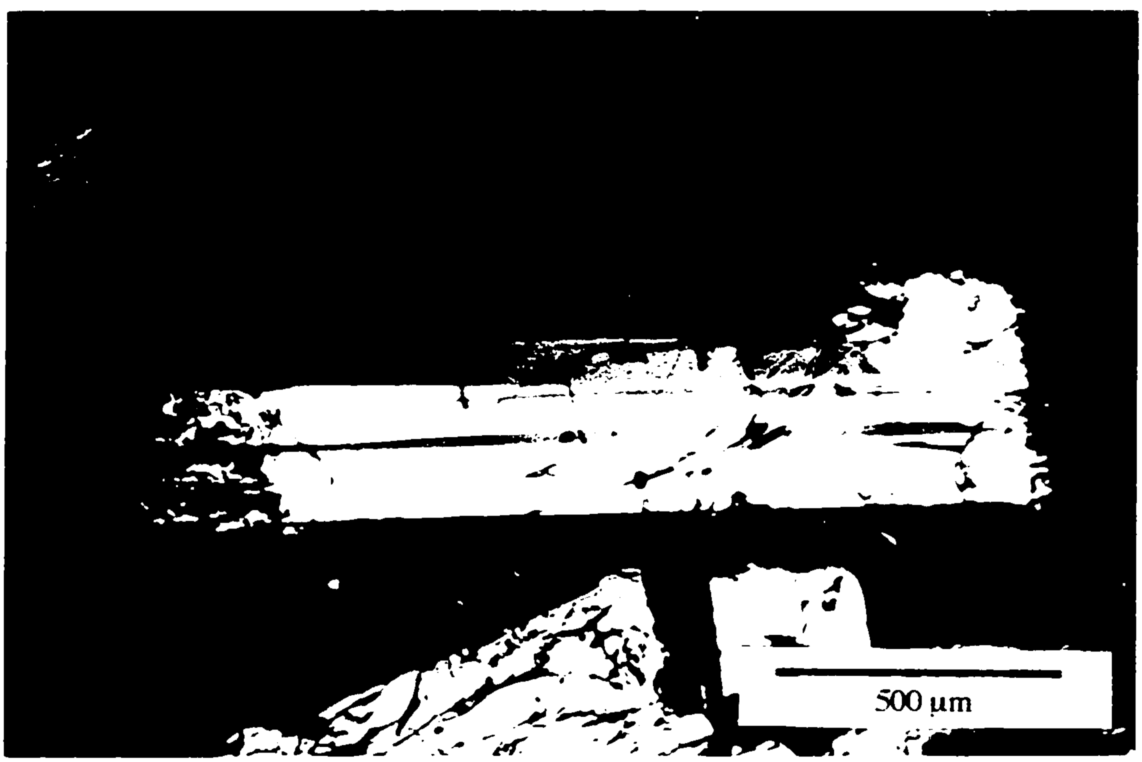

Plate 4.11: NDIC microphotograph of sieved tabular end of transitional feldspar crystal. Zoning pattern mimics that shown for Type IB feldspars. Main body of crystal shown by (C).

Plate 4.12: NDIC microphotograph of sieved tabular end of transitional feldspar crystal. Sharp contacts between more sodic feldspar (≈ An_{58}) and calcic feldspar (≈ An_{68}). Several EMP analysis shown.

Plate 4.11

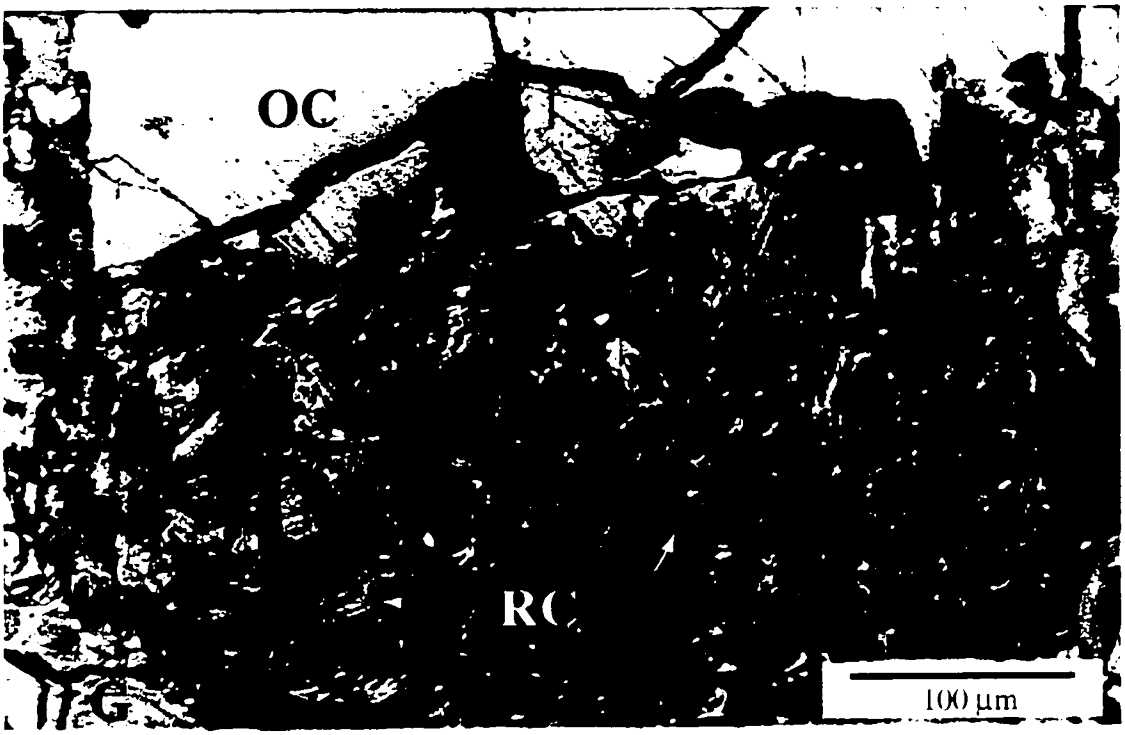

Plate 4.12

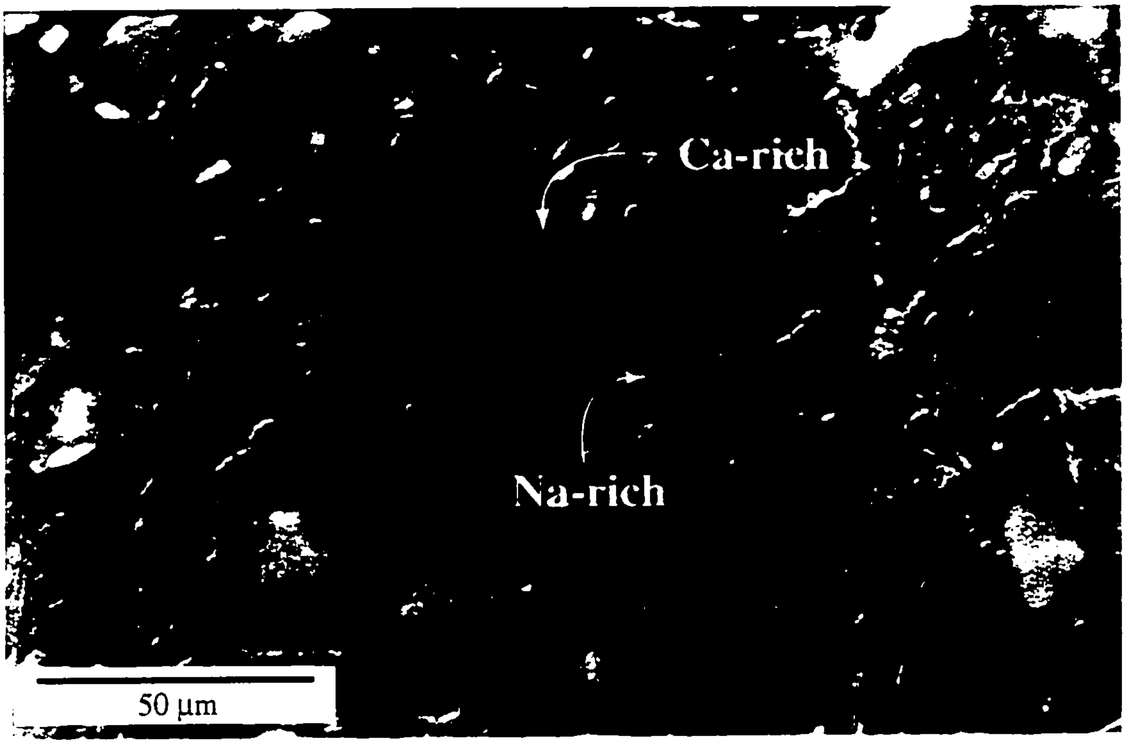

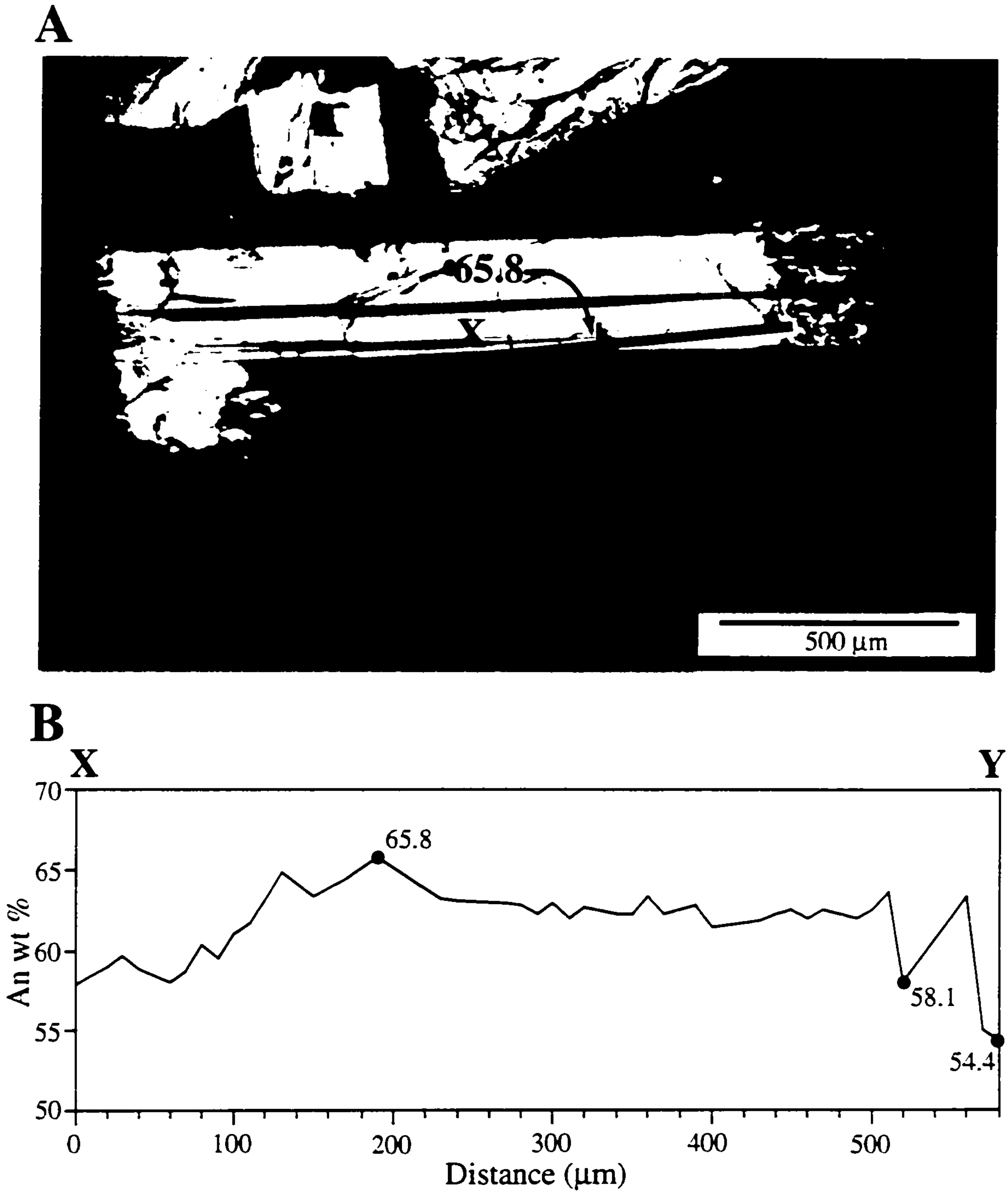

Figure 4.6: EMP line traverse of transitional feldspar from core to rim. Reverse zoning evident from core to mantle, marked by discontinunity visible in crossed polars photo (in A) and on traverse line (in B). Zoning is normal from mantle to rim with two large drops in An content.

before the process was completed it was removed from the heat source thereby saving this intermediate phase. Thus these feldspars probably originate from a basic melt with an 'equilibrium' feldspar composition of ≈ An_{60}. This feldspar composition is interpreted from lath-shaped Type II feldspar and core composition of the above transitional feldspar. As these feldspar laths are transported from its source region into the sub-volcanic environment they undergo rapid decompression that lowers the liquidus temperature (Nelson and Montana 1992; Pearce et al. 1987) thereby inducing melting in the form of a dissolution/repreciptation mechanism (Johannes et al. 1993).

Feldspar - Type IC

Type IC feldspars are more ambiguous as they represent « 1 vol % of the total phenocryst population. Morphologically they are distinctive from all other feldspars observed due to their rounded/oval appearance (Plate 4.13). In this case resorption is restricted to outer crystal surfaces without penetration, as cores are intact and unaffected. Crystal sizes range from 100 to 300 μm. Unfortunately no EMP analysis were performed on Type IC feldspar so their chemical composition is unknown. Type IC feldspars are all hosted in medium brown glass from banded pumice samples. When viewed in NDIC there is no internal zoning, but the rough interface with glass is very obvious. No Type IC feldspars are observed in felsic pumice (TK-25B).

Interpretation of Type IC Feldspar

Without the aid of chemical data it is hard to comment to any large degree on the possible origin of Type IC feldspars. If the analogy to Diego Hernández holds, then these feldspars are alkali in composition, probably in the anorthoclase range (≈ Or_{35}). All identified

Plate 4.13: Transmitted light (PPL) microphotograph of anhedral Type IC feldspar phenocryst hosted in black glass. Crystal has rough interface with host indicating simple dissolution.

Plate 4.14: Transmitted light (PPL) microphotograph of euhedral, tabular Type II feldspar hosted in pale green glass.

Plate 4.13

Plate 4.14

Type IC feldspar are hosted in medium brown glass, which is probably not the host it crystallized from based on its anhedral, rough interface with this glass. Tsuchiyama (1985) interprets rough interfaces as a result of a more sodic feldspar immersed in a more calcic melt, which complies with an alkali feldspar in a intermediate melt.

Type IC feldspars are envisioned to have crystallized in a trachytic to phonolitic melt close to the boundary layer with underlying intermediate melt. During the eruption these alkalic feldspars mingled with the intermediate melt, accompanied by an increase in temperature. These combined conditions were sufficient to cause simple dissolution, hence rounding of crystal morphology (Tsuchiyama 1985; Tsuchiyama and Takahashi 1983).

Feldspar - Type II

All feldspars grouped in this feldspar type have little to no resorption features. These crystals vary from euhedral to subhedral with rectangular or lath-shaped morphology (Plate 4.14). Type II feldspars make up about 2 vol % of the total phenocryst population. Compositions range from Ca-plagioclase (An_{65}) to alkali feldspar (Or_{43}) (Fig. 4.5).

Type II alkali feldspars are the largest phenocrysts observed having sizes up to 2.4 mm. Alkali feldspars are dominantly hosted in felsic pumice (TK-25B), but an EMP analysis identified one in banded pumice. Alkali feldspars are more rectangular than Type II plagioclase feldspars and tend to be euhedral when hosted in pale green glass. Those that are in light to medium brown glass are subhedral and have slightly rounded corners. Typically Type II alkali feldspars have a Carlsbad twins that separates a side of cross-hatch twinning with an enhanced cleavage pattern, giving a dirty/dusty appearance. On the other side of the Carlsbad twins the crystals are more homogeneous, with no sign of defects. Due to their large size these crystal are commonly fragmented.

Plagioclase feldspars are more lath-shaped to tabular, having an euhedral habit when hosted in medium to dark brown/black glass. Crystal sizes range from 0.35 to 1.4 mm. Albite twinning is common but not diagnostic. Lath-shaped plagioclase feldspar of this type that has experienced resorption on both lath ends is described in section on Type IB. As mentioned previously, this particular crystal is hosted in pale green glass rather than the more typical brown glass.

Interpretation of Type II feldspars

Overall Type II feldspars have a euhedral morphology in comparison to Type I feldspars. Zoning in NDIC is weak to non-existent with a few rare cases of oscillatory-like zoning in small plagioclase laths hosted in dark brown glass. The two populations illustrated on the ternary diagram (Fig. 4.5) represent two separate near-equilibrium growth phases resulting in the growth of these euhedral feldspar crystals, one from a mafic end member, the other from a felsic end member.

Of interest is that the alkali feldspars seem to have two trends on the An-Ab-Or diagram (Fig. 4.5), with those analyzed from the felsic pumice (TK-25B) being depleted in Ca compared to those from banded pumice. This may indicate a possible interaction between felsic and mafic glass in banded pumice.

Type II plagioclase feldspars probably represent entrained crystals from a basic melt that was injected into the sub-volcanic magma chamber that was subsequently mixed to form an intermediate host. Most of these entrained feldspars underwent dissolution followed by reprecipitation to form Type IB feldspars, but a small proportion survived.

Feldspar - Type III

Type III feldspars describe microphenocrysts and skeletal feldspars found throughout banded pumice samples. Both feldspar types are related to a period of rapid growth probably due to undercooling of their host melts. Unfortunately no EMP analysis were performed on either microphenocrysts or skeletal feldspars.

Microphenocrysts are concentrated in brown, or mafic glass, with the ground mass sometimes being comprised of a mass of microlites (Plate 4.15). Microphenocrysts reach a maximum of 150 μm and have an acicular habit. A very rough estimate of their abundance has microphenocrysts making up about 1 vol % of total phenocryst population. Overall 90 % of all microphenocrysts are hosted in mafic glass with scattered microphenocrysts found throughout felsic glass. However, the felsic glass does contain swallow-tailed feldspars (Plate 4.16) that are conspicuous by their absence in mafic glass. Swallow-tailed feldspars are slightly thicker than the acicular microphenocrysts and measure between 50 and 100 μm in size. No microphenocrysts are observed in felsic pumice (TK-25B).

Skeletal feldspar crystals are observed in trace amounts in banded pumice with none in felsic pumice. Both felsic and mafic glass host skeletal crystals with no evident of resorption. Skeletal crystals hosted in mafic glass are more abundant that those in felsic glass, with the latter type being more equant and square, whereas the former is more lath-shaped. The largest observed skeletal crystal measures 300 μm.

Both microphenocrysts and skeletal crystals from felsic and mafic glass are thought to represent near-equilibrium growth during minor undercooling of their respective melts. For Type III feldspars from mafic glass, undercooling is thought to have occurred during the initial injection of a basic magma into the base of the sub-volcanic chamber where it cooled in response to mixing with an intermediate magma. Type III feldspars from felsic glass are

Plate 4.15: NDIC microphotograph of a mass of microlites hosted in brown (mafic) glass.

Plate 4.16: NDIC microphotograph of swallow-tailed feldspar crystal hosted in pale green (felsic) glass.

Plate 4.15

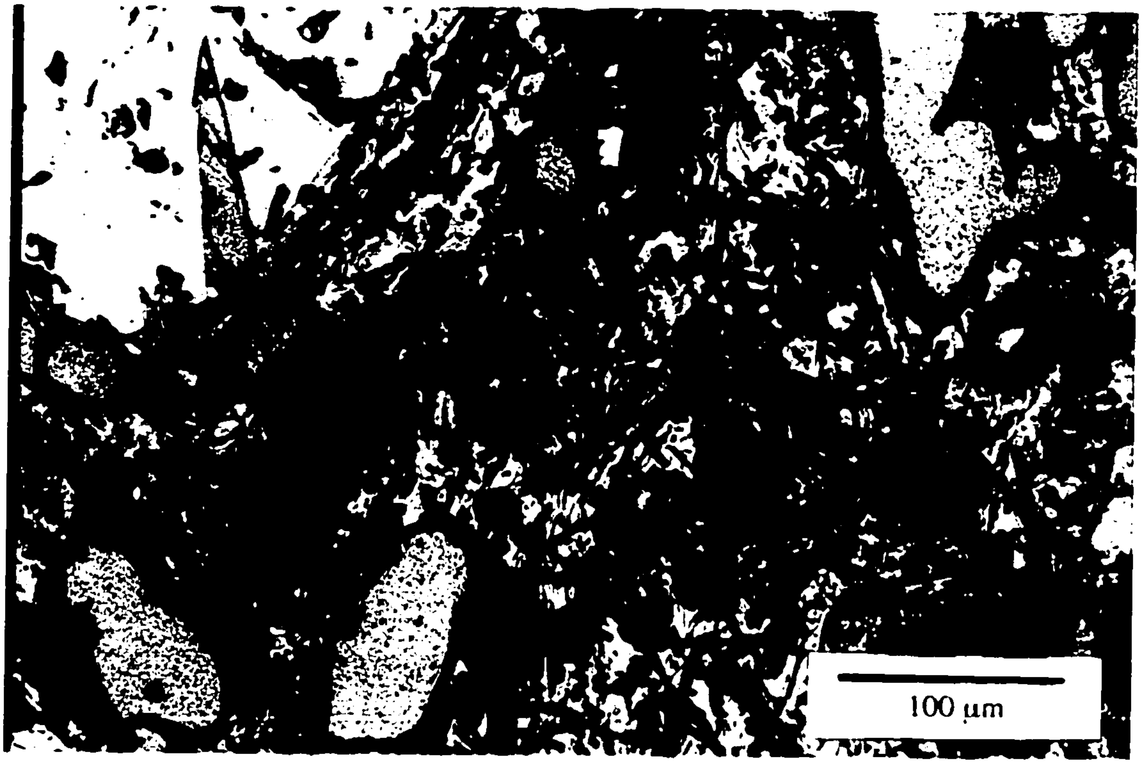

Plate 4.16

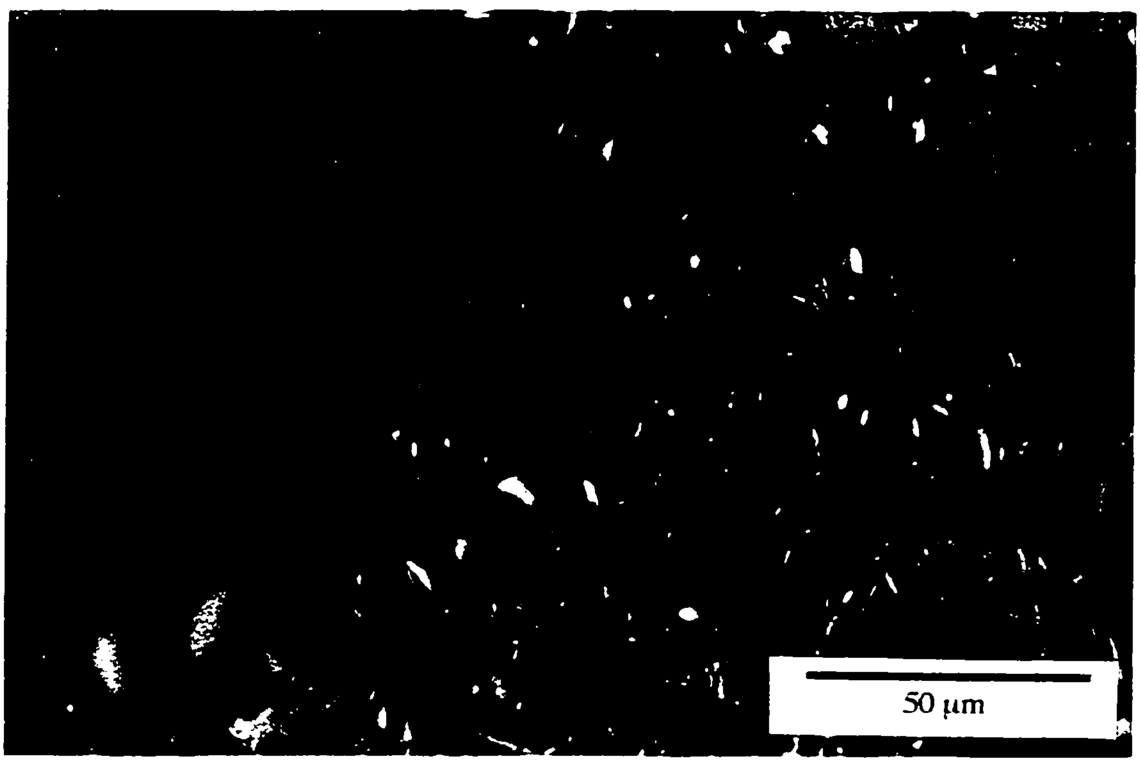

probably the result of undercooling during the eruptive event as the felsic magma was extruded onto the surface.

4.2.3 Pyroxene

At an estimated 1 vol % of the total population pyroxene is the most abundant ferromagnesium mineral identified in El Abrigo samples. No pyroxene is observed in felsic pumice (TK-25B), whereas in banded pumice pyroxene varies from trace amounts (CS-015A) to 2 vol % (CS-002). At least two different pyroxenes can be recognized based on crystal habit and pleochroism. Chemical composition is lacking, with only one pyroxene analyzed from El Abrigo.

The most abundant pyroxene make up about two-thirds of the total pyroxene population. These pyroxenes are lath-shaped with a subhedral habit. Crystal sizes range from 0.4 to 1 mm. Pleochroism varies from a lime green, yellowish brown and bluish green. The one EMP analysis is done on this sub-type of pyroxene (Table 4.3), and can be classified as a salite. Fe-Ti oxide inclusions are common, along with acicular microphenocrysts of apatite. These salites phenocrysts are typically hosted in medium to dark brown glass, with medium brown the more common.

The less abundant pyroxene occurs as phenocrysts that are distinctive due to their euhedral habit and blocky to rectangular morphology. These pyroxenes are found only in trace amounts with crystal sizes ranging from 600 to 800 μm. Pleochroism varies from pale greenish brown to a distinctive bleached pink (Plate 4.17). Another feature that sets these pyroxene phenocrysts apart is their zoning. Oscillatory zoning is common as is sector zoning, or hourglass zoning (Plate 4.18). These pyroxene phenocrysts are typically hosted in medium to dark brown glass and normally have inclusions of Fe-Ti oxides.

Table 4.3: Represenative EMP analyses for Pyroxene & Amphibole.
See Appendix B for complete data.

	Pyroxene		Amphibole			
	C007-001	C007-004	AM007-001 rim	AM007-004 core	AM008-001 rim	AM008-007 core
SiO_2	51.093	50.032	38.2	39.73	39.59	40.322
TiO_2	0.976	1.21	6.616	6.371	4.832	5.068
Al_2O_3	2.258	3.027	14.086	13.017	12.022	11.989
FeO_T	7.817	8.287	11.843	11.521	13.994	13.659
Cr_2O_3	0.007	0.014	0	0	0	0
MnO	0.602	0.573	0.156	0.229	0.378	0.442
MgO	13.859	13.229	12.731	13.166	11.634	12.182
CaO	22.983	22.852	12.179	12.086	11.733	11.61
Na_2O	0.902	1.118	2.696	2.714	2.811	2.929
K_2O	0.017	0.018	0.98	0.995	1.294	1.224
F	*	*	0.063	0.027	0.056	0.091
Cl	*	*	0.009	0.013	0.026	0.019
Total	100.514	100.36	99.56	99.87	98.37	99.54
	Oxygen = 6.000		Oxygen = 23.000			
Si	1.882	1.847	5.763	5.879	6.132	6.216
Al	0.098	0.132	2.503	2.268	2.193	2.177
Ti	0.027	0.034	0	0	0	0
Fe*	0.241	0.255	0.751	0.709	0.563	0.588
Cr	0	0	2.863	2.904	2.686	2.8
Mg	0.761	0.728	1.494	1.425	1.812	1.761
Mn	0.019	0.018	0.02	0.029	0.05	0.058
Ca	0.907	0.904	1.969	1.916	1.947	1.917
Na	0.064	0.08	0.789	0.779	0.844	0.876
K	0.001	0.001	0.189	0.188	0.256	0.241
Cl	*	*	0.002	0.003	0.007	0.005
F	*	*	0.03	0.013	0.027	0.044
WO	47.054	47.43	*	*	*	*
EN	39.48	38.204	*	*	*	*
FS	13.466	14.366	*	*	*	*

* not applicable

Plate 4.17: Transmitted light (PPL) microphotograph of euhedral pyroxene hosted in dark brown to black (mafic) glass.

Plate 4.18: Transmitted light (X-Nicols) microphotograph of hourglass zoning in euhedral pyroxene crystal hosted in dark brown to black (mafic) glass.

Plate 4.17

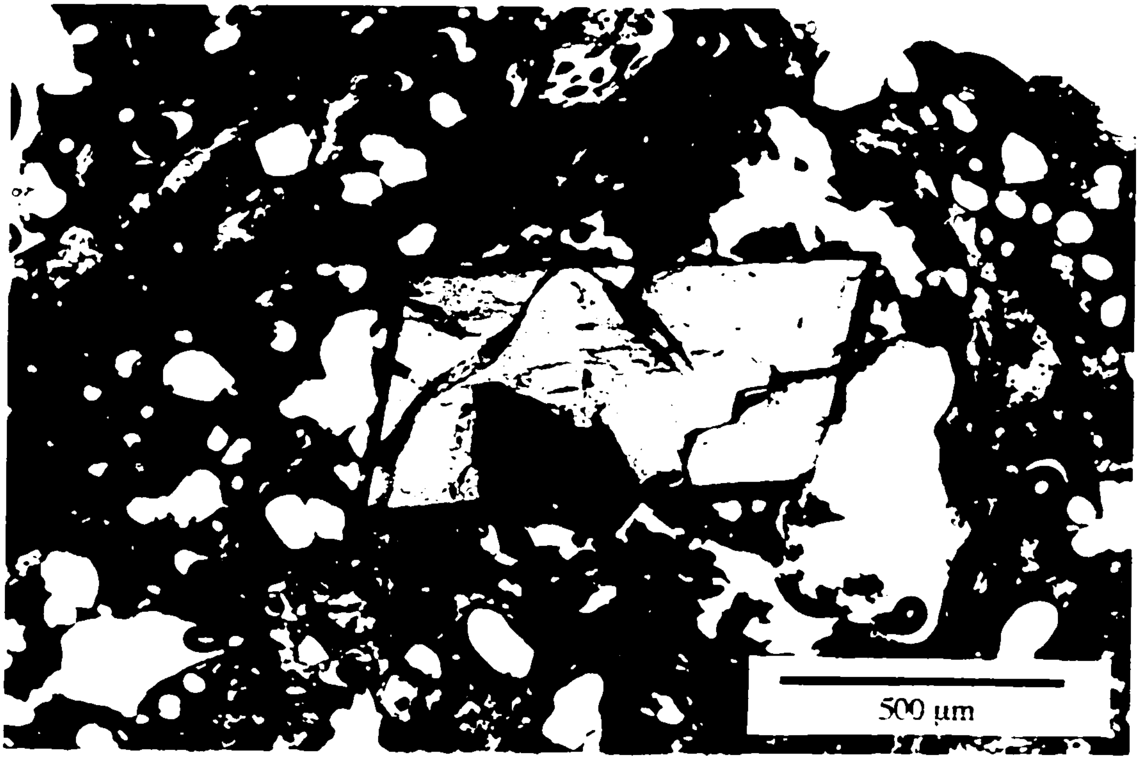

Plate 4.18

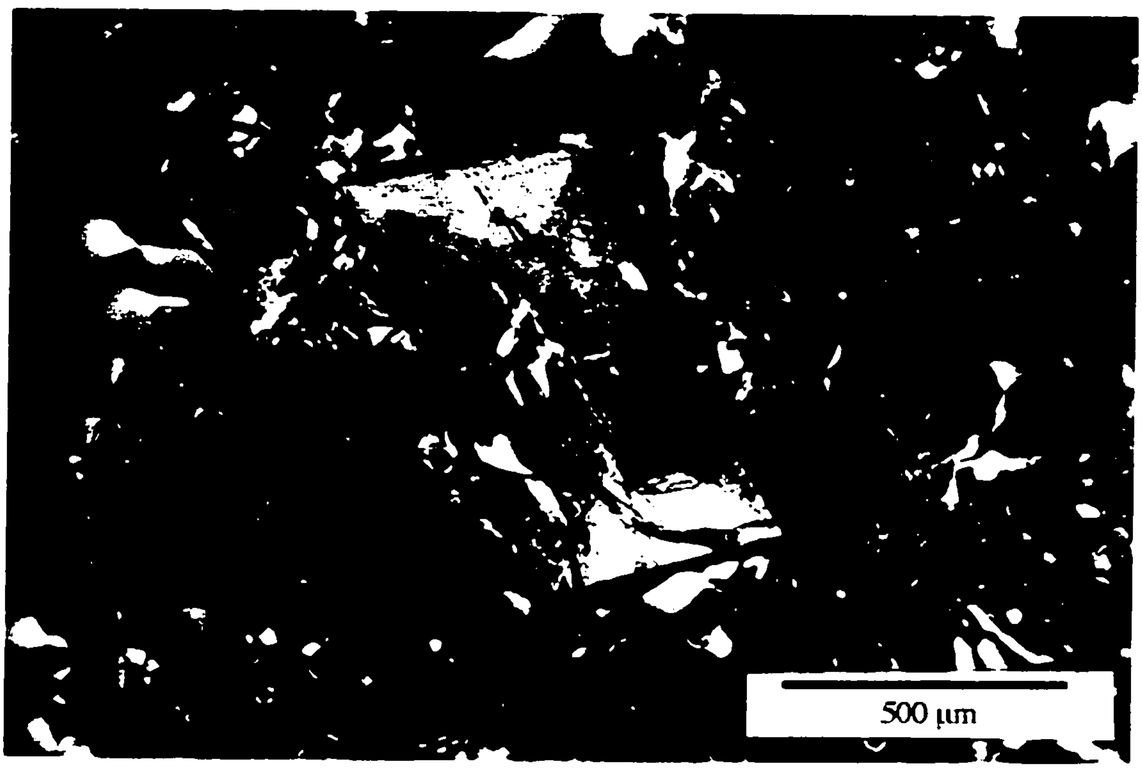

The last sub-type of pyroxenes are very rare with an average crystal size of 600 μm. They have an anhedral habit with a blue-green pleochroism. Only identifiable pyroxenes of this sub-type are observed in felsic glass from banded pumice, none are observed from felsic pumice (TK-25B).

El Abrigo pyroxenes resemble those described from Diego Hernández in certain aspects. Unfortunately their chemical compositions cannot be directly compared. The one EMP analysis obtained is comparable to the salites identified from Diego Hernández, as are their pleochroism and crystal habits. The euhedral pyroxenes with hourglass zoning correlate well with the titanaugites from Diego Hernández based on crystal habit and pleochroism. Anhedral pyroxenes do not match with any observed pyroxenes from Diego Hernández. No observed pyroxene from El Abrigo has been found to compare to assemblage three feldspar of Diego Hernández. The only major discrepancy has to deal with the actual amount of pyroxene present from each deposit, with El Abrigo having about half as much as Diego Hernández, but this only translates to a difference of 1 vol %.

4.2.4 Amphibole

Amphiboles make up the second most abundant ferromagnesium mineral with an estimated 1 vol % of total phenocryst population. These hydrous minerals typically have a euhedral habit with a blocky morphology and crystal sizes from 200 to 800 μm. While most amphibole phenocrysts are euhedral, many have experienced weak to moderate resorption, with a few having been almost completely resorbed. In most cases resorption has penetrated the crystal structure giving an embayed appearance (Plate 4.19). Another distinctive feature of these amphiboles is that their cleavage is enhanced so that it is very noticeable. Pleochroism varies from dark brown to yellowish brown depending on crystal orientation. Limited EMP

Plate 4.19: Transmitted light (PPL) microphotograph of resorbed amphibole crystal hosted in brown (mafic) glass. Resorption has penetrated crystal structure giving an embayed morphology.

Plate 4.20: Transmitted light (PPL) microphotograph of euhedral titanite crystal hosted in pale green (felsic) glass. Crystal edge close to black (mafic) glass is slightly rounded indicating possible simple dissolution.

Plate 4.19

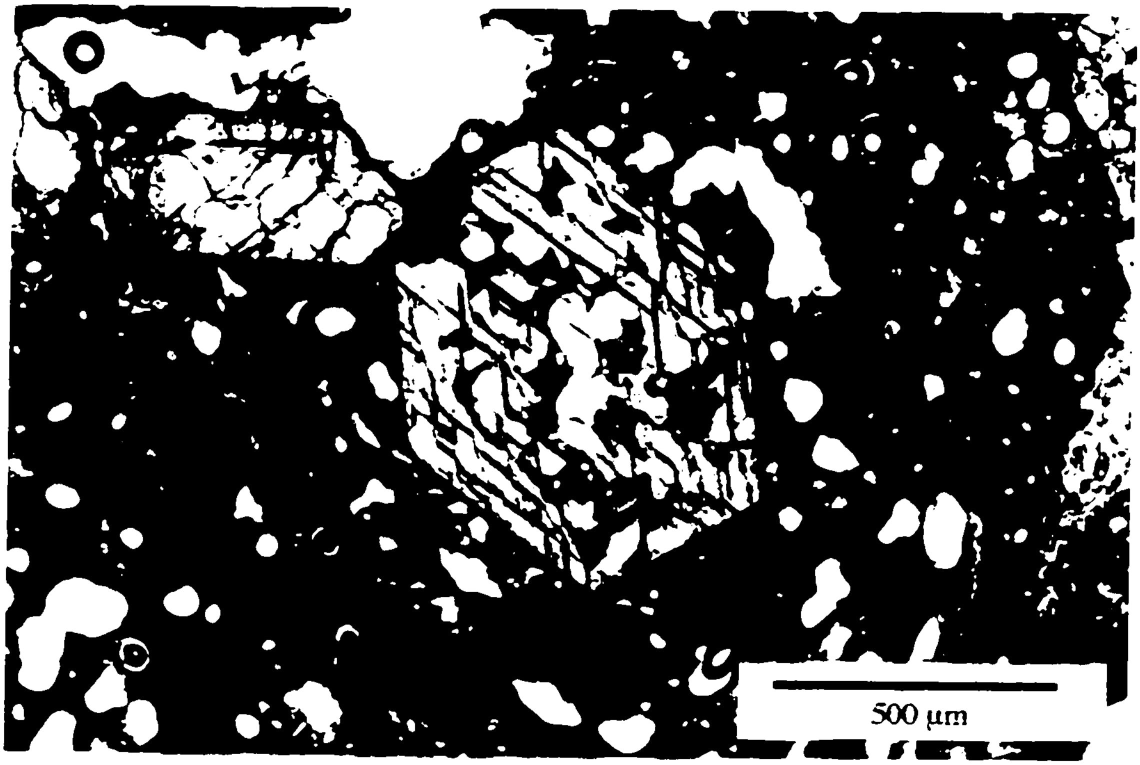

Plate 4.20

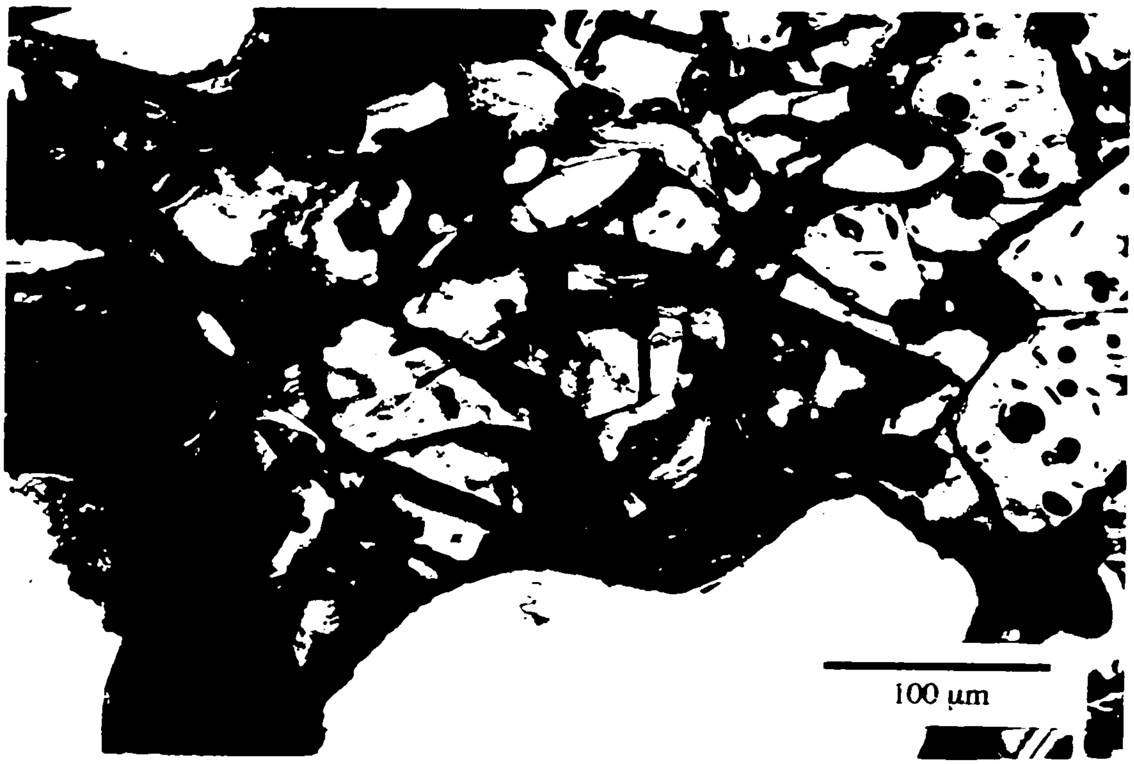

analysis on just two amphibole phenocrysts (Table 4.3) indicates that these amphiboles are kaersutite. Amphibole phenocrysts are observed from pale green all the way to dark brown glass. Those crystals hosted in dark brown glass are usually rounded and are more resorbed, (ie. anhedral) and commonly have a single twin plane.

4.2.5 Biotite

Biotite is a minor phase in all thin sections except for one of the banded pumice samples (CS-015A) where it makes up < 1 vol % of total phenocryst population. Crystal sizes range from 0.25 to 1.4 mm. No EMP analysis where done on any biotite phenocrysts from El Abrigo making detailed study and comparisons difficult. Crystal habits are subhedral to anhedral, with rare euhedral laths, with typical morphologies ranging from lath to tabular. Pleochroism varies from yellowish brown to dark red and birds eye extinction is common. Biotite is present in both banded and felsic pumice, normally hosted in pale green glass, but biotite in light to medium brown glass is observed occasionally. In felsic pumice biotite is conspicuous by its small crystal size (average ≈ 300 μm) and deep red pleochroism.

4.2.6 Feldspathoids

The feldspathoid population is limited to sodalite group minerals, namely sodalite and haüyne. Sodalite is found in trace amounts in all pumice samples studied with rare haüyne present only in banded pumice. Both sodalite and haüyne are recognized in thin section by their distinctive isotropic behaviour. Haüyne is larger, with crystals about 800 μm whereas sodalite crystal size range from 200 to 400 μm. Haüyne is distinguished from sodalite by its grey appearance in plane polarized light and by being hosted in medium brown glass. Sodalite is more equant with numerous cracks running across its crystal surface. When sodalite is hosted in pale green glass it is clear or white in appearance, but in light to medium brown glass the crystal surface becomes cloudy. Both minerals are euhedral overall, with some instances of subhedral to anhedral sodalite crystals when hosted in brown glass. In rare cases sodalite is associated with resorbed amphibole and biotite, and may be a reaction product.

4.2.7 Fe-Ti Oxides

Fe-Ti oxides are minor phases with only trace amounts found in banded pumice and rarely in felsic pumice. All oxides are typically equant with blocky to rectangular morphology, having crystals sizes ranging from 100 to 350 μm. Crystals habits are subhedral to anhedral depending on the degree of resorption. All oxides observed are rounded to some extent with one or more embayments common. Two oxides are identified in banded pumice, namely magnetite and ilmenite. Ilmenite is more rectangular than magnetite. Both oxides are observed in all glass types in banded pumice with various styles of resorption, but only magnetite is present in felsic pumice (TK-25B). No EMP analysis are done on any oxide. More euhedral oxides are observed as inclusions within silicate minerals, particularly pyroxene.

4.2.8 Accessory Phases

Accessory phases present in pumice samples include titanite, apatite and pyrrhotite. All three are very rare, with both apatite and pyrrhotite being restricted to being inclusions within silicates and oxides, respectively. Titanite is the more abundant accessory phase occurring as discrete crystals hosted in pale green glass close to contacts with brown glass (Plate 4.20). Titanite has a distinct pale yellow-brown pleochroism with a diamond-shaped euhedral habit. All crystals identified are about 200 μm in size. No titanite is observed in felsic pumice samples.

4.3 Discussion

By careful examination of zoning, textures and glass hosts some assumptions can be made in regard to possible mineral assemblages. At least two different assemblages exist, with a possible third, depending on the origin postulated for Type IB feldspars. A third assemblage is also suggested by two varieties of pyroxene observed in mafic glass. This implies either the pyroxene population from the felsic melt has somehow been incorporated into the mafic glass or that the mafic glass is a hybrid of two contrasting magmas, each with its own pyroxene population. Only a few pyroxenes are present in felsic glass and they do not look like either of the two pyroxenes described from mafic glass, thus it is concluded that the brown glass is a hybrid that is dominantly an intermediate magma of trachyandesite composition (Fig. 4.2).

Assemblage one is considered to be derived from the basic magma that contributed to the intermediate hybrid. Calcic plagioclase of Type IB and Type II affinity are possible crystals from such a magma. Type II plagioclase feldspars probably crystallized from a basic melt at or close to its source and then were subsequently emplaced in the sub-volcanic chamber. Most Type II feldspars have gone through a dissolution/reprecipitation (Johannes et al. 1993) process triggered by rapid decompression (Nelson and Montana 1992; Pearce et al. 1987) during their emplacement from depth. This results in Type IB sieved feldspars that are Ca-enriched. Without the aid of chemical composition, deciding which of the two pyroxene phenocrysts originates from the basic magma is difficult. From the abundance of phenocrysts and correlation to the first eruptive event from Diego Hernández, it is speculated that the euhedral pyroxenes with blocky to rectangular morphology (Plate 4.17) are derived from the basic melt. Where the mafic melt is dominated by that of the intermediate melt then it is assumed that the basic melt component of the hybrid is minor such that any entrained phenocrysts will be subordinate to those from the more 'felsic' component. Also basic pyroxenes (titanaugites) from Diego Hernández are nearly identical to those described from El Abrigo. The lack of chemical analyses for Fe-Ti oxides precludes them being assigned to either the basic or intermediate end-members for the hybrid. However, the likelihood that both basic and intermediate melts had their own Fe-Ti oxide population is high.

Assemblage two is probably an intermediate melt that mixed with the basic melt of assemblage one to form the hybrid present in banded pumice. All feldspars with chemical compositions in the andesine range probably crystallized either from the pre-existing intermediate magma or from the intermediate hybrid. If from the pre-existing melt, then they should have some form of resorption texture whereas those from the hybrid would probably be more euhedral, crystallizing under near-equilibrium conditions. The only feldspars that comply with these restrictions are Type IA_1. Type IA_1 feldspars range from andesine to oligoclase in composition (Fig. 4.5) and have experienced resorption. Another feature of Type IA_1 feldspars is that their euhedral-like mantle probably represents growth from the intermediate hybrid. No completely euhedral feldspars of andesine to oligoclase composition have been analyzed. If similar crystal morphologies and habits are correlated from Diego Hernández to El Abrigo, then in addition no euhedral andesine feldspars are observed in El Abrigo pumice samples. Through the process of elimination, overall abundance and correlation to Diego Hernández, the pyroxene population for the intermediate melt can be identified. With one of the two observed pyroxenes in the hybrid melt already associated to the basic magma, the other pyroxene must represent the intermediate melt. Again, if the intermediate melt dominates the hybrid mixture, then it is more probable that they will be more intermediate pyroxenes contained in the newly formed melt. Correlation with Diego Hernández is two-fold, with similar optical and chemical crystal characteristics. Kaersutite amphiboles probably originate from this intermediate melt, based on their composition. As with assemblage one, Fe-Ti oxides cannot be precisely identified to originate from this intermediate melt, but it assumed that a specific population that was in 'equilibrium' with this intermediate does exist.

The final assemblage is an acidic melt, represented by the pale green glass in thin section, of phonolitic composition. The feldspars belonging to this assemblage are all alkali feldspars and are represented by Type IA_2 and Type II feldspars (Fig. 4.5). Biotite crystals are present in pale green glass and are therefore placed in this assemblage as are titanite crystals. Sodalite is interpreted to be from assemblage three based on its host and overall morphology. When sodalite is hosted in felsic glass it is more euhedral as compared to when it is hosted in mafic glass when it is more apt to be subhedral to anhedral, with a dusty or cloudy core. Haüyne is hosted in felsic glass, even though it is only thin veneer separating it from mafic glass, so it lumped into assemblage three. For Fe-Ti oxides the same argument used in the first two assemblages is used again.

It is concluded that three separate magmas existed at one time in the sub-volcanic chamber under Diego Hernández during the second volcanic event that culminated in collapse of the caldera. Each magma is recognizable by its distinct mineral assemblages described above. As mentioned, each assemblage corresponds to different magma type, in this case a acidic, intermediate and basic magma member.

Timing the formation of each member is basically impossible. However, some very basic assumptions can be made in regard to crystal morphologies and their interactions that give a very simplistic view of what may have happened just prior to and during the eruption.

The felsic or acidic magma is identified as being phonolitic in composition. While felsic pumice (TK-25B) was aphyric, it still had a significant phenocryst population (≈ 4 vol %), having alkali feldspar, biotite, sodalite and titanite, in order of decreasing abundance. Alkali feldspars dominated the phenocryst population and are conspicuous due to their size (up to 2.4

mm), as compared to feldspars from banded pumice. This size indicates that this acidic magma member has been around for a significant period of time (ie. around 1000 years).

The intermediate hybrid magma constitutes an intermediate and basic magma that mixed prior to the eruptive event. The hybrid that results plots in the trachyandesite field on a total alkali-silica diagram indicating that the original intermediate melt dominants the hybrid. Near-equilibrium feldspar compositions are estimated to be about An_{45}, from Type IA_1 feldspars, for the original intermediate melt. An overgrowth on Type IA_1 of An_{48} is hypothesized to be 'equilibrium' growth from the hybrid, thus indicating very little change from the original intermediate melt. The basic melt contributing to the hybrid is not overly basic with 'equilibrium' feldspars being $\approx An_{65}$. This means that chemically these two melts were probably not that different, thereby increasing the likelihood of complete hybrization (see chapter two). Mixing is fairly complete as there is no basic melt identified on TAS diagram, but there was also no mafic pumice sample to work on for this deposit. The basic melt is envisioned to have been injected into the intermediate melt from its source region, carrying several phenocryst phases along with it that have reacted to the change in pressure and temperature in various ways. Most notable are feldspar phenocrysts that have gone through a dissolution phase, then recrystallized to higher An contents.

Overgrowths on feldspars thought to be from the hybrid range in size from 5 to 15 µm that represent about 50 to 150 days of growth (based on growth rate of 0.1 µm/day, from Pearce et al. 1987). This growth rate is a rough estimate and is considered to be accurate within one order of magnitude (Pearce et al. 1987). No euhedral feldspar crystals of andesine composition are identified.

Interaction between the overlying capping layer of trachyte and the underlying layer of trachyandesite is limited to an exchange of a few phenocrysts and very intimate mingling. Evidence of their interaction is preserved in Type IC feldspars, where alkali feldspars in 'equilibrium' with the trachytic melt are now hosted in the hybrid and have subsequently been rounded due to simple dissolution (Tsuchiyama 1985). Glass diffusion profiles show slight evidence of exchange of elements, but is limited to the alkalies (Na, K). Contacts between glass types are very sharp, showing no sign of interaction optically.

The injection of the basic magma was probably a trigger for this major collapse event since the hybrid magma only had an estimated 150 days of growth, before erupting. Injection of basic magma resulted in an increase in the volatile content as it probably carried along a certain amount of volatiles, that at lower pressure will exsolve, plus the resorption of kaersutite released more volatiles which may have been enough to saturate the melt. Add this to an increase in the magma chamber pressure due added mass could be enough to cause failure in the roof rocks. All these factors could act together resulting in a major volcanic eruption. It is during the eruptive stage that the interfingering of trachytic and hybrid magma probably took place, either at the boundary between contrasting layers or in the volcanic conduit.

5 Conclusions

5.1 Summary

An integral part of this thesis has been the use of Nomarski (DIC) to distinguish subtle zoning changes in feldspars. Through interpretation of zoning changes and comprehensive chemical work using a electron microprobe, a viable magmatic history of feldspar phenocrysts is hypothesized. Feldspar history can be translated to the sub-volcanic environment as a whole giving a feasible model for the development of the magma chamber beneath Diego Hernández.

Diego Hernández Formation is divided into two major volcanic episodes, with the second event culminating in collapse of the caldera, forming the third and final stage of Las Cañadas Caldera (Martí and Mitijavila 1995; Martí et al. 1994b). The first eruptive event from Diego Hernández is an example of two separate mixing phenomena, one resulting in the formation of a hybrid, the other in physically banded magma. Feldspar populations and their characteristic zoning can be used to identify each mixing episode along with the magmas involved in each.

The magma chamber beneath Diego Hernández is thought to have initially been filled by an intermediate melt. This intermediate melt experienced undercooling on emplacement in the sub-volcanic chamber, as depicted by skeletal growth of plagioclase of andesine composition ($\approx An_{40}$). Differentiation of this intermediate melt formed a phonolitic magma, containing euhedral alkali feldspars (sanidine). Due to a density contrast the phonolite magma segregated from its parental melt to develop a separate capping layer. The homogeneity of euhedral alkali feldspars indicates that this phonolite capping layer remained fairly stable over its lifetime.

Closely following the segregation of the phonolite magma a basic magma was injected into the intermediate melt. A short time between phonolite segregation and basic magma injection is postulated based on evidence of resorption of skeletal plagioclase crystals derived from the intermediate melt. These skeletal feldspar crystals show no evidence of renewed growth *prior* to resorption, therefore basic melt injection predates mantle growth around skeletal feldspars. The basic melt is probably an alkali basalt originating from deep within the mantle and travels unimpeded to the sub-volcanic magma chamber. Support for this hypothesis stems from the sieved nature of entrained Ca-rich plagioclase phenocrysts that are interpreted to have formed in response to rapid decompression that occurs as basic melt is emplaced. Compositionally the intermediate and basic melts are interpreted not to be significantly different as the original plagioclase from the basic melt had an equilibrium composition of about An_{58} as compared to An_{40} for the intermediate melt. This lack of chemical contrast enabled the basic and intermediate magmas to mix more readily.

Crystallization was renewed before hybridization was completed, evidence of which is shown by reverse zoned euhedral plagioclase feldspars. These feldspars result from inhomogeneities in the hybrid melt where crystallization occurred in areas of higher Ca-content. Overgrowths on moderately resorbed skeletal plagioclase, from the original intermediate melt, also indicate renewed growth from the hybrid.

Residence time for the hybrid was short based on the largest feldspar phenocryst crystallized from this mixture. The largest observed euhedral plagioclase feldspar is 850 μm and if a growth time of 0.1 μm/day is taken as an estimate (Pearce et al. 1987) then it would take about 23.3 years to grow. However, this calculated growth time is just an order of magnitude approximation. Nevertheless, it is logical that the injection of a basic melt would induce the eventual eruption so this time frame seems reasonable.

There is evidence of limited interaction between the capping phonolite and the underlying intermediate hybrid in the form of resorbed alkali feldspars. Resorbed alkali feldspars are all rounded due to simple dissolution probably as a direct result of heating from the underlying intermediate melt. This interaction is interpreted to have been in the form of heat exchange as these resorbed alkali feldspars are still hosted in felsic glass. Heat exchange could have taken place while magma was in situ, with heat moving across the density barrier in the magma chamber, or during physical mingling enroute to the surface.

Undercooling of both phonolite and intermediate hybrid results in a period of rapid growth. This is indicated in the phonolite melt by the swallow-tailed growth forms on microphenocrysts whereas most feldspars in the intermediate melt have dendrite-like thin overgrowths.

The second major volcanic event from Diego Hernández, studied in the distal deposits of El Abrigo, mimics the model for the first eruptive episode from Diego Hernández (DH-1). Slight variations observed may indicate why the second event resulted in collapse of the caldera whereas the first did not. Only the differences will be emphasized and possible explanations for these variations.

Moderately resorbed skeletal feldspars that form the cores of plagioclase feldspars (Type IA) are subordinate in El Abrigo when compared to DH-1. This may indicate that the original intermediate melt did not undercool to the same degree with very few feldspars crystallizing or that most of these skeletal crystals were completely resorbed by injection of the basic melt.

El Abrigo has a large population of embayed alkali feldspars crystals that are absent in DH-1 pumice samples. Due to their resorbed nature, chemical composition ($\approx Or_{20}$) and felsic host these feldspars are interpreted to have crystallized in close proximity to the phonolite/intermediate boundary. If the phonolite is assumed to be stratified and not convecting then feldspars crystallizing in the lower portions of the melt will have lower Or contents. Close proximity to the boundary layer allows these crystals to be affected by any heat exchange across the boundary, hence they were resorbed. These embayed feldspars differ from rounded alkali feldspars from DH-1 in their morphology and crystal size. The fact that El Abrigo alkali feldspars are larger indicates a possible longer residence time for the phonolitic melt in the magma chamber.

Absent in El Abrigo pumice samples are euhedral plagioclase feldspars that are thought to represent near-equilibrium growth from the hybrid melt of DH-1. Their absence may indicate a short time frame between mixing of basic and intermediate melt and eruption. Hybridization is probably incomplete for El Abrigo as shown by the larger range in glass analysis on TAS diagram as compared to DH-1 (Fig. 5.1).

Anhedral alkali feldspars from El Abrigo are hosted in brown glass (intermediate) whereas in DH-1 they are hosted in pale green glass (acidic), yet both crystallize from an acidic magma. Resorption of these feldspars is similar, but the different magma host suggests more vigorous physical mixing either in the magma chamber or in the volcanic conduit. This implies a larger magnitude of volcanic energy associated with the El Abrigo eruptive event as compared to DH-1.

These discrepancies indicate that the injection or recharge of the sub-volcanic chamber promptly initiated the eruption leading to collapse of the caldera. The intensity of this eruption vigorously mixed the basic and intermediate magmas, waned briefly, then disrupted the density barrier separating the phonolitic and intermediate magmas. This disruption probably occurred just prior to eruption due to evidence of a diffusion profile for alkalies between mafic and felsic glass (Fig. 4.4). The eruption commenced with the chamber roof collapsing resulting in the

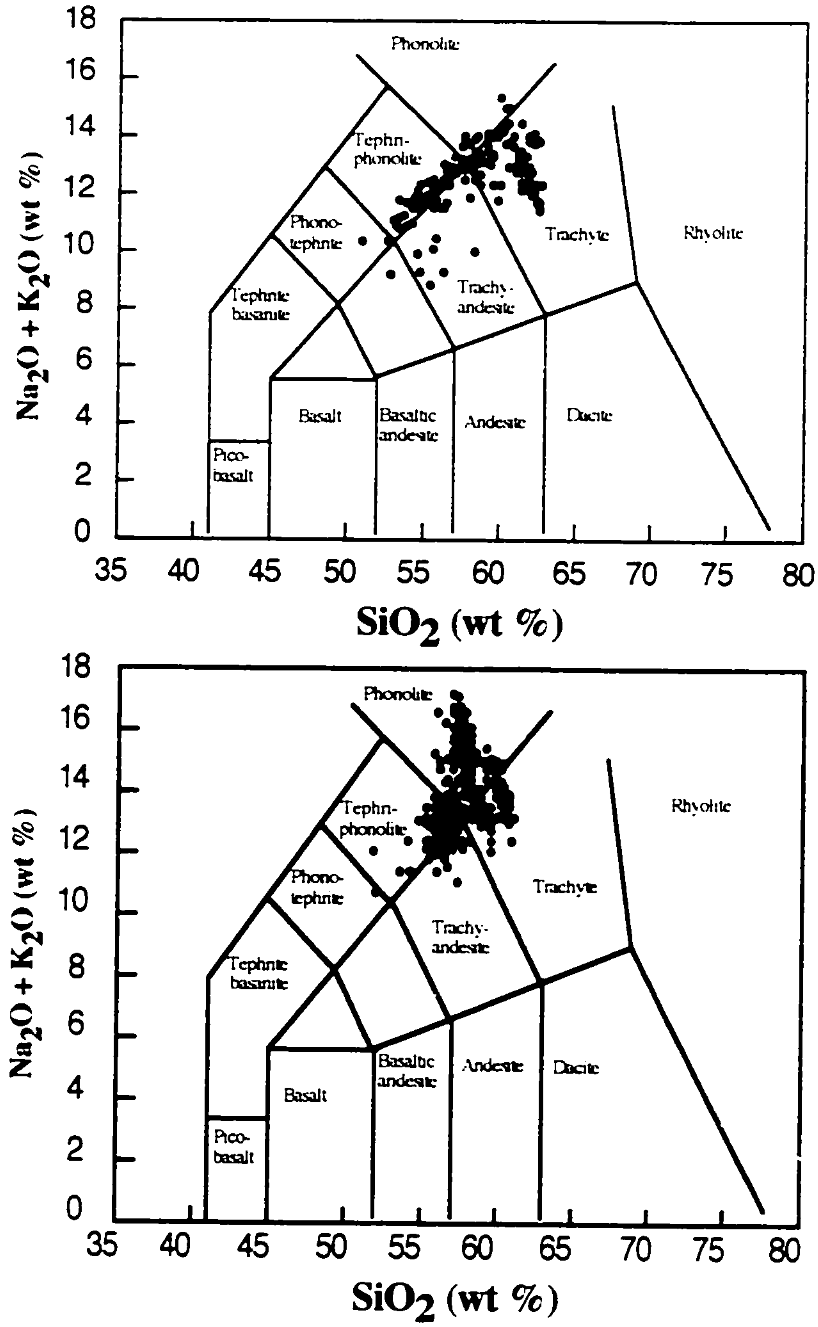

Figure 5.1: Total alkali-silica comparison for El Abrigo (top) and Diego Hernández (bottom) glasses.

extensive El Abrigo Ignimbrite.

5.2 Correlation of Tajao to Lower Eruptive Unit - Diego Hernández Formation

The Tajao ignimbrite is an informal name for a ignimbrite that stratigraphically overlies the Granadilla Fall and Ignimbrite, separated by basaltic and tephritic lavas and a palaeosol (Fig. 5.2 & 5.3) (Bryan et al. 1997; Wolff 1985). Wolff (1985) describes this ignimbrite as a non-welded deposit with porphyritic pumice and lithic fragments in a matrix of fine ash and loose crystals. What is characteristic of this ignimbrite deposit is its abundant banded pumice fragments.

Through Wolff's descriptions of mineral assemblages and limited chemical data it was noted that a correlation seems to exist between the Tajao ignimbrite and the first eruptive event from Diego Hernández (DH-1), described in detail in chapter 3. To date DH-1 has not been traced out of Las Cañadas Caldera to the coastline in the south. Recent stratigraphic work on pyroclastic deposits on the south coast of Tenerife has placed the Tajao ignimbrite in a favorable setting to be correlated to DH-1 (Fig. 5.2). The only age data positions Tajao between 0.372 Ma (El Medano Ignimbrite) and 0.179 Ma (El Abrigo Ignimbrite) with DH-1 dated at 0.266 Ma (Bryan et al. 1997; Martí et al. 1994b).

This comparison should only be taken at face value since the amount of chemical data available from Tajao is very restricted. A direct correlation can be made with feldspars, pyroxenes and Fe-Ti oxides. Physical descriptions of feldspar phenocryst from Wolff's assemblage 1 and 2 are nearly identical to those from assemblage 1 and 2 from DH-1. Plotted feldspar compositions on An-Ab-Or ternary diagram also mimic feldspars analyzed from DH-1 (Fig. 5.4). However, feldspar from El Abrigo also agree with both Wolff and DH-1, so cannot be used as a diagnostic tool for correlation.

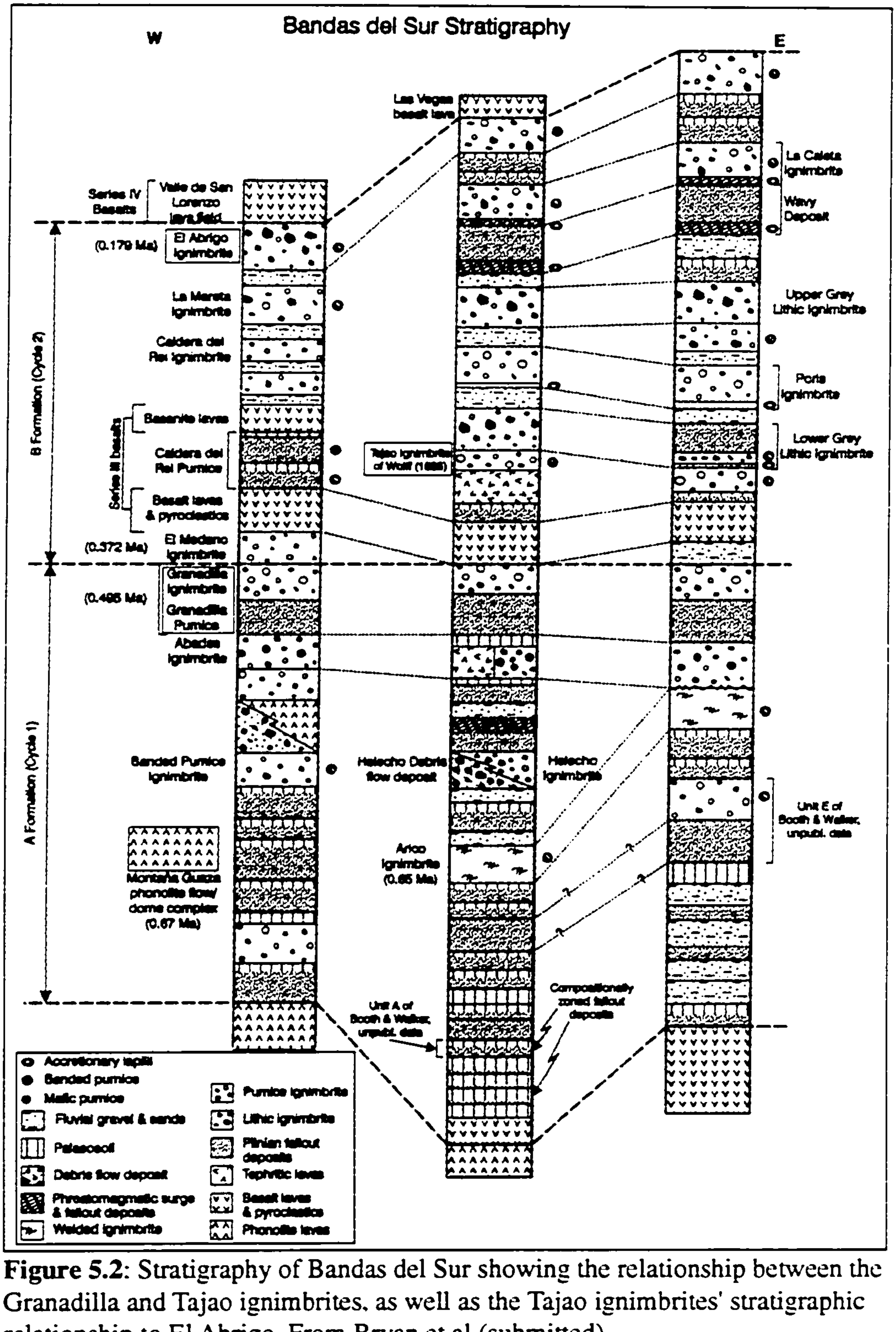

Figure 5.2: Stratigraphy of Bandas del Sur showing the relationship between the Granadilla and Tajao ignimbrites, as well as the Tajao ignimbrites' stratigraphic relationship to El Abrigo. From Bryan et al (submitted).

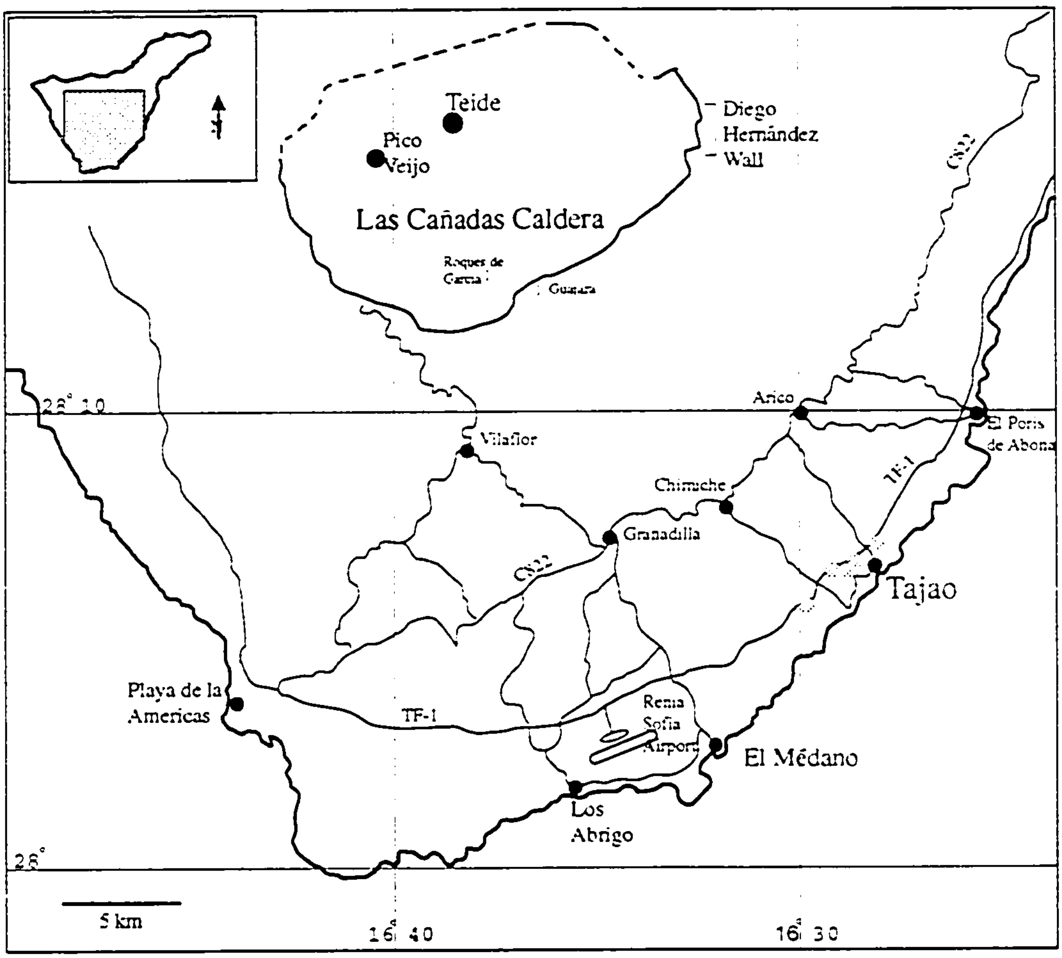

Figure 5.3: South coast of Tenerife showing the relationship of Tajao ignimbrite and Diego Hernández wall. Wolff (1985) approximate sample locations are shown (◌).

Pyroxene analysis provided by Wolff (1985) allow for three populations to be identified on a MgO vs Al_2O_3 plot. As mentioned in chapter three, two pyroxene populations are identified which agree with assemblage one and two of Wolff (Fig. 5.4).

Wolff identifies three Ti-magnetites and two ilmenites populations by plotting minor elements. In plotting DH-1 oxides on the same ternary diagram as Wolff it is noted that all five populations are almost identical (Fig 5.5). Wolff explains the absence of assemblage three ilmenite by the presence of titanite, which also occurs in DH-1 pumice.

In both pyroxene and Fe-Ti oxides a comparison to El Abrigo cannot be done due to the lack of analysis on pyroxene and oxides from this deposit. However, a close examination of glass data from El Abrigo shows a silica enrichment trend, whereas both DH-1 and Tajao have an alkali enrichment trend (Fig. 5.6).

As noted previously a more complete data set is required to truly correlate Tajao and DH-1, especially a radiometric age for the Tajao. At present the information presented indicates that it is possible that the Tajao ignimbrite is the distal equivalent to the lower pumice-rich pyroclastic deposit from the Diego Hernández Formation.

5.3 Final Word

A more complete model of the Diego Hernández Formation would have benefited from additional work in the following areas:

(1) Isotopic data would have aided in correlating glasses to their respective source regions and help determined whether these melts were co-genetic. This idea could be expanded to the other pre-calderan rocks of the Ucanca and Guarjara Formations to possibly come up with a model for the formation of Las Cañadas Caldera as a whole.

(2) More detailed sampling on more of a stratigraphic scale of both Diego Hernández

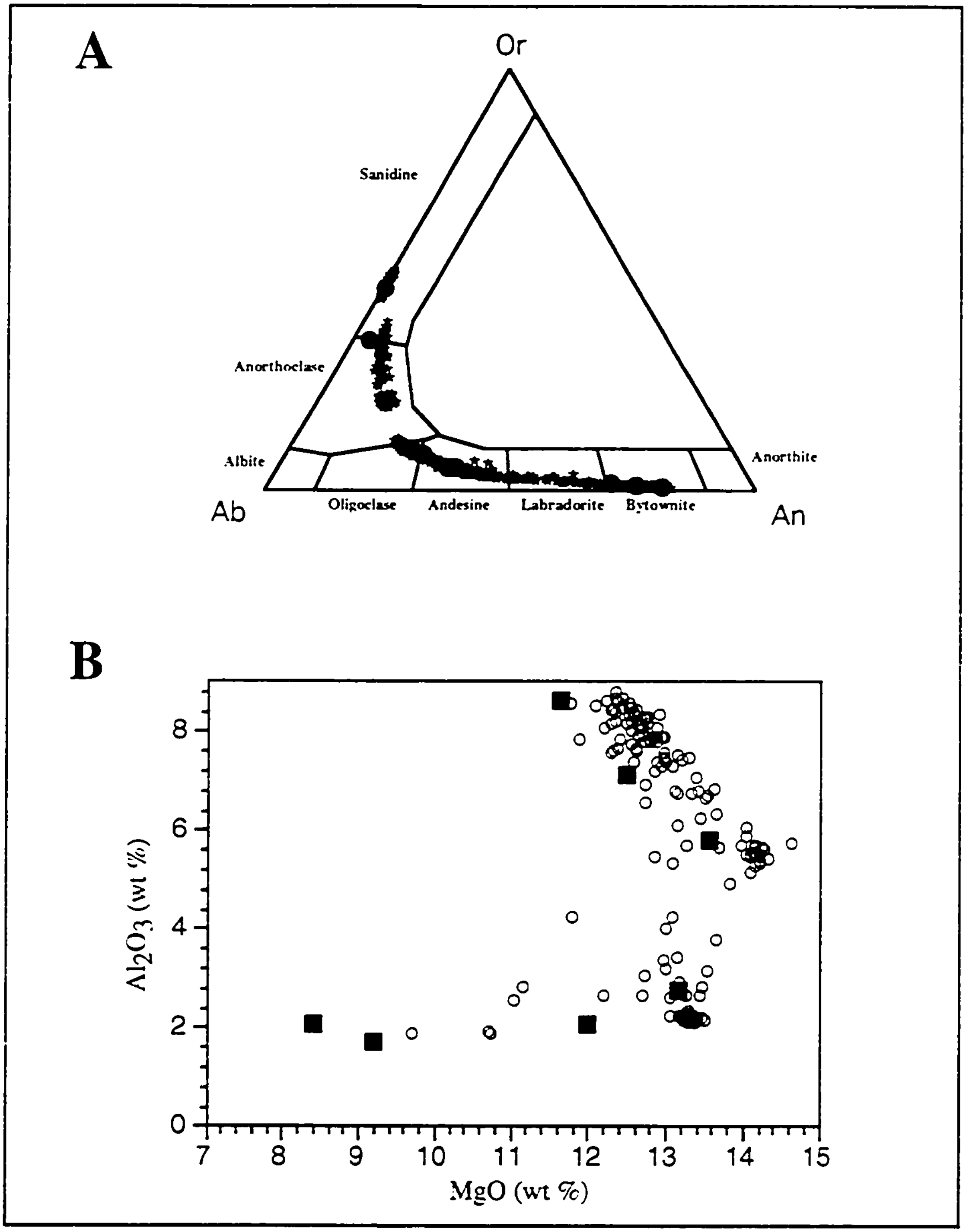

Figure 5.4: Comparison plots (A) Feldspar comparison on An-Ab-Or ternary diagram between DH (★) and Tajao (●) ignimbrites; (B) Pyroxene comparison on MgO vs Al_2O_3 binary diagram between DH (○) and Tajao (■) ignimbrites.

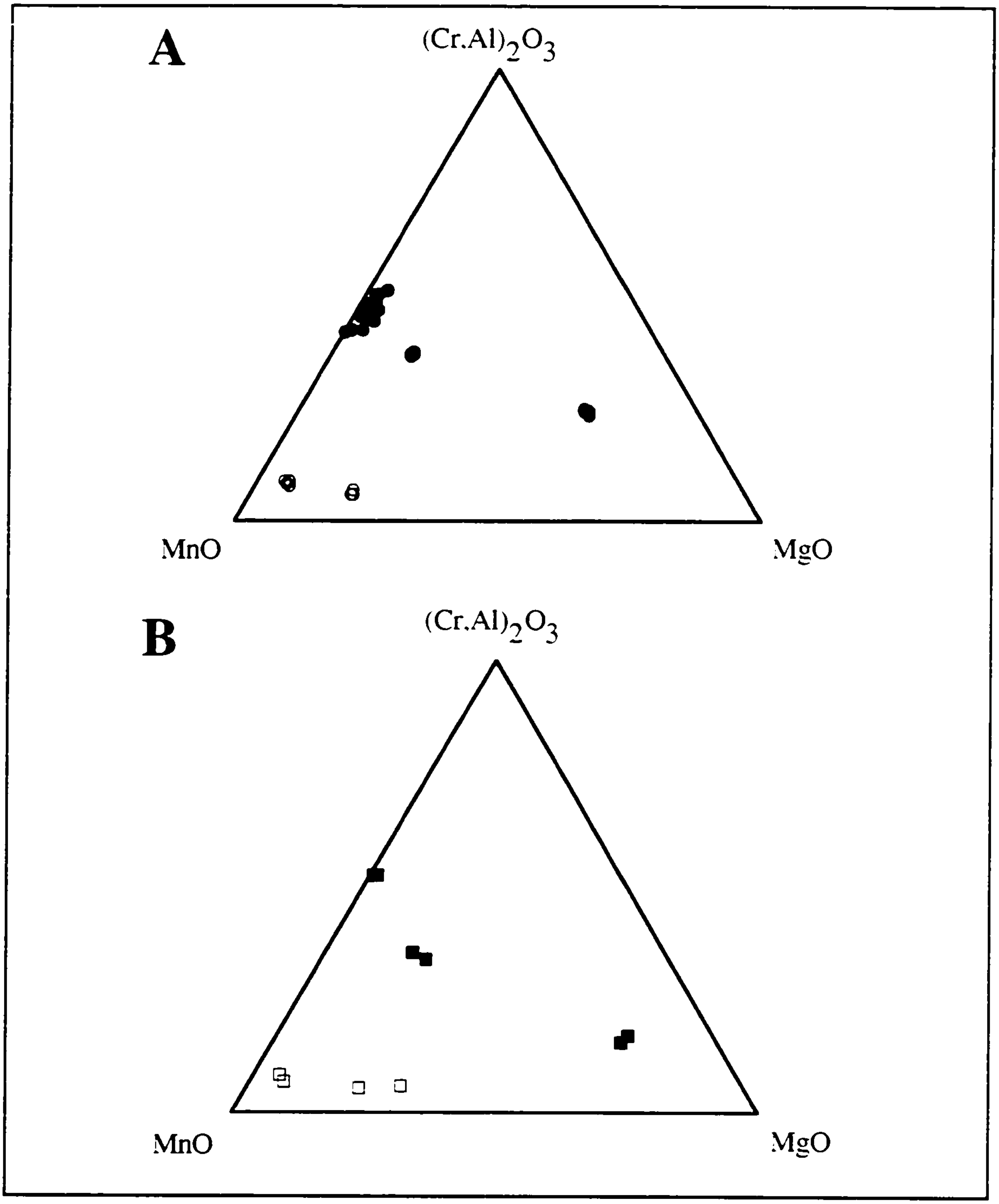

Figure 5.5: Comparison of minor elements in ternary diagram for Fe-Ti oxides. Closed symbols are Ti-magnetite whereas open symbols are ilmenite. (A) Plot of Fe-Ti oxides from DH (circles): (B) Plot of Fe-Ti oxides from Tajao (squares). Data for Tajao from Wolff (1985).

A

B

C

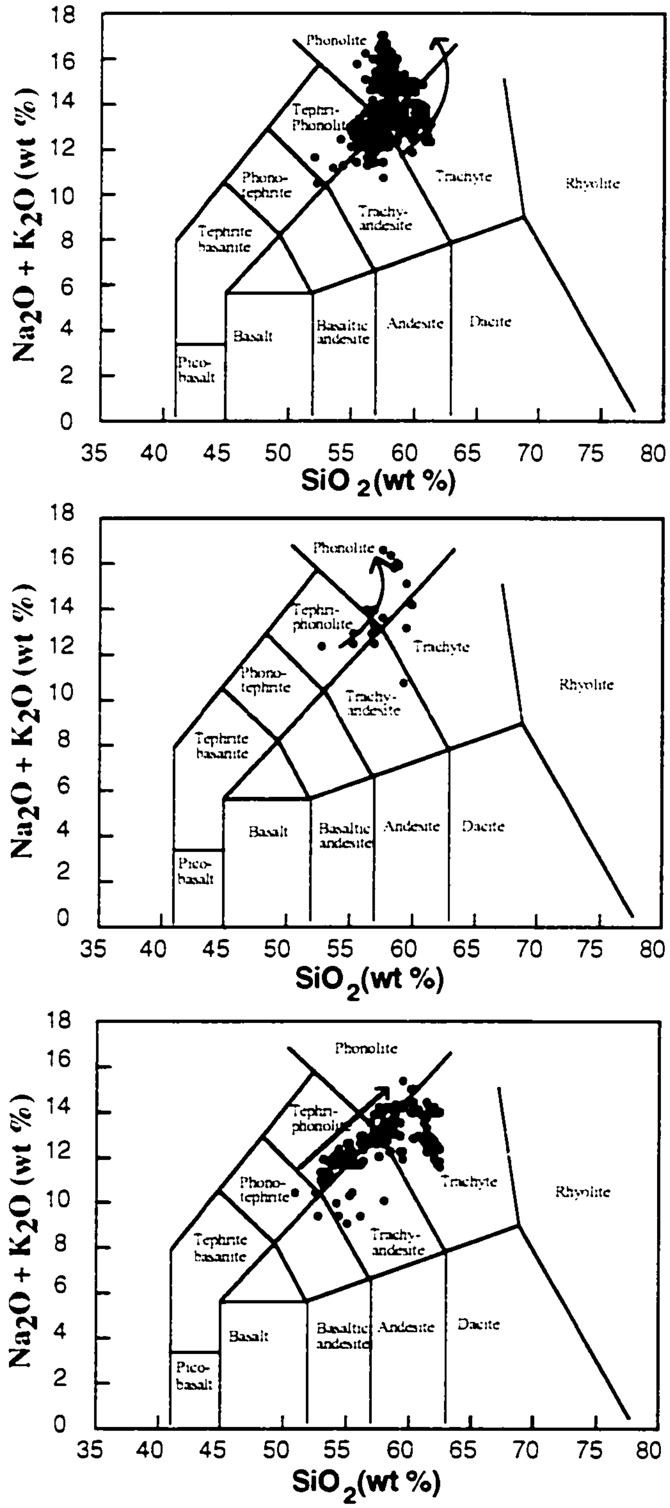

Figure 5.6: Comparison of glass data on total alkali-silica diagrams from (A) Diego Hernández; (B) Tajao (Wolff 1985); and (C) El Abrigo. Projected trends are added to each figure for added comparison.

and El Abrigo may have given a more complete picture of the magma chamber prior to eruption. As it is sampling was limited due to time constraints as part of the attended field trip.

(3) Many of the textures described have been misinterpreted by previous workers due to incomplete work and the knowledge base of the time. It is quite possible that the textures here may be re-interpreted as a better understanding of growth and dissolution crystals, particularly feldspars, under non-equilibrium conditions becomes available through experimental work. Such is the case for the dissolution/reprecipitation mechanism described by Johannes et al. (1993). Their experimental work has shown that a plagioclase crystal will melt and reprecipitate a plagioclase crystal more calcic than its original crystal. A literature search revealed no natural examples considered to originate from this process, but feldspars from Diego Hernández seem to compare to their described mechanism.

References Cited

Alvarez, W. 1990. Geologic evidence for the plate-driving mechanism: the continental undertow hypothesis and the Australian-Antarctic discordance. Tectonics, **9**: 1213-1220.

Anderson, A. T. 1976. Magma mixing: petrological process and volcanological tool. Journ. Volcanol. Geotherm. Res., **1**: 3-33.

Anderson, A. T., Jr. 1984. Probable relations between plagioclase zoning and magma dynamics, Fuego Volcano, Guatemala. Amer. Mineral., **69**: 660-676.

Arana, V., Marti, J., Aparicio, A., Garcia-Cacho, L., and Garcia-Garcia, R. 1994. Magma mixing in alkaline magmas: An example from Tenerife, Canary Islands. Lithos, **32**: 1-19.

Bacon, C. R. 1986. Magmatic inclusions in silicic and intermediate volcanic rocks. Journal of Geophysical Research, **91**: 6091-6112.

Baker, D. R. 1990. Chemical interdiffusion of dacite and rhyolite: anhydrous measurements at 1 atm and 10 kbar, application of transition state theory, and diffusion in zoned magma chambers. Contrib. Mineral. Petrol., **104**: 407-423.

Bardintzeff, J.-M. 1992. Magma mixing processes in volcanic contexts; a thermodynamic approach with the examples of St. Vincent Soufriere Volcano, West Indies and Cerro Chiquito, Guatemala. Terra Nova, **4**: 553-566.

Blake, S., and Campbell, I. H. 1986. The dynamics of magma-mixing during flow in volcanic conduits. Contrib. Mineral. Petrol, **94**: 72-81.

Blake, S., and Ivey, G. N. 1986. Magma-mixing and the dynamics of withdrawal from stratified reservoirs. Journ. Volcanol. Geotherm. Res., **27**: 153-178.

Blake, S., and Koyaguchi, T. 1991. Insights on magma mixing model from volcanic rocks. *In* Enclaves and Granitic Petrology. *Edited by* Didier, J. and Barbarin, B. Elsevier, pp. 403-413.

Borley, G. D. 1974. Aspects of volcanic history and petrology of the island of Tenerife, Canary Islands. Proc. Geol. Ass., **85**: 259-279.

Brooks, C. K., and Printzlau, I. 1978. Magma mixing in mafic alkaline volcanic rocks: the evidence from relict phenocryst phases and other inclusions. Journ. Vol. Geotherm. Res, **4**: 315-331.

Brown, W. L., and Parsons, I. 1994. Feldspars in igneous rocks. *In* Feldspars and Their Reactions. *Edited by* Parsons, I. Kluwer Academic Publishers, pp. 449-499.

Bryan, S. 1995. Bandas del Sur pyroclastics, southern Tenerife. *In* A Field Guide to the Central Volcanic Complex of Tenerife (Canary Islands). *Edited by* Marti, J. and Mitjavilla, J. pp. 39-45.

Bryan, S. E., Cas, R. A. F., Martí, J., and Foster, D. A. 1997. The outercaldera record of phonolitic explosive volcanism from the Las Cañadas edifice, Tenerife Canary Islands. Submitted

Bunsen. 1851. Über die Prozesse der vulkanischen Gesteinsbildurgen Islands. Annal Phys. Chem., **83**: 197-272.

Cas, R. A. F., and Wright, J. V. 1987. Volcanic Successions: Modern & Ancient. *Edited by* Cas, R. A. F. and Wright, J. V. Chapmen & Hall, pp. 528p.

Deer, W. A., Howie, R. A., and Zussman, J. 1989. An Introduction to the Rock Forming Minerals. Lngman Scientific & Technical, pp. 528.

Dungan, M. A., and Rhodes, J. M. 1978. Residual glasses and melt inclusions in basalts from DSDP legs 45 and 46: evidence for magma mixing. Contrib. Mineral. Petrol., **67**: 417-431.

Eichelberger, J. C. 1978. Andesitic volcanism and crustal evolution. Nature, **275**: 21-27.

Fisher, R. V., and Schmincke, H.-U. 1984. Pyroclastic Rocks. Springer-Verlag, pp. 472.

Freundt, A., and Schmincke, H.-U. 1992. Mixing of rhyolite, trachyte and basalt magma erupted from a vertically and laterally zoned reservoir, composite flow P1, Gran Canaria. Contrib. Mineral. Petrol., **112**: 1-19.

Freundt, A., and Tait, S. R. 1986. The entrainment of high-viscosity magma into low-viscosity magma in eruption conduits. Bull. Volcanol., **48**: 325-339.

Frost, T. P., and Mahood, G. A. 1987. Field, chemical and physical constraints on mafic-felsic interaction in the Lamark Granodiorite, Sierra Nevada, California. Geol. Soc. Am. Bull., **99**: 272-291.

Gardner, J. E., Carey, S., Rutherford, M. J., and Sigurdsson, H. 1995. Petrologic diversity in Mount St. Helens dacites during the last 4,000 years: implications for magma mixing. Contrib. Mineral. Petrol., **119**: 224-238.

Hildreth, W. 1981. Gradients in silicic magma chambers: implications for lithospheric magmatism. Journ. Geophys. Res., **86**: 10,153-10,192.

Hildreth, W. 1984. The compositionally zoned eruption of 1912 in the Valley of Ten Thousand Smokes, Katmai National Park, Alaska. Journ. Volcanol. Geotherm. Res., **18**: 1-56.

Hofmann, A. W. 1980. Diffusion in natural silicate melts: a critical review. *In* Physics of Magmatic Processes. *Edited by* Hargraves, R. B. Princeton University Press, pp. 385-417.

Johannes, W., Koepke, J., and Behrens, H. 1993. Partial melting reactions of plagioclase and plagioclase-bearing systems. *In* Feldspars and Their Reactions. *Edited by* Parsons, I. Kluwer Academic Publishers, pp. 161-194.

Kouchi, A., and Sunagawa, I. 1985. A model for mixing basaltic and dacitic magmas as deduced from experimental data. Contrib. Mineral. Petrol., **89**: 17-23.

Koyaguchi, T. 1985. Magma mixing in a conduit. Journal of Volcanology and Geothermal Research, **25**: 365-369.

Marsh, B. D. 1988. Crystal capture, sorting, and retention in convecting magma. Geol. Soc. Amer. Bull., **100**: 1720-1737.

Marsh, B. D. 1989. Magma chambers. Ann. Rev. Earth Planet. Sci., **17**: 439-474.

Marsh, B. D. 1996. Solidification fronts and magmatic evolution. MIneral. Mag., **60**: 5-40.

Martí, J., Ablay, G. L., Redshaw, L. T., and Sparks, R. S. J. 1994a. Experimental studies of collapse calderas. Journ. Geolo. Soc. London, **151**: 919-929.

Martí, J., and Mitjavilla, J. 1995. A Field Guide to the Central Volcanic Complex of Tenerife (Canary Islands). Casa de Los Volcanoes No. 4. pp. 156.

Martí, J., Mitjavila, J., and Araña, V. 1994b. Stratigraphy, structure and geochronology of the Las Cañadas caldera (Tenerife, Canary Islands). Geol. Mag., **131**: 715-727.

Martí, J., Mitjavila, J., and Villa, I. M. 1990. Stratigraphy and K-Ar ages of the Diego Hernández wall and their significance on the Las Cañadas caldera formation (Tenerife, Canary Islands). Terra Nova, **2**: 148-153.

Martí, J., Mitjavila, J. M., and Arana, V. 1995. The Las Canadas Edifice and caldera. *In* A Field Guide to the Central Volcanic Complex of Tenerife (Canary Islands). *Edited by* Marti, J. and Mitjavila, J. M. pp. 19-38.

Mitjavila, J., and Villa, I. M. 1993. Temporal evolution of the Diego Hernández Formation (Las Cañadas, Tenerife) and confirmation of the age of the caldera using the 40Ar/39Ar method. Revista de la Sociedad Geológica de Españdas, **6**: 61-65.

Nelson, S. T., and Montana, A. 1992. Sieve-textured plagioclase in volcanic rocks produced by rapid decompression. American Mineralogist, **77**: 1242-1249.

Nixon, G. T., and Pearce, T. H. 1987. Laser-interferometry study of oscillatory zoning in plagioclase: the record of magma mixing and phenocryst recycling in calc-alkaline magma chambers, Iztaccihuatl volcano, Mexico. Amer. Mineral., **72**: 1144-1162.

Pearce, T. H. 1993. Recent work on oscillatory zoning in plagioclase. *In* Feldspars and their reactions. *Edited by* Parsons, I. Kluwer Academic Publishers, pp. 313-349.

Pearce, T. H., and Clark, A. H. 1989. Nomarski interference contrast observations of textural details in volcanic rocks. Geology, **17**: 757-759.

Pearce, T. H., and Kolisnik, A. M. 1990. Observations of plagioclase zoning using interference imaging. Earth-Science Reviews, **29**: 9-26.

Pearce, T. H., Russell, J. K., and Wolfson, I. 1987. Laser-interference and Nomarski interference imaging of zoning profiles in plagioclase phenocrysts from the May 18, 1980, eruption of Mount St. Helens, Washington. Amer. Mineral., **72**: 1131-1143.

Shelley, D. 1993. Igneous and metamorphic rocks under the microscope: classification, textures, microstructures and mineral preferred orientations. Chapman & Hall, pp. 445.

Sigurdsson, H., and Sparks, R. S. J. 1981. Petrology of rhyolitic and mixed magma ejecta from the 1975 eruption of Askja, Iceland. Journ. Petrol., **22**: 41-84.

Singer, B. S., Dungan, M. A., and Layne, G. D. 1995. Textures and Sr, Mg, Fe, K, and Ti compositional profiles in volcanic plagioclase: clues to the dynamics of calc-alkaline magma chambers. Amer. Mineral., **80**: 776-798.

Singer, B. S., Pearce, T. H., Kolisnik, A. M., and Myers, J. D. 1993. Plagioclase zoning in Mid-Pleistocene lavas from the Seguam volcanic center, central Aleutian arc, Alaska. Amer. Mineral., **78**: 143-157.

Smith, J. V., and Brown, W. L. 1988. Feldspar Minerals. Springer-Verlag, pp. 828.

Sparks, R. S. J., and Marshall, L. A. 1986. Thermal and mechanical constraints on mixing between mafic and silicic magmas. Journ. Volcanol. Geotherm. Res., **29**: 99-124.

Sparks, R. S. J., and Sigurdsson, H. 1977. Magma mixing: a mechanism for triggering acid explosive eruptions. Nature, **267**: 315-318.

Sparks, R. S. J., and Wilson, L. 1976. A model for the formation of ignimbrite by gravitational column collapse. J. Geol. Soc. Lon., **132**: 441-451.

St. Seymour, K., Vlassopoulos, D., Pearce, T. H., and Rice, C. 1990. The record of magma chamber processes in plagioclase phenocrysts at Thera volcano, Aegean volcanic arc, Greece. Contrib. Mineral. Petrol., **104**: 73-84.

Stimac, J. A., and Pearce, T. H. 1992. Textural evidence of mafic-felsic magma interaction in dacite lavas, Clear Lake, California. Amer. Mineral., **77**: 795-809.

Swanson, S. E., Nye, C. J., Miller, T. P., and Avery, V. F. 1994. Geochemistry of the 1989-1990 eruption of Redoubt Volcano: Part II. Evidence from mineral and glass chemistry. Journal of Volcan. Geotherm. Res., **62**: 453-468.

Thompson, R. A., and Dungan, M. A. 1985. The petrology and geochemistry of the Handkerchief Mesa mixed magma complex, San Juan Mountains, Colorado. Journ. Volcanol. Geotherm. Res., **26**: 251-274.

Tsuchiyama, A. 1985. Dissolution kinetics of plagioclase in the melt of the system diopside-albite-anorthite, and the origin of dusty plagioclase in andesites. Contrib. Mineral. Petrol., **89**: 1-16.

Tsuchiyama, A., and Takahashi, E. 1983. Melting kinetics of a plagioclase feldspar. Contrib. Mineral. Petrol., **84**: 345-354.

Valentin, A., Albert-Beltran, J. F., and Diez, J. L. 1990. Geochemical and geothermal constraints on magma bodies associated with historic activity, Tenerife (Canary Islands). Journ. Volcanol. Geotherm. Res., **44**: 251-264.

Vogel, T. A., Ryerson, F. J., Nobel, D. C., and Younker, L. W. 1987. Limits to magma mixing based on chemistry and mineralogy of pumice fragments erupted from a chemically zoned magma body. Journ. Geol., **95**: 659-670.

Walker, G. P. L. 1981. Volcanological applications of pyroclastic studies. *In* Tephra Studies. *Edited by* Self, S. and Sparks, R. S. J. pp. 391-404.

Watson, E. B., and Baker, D. R. 1990. Chemical diffusion in magmas: an overview of experimental results and geochemcial applications. *In* Physical Chemistry of Magmas. *Edited by* Kushiro, L. L. P. I. pp. 120-151.

Wiede, R. A. 1987. Evidence for stratification of basic, silicic and hybrid magmas in the Newark Island layered intrusion, Nain, Labrador. Geology, **15**: 349-352.

Wilson, L., Sparks, R. S. J., and Walker, G. P. L. 1980. Explosive volcanic eruptions - IV. The control of magma properties and conduit geometry on eruption column behavior. Geophys. J. R. Soc., **63**: 117-148.

Wolff, J. A. 1985. Zonation, mixing and eruption of silica-undersaturated alkaline magma: a case study from Tenerife, Canary Islands. Geol. Mag., **122**: 623-640.

Wolff, J. A., and Storey, M. 1984. Zoning in highly alkaline magma bodies. Geol. Mag., **121**: 563-575.

Wright, J. V., Smith, A. L., and Self, S. 1980. A working terminology of pyroclastic deposits. Journ. Volcanol. Res., **8**: 315-336.

Appendix A

The following five tables are intended to show from where each electron microprobe analysis comes from in terms of a particular pumice type.

Table A.A: Diego Hernández Wall - Mafic Pumice (CS-010A)

Mineral	Analyses id				
Feldspar	LT009	LT011	011	013	015
	LT010	LT016	012	014	016
Glass	G003	G008	G013	LT046	
	G004	G009	G014	LT047	
	G005	G010	G015	LT048	
	G006	G011	G016	LT052	
	G007	G012	G017	LT053	
Pyroxene	LT049	LT050	LT020		
Nepheline	LT012	LT013			
Biotite	BT003				
Amphibole	LT051	AM006			

Table A.B: Diego Hernández Wall - Mixed Pumice (CS-010)

Mineral	Analyses id				
Feldspar	017	LT017	LT019	LT068	LT070
	038		LT067	LT069	
Glass	G018	G023	LT034	LT039	LT044
	G019	G024	LT035	LT040	LT045
	G020	G025	LT036	LT041	
	G021	G026	LT037	LT042	
	G022	G045	LT038	LT043	
Biotite	BT002				
Pyroxene	C001	C002	C003	LT018	
Amphibole	AM004	AM005			
Oxides	036	040	042	044	
	037	041	043		

Table A.C: Diego Hernández Wall - Mafic Pumice (TK-9C)

Mineral	Analyses id				
Feldspar	001E	006	LT001	LT006	LT066
	001F	007	LT002	LT007	
	001G	008	LT003	LT008	
	003	009	LT004	LT064	
	004	010	LT005	LT065	
Glass	LT028	LT031	G040	G043	
	LT029	LT032	G041	G044	
	LT030	LT033	G042		
Biotite	BT001				
Pyroxene	C004	C005	C006		
Amphibole	AM001	AM002	AM003		
Oxides	025	030	034		
	026	031	035		

Table A.D: Diego Hernández Wall - Mixed Pumice (CS-011)

Mineral	Analyses id	
Feldspar	018	
Nepheline	LT014	LT015

Table A.E: Diego Hernández Wall - Felsic Pumice (TK-19D)

Mineral	Analyses id			
Feldspar	LT058	LT059	LT060	LT061
Glass	G048	G051		

LT - line traverse

Table A.1: All EMP analysis of glass for Diego Hernandez wall

	G003-001	G003-002	G003-003	G003-004	G003-005	G003-006	G003-007	G003-008	G003-009	G004-001
Na_2O	10.558	10.836	10.399	10.068	9.764	9.557	9.802	9.789	9.749	7.146
Al_2O_3	20.784	20.665	20.732	20.899	20.539	20.408	20.523	20.585	20.798	18.304
SiO_2	57.21	57.239	57.26	58.12	57.248	57.415	57.388	57.92	57.367	54.628
MgO	0.188	0.181	0.204	0.23	0.235	0.295	0.263	0.316	0.231	1.056
TiO_2	0.359	0.334	0.376	0.414	0.441	0.505	0.475	0.506	0.418	1.275
K_2O	5.681	5.565	5.696	5.635	5.808	5.718	5.634	5.862	5.777	5.582
CaO	0.768	0.639	0.824	0.899	1.088	1.066	1.157	1.057	0.836	2.505
FeO_t	2.696	2.815	2.799	2.783	2.806	2.943	2.946	2.76	2.697	3.77
MnO	0.235	0.223	0.259	0.226	0.219	0.223	0.22	0.186	0.182	0.146
F										
Cl										
Total	98.479	98.497	98.549	99.274	98.148	98.13	98.408	98.981	98.055	94.412

Table A.1: Con't

	G004-002	G004-003	G005-001	G005-002	G005-003	G005-004	G006-001	G007-002	G007-003	G007-004
Na_2O	7.298	6.932	6.763	6.682	6.95	7.228	6.868	9.853	9.424	9.804
Al_2O_3	18.789	18.581	18.333	18.05	18.174	18.594	18.334	20.961	21.031	20.985
SiO_2	55.896	54.769	54.359	53.784	53.78	55.194	54.131	57.749	57.341	57.314
MgO	1.209	1.582	1.218	1.582	1.773	1.29	1.727	0.146	0.134	0.197
TiO_2	1.367	1.528	1.438	1.717	1.763	1.482	1.706	0.32	0.355	0.35
K_2O	5.535	5.324	4.83	4.786	5.213	4.859	4.597	5.901	5.826	5.923
CaO	2.591	2.923	3.311	3.391	3.266	3.086	4.197	0.803	0.766	0.795
FeO_t	4.079	4.442	4.402	4.952	4.891	4.516	4.665	2.632	2.701	2.75
MnO	0.154	0.116	0.115	0.152	0.165	0.116	0.142	0.198	0.21	0.205
F										
Cl										
Total	96.918	96.197	94.769	95.096	95.975	96.365	96.667	98.563	97.788	98.323

Table A.1: Con't

	G007-005	G007-006	G007-007	G008-001	G008-002	G008-003	G008-004	G008-005	G009-001	G009-002
Na_2O	9.556	9.511	9.38	6.917	6.63	6.666	6.816	6.67	6.749	6.896
Al_2O_3	20.772	20.913	20.769	18.613	18.333	18.27	18.418	18.248	18.247	18.265
SiO_2	57.352	57.577	57.26	54.744	53.395	54.04	54.832	54.389	53.26	53.731
MgO	0.167	0.193	0.201	1.179	1.417	1.297	1.655	1.375	1.559	1.085
TiO_2	0.328	0.382	0.353	1.544	1.569	1.525	1.659	1.577	1.656	1.393
K_2O	5.887	6.013	5.945	4.865	5.082	4.763	4.974	5.156	5.247	5.584
CaO	0.972	0.814	0.813	3.362	3.347	3.6	3.517	3.239	3.457	2.793
FeO_T	2.855	2.802	2.855	4.515	4.984	4.533	5.053	4.593	4.973	4.285
MnO	0.246	0.259	0.224	0.131	0.167	0.174	0.157	0.164	0.146	0.165
F										
Cl										
Total	98.135	98.464	97.8	95.87	94.924	94.868	97.081	95.411	95.294	94.197

Table A.1: Con't

	G010-003	G010-004	G011-001	G011-002	G011-003	G011-004	G011-005	G011-006	G011-007	G011-008
Na_2O	6.61	6.625	10.024	10.161	10.28	9.728	9.466	10.55	9.26	10.368
Al_2O_3	18.02	17.987	20.573	20.646	20.672	20.786	19.282	20.962	18.479	21.172
SiO_2	54.166	54.076	57.585	57.425	57.945	57.527	58.031	56.876	57.927	57.71
MgO	1.608	1.88	0.249	0.268	0.259	0.267	0.547	0.163	0.765	0.246
TiO_2	1.569	1.736	0.51	0.457	0.453	0.458	0.854	0.347	1.128	0.368
K_2O	4.91	5.168	5.549	5.563	5.567	5.62	5.577	5.46	5.495	5.574
CaO	3.549	3.512	0.985	0.96	0.939	1.054	1.412	0.788	1.679	0.784
FeO_T	4.823	4.923	2.804	2.806	2.626	2.863	3.175	2.698	3.538	2.463
MnO	0.194	0.129	0.235	0.218	0.152	0.279	0.19	0.217	0.215	0.151
F										
Cl										
Total	95.449	96.036	98.514	98.504	98.893	98.582	98.534	98.061	98.486	98.836

Table A.1: Con't

	G011-009	G011-010	G011-011	G011-012	G011-013	G011-014	G012-001	G012-002	G012-003	G012-004
Na_2O	8.18	9.27	9.237	9.424	10.173	8.915	9.365	9.706	9.688	10.29
Al_2O_3	18.722	20.168	20.301	20.341	20.67	19.763	19.765	20.378	20.431	21.164
SiO_2	57.651	57.332	57.121	56.9	57.133	58.963	57.957	57.986	57.754	57.564
MgO	0.724	0.375	0.281	0.281	0.249	0.355	0.404	0.346	0.302	0.157
TiO_2	1.151	0.591	0.453	0.5	0.391	0.729	0.651	0.502	0.553	0.347
K_2O	5.661	5.487	5.412	5.489	5.576	5.89	5.634	5.564	5.476	5.529
CaO	1.641	1.201	1.101	1.1	0.904	0.979	1.232	1.252	1.061	0.894
FeO_T	3.65	2.834	2.857	2.934	2.675	2.606	3.018	2.781	2.79	2.691
MnO	0.156	0.211	0.156	0.2	0.204	0.124	0.209	0.184	0.199	0.215
F										
Cl										
Total	97.536	97.469	96.919	97.169	97.975	98.324	98.235	98.699	98.254	98.851

Table A.1: Con't

	G012-005	G012-006	G013-001	G013-002	G013-003	G013-004	G013-005	G013-006	G014-001	G014-002
Na_2O	9.893	9.109	6.813	6.837	7.072	6.927	6.887	6.703	6.061	6.749
Al_2O_3	21.089	20.949	18.606	18.328	18.066	18.868	18.424	18.288	17.503	18.386
SiO_2	57.259	57.636	54.553	53.971	53.906	55.055	55.423	55.225	52.166	55.06
MgO	0.186	0.191	1.678	1.778	1.539	1.328	1.84	1.303	2.98	1.441
TiO_2	0.328	0.361	1.725	1.618	1.503	1.594	1.743	1.55	2.34	1.625
K_2O	5.594	5.706	5.05	4.526	4.929	4.559	4.675	4.708	4.502	5.047
CaO	0.926	0.994	3.604	4.206	3.743	3.532	3.83	3.318	4.498	3.328
FeO_T	2.778	2.736	4.976	5.205	4.388	4.834	4.887	4.889	5.854	4.933
MnO	0.272	0.174	0.155	0.127	0.156	0.153	0.158	0.143	0.103	0.163
F										
Cl										
Total	98.325	97.856	97.16	96.596	95.302	96.85	97.867	96.127	96.007	96.732

Table A.1: Con't

	G014-003	G014-004	G014-005	G014-006	G014-007	G014-008	G015-001	G015-002	G015-003	G016-001
Na_2O	6.672	6.825	6.666	6.587	6.812	6.473	7.697	7.71	7.927	9.588
Al_2O_3	18.638	18.803	19.063	18.634	18.489	18.319	18.67	18.756	18.88	20.307
SiO_2	55.814	55.332	56.018	55.765	55.314	54.299	59.536	59.486	59.617	58.193
MgO	1.393	1.325	1.173	1.34	1.213	1.574	0.561	0.598	0.555	0.389
TiO_2	1.615	1.626	1.417	1.533	1.579	1.588	0.941	0.846	0.805	0.529
K_2O	4.809	4.884	3.447	4.258	4.739	4.079	5.793	5.832	5.954	5.719
CaO	3.323	3.176	3.869	3.809	3.072	4.214	1.5	1.138	1.333	1.129
FeO_T	4.537	4.869	4.312	4.713	4.699	4.989	3.068	2.879	2.88	2.843
MnO	0.149	0.16	0.116	0.147	0.164	0.157	0.147	0.139	0.114	0.165
F										
Cl										
Total	96.95	97	96.081	96.786	96.081	95.692	97.913	97.384	98.065	98.862

Table A.1: Con't

	G016-002	G016-003	G016-005	G016-006	G016-007	G017-001	G017-002	G017-003	G017-004	G018-001
Na_2O	9.092	9.471	9.168	9.077	9.456	6.711	6.716	6.918	7.275	9.535
Al_2O_3	19.876	20.297	19.887	19.72	20.101	18.249	18.494	19.07	18.684	21.244
SiO_2	58.014	57.574	57.963	57.678	57.809	53.539	54.932	55.671	55.508	57.496
MgO	0.404	0.383	0.527	0.512	0.4	1.418	1.426	1.348	1.45	0.194
TiO_2	0.668	0.548	0.815	0.783	0.554	1.61	1.507	1.583	1.649	0.386
K_2O	5.662	5.586	5.699	5.437	5.562	5.081	4.75	4.164	5.274	5.749
CaO	1.324	1.222	1.538	1.429	1.227	3.288	3.556	3.73	3.101	0.996
FeO_T	2.969	2.882	3.174	3.033	2.928	5.076	4.701	4.494	4.736	2.545
MnO	0.175	0.193	0.145	0.184	0.167	0.155	0.161	0.191	0.134	0.175
F										
Cl										
Total	98.184	98.156	98.916	97.853	98.204	95.127	96.243	97.169	97.811	98.32

Table A.1: Con't

	G018-002	G018-003	G018-004	G018-005	G018-006	G018-007	G018-008	G018-009	G019-001	G019-002
Na_2O	9.518	9.33	8.78	9.676	9.181	9.013	9.45	8.164	9.341	9.218
Al_2O_3	21.221	20.443	20.561	21.406	19.949	19.801	20.6	18.756	20.508	20.508
SiO_2	57.195	57.92	58.763	57.109	57.588	58.15	56.368	59.321	57.348	58.074
MgO	0.202	0.354	0.31	0.196	0.41	0.46	0.313	0.511	0.289	0.268
TiO_2	0.395	0.548	0.567	0.353	0.663	0.703	0.465	0.87	0.469	0.465
K_2O	5.698	5.701	5.932	5.746	5.69	5.821	5.735	6.041	5.447	5.728
CaO	0.989	1.182	0.986	0.891	1.136	1.3	1.119	1.477	1.144	1.125
FeO_T	2.61	2.818	2.515	2.6	2.922	3.034	2.787	2.849	2.76	2.623
MnO	0.196	0.198	0.132	0.19	0.2	0.196	0.198	0.118	0.191	0.18
F										
Cl										
Total	98.024	98.494	98.546	98.167	97.739	98.478	97.035	98.107	97.497	98.189

Table A.1: Con't

	G020-001	G020-002	G020-003	G020-004	G020-005	G020-006	G020-007	G020-008	G020-009	G020-010
Na_2O	6.054	6.224	6.925	6.975	6.544	6.767	6.809	6.78	6.741	6.812
Al_2O_3	17.637	17.816	18.526	18.467	17.872	18.192	18.16	18.41	18.465	18.013
SiO_2	54.157	52.792	55.056	55.22	53.999	54.226	55.772	55.137	55.746	53.894
MgO	1.24	1.828	1.159	1.222	1.503	1.449	1.124	1.092	1.244	1.491
TiO_2	1.545	1.685	1.442	1.482	1.575	1.626	1.448	1.322	1.317	1.567
K_2O	4.494	4.448	4.907	5.005	4.563	4.88	5.335	5.367	5.164	4.855
CaO	3.268	4.126	2.448	2.935	3.547	3.248	2.685	2.474	2.899	3.485
FeO_T	4.751	4.952	4.304	4.334	4.992	4.526	4.149	4.111	4.195	4.749
MnO	0.163	0.143	0.145	0.128	0.164	0.142	0.144	0.176	0.146	0.136
F										
Cl										
Total	93.309	94.014	94.912	95.768	94.759	95.056	95.626	94.869	95.917	95.002

Table A.1: Con't

	G020-011	G020-012	G020-013	G021-001	G021-003	G022-001	G022-002	G022-003	G022-004	G022-005
Na_2O	6.796	6.943	6.605	7.043	6.822	3.4	7.854	8.889	8.103	7.808
Al_2O_3	18.11	18.223	18.394	18.604	18.049	21.354	18.72	20.525	18.849	18.748
SiO_2	54.652	54.515	55.019	54.747	55.49	60.504	59.831	59.045	57.985	58.107
MgO	1.45	1.555	1.178	1.403	1.327	0.29	0.604	0.39	0.961	0.957
TiO_2	1.606	1.635	1.468	1.582	1.364	0.494	0.89	0.64	1.095	1.139
K_2O	4.865	4.764	5.073	5.362	5.038	5.718	5.836	5.763	5.592	5.614
CaO	3.402	3.363	3.144	3.018	3.247	1.187	1.415	1.4	1.957	1.977
FeO_T	4.802	4.91	4.305	4.551	4.519	2.8	2.857	2.911	3.991	3.825
MnO	0.133	0.167	0.165	0.168	0.171	0.202	0.149	0.169	0.161	0.139
F										
Cl										
Total	95.816	96.075	95.351	96.478	96.027	95.949	98.156	99.732	98.694	98.314

Table A.1: Con't

	G023-001	G023-002	G023-003	G023-004	G023-005	G023-006	G023-007	G023-008	G023-009	G023-010
Na_2O	6.155	6.894	6.895	6.779	6.84	6.61	6.662	6.775	6.581	6.534
Al_2O_3	17.676	18.557	18.606	18.398	18.537	18.041	18.289	18.613	18.607	18.358
SiO_2	52.488	55.874	54.881	55.671	54.995	54.688	54.722	56.476	55.961	55.903
MgO	2.336	1.129	1.192	1.317	1.368	1.52	1.46	1.076	1.48	1.074
TiO_2	1.991	1.481	1.47	1.521	1.619	1.629	1.645	1.342	1.404	1.279
K_2O	4.313	5.372	5.212	4.567	4.811	5.173	5.244	5.357	4.784	4.956
CaO	4.348	2.778	2.991	3.187	3.443	3.338	3.131	2.706	3.567	2.969
FeO_T	5.528	4.506	4.441	4.535	4.667	4.878	4.772	4.068	4.514	4.117
MnO	0.157	0.146	0.144	0.175	0.106	0.164	0.163	0.155	0.136	0.134
F										
Cl										
Total	94.992	96.737	95.832	96.15	96.386	96.041	96.088	96.568	97.034	95.324

Table A.1: Con't

	G023-011	G023-012	G024-001	G024-002	G024-003	G024-004	G024-005	G024-006	G024-007	G024-008
Na_2O	6.692	6.919	9.171	8.817	8.79	8.663	8.562	8.487	8.93	9.389
Al_2O_3	18.425	18.532	20.463	20.147	20.559	20.157	19.337	19.379	21.109	21.35
SiO_2	56.516	57.573	58.713	57.621	57.342	59.288	59.11	59.741	57.193	57.707
MgO	1.166	1.111	0.401	0.337	0.357	0.401	0.567	0.58	0.255	0.221
TiO_2	1.371	1.293	0.615	0.572	0.551	0.674	0.858	0.912	0.444	0.397
K_2O	5.402	5.49	5.522	5.69	5.529	5.859	5.862	5.717	5.722	5.794
CaO	2.8	2.455	1.128	1.249	1.209	1.085	1.427	1.393	1.108	1.177
FeO_T	4.126	3.81	2.985	2.875	2.984	3.013	3.195	3.014	2.532	2.816
MnO	0.15	0.111	0.16	0.181	0.199	0.154	0.161	0.138	0.158	0.174
F										
Cl										
Total	96.648	97.294	99.158	97.489	97.52	99.294	99.079	99.361	97.451	99.025

Table A.1: Con't

	G024-009	G025-001	G025-002	G025-003	G025-004	G025-005	G025-006	G025-007	G025-008	G025-009
Na_2O	8.508	9.43	10.01	10.68	9.593	9.661	9.719	10.387	10.402	10.663
Al_2O_3	20.077	20.913	20.5	20.915	20.817	20.979	20.971	20.802	20.741	20.858
SiO_2	56.77	57.411	56.269	57.234	57.643	56.854	57.53	57.748	57.27	57.204
MgO	0.395	0.19	0.198	0.196	0.22	0.189	0.177	0.213	0.166	0.16
TiO_2	0.601	0.323	0.403	0.354	0.417	0.369	0.383	0.406	0.351	0.31
K_2O	5.688	5.724	5.646	5.822	5.735	5.445	5.599	5.472	5.591	5.706
CaO	1.28	1.05	0.914	0.698	1.022	1.084	0.753	0.743	0.71	0.72
FeO_T	3.026	2.638	2.774	2.629	2.762	2.725	2.631	2.709	2.824	2.63
MnO	0.137	0.171	0.218	0.239	0.196	0.218	0.174	0.206	0.229	0.221
F										
Cl										
Total	96.482	97.85	96.932	98.767	98.405	97.524	97.937	98.686	98.284	98.472

Table A.1: Con't

	G025-010	G025-011	G025-012	G025-013	G025-014	G025-015	G025-016	G025-017	G025-018	G025-019
Na_2O	10.44	10.022	9.012	8.875	9.8	9.646	10.44	7.709	7.8	7.739
Al_2O_3	20.714	20.911	19.762	19.862	20.919	20.824	20.702	18.719	18.489	18.598
SiO_2	57.295	57.181	58.014	56.894	56.768	56.479	57.62	58.851	58.263	58.253
MgO	0.168	0.183	0.461	0.52	0.198	0.204	0.181	0.823	0.953	0.992
TiO_2	0.356	0.39	0.719	0.634	0.379	0.339	0.332	1.118	1.24	1.186
K_2O	5.737	5.787	5.89	5.825	5.994	5.747	5.812	5.783	5.733	5.813
CaO	0.761	0.804	1.313	1.369	0.888	1.075	0.718	1.666	1.725	1.976
FeO_T	2.671	2.673	3.01	2.947	2.547	2.885	2.576	3.659	3.926	3.976
MnO	0.228	0.242	0.164	0.186	0.186	0.215	0.201	0.159	0.155	0.131
F										
Cl										
Total	98.37	98.193	98.375	97.112	97.679	97.414	98.582	98.487	98.284	98.664

Table A.1: Con't

	G025-020	G025-021	G025-022	G026-001	G026-002	G026-003	G026-004	G040-001	G040-002	G040-003
Na_2O	8.24	8.14	7.688	7.117	7.102	7.351	6.927	6.734	7.592	7.535
Al_2O_3	18.84	19.002	18.953	18.829	19.01	18.323	18.171	18.356	18.497	18.379
SiO_2	58.952	59.734	59.07	56.557	58.458	56.222	55.411	59.985	59.599	60.004
MgO	0.607	0.438	0.597	1.101	0.886	1.206	1.294	0.572	0.559	0.56
TiO_2	0.931	0.752	0.873	1.368	1.125	1.287	1.504	0.679	0.663	0.694
K_2O	5.841	5.908	5.982	5.589	5.012	5.57	5.211	5.685	5.54	5.719
CaO	1.373	1.212	1.384	2.573	2.594	2.748	2.766	1.804	1.718	1.713
FeO_T	3.06	2.873	3.151	4.207	3.625	3.999	4.481	2.587	2.669	2.566
MnO	0.136	0.167	0.131	0.12	0.124	0.162	0.138	0.102	0.136	0.107
F								0.133	0.145	0.118
Cl								0.153	0.153	0.151
Total	97.98	98.226	97.829	97.461	97.936	96.868	95.903	96.699	97.175	97.462

Table A.1: Con't

	G040-004	G041-001	G041-002	G042-001	G042-002	G042-003	G042-004	G042-005	G043-001	G043-002
Na_2O	7.629	7.431	7.099	7.21	7.188	7.144	7.083	7.32	7.397	7.862
Al_2O_3	18.407	18.643	18.621	18.757	18.826	18.513	18.257	18.106	18.464	18.96
SiO_2	59.878	59.534	58.909	57.532	58.54	57.642	57.072	57.377	57.519	60.44
MgO	0.567	0.547	0.555	0.982	0.915	0.999	0.983	1.048	1.387	0.618
TiO_2	0.677	0.703	0.654	1.116	1.057	1.054	1.108	1.109	1.455	0.864
K_2O	5.696	5.61	5.47	5.017	5.171	4.941	5.17	5.038	5.017	5.782
CaO	1.778	1.771	1.713	1.955	2.098	2.058	2.095	2.326	3.013	1.597
FeO_T	2.569	2.397	2.481	3.305	3.223	3.402	3.449	3.508	4.427	2.853
MnO	0.093	0.079	0.098	0.141	0.157	0.147	0.169	0.148	0.171	0.134
F	0.132									
Cl	0.15									
Total	97.486	96.715	95.6	96.015	97.175	95.9	95.386	95.98	98.85	99.11

Table A.1: Con't

	G043-003	G044-001	G044-003	G044-004	G045-001	G045-002	G045-003	G048-001	G048-002	G048-003
Na_2O	8.644	7.011	7.242	7.527	8.67	8.725	8.867	8.199	7.637	7.23
Al_2O_3	20.441	17.908	18.271	18.64	19.253	19.649	19.637	22.476	22.249	22.193
SiO_2	57.58	50.331	55.083	54.027	56.9	57.183	56.558	57.722	57.448	57.255
MgO	0.625	1.833	1.477	1.41	0.601	0.721	0.687	0.196	0.176	0.179
TiO_2	0.658	1.913	1.585	1.591	0.898	0.935	0.944	0.283	0.3	0.329
K_2O	5.319	4.123	4.748	4.749	5.811	5.682	5.755	5.537	5.441	5.516
CaO	2.075	5.361	3.144	3.156	1.592	1.758	1.741	0.65	0.497	0.547
FeO_T	3.294	6.997	4.816	4.557	3.015	3.35	3.118	2.571	2.541	2.464
MnO	0.151	0.23	0.155	0.162	0.168	0.19	0.171	0.234	0.25	0.26
F										
Cl										
Total	98.787	95.707	96.521	95.819	96.938	98.193	97.478	97.868	96.539	95.973

Table A.1: Con't

	G048-005	G048-006	G048-009	G048-010	G048-011	G048-012	G048-013	G048-014	G048-015	G048-016
Na_2O	7.393	8	7.757	7.216	7.727	8.098	6.931	6.706	6.937	6.24
Al_2O_3	22.067	22.142	22.278	21.958	22.026	22.202	20.459	21.907	22.118	22.076
SiO_2	57.404	57.604	57.355	57.56	57.556	57.555	58.403	57.864	57.542	57.499
MgO	0.192	0.183	0.188	0.191	0.187	0.185	0.292	0.251	0.178	0.174
TiO_2	0.324	0.38	0.321	0.286	0.28	0.324	0.548	0.457	0.315	0.289
K_2O	5.482	5.546	5.36	5.379	5.5	5.513	5.45	5.5	5.387	5.386
CaO	0.611	0.682	0.723	0.537	0.672	0.628	0.805	0.482	0.52	0.543
FeO_T	2.573	2.667	2.556	2.541	2.584	2.615	2.517	2.309	2.57	2.593
MnO	0.255	0.248	0.247	0.245	0.241	0.297	0.174	0.183	0.237	0.228
F										
Cl										
Total	96.301	97.452	96.785	95.913	96.773	97.417	95.579	95.659	95.804	95.028

Table A.1: Con't

	G048-018	G048-020	G048-022	G048-023	G048-024	G048-025	G048-026	G048-027	G048-028	G048-029
Na_2O	7.054	8.206	7.474	7.205	6.779	7.218	7.535	7.987	6.432	7.542
Al_2O_3	21.864	22.535	22.406	22.416	22.428	21.822	22.287	22.356	21.954	22.364
SiO_2	56.199	57.634	57.409	57.402	57.507	56.563	57.093	57.749	57.474	56.96
MgO	0.184	0.173	0.198	0.188	0.182	0.197	0.181	0.178	0.165	0.198
TiO_2	0.286	0.314	0.344	0.316	0.345	0.332	0.332	0.333	0.342	0.32
K_2O	5.416	5.481	5.485	5.483	5.472	5.402	5.414	5.536	5.258	5.48
CaO	0.484	0.663	0.603	0.65	0.567	0.689	0.703	0.679	0.529	0.629
FeO_T	2.578	2.572	2.559	2.53	2.587	2.528	2.616	2.594	2.662	2.513
MnO	0.228	0.235	0.225	0.229	0.234	0.203	0.253	0.3	0.271	0.227
F										
Cl										
Total	94.293	97.813	96.703	96.419	96.101	94.954	96.414	97.712	95.087	96.233

Table A.1: Con't

	G048-030	G048-031	G048-033	G048-034	G048-035	G048-036	G048-037	G048-040	G048-041	G048-042
Na_2O	7.721	7.806	7.55	7.741	7.904	8.416	7.218	7.74	8.055	6.223
Al_2O_3	22.553	22.437	22.248	22.48	22.686	22.508	22.365	22.281	22.214	21.611
SiO_2	57.226	57.432	57.357	57.333	57.23	57.646	57.539	57.378	57.429	56.86
MgO	0.181	0.193	0.188	0.177	0.207	0.175	0.187	0.178	0.173	0.188
TiO_2	0.373	0.333	0.328	0.332	0.358	0.34	0.344	0.298	0.344	0.295
K_2O	5.322	5.506	5.413	5.423	5.363	5.565	5.424	5.427	5.518	5.257
CaO	0.62	0.643	0.472	0.609	0.553	0.667	0.592	0.619	0.677	0.574
FeO_T	2.568	2.606	2.451	2.574	2.368	2.654	2.615	2.588	2.595	2.574
MnO	0.245	0.237	0.209	0.23	0.194	0.252	0.248	0.23	0.261	0.247
F										
Cl										
Total	96.809	97.193	96.216	96.899	96.863	98.223	96.532	96.739	97.266	93.829

Table A.1: Con't

	G048-043	G048-044	G048-046	G051-001	G051-002	G051-003	G051-004	G051-006	G051-007	G051-008
Na_2O	7.971	7.966	7.061	6.361	6.894	6.21	7.534	6.793	8.19	7.25
Al_2O_3	22.441	22.3	21.771	22.097	22.1	22.217	22.227	22.225	22.408	22.203
SiO_2	57.249	57.451	57.481	57.289	57.166	57.098	57.271	57.639	57.518	57.558
MgO	0.189	0.174	0.195	0.174	0.173	0.174	0.168	0.18	0.173	0.164
TiO_2	0.334	0.365	0.296	0.309	0.322	0.288	0.327	0.303	0.304	0.352
K_2O	5.43	5.42	5.37	5.353	5.342	5.283	5.464	5.391	5.577	5.37
CaO	0.606	0.607	0.54	0.479	0.494	0.5	0.545	0.609	0.667	0.579
FeO_T	2.551	2.538	2.577	2.618	2.586	2.515	2.584	2.646	2.652	2.625
MnO	0.214	0.268	0.219	0.193	0.256	0.226	0.237	0.234	0.238	0.271
F										
Cl										
Total	96.985	97.089	95.51	94.873	95.333	94.511	96.357	96.02	97.727	96.372

Table A.1: Con't

	G051-009	G051-010	G051-012	G051-013	G051-015	G051-017	G051-019	G051-020	G051-021	G051-023
Na_2O	7.209	6.99	7.02	7.578	6.386	7.936	6.782	7.445	7.619	8.822
Al_2O_3	22.213	22.23	21.968	22.133	22.135	22.407	21.984	21.986	22.235	22.378
SiO_2	57.487	57.961	57.396	57.591	57.371	57.375	56.49	57.545	56.412	57.12
MgO	0.167	0.164	0.168	0.172	0.176	0.178	0.155	0.177	0.181	0.175
TiO_2	0.349	0.302	0.334	0.349	0.324	0.29	0.302	0.308	0.284	0.333
K_2O	5.335	5.322	5.346	5.373	5.376	5.522	5.38	5.443	5.502	5.49
CaO	0.553	0.586	0.53	0.579	0.587	0.608	0.391	0.542	0.658	0.631
FeO_T	2.646	2.591	2.638	2.594	2.619	2.667	2.541	2.608	2.579	2.598
MnO	0.229	0.263	0.266	0.254	0.223	0.247	0.252	0.244	0.27	0.261
F										
Cl										
Total	96.188	96.409	95.666	96.623	95.197	97.23	94.277	96.298	95.74	97.808

Table A.1: Con't

	G051-024	G051-025	LT028-001	LT028-002	LT028-004	LT028-005	LT028-006	LT028-007	LT028-008	LT028-010
Na_2O	8.115	7.476	7.437	7.538	6.754	6.756	7.341	6.678	7.42	7.598
Al_2O_3	22.365	22.267	18.545	18.252	17.899	18.676	18.761	18.671	18.711	18.904
SiO_2	57.376	57.007	57.387	56	57.324	59.922	59.818	59.716	60.303	60.09
MgO	0.194	0.184	1.404	1.163	0.796	0.663	0.606	0.588	0.615	0.604
TiO_2	0.324	0.323	1.444	1.391	1.027	0.875	0.901	0.813	0.914	0.876
K_2O	5.63	5.385	5.03	4.479	5.272	5.651	5.536	5.614	5.715	5.728
CaO	0.628	0.663	3.161	2.938	1.968	1.664	1.66	1.545	1.521	1.387
FeO_T	2.699	2.624	4.418	4.267	3.33	2.966	2.82	2.934	2.947	2.948
MnO	0.266	0.237	0.141	0.147	0.107	0.136	0.121	0.101	0.156	0.182
F										
Cl										
Total	97.597	96.166	98.967	96.175	94.477	97.309	97.564	96.66	98.302	98.317

Table A.1: Con't

	LT028-011	LT028-012	LT028-013	LT028-014	LT028-015	LT029-001	LT029-002	LT029-006	LT029-011	LT029-012
Na_2O	7.133	7.579	7.13	7.583	7.069	7.095	7.003	6.749	7.793	7.406
Al_2O_3	18.786	18.874	18.954	18.855	18.894	18.082	18.177	18.213	19.186	19.103
SiO_2	60.353	60.542	60.702	60.566	60.498	56.929	57.122	55.44	60.623	60.249
MgO	0.626	0.617	0.609	0.567	0.591	1.646	1.411	1.464	0.645	0.606
TiO_2	0.866	0.854	0.873	0.922	0.88	1.543	1.452	1.553	0.853	0.906
K_2O	5.913	5.847	5.985	5.805	5.924	5.033	5.169	4.804	5.688	5.689
CaO	1.497	1.569	1.491	1.456	1.43	3.333	3.115	3.202	1.652	1.602
FeO_T	2.956	2.901	2.823	2.893	2.808	4.621	4.538	4.632	2.854	2.839
MnO	0.157	0.126	0.156	0.132	0.137	0.124	0.128	0.16	0.121	0.126
F										
Cl										
Total	98.287	98.909	98.723	98.779	98.231	98.406	98.115	96.217	99.415	98.526

Table A.1: Con't

	LT029-013	LT030-001	LT030-005	LT030-007	LT030-008	LT030-010	LT030-011	LT030-012	LT030-013	LT030-014
Na_2O	4.294	7.427	6.532	6.951	7.231	7.573	7.408	7.432	7.707	7.708
Al_2O_3	19.177	18.422	17.215	17.496	18.183	18.745	19.012	18.82	18.933	19.008
SiO_2	61.054	57.407	56.887	56.751	54.722	59.572	60.408	60.14	60.743	60.218
MgO	0.583	1.416	1.699	1.218	1.135	0.612	0.6	0.577	0.58	0.594
TiO_2	0.871	1.443	1.61	1.357	1.347	0.882	0.875	0.871	0.886	0.866
K_2O	5.87	5.115	4.896	4.597	4.324	5.588	5.719	5.845	5.837	5.719
CaO	1.533	3.013	3.28	2.951	3.073	1.546	1.544	1.519	1.471	1.464
FeO_T	2.946	4.206	4.815	4.284	4.407	2.961	2.799	2.95	2.747	2.931
MnO	0.157	0.128	0.167	0.135	0.167	0.124	0.105	0.141	0.156	0.129
F										
Cl										
Total	96.485	98.577	97.101	95.74	94.589	97.603	98.47	98.295	99.06	98.637

Table A.1: Con't

	LT031-001	LT031-002	LT031-003	LT031-004	LT031-005	LT032-001	LT032-002	LT032-007	LT032-008	LT033-001
Na_2O	7.024	6.592	6.287	6.536	6.699	7.87	7.366	7.217	7.426	7.347
Al_2O_3	18.282	18.844	18.911	18.873	18.652	19.03	18.697	18.728	18.869	18.275
SiO_2	57.174	59.17	59.619	59.426	58.984	56.399	55.857	60.015	60.625	56.589
MgO	0.595	0.579	0.579	0.612	0.691	1.27	1.318	0.734	0.583	1.529
TiO_2	0.843	0.906	0.916	0.916	0.932	1.268	1.353	1.002	0.887	1.539
K_2O	5.555	5.742	5.503	5.551	5.742	5.07	5.11	5.766	5.805	4.883
CaO	1.634	1.44	1.558	1.471	1.601	3.089	3.116	1.776	1.562	3.04
FeO_T	2.743	2.854	2.844	2.761	2.903	4.366	4.571	3.056	2.982	4.389
MnO	0.127	0.119	0.141	0.171	0.153	0.152	0.158	0.132	0.137	0.135
F	0.114	0.161	0.139	0.16	0.163					
Cl	0.146	0.143	0.154	0.144	0.139					
Total	94.156	96.45	96.557	96.522	96.559	98.514	97.546	98.426	98.876	97.726

Table A.1: Con't

	LT033-002	LT033-003	LT033-004	LT033-007	LT033-008	LT033-009	LT033-010	LT033-011	LT034-001	LT034-002
Na_2O	6.852	7.005	7.457	6.969	6.82	7.83	7.736	7.291	7.523	6.846
Al_2O_3	18.051	18.417	19.034	18.234	18.289	19.11	19.094	18.902	18.452	18.533
SiO_2	56.298	56.603	58.88	54.553	55.744	56.167	59.082	58.742	55.506	55.739
MgO	1.537	1.456	1.13	1.26	1.521	1.255	0.957	0.722	1.267	1.468
TiO_2	1.574	1.406	1.182	1.455	1 669	1.486	1.103	1.029	1.471	1.541
K_2O	4.937	4.931	5.164	4.689	4.81	4.881	5.237	5.43	5.248	5.132
CaO	3.174	3.093	2.466	2.918	3.229	2.63	2.262	1.927	2.969	3.224
FeO_T	4.286	4.346	3.62	4.046	4.805	4.38	3.527	3.142	4.518	4.685
MnO	0.131	0.124	0.118	0.1	0.152	0.161	0.142	0.136	0.138	0.176
F										
Cl										
Total	96.84	97.381	99.051	94.224	97.039	97.9	99.14	97.321	97.092	97.344

Table A.1: Con't

	LT034-003	LT034-004	LT034-009	LT034-010	LT034-011	LT034-012	LT034-013	LT034-014	LT034-015	LT035-001
Na_2O	7.154	7.051	9.036	8.855	8.26	7.992	9.249	8.898	8.934	8.783
Al_2O_3	18.527	18.725	21.127	21.116	22.092	19.584	20.797	20.687	20.559	19.411
SiO_2	56.052	56.136	57.326	57.032	53.657	56.43	57.915	57.739	57.552	55.41
MgO	1.343	1.231	0.264	0.224	0.264	0.318	0.329	0.332	0.293	0.807
TiO_2	1.409	1.442	0.411	0.394	0.379	0.555	0.57	0.57	0.551	0.96
K_2O	5.119	5.226	5.409	5.465	5.186	5.303	5.491	5.617	5.515	5.364
CaO	3.164	2.866	1.142	1.08	1.14	1.155	1.178	1.223	1.218	1.744
FeO_T	4.364	4.549	2.742	2.632	2.68	2.696	2.764	2.746	2.773	3.62
MnO	0.166	0.141	0.229	0.21	0.217	0.216	0.197	0.21	0.244	0.129
F										
Cl										
Total	97.298	97.367	97.686	97.008	93.875	94.249	98.49	98.022	97.639	96.228

Table A.1: Con't

	LT035-002	LT035-003	LT035-004	LT035-005	LT035-006	LT035-007	LT035-008	LT035-009	LT035-010	LT036-001
Na_2O	8.645	8.431	8.746	8.485	8.907	9.234	9.347	9.226	9.458	8.504
Al_2O_3	20.259	19.516	19.646	19.216	19.827	20.935	21.221	21.18	21.465	19.312
SiO_2	55.405	55.075	55.559	55.585	55.279	55.784	57.32	57.274	57.295	55.562
MgO	0.612	0.899	0.837	0.939	0.922	0.207	0.186	0.198	0.19	1.081
TiO_2	0.761	1.012	0.975	1.069	0.839	0.361	0.355	0.332	0.362	1.218
K_2O	5.089	4.979	5.382	5.139	5.198	5.582	5.806	5.741	5.635	5.474
CaO	1.612	2.305	1.695	2.237	2.169	1.177	1.04	0.836	0.817	2.209
FeO_T	3.212	3.668	3.353	3.77	3.457	2.723	2.518	2.553	2.606	3.912
MnO	0.127	0.138	0.162	0.229	0.187	0.227	0.185	0.176	0.198	0.143
F										
Cl										
Total	95.722	96.023	96.355	96.669	96.785	96.23	97.978	97.516	98.026	97.415

Table A.1: Con't

	LT036-002	LT036-006	LT036-007	LT037-001	LT037-002	LT037-003	LT037-007	LT037-008	LT037-009	LT037-010
Na_2O	8.176	10.174	9.474	6.826	6.615	6.247	8.982	8.686	9.098	8.713
Al_2O_3	18.963	21.159	21.351	18.089	19.043	18.422	20.651	20.96	20.713	20.917
SiO_2	53.13	57.164	57.835	55.581	54.775	53.932	56.64	57.764	57.532	57.33
MgO	1.002	0.213	0.183	1.179	1.398	1.502	0.406	0.361	0.352	0.341
TiO_2	1.16	0.381	0.391	1.24	1.383	1.453	0.644	0.517	0.601	0.525
K_2O	5.157	5.544	5.614	4.756	4.824	4.662	5.459	5.475	5.477	5.581
CaO	1.784	0.83	0.821	2.773	3.412	3.649	1.2	1.256	1.305	1.25
FeO_t	3.814	2.736	2.638	4.347	4.555	4.855	2.91	2.803	2.749	2.543
MnO	0.15	0.195	0.182	0.119	0.182	0.136	0.168	0.179	0.149	0.175
F										
Cl										
Total	93.336	98.396	98.489	94.91	96.187	94.858	97.06	98.001	97.976	97.375

Table A.1: Con't

	LT038-003	LT038-005	LT038-006	LT038-007	LT038-008	LT038-009	LT038-010	LT038-011	LT038-012	LT038-013
Na_2O	6.422	7.417	9.334	8.894	9.26	8.849	9.547	8.829	9.479	9.18
Al_2O_3	17.983	19.475	20.447	20.606	20.398	20.579	21.257	20.52	20.73	20.751
SiO_2	52.646	57.783	55.472	57.105	57.619	57.547	57.331	56.649	57.206	57.531
MgO	1.606	0.34	0.404	0.334	0.408	0.44	0.316	0.603	0.347	0.369
TiO_2	1.518	0.713	0.634	0.555	0.582	0.63	0.562	0.71	0.6	0.596
K_2O	4.914	3.744	5.33	5.53	5.557	5.439	5.649	5.748	5.644	5.634
CaO	3.5	3.031	1.425	1.412	1.332	1.159	0.963	1.131	1.038	1.136
FeO_t	4.898	2.884	2.927	2.821	2.885	2.975	2.514	2.985	2.677	2.708
MnO	0.177	0.112	0.206	0.234	0.19	0.169	0.177	0.133	0.16	0.173
F										
Cl										
Total	93.664	95.499	96.179	97.491	98.231	97.787	98.316	97.308	97.881	98.078

Table A.1: Con't

	LT038-014	LT038-015	LT038-016	LT039-001	LT039-002	LT039-003	LT039-005	LT039-006	LT039-007	LT039-008
Na_2O	9.321	9.172	9.494	8.127	8.17	8.288	9.154	9.378	9.106	9.719
Al_2O_3	20.204	20.796	20.419	18.896	18.81	19.05	20.099	20.588	19.826	20.873
SiO_2	58.013	57.66	57.102	58.561	58.703	58.741	56.952	55.508	57.682	56.916
MgO	0.394	0.356	0.379	0.42	0.41	0.413	0.374	0.259	0.388	0.272
TiO_2	0.671	0.591	0.665	0.825	0.779	0.758	0.657	0.486	0.693	0.495
K_2O	5.659	5.667	5.561	6.054	6.021	6.009	5.946	5.932	6.062	5.92
CaO	1.039	0.991	1.176	1.112	1.083	1.024	1.106	0.938	1.05	0.93
FeO_T	2.612	2.719	2.897	2.46	2.486	2.491	2.556	2.367	2.578	2.43
MnO	0.149	0.201	0.187	0.134	0.153	0.14	0.171	0.172	0.159	0.167
F										
Cl										
Total	98.062	98.153	97.88	96.589	96.615	96.914	97.015	95.628	97.544	97.722

Table A.1: Con't

	LT039-010	LT039-011	LT039-012	LT039-013	LT039-014	LT039-015	LT040-001	LT040-002	LT040-003	LT040-004
Na_2O	9.478	10.103	9.672	10.097	9.775	9.67	8.084	8.187	9.539	8.804
Al_2O_3	20.248	20.852	20.263	21.122	20.297	20.405	18.701	18.831	20.826	19.931
SiO_2	56.999	56.802	57.637	57.03	57.901	57.441	59.123	58.328	57.798	55.078
MgO	0.306	0.288	0.236	0.246	0.322	0.301	0.409	0.434	0.321	0.291
TiO_2	0.544	0.514	0.425	0.401	0.622	0.506	0.721	0.72	0.573	0.568
K_2O	6.089	5.856	5.655	5.887	6.075	6.027	5.919	5.819	5.717	5.752
CaO	0.996	0.896	0.813	0.864	0.869	0.844	1.04	1.098	1.131	1.031
FeO_T	2.542	2.517	2.398	2.431	2.403	2.512	2.505	2.46	2.522	2.371
MnO	0.147	0.168	0.169	0.171	0.169	0.173	0.118	0.158	0.141	0.175
F										
Cl										
Total	97.349	97.996	97.268	98.249	98.433	97.879	96.62	96.035	98.568	94.001

Table A.1: Con't

	LT040-005	LT040-006	LT040-007	LT040-008	LT041-001	LT041-002	LT041-003	LT041-004	LT041-005	LT041-006
Na_2O	9.191	9.282	9.489	8.941	8.303	8.309	7.456	8.428	7.746	8.069
Al_2O_3	19.92	20.515	20.321	19.751	18.949	18.93	18.946	18.902	19.15	18.649
SiO_2	57.184	55.832	57.397	55.488	59.154	59.063	59.155	59.038	59.489	57.524
MgO	0.358	0.328	0.351	0.315	0.505	0.481	0.478	0.493	0.484	0.515
TiO_2	0.611	0.54	0.586	0.519	0.809	0.811	0.807	0.835	0.806	0.81
K_2O	5.807	5.619	5.848	5.873	5.852	5.919	5.937	5.987	5.902	5.868
CaO	1.135	1.047	1.086	0.998	1.153	1.161	1.178	1.205	1.216	1.264
FeO_T	2.669	2.521	2.626	2.462	2.565	2.551	2.643	2.646	2.621	2.674
MnO	0.172	0.17	0.196	0.163	0.11	0.13	0.151	0.139	0.125	0.12
F										
Cl										
Total	97.047	95.854	97.9	94.51	97.4	97.355	96.751	97.673	97.539	95.493

Table A.1: Con't

	LT041-007	LT041-012	LT041-013	LT041-014	LT042-001	LT042-002	LT042-003	LT042-004	LT042-005	LT042-006
Na_2O	8.064	9.451	8.586	9.266	9.077	9.365	9.193	8.641	9.102	9.358
Al_2O_3	19.404	20.133	20.082	19.877	20.465	20.939	20.514	19.194	20.494	20.751
SiO_2	59.479	58.047	57.927	57.721	57.397	57.686	57.455	58.889	56.08	57.845
MgO	0.486	0.445	0.522	0.607	0.374	0.343	0.459	0.731	0.36	0.391
TiO_2	0.789	0.7	0.754	0.835	0.576	0.545	0.688	0.943	0.577	0.586
K_2O	6.036	5.87	5.891	6.008	5.767	5.753	5.731	5.815	5.76	5.776
CaO	1.176	1.195	1.268	1.38	1.28	1.349	1.337	1.457	1.192	1.255
FeO_T	2.693	2.814	2.929	3.041	2.83	2.603	2.922	3.29	2.679	2.641
MnO	0.112	0.157	0.177	0.15	0.141	0.156	0.145	0.176	0.183	0.179
F										
Cl										
Total	98.239	98.812	98.136	98.885	97.907	98.739	98.444	99.136	96.427	98.782

Table A.1: Con't

	LT042-007	LT042-008	LT043-001	LT043-002	LT043-003	LT043-004	LT043-005	LT043-006	LT043-007	LT043-008
Na_2O	9.543	9.342	8.564	8.625	8.73	8.729	9.275	8.061	7.735	8.782
Al_2O_3	20.374	20.866	19.929	20.162	19.281	19.87	20.662	19.202	18.78	19.507
SiO_2	57.505	57.51	55.822	54.794	58.242	57.245	56.502	55.152	53.364	54.173
MgO	0.473	0.314	0.672	0.354	0.802	0.721	0.489	0.758	1.01	0.793
TiO_2	0.681	0.511	0.925	0.484	1.024	0.916	0.614	1.024	1.597	1.141
K_2O	5.663	5.894	5.831	5.626	5.61	5.582	5.567	5.045	4.96	5.506
CaO	1.353	1.152	1.609	1.27	1.786	1.773	1.333	2.375	2.636	2.016
FeO_T	3.026	2.781	3.33	2.81	3.42	3.321	2.81	3.719	4.261	3.884
MnO	0.156	0.177	0.113	0.155	0.188	0.193	0.134	0.182	0.183	0.202
F										
Cl										
Total	98.774	98.547	96.795	94.28	99.083	98.35	97.386	95.518	94.526	96.004

Table A.1: Con't

	LT043-009	LT043-010	LT043-011	LT043-012	LT043-013	LT044-001	LT044-005	LT044-007	LT044-008	LT045-001
Na_2O	9.704	10.526	9.595	9.378	9.272	7.556	7.174	7.537	8.098	9.577
Al_2O_3	21.096	21.874	20.765	20.406	20.181	19.043	19.378	20.003	18.888	20.801
SiO_2	56.797	57.162	58.017	58.112	56.796	55.978	55.616	58.214	56.368	57.464
MgO	0.376	0.397	0.439	0.454	0.442	1.124	0.944	0.365	0.611	0.351
TiO_2	0.587	0.581	0.61	0.73	0.626	1.416	1.189	0.655	0.865	0.518
K_2O	5.754	5.344	5.733	5.862	5.816	5.648	5.465	5.915	5.559	5.908
CaO	1.029	1.085	1.199	1.241	1.278	2.309	2.078	1.131	1.504	0.994
FeO_T	2.623	2.743	2.986	2.965	3.012	3.997	3.59	2.641	3.068	2.756
MnO	0.182	0.17	0.188	0.183	0.183	0.139	0.174	0.133	0.155	0.167
F										
Cl										
Total	98.148	99.882	99.532	99.331	97.606	97.21	95.608	96.594	95.116	98.536

Table A.1: Con't

	LT045-002	LT045-003	LT045-004	LT045-005	LT045-006	LT045-007	LT045-008	LT045-009	LT045-010	LT045-011
Na_2O	9.572	9.311	9.269	9.134	8.91	7.484	7.559	7.327	7.355	7.211
Al_2O_3	20.745	20.957	20.825	20.422	20.584	19.072	18.39	18.706	18.733	18.526
SiO_2	57.332	56.957	57.727	58.283	58.553	56.492	55.877	56.218	56.533	56.022
MgO	0.312	0.229	0.268	0.436	0.415	1.189	1.423	1.33	1.428	1.629
TiO_2	0.514	0.422	0.478	0.625	0.623	1.318	1.566	1.559	1.594	1.574
K_2O	5.841	5.904	5.877	5.958	5.889	5.534	4.88	5.473	5.028	5.089
CaO	1.078	1.071	1.09	1.216	1.006	2.745	3.127	2.72	3.502	3.93
FeO_T	2.847	2.698	2.562	2.906	2.718	3.919	4.237	4.247	4.427	4.585
MnO	0.209	0.198	0.161	0.162	0.12	0.135	0.183	0.166	0.165	0.156
F										
Cl										
Total	98.45	97.747	98.257	99.142	98.818	97.888	97.242	97.746	98.765	98.722

Table A.1: Con't

	LT045-012	LT045-013	LT045-014	LT045-015	LT045-019	LT045-020	LT045-021	LT045-022	LT046-001	LT046-002
Na_2O	6.988	7.477	7.173	7.575	8.94	9.326	9.082	9.233	7.588	7.455
Al_2O_3	18.244	18.62	18.799	18.928	20.657	20.891	20.915	20.552	18.391	18.678
SiO_2	53.885	55.437	56.11	56.291	57.098	57.753	57.493	57.804	55.797	56.7
MgO	2.528	1.92	1.57	1.31	0.274	0.309	0.277	0.422	1.499	1.107
TiO_2	1.836	1.76	1.485	1.435	0.525	0.484	0.448	0.646	1.565	1.526
K_2O	4.899	5.184	5.353	5.381	5.939	5.909	5.846	5.844	5.17	4.987
CaO	4.26	3.599	3.313	3.06	0.955	0.982	0.99	1.267	3.454	2.83
FeO_T	5.304	4.682	4.314	4.145	2.565	2.802	2.596	2.786	4.733	4.422
MnO	0.131	0.14	0.163	0.181	0.175	0.187	0.195	0.173	0.191	0.186
F										
Cl										
Total	98.075	98.819	98.28	98.306	97.128	98.643	97.842	98.727	98.388	97.891

Table A.1: Con't

	LT046-003	LT046-004	LT046-005	LT046-006	LT046-007	LT046-008	LT046-009	LT046-010	LT046-012	LT046-013
Na_2O	7.56	7.056	7.423	7.857	7.52	7.599	7.602	8.811	9.344	9.139
Al_2O_3	18.808	18.454	18.414	19.005	18.264	18.631	18.45	20.483	21.544	21.468
SiO_2	56.317	55.659	55.567	57.13	55.154	56.067	55.272	55.822	58.76	58.28
MgO	1.153	1.418	1.745	1.027	1.201	1.574	1.73	0.366	0.173	0.145
TiO_2	1.544	1.552	1.617	1.474	1.496	1.538	1.565	0.409	0.34	0.349
K_2O	5.194	4.811	4.331	5.006	4.053	5.195	5.267	5.848	6.132	6.16
CaO	2.638	3.554	4.413	2.508	3.531	3.173	3.576	0.861	0.671	0.566
FeO_T	4.281	4.508	4.564	3.934	4.293	4.48	4.465	2.912	2.412	2.268
MnO	0.176	0.151	0.158	0.199	0.166	0.145	0.206	0.155	0.143	0.193
F										
Cl										
Total	97.671	97.163	98.232	98.14	95.678	98.402	98.133	95.667	99.519	98.568

Table A.1: Con't

	LT046-014	LT046-015	LT046-016	LT047-001	LT047-002	LT047-003	LT047-004	LT047-005	LT047-006	LT047-007
Na_2O	9.173	9.081	8.99	8.12	7.852	7.182	7.558	6.976	7.293	6.846
Al_2O_3	21.275	21.236	21.188	18.959	18.679	18.474	18.171	18.729	18.044	18.5
SiO_2	57.655	57.726	57.657	58.331	57.412	56.869	55.038	55.752	54.574	55.885
MgO	0.197	0.215	0.206	0.704	0.977	1.363	1.831	1.509	2.012	1.647
TiO_2	0.368	0.396	0.387	1.188	1.154	1.45	1.652	1.55	1.775	1.601
K_2O	5.954	5.852	5.92	5.782	5.417	4.717	5.226	5.591	5.079	4.504
CaO	0.713	0.672	0.61	1.555	2.275	3.628	3.984	3.085	3.931	4.215
FeO_T	2.862	2.979	2.883	3.735	3.898	4.182	4.863	4.737	5.164	4.953
MnO	0.226	0.24	0.2	0.147	0.191	0.129	0.169	0.17	0.183	0.165
F										
Cl										
Total	98.423	98.397	98.041	98.521	97.855	97.994	98.492	98.099	98.055	98.316

Table A.1: Con't

	LT047-008	LT047-009	LT047-010	LT047-011	LT047-012	LT047-016	LT047-017	LT047-018	LT047-019	LT048-001
Na_2O	7.318	5.956	7.761	7.691	8.948	10.477	9.222	9.481	8.283	7.789
Al_2O_3	18.218	16.92	18.599	19.445	20.297	21.676	20.908	20.931	21.042	18.512
SiO_2	55.012	51.972	55.67	56.267	57.258	53.799	58.241	57.185	57.362	55.53
MgO	2.063	4.141	1.27	0.811	0.541	0.202	0.221	0.199	0.196	1.102
TiO_2	1.743	2.632	1.499	1.032	0.601	0.313	0.297	0.35	0.356	1.393
K_2O	4.692	4.207	5.458	5.812	5.934	4.818	4.912	6.06	5.937	4.7
CaO	4.085	5.724	3.233	2.096	1.356	0.726	0.704	0.861	0.896	3.004
FeO_T	5.058	6.621	4.197	3.477	3.151	2.68	2.667	2.897	2.918	4.592
MnO	0.153	0.171	0.16	0.191	0.193	0.217	0.159	0.214	0.206	0.137
F										
Cl										
Total	98.342	98.344	97.847	96.822	98.279	94.908	97.331	98.178	97.196	96.759

Table A.1: Con't

	LT048-002	LT048-003	LT048-004	LT048-005	LT048-006	LT048-007	LT048-008	LT048-009	LT048-011	LT048-012
Na_2O	7.634	8.163	7.264	7.167	7.418	7.794	7.799	7.957	9.279	7.303
Al_2O_3	19.043	19.398	18.506	18.466	18.473	19.375	19.418	19.112	20.68	18.859
SiO_2	57.247	56.653	53.453	54.985	54.683	56.893	57.126	56.764	56.228	55.724
MgO	0.728	1.106	1.166	1.766	1.408	0.836	0.917	1.248	0.253	0.202
TiO_2	1.298	1.527	1.468	1.699	1.505	1.251	1.368	1.338	0.358	0.416
K_2O	4.867	4.889	5.431	4.909	4.871	5.828	4.875	4.266	5.757	5.984
CaO	2.234	2.446	2.261	3.612	3.016	1.376	2.074	3.312	0.823	0.955
FeO_T	3.838	4.178	4.414	4.866	4.466	3.602	3.837	4.527	2.713	2.698
MnO	0.132	0.17	0.165	0.182	0.177	0.172	0.159	0.219	0.21	0.192
F										
Cl										
Total	97.021	98.53	94.128	97.652	96.017	97.127	97.573	98.743	96.301	92.333

Table A.1: Con't

	LT048-013	LT048-014	LT048-015	LT048-016	LT048-017	LT048-018	LT052-001	LT052-002	LT052-003	LT052-004
Na_2O	8.459	9.048	9.178	9.207	8.949	8.732	9.809	8.089	9.741	8.613
Al_2O_3	20.177	20.746	20.858	21.016	21.154	21.174	21.137	21.105	21.014	21.36
SiO_2	55.397	56.468	57.201	57.236	57.531	57.575	57.409	56.695	57.409	57.339
MgO	0.196	0.211	0.201	0.202	0.197	0.186	0.229	0.172	0.166	0.185
TiO_2	0.366	0.347	0.369	0.376	0.372	0.397	0.333	0.328	0.369	0.34
K_2O	6.093	5.838	5.898	5.95	5.983	5.869	5.671	5.672	5.641	5.685
CaO	0.98	0.98	0.943	0.921	0.808	0.765	0.77	0.769	0.84	0.949
FeO_T	2.786	2.667	2.722	2.812	2.809	2.66	2.89	2.884	2.773	2.954
MnO	0.238	0.247	0.262	0.252	0.216	0.22	0.199	0.196	0.223	0.271
F										
Cl										
Total	94.692	96.552	97.632	97.972	98.019	97.578	98.447	95.91	98.176	97.696

Table A.1: Con't

	LT052-005	LT052-006	LT052-008	LT052-009	LT052-010	LT052-011	LT052-012	LT052-013	LT052-015	LT052-016
Na_2O	9.583	8.368	8.922	9.684	8.456	9.76	8.686	10.08	9.827	8.737
Al_2O_3	20.879	21.372	21.196	21.286	21.532	21.124	21.347	21.489	21.272	21.544
SiO_2	56.989	57.508	57.076	57.664	58.115	57.36	57.821	57.864	57.612	58.061
MgO	0.291	0.281	0.165	0.164	0.135	0.173	0.163	0.177	0.196	0.177
TiO_2	0.437	0.47	0.279	0.325	0.359	0.307	0.32	0.336	0.348	0.343
K_2O	5.582	5.716	5.781	5.724	5.859	5.68	5.729	5.716	5.857	5.768
CaO	0.986	0.962	0.839	0.789	0.679	0.818	0.785	0.76	0.752	0.771
FeO_T	3.133	2.948	2.89	2.584	2.322	2.787	2.906	2.557	2.643	2.815
MnO	0.26	0.141	0.23	0.207	0.197	0.199	0.251	0.209	0.26	0.203
F										
Cl										
Total	98.14	97.766	97.378	98.427	97.654	98.208	98.008	99.188	98.767	98.419

Table A.1: Con't

	LT052-017	LT052-018	LT052-019	LT052-020	LT052-021	LT053-001	LT053-002	LT053-003	LT053-004	LT053-005
Na_2O	9.826	8.102	9.604	8.853	9.935	8.033	8.054	9.07	9.569	9.681
Al_2O_3	21.176	20.106	20.407	21.384	21.125	18.516	18.778	19.768	20.721	20.572
SiO_2	57.891	56.38	56.235	57.732	57.137	56.889	57.636	55.734	57.25	57.782
MgO	0.229	0.896	0.367	0.227	0.186	1.261	0.874	0.538	0.289	0.391
TiO_2	0.337	0.841	0.452	0.349	0.318	1.441	1.251	0.632	0.405	0.551
K_2O	5.663	5.373	5.735	5.756	5.753	5.248	4.672	5.508	5.681	5.698
CaO	0.744	2.081	0.83	0.833	0.864	3.201	2.916	1.45	0.871	1.08
FeO_T	2.782	3.57	3.004	2.836	2.794	4.137	4.012	3.175	2.993	3.025
MnO	0.162	0.197	0.172	0.242	0.25	0.176	0.2	0.178	0.163	0.175
F										
Cl										
Total	98.81	97.546	96.806	98.212	98.362	98.902	98.423	96.053	97.942	98.955

Table A.1: Con't

	LT053-006	LT053-007	LT053-008	LT053-009	LT053-010	LT053-011	LT053-012	LT053-013	LT053-014	LT053-015
Na_2O	9.127	9.259	9.033	9.267	9.454	9.873	9.677	10.18	9.919	10.25
Al_2O_3	20.024	19.922	20.108	20.304	20.219	20.603	20.556	20.928	21.017	21.277
SiO_2	57.159	56.911	57.481	57.311	57.772	57.99	57.858	57.983	57.614	58.061
MgO	0.53	0.509	0.644	0.64	0.585	0.393	0.388	0.237	0.206	0.191
TiO_2	0.835	0.633	0.82	0.803	0.739	0.532	0.542	0.38	0.376	0.387
K_2O	5.422	5.345	5.625	5.563	5.567	5.683	5.697	5.713	5.674	5.637
CaO	1.53	1.302	1.615	1.452	1.434	1.046	1.178	0.781	0.83	0.828
FeO_T	3.62	3.39	3.657	3.45	3.394	3.023	3.123	2.657	2.683	2.585
MnO	0.182	0.174	0.166	0.177	0.219	0.144	0.179	0.182	0.211	0.202
F										
Cl										
Total	98.429	97.445	99.149	98.967	99.383	99.287	99.198	99.041	98.53	99.418

Table A.1: Con't

	LT053-016	LT053-018	LT053-019	LT053-020	LT053-021	LT053-022	LT053-023	LT053-024	LT053-025	LT053-026
Na_2O	10.142	9.925	10.525	10.273	10.621	10.379	10.89	10.352	10.699	10.369
Al_2O_3	21.435	21.354	21.213	21.117	21.141	21.085	21.274	21.112	21.188	21.25
SiO_2	58.158	58.192	57.971	57.806	57.108	57.857	57.86	56.909	57.672	57.895
MgO	0.18	0.144	0.171	0.191	0.172	0.163	0.15	0.146	0.169	0.161
TiO_2	0.374	0.355	0.31	0.304	0.307	0.323	0.349	0.306	0.36	0.361
K_2O	5.698	5.813	5.603	5.601	5.518	5.616	5.472	5.596	5.568	5.566
CaO	0.757	0.677	0.835	0.902	0.988	1.024	0.997	0.945	0.906	0.857
FeO_T	2.54	2.412	2.967	2.826	2.712	2.726	2.759	2.648	2.696	2.726
MnO	0.181	0.174	0.236	0.27	0.248	0.255	0.216	0.199	0.237	0.213
F										
Cl										
Total	99.465	99.046	99.831	99.29	98.815	99.428	99.967	98.213	99.495	99.398

Table A.1: Con't

	LT053-027	LT053-028	LT053-029
Na_2O	10.555	10.499	10.822
Al_2O_3	21.136	21.371	21.432
SiO_2	57.506	57.751	57.882
MgO	0.146	0.174	0.168
TiO_2	0.3	0.328	0.301
K_2O	5.556	5.607	5.625
CaO	0.835	0.818	0.771
FeO_T	2.63	2.522	2.545
MnO	0.248	0.196	0.231
F			
Cl			
Total	98.912	99.266	99.777

Table A.2: All EMP analysis of feldspar from Diego Hernandez wall.

	001-083	001-084	001-085	001-086	001-087	001-088	001-089	001-090
SiO_2	59.022	59.498	58.879	59.14	58.713	59.284	58.656	59.302
Al_2O_3	24.953	24.477	25.315	24.889	25.148	24.837	25.377	24.392
FeOT	0.376	0.423	0.431	0.399	0.45	0.411	0.426	0.403
MgO	0.013	0.029	0.018	0.031	0.017	0.032	0.025	0.02
BaO	0.259	0.26	0.225	0.252	0.242	0.267	0.253	0.273
SrO	0.369	0.377	0.343	0.374	0.343	0.279	0.39	0.386
CaO	6.626	6.258	7.1	6.556	6.852	6.583	7.164	5.984
Na_2O	6.719	6.916	6.471	6.79	6.574	6.693	6.567	6.954
K_2O	1.022	1.122	0.957	1.057	0.975	1.042	0.934	1.197
Total	99.36	99.36	99.74	99.49	99.31	99.43	99.79	98.91
				Oxygen = 32.000				
Si	10.666	10.749	10.604	10.676	10.619	10.697	10.572	10.761
Al	5.31	5.208	5.369	5.291	5.357	5.278	5.387	5.212
Fe	0.057	0.064	0.065	0.06	0.068	0.062	0.064	0.061
Mg	0.004	0.008	0.005	0.008	0.005	0.009	0.007	0.005
Ba	0.018	0.018	0.016	0.018	0.017	0.019	0.018	0.019
Ca	1.283	1.211	1.37	1.268	1.328	1.273	1.383	1.163
Na	2.354	2.423	2.26	2.377	2.306	2.342	2.295	2.447
K	0.236	0.259	0.22	0.243	0.225	0.24	0.215	0.277
Ab	60.8	62.2	58.7	61.1	59.8	60.8	59	63
An	33.1	31.1	35.6	32.6	34.4	33	35.5	29.9
Or	6.1	6.7	5.7	6.3	5.8	6.2	5.5	7.1

Table A.2: Con't

	001-091	001-092	001-093	001-094	001-097	001-098	001-099	001-100
SiO_2	58.113	58.835	58.59	58.91	57.768	58.461	59.664	58.142
Al_2O_3	24.816	24.978	24.673	24.863	25.387	25.385	24.537	25.302
FeOT	0.408	0.417	0.396	0.405	0.358	0.43	0.374	0.431
MgO	0.036	0.026	0.016	0.026	0.021	0.01	0.012	0.03
BaO	0.284	0.28	0.224	0.223	0.229	0.154	0.266	0.166
SrO	0.345	0.309	0.352	0.369	0.286	0.34	0.33	0.398
CaO	6.591	6.861	6.255	6.581	7.031	7.231	6.376	7.153
Na_2O	6.816	6.739	6.834	6.787	6.497	6.415	6.772	6.351
K_2O	1.021	1.019	1.124	1.071	0.937	0.905	1.107	0.921
Total	98.43	99.46	98.46	99.24	98.51	99.33	99.44	98.89
				Oxygen = 32.000				
Si	10.618	10.634	10.683	10.664	10.537	10.57	10.76	10.563
Al	5.34	5.317	5.298	5.3	5.453	5.405	5.211	5.414
Fe	0.062	0.063	0.06	0.061	0.055	0.065	0.056	0.065
Mg	0.01	0.007	0.004	0.007	0.006	0.003	0.003	0.008
Ba	0.02	0.02	0.016	0.016	0.016	0.011	0.019	0.012
Ca	1.29	1.329	1.222	1.276	1.374	1.401	1.232	1.392
Na	2.415	2.362	2.416	2.382	2.298	2.249	2.368	2.237
K	0.238	0.235	0.261	0.247	0.218	0.209	0.255	0.213
Ab	61.2	60.2	62	61	59.1	58.3	61.4	58.2
An	32.7	33.9	31.3	32.7	35.3	36.3	32	36.2
Or	6	6	6.7	6.3	5.6	5.4	6.6	5.5

Table A.2: Con't

	001-101	001-102	001-103	001-104	001-105	001-106	001-107	001-108
SiO_2	57.304	60.16	57.612	59.519	57.986	57.475	59.945	57.402
Al_2O_3	25.525	24.016	25.672	24.644	25.731	26.098	24.154	25.392
FeOT	0.35	0.359	0.449	0.397	0.457	0.376	0.392	0.399
MgO	0.023	0.033	0.023	0.027	0.023	0.024	0.025	0.02
BaO	0.169	0.272	0.162	0.239	0.162	0.189	0.319	0.165
SrO	0.317	0.275	0.367	0.351	0.362	0.338	0.375	0.373
CaO	8.115	5.68	7.616	6.606	7.804	8.171	5.757	7.698
Na_2O	5.924	7.134	6.14	6.656	6.045	6.055	7.013	6.21
K_2O	0.729	1.289	0.833	1.057	0.807	0.771	1.322	0.866
Total	98.46	99.22	98.87	99.5	99.38	99.5	99.3	98.53
				Oxygen = 32.000				
Si	10.465	10.862	10.478	10.731	10.489	10.401	10.83	10.486
Al	5.49	5.107	5.498	5.232	5.482	5.562	5.139	5.463
Fe	0.053	0.054	0.068	0.06	0.069	0.057	0.059	0.061
Mg	0.006	0.009	0.006	0.007	0.006	0.006	0.007	0.005
Ba	0.012	0.019	0.012	0.017	0.011	0.013	0.023	0.012
Ca	1.588	1.099	1.484	1.276	1.513	1.584	1.114	1.507
Na	2.098	2.498	2.165	2.327	2.12	2.125	2.457	2.2
K	0.17	0.297	0.193	0.243	0.186	0.178	0.305	0.202
Ab	54.4	64.1	56.4	60.5	55.5	54.7	63.4	56.3
An	41.2	28.2	38.6	33.2	39.6	40.8	28.7	38.6
Or	4.4	7.6	5	6.3	4.9	4.6	7.9	5.2

Table A.2: Con't

	001-109	001-110	001-111	001-112	001-113	001-114	001-115	001-116
SiO_2	58.94	60.133	59.42	58.906	57.348	59.831	64.54	64.884
Al_2O_3	24.889	23.662	24.661	24.377	25.792	24.699	20.035	19.737
FeOT	0.473	0.382	0.376	0.427	0.424	0.374	0.245	0.242
MgO	0.021	0.027	0.032	0.02	0.025	0.02	0.002	0.007
BaO	0.248	0.298	0.272	0.284	0.186	0.291	0.313	0.00
SrO	0.406	0.359	0.332	0.328	0.387	0.39	0.081	0.00
CaO	6.749	5.7	6.402	6.397	7.676	6.32	1.445	1.162
Na_2O	6.587	7.063	6.74	6.653	6.226	6.776	6.602	6.164
K_2O	1.037	1.333	1.108	1.078	0.842	1.16	6.025	6.892
Total	99.35	98.96	99.34	98.47	98.91	99.86	99.29	99.09
				Oxygen = 32.000				
Si	10.66	10.896	10.73	10.735	10.439	10.75	11.69	11.764
Al	5.301	5.049	5.244	5.232	5.529	5.226	4.273	4.214
Fe	0.072	0.058	0.057	0.065	0.065	0.056	0.037	0.037
Mg	0.006	0.007	0.009	0.005	0.007	0.005	0.001	0.002
Ba	0.018	0.021	0.019	0.02	0.013	0.02	0.022	0
Ca	1.308	1.107	1.239	1.249	1.497	1.217	0.28	0.226
Na	2.31	2.482	2.36	2.351	2.198	2.361	2.319	2.167
K	0.239	0.308	0.255	0.251	0.196	0.266	1.392	1.594
Ab	59.9	63.7	61.2	61	56.5	61.4	58.1	54.4
An	33.9	28.4	32.1	32.4	38.5	31.7	7	5.7
Or	6.2	7.9	6.6	6.5	5	6.9	34.9	40

Table A.2: Con't

	001-117	001-118	001-119	001-120	001-121	001-122	001-123	001-124
SiO_2	65.181	64.761	64.698	63.893	65.1	64.181	64.271	64.056
Al_2O_3	19.816	19.483	20.051	20.82	19.888	20.887	20.806	21.082
FeOT	0.202	0.186	0.239	0.296	0.245	0.289	0.271	0.28
MgO	0.00	0.00	0.006	0.008	0.00	0.002	0.00	0.00
BaO	0.026	0.056	0.061	0.46	0.093	0.146	0.162	0.14
SrO	0.013	0.00	0.022	0.105	0.00	0.07	0.028	0.035
CaO	1.238	0.946	1.385	2.023	1.176	2.154	2.169	2.315
Na_2O	6.365	6.081	6.327	6.747	6.268	6.856	6.735	7.034
K_2O	6.82	7.306	6.29	4.946	6.699	4.83	4.969	4.554
Total	99.66	98.82	99.08	99.3	99.47	99.41	99.41	99.5
				Oxygen = 32.000				
Si	11.755	11.793	11.715	11.554	11.755	11.559	11.576	11.522
Al	4.209	4.178	4.276	4.434	4.229	4.43	4.413	4.466
Fe	0.03	0.028	0.036	0.045	0.037	0.044	0.041	0.042
Mg	0	0	0.002	0.002	0	0.001	0	0
Ba	0.002	0.004	0.004	0.033	0.007	0.01	0.011	0.01
Ca	0.239	0.185	0.269	0.392	0.228	0.416	0.419	0.446
Na	2.226	2.147	2.221	2.366	2.195	2.394	2.352	2.453
K	1.569	1.697	1.453	1.141	1.543	1.11	1.142	1.045
Ab	55.2	53.3	56.3	60.7	55.3	61.1	60.1	62.2
An	5.9	4.6	6.8	10.1	5.7	10.6	10.7	11.3
Or	38.9	42.1	36.9	29.3	38.9	28.3	29.2	26.5

Table A.2: Con't

	003-001	003-002	003-003	003-004	003-005	003-007	003-008	003-009
SiO_2	48.163	48.651	56.773	56.008	49.747	48.727	49.653	49.498
Al_2O_3	31.835	31.713	21.386	25.752	30.902	31.714	30.989	31.158
FeOT	0.55	0.54	3.008	1.017	0.606	0.541	0.548	0.544
MgO	0.07	0.066	0.805	0.293	0.07	0.065	0.069	0.063
BaO	na	na	na	na	na	na	na	na
SrO	na	na	na	na	na	na	na	na
CaO	15.645	15.41	5.778	8.859	14.401	15.596	14.542	14.77
Na_2O	2.286	2.401	5.85	5.457	2.908	2.424	2.789	2.808
K_2O	0.154	0.164	3.236	0.815	0.265	0.174	0.203	0.195
Total	98.7	98.95	96.84	98.2	98.9	99.24	98.79	99.04
				Oxygen = 32.000				
Si	8.947	9.006	10.75	10.292	9.193	9	9.18	9.139
Al	6.965	6.913	4.769	5.573	6.725	6.898	6.747	6.775
Fe	0.085	0.084	0.476	0.156	0.094	0.084	0.085	0.084
Mg	0.019	0.018	0.227	0.08	0.019	0.018	0.019	0.017
Ba	na	na	na	na	na	na	na	na
Ca	3.114	3.056	1.172	1.744	2.851	3.086	2.881	2.922
Na	0.823	0.862	2.148	1.944	1.042	0.868	1	1.005
K	0.036	0.039	0.782	0.191	0.062	0.041	0.048	0.046
Ab	20.7	21.8	52.4	50.1	26.3	21.7	25.5	25.3
An	78.4	77.2	28.6	45	72.1	77.2	73.3	73.5
Or	0.9	1	19.1	4.9	1.6	1	1.2	1.2

Table A.2: Con't

	003-010	003-011	003-012	003-013	003-014	003-015	003-016	003-017
SiO_2	49.121	49.734	52.782	50.466	53.198	52.415	48.333	48.615
Al_2O_3	31.4	31.054	29.047	30.688	28.415	29.301	32.029	31.739
FeOT	0.524	0.517	0.61	0.54	0.647	0.6	0.559	0.552
MgO	0.064	0.07	0.08	0.093	0.094	0.085	0.064	0.067
BaO	na	na	na	na	na	na	na	na
SrO	na	na	na	na	na	na	na	na
CaO	15.156	14.543	12.141	13.934	11.514	12.512	15.832	15.477
Na_2O	2.696	2.912	4.14	3.238	4.349	3.831	2.23	2.406
K_2O	0.188	0.203	0.393	0.229	0.524	0.38	0.143	0.186
Total	99.15	99.03	99.19	99.19	98.74	99.12	99.19	99.04
				Oxygen = 32.000				
Si	9.072	9.175	9.661	9.281	9.772	9.605	8.936	8.995
Al	6.829	6.747	6.261	6.646	6.147	6.323	6.974	6.916
Fe	0.081	0.08	0.093	0.083	0.099	0.092	0.086	0.085
Mg	0.018	0.019	0.022	0.025	0.026	0.023	0.018	0.018
Ba	na	na	na	na	na	na	na	na
Ca	2.999	2.875	2.381	2.746	2.266	2.456	3.136	3.068
Na	0.965	1.042	1.469	1.155	1.549	1.361	0.799	0.863
K	0.044	0.048	0.092	0.054	0.123	0.089	0.034	0.044
Ab	24.1	26.3	37.3	29.2	39.3	34.8	20.1	21.7
An	74.8	72.5	60.4	69.4	57.5	62.9	79	77.2
Or	1.1	1.2	2.3	1.4	3.1	2.3	0.9	1.1

Table A.2: Con't

	003-018	003-019	003-020	003-021	003-022	003-023	004-002	004-004
SiO_2	54.525	51.597	51.566	49.344	48.443	48.34	49.059	49.176
Al_2O_3	27.482	29.811	29.653	31.232	31.799	32.149	31.448	31.286
FeOT	0.685	0.531	0.556	0.546	0.575	0.556	0.544	0.597
MgO	0.074	0.079	0.072	0.069	0.072	0.062	0.066	0.065
BaO	na	na	na	na	na	na	na	na
SrO	na	na	na	na	na	na	na	na
CaO	10.568	13.381	13.17	14.759	15.493	15.649	14.939	14.653
Na_2O	4.84	3.515	3.709	2.833	2.361	2.239	2.78	2.836
K_2O	0.57	0.272	0.279	0.202	0.158	0.172	0.199	0.181
Total	98.74	99.19	99.01	98.99	98.9	99.17	99.04	98.79
				Oxygen = 32.000				
Si	9.987	9.468	9.482	9.119	8.977	8.935	9.069	9.105
Al	5.928	6.442	6.421	6.797	6.939	6.998	6.846	6.822
Fe	0.105	0.081	0.086	0.084	0.089	0.086	0.084	0.092
Mg	0.02	0.022	0.02	0.019	0.02	0.017	0.018	0.018
Ba	na	na	na	na	na	na	na	na
Ca	2.074	2.631	2.595	2.922	3.076	3.099	2.959	2.907
Na	1.719	1.251	1.322	1.015	0.848	0.802	0.996	1.018
K	0.133	0.064	0.065	0.048	0.037	0.041	0.047	0.043
Ab	43.8	31.7	33.2	25.5	21.4	20.3	24.9	25.7
An	52.8	66.7	65.2	73.3	77.7	78.6	73.9	73.3
Or	3.4	1.6	1.6	1.2	0.9	1	1.2	1.1

Table A.2: Con't

	004-005	004-006	004-007	004-008	004-009	004-010	004-011	004-012
SiO_2	50.285	49.635	49.209	49.169	49.597	48.913	48.866	49.521
Al_2O_3	30.586	31.067	31.512	31.191	31.281	31.445	31.587	31.164
FeOT	0.571	0.539	0.549	0.555	0.622	0.561	0.584	0.579
MgO	0.064	0.063	0.069	0.073	0.066	0.061	0.051	0.081
BaO	na	na	na	na	na	na	na	na
SrO	na	na	na	na	na	na	na	na
CaO	13.992	14.642	14.939	14.845	14.662	15.105	15.112	14.527
Na_2O	3.26	2.902	2.67	2.847	2.859	2.583	2.594	2.753
K_2O	0.23	0.187	0.18	0.203	0.225	0.159	0.174	0.196
Total	98.99	99.04	99.13	98.88	99.31	98.83	98.97	98.82
				Oxygen = 32.000				
Si	9.273	9.161	9.081	9.102	9.134	9.059	9.04	9.154
Al	6.642	6.753	6.848	6.8	6.785	6.859	6.882	6.784
Fe	0.088	0.083	0.085	0.086	0.096	0.087	0.09	0.09
Mg	0.018	0.017	0.019	0.02	0.018	0.017	0.014	0.022
Ba	na	na	na	na	na	na	na	na
Ca	2.765	2.896	2.954	2.944	2.893	2.997	2.995	2.877
Na	1.166	1.039	0.955	1.022	1.021	0.928	0.931	0.987
K	0.054	0.044	0.042	0.048	0.053	0.038	0.041	0.046
Ab	29.3	26.1	24.2	25.5	25.7	23.4	23.5	25.2
An	69.4	72.8	74.8	73.3	72.9	75.6	75.5	73.6
Or	1.4	1.1	1.1	1.2	1.3	1	1	1.2

Table A.2: Con't

	004-013	004-014	004-015	004-016	004-017	004-018	004-019	004-020
SiO_2	49.623	49.515	50.992	57.445	49.485	48.724	53.144	49.58
Al_2O_3	30.979	31.373	30.22	25.386	31.032	31.626	28.821	31.033
FeOT	0.54	0.63	0.571	0.834	0.584	0.571	0.511	0.588
MgO	0.06	0.075	0.071	0.089	0.064	0.069	0.069	0.071
BaO	na	na	na	na	na	na	na	na
SrO	na	na	na	na	na	na	na	na
CaO	14.573	14.78	13.581	8.05	14.633	15.278	11.964	14.73
Na_2O	2.866	2.78	3.429	5.822	2.793	2.455	4.292	2.797
K_2O	0.209	0.198	0.263	1.167	0.215	0.162	0.334	0.216
Total	98.85	99.35	99.13	98.79	98.81	98.89	99.14	98.82
				Oxygen = 32.000				
Si	9.174	9.117	9.375	10.467	9.156	9.023	9.719	9.141
Al	6.745	6.803	6.543	5.447	6.762	6.897	6.207	6.765
Fe	0.083	0.097	0.088	0.127	0.09	0.088	0.078	0.091
Mg	0.017	0.021	0.019	0.024	0.018	0.019	0.019	0.02
Ba	na	na	na	na	na	na	na	na
Ca	2.887	2.916	2.675	1.572	2.901	3.031	2.344	2.922
Na	1.027	0.992	1.222	2.057	1.002	0.882	1.522	1.004
K	0.049	0.047	0.062	0.271	0.051	0.038	0.078	0.051
Ab	25.9	25.1	30.9	52.7	25.3	22.3	38.6	25.2
An	72.8	73.7	67.6	40.3	73.4	76.7	59.4	73.5
Or	1.2	1.2	1.6	6.9	1.3	1	2	1.3

Table A.2: Con't

	004-021	004-022	004-023	004-024	005-001	005-002	005-003	005-004
SiO_2	55.973	54.65	49.262	49.206	51.548	52.127	51.657	51.171
Al_2O_3	25.786	26.85	31.302	31.483	29.507	29.121	29.878	29.828
FeOт	0.754	0.843	0.606	0.603	0.589	0.519	0.534	0.577
MgO	0.119	0.107	0.072	0.06	0.063	0.056	0.056	0.066
BaO	na	na	na	na	na	na	na	na
SrO	na	na	na	na	na	na	na	na
CaO	9.037	10.044	14.713	14.852	12.705	12.23	13.042	13.151
Na_2O	5.566	5.182	2.789	2.729	3.847	4.103	3.763	3.549
K_2O	0.858	0.634	0.202	0.19	0.32	0.332	0.28	0.262
Total	98.09	98.31	98.95	99.12	98.58	98.49	99.21	98.6
				Oxygen = 32.000				
Si	10.295	10.06	9.108	9.083	9.513	9.611	9.474	9.445
Al	5.586	5.821	6.815	6.844	6.413	6.323	6.453	6.484
Fe	0.116	0.13	0.094	0.093	0.091	0.08	0.082	0.089
Mg	0.033	0.029	0.02	0.017	0.017	0.015	0.015	0.018
Ba	na	na	na	na	na	na	na	na
Ca	1.781	1.981	2.914	2.937	2.512	2.416	2.563	2.601
Na	1.985	1.85	1	0.977	1.377	1.467	1.338	1.27
K	0.201	0.149	0.048	0.045	0.075	0.078	0.066	0.062
Ab	50	46.5	25.2	24.7	34.7	37	33.7	32.3
An	44.9	49.8	73.5	74.2	63.4	61	64.6	66.1
Or	5.1	3.7	1.2	1.1	1.9	2	1.7	1.6

Table A.2: Con't

	005-005	005-006	005-007	005-008	005-009	005-010	005-011	005-012
SiO_2	52.801	51.445	51.016	51.34	52.096	51.821	50.252	52.619
Al_2O_3	29.122	29.747	30.205	29.841	29.506	29.092	30.764	28.942
FeOт	0.543	0.528	0.581	0.562	0.582	0.564	0.539	0.568
MgO	0.061	0.067	0.057	0.058	0.072	0.056	0.065	0.059
BaO	na	na	na	na	na	na	na	na
SrO	na	na	na	na	na	na	na	na
CaO	12.342	12.842	13.533	13.299	12.412	12.487	14.093	12.112
Na_2O	4	3.58	3.34	3.576	3.787	3.82	3.218	4.065
K_2O	0.336	0.266	0.251	0.257	0.286	0.313	0.205	0.337
Total	99.21	98.48	98.98	98.93	98.74	98.15	99.14	98.7
				Oxygen = 32.000				
Si	9.657	9.492	9.387	9.448	9.575	9.59	9.252	9.671
Al	6.273	6.464	6.545	6.467	6.386	6.34	6.671	6.264
Fe	0.083	0.081	0.089	0.086	0.089	0.087	0.083	0.087
Mg	0.017	0.018	0.016	0.016	0.02	0.015	0.018	0.016
Ba	na	na	na	na	na	na	na	na
Ca	2.419	2.539	2.668	2.622	2.444	2.476	2.78	2.385
Na	1.419	1.281	1.192	1.276	1.35	1.371	1.149	1.449
K	0.078	0.063	0.059	0.06	0.067	0.074	0.048	0.079
Ab	36.2	33	30.4	32.2	35	35	28.9	37
An	61.8	65.4	68.1	66.2	63.3	63.1	69.9	61
Or	2	1.6	1.5	1.5	1.7	1.9	1.2	2

Table A.2: Con't

	006-001	006-002	006-003	006-004	006-005	006-006	006-007	006-008
SiO_2	47.94	47.983	47.971	48.174	48.951	49.921	48.813	47.79
Al_2O_3	32.005	32.006	31.932	32.05	31.417	30.673	31.671	32.006
FeOT	0.532	0.496	0.55	0.566	0.596	0.48	0.535	0.593
MgO	0.075	0.08	0.066	0.068	0.058	0.081	0.063	0.072
BaO	na	na	na	na	na	na	na	na
SrO	na	na	na	na	na	na	na	na
CaO	15.607	15.654	15.59	15.601	15.015	14.267	15.211	15.924
Na_2O	2.254	2.246	2.391	2.434	2.697	3.044	2.443	2.203
K_2O	0.149	0.16	0.163	0.152	0.178	0.239	0.177	0.167
Total	98.56	98.62	98.66	99.04	98.91	98.71	98.91	98.75
				Oxygen = 32.000				
Si	8.917	8.919	8.92	8.923	9.062	9.234	9.032	8.887
Al	7.011	7.007	6.993	6.991	6.849	6.682	6.901	7.009
Fe	0.083	0.077	0.086	0.088	0.092	0.074	0.083	0.092
Mg	0.021	0.022	0.018	0.019	0.016	0.022	0.017	0.02
Ba	na	na	na	na	na	na	na	na
Ca	3.11	3.118	3.106	3.096	2.978	2.828	3.015	3.173
Na	0.813	0.81	0.862	0.874	0.968	1.092	0.876	0.794
K	0.035	0.038	0.039	0.036	0.042	0.056	0.042	0.04
Ab	20.5	20.4	21.5	21.8	24.3	27.5	22.3	19.8
An	78.6	78.6	77.5	77.3	74.7	71.1	76.7	79.2
Or	0.9	1	1	0.9	1.1	1.4	1.1	1

Table A.2: Con't

	006-009	006-010	006-012	006-013	006-014	007-001	007-002	007-003
SiO_2	48.7	48.426	48.996	49.019	47.795	50.554	49.024	49.664
Al_2O_3	31.732	31.82	31.617	31.59	31.849	30.962	31.65	30.861
FeOT	0.52	0.523	0.484	0.55	0.479	0.537	0.556	0.539
MgO	0.068	0.056	0.075	0.088	0.069	0.07	0.065	0.074
BaO	na	na	na	na	na	na	na	na
SrO	na	na	na	na	na	na	na	na
CaO	15.472	15.526	14.93	14.913	15.728	14.198	15.374	14.596
Na_2O	2.444	2.339	2.556	2.731	2.213	3.008	2.473	2.918
K_2O	0.16	0.168	0.193	0.177	0.242	0.231	0.169	0.216
Total	99.1	98.86	98.85	99.07	98.38	99.56	99.31	98.87
				Oxygen = 32.000				
Si	9.003	8.976	9.062	9.055	8.915	9.261	9.039	9.183
Al	6.908	6.946	6.887	6.872	6.996	6.679	6.872	6.72
Fe	0.08	0.081	0.075	0.085	0.075	0.082	0.086	0.083
Mg	0.019	0.015	0.021	0.024	0.019	0.019	0.018	0.02
Ba	na	na	na	na	na	na	na	na
Ca	3.065	3.083	2.959	2.952	3.143	2.787	3.037	2.892
Na	0.876	0.841	0.917	0.978	0.8	1.068	0.884	1.046
K	0.038	0.04	0.046	0.042	0.058	0.054	0.04	0.051
Ab	22	21.2	23.4	24.6	20	27.3	22.3	26.2
An	77	77.8	75.4	74.3	78.6	71.3	76.7	72.5
Or	1	1	1.2	1.1	1.4	1.4	1	1.3

Table A.2: Con't

	007-004	007-005	008-001	008-002	008-004	008-005	008-006	008-007
SiO_2	48.506	48.368	60.027	59.163	59.369	59.861	60.04	59.857
Al_2O_3	31.422	31.867	24.389	24.765	24.177	24.25	24.243	24.108
FeOT	0.525	0.603	0.385	0.447	0.369	0.415	0.394	0.392
MgO	0.075	0.071	0.028	0.025	0.028	0.039	0.021	0.021
BaO	na	na	na	na	na	na	na	na
SrO	na	na	na	na	na	na	na	na
CaO	15.27	15.457	6.336	6.794	6.243	6.263	6.257	5.97
Na_2O	2.509	2.201	6.77	6.705	6.773	6.953	6.889	6.945
K_2O	0.18	0.152	1.197	1.079	1.196	1.244	1.262	1.242
Total	98.49	98.72	99.13	98.98	98.15	99.03	99.11	98.54
				Oxygen = 32.000				
Si	9.023	8.973	10.812	10.696	10.803	10.807	10.824	10.845
Al	6.883	6.962	5.173	5.273	5.181	5.156	5.147	5.144
Fe	0.082	0.094	0.058	0.068	0.056	0.063	0.059	0.059
Mg	0.021	0.02	0.008	0.007	0.008	0.01	0.006	0.006
Ba	na	na	na	na	na	na	na	na
Ca	3.043	3.072	1.223	1.316	1.217	1.211	1.209	1.159
Na	0.905	0.792	2.364	2.351	2.39	2.434	2.408	2.44
K	0.043	0.036	0.275	0.249	0.278	0.287	0.29	0.287
Ab	22.7	20.3	61.2	60	61.5	61.9	61.6	62.8
An	76.2	78.8	31.7	33.6	31.3	30.8	30.9	29.8
Or	1.1	0.9	7.1	6.4	7.2	7.3	7.4	7.4

Table A.2: Con't

	008-008	008-010	008-012	008-013	009-001	009-002	009-003	009-004
SiO_2	59.016	59.393	59	60.049	57.222	57.958	57.976	59.499
Al_2O_3	24.834	24.553	24.563	24.424	26.137	25.209	25.821	24.76
FeOT	0.453	0.374	0.417	0.407	0.377	0.393	0.373	0.388
MgO	0.025	0.009	0.024	0.006	0.028	0.019	0.022	0.016
BaO	na	na	na	na	na	na	na	na
SrO	na	na	na	na	na	na	na	na
CaO	6.756	6.504	6.55	6.263	8.519	7.585	7.87	6.783
Na_2O	6.68	6.646	6.508	6.742	5.828	6.199	6.036	6.49
K_2O	1.038	1.186	1.092	1.212	0.745	0.901	0.838	1.071
Total	98.8	98.66	98.15	99.1	98.86	98.26	98.94	99.01
				Oxygen = 32.000				
Si	10.685	10.756	10.737	10.816	10.388	10.564	10.495	10.734
Al	5.295	5.237	5.264	5.181	5.588	5.411	5.505	5.261
Fe	0.069	0.057	0.063	0.061	0.057	0.06	0.056	0.059
Mg	0.007	0.002	0.007	0.002	0.008	0.005	0.006	0.004
Ba	na	na	na	na	na	na	na	na
Ca	1.311	1.262	1.277	1.209	1.657	1.481	1.526	1.311
Na	2.345	2.334	2.296	2.355	2.051	2.191	2.119	2.27
K	0.24	0.274	0.254	0.279	0.173	0.21	0.194	0.247
Ab	60.2	60.3	60	61.3	52.8	56.4	55.2	59.3
An	33.6	32.6	33.4	31.5	42.7	38.2	39.7	34.2
Or	6.2	7.1	6.6	7.3	4.5	5.4	5.1	6.5

Table A.2: Con't

	009-005	009-006	009-007	009-008	009-009	009-010	009-011	009-012
SiO_2	57.117	58.077	58.521	57.861	58.264	57.335	57.354	58.655
Al_2O_3	26.071	25.265	25.57	25.559	25.602	26.076	25.621	25.624
FeOT	0.378	0.374	0.413	0.388	0.47	0.41	0.394	0.424
MgO	0.018	0.021	0.022	0.024	0.035	0.026	0.017	0.031
BaO	na	na	na	na	na	na	na	na
SrO	na	na	na	na	na	na	na	na
CaO	8.296	7.569	7.723	7.795	7.668	8.259	7.949	7.477
Na_2O	5.8	6.246	6.149	6.014	6.233	5.832	5.935	6.329
K_2O	0.748	0.906	0.882	0.852	0.888	0.777	0.841	0.935
Total	98.43	98.46	99.28	98.49	99.16	98.71	98.11	99.48
				Oxygen = 32.000				
Si	10.405	10.564	10.554	10.52	10.529	10.415	10.477	10.559
Al	5.593	5.412	5.431	5.473	5.449	5.578	5.512	5.432
Fe	0.058	0.057	0.062	0.059	0.071	0.062	0.06	0.064
Mg	0.005	0.006	0.006	0.007	0.009	0.007	0.005	0.008
Ba	na	na	na	na	na	na	na	na
Ca	1.619	1.475	1.492	1.518	1.485	1.607	1.556	1.442
Na	2.049	2.203	2.15	2.12	2.184	2.054	2.102	2.209
K	0.174	0.21	0.203	0.198	0.205	0.18	0.196	0.215
Ab	53.3	56.7	55.9	55.3	56.4	53.5	54.5	57.1
An	42.1	37.9	38.8	39.6	38.3	41.8	40.4	37.3
Or	4.5	5.4	5.3	5.2	5.3	4.7	5.1	5.6

Table A.2: Con't

	009-013	009-014	009-016	010-001	010-002	010-003	010-004	010-005
SiO_2	58.245	56.594	59.228	50.63	49.573	49.778	52.256	50.325
Al_2O_3	25.909	26.272	24.188	30.784	31.272	31.446	30.248	31.006
FeOT	0.411	0.401	0.448	0.588	0.588	0.582	0.579	0.491
MgO	0.029	0.026	0.018	0.081	0.058	0.072	0.079	0.075
BaO	na	na	na	na	na	na	na	na
SrO	na	na	na	na	na	na	na	na
CaO	8.013	8.73	6.426	14.107	14.82	14.931	12.987	14.185
Na_2O	6.213	5.699	6.595	3.197	2.749	2.796	3.711	3.096
K_2O	0.818	0.68	1.178	0.226	0.188	0.188	0.257	0.217
Total	99.64	98.4	98.08	99.61	99.25	99.79	100.12	99.4
				Oxygen = 32.000				
Si	10.482	10.329	10.79	9.276	9.133	9.124	9.486	9.237
Al	5.491	5.647	5.189	6.642	6.785	6.788	6.467	6.702
Fe	0.062	0.061	0.068	0.09	0.091	0.089	0.088	0.075
Mg	0.008	0.007	0.005	0.022	0.016	0.02	0.021	0.021
Ba	na	na	na	na	na	na	na	na
Ca	1.545	1.707	1.254	2.769	2.925	2.932	2.526	2.79
Na	2.168	2.017	2.33	1.136	0.982	0.994	1.306	1.102
K	0.188	0.158	0.274	0.053	0.044	0.044	0.06	0.051
Ab	55.6	52	60.4	28.7	24.9	25	33.6	27.9
An	39.6	44	32.5	70	74	73.9	64.9	70.8
Or	4.8	4.1	7.1	1.3	1.1	1.1	1.5	1.3

Table A.2: Con't

	010-006	010-007	010-008	011-001	011-003	011-004	011-005	011-006
SiO_2	49.623	50.24	49.53	48.341	48.073	48.534	48.325	48.289
Al_2O_3	31.802	31.216	31.642	32.158	31.421	32.374	31.774	32.246
FeOT	0.612	0.614	0.548	0.669	0.788	0.602	0.626	0.608
MgO	0.072	0.071	0.066	0.073	0.059	0.069	0.045	0.066
BaO	na	na	na	na	na	na	na	na
SrO	na	na	na	na	na	na	na	na
CaO	15.177	14.606	15.246	15.916	15.426	15.874	15.442	15.901
Na_2O	2.685	2.984	2.657	2.298	2.398	2.343	2.337	2.3
K_2O	0.171	0.221	0.202	0.173	0.207	0.172	0.16	0.155
Total	100.14	99.95	99.89	99.63	98.37	99.97	98.71	99.57
				Oxygen = 32.000				
Si	9.07	9.188	9.077	8.911	8.973	8.91	8.973	8.903
Al	6.846	6.723	6.829	6.981	6.907	6.999	6.948	7.001
Fe	0.094	0.094	0.084	0.103	0.123	0.092	0.097	0.094
Mg	0.02	0.019	0.018	0.02	0.016	0.019	0.012	0.018
Ba	na	na	na	na	na	na	na	na
Ca	2.972	2.862	2.994	3.143	3.085	3.122	3.072	3.141
Na	0.952	1.058	0.944	0.821	0.868	0.834	0.841	0.822
K	0.04	0.052	0.047	0.041	0.049	0.04	0.038	0.036
Ab	24	26.6	23.7	20.5	21.7	20.9	21.3	20.6
An	75	72.1	75.1	78.5	77.1	78.1	77.8	78.5
Or	1	1.3	1.2	1	1.2	1	1	0.9

Table A.2: Con't

	011-007	011-008	012-003	012-004	012-005	012-007	012-008	012-009
SiO_2	48.127	53.26	48.571	48.868	49.179	49.069	49.808	48.368
Al_2O_3	32.064	29.2	31.776	32.928	32.087	31.881	31.943	32.139
FeOT	0.6	0.719	0.596	0.622	0.598	0.617	0.573	0.572
MgO	0.084	0.107	0.053	0.069	0.064	0.053	0.068	0.064
BaO	na	na	na	na	na	na	na	na
SrO	na	na	na	na	na	na	na	na
CaO	15.76	12.213	15.807	15.697	15.364	15.724	15.247	15.696
Na_2O	2.352	4.356	2.473	2.408	2.613	2.464	2.667	2.262
K_2O	0.159	0.337	0.151	0.157	0.16	0.141	0.144	0.117
Total	99.15	100.19	99.43	100.75	100.07	99.95	100.45	99.22
				Oxygen = 32.000				
Si	8.91	9.66	8.967	8.893	9.004	9.002	9.072	8.935
Al	6.991	6.237	6.908	7.057	6.918	6.888	6.852	6.992
Fe	0.093	0.109	0.092	0.095	0.092	0.095	0.087	0.088
Mg	0.023	0.029	0.015	0.019	0.017	0.014	0.018	0.018
Ba	na	na	na	na	na	na	na	na
Ca	3.126	2.373	3.127	3.061	3.014	3.091	2.975	3.107
Na	0.844	1.532	0.885	0.85	0.928	0.876	0.942	0.81
K	0.038	0.078	0.036	0.036	0.037	0.033	0.033	0.028
Ab	21.1	38.5	21.9	21.5	23.3	21.9	23.8	20.5
An	78	59.6	77.2	77.6	75.7	77.3	75.3	78.8
Or	0.9	2	0.9	0.9	0.9	0.8	0.8	0.7

Table A.2: Con't

	012-010	013-001	013-002	013-003	013-004	013-005	013-006	013-007
SiO_2	48.453	61.534	61.03	61.566	62.112	62.162	61.658	61.876
Al_2O_3	32.092	22.903	23.181	23.181	22.856	22.662	22.89	23.021
FeOT	0.619	0.355	0.377	0.384	0.383	0.405	0.405	0.401
MgO	0.051	0.024	0.027	0	0.012	0.006	0.02	0.025
BaO	na	na	na	na	na	na	na	na
SrO	na	na	na	na	na	na	na	na
CaO	15.847	4.712	5.122	5.075	4.666	4.575	4.771	4.579
Na_2O	2.3	7.221	7.16	7.234	7.247	7.395	7.307	7.256
K_2O	0.151	1.882	1.664	1.68	1.878	2.012	1.833	1.828
Total	99.51	98.63	98.56	99.12	99.15	99.22	98.88	98.99
				Oxygen = 32.000				
Si	8.934	11.115	11.04	11.07	11.154	11.169	11.114	11.128
Al	6.968	4.872	4.938	4.909	4.833	4.795	4.859	4.876
Fe	0.095	0.054	0.057	0.058	0.058	0.061	0.061	0.06
Mg	0.014	0.006	0.007	0	0.003	0.002	0.005	0.007
Ba	na	na	na	na	na	na	na	na
Ca	3.131	0.912	0.993	0.978	0.898	0.881	0.921	0.882
Na	0.822	2.529	2.511	2.522	2.523	2.576	2.554	2.53
K	0.036	0.434	0.384	0.385	0.43	0.461	0.422	0.419
Ab	20.6	65.3	64.6	64.9	65.5	65.7	65.5	66
An	78.5	23.5	25.5	25.2	23.3	22.5	23.6	23
Or	0.9	11.2	9.9	9.9	11.2	11.8	10.8	10.9

Table A.2: Con't

	013-008	013-009	013-010	013-011	013-012	013-013	013-014	013-015
SiO_2	61.648	61.706	61.557	61.673	61.813	61.984	61.843	61.962
Al_2O_3	22.847	22.518	23.048	22.945	22.864	23.074	22.872	22.943
FeOT	0.381	0.386	0.418	0.433	0.41	0.404	0.38	0.365
MgO	0.011	0.004	0.015	0.021	0.017	0.023	0.014	0.006
BaO	na	na	na	na	na	na	na	na
SrO	na	na	na	na	na	na	na	na
CaO	4.751	4.359	5.051	4.865	4.709	4.961	4.655	4.855
Na_2O	7.25	7.285	7.381	7.262	7.213	7.306	7.419	7.338
K_2O	1.93	2.053	1.745	1.737	1.919	1.767	1.904	1.783
Total	98.82	98.31	99.22	98.94	98.94	99.52	99.09	99.25
				Oxygen = 32.000				
Si	11.121	11.181	11.071	11.108	11.132	11.102	11.126	11.123
Al	4.854	4.805	4.882	4.867	4.849	4.867	4.846	4.85
Fe	0.057	0.058	0.063	0.065	0.062	0.061	0.057	0.055
Mg	0.003	0.001	0.004	0.006	0.005	0.006	0.004	0.002
Ba	na	na	na	na	na	na	na	na
Ca	0.918	0.846	0.973	0.939	0.909	0.952	0.897	0.934
Na	2.536	2.56	2.574	2.536	2.519	2.537	2.588	2.554
K	0.444	0.475	0.4	0.399	0.441	0.404	0.437	0.408
Ab	65.1	66	6	65.5	65.1	65.2	66	65.6
An	23.6	21.8	24.7	24.2	23.5	24.5	22.9	24
Or	11.4	12.2	10.1	10.3	11.4	10.4	11.1	10.5

Table A.2: Con't

	013-016	013-017	013-018	013-019	013-020	013-021	013-022	013-023
SiO_2	61.859	61.61	61.782	62.01	61.433	61.224	61.29	61.542
Al_2O_3	22.776	23.075	23.064	22.765	23.018	23.095	22.485	22.74
FeOT	0.463	0.381	0.4	0.341	0.398	0.395	0.413	0.42
MgO	0.006	0.024	0.009	0.002	0.006	0.013	0.011	0.015
BaO	na	na	na	na	na	na	na	na
SrO	na	na	na	na	na	na	na	na
CaO	4.588	4.887	4.945	4.507	4.914	4.977	4.683	4.769
Na_2O	7.418	7.298	7.395	7.357	7.369	7.177	7.278	7.228
K_2O	1.91	1.757	1.74	2.017	1.755	1.708	1.925	1.859
Total	99.02	99.03	99.34	99	98.89	98.59	98.09	98.57
				Oxygen = 32.000				
Si	11.139	11.088	11.09	11.16	11.079	11.068	11.143	11.128
Al	4.83	4.891	4.876	4.825	4.889	4.917	4.814	4.842
Fe	0.07	0.057	0.06	0.051	0.06	0.06	0.063	0.064
Mg	0.002	0.006	0.002	0.001	0.002	0.004	0.003	0.004
Ba	na	na	na	na	na	na	na	na
Ca	0.885	0.942	0.951	0.869	0.95	0.964	0.912	0.924
Na	2.59	2.547	2.574	2.567	2.577	2.516	2.566	2.534
K	0.439	0.403	0.398	0.463	0.404	0.394	0.447	0.429
Ab	66.2	65.4	65.6	65.8	65.6	64.9	65.4	65.2
An	22.6	24.2	24.2	22.3	24.2	24.9	23.2	23.8
Or	11.2	10.4	10.1	11.9	10.3	10.2	11.4	11

Table A.2: Con't

	013-024	014-003	014-004	014-005	014-006	014-007	014-008	014-009
SiO_2	61.309	48.661	49.342	49.531	48.846	48.542	49.8	48.548
Al_2O_3	22.843	31.818	31.251	31.336	31.791	31	31.323	31.838
FeOT	0.373	0.661	0.633	0.651	0.612	0.788	0.553	0.604
MgO	0.022	0.07	0.084	0.065	0.073	0.144	0.07	0.055
BaO	na	na	na	na	na	na	na	na
SrO	na	na	na	na	na	na	na	na
CaO	4.922	15.612	15.281	15.157	15.504	15.284	14.954	15.671
Na_2O	7.218	2.37	2.653	2.673	2.364	2.458	2.709	2.377
K_2O	1.802	0.158	0.163	0.16	0.162	0.18	0.174	0.163
Total	98.49	99.29	99.41	99.57	99.35	98.4	99.58	99.26
				Oxygen = 32.000				
Si	11.098	8.977	9.093	9.107	9.007	9.05	9.142	8.971
Al	4.87	6.921	6.782	6.785	6.904	6.806	6.772	6.928
Fe	0.056	0.102	0.098	0.1	0.094	0.123	0.085	0.093
Mg	0.006	0.019	0.023	0.018	0.02	0.04	0.019	0.015
Ba	na	na	na	na	na	na	na	na
Ca	0.955	3.09	3.017	2.986	3.063	3.053	2.941	3.102
Na	2.534	0.849	0.948	0.953	0.845	0.889	0.964	0.852
K	0.416	0.037	0.038	0.038	0.038	0.043	0.041	0.038
Ab	64.9	21.4	23.7	24	21.4	22.3	24.4	21.3
An	24.5	77.7	75.4	75.1	77.6	76.6	74.5	77.7
Or	10.7	0.9	0.9	1	1	1.1	1	1

Table A.2: Con't

	014-010	014-011	014-012	014-013	015-002	015-003	015-004	015-005
SiO_2	50.093	49.643	48.087	47.961	52.212	51.179	50.083	52.752
Al_2O_3	31.663	31.124	31.56	31.445	28.88	29.854	30.141	28.982
FeOт	0.576	0.575	0.637	0.545	0.624	0.527	0.718	0.561
MgO	0.068	0.076	0.053	0.06	0.105	0.087	0.081	0.07
BaO	na	na	na	na	na	na	na	na
SrO	na	na	na	na	na	na	na	na
CaO	14.912	14.715	15.541	15.795	12.158	13.57	13.981	12.164
Na_2O	2.792	2.865	2.358	2.325	4.304	3.415	3.126	4.153
K_2O	0.194	0.187	0.146	0.141	0.388	0.214	0.177	0.311
Total	100.3	99.18	98.38	98.27	98.67	98.85	98.31	98.99
				Oxygen = 32.000				
Si	9.13	9.152	8.966	8.957	9.623	9.428	9.301	9.669
Al	6.796	6.757	6.93	6.916	6.269	6.477	6.592	6.256
Fe	0.088	0.089	0.099	0.085	0.096	0.081	0.112	0.086
Mg	0.018	0.021	0.015	0.017	0.029	0.024	0.022	0.019
Ba	na	na	na	na	na	na	na	na
Ca	2.912	2.907	3.105	3.161	2.401	2.678	2.782	2.389
Na	0.987	1.024	0.853	0.842	1.538	1.22	1.126	1.476
K	0.045	0.044	0.035	0.034	0.091	0.05	0.042	0.073
Ab	25	25.8	21.4	20.9	38.2	30.9	28.5	37.5
An	73.8	73.1	77.8	78.3	59.6	67.8	70.4	60.7
Or	1.1	1.1	0.9	0.8	2.3	1.3	1.1	1.9

Table A.2: Con't

	015-006	015-007	015-008	015-009	015-010	015-012	017-004	017-006
SiO_2	54.5	50.311	52.53	51.149	52.671	52.4	48.626	48.362
Al_2O_3	27.186	30.562	28.759	29.827	29.276	28.806	31.874	31.558
FeOт	0.687	0.597	0.557	0.59	0.552	0.545	0.596	0.612
MgO	0.095	0.079	0.071	0.054	0.064	0.08	0.077	0.078
BaO	na	na	na	na	na	na	na	na
SrO	na	na	na	na	na	na	na	na
CaO	10.492	14.22	12.083	13.227	12.463	12.162	15.442	15.416
Na_2O	4.879	3.059	4.213	3.667	4.225	4.104	2.507	2.515
K_2O	0.529	0.189	0.28	0.232	0.29	0.287	0.133	0.161
Total	98.37	99.02	98.49	98.75	99.54	98.38	99.26	98.7
				Oxygen = 32.000				
Si	10.017	9.274	9.678	9.434	9.615	9.664	8.98	8.986
Al	5.885	6.634	6.24	6.479	6.294	6.257	6.932	6.906
Fe	0.106	0.092	0.086	0.091	0.084	0.084	0.092	0.095
Mg	0.026	0.022	0.019	0.015	0.017	0.022	0.021	0.022
Ba	na	na	na	na	na	na	na	na
Ca	2.066	2.808	2.385	2.614	2.438	2.403	3.055	3.069
Na	1.739	1.093	1.505	1.312	1.495	1.468	0.898	0.906
K	0.124	0.044	0.066	0.055	0.068	0.068	0.031	0.038
Ab	44.3	27.7	38	33	37.4	37.3	22.5	22.6
An	52.6	71.2	60.3	65.7	60.9	61	76.7	76.5
Or	3.2	1.1	1.7	1.4	1.7	1.7	0.8	0.9

Table A.2: Con't

	017-007	017-011	017-012	018-001	018-002	018-003	018-004	018-005
SiO_2	48.003	49.613	48.997	56.45	52.364	50.022	50.783	50.026
Al_2O_3	31.62	31.295	31.219	26.061	29.734	30.512	30.717	31.068
FeOT	0.538	0.611	0.573	0.803	0.603	0.671	0.618	0.612
MgO	0.059	0.058	0.066	0.088	0.079	0.065	0.06	0.055
BaO	na	na	na	na	na	na	na	na
SrO	na	na	na	na	na	na	na	na
CaO	15.319	14.977	15.321	9.313	12.769	14.219	14.065	14.409
Na_2O	2.473	2.741	2.545	5.806	3.833	3.055	3.153	3.056
K_2O	0.186	0.177	0.157	0.741	0.305	0.219	0.213	0.191
Total	98.2	99.47	98.88	99.26	99.69	98.76	99.61	99.42
				Oxygen = 32.000				
Si	8.963	9.125	9.076	10.272	9.547	9.253	9.299	9.195
Al	6.953	6.779	6.81	5.584	6.384	6.647	6.624	6.725
Fe	0.084	0.094	0.089	0.122	0.092	0.104	0.095	0.094
Mg	0.016	0.016	0.018	0.024	0.021	0.018	0.016	0.015
Ba								
Ca	3.065	2.951	3.041	1.816	2.494	2.818	2.76	2.837
Na	0.895	0.978	0.914	2.048	1.355	1.096	1.12	1.089
K	0.044	0.042	0.037	0.172	0.071	0.052	0.05	0.045
Ab	22.4	24.6	22.9	50.7	34.6	27.6	28.5	27.4
An	76.5	74.3	76.2	45	63.6	71.1	70.2	71.4
Or	1.1	1.1	0.9	4.3	1.8	1.3	1.3	1.1

Table A.2: Con't

	018-006	018-007	018-008	018-009	018-010	038-001	LT001-003	LT001-004
SiO_2	50.54	50.682	53.792	50.575	51.246	61.238	60.482	60.944
Al_2O_3	30.676	30.938	28.771	30.899	30.267	20.992	23.43	23.078
FeOT	0.658	0.719	0.578	0.64	0.621	2.748	0.367	0.355
MgO	0.062	0.076	0.074	0.061	0.069	0.56	0.013	0.021
BaO	na	na	na	na	na	0.049	na	na
SrO	na	na	na	na	na	0	na	na
CaO	13.924	14.302	11.709	14.145	13.775	1.508	5.337	5.09
Na_2O	3.257	3.227	4.563	3.186	3.34	6.708	6.96	7.015
K_2O	0.24	0.224	0.359	0.198	0.258	6.564	1.585	1.593
Total	99.36	100.17	99.85	99.7	99.58	100.37	98.17	98.1
				Oxygen = 32.000				
Si	9.284	9.247	9.766	9.259	9.382	11.194	10.984	11.062
Al	6.636	6.648	6.152	6.662	6.525	4.519	5.011	4.933
Fe	0.101	0.11	0.088	0.098	0.095	0.42	0.056	0.054
Mg	0.017	0.021	0.02	0.017	0.019	0.153	0.004	0.006
Ba						0.004		
Ca	2.741	2.796	2.278	2.775	2.702	0.295	1.039	0.99
Na	1.16	1.142	1.606	1.131	1.186	2.378	2.451	2.469
K	0.056	0.052	0.083	0.046	0.06	1.531	0.367	0.369
Ab	29.3	28.6	40.5	28.6	30	56.6	63.5	64.5
An	69.3	70.1	57.4	70.2	68.4	7	26.9	25.9
Or	1.4	1.3	2.1	1.2	1.5	36.4	9.5	9.6

Table A.2: Con't

	LT001-005	LT001-009	LT001-010	LT001-012	LT001-013	LT001-014	LT001-015	LT001-016
SiO_2	60.981	60.089	60.064	59.964	59.636	60.508	61.045	60.847
Al_2O_3	23.047	23.686	23.607	23.809	23.837	23.246	23.339	23.563
FeOT	0.335	0.369	0.43	0.401	0.414	0.439	0.388	0.382
MgO	0.017	0.015	0.023	0.006	0.01	0.019	0.01	0.015
BaO	na	na	na	na	na	na	na	na
SrO	na	na	na	na	na	na	na	na
CaO	5.023	5.892	5.583	5.714	5.866	5.35	5.259	5.568
Na_2O	7.149	6.952	6.895	6.889	6.88	7.029	7.226	6.871
K_2O	1.719	1.356	1.403	1.352	1.39	1.487	1.575	1.532
Total	98.27	98.36	98.01	98.13	98.03	98.08	98.84	98.78
				Oxygen = 32.000				
Si	11.06	10.906	10.931	10.9	10.866	11.001	11.015	10.982
Al	4.923	5.063	5.06	5.097	5.115	4.977	4.959	5.008
Fe	0.051	0.056	0.065	0.061	0.063	0.067	0.059	0.058
Mg	0.005	0.004	0.006	0.002	0.003	0.005	0.003	0.004
Ba	na	na	na	na	na	na	na	na
Ca	0.976	1.146	1.089	1.113	1.145	1.042	1.017	1.077
Na	2.514	2.447	2.433	2.428	2.431	2.478	2.528	2.405
K	0.398	0.314	0.326	0.314	0.323	0.345	0.363	0.353
Ab	64.7	62.6	63.2	63	62.3	64.1	64.7	62.7
An	25.1	29.3	28.3	28.9	29.4	27	26	28.1
Or	10.2	8	8.5	8.1	8.3	8.9	9.3	9.2

Table A.2: Con't

	LT001-017	LT001-021	LT001-022	LT001-023	LT001-024	LT001-025	LT001-026	LT001-027
SiO_2	60.331	60.087	60.674	60.515	60.434	60.64	61.1	60.902
Al_2O_3	23.875	23.663	23.73	23.733	23.746	23.436	23.194	23.038
FeOT	0.408	0.413	0.324	0.374	0.333	0.403	0.347	0.363
MgO	0.025	0.009	0.019	0.023	0.027	0.01	0.016	0.012
BaO	na	na	na	na	na	na	na	na
SrO	na	na	na	na	na	na	na	na
CaO	5.983	5.76	5.485	5.883	5.709	5.532	5.192	5.148
Na_2O	6.811	6.929	7.127	6.929	7.003	7.097	7.06	7.152
K_2O	1.388	1.421	1.55	1.518	1.432	1.537	1.705	1.744
Total	98.82	98.28	98.91	98.98	98.68	98.66	98.61	98.36
				Oxygen = 32.000				
Si	10.898	10.914	10.946	10.92	10.926	10.972	11.045	11.046
Al	5.079	5.062	5.041	5.044	5.056	4.994	4.938	4.921
Fe	0.062	0.063	0.049	0.056	0.05	0.061	0.052	0.055
Mg	0.007	0.002	0.005	0.006	0.007	0.003	0.004	0.003
Ba	na	na	na	na	na	na	na	na
Ca	1.158	1.121	1.06	1.137	1.106	1.072	1.006	1
Na	2.386	2.44	2.493	2.424	2.455	2.49	2.475	2.515
K	0.32	0.329	0.357	0.349	0.33	0.355	0.393	0.404
Ab	61.7	62.7	63.8	62	63.1	63.6	63.9	64.2
An	30	28.8	27.1	29.1	28.4	27.4	26	25.5
Or	8.3	8.5	9.1	8.9	8.5	9.1	10.1	10.3

Table A.2: Con't

	LT001-032	LT001-033	LT001-045	LT001-046	LT001-047	LT001-049	LT001-050	LT001-051
SiO_2	61.043	60.822	60.445	60.581	60.777	60.109	59.86	60.042
Al_2O_3	23.429	23.452	23.467	23.527	23.074	23.628	23.746	23.578
FeOт	0.426	0.36	0.445	0.439	0.427	0.369	0.374	0.408
MgO	0.006	0.002	0.015	0.025	0.03	0.027	0.019	0.008
BaO	na	na	na	na	na	na	na	na
SrO	na	na	na	na	na	na	na	na
CaO	5.301	5.408	5.638	5.677	5.334	5.494	5.793	5.871
Na_2O	7.065	6.924	6.935	6.908	7.157	7.074	6.957	6.872
K_2O	1.663	1.545	1.482	1.424	1.637	1.438	1.352	1.392
Total	98.93	98.51	98.43	98.58	98.44	98.14	98.1	98.17
				Oxygen = 32.000				
Si	11.007	11.002	10.959	10.961	11.022	10.928	10.892	10.919
Al	4.975	4.996	5.011	5.013	4.928	5.059	5.088	5.049
Fe	0.064	0.054	0.067	0.066	0.065	0.056	0.057	0.062
Mg	0.002	0.001	0.004	0.007	0.008	0.007	0.005	0.002
Ba	na	na	na	na	na	na	na	na
Ca	1.024	1.048	1.095	1.101	1.036	1.07	1.129	1.144
Na	2.47	2.428	2.438	2.424	2.517	2.494	2.455	2.423
K	0.383	0.357	0.343	0.329	0.379	0.334	0.314	0.323
Ab	63.7	63.3	62.9	62.9	64	64	63	62.3
An	26.4	27.3	28.3	28.6	26.3	27.4	29	29.4
Or	9.9	9.3	8.8	8.5	9.6	8.6	8.1	8.3

Table A.2: Con't

	LT001-053	LT001-054	LT001-055	LT001-057	LT001-058	LT001-059	LT001-060	LT001-062
SiO_2	59.875	60.231	60.654	60.545	61.066	61.074	61.444	60.964
Al_2O_3	23.772	23.675	23.217	23.307	23.069	23.024	23.093	22.884
FeOт	0.374	0.347	0.408	0.395	0.378	0.397	0.366	0.41
MgO	0.022	0.022	0.024	0.015	0.018	0.029	0.01	0.022
BaO	na	na	na	na	na	na	na	na
SrO	na	na	na	na	na	na	na	na
CaO	5.881	5.648	5.24	5.406	5	5.126	5.042	5.011
Na_2O	6.807	6.933	7.061	6.92	7.147	7.111	7.105	7.029
K_2O	1.413	1.447	1.711	1.566	1.825	1.74	1.826	1.788
Total	98.14	98.3	98.32	98.15	98.5	98.5	98.89	98.11
				Oxygen = 32.000				
Si	10.891	10.93	11.01	10.998	11.058	11.058	11.077	11.079
Al	5.092	5.059	4.963	4.986	4.919	4.909	4.903	4.897
Fe	0.057	0.053	0.062	0.06	0.057	0.06	0.055	0.062
Mg	0.006	0.006	0.006	0.004	0.005	0.008	0.003	0.006
Ba	na	na	na	na	na	na	na	na
Ca	1.146	1.098	1.019	1.052	0.97	0.994	0.974	0.976
Na	2.401	2.439	2.485	2.437	2.509	2.497	2.484	2.477
K	0.328	0.335	0.396	0.363	0.422	0.402	0.42	0.415
Ab	62	63	63.7	63.3	64.3	64.1	64.1	64
An	29.6	28.4	26.1	27.3	24.9	25.5	25.1	25.2
Or	8.5	8.7	10.2	9.4	10.8	10.3	10.8	10.7

Table A.2: Con't

	LT001-065	LT001-066	LT001-067	LT001-068	LT001-070	LT001-071	LT001-072	LT001-073
SiO_2	60.875	60.919	60.857	60.511	61.125	60.551	60.961	60.669
Al_2O_3	23.043	22.883	23.108	23.326	22.893	23.635	23.569	23.718
FeOт	0.384	0.344	0.376	0.404	0.353	0.393	0.335	0.379
MgO	0.02	0.023	0.014	0.01	0.019	0.017	0.005	0.037
BaO	na	na	na	na	na	na	na	na
SrO	na	na	na	na	na	na	na	na
CaO	4.947	4.994	5.084	5.416	4.971	5.608	5.614	5.691
Na_2O	7.173	7.122	7.188	6.999	6.992	6.72	6.852	6.966
K_2O	1.713	1.774	1.725	1.569	1.672	1.469	1.575	1.45
Total	98.16	98.06	98.35	98.24	98.03	98.39	98.91	98.91
				Oxygen = 32.000				
Si	11.056	11.076	11.038	10.989	11.099	10.965	10.987	10.942
Al	4.929	4.899	4.936	4.989	4.896	5.04	5.003	5.038
Fe	0.058	0.052	0.057	0.061	0.054	0.06	0.05	0.057
Mg	0.005	0.006	0.004	0.003	0.005	0.005	0.001	0.01
Ba	na	na	na	na	na	na	na	na
Ca	0.963	0.973	0.988	1.054	0.967	1.088	1.084	1.1
Na	2.526	2.511	2.528	2.465	2.462	2.36	2.395	2.436
K	0.397	0.411	0.399	0.364	0.387	0.339	0.362	0.334
Ab	65	64.5	64.6	63.5	64.5	62.3	62.4	62.9
An	24.8	25	25.2	27.1	25.3	28.7	28.2	28.4
Or	10.2	10.6	10.2	9.4	10.1	9	9.4	8.6

Table A.2: Con't

	LT001-074	LT001-075	LT001-078	LT001-079	LT001-080	LT001-081	LT001-082	LT001-083
SiO_2	60.222	60.333	61.175	60.684	60.754	60.384	60.932	60.586
Al_2O_3	23.864	23.404	23.35	23.457	23.589	23.453	23.051	23.211
FeOт	0.376	0.334	0.354	0.352	0.43	0.36	0.388	0.368
MgO	0.028	0.007	0.022	0.012	0.012	0.012	0.009	0.008
BaO	na	na	na	na	na	na	na	na
SrO	na	na	na	na	na	na	na	na
CaO	5.818	5.839	5.203	5.583	5.542	5.579	5.017	5.277
Na_2O	6.992	6.93	7.105	7.055	7.097	6.893	6.97	6.891
K_2O	1.364	1.492	1.639	1.552	1.498	1.557	1.778	1.679
Total	98.66	98.34	98.85	98.7	98.92	98.24	98.15	98.02
				Oxygen = 32.000				
Si	10.895	10.953	11.03	10.973	10.961	10.966	11.064	11.019
Al	5.084	5.004	4.958	4.995	5.012	5.016	4.929	4.972
Fe	0.057	0.051	0.053	0.053	0.065	0.055	0.059	0.056
Mg	0.008	0.002	0.006	0.003	0.003	0.003	0.002	0.002
Ba	na	na	na	na	na	na	na	na
Ca	1.128	1.136	1.005	1.082	1.071	1.086	0.976	1.028
Na	2.453	2.439	2.484	2.474	2.483	2.427	2.454	2.43
K	0.315	0.346	0.377	0.358	0.345	0.361	0.412	0.39
Ab	63	62.2	64.3	63.2	63.7	62.6	63.9	63.1
An	29	29	26	27.6	27.5	28	25.4	26.7
Or	8.1	8.8	9.8	9.1	8.8	9.3	10.7	10.1

Table A.2: Con't

	LT001-086	LT002-001	LT002-002	LT002-003	LT002-004	LT002-005	LT002-006	LT002-007
SiO_2	61.295	59.442	59.226	59.335	59.134	59.924	59.323	60.579
Al_2O_3	22.681	24.754	24.735	24.479	24.708	23.885	24.654	23.983
FeOT	0.387	0.413	0.424	0.436	0.406	0.425	0.387	0.411
MgO	0.019	0.03	0.029	0.028	0.031	0.022	0.022	0.033
BaO	na	na	na	na	na	na	na	na
SrO	na	na	na	na	na	na	na	na
CaO	4.465	6.849	6.9	6.74	6.958	6.139	6.876	5.867
Na_2O	7.274	6.686	6.699	6.673	6.632	6.893	6.586	6.968
K_2O	1.941	1.027	1.045	1.147	0.989	1.268	1.032	1.363
Total	98.06	99.2	99.06	98.84	98.86	98.56	98.88	99.2
				Oxygen = 32.000				
Si	11.137	10.715	10.699	10.74	10.699	10.862	10.725	10.899
Al	4.853	5.255	5.262	5.218	5.265	5.099	5.249	5.081
Fe	0.059	0.062	0.064	0.066	0.061	0.064	0.059	0.062
Mg	0.005	0.008	0.008	0.008	0.008	0.006	0.006	0.009
Ba	na	na	na	na	na	na	na	na
Ca	0.869	1.323	1.335	1.307	1.349	1.192	1.332	1.131
Na	2.563	2.337	2.346	2.342	2.327	2.423	2.309	2.431
K	0.45	0.236	0.241	0.265	0.228	0.293	0.238	0.313
Ab	66	60	59.8	59.8	59.6	62	59.5	62.7
An	22.4	34	34	33.4	34.6	30.5	34.3	29.2
Or	11.6	6.1	6.1	6.8	5.8	7.5	6.1	8.1

Table A.2: Con't

	LT002-008	LT002-009	LT002-010	LT002-011	LT002-012	LT002-013	LT002-014	LT002-016
SiO_2	59.28	59.164	59.215	58.875	59.868	60.615	60.172	59.323
Al_2O_3	24.666	24.809	25.008	24.805	24.217	23.609	23.873	24.643
FeOT	0.358	0.44	0.408	0.414	0.4	0.414	0.359	0.445
MgO	0.03	0.027	0.014	0.016	0.019	0.013	0.026	0.017
BaO	na	na	na	na	na	na	na	na
SrO	na	na	na	na	na	na	na	na
CaO	6.951	7.117	6.956	7.116	6.386	5.724	6.027	6.783
Na_2O	6.547	6.53	6.615	6.351	6.718	6.967	6.623	6.583
K_2O	1.048	1.03	1.002	1.039	1.15	1.391	1.19	1.081
Total	98.88	99.12	99.22	98.62	98.76	98.73	98.27	98.88
				Oxygen = 32.000				
Si	10.718	10.683	10.674	10.679	10.823	10.951	10.907	10.728
Al	5.252	5.276	5.309	5.298	5.156	5.023	5.096	5.248
Fe	0.054	0.066	0.062	0.063	0.06	0.063	0.054	0.067
Mg	0.008	0.007	0.004	0.004	0.005	0.004	0.007	0.005
Ba	na	na	na	na	na	na	na	na
Ca	1.347	1.377	1.343	1.383	1.237	1.108	1.171	1.314
Na	2.295	2.286	2.312	2.234	2.355	2.441	2.328	2.308
K	0.242	0.237	0.23	0.24	0.265	0.321	0.275	0.249
Ab	59.1	58.6	59.5	57.9	61.1	63.1	61.7	59.6
An	34.7	35.3	34.6	35.9	32.1	28.6	31	33.9
Or	6.2	6.1	5.9	6.2	6.9	8.3	7.3	6.4

Table A.2: Con't

	LT002-017	LT002-018	LT002-019	LT002-023	LT002-024	LT002-025	LT002-026	LT002-027
SiO_2	59.882	59.537	59.756	58.814	59.133	58.922	59.152	59.908
Al_2O_3	23.94	24.061	24.106	24.756	24.613	24.694	24.878	24.256
FeOT	0.378	0.396	0.395	0.394	0.398	0.441	0.397	0.395
MgO	0.012	0.028	0.033	0.021	0.022	0.025	0.025	0.028
BaO	na	na	na	na	na	na	na	na
SrO	na	na	na	na	na	na	na	na
CaO	6.326	6.345	6.255	7.084	6.995	7.015	7.049	6.404
Na_2O	6.648	6.742	6.81	6.546	6.582	6.519	6.626	6.774
K_2O	1.181	1.121	1.24	1.053	1.058	0.96	1.042	1.088
Total	98.37	98.23	98.59	98.67	98.8	98.58	99.17	98.85
				Oxygen = 32.000				
Si	10.863	10.822	10.827	10.671	10.709	10.691	10.676	10.818
Al	5.114	5.151	5.144	5.29	5.249	5.277	5.288	5.158
Fe	0.057	0.06	0.06	0.06	0.06	0.067	0.06	0.06
Mg	0.003	0.008	0.009	0.006	0.006	0.007	0.007	0.008
Ba	na	na	na	na	na	na	na	na
Ca	1.229	1.236	1.214	1.377	1.357	1.364	1.363	1.239
Na	2.338	2.376	2.393	2.303	2.311	2.294	2.319	2.372
K	0.273	0.26	0.287	0.244	0.244	0.222	0.24	0.251
Ab	60.9	61.4	61.5	58.7	59.1	59.1	59.1	61.4
An	32	31.9	31.2	35.1	34.7	35.2	34.8	32.1
Or	7.1	6.7	7.4	6.2	6.2	5.7	6.1	6.5

Table A.2: Con't

	LT002-028	LT002-029	LT002-030	LT002-031	LT002-032	LT002-033	LT002-034	LT002-035
SiO_2	59.647	59.809	59.089	59.378	58.779	58.895	59.165	59.535
Al_2O_3	24.193	24.472	24.353	24.503	24.868	24.904	24.659	24.624
FeOT	0.387	0.42	0.413	0.432	0.397	0.434	0.398	0.396
MgO	0.016	0.033	0.016	0.019	0.019	0.017	0.029	0.029
BaO	na	na	na	na	na	na	na	na
SrO	na	na	na	na	na	na	na	na
CaO	6.246	6.504	6.571	6.921	7.26	7.021	6.98	6.714
Na_2O	6.832	6.762	6.617	6.651	6.375	6.49	6.572	6.641
K_2O	1.146	1.15	1.058	1.026	0.969	0.966	0.987	1.067
Total	98.47	99.15	98.12	98.93	98.67	98.73	98.79	99.01
				Oxygen = 32.000				
Si	10.816	10.779	10.759	10.736	10.659	10.669	10.709	10.745
Al	5.166	5.194	5.222	5.217	5.311	5.313	5.256	5.234
Fe	0.059	0.063	0.063	0.065	0.06	0.066	0.06	0.06
Mg	0.004	0.009	0.004	0.005	0.005	0.005	0.008	0.008
Ba	na	na	na	na	na	na	na	na
Ca	1.214	1.256	1.282	1.341	1.411	1.363	1.354	1.298
Na	2.402	2.363	2.336	2.332	2.242	2.28	2.307	2.324
K	0.265	0.264	0.246	0.237	0.224	0.223	0.228	0.246
Ab	61.9	60.9	60.5	59.6	57.8	59	59.3	60.1
An	31.3	32.3	33.2	34.3	36.4	35.3	34.8	33.6
Or	6.8	6.8	6.4	6.1	5.8	5.8	5.9	6.4

Table A.2: Con't

	LT002-036	LT002-037	LT002-040	LT002-041	LT002-042	LT002-043	LT002-044	LT002-045
SiO_2	59.09	57.751	58.776	58.868	58.811	58.647	58.781	58.687
Al_2O_3	24.725	25.682	24.875	24.805	24.879	24.981	24.835	24.956
FeOт	0.43	0.439	0.48	0.453	0.482	0.449	0.444	0.437
MgO	0.017	0.033	0.028	0.047	0.026	0.035	0.014	0.015
BaO	na	na	na	na	na	na	na	na
SrO	na	na	na	na	na	na	na	na
CaO	7.01	7.99	7.255	7.214	7.315	7.258	7.333	7.128
Na_2O	6.561	6.027	6.372	6.608	6.496	6.407	6.495	6.514
K_2O	0.971	0.793	0.949	0.957	0.96	0.921	0.978	0.912
Total	98.8	98.71	98.74	98.95	98.97	98.7	98.88	98.65
				Oxygen = 32.000				
Si	10.696	10.486	10.654	10.655	10.644	10.635	10.648	10.645
Al	5.271	5.492	5.31	5.287	5.303	5.335	5.298	5.331
Fe	0.065	0.067	0.073	0.069	0.073	0.068	0.067	0.066
Mg	0.005	0.009	0.008	0.013	0.007	0.009	0.004	0.004
Ba	na	na	na	na	na	na	na	na
Ca	1.36	1.554	1.409	1.399	1.419	1.41	1.423	1.385
Na	2.303	2.122	2.24	2.319	2.28	2.253	2.281	2.291
K	0.224	0.184	0.219	0.221	0.222	0.213	0.226	0.211
Ab	59.2	55	57.9	58.9	58.1	58.1	58	58.9
An	35	40.3	36.4	35.5	36.2	36.4	36.2	35.6
Or	5.8	4.8	5.7	5.6	5.7	5.5	5.8	5.4

Table A.2: Con't

	LT002-048	LT002-049	LT003-001	LT003-002	LT003-003	LT003-006	LT003-007	LT003-009
SiO_2	59.074	59.389	57.127	57.149	57.38	57.262	57.603	57.621
Al_2O_3	24.702	24.334	25.552	25.479	25.582	25.572	25.683	25.483
FeOт	0.453	0.45	0.483	0.451	0.497	0.452	0.449	0.465
MgO	0.027	0.021	0.036	0.031	0.022	0.024	0.037	0.046
BaO	na	na	na	na	na	na	na	na
SrO	na	na	na	na	na	na	na	na
CaO	7.054	6.684	8.003	8.143	7.993	8.082	7.916	7.827
Na_2O	6.696	6.75	6.048	6.107	6.054	6.114	6.096	6.135
K_2O	1.036	1.07	0.752	0.771	0.754	0.735	0.751	0.769
Total	99.04	98.7	98	98.13	98.28	98.24	98.54	98.35
				Oxygen = 32.000				
Si	10.683	10.761	10.457	10.455	10.471	10.458	10.478	10.501
Al	5.261	5.193	5.508	5.49	5.498	5.5	5.502	5.469
Fe	0.069	0.068	0.074	0.069	0.076	0.069	0.068	0.071
Mg	0.007	0.006	0.01	0.008	0.006	0.007	0.01	0.012
Ba	na	na	na	na	na	na	na	na
Ca	1.367	1.298	1.57	1.596	1.563	1.581	1.543	1.528
Na	2.348	2.372	2.147	2.166	2.142	2.165	2.15	2.168
K	0.239	0.247	0.176	0.18	0.176	0.171	0.174	0.179
Ab	59.4	60.6	55.2	54.9	55.2	55.3	55.6	55.9
An	34.6	33.1	40.3	40.5	40.3	40.4	39.9	39.4
Or	6	6.3	4.5	4.6	4.5	4.4	4.5	4.6

Table A.2: Con't

	LT003-010	LT003-011	LT003-012	LT003-013	LT003-014	LT003-015	LT003-016	LT003-017
SiO_2	57.776	58.058	58.148	57.865	57.764	57.683	57.745	57.79
Al_2O_3	25.557	25.352	25.027	25.234	25.482	25.396	25.333	25.501
FeOT	0.478	0.457	0.506	0.429	0.463	0.483	0.505	0.446
MgO	0.028	0.019	0.022	0.023	0.022	0.03	0.022	0.025
BaO	na	na	na	na	na	na	na	na
SrO	na	na	na	na	na	na	na	na
CaO	7.574	7.583	7.358	7.627	7.834	7.682	7.72	7.727
Na_2O	6.234	6.284	6.208	6.186	6.236	6.27	6.064	6.271
K_2O	0.82	0.805	0.815	0.802	0.803	0.751	0.775	0.814
Total	98.47	98.56	98.08	98.17	98.6	98.3	98.16	98.57
				Oxygen = 32.000				
Si	10.513	10.551	10.607	10.555	10.505	10.517	10.536	10.51
Al	5.476	5.426	5.376	5.421	5.458	5.453	5.443	5.462
Fe	0.073	0.069	0.077	0.065	0.07	0.074	0.077	0.068
Mg	0.008	0.005	0.006	0.006	0.006	0.008	0.006	0.007
Ba	na	na	na	na	na	na	na	na
Ca	1.477	1.476	1.438	1.491	1.526	1.501	1.509	1.506
Na	2.199	2.214	2.196	2.188	2.199	2.217	2.145	2.211
K	0.19	0.187	0.19	0.187	0.186	0.175	0.18	0.189
Ab	56.9	57.1	57.4	56.6	56.2	56.9	55.9	56.6
An	38.2	38.1	37.6	38.6	39	38.6	39.4	38.6
Or	4.9	4.8	5	4.8	4.8	4.5	4.7	4.8

Table A.2: Con't

	LT003-018	LT003-019	LT003-020	LT003-021	LT003-022	LT003-023	LT003-024	LT003-025
SiO_2	57.562	57.788	57.939	57.766	57.536	57.36	57.329	57.272
Al_2O_3	25.4	25.408	25.352	25.452	25.439	25.602	25.647	25.713
FeOT	0.466	0.442	0.475	0.451	0.428	0.477	0.486	0.46
MgO	0.02	0.032	0.034	0.035	0.031	0.03	0.031	0.013
BaO	na	na	na	na	na	na	na	na
SrO	na	na	na	na	na	na	na	na
CaO	7.762	7.787	7.62	7.659	7.806	7.858	7.919	8.058
Na_2O	6.092	6.256	6.27	6.2	6.208	6.153	6.147	6.102
K_2O	0.823	0.809	0.761	0.79	0.761	0.74	0.737	0.765
Total	98.12	98.52	98.45	98.35	98.21	98.22	98.3	98.38
				Oxygen = 32.000				
Si	10.513	10.516	10.541	10.522	10.501	10.471	10.461	10.446
Al	5.463	5.445	5.432	5.459	5.468	5.504	5.511	5.523
Fe	0.071	0.067	0.072	0.069	0.065	0.073	0.074	0.07
Mg	0.005	0.009	0.009	0.01	0.008	0.008	0.008	0.004
Ba	na	na	na	na	na	na	na	na
Ca	1.519	1.518	1.485	1.495	1.526	1.537	1.548	1.575
Na	2.157	2.207	2.212	2.19	2.197	2.178	2.175	2.158
K	0.192	0.188	0.177	0.184	0.177	0.172	0.172	0.178
Ab	55.8	56.4	57.1	56.6	56.3	56	55.8	55.2
An	39.3	38.8	38.3	38.6	39.1	39.5	39.7	40.3
Or	5	4.8	4.6	4.8	4.5	4.4	4.4	4.6

Table A.2: Con't

	LT003-026	LT003-027	LT003-028	LT003-029	LT003-030	LT003-031	LT003-032	LT003-033
SiO_2	57.718	56.792	57.054	58.114	57.848	57.815	57.634	57.889
Al_2O_3	26.16	25.981	26.045	25.41	25.301	25.535	25.367	25.538
FeOт	0.452	0.466	0.438	0.442	0.445	0.454	0.443	0.482
MgO	0.014	0.033	0.032	0.034	0.022	0.017	0.033	0.037
BaO	na	na	na	na	na	na	na	na
SrO	na	na	na	na	na	na	na	na
CaO	8.357	8.432	8.432	7.605	7.722	7.789	7.785	7.804
Na_2O	5.973	5.849	5.786	6.171	6.196	6.147	6.202	5.893
K_2O	0.688	0.685	0.68	0.844	0.82	0.793	0.805	0.804
Total	99.36	98.24	98.47	98.62	98.35	98.55	98.27	98.45
				Oxygen = 32.000				
Si	10.419	10.379	10.394	10.551	10.539	10.512	10.514	10.526
Al	5.561	5.591	5.588	5.433	5.428	5.468	5.45	5.469
Fe	0.068	0.071	0.067	0.067	0.068	0.069	0.068	0.073
Mg	0.004	0.009	0.009	0.009	0.006	0.005	0.009	0.01
Ba	na	na	na	na	na	na	na	na
Ca	1.616	1.651	1.646	1.479	1.507	1.517	1.522	1.52
Na	2.091	2.073	2.044	2.172	2.189	2.167	2.194	2.078
K	0.158	0.16	0.158	0.195	0.191	0.184	0.187	0.187
Ab	54.1	53.4	53.1	56.5	56.3	56	56.2	54.9
An	41.8	42.5	42.8	38.5	38.8	39.2	39	40.2
Or	4.1	4.1	4.1	5.1	4.9	4.8	4.8	4.9

Table A.2: Con't

	LT003-034	LT004-002	LT004-003	LT004-004	LT004-005	LT004-006	LT004-007	LT004-012
SiO_2	58.023	59.253	58.847	58.36	58.446	57.442	57.787	57.949
Al_2O_3	25.249	24.433	24.606	24.812	25.071	25.585	25.288	25.316
FeOт	0.446	0.387	0.399	0.418	0.413	0.429	0.411	0.446
MgO	0.026	0.031	0.039	0.04	0.027	0.016	0.04	0.021
BaO	na	na	na	na	na	na	na	na
SrO	na	na	na	na	na	na	na	na
CaO	7.506	6.547	6.764	7.319	7.258	7.935	7.623	7.558
Na_2O	6.251	6.597	6.545	6.35	6.371	6.138	6.253	6.284
K_2O	0.829	1.098	1.037	0.905	0.914	0.813	0.823	0.837
Total	98.33	98.35	98.24	98.2	98.5	98.36	98.23	98.41
				Oxygen = 32.000				
Si	10.565	10.762	10.709	10.636	10.618	10.475	10.54	10.549
Al	5.414	5.226	5.273	5.326	5.364	5.495	5.432	5.427
Fe	0.068	0.059	0.061	0.064	0.063	0.065	0.063	0.068
Mg	0.007	0.008	0.011	0.011	0.007	0.004	0.011	0.006
Ba	na	na	na	na	na	na	na	na
Ca	1.464	1.274	1.319	1.429	1.413	1.55	1.49	1.474
Na	2.207	2.323	2.309	2.244	2.244	2.17	2.211	2.218
K	0.193	0.254	0.241	0.21	0.212	0.189	0.191	0.194
Ab	57.1	60.3	59.7	57.8	58	55.5	56.8	57.1
An	37.9	33.1	34.1	36.8	36.5	39.7	38.3	37.9
Or	5	6.6	6.2	5.4	5.5	4.8	4.9	5

Table A.2: Con't

	LT004-013	LT004-014	LT004-016	LT004-017	LT004-018	LT004-020	LT004-022	LT004-024
SiO_2	58.358	57.814	58.036	58.073	58.032	58.164	57.929	57.977
Al_2O_3	25.317	25.243	25.092	25.191	25.23	24.921	25.237	25.434
FeOT	0.442	0.441	0.47	0.454	0.415	0.441	0.516	0.404
MgO	0.031	0.025	0.03	0.021	0.032	0.024	0.032	0.029
BaO	na	na	na	na	na	na	na	na
SrO	na	na	na	na	na	na	na	na
CaO	7.642	7.48	7.482	7.454	7.613	7.223	7.622	7.627
Na_2O	6.217	6.291	6.297	6.258	6.272	6.496	6.265	6.286
K_2O	0.82	0.826	0.813	0.843	0.821	0.817	0.803	0.777
Total	98.83	98.12	98.22	98.29	98.42	98.09	98.4	98.53
				Oxygen = 32.000				
Si	10.572	10.553	10.581	10.577	10.561	10.614	10.55	10.537
Al	5.401	5.426	5.387	5.403	5.407	5.356	5.413	5.444
Fe	0.067	0.067	0.072	0.069	0.063	0.067	0.079	0.061
Mg	0.008	0.007	0.008	0.006	0.009	0.007	0.009	0.008
Ba	na	na	na	na	na	na	na	na
Ca	1.483	1.463	1.462	1.455	1.484	1.412	1.487	1.485
Na	2.184	2.227	2.226	2.21	2.213	2.299	2.212	2.215
K	0.19	0.192	0.189	0.196	0.191	0.19	0.187	0.18
Ab	56.6	57.4	57.4	57.2	56.9	58.9	56.9	57.1
An	38.4	37.7	37.7	37.7	38.2	36.2	38.3	38.3
Or	4.9	4.9	4.9	5.1	4.9	4.9	4.8	4.6

Table A.2: Con't

	LT004-025	LT004-026	LT004-027	LT004-028	LT004-030	LT004-031	LT004-032	LT004-033
SiO_2	57.586	57.656	57.641	57.56	57.342	57.577	57.644	57.789
Al_2O_3	25.284	25.37	25.542	25.491	25.431	25.556	25.467	25.396
FeOT	0.458	0.405	0.474	0.43	0.483	0.455	0.435	0.41
MgO	0.027	0.023	0.043	0.021	0.032	0.034	0.04	0.024
BaO	na	na	na	na	na	na	na	na
SrO	na	na	na	na	na	na	na	na
CaO	7.733	7.768	7.795	7.871	7.937	7.949	7.85	7.822
Na_2O	6.229	6.249	6.266	6.216	6.085	6.062	6.099	6.138
K_2O	0.805	0.768	0.744	0.753	0.737	0.746	0.794	0.794
Total	98.12	98.24	98.51	98.34	98.05	98.38	98.33	98.37
				Oxygen = 32.000				
Si	10.521	10.518	10.492	10.494	10.487	10.49	10.506	10.525
Al	5.44	5.45	5.475	5.473	5.477	5.483	5.466	5.447
Fe	0.07	0.062	0.072	0.066	0.074	0.069	0.066	0.062
Mg	0.007	0.006	0.012	0.006	0.009	0.009	0.011	0.007
Ba	na	na	na	na	na	na	na	na
Ca	1.514	1.518	1.52	1.537	1.555	1.552	1.533	1.526
Na	2.207	2.21	2.211	2.197	2.158	2.141	2.155	2.168
K	0.188	0.179	0.173	0.175	0.172	0.173	0.185	0.184
Ab	56.5	56.6	56.6	56.2	55.5	55.4	55.6	55.9
An	38.7	38.9	38.9	39.3	40	40.1	39.6	39.4
Or	4.8	4.6	4.4	4.5	4.4	4.5	4.8	4.7

Table A.2: Con't

	LT004-036	LT004-037	LT004-038	LT004-039	LT004-040	LT004-042	LT004-045	LT004-046
SiO_2	57.792	57.996	58.092	57.948	57.911	58.722	58.799	56.969
Al_2O_3	25.23	25.164	25.153	25.214	25.153	24.795	24.723	25.829
FeOT	0.461	0.44	0.425	0.456	0.444	0.447	0.384	0.422
MgO	0.029	0.017	0.031	0.029	0.027	0.033	0.025	0.027
BaO	na	na	na	na	na	na	na	na
SrO	na	na	na	na	na	na	na	na
CaO	7.5	7.495	7.473	7.382	7.492	7.048	7	8.396
Na_2O	6.231	6.236	6.065	6.243	6.215	6.533	6.551	5.926
K_2O	0.81	0.823	0.792	0.81	0.828	0.904	0.914	0.78
Total	98.05	98.17	98.03	98.08	98.07	98.48	98.4	98.35
				Oxygen = 32.000				
Si	10.554	10.576	10.595	10.573	10.572	10.666	10.684	10.403
Al	5.426	5.404	5.403	5.418	5.408	5.304	5.29	5.554
Fe	0.07	0.067	0.065	0.07	0.068	0.068	0.058	0.064
Mg	0.008	0.005	0.008	0.008	0.007	0.009	0.007	0.007
Ba	na	na	na	na	na	na	na	na
Ca	1.468	1.464	1.46	1.443	1.465	1.372	1.363	1.643
Na	2.207	2.205	2.145	2.209	2.2	2.301	2.308	2.098
K	0.189	0.191	0.184	0.189	0.193	0.209	0.212	0.182
Ab	57.1	57.1	56.6	57.5	57	59.3	59.4	53.5
An	38	37.9	38.5	37.6	38	35.3	35.1	41.9
Or	4.9	4.9	4.9	4.9	5	5.4	5.5	4.6

Table A.2: Con't

	LT004-048	LT004-050	LT006-001	LT006-002	LT006-003	LT006-004	LT006-005	LT006-006
SiO_2	57.222	58.114	63.526	64.504	64.308	63.901	64.373	63.973
Al_2O_3	25.472	25.191	20.707	19.894	19.767	20.383	19.897	20.34
FeOT	0.434	0.442	0.287	0.254	0.267	0.301	0.288	0.289
MgO	0.034	0.032	0.002	0.001	0	0	0.001	0.003
BaO	na	na	na	na	na	na	na	na
SrO	na	na	na	na	na	na	na	na
CaO	7.91	7.589	2.33	1.586	1.375	1.863	1.463	1.898
Na_2O	6.246	6.274	6.766	6.494	6.328	6.493	6.195	6.438
K_2O	0.832	0.868	4.556	5.934	6.226	5.412	6.102	5.353
Total	98.15	98.51	98.17	98.67	98.27	98.35	98.32	98.29
				Oxygen = 32.000				
Si	10.466	10.569	11.559	11.716	11.734	11.629	11.728	11.641
Al	5.486	5.395	4.437	4.255	4.248	4.368	4.269	4.359
Fe	0.066	0.067	0.044	0.039	0.041	0.046	0.044	0.044
Mg	0.009	0.009	0.001	0	0	0	0	0.001
Ba	na	na	na	na	na	na	na	na
Ca	1.55	1.479	0.454	0.309	0.269	0.363	0.286	0.37
Na	2.215	2.212	2.387	2.287	2.239	2.291	2.189	2.272
K	0.194	0.201	1.058	1.375	1.449	1.256	1.418	1.243
Ab	55.9	56.8	61.2	57.6	56.6	58.6	56.2	58.5
An	39.2	38	11.6	7.8	6.8	9.3	7.3	9.5
Or	4.9	5.2	27.1	34.6	36.6	32.1	36.4	32

Table A.2: Con't

	LT006-007	LT006-008	LT006-009	LT006-011	LT006-014	LT006-015	LT006-016	LT006-017
SiO_2	64.264	64.372	62.916	62.801	62.428	62.617	62.959	62.533
Al_2O_3	20.206	20.431	21.318	21.529	21.631	21.557	21.327	21.562
FeOT	0.286	0.297	0.307	0.324	0.306	0.3	0.338	0.345
MgO	0.008	0	0.012	0.002	0	0.006	0.004	0
BaO	na	na	na	na	na	na	na	na
SrO	na	na	na	na	na	na	na	na
CaO	1.644	1.897	2.994	3.02	3.264	3.292	2.906	3.095
Na_2O	6.432	6.392	6.765	6.836	6.925	6.939	6.986	6.916
K_2O	5.743	5.257	3.783	3.703	3.427	3.433	3.786	3.619
Total	98.58	98.65	98.1	98.22	97.98	98.14	98.31	98.07
				Oxygen = 32.000				
Si	11.673	11.657	11.44	11.407	11.366	11.381	11.433	11.382
Al	4.322	4.357	4.565	4.605	4.638	4.614	4.561	4.622
Fe	0.043	0.045	0.047	0.049	0.047	0.046	0.051	0.053
Mg	0.002	0	0.003	0.001	0	0.002	0.001	0
Ba	na	na	na	na	na	na	na	na
Ca	0.32	0.368	0.583	0.588	0.637	0.641	0.565	0.604
Na	2.265	2.245	2.385	2.408	2.445	2.446	2.46	2.441
K	1.331	1.215	0.878	0.858	0.796	0.796	0.877	0.84
Ab	57.8	58.6	62	62.5	63	63	63	62.8
An	8.2	9.6	15.2	15.3	16.4	16.5	14.5	15.5
Or	34	31.7	22.8	22.3	20.5	20.5	22.5	21.6

Table A.2: Con't

	LT006-018	LT006-020	LT006-021	LT006-023	LT006-025	LT007-001	LT007-002	LT007-003
SiO_2	62.508	63.183	62.652	63.376	63.289	54.208	48.839	48.387
Al_2O_3	21.432	21.002	21.403	21.376	19.839	27.502	31.523	32.093
FeOT	0.326	0.296	0.336	0.301	1.143	0.673	0.613	0.553
MgO	0	0.005	0.004	0.015	0.165	0.079	0.084	0.072
BaO	na	na	na	na	na	na	na	na
SrO	na	na	na	na	na	na	na	na
CaO	2.99	2.472	2.964	2.796	1.514	10.726	15.056	15.876
Na_2O	6.977	6.681	6.819	7.006	6.541	4.69	2.576	2.29
K_2O	3.794	4.428	3.821	3.864	5.743	0.514	0.178	0.131
Total	98.03	98.07	98	98.73	98.23	98.39	98.87	99.4
				Oxygen = 32.000				
Si	11.393	11.507	11.413	11.453	11.607	9.964	9.044	8.929
Al	4.6	4.504	4.592	4.549	4.285	5.953	6.875	6.975
Fe	0.05	0.045	0.051	0.045	0.175	0.103	0.095	0.085
Mg	0	0.001	0.001	0.004	0.045	0.022	0.023	0.02
Ba	na	na	na	na	na	na	na	na
Ca	0.584	0.482	0.579	0.541	0.297	2.112	2.987	3.139
Na	2.466	2.359	2.409	2.455	2.326	1.672	0.925	0.819
K	0.882	1.029	0.888	0.891	1.344	0.121	0.042	0.031
Ab	62.7	61	62.2	63.2	58.6	42.8	23.4	20.5
An	14.9	12.5	14.9	13.9	7.5	54.1	75.5	78.7
Or	22.4	26.6	22.9	22.9	33.9	3.1	1.1	0.8

Table A.2: Con't

	LT007-004	LT007-005	LT007-006	LT007-007	LT007-008	LT007-009	LT007-010	LT007-011
SiO_2	48.85	48.589	50.268	49.789	49.919	48.834	50.795	49.506
Al_2O_3	31.825	31.644	30.974	30.962	30.984	31.074	28.646	31.13
FeOT	0.534	0.588	0.518	0.582	0.52	0.584	1.158	0.534
MgO	0.053	0.069	0.079	0.053	0.07	0.069	0.225	0.068
BaO	na	na	na	na	na	na	na	na
SrO	na	na	na	na	na	na	na	na
CaO	15.518	15.232	14.065	14.63	14.132	15.111	13.325	14.709
Na_2O	2.393	2.587	3.034	3.03	2.949	3.043	3.64	2.785
K_2O	0.156	0.182	0.22	0.189	0.205	0.198	0.344	0.192
Total	99.33	98.89	99.16	99.23	98.78	98.91	98.13	98.92
				Oxygen = 32.000				
Si	9.007	9.005	9.244	9.176	9.218	9.06	9.474	9.147
Al	6.911	6.906	6.708	6.72	6.738	6.79	6.292	6.774
Fe	0.082	0.091	0.08	0.09	0.08	0.091	0.181	0.083
Mg	0.015	0.019	0.022	0.015	0.019	0.019	0.063	0.019
Ba	na	na	na	na	na	na	na	na
Ca	3.066	3.024	2.771	2.889	2.796	3.004	2.663	2.912
Na	0.856	0.93	1.082	1.083	1.056	1.095	1.316	0.998
K	0.037	0.043	0.052	0.044	0.048	0.047	0.082	0.045
Ab	21.6	23.3	27.7	27	27.1	26.4	32.4	25.2
An	77.4	75.7	71	71.9	71.7	72.5	65.6	73.6
Or	0.9	1.1	1.3	1.1	1.2	1.1	2	1.1

Table A.2: Con't

	LT007-012	LT007-014	LT007-015	LT007-016	LT007-017	LT007-018	LT007-019	LT007-020
SiO_2	47.961	47.957	48.144	48.097	48.634	49.406	49.198	49.471
Al_2O_3	32.09	32.076	32.194	32.166	31.73	30.997	31.185	31.359
FeOT	0.564	0.546	0.563	0.536	0.544	0.603	0.563	0.498
MgO	0.066	0.058	0.053	0.068	0.069	0.058	0.071	0.075
BaO	na	na	na	na	na	na	na	na
SrO	na	na	na	na	na	na	na	na
CaO	15.583	15.864	15.726	15.96	15.451	14.611	14.87	14.842
Na_2O	2.245	2.141	2.214	2.195	2.527	2.832	2.74	2.796
K_2O	0.147	0.148	0.148	0.128	0.172	0.227	0.192	0.194
Total	98.66	98.79	99.04	99.15	99.13	98.73	98.82	99.24
				Oxygen = 32.000				
Si	8.913	8.904	8.913	8.9	8.993	9.151	9.109	9.116
Al	7.023	7.014	7.019	7.01	6.91	6.762	6.8	6.805
Fe	0.088	0.085	0.087	0.083	0.084	0.093	0.087	0.077
Mg	0.018	0.016	0.015	0.019	0.019	0.016	0.02	0.021
Ba	na	na	na	na	na	na	na	na
Ca	3.103	3.156	3.119	3.164	3.061	2.9	2.95	2.93
Na	0.809	0.771	0.795	0.788	0.906	1.017	0.984	0.999
K	0.035	0.035	0.035	0.03	0.041	0.054	0.045	0.046
Ab	20.5	19.5	20.1	19.8	22.6	25.6	24.7	25.1
An	78.6	79.7	79	79.5	76.4	73	74.1	73.7
Or	0.9	0.9	0.9	0.8	1	1.4	1.1	1.2

Table A.2: Con't

	LT007-021	LT007-022	LT007-023	LT007-025	LT007-026	LT007-027	LT007-028	LT007-029
SiO_2	48.163	48.023	49.228	51.187	49.066	48.222	49.248	48.488
Al_2O_3	32.117	32.365	31.543	29.917	31.307	32.049	31.265	31.755
FeOт	0.52	0.532	0.518	0.608	0.505	0.56	0.569	0.532
MgO	0.067	0.065	0.071	0.047	0.066	0.062	0.053	0.061
BaO	na	na	na	na	na	na	na	na
SrO	na	na	na	na	na	na	na	na
CaO	15.612	15.89	15.083	13.421	15.013	15.712	15.031	15.283
Na_2O	2.277	2.22	2.609	3.446	2.572	2.288	2.708	2.422
K_2O	0.148	0.144	0.189	0.25	0.177	0.151	0.173	0.166
Total	98.9	99.24	99.24	98.88	98.71	99.04	99.05	98.71
				Oxygen = 32.000				
Si	8.925	8.878	9.075	9.428	9.091	8.929	9.1	8.995
Al	7.009	7.047	6.848	6.489	6.831	6.988	6.804	6.938
Fe	0.081	0.082	0.08	0.094	0.078	0.087	0.088	0.083
Mg	0.019	0.018	0.02	0.013	0.018	0.017	0.015	0.017
Ba	na	na	na	na	na	na	na	na
Ca	3.1	3.148	2.979	2.649	2.98	3.117	2.976	3.038
Na	0.818	0.796	0.933	1.231	0.924	0.821	0.97	0.871
K	0.035	0.034	0.044	0.059	0.042	0.036	0.041	0.039
Ab	20.7	20	23.6	31.3	23.4	20.7	24.3	22.1
An	78.4	79.1	75.3	67.3	75.5	78.4	74.6	77
Or	0.9	0.9	1.1	1.5	1.1	0.9	1	1

Table A.2: Con't

	LT007-030	LT007-031	LT007-032	LT007-034	LT007-039	LT007-040	LT007-041	LT007-042
SiO_2	47.548	49.1	50.683	48.67	51.852	48.694	49.149	48.909
Al_2O_3	31.943	31.381	29.776	31.26	28.395	32.408	31.569	31.584
FeOт	0.543	0.55	0.626	0.545	1.626	0.586	0.529	0.533
MgO	0.071	0.069	0.107	0.072	0.392	0.056	0.074	0.051
BaO	na	na	na	na	na	na	na	na
SrO	na	na	na	na	na	na	na	na
CaO	15.795	14.882	13.208	15.072	12.302	15.852	15.097	15.2
Na_2O	2.3	2.649	3.451	2.581	3.771	2.311	2.644	2.564
K_2O	0.171	0.212	0.322	0.201	0.668	0.164	0.183	0.16
Total	98.37	98.84	98.17	98.4	99.01	100.07	99.25	99
				Oxygen = 32.000				
Si	8.877	9.087	9.407	9.057	9.584	8.925	9.063	9.044
Al	7.023	6.84	6.509	6.851	6.181	6.995	6.856	6.878
Fe	0.085	0.085	0.097	0.085	0.251	0.09	0.082	0.082
Mg	0.02	0.019	0.03	0.02	0.108	0.015	0.02	0.014
Ba	na	na	na	na	na	na	na	na
Ca	3.159	2.951	2.627	3.005	2.436	3.113	2.983	3.011
Na	0.833	0.951	1.242	0.931	1.352	0.821	0.945	0.919
K	0.041	0.05	0.076	0.048	0.158	0.038	0.043	0.038
Ab	20.7	24.1	31.5	23.4	34.3	20.7	23.8	23.2
An	78.3	74.7	66.6	75.4	61.7	78.4	75.1	75.9
Or	1	1.3	1.9	1.2	4	1	1.1	1

Table A.2: Con't

	LT007-043	LT007-044	LT007-045	LT007-046	LT007-050	LT007-052	LT007-053	LT007-054
SiO_2	48.466	49.241	49.178	50.858	48.256	49.169	52.354	50.015
Al_2O_3	31.382	31.257	31.518	30.439	31.922	31.062	29.093	30.375
FeOT	0.533	0.508	0.538	0.491	0.554	0.535	0.5	0.516
MgO	0.081	0.081	0.069	0.078	0.052	0.056	0.067	0.061
BaO	na	na	na	na	na	na	na	na
SrO	na	na	na	na	na	na	na	na
CaO	15.213	14.69	14.988	13.508	15.495	14.549	12.163	13.982
Na_2O	2.431	2.665	2.639	3.265	2.336	2.731	4.013	3.159
K_2O	0.159	0.195	0.195	0.248	0.15	0.213	0.329	0.238
Total	98.27	98.64	99.12	98.89	98.77	98.32	98.52	98.35
				Oxygen = 32.000				
Si	9.03	9.122	9.076	9.361	8.954	9.139	9.639	9.28
Al	6.886	6.819	6.851	6.598	6.975	6.799	6.308	6.637
Fe	0.083	0.079	0.083	0.076	0.086	0.083	0.077	0.08
Mg	0.022	0.022	0.019	0.021	0.014	0.016	0.018	0.017
Ba	na	na	na	na	na	na	na	na
Ca	3.037	2.916	2.964	2.664	3.08	2.897	2.399	2.78
Na	0.878	0.957	0.944	1.165	0.84	0.984	1.433	1.137
K	0.038	0.046	0.046	0.058	0.036	0.051	0.077	0.056
Ab	22.2	24.4	23.9	30	21.2	25	36.7	28.6
An	76.8	74.4	75	68.5	77.9	73.7	61.4	70
Or	1	1.2	1.2	1.5	0.9	1.3	2	1.4

Table A.2: Con't

	LT007-057	LT007-059	LT007-063	LT007-064	LT007-065	LT007-066	LT007-067	LT007-069
SiO_2	48.055	48.409	48.179	48.313	49.191	49.932	52.893	48.343
Al_2O_3	31.822	31.65	31.985	32.03	31.368	30.938	27.569	31.659
FeOT	0.509	0.576	0.576	0.571	0.558	0.582	0.909	0.524
MgO	0.063	0.07	0.069	0.05	0.055	0.052	0.219	0.055
BaO	na	na	na	na	na	na	na	na
SrO	na	na	na	na	na	na	na	na
CaO	15.609	15.272	15.633	15.722	14.917	14.491	11.719	15.654
Na_2O	2.179	2.428	2.368	2.347	2.708	2.844	4.309	2.3
K_2O	0.155	0.146	0.135	0.149	0.17	0.208	0.581	0.144
Total	98.39	98.55	98.94	99.18	98.97	99.05	98.2	98.68
				Oxygen = 32.000				
Si	8.949	8.997	8.931	8.935	9.093	9.207	9.799	8.979
Al	6.979	6.927	6.982	6.976	6.829	6.718	6.015	6.925
Fe	0.079	0.09	0.089	0.088	0.086	0.09	0.141	0.081
Mg	0.017	0.019	0.019	0.014	0.015	0.014	0.06	0.015
Ba	na	na	na	na	na	na	na	na
Ca	3.114	3.041	3.105	3.115	2.954	2.863	2.326	3.115
Na	0.787	0.875	0.851	0.842	0.971	1.017	1.548	0.828
K	0.037	0.035	0.032	0.035	0.04	0.049	0.137	0.034
Ab	20	22.1	21.3	21.1	24.5	25.9	38.6	20.8
An	79.1	77	77.9	78	74.5	72.9	58	78.3
Or	0.9	0.9	0.8	0.9	1	1.2	3.4	0.9

Table A.2: Con't

	LT007-070	LT007-071	LT007-072	LT007-073	LT007-074	LT008-001	LT008-002	LT008-003
SiO_2	49.763	48.246	49.777	48.307	53.733	66.026	65.896	66.01
Al_2O_3	31.085	31.939	30.981	32.065	28.124	18.664	18.782	18.774
FeOT	0.529	0.574	0.501	0.572	0.653	0.237	0.199	0.205
MgO	0.061	0.073	0.073	0.085	0.1	0	0.004	0
BaO	na	na	na	na	na	na	na	na
SrO	na	na	na	na	na	na	na	na
CaO	14.75	15.916	14.616	15.901	11.187	0.143	0.145	0.169
Na_2O	2.849	2.132	2.867	2.209	4.489	5.478	5.459	5.493
K_2O	0.215	0.141	0.186	0.15	0.477	8.772	8.686	8.645
Total	99.25	99.02	99	99.29	98.76	99.32	99.17	99.3
				Oxygen = 32.000				
Si	9.166	8.936	9.185	8.925	9.852	11.983	11.97	11.974
Al	6.743	6.967	6.732	6.977	6.072	3.989	4.018	4.011
Fe	0.081	0.089	0.077	0.088	0.1	0.036	0.03	0.031
Mg	0.017	0.02	0.02	0.023	0.027	0	0.001	0
Ba	na	na	na	na	na	na	na	na
Ca	2.911	3.159	2.89	3.148	2.198	0.028	0.028	0.033
Na	1.018	0.766	1.026	0.791	1.596	1.928	1.923	1.932
K	0.051	0.033	0.044	0.035	0.112	2.031	2.013	2.001
Ab	25.6	19.4	25.9	19.9	40.9	48.4	48.5	48.7
An	73.1	79.8	73	79.2	56.3	0.7	0.7	0.8
Or	1.3	0.8	1.1	0.9	2.9	50.9	50.8	50.5

Table A.2: Con't

	LT008-004	LT008-005	LT008-006	LT008-007	LT008-009	LT008-010	LT008-012	LT008-013
SiO_2	66.108	66.126	66.044	65.695	66.401	65.997	65.808	66.137
Al_2O_3	18.642	18.721	18.878	18.633	18.75	18.728	18.648	18.775
FeOT	0.246	0.19	0.239	0.228	0.235	0.235	0.19	0.222
MgO	0.001	0.014	0.007	0	0	0	0.003	0.004
BaO	na	na	na	na	na	na	na	na
SrO	na	na	na	na	na	na	na	na
CaO	0.142	0.179	0.166	0.168	0.132	0.172	0.167	0.167
Na_2O	5.504	5.584	5.616	5.584	5.419	5.581	5.395	5.322
K_2O	8.749	8.612	8.54	8.615	8.955	8.68	8.979	9.062
Total	99.39	99.43	99.49	98.92	99.89	99.39	99.19	99.69
				Oxygen = 32.000				
Si	11.989	11.98	11.957	11.971	11.987	11.97	11.973	11.972
Al	3.981	3.994	4.025	3.998	3.986	4	3.995	4.002
Fe	0.037	0.029	0.036	0.035	0.035	0.036	0.029	0.034
Mg	0	0.004	0.002	0	0	0	0.001	0.001
Ba	na	na	na	na	na	na	na	na
Ca	0.028	0.035	0.032	0.033	0.026	0.033	0.033	0.032
Na	1.935	1.962	1.972	1.973	1.897	1.963	1.903	1.868
K	2.024	1.99	1.972	2.003	2.062	2.008	2.084	2.093
Ab	48.5	49.2	49.6	49.2	47.6	49	47.3	46.8
An	0.7	0.9	0.8	0.8	0.7	0.8	0.8	0.8
Or	50.8	49.9	49.6	50	51.7	50.1	51.8	52.4

Table A.2: Con't

	LT008-014	LT008-015	LT008-016	LT008-017	LT008-018	LT008-019	LT008-020	LT008-021
SiO_2	65.795	66.352	66.185	65.946	65.646	65.565	65.687	65.589
Al_2O_3	18.735	18.703	18.765	18.637	18.766	18.646	18.78	18.624
FeOT	0.223	0.245	0.207	0.216	0.198	0.256	0.224	0.257
MgO	0	0.001	0.014	0.002	0	0	0.005	0.004
BaO	na	na	na	na	na	na	na	na
SrO	na	na	na	na	na	na	na	na
CaO	0.177	0.17	0.165	0.181	0.162	0.168	0.14	0.162
Na_2O	5.433	5.494	5.467	5.536	5.392	5.45	5.365	5.462
K_2O	8.698	8.727	8.739	8.691	8.825	8.779	9.035	9.082
Total	99.06	99.69	99.54	99.21	98.99	98.86	99.24	99.18
				Oxygen = 32.000				
Si	11.969	11.992	11.979	11.981	11.958	11.963	11.95	11.953
Al	4.014	3.981	4	3.987	4.026	4.007	4.024	3.997
Fe	0.034	0.037	0.031	0.033	0.03	0.039	0.034	0.039
Mg	0	0	0.004	0.001	0	0	0.001	0.001
Ba	na	na	na	na	na	na	na	na
Ca	0.034	0.033	0.032	0.035	0.032	0.033	0.027	0.032
Na	1.916	1.925	1.919	1.95	1.904	1.928	1.893	1.93
K	2.019	2.012	2.018	2.014	2.051	2.044	2.097	2.111
Ab	48.3	48.5	48.3	48.8	47.8	48.1	47.1	47.4
An	0.9	0.8	0.8	0.9	0.8	0.8	0.7	0.8
Or	50.9	50.7	50.8	50.4	51.4	51	52.2	51.8

Table A.2: Con't

	LT008-022	LT009-002	LT009-003	LT009-006	LT009-007	LT009-008	LT009-009	LT009-010
SiO_2	64.995	49.408	50.754	48.235	48.253	47.217	47.415	47.874
Al_2O_3	18.522	30.421	30.635	31.224	31.789	31.822	32.088	31.779
FeOT	0.301	0.592	0.542	0.591	0.601	0.605	0.61	0.664
MgO	0.013	0.08	0.053	0.07	0.07	0.059	0.073	0.064
BaO	na	na	na	na	na	na	na	na
SrO	na	na	na	na	na	na	na	na
CaO	0.181	14.551	14.168	15.218	15.479	15.937	16.065	15.959
Na_2O	5.338	2.985	3.223	2.64	2.393	2.285	2.229	2.267
K_2O	8.84	0.17	0.242	0.162	0.163	0.176	0.14	0.175
Total	98.19	98.21	99.62	98.14	98.75	98.1	98.62	98.78
				Oxygen = 32.000				
Si	11.952	9.202	9.298	9.013	8.96	8.851	8.839	8.907
Al	4.011	6.672	6.61	6.871	6.952	7.025	7.045	6.963
Fe	0.046	0.092	0.083	0.092	0.093	0.095	0.095	0.103
Mg	0.004	0.022	0.014	0.019	0.019	0.016	0.02	0.018
Ba	na	na	na	na	na	na	na	na
Ca	0.036	2.904	2.781	3.047	3.08	3.201	3.209	3.181
Na	1.903	1.078	1.145	0.957	0.862	0.831	0.806	0.818
K	2.074	0.04	0.057	0.039	0.039	0.042	0.033	0.042
Ab	47.4	26.8	28.7	23.7	21.7	20.4	19.9	20.2
An	0.9	72.2	69.8	75.4	77.4	78.6	79.3	78.7
Or	51.7	1	1.4	1	1	1	0.8	1

Table A.2: Con't

	LT009-011	LT009-012	LT009-013	LT009-017	LT009-018	LT009-020	LT010-001	LT010-003
SiO_2	48.243	47.951	48.151	49.28	48.734	53.914	54.192	54.468
Al_2O_3	32.328	32.197	32.33	31.025	32.051	27.647	28.336	28.021
FeOт	0.571	0.546	0.565	0.639	0.615	0.762	0.576	0.528
MgO	0.059	0.071	0.046	0.062	0.062	0.096	0.076	0.049
BaO	na	na	na	na	na	na	na	na
SrO	na	na	na	na	na	na	na	na
CaO	15.958	15.98	15.882	14.776	15.92	10.979	11.039	10.705
Na_2O	2.296	2.333	2.273	2.727	2.286	4.846	4.785	4.927
K_2O	0.154	0.127	0.15	0.186	0.138	0.495	0.409	0.438
Total	99.61	99.21	99.4	98.7	99.81	98.74	99.41	99.14
				Oxygen = 32.000				
Si	8.891	8.877	8.89	9.134	8.957	9.9	9.864	9.93
Al	7.016	7.019	7.029	6.772	6.937	5.978	6.074	6.016
Fe	0.088	0.085	0.087	0.099	0.095	0.117	0.088	0.081
Mg	0.016	0.02	0.013	0.017	0.017	0.026	0.021	0.013
Ba	na	na	na	na	na	na	na	na
Ca	3.151	3.169	3.142	2.934	3.135	2.16	2.153	2.091
Na	0.82	0.837	0.814	0.98	0.815	1.725	1.689	1.742
K	0.036	0.03	0.035	0.044	0.032	0.116	0.095	0.102
Ab	20.5	20.7	20.4	24.8	20.5	43.1	42.9	44.3
An	78.6	78.5	78.7	74.1	78.7	54	54.7	53.1
Or	0.9	0.7	0.9	1.1	0.8	2.9	2.4	2.6

Table A.2: Con't

	LT010-004	LT010-005	LT010-006	LT010-007	LT010-008	LT010-009	LT010-010	LT011-003
SiO_2	55.206	55.074	54.878	54.631	54.712	53.641	53.818	48.578
Al_2O_3	27.662	27.299	27.497	27.457	27.505	27.796	28.169	31.388
FeOт	0.504	0.541	0.51	0.487	0.5	0.584	0.571	0.548
MgO	0.048	0.048	0.046	0.049	0.061	0.044	0.058	0.069
BaO	na	na	na	na	na	na	na	na
SrO	na	na	na	na	na	na	na	na
CaO	10.286	10.294	10.373	10.419	10.17	10.824	10.926	15.368
Na_2O	5.115	5.212	5.148	5.123	5.177	4.903	4.856	2.456
K_2O	0.458	0.452	0.438	0.44	0.485	0.415	0.432	0.144
Total	99.28	98.92	98.89	98.61	98.61	98.21	98.83	98.55
				Oxygen = 32.000				
Si	10.032	10.053	10.02	10.007	10.016	9.888	9.858	9.029
Al	5.92	5.868	5.913	5.923	5.93	6.034	6.076	6.871
Fe	0.077	0.083	0.078	0.075	0.077	0.09	0.087	0.085
Mg	0.013	0.013	0.013	0.013	0.017	0.012	0.016	0.019
Ba	na	na	na	na	na	na	na	na
Ca	2.003	2.013	2.029	2.045	1.995	2.138	2.144	3.061
Na	1.802	1.845	1.823	1.819	1.838	1.752	1.725	0.885
K	0.106	0.105	0.102	0.103	0.113	0.098	0.101	0.034
Ab	46.1	46.6	46.1	45.9	46.6	43.9	43.5	22.2
An	51.2	50.8	51.3	51.6	50.6	53.6	54	76.9
Or	2.7	2.6	2.6	2.6	2.9	2.5	2.5	0.9

Table A.2: Con't

	LT011-004	LT016-002	LT016-003	LT016-004	LT016-005	LT016-006	LT016-007	LT016-008
SiO_2	49.994	52.749	50.817	48.033	47.98	47.351	47.644	47.576
Al_2O_3	31.225	28.082	31.044	31.321	31.707	31.934	31.625	31.834
FeOT	0.534	0.686	0.641	0.542	0.571	0.602	0.555	0.566
MgO	0.073	0.078	0.091	0.054	0.052	0.047	0.05	0.055
BaO	na	na	na	na	na	na	na	na
SrO	na	na	na	na	na	na	na	na
CaO	14.932	12.178	14.552	15.546	15.638	16.072	15.843	16.03
Na_2O	2.865	4.155	3.132	2.437	2.403	2.189	2.289	2.233
K_2O	0.17	0.376	0.188	0.173	0.152	0.128	0.154	0.152
Total	99.79	98.3	100.47	98.11	98.5	98.32	98.16	98.45
				Oxygen = 32.000				
Si	9.161	9.748	9.242	8.983	8.939	8.852	8.914	8.881
Al	6.738	6.112	6.649	6.898	6.957	7.031	6.968	6.998
Fe	0.082	0.106	0.097	0.085	0.089	0.094	0.087	0.088
Mg	0.02	0.021	0.025	0.015	0.014	0.013	0.014	0.015
Ba	na	na	na	na	na	na	na	na
Ca	2.931	2.411	2.836	3.115	3.122	3.219	3.176	3.206
Na	1.018	1.489	1.105	0.884	0.868	0.794	0.83	0.808
K	0.04	0.089	0.044	0.041	0.036	0.031	0.037	0.036
Ab	25.5	37.3	27.7	21.9	21.6	19.6	20.5	20
An	73.5	60.4	71.2	77.1	77.5	79.6	78.6	79.2
Or	1	2.2	1.1	1	0.9	0.8	0.9	0.9

Table A.2: Con't

	LT016-009	LT016-010	LT016-012	LT016-013	LT016-014	LT016-015	LT017-002	LT017-006
SiO_2	48.289	47.909	48.019	48.396	48.216	48.186	47.528	48.09
Al_2O_3	31.633	31.951	31.689	31.78	31.695	31.75	31.618	31.805
FeOT	0.611	0.598	0.6	0.542	0.543	0.599	0.558	0.53
MgO	0.055	0.059	0.044	0.053	0.071	0.067	0.064	0.063
BaO	na	na	na	na	na	na	na	na
SrO	na	na	na	na	na	na	na	na
CaO	15.834	15.865	16.042	15.874	15.829	15.759	15.881	15.855
Na_2O	2.445	2.213	2.294	2.302	2.35	2.355	2.289	2.312
K_2O	0.173	0.129	0.161	0.137	0.141	0.168	0.133	0.14
Total	99.04	98.7	98.85	99.08	98.85	98.88	98.07	98.8
				Oxygen = 32.000				
Si	8.955	8.908	8.926	8.96	8.951	8.945	8.902	8.933
Al	6.909	6.992	6.937	6.929	6.93	6.941	6.974	6.957
Fe	0.095	0.093	0.093	0.084	0.084	0.093	0.087	0.082
Mg	0.015	0.016	0.012	0.015	0.02	0.019	0.018	0.017
Ba	na	na	na	na	na	na	na	na
Ca	3.146	3.161	3.195	3.149	3.149	3.134	3.187	3.155
Na	0.879	0.798	0.827	0.826	0.846	0.848	0.831	0.833
K	0.041	0.031	0.038	0.032	0.033	0.04	0.032	0.033
Ab	21.6	20	20.4	20.6	21	21.1	20.5	20.7
An	77.4	79.2	78.7	78.6	78.2	77.9	78.7	78.5
Or	1	0.8	0.9	0.8	0.8	1	0.8	0.8

Table A.2: Con't

	LT017-013	LT017-014	LT017-015	LT017-016	LT017-017	LT017-020	LT017-021	LT017-022
SiO_2	47.227	47.645	50.241	47.147	56.136	48.606	48.074	48.093
Al_2O_3	30.283	32.066	30.927	31.993	24.076	32.337	31.496	31.407
FeOT	1.728	0.527	0.574	0.524	2.574	0.568	0.584	0.534
MgO	0.352	0.056	0.078	0.066	0.658	0.058	0.065	0.061
BaO	na	na	na	na	na	na	na	na
SrO	na	na	na	na	na	na	na	na
CaO	15.998	16.161	14.515	16.115	9.174	15.881	15.658	15.771
Na_2O	2.296	2.257	3.125	2.193	5.953	2.215	2.358	2.301
K_2O	0.137	0.148	0.231	0.137	1.196	0.113	0.143	0.158
Total	98.02	98.86	99.69	98.18	99.77	99.78	98.38	98.33
				Oxygen = 32.000				
Si	8.92	8.858	9.214	8.829	10.304	8.929	8.966	8.974
Al	6.736	7.021	6.679	7.056	5.204	6.996	6.918	6.902
Fe	0.273	0.082	0.088	0.082	0.395	0.087	0.091	0.083
Mg	0.099	0.016	0.021	0.018	0.18	0.016	0.018	0.017
Ba	na	na	na	na	na	na	na	na
Ca	3.237	3.219	2.852	3.233	1.804	3.126	3.129	3.153
Na	0.841	0.814	1.111	0.796	2.119	0.789	0.853	0.833
K	0.033	0.035	0.054	0.033	0.28	0.026	0.034	0.038
Ab	20.5	20	27.7	19.6	50.4	20	21.2	20.7
An	78.7	79.1	71	79.6	42.9	79.3	77.9	78.4
Or	0.8	0.9	1.3	0.8	6.7	0.7	0.8	0.9

Table A.2: Con't

	LT017-023	LT017-024	LT017-025	LT017-026	LT017-027	LT017-028	LT017-029	LT017-032
SiO_2	46.807	46.707	47.848	47.484	46.951	47.436	47.489	46.607
Al_2O_3	32.438	32.495	32.275	32.026	32.504	32.163	31.785	32.562
FeOT	0.545	0.54	0.552	0.544	0.548	0.516	0.531	0.564
MgO	0.053	0.045	0.058	0.062	0.071	0.069	0.064	0.057
BaO	na	na	na	na	na	na	na	na
SrO	na	na	na	na	na	na	na	na
CaO	16.489	16.788	15.903	16.055	16.548	16.334	15.947	16.774
Na_2O	1.822	1.868	2.278	2.247	1.907	1.927	2.235	1.854
K_2O	0.109	0.124	0.123	0.12	0.11	0.115	0.132	0.114
Total	98.26	98.57	99.04	98.54	98.64	98.56	98.18	98.53
				Oxygen = 32.000				
Si	8.759	8.727	8.869	8.855	8.756	8.84	8.884	8.712
Al	7.148	7.15	7.045	7.033	7.139	7.058	7.002	7.168
Fe	0.085	0.084	0.086	0.085	0.085	0.08	0.083	0.088
Mg	0.015	0.013	0.016	0.017	0.02	0.019	0.018	0.016
Ba	na	na	na	na	na	na	na	na
Ca	3.306	3.361	3.158	3.208	3.306	3.261	3.196	3.359
Na	0.661	0.677	0.819	0.812	0.69	0.696	0.811	0.672
K	0.026	0.03	0.029	0.029	0.026	0.027	0.032	0.027
Ab	16.6	16.6	20.4	20.1	17.2	17.5	20.1	16.6
An	82.8	82.6	78.8	79.2	82.2	81.9	79.1	82.8
Or	0.7	0.7	0.7	0.7	0.6	0.7	0.8	0.7

Table A.2: Con't

	LT017-033	LT017-034	LT017-035	LT017-036	LT017-037	LT017-038	LT017-039	LT017-040
SiO_2	48.325	46.753	46.986	47	46.605	46.74	47.481	48.556
Al_2O_3	32.579	32.299	31.89	32.75	32.681	32.558	32.32	31.22
FeOT	0.605	0.6	0.633	0.573	0.615	0.659	0.605	0.635
MgO	0.053	0.075	0.055	0.078	0.069	0.059	0.068	0.066
BaO	na	na	na	na	na	na	na	na
SrO	na	na	na	na	na	na	na	na
CaO	15.958	16.577	16.428	16.649	16.636	16.644	16.229	15.447
Na_2O	2.251	1.928	1.987	1.856	1.854	1.869	2.216	2.544
K_2O	0.149	0.117	0.117	0.088	0.125	0.121	0.143	0.178
Total	99.92	98.35	98.1	98.99	98.59	98.65	99.06	98.65
				Oxygen = 32.000				
Si	8.876	8.752	8.815	8.734	8.705	8.726	8.816	9.03
Al	7.047	7.121	7.045	7.167	7.189	7.158	7.067	6.837
Fe	0.093	0.094	0.099	0.089	0.096	0.103	0.094	0.099
Mg	0.015	0.021	0.015	0.022	0.019	0.016	0.019	0.018
Ba	na	na	na	na	na	na	na	na
Ca	3.14	3.325	3.302	3.315	3.329	3.329	3.228	3.078
Na	0.802	0.7	0.723	0.669	0.671	0.677	0.798	0.917
K	0.035	0.028	0.028	0.021	0.03	0.029	0.034	0.042
Ab	20.2	17.3	17.8	16.7	16.7	16.8	19.7	22.7
An	79	82	81.5	82.8	82.6	82.5	79.5	76.2
Or	0.9	0.7	0.7	0.5	0.7	0.7	0.8	1

Table A.2: Con't

	LT017-041	LT017-042	LT017-043	LT017-044	LT017-045	LT017-046	LT019-003	LT019-004
SiO_2	48.394	48.776	47.103	46.994	46.954	46.962	55.921	56.77
Al_2O_3	32.017	31.793	32.474	32.556	32.532	32.605	26.381	26.972
FeOT	0.602	0.597	0.577	0.566	0.601	0.572	0.526	0.479
MgO	0.062	0.077	0.073	0.065	0.053	0.063	0.045	0.049
BaO	na	na	na	na	na	na	na	na
SrO	na	na	na	na	na	na	na	na
CaO	15.552	15.423	16.531	16.582	16.566	16.752	9.248	9.338
Na_2O	2.364	2.483	1.896	1.909	1.839	1.841	5.566	5.609
K_2O	0.163	0.188	0.13	0.104	0.128	0.11	0.58	0.561
Total	99.15	99.34	98.78	98.78	98.67	98.91	98.27	99.78
				Oxygen = 32.000				
Si	8.949	8.999	8.771	8.753	8.755	8.739	10.245	10.234
Al	6.972	6.908	7.121	7.141	7.143	7.146	5.692	5.726
Fe	0.093	0.092	0.09	0.088	0.094	0.089	0.081	0.072
Mg	0.017	0.021	0.02	0.018	0.015	0.017	0.012	0.013
Ba	na	na	na	na	na	na	na	na
Ca	3.081	3.049	3.298	3.309	3.309	3.34	1.815	1.804
Na	0.848	0.888	0.685	0.689	0.665	0.664	1.977	1.961
K	0.038	0.044	0.031	0.025	0.03	0.026	0.136	0.129
Ab	21.4	22.3	17.1	17.1	16.6	16.5	50.3	50.4
An	77.7	76.6	82.2	82.3	82.6	82.9	46.2	46.3
Or	1	1.1	0.8	0.6	0.7	0.6	3.5	3.3

Table A.2: Con't

	LT019-006	LT019-007	LT019-008	LT019-009	LT019-013	LT019-014	LT019-015	LT019-016
SiO_2	56.587	54.95	54.689	54.204	55.752	55.912	57.241	56.283
Al_2O_3	26.235	27.132	27.362	27.527	26.767	26.369	25.949	26.273
FeOT	0.531	0.52	0.561	0.531	0.532	0.468	0.485	0.532
MgO	0.044	0.044	0.038	0.048	0.038	0.037	0.043	0.059
BaO	na	na	na	na	na	na	na	na
SrO	na	na	na	na	na	na	na	na
CaO	8.876	9.928	10.206	10.232	9.386	9.248	8.458	8.881
Na_2O	5.758	5.391	5.163	5.159	5.542	5.649	6.142	5.787
K_2O	0.643	0.475	0.484	0.462	0.575	0.593	0.654	0.621
Total	98.67	98.44	98.5	98.16	98.59	98.28	98.97	98.44
				Oxygen = 32.000				
Si	10.313	10.074	10.027	9.977	10.187	10.244	10.391	10.287
Al	5.631	5.858	5.908	5.967	5.76	5.689	5.548	5.655
Fe	0.081	0.08	0.086	0.082	0.081	0.072	0.074	0.081
Mg	0.012	0.012	0.01	0.013	0.01	0.01	0.012	0.016
Ba	na	na	na	na	na	na	na	na
Ca	1.733	1.95	2.005	2.018	1.837	1.815	1.645	1.739
Na	2.035	1.916	1.835	1.841	1.963	2.007	2.162	2.051
K	0.15	0.111	0.113	0.108	0.134	0.139	0.151	0.145
Ab	51.9	48.2	46.4	46.4	49.9	50.7	54.6	52.1
An	44.2	49	50.7	50.9	46.7	45.8	41.6	44.2
Or	3.8	2.8	2.9	2.7	3.4	3.5	3.8	3.7

Table A.2: Con't

	LT019-019	LT019-020	LT058-001	LT058-002	LT058-003	LT058-004	LT058-005	LT058-006
SiO_2	55.089	54.558	65.262	65.179	65.408	65.127	65.697	65.579
Al_2O_3	27.424	27.24	18.83	18.69	18.606	18.603	18.566	18.562
FeOT	0.509	0.495	0.282	0.208	0.218	0.243	0.254	0.197
MgO	0.046	0.055	0.003	0	0	0.005	0	0.002
BaO	na	na	0	0	0	0.007	0.013	0.042
SrO	na	na	0	0	0	0	0	0
CaO	10.211	10.124	0.155	0.164	0.172	0.16	0.145	0.142
Na_2O	5.249	5.162	5.864	5.965	5.881	5.899	5.914	5.949
K_2O	0.469	0.499	8.981	8.944	8.925	8.963	8.824	8.851
Total	99	98.13	99.38	99.15	99.21	99.01	99.41	99.32
				Oxygen = 32.000				
Si	10.045	10.037	11.89	11.902	11.928	11.911	11.948	11.942
Al	5.889	5.901	4.04	4.019	3.996	4.007	3.976	3.981
Fe	0.078	0.076	0.043	0.032	0.033	0.037	0.039	0.03
Mg	0.013	0.015	0.001	0	0	0.001	0	0.001
Ba	na	na	0	0	0	0.001	0.001	0.003
Ca	1.995	1.995	0.03	0.032	0.034	0.031	0.028	0.028
Na	1.856	1.841	2.072	2.112	2.08	2.092	2.085	2.101
K	0.109	0.117	2.087	2.084	2.076	2.091	2.047	2.056
Ab	46.9	46.6	49.5	50	49.6	49.6	50.1	50.2
An	50.4	50.5	0.7	0.8	0.8	0.7	0.7	0.7
Or	2.8	3	49.8	49.3	49.5	49.6	49.2	49.1

Table A.2: Con't

	LT058-007	LT058-008	LT058-010	LT058-011	LT058-012	LT058-013	LT058-014	LT058-016
SiO_2	65.413	65.254	65.455	65.549	65.597	65.323	65.297	64.849
Al_2O_3	18.608	18.54	18.389	18.448	18.417	18.673	18.552	18.673
FeOт	0.238	0.174	0.23	0.168	0.213	0.171	0.196	0.194
MgO	0	0	0.004	0	0	0	0	0
BaO	0.017	0.014	0.03	0	0	0	0.021	0.035
SrO	0	0	0	0	0	0	0	0
CaO	0.195	0.247	0.204	0.208	0.166	0.136	0.145	0.154
Na_2O	5.907	5.911	6.038	6.224	5.79	5.801	5.575	5.983
K_2O	8.794	8.599	8.53	8.293	9.158	9.09	9.284	8.793
Total	99.17	98.74	98.88	98.89	99.34	99.19	99.07	98.68
				Oxygen = 32.000				
Si	11.928	11.937	11.959	11.958	11.956	11.919	11.936	11.894
Al	3.996	3.994	3.957	3.963	3.953	4.012	3.994	4.033
Fe	0.036	0.027	0.035	0.026	0.032	0.026	0.03	0.03
Mg	0	0	0.001	0	0	0	0	0
Ba	0.001	0.001	0.002	0	0	0	0.002	0.003
Ca	0.038	0.048	0.04	0.041	0.032	0.027	0.028	0.03
Na	2.089	2.097	2.139	2.202	2.046	2.052	1.976	2.128
K	2.046	2.007	1.988	1.93	2.129	2.116	2.165	2.057
Ab	50.1	50.5	51.3	52.8	48.6	48.9	47.4	50.5
An	0.9	1.2	1	1	0.8	0.6	0.7	0.7
Or	49	48.3	47.7	46.2	50.6	50.4	51.9	48.8

Table A.2: Con't

	LT058-017	LT058-018	LT058-019	LT058-020	LT058-021	LT058-022	LT058-023	LT058-024
SiO_2	65.25	65.133	65.322	64.481	65.733	65.991	65.72	66.09
Al_2O_3	18.634	18.793	18.771	18.686	18.83	18.786	18.853	18.909
FeOт	0.21	0.226	0.189	0.24	0.232	0.175	0.232	0.241
MgO	0.007	0.001	0	0.006	0	0	0.015	0
BaO	0.036	0.041	0.018	0.024	0.055	0.011	0.043	0
SrO	0	0	0	0	0	0	0	0
CaO	0.158	0.197	0.189	0.199	0.158	0.117	0.181	0.151
Na_2O	5.961	5.943	5.831	5.951	5.81	5.773	5.862	5.8
K_2O	8.775	8.955	9.088	8.888	9.046	9.142	9.023	9.15
Total	99.03	99.29	99.41	98.48	99.86	99.99	99.93	100.34
				Oxygen = 32.000				
Si	11.918	11.884	11.9	11.867	11.914	11.937	11.906	11.919
Al	4.008	4.038	4.027	4.05	4.019	4.002	4.022	4.016
Fe	0.032	0.034	0.029	0.037	0.035	0.026	0.035	0.036
Mg	0.002	0	0	0.002	0	0	0.004	0
Ba	0.003	0.003	0.001	0.002	0.004	0.001	0.003	0
Ca	0.031	0.039	0.037	0.039	0.031	0.023	0.035	0.029
Na	2.111	2.102	2.06	2.124	2.042	2.025	2.059	2.028
K	2.045	2.084	2.112	2.087	2.092	2.11	2.085	2.105
Ab	50.4	49.8	48.9	50	49	48.7	49.3	48.7
An	0.7	0.9	0.9	0.9	0.7	0.6	0.8	0.7
Or	48.8	49.3	50.2	49.1	50.2	50.7	49.9	50.6

Table A.2: Con't

	LT059-001	LT059-002	LT059-003	LT059-004	LT059-005	LT059-006	LT059-007	LT059-008
SiO_2	65.893	65.941	65.696	65.376	65.215	65.525	65.584	65.556
Al_2O_3	18.769	18.687	18.741	18.769	18.61	18.639	18.811	18.824
FeOт	0.2	0.228	0.188	0.265	0.175	0.282	0.249	0.243
MgO	0	0	0.011	0.005	0	0.001	0	0
BaO	0.045	0.003	0.012	0.008	0.021	0.024	0.005	0.04
SrO	0	0	0	0	0	0	0	0
CaO	0.236	0.263	0.217	0.277	0.31	0.309	0.257	0.284
Na_2O	6.258	6.307	6.241	6.278	6.158	6.251	6.165	6.195
K_2O	8.406	8.187	8.286	8.389	8.196	8.197	8.409	8.377
Total	99.81	99.62	99.39	99.37	98.69	99.23	99.48	99.52
				Oxygen = 32.000				
Si	11.924	11.939	11.926	11.893	11.924	11.922	11.907	11.901
Al	4	3.985	4.007	4.021	4.007	3.994	4.022	4.024
Fe	0.03	0.035	0.029	0.04	0.027	0.043	0.038	0.037
Mg	0	0	0.003	0.001	0	0	0	0
Ba	0.003	0	0.001	0.001	0.002	0.002	0	0.003
Ca	0.046	0.051	0.042	0.054	0.061	0.06	0.05	0.055
Na	2.196	2.214	2.197	2.214	2.183	2.205	2.17	2.181
K	1.941	1.891	1.919	1.947	1.912	1.903	1.948	1.94
Ab	52.5	53.3	52.8	52.5	52.5	52.9	52.1	52.2
An	1.1	1.2	1	1.3	1.5	1.4	1.2	1.3
Or	46.4	45.5	46.2	46.2	46	45.7	46.7	46.5

Table A.2: Con't

	LT059-009	LT059-010	LT059-011	LT059-012	LT059-013	LT059-014	LT059-015	LT059-016
SiO_2	65.379	64.176	64.763	64.663	64.883	64.8	65.156	65.349
Al_2O_3	18.816	18.737	18.743	18.689	18.688	18.652	18.649	18.618
FeOт	0.239	0.186	0.247	0.203	0.227	0.22	0.256	0.243
MgO	0	0	0	0.005	0.001	0.002	0	0
BaO	0.008	0.05	0.019	0.018	0	0.004	0.021	0.021
SrO	0	0	0	0	0	0	0	0
CaO	0.254	0.286	0.236	0.237	0.194	0.224	0.178	0.173
Na_2O	6.237	6.334	6.196	6.022	6.069	6.124	5.993	5.967
K_2O	8.199	8.322	8.61	8.598	8.55	8.633	8.774	8.903
Total	99.13	98.09	98.81	98.44	98.61	98.66	99.03	99.27
				Oxygen = 32.000				
Si	11.902	11.842	11.867	11.883	11.895	11.886	11.907	11.917
Al	4.034	4.072	4.045	4.045	4.035	4.029	4.013	3.998
Fe	0.036	0.029	0.038	0.031	0.035	0.034	0.039	0.037
Mg	0	0	0	0.001	0	0.001	0	0
Ba	0.001	0.004	0.001	0.001	0	0	0.002	0.002
Ca	0.05	0.057	0.046	0.047	0.038	0.044	0.035	0.034
Na	2.202	2.266	2.201	2.146	2.157	2.178	2.124	2.11
K	1.904	1.959	2.013	2.016	2	2.02	2.046	2.071
Ab	53	52.9	51.7	51	51.4	51.3	50.5	50.1
An	1.2	1.3	1.1	1.1	0.9	1	0.8	0.8
Or	45.8	45.7	47.3	47.9	47.7	47.6	48.7	49.1

Table A.2: Con't

	LT059-017	LT059-018	LT059-019	LT059-020	LT059-021	LT059-022	LT059-023	LT059-024
SiO_2	65.366	65.151	65.654	65.624	65.484	65.378	65.508	65.351
Al_2O_3	18.693	18.576	18.541	18.684	18.591	18.518	18.589	18.534
FeOT	0.26	0.263	0.199	0.199	0.238	0.236	0.255	0.229
MgO	0	0.009	0	0	0	0	0.008	0.001
BaO	0.014	0.021	0.022	0.035	0.033	0.013	0	0.024
SrO	0	0	0	0	0	0	0	0
CaO	0.16	0.166	0.158	0.192	0.177	0.22	0.2	0.256
Na_2O	6.022	5.969	5.917	5.958	6.077	5.994	5.907	6.046
K_2O	8.963	8.867	8.893	8.81	8.737	8.795	8.84	8.73
Total	99.48	99.02	99.38	99.5	99.34	99.15	99.31	99.17
				Oxygen = 32.000				
Si	11.903	11.913	11.947	11.927	11.926	11.93	11.931	11.924
Al	4.009	4	3.973	3.999	3.987	3.98	3.987	3.982
Fe	0.04	0.04	0.03	0.03	0.036	0.036	0.039	0.035
Mg	0	0.002	0	0	0	0	0.002	0
Ba	0.001	0.002	0.002	0.002	0.002	0.001	0	0.002
Ca	0.031	0.033	0.031	0.037	0.035	0.043	0.039	0.05
Na	2.126	2.116	2.088	2.1	2.146	2.121	2.086	2.139
K	2.082	2.068	2.065	2.043	2.03	2.047	2.054	2.032
Ab	50.2	50.2	49.9	50.2	51	50.4	49.9	50.7
An	0.7	0.8	0.7	0.9	0.8	1	0.9	1.2
Or	49.1	49	49.4	48.9	48.2	48.6	49.2	48.1

Table A.2: Con't

	LT059-025	LT059-026	LT059-027	LT059-028	LT059-029	LT059-030	LT059-031	LT059-032
SiO_2	65.43	65.251	65.245	64.978	65.316	65.169	64.805	65.166
Al_2O_3	18.657	18.561	18.664	18.609	18.586	18.498	18.446	18.656
FeOT	0.284	0.222	0.259	0.226	0.24	0.231	0.247	0.241
MgO	0.008	0	0	0	0	0	0	0
BaO	0.031	0.015	0	0	0.002	0	0.025	0
SrO	0	0	0	0	0	0	0	0
CaO	0.212	0.192	0.197	0.203	0.18	0.152	0.138	0.173
Na_2O	6.067	5.949	6.005	5.825	5.975	5.816	5.87	5.981
K_2O	8.713	8.901	8.781	8.853	8.961	8.994	9.043	8.941
Total	99.4	99.09	99.15	98.69	99.26	98.86	98.57	99.16
				Oxygen = 32.000				
Si	11.911	11.92	11.907	11.911	11.916	11.932	11.915	11.902
Al	4	3.993	4.011	4.017	3.993	3.988	3.994	4.013
Fe	0.043	0.034	0.04	0.035	0.037	0.035	0.038	0.037
Mg	0.002	0	0	0	0	0	0	0
Ba	0.002	0.001	0	0	0	0	0.002	0
Ca	0.041	0.038	0.039	0.04	0.035	0.03	0.027	0.034
Na	2.142	2.107	2.125	2.07	2.114	2.065	2.093	2.118
K	2.024	2.074	2.044	2.07	2.086	2.101	2.121	2.083
Ab	50.9	49.9	50.5	49.5	49.9	49.2	49.4	50
An	1	0.9	0.9	1	0.8	0.7	0.6	0.8
Or	48.1	49.2	48.6	49.5	49.3	50.1	50	49.2

Table A.2: Con't

	LT059-033	LT059-034	LT059-035	LT059-036	LT059-037	LT059-038	LT059-039	LT059-040
SiO_2	65.482	65.161	65.122	65.204	65.477	65.326	64.937	65.522
Al_2O_3	18.604	18.704	18.45	18.557	18.615	18.521	18.388	18.512
FeOT	0.215	0.226	0.232	0.193	0.241	0.212	0.217	0.263
MgO	0.009	0.001	0	0.009	0.005	0.009	0	0.007
BaO	0.03	0.005	0.001	0.011	0	0.022	0	0.003
SrO	0	0	0	0	0	0	0	0
CaO	0.142	0.143	0.159	0.156	0.115	0.106	0.186	0.152
Na_2O	5.864	5.811	5.882	5.773	5.887	5.938	5.859	5.705
K_2O	9.023	9.113	8.912	9.064	9.124	9.077	8.994	9.169
Total	99.37	99.16	98.76	98.97	99.46	99.21	98.58	99.33
				Oxygen = 32.000				
Si	11.929	11.902	11.934	11.927	11.923	11.927	11.93	11.943
Al	3.991	4.023	3.982	3.997	3.992	3.982	3.978	3.974
Fe	0.033	0.035	0.036	0.03	0.037	0.032	0.033	0.04
Mg	0.002	0	0	0.002	0.001	0.002	0	0.002
Ba	0.002	0	0	0.001	0	0.002	0	0
Ca	0.028	0.028	0.031	0.031	0.022	0.021	0.037	0.03
Na	2.071	2.058	2.09	2.048	2.079	2.102	2.087	2.016
K	2.097	2.124	2.084	2.115	2.12	2.114	2.108	2.132
Ab	49.4	48.9	49.7	48.8	49.3	49.6	49.3	48.3
An	0.7	0.7	0.7	0.7	0.5	0.5	0.9	0.7
Or	50	50.5	49.6	50.4	50.2	49.9	49.8	51

Table A.2: Con't

	LT059-041	LT059-042	LT059-043	LT059-044	LT059-045	LT059-046	LT059-047	LT059-048
SiO_2	65.817	65.586	65.497	65.522	65.141	65.19	65.066	65.088
Al_2O_3	18.436	18.425	18.458	18.43	18.391	18.303	18.465	18.478
FeOT	0.233	0.206	0.243	0.206	0.232	0.246	0.227	0.236
MgO	0	0	0	0	0	0	0.009	0
BaO	0	0	0	0.056	0.011	0	0.024	0.031
SrO	0	0	0	0	0	0	0	0
CaO	0.113	0.137	0.153	0.151	0.123	0.129	0.144	0.139
Na_2O	5.785	5.844	5.839	5.758	5.811	5.865	5.752	5.798
K_2O	9.167	9.118	9.214	9.174	8.961	9.165	9.065	9.211
Total	99.55	99.32	99.4	99.3	98.67	98.9	98.75	98.98
				Oxygen = 32.000				
Si	11.966	11.955	11.94	11.952	11.947	11.946	11.931	11.922
Al	3.947	3.955	3.963	3.959	3.972	3.95	3.988	3.986
Fe	0.035	0.031	0.037	0.031	0.036	0.038	0.035	0.036
Mg	0	0	0	0	0	0	0.002	0
Ba	0	0	0	0.004	0.001	0	0.002	0.002
Ca	0.022	0.027	0.03	0.03	0.024	0.025	0.028	0.027
Na	2.039	2.066	2.064	2.037	2.066	2.084	2.045	2.059
K	2.126	2.12	2.143	2.135	2.097	2.143	2.121	2.152
Ab	48.7	49	48.7	48.5	49.3	49	48.8	48.6
An	0.5	0.6	0.7	0.7	0.6	0.6	0.7	0.6
Or	50.8	50.3	50.6	50.8	50.1	50.4	50.6	50.8

Table A.2: Con't

	LT060-001	LT060-002	LT060-003	LT060-005	LT060-006	LT060-007	LT060-008	LT060-009
SiO_2	64.782	64.554	64.715	64.905	65.788	65.475	64.934	65.272
Al_2O_3	18.697	18.488	18.612	18.732	18.852	18.905	18.592	18.612
FeOT	0.205	0.215	0.212	0.19	0.277	0.241	0.172	0.207
MgO	0	0.007	0	0	0	0	0.01	0
BaO	0	0	0	0.021	0.025	0	0.02	0.009
SrO	0	0	0	0	0	0	0	0
CaO	0.207	0.187	0.243	0.255	0.274	0.237	0.223	0.218
Na_2O	5.662	5.599	5.777	5.898	6.078	6.111	6.025	5.909
K_2O	9.258	9.237	8.987	8.922	8.566	8.526	8.771	8.996
Total	98.81	98.29	98.55	98.92	99.86	99.49	98.75	99.22
				Oxygen = 32.000				
Si	11.886	11.905	11.894	11.883	11.907	11.891	11.902	11.913
Al	4.04	4.015	4.028	4.039	4.018	4.043	4.013	4
Fe	0.031	0.033	0.033	0.029	0.042	0.037	0.026	0.032
Mg	0	0.002	0	0	0	0	0.003	0
Ba	0	0	0	0.002	0.002	0	0.001	0.001
Ca	0.041	0.037	0.048	0.05	0.053	0.046	0.044	0.043
Na	2.014	2.002	2.059	2.094	2.133	2.152	2.141	2.091
K	2.167	2.173	2.107	2.084	1.978	1.975	2.051	2.095
Ab	47.7	47.5	48.9	49.5	51.2	51.6	50.5	49.4
An	1	0.9	1.1	1.2	1.3	1.1	1	1
Or	51.3	51.6	50	49.3	47.5	47.3	48.4	49.5

Table A.2: Con't

	LT060-010	LT060-011	LT060-012	LT060-013	LT060-014	LT060-015	LT060-016	LT060-017
SiO_2	65.546	66.026	64.864	65.798	66.069	65.502	65.551	65.294
Al_2O_3	18.62	18.489	18.276	18.671	18.592	18.535	18.429	18.452
FeOT	0.202	0.187	0.197	0.187	0.201	0.197	0.209	0.231
MgO	0.006	0.004	0.002	0	0	0	0	0
BaO	0.017	0.03	0	0.036	0.001	0	0	0
SrO	0	0	0	0	0	0	0	0
CaO	0.19	0.189	0.207	0.189	0.22	0.167	0.19	0.161
Na_2O	5.788	6.039	5.764	5.911	5.783	5.852	5.775	5.878
K_2O	8.838	8.96	9.045	8.997	9.118	9.169	9.15	9.181
Total	99.21	99.92	98.35	99.79	99.98	99.42	99.3	99.2
				Oxygen = 32.000				
Si	11.941	11.958	11.943	11.933	11.955	11.934	11.952	11.93
Al	3.995	3.943	3.963	3.988	3.962	3.977	3.957	3.97
Fe	0.031	0.028	0.03	0.028	0.03	0.03	0.032	0.035
Mg	0.002	0.001	0.001	0	0	0	0	0
Ba	0.001	0.002	0	0.003	0	0	0	0
Ca	0.037	0.037	0.041	0.037	0.043	0.033	0.037	0.032
Na	2.045	2.121	2.058	2.079	2.029	2.067	2.042	2.082
K	2.054	2.07	2.125	2.082	2.105	2.131	2.128	2.14
Ab	49.4	50.2	48.7	49.5	48.6	48.9	48.5	48.9
An	0.9	0.9	1	0.9	1	0.8	0.9	0.8
Or	49.7	49	50.3	49.6	50.4	50.4	50.6	50.3

Table A.2: Con't

	LT060-019	LT060-020	LT060-021	LT060-022	LT060-023	LT060-024	LT060-025	LT060-026
SiO_2	65.711	65.186	64.8	65.264	65.752	65.196	65.204	65.221
Al_2O_3	18.571	18.553	18.667	18.51	18.74	18.602	18.643	18.603
FeOT	0.206	0.254	0.169	0.245	0.191	0.235	0.194	0.185
MgO	0	0.006	0	0.007	0	0	0	0
BaO	0.007	0.002	0.012	0.003	0	0	0.032	0.031
SrO	0	0	0	0	0	0	0	0
CaO	0.182	0.149	0.143	0.145	0.145	0.162	0.158	0.163
Na_2O	5.716	5.798	5.744	5.775	5.915	5.754	5.745	5.822
K_2O	9.078	9.235	9.105	9.193	9.237	9.069	9.204	9.113
Total	99.47	99.18	98.64	99.14	99.98	99.02	99.18	99.14
				Oxygen = 32.000				
Si	11.95	11.915	11.898	11.928	11.915	11.92	11.912	11.917
Al	3.977	3.994	4.036	3.984	3.999	4.005	4.011	4.003
Fe	0.031	0.039	0.026	0.037	0.029	0.036	0.03	0.028
Mg	0	0.002	0	0.002	0	0	0	0
Ba	0	0	0.001	0	0	0	0.002	0.002
Ca	0.035	0.029	0.028	0.028	0.028	0.032	0.031	0.032
Na	2.016	2.055	2.045	2.047	2.078	2.04	2.035	2.063
K	2.106	2.153	2.133	2.143	2.135	2.115	2.145	2.124
Ab	48.5	48.5	48.6	48.5	49	48.7	48.3	48.9
An	0.8	0.7	0.7	0.7	0.7	0.8	0.7	0.8
Or	50.7	50.8	50.7	50.8	50.3	50.5	50.9	50.3

Table A.2: Con't

	LT060-027	LT060-028	LT060-029	LT060-030	LT060-031	LT060-032	LT060-033	LT060-034
SiO_2	65.64	65.645	65.768	65.08	65.995	66.093	65.56	65.639
Al_2O_3	18.693	18.665	18.619	18.44	18.444	18.638	18.508	18.449
FeOT	0.177	0.248	0.207	0.22	0.252	0.214	0.207	0.236
MgO	0	0.003	0	0	0	0	0	0.007
BaO	0	0.048	0.015	0.038	0.006	0	0.026	0
SrO	0	0	0	0	0	0	0	0
CaO	0.111	0.14	0.132	0.14	0.099	0.18	0.158	0.137
Na_2O	5.812	5.827	5.765	5.821	5.812	5.855	5.775	5.739
K_2O	9.184	9.146	9.221	9.183	9.371	9.28	9.376	9.156
Total	99.62	99.72	99.73	98.92	99.98	100.26	99.61	99.36
				Oxygen = 32.000				
Si	11.928	11.925	11.941	11.926	11.963	11.942	11.935	11.957
Al	4	3.993	3.981	3.98	3.937	3.966	3.968	3.958
Fe	0.027	0.038	0.031	0.034	0.038	0.032	0.032	0.036
Mg	0	0.001	0	0	0	0	0	0.002
Ba	0	0.003	0.001	0.003	0	0	0.002	0
Ca	0.022	0.027	0.026	0.027	0.019	0.035	0.031	0.027
Na	2.048	2.052	2.03	2.068	2.043	2.051	2.039	2.027
K	2.129	2.12	2.136	2.147	2.167	2.139	2.178	2.128
Ab	48.8	48.9	48.4	48.8	48.3	48.5	48	48.5
An	0.5	0.6	0.6	0.6	0.4	0.8	0.7	0.6
Or	50.7	50.5	51	50.6	51.2	50.6	51.3	50.9

Table A.2: Con't

	LT060-035	LT060-036	LT060-037	LT060-039	LT060-040	LT060-041	LT060-042	LT060-044
SiO_2	65.02	65.346	65.672	65.506	65.441	65.931	65.545	66.397
Al_2O_3	18.257	18.517	18.544	18.566	18.658	18.85	18.615	18.746
FeOT	0.199	0.242	0.233	0.201	0.236	0.229	0.25	0.232
MgO	0	0	0	0	0	0	0.007	0
BaO	0	0.006	0	0.024	0.009	0.001	0.008	0.057
SrO	0	0	0	0	0	0	0	0
CaO	0.19	0.142	0.177	0.162	0.157	0.15	0.12	0.117
Na_2O	5.714	5.622	5.729	5.763	5.682	5.658	5.758	5.757
K_2O	9.317	9.295	9.34	9.31	9.421	9.366	9.457	9.522
Total	98.7	99.17	99.7	99.53	99.6	100.19	99.76	100.83
				Oxygen = 32.000				
Si	11.946	11.937	11.938	11.929	11.915	11.919	11.919	11.941
Al	3.95	3.984	3.97	3.982	4	4.013	3.986	3.97
Fe	0.031	0.037	0.035	0.031	0.036	0.035	0.038	0.035
Mg	0	0	0	0	0	0	0.002	0
Ba	0	0	0	0.002	0.001	0	0.001	0.004
Ca	0.037	0.028	0.034	0.032	0.031	0.029	0.023	0.023
Na	2.036	1.991	2.019	2.035	2.006	1.983	2.03	2.008
K	2.184	2.166	2.166	2.163	2.188	2.16	2.194	2.185
Ab	47.8	47.6	47.9	48.1	47.5	47.5	47.8	47.6
An	0.9	0.7	0.8	0.8	0.7	0.7	0.5	0.5
Or	51.3	51.8	51.3	51.1	51.8	51.8	51.7	51.8

Table A.2: Con't

	LT061-001	LT061-002	LT061-003	LT061-004	LT061-005	LT061-006	LT061-007	LT061-008
SiO_2	65.463	65.087	66.134	65.537	65.714	65.707	65.966	66.277
Al_2O_3	18.77	18.68	18.775	18.641	18.792	18.673	18.728	18.69
FeOT	0.208	0.262	0.203	0.205	0.216	0.244	0.23	0.237
MgO	0.001	0	0	0.001	0	0.009	0.002	0.006
BaO	0.044	0.017	0	0.015	0.062	0.01	0.021	0.024
SrO	0	0	0	0	0	0	0	0
CaO	0.19	0.14	0.147	0.204	0.176	0.179	0.175	0.156
Na_2O	6.102	6.065	5.868	5.866	5.97	5.831	5.742	5.861
K_2O	8.826	8.883	9.082	8.985	8.988	9.079	9.19	9.241
Total	99.6	99.13	100.21	99.45	99.92	99.73	100.05	100.49
				Oxygen = 32.000				
Si	11.898	11.893	11.938	11.926	11.909	11.927	11.935	11.944
Al	4.018	4.02	3.991	3.995	4.011	3.992	3.99	3.967
Fe	0.032	0.04	0.031	0.031	0.033	0.037	0.035	0.036
Mg	0	0	0	0	0	0.002	0.001	0.002
Ba	0.003	0.001	0	0.001	0.004	0.001	0.001	0.002
Ca	0.037	0.027	0.028	0.04	0.034	0.035	0.034	0.03
Na	2.151	2.149	2.054	2.07	2.098	2.052	2.014	2.048
K	2.047	2.071	2.091	2.086	2.078	2.102	2.121	2.125
Ab	50.8	50.6	49.2	49.3	49.8	49	48.3	48.7
An	0.9	0.6	0.7	1	0.8	0.8	0.8	0.7
Or	48.3	48.8	50.1	49.7	49.4	50.2	50.9	50.6

Table A.2: Con't

	LT061-009	LT061-010	LT061-011	LT061-012	LT061-013	LT064-003	LT064-004	LT064-005
SiO_2	66.025	66.015	66.003	65.767	65.502	57.199	56.451	56.589
Al_2O_3	18.553	18.465	18.507	18.463	18.542	26.654	26.539	26.309
FeOT	0.221	0.239	0.2	0.197	0.233	0.468	0.469	0.527
MgO	0.006	0	0	0.019	0.003	0.016	0.03	0.009
BaO	0.012	0.037	0.023	0	0	0.143	0.171	0.122
SrO	0	0	0	0	0	0.272	0.23	0.228
CaO	0.154	0.149	0.151	0.138	0.131	8.843	9	8.847
Na_2O	5.814	5.691	5.695	5.689	5.747	5.965	5.93	6.131
K_2O	9.041	9.434	9.406	9.448	9.341	0.661	0.621	0.652
Total	99.83	100.03	99.99	99.72	99.5	100.22	99.44	99.41
				Oxygen = 32.000				
Si	11.962	11.963	11.96	11.953	11.932	10.292	10.249	10.279
Al	3.959	3.941	3.949	3.952	3.978	5.648	5.674	5.628
Fe	0.033	0.036	0.03	0.03	0.035	0.07	0.071	0.08
Mg	0.002	0	0	0.005	0.001	0.004	0.008	0.002
Ba	0.001	0.003	0.002	0	0	0.01	0.012	0.009
Ca	0.03	0.029	0.029	0.027	0.026	1.705	1.751	1.722
Na	2.042	2	2.001	2.005	2.03	2.081	2.088	2.159
K	2.09	2.181	2.174	2.191	2.171	0.152	0.144	0.151
Ab	49.1	47.5	47.6	47.5	48	52.8	52.4	53.5
An	0.7	0.7	0.7	0.6	0.6	43.3	44	42.7
Or	50.2	51.8	51.7	51.9	51.4	3.9	3.6	3.7

Table A.2: Con't

	LT064-006	LT064-007	LT064-008	LT064-009	LT064-010	LT064-011	LT064-012	LT064-013
SiO_2	57.087	56.643	56.131	56.444	56.676	56.733	56.804	56.78
Al_2O_3	26.541	26.905	25.652	26.46	26.378	26.342	26.629	26.251
FeOT	0.499	0.496	0.483	0.499	0.424	0.51	0.487	0.434
MgO	0.04	0.022	0.027	0.035	0.023	0.035	0.039	0.028
BaO	0.189	0.141	0.153	0.118	0.147	0.161	0.138	0.135
SrO	0.239	0.274	0.263	0.312	0.292	0.269	0.296	0.243
CaO	8.61	9.115	8.695	9.117	8.704	8.906	8.671	8.532
Na_2O	6.123	5.934	6.05	5.876	5.951	6.092	6.103	5.941
K_2O	0.67	0.617	0.651	0.614	0.641	0.643	0.648	0.685
Total	100	100.15	98.11	99.47	99.24	99.69	99.82	99.05
				Oxygen = 32.000				
Si	10.298	10.215	10.33	10.249	10.298	10.28	10.269	10.329
Al	5.639	5.714	5.56	5.658	5.644	5.621	5.669	5.624
Fe	0.075	0.075	0.074	0.076	0.064	0.077	0.074	0.066
Mg	0.011	0.006	0.007	0.009	0.006	0.009	0.011	0.008
Ba	0.013	0.01	0.011	0.008	0.01	0.011	0.01	0.01
Ca	1.664	1.761	1.715	1.774	1.694	1.729	1.68	1.663
Na	2.142	2.075	2.159	2.069	2.097	2.14	2.139	2.095
K	0.154	0.142	0.153	0.142	0.149	0.149	0.149	0.159
Ab	54.1	52.2	53.6	51.9	53.2	53.3	53.9	53.5
An	42	44.3	42.6	44.5	43	43	42.3	42.5
Or	3.9	3.6	3.8	3.6	3.8	3.7	3.8	4.1

Table A.2: Con't

	LT064-014	LT064-015	LT064-017	LT064-018	LT065-001	LT065-002	LT065-004	LT065-005
SiO_2	57.547	57.704	58.429	56.303	56.777	56.4	57.944	58.917
Al_2O_3	26.286	25.699	24.449	26.091	26.504	26.505	26.457	25.51
FeOT	0.466	0.514	0.446	0.525	0.511	0.466	0.467	0.457
MgO	0.033	0.043	0.026	0.038	0.023	0.025	0.03	0.028
BaO	0.13	0.173	0.205	0.086	0.129	0.103	0.127	0.173
SrO	0.271	0.234	0.227	0.26	0.265	0.255	0.289	0.254
CaO	8.432	7.717	6.845	9.062	9.096	8.999	8.461	7.477
Na_2O	6.241	6.502	6.961	5.791	5.974	5.923	6.406	6.84
K_2O	0.692	0.819	0.968	0.646	0.611	0.66	0.649	0.812
Total	100.1	99.41	98.56	98.8	99.89	99.34	100.83	100.47
				Oxygen = 32.000				
Si	10.36	10.453	10.659	10.286	10.264	10.249	10.358	10.548
Al	5.573	5.483	5.253	5.613	5.643	5.672	5.57	5.378
Fe	0.07	0.078	0.068	0.08	0.077	0.071	0.07	0.068
Mg	0.009	0.012	0.007	0.01	0.006	0.007	0.008	0.007
Ba	0.009	0.012	0.015	0.006	0.009	0.007	0.009	0.012
Ca	1.626	1.498	1.338	1.774	1.762	1.752	1.62	1.434
Na	2.179	2.284	2.462	2.051	2.094	2.087	2.22	2.374
K	0.159	0.189	0.225	0.151	0.141	0.153	0.148	0.185
Ab	55	57.5	61.2	51.6	52.4	52.3	55.7	59.5
An	41	37.7	33.2	44.6	44.1	43.9	40.6	35.9
Or	4	4.8	5.6	3.8	3.5	3.8	3.7	4.6

Table A.2: Con't

	LT065-006	LT065-007	LT065-008	LT065-009	LT065-010	LT065-011	LT065-012	LT065-013
SiO_2	56.283	56.584	56.157	56.603	56.355	56.398	56.206	57.376
Al_2O_3	26.674	26.621	26.867	26.847	26.804	27.039	26.136	25.964
FeOT	0.446	0.485	0.456	0.467	0.465	0.437	0.45	0.474
MgO	0.039	0.035	0.028	0.038	0.043	0.038	0.03	0.043
BaO	0.093	0.096	0.102	0.107	0.128	0.082	0.114	0.099
SrO	0.266	0.234	0.256	0.23	0.241	0.225	0.268	0.223
CaO	8.829	8.827	9.103	9.061	8.963	8.892	8.849	8.255
Na_2O	5.938	6.054	5.825	5.966	5.891	5.816	5.973	6.28
K_2O	0.584	0.582	0.577	0.532	0.573	0.55	0.613	0.7
Total	99.15	99.52	99.37	99.85	99.46	99.48	98.64	99.42
				Oxygen = 32.000				
Si	10.237	10.255	10.199	10.226	10.221	10.213	10.283	10.392
Al	5.713	5.682	5.746	5.712	5.725	5.766	5.631	5.538
Fe	0.068	0.074	0.069	0.071	0.071	0.066	0.069	0.072
Mg	0.011	0.009	0.008	0.01	0.012	0.01	0.008	0.012
Ba	0.007	0.007	0.007	0.008	0.009	0.006	0.008	0.007
Ca	1.72	1.714	1.771	1.754	1.742	1.725	1.735	1.602
Na	2.094	2.127	2.051	2.09	2.072	2.042	2.119	2.206
K	0.136	0.135	0.134	0.123	0.133	0.127	0.143	0.162
Ab	53	53.5	51.8	52.7	52.5	52.4	53	55.6
An	43.5	43.1	44.8	44.2	44.1	44.3	43.4	40.4
Or	3.4	3.4	3.4	3.1	3.4	3.3	3.6	4.1

Table A.2: Con't

	LT065-014	LT065-015	LT065-016	LT065-017	LT065-019	LT065-020	LT065-021	LT065-023
SiO_2	58.003	57.664	57.468	57.373	56.064	55.956	55.784	55.664
Al_2O_3	26.013	25.618	25.501	25.653	27.018	26.828	26.281	26.761
FeOT	0.426	0.472	0.454	0.49	0.511	0.492	0.487	0.529
MgO	0.044	0.035	0.034	0.026	0.052	0.047	0.052	0.046
BaO	0.158	0.176	0.131	0.169	0.076	0.101	0.144	0.111
SrO	0.254	0.268	0.275	0.234	0.236	0.268	0.216	0.258
CaO	8.077	7.981	8.084	8.213	9.593	9.358	9.006	9.491
Na_2O	6.452	6.279	6.3	6.34	5.698	5.797	5.657	5.685
K_2O	0.697	0.693	0.691	0.67	0.524	0.547	0.541	0.529
Total	100.12	99.19	98.94	99.17	99.77	99.39	98.17	99.07
				Oxygen = 32.000				
Si	10.428	10.462	10.456	10.424	10.152	10.172	10.248	10.157
Al	5.508	5.474	5.464	5.489	5.762	5.744	5.686	5.751
Fe	0.064	0.072	0.069	0.074	0.077	0.075	0.075	0.081
Mg	0.012	0.009	0.009	0.007	0.014	0.013	0.014	0.013
Ba	0.011	0.013	0.009	0.012	0.005	0.007	0.01	0.008
Ca	1.556	1.551	1.576	1.599	1.861	1.823	1.773	1.856
Na	2.249	2.209	2.223	2.233	2.001	2.043	2.015	2.011
K	0.16	0.16	0.16	0.155	0.121	0.127	0.127	0.123
Ab	56.7	56.4	56.2	56	50.2	51.2	51.5	50.4
An	39.2	39.6	39.8	40.1	46.7	45.7	45.3	46.5
Or	4	4.1	4	3.9	3	3.2	3.2	3.1

Table A.2: Con't

	LT065-024	LT065-025	LT065-026	LT065-027	LT065-029	LT065-030	LT065-031	LT065-032
SiO_2	54.897	56.099	55.083	56.404	56.522	57.139	56.732	56.871
Al_2O_3	26.872	26.974	26.455	26.607	25.909	26.055	25.511	25.549
FeOT	0.515	0.513	0.485	0.482	0.495	0.502	0.453	0.496
MgO	0.035	0.028	0.04	0.043	0.029	0.029	0.034	0.038
BaO	0.062	0.104	0.085	0.086	0.161	0.144	0.117	0.114
SrO	0.246	0.254	0.276	0.268	0.284	0.244	0.287	0.256
CaO	9.942	9.442	9.398	8.972	8.611	8.423	8.442	8.311
Na_2O	5.5	5.824	5.665	5.932	6.105	6.144	6.294	6.217
K_2O	0.473	0.532	0.555	0.559	0.624	0.657	0.639	0.66
Total	98.54	99.77	98.04	99.35	98.74	99.34	98.51	98.51
				Oxygen = 32.000				
Si	10.082	10.162	10.158	10.242	10.33	10.365	10.387	10.403
Al	5.812	5.754	5.746	5.69	5.577	5.566	5.501	5.504
Fe	0.079	0.078	0.075	0.073	0.076	0.076	0.069	0.076
Mg	0.01	0.008	0.011	0.012	0.008	0.008	0.009	0.01
Ba	0.004	0.007	0.006	0.006	0.012	0.01	0.008	0.008
Ca	1.956	1.833	1.857	1.745	1.686	1.637	1.656	1.629
Na	1.959	2.046	2.026	2.089	2.164	2.161	2.235	2.205
K	0.111	0.123	0.131	0.129	0.145	0.152	0.149	0.154
Ab	48.7	51.1	50.5	52.7	54.2	54.7	55.3	55.3
An	48.6	45.8	46.3	44	42.2	41.4	41	40.8
Or	2.8	3.1	3.3	3.3	3.6	3.8	3.7	3.9

Table A.2: Con't

	LT065-033	LT065-034	LT065-035	LT065-037	LT066-001	LT066-002	LT066-004	LT066-007
SiO_2	57.54	57.881	58.036	58.418	57.279	56.668	57.779	56.632
Al_2O_3	25.622	25.574	25.501	24.904	26.244	26.631	26.543	26.677
FeOT	0.491	0.445	0.467	0.469	0.476	0.473	0.475	0.445
MgO	0.049	0.033	0.015	0.025	0.033	0.021	0.035	0.033
BaO	0.143	0.116	0.143	0.22	0.164	0.158	0.144	0.162
SrO	0.239	0.236	0.287	0.206	0.23	0.249	0.222	0.296
CaO	7.94	7.656	7.577	7.297	8.546	8.892	8.267	8.755
Na_2O	6.439	6.632	6.645	6.712	6.163	5.919	6.405	5.976
K_2O	0.703	0.773	0.765	0.843	0.719	0.635	0.698	0.684
Total	99.17	99.35	99.44	99.09	99.85	99.65	100.57	99.66
				Oxygen = 32.000				
Si	10.446	10.481	10.501	10.599	10.344	10.261	10.35	10.256
Al	5.478	5.454	5.434	5.321	5.581	5.679	5.599	5.689
Fe	0.075	0.067	0.071	0.071	0.072	0.072	0.071	0.067
Mg	0.013	0.009	0.004	0.007	0.009	0.006	0.009	0.009
Ba	0.01	0.008	0.01	0.016	0.012	0.011	0.01	0.011
Ca	1.544	1.485	1.469	1.418	1.654	1.725	1.587	1.699
Na	2.267	2.329	2.331	2.361	2.158	2.078	2.225	2.098
K	0.163	0.179	0.177	0.195	0.166	0.147	0.16	0.158
Ab	57	58.3	58.6	59.4	54.2	52.6	56	53
An	38.9	37.2	36.9	35.7	41.6	43.7	40	43
Or	4.1	4.5	4.5	4.9	4.2	3.7	4	4

Table A.2: Con't

	LT066-008	LT066-009	LT066-010	LT066-012	LT066-013	LT066-014	LT066-015	LT066-017
SiO_2	56.261	56.801	56.478	56.911	57.151	55.914	57.29	56.814
Al_2O_3	25.985	26.042	25.952	25.793	26.193	26.256	26.634	26.025
FeOT	0.462	0.493	0.46	0.434	0.503	0.484	0.571	0.466
MgO	0.042	0.037	0.034	0.027	0.041	0.036	0.039	0.054
BaO	0.136	0.144	0.14	0.136	0.096	0.103	0.122	0.122
SrO	0.249	0.274	0.236	0.267	0.293	0.255	0.27	0.294
CaO	8.463	8.558	8.551	8.439	8.587	9.144	8.963	8.95
Na_2O	6.003	6.154	6.038	6.25	6.118	5.95	6.093	5.963
K_2O	0.702	0.657	0.664	0.686	0.668	0.597	0.564	0.596
Total	98.3	99.16	98.55	98.94	99.65	98.74	100.55	99.28
				Oxygen = 32.000				
Si	10.32	10.334	10.333	10.372	10.34	10.233	10.283	10.325
Al	5.613	5.58	5.591	5.536	5.581	5.659	5.63	5.57
Fe	0.071	0.075	0.07	0.066	0.076	0.074	0.086	0.071
Mg	0.011	0.01	0.009	0.007	0.011	0.01	0.01	0.015
Ba	0.01	0.01	0.01	0.01	0.007	0.007	0.009	0.009
Ca	1.663	1.668	1.676	1.648	1.665	1.793	1.724	1.743
Na	2.135	2.171	2.142	2.209	2.146	2.111	2.121	2.101
K	0.164	0.152	0.155	0.16	0.154	0.139	0.129	0.138
Ab	53.9	54.4	53.9	55	54.1	52.2	53.4	52.8
An	42	41.8	42.2	41	42	44.3	43.4	43.8
Or	4.1	3.8	3.9	4	3.9	3.4	3.2	3.5

Table A.2: Con't

	LT066-018	LT066-019	LT066-020	LT066-021	LT066-022	LT066-023	LT066-024	LT066-025
SiO_2	57.381	57.594	57.414	56.511	56.841	57.499	57.867	56.985
Al_2O_3	25.674	25.633	25.873	25.708	25.813	25.557	26.24	25.227
FeOT	0.486	0.479	0.472	0.449	0.399	0.482	0.439	0.509
MgO	0.037	0.043	0.055	0.045	0.038	0.038	0.03	0.039
BaO	0.133	0.158	0.15	0.133	0.142	0.159	0.132	0.15
SrO	0.238	0.278	0.231	0.242	0.242	0.273	0.288	0.269
CaO	8.321	7.988	8.264	8.284	8.204	8.008	8.301	8.363
Na_2O	6.347	6.352	6.327	6.175	6.265	6.454	6.341	6.311
K_2O	0.664	0.707	0.695	0.65	0.655	0.746	0.668	0.704
Total	99.28	99.23	99.48	98.2	98.6	99.22	100.31	98.56
				Oxygen = 32.000				
Si	10.415	10.45	10.399	10.369	10.382	10.444	10.39	10.432
Al	5.488	5.477	5.519	5.555	5.553	5.467	5.548	5.439
Fe	0.074	0.073	0.071	0.069	0.061	0.073	0.066	0.078
Mg	0.01	0.012	0.015	0.012	0.01	0.01	0.008	0.011
Ba	0.009	0.011	0.011	0.01	0.01	0.011	0.009	0.011
Ca	1.618	1.553	1.604	1.629	1.606	1.558	1.597	1.64
Na	2.234	2.235	2.222	2.197	2.219	2.273	2.208	2.24
K	0.154	0.164	0.161	0.152	0.153	0.173	0.153	0.164
Ab	55.8	56.6	55.7	55.2	55.8	56.8	55.8	55.4
An	40.4	39.3	40.2	41	40.4	38.9	40.3	40.6
Or	3.8	4.1	4	3.8	3.8	4.3	3.9	4.1

Table A.2: Con't

	LT066-026	LT066-027	LT066-028	LT066-029	LT066-030	LT066-034	LT066-035	LT066-036
SiO_2	57.218	55.295	55.889	55.73	55.37	57.025	57.805	58.102
Al_2O_3	26.926	26.659	26.122	26.746	26.764	25.646	25.032	24.64
FeOT	0.516	0.478	0.483	0.5	0.528	0.442	0.412	0.449
MgO	0.045	0.035	0.039	0.053	0.041	0.03	0.039	0.033
BaO	0.081	0.122	0.065	0.096	0.109	0.138	0.169	0.176
SrO	0.254	0.249	0.283	0.245	0.26	0.281	0.256	0.254
CaO	9.155	9.772	9.268	9.721	9.72	8.441	7.834	7.392
Na_2O	5.982	5.607	5.834	5.724	5.527	6.196	6.433	6.686
K_2O	0.569	0.546	0.587	0.54	0.553	0.674	0.768	0.855
Total	100.75	98.76	98.57	99.36	98.87	98.87	98.75	98.59
				Oxygen = 32.000				
Si	10.246	10.133	10.244	10.148	10.131	10.397	10.533	10.602
Al	5.678	5.753	5.639	5.735	5.767	5.507	5.372	5.295
Fe	0.077	0.073	0.074	0.076	0.081	0.067	0.063	0.069
Mg	0.012	0.01	0.011	0.014	0.011	0.008	0.011	0.009
Ba	0.006	0.009	0.005	0.007	0.008	0.01	0.012	0.013
Ca	1.757	1.919	1.82	1.896	1.906	1.649	1.529	1.445
Na	2.077	1.992	2.073	2.021	1.961	2.19	2.273	2.366
K	0.13	0.128	0.137	0.125	0.129	0.157	0.179	0.199
Ab	52.4	49.3	51.4	50	49.1	54.8	57.1	59
An	44.3	47.5	45.2	46.9	47.7	41.3	38.4	36
Or	3.3	3.2	3.4	3.1	3.2	3.9	4.5	5

Table A.2: Con't

	LT066-037	LT066-038	LT066-039	LT066-040	LT066-041	LT067-001	LT067-002	LT067-003
SiO_2	58.525	59.152	59.501	59.009	60.591	61.118	61.667	61.363
Al_2O_3	24.971	24.776	24.892	24.547	23.563	23.61	23.094	22.937
FeOT	0.419	0.451	0.447	0.411	0.413	0.36	0.357	0.371
MgO	0.017	0.019	0.031	0.023	0.02	0.012	0.023	0.021
BaO	0.228	0.185	0.206	0.221	0.3	0.361	0.325	0.276
SrO	0.245	0.191	0.163	0.138	0.107	0.14	0.087	0.118
CaO	7.346	6.951	6.91	6.709	5.565	5.347	5.088	5.181
Na_2O	6.726	7.02	7.081	6.947	7.35	7.559	7.681	7.506
K_2O	0.897	0.981	0.962	1.02	1.365	1.543	1.632	1.566
Total	99.37	99.73	100.19	99.03	99.27	100.05	99.95	99.34
				Oxygen = 32.000				
Si	10.594	10.659	10.667	10.696	10.932	10.953	11.048	11.055
Al	5.323	5.258	5.255	5.24	5.007	4.983	4.872	4.866
Fe	0.063	0.068	0.067	0.062	0.062	0.054	0.053	0.056
Mg	0.005	0.005	0.008	0.006	0.005	0.003	0.006	0.006
Ba	0.016	0.013	0.014	0.016	0.021	0.025	0.023	0.019
Ca	1.425	1.342	1.327	1.303	1.076	1.027	0.977	1
Na	2.361	2.453	2.461	2.442	2.571	2.627	2.668	2.622
K	0.207	0.226	0.22	0.236	0.314	0.353	0.373	0.36
Ab	59.1	61	61.4	61.3	64.9	65.6	66.4	65.8
An	35.7	33.4	33.1	32.7	27.2	25.6	24.3	25.1
Or	5.2	5.6	5.5	5.9	7.9	8.8	9.3	9

Table A.2: Con't

	LT067-004	LT067-005	LT067-006	LT067-007	LT067-008	LT067-009	LT067-010	LT067-011
SiO_2	60.769	59.791	61.786	62.137	61.419	61.764	60.627	60.619
Al_2O_3	23.249	23.849	22.32	22.216	22.997	22.718	23.238	23.502
FeOT	0.38	0.394	0.402	0.383	0.418	0.395	0.384	0.374
MgO	0.024	0.016	0.003	0.018	0.021	0.018	0.009	0.009
BaO	0.262	0.274	0.34	0.391	0.35	0.377	0.305	0.303
SrO	0.095	0.112	0.095	0.117	0.107	0.106	0.092	0.087
CaO	5.499	6.225	4.612	4.451	5.226	4.764	5.31	5.401
Na_2O	7.463	7.191	7.812	7.75	7.556	7.736	7.414	7.532
K_2O	1.56	1.252	1.889	2.048	1.612	1.776	1.593	1.504
Total	99.3	99.1	99.26	99.51	99.71	99.65	98.97	99.33
				Oxygen = 32.000				
Si	10.969	10.827	11.152	11.189	11.039	11.103	10.977	10.938
Al	4.942	5.086	4.744	4.711	4.868	4.81	4.955	4.994
Fe	0.057	0.06	0.061	0.058	0.063	0.059	0.058	0.056
Mg	0.006	0.004	0.001	0.005	0.006	0.005	0.002	0.002
Ba	0.019	0.019	0.024	0.028	0.025	0.027	0.022	0.021
Ca	1.063	1.208	0.892	0.859	1.006	0.918	1.03	1.044
Na	2.612	2.525	2.734	2.706	2.633	2.697	2.603	2.635
K	0.359	0.289	0.435	0.47	0.37	0.407	0.368	0.346
Ab	64.7	62.8	67.3	67.1	65.7	67.1	65.1	65.5
An	26.4	30	22	21.3	25.1	22.8	25.7	25.9
Or	8.9	7.2	10.7	11.6	9.2	10.1	9.2	8.6

Table A.2: Con't

	LT067-014	LT067-015	LT067-016	LT067-017	LT067-018	LT067-019	LT067-020	LT067-021
SiO_2	60.444	60.079	60.989	60.931	61.274	60.951	61.001	60.885
Al_2O_3	23.495	23.469	23.639	23.649	23.321	23.072	23.252	23.263
FeCr	0.407	0.346	0.405	0.368	0.347	0.383	0.337	0.318
MgO	0.005	0.019	0.024	0.027	0.017	0.004	0.005	0.016
BaO	0.435	0.31	0.357	0.372	0.343	0.346	0.348	0.323
SrO	0.138	0.144	0.116	0.128	0.131	0.096	0.117	0.118
CaO	5.737	5.608	5.526	5.417	5.346	5.343	5.272	5.284
Na_2O	7.325	7.267	7.462	7.525	7.461	7.637	7.54	7.525
K_2O	1.437	1.437	1.533	1.522	1.594	1.611	1.577	1.616
Total	99.42	98.68	100.05	99.94	99.83	99.44	99.45	99.35
				Oxygen = 32.000				
Si	10.916	10.914	10.934	10.934	10.998	10.996	10.993	10.984
Al	4.997	5.021	4.991	4.998	4.929	4.902	4.935	4.942
Fe	0.061	0.053	0.061	0.055	0.052	0.058	0.051	0.048
Mg	0.001	0.005	0.006	0.007	0.005	0.001	0.001	0.004
Ba	0.031	0.022	0.025	0.026	0.024	0.024	0.025	0.023
Ca	1.11	1.092	1.061	1.042	1.028	1.033	1.018	1.021
Na	2.565	2.56	2.594	2.618	2.597	2.672	2.635	2.632
K	0.331	0.333	0.351	0.348	0.365	0.371	0.363	0.372
Ab	64	64.2	64.8	65.3	65.1	65.6	65.6	65.4
An	27.7	27.4	26.5	26	25.8	25.3	25.3	25.4
Or	8.3	8.4	8.8	8.7	9.1	9.1	9	9.2

Table A.2: Con't

	LT067-024	LT067-025	LT067-026	LT067-027	LT067-028	LT067-029	LT067-030	LT067-031
SiO_2	59.925	60.311	60.964	61.363	61.553	61.752	60.767	60.97
Al_2O_3	23.914	23.796	23.347	23.204	23.157	22.869	23.364	23.614
FeCr	0.394	0.395	0.369	0.367	0.401	0.368	0.394	0.395
MgO	0.017	0.006	0.032	0.009	0.01	0.003	0.017	0.013
BaO	0.295	0.29	0.33	0.334	0.368	0.325	0.331	0.309
SrO	0.159	0.157	0.148	0.171	0.162	0.133	0.197	0.09
CaO	6.16	5.909	5.674	5.079	4.898	4.863	5.427	5.653
Na_2O	7.171	7.375	7.504	7.558	7.541	7.655	7.455	7.511
K_2O	1.215	1.297	1.511	1.618	1.635	1.735	1.431	1.463
Total	99.25	99.54	99.88	99.7	99.73	99.7	99.38	100.02
				Oxygen = 32.000				
Si	10.832	10.87	10.954	11.025	11.051	11.089	10.961	10.931
Al	5.091	5.051	4.94	4.91	4.896	4.836	4.963	4.986
Fe	0.06	0.06	0.055	0.055	0.06	0.055	0.059	0.059
Mg	0.005	0.002	0.009	0.002	0.003	0.001	0.005	0.003
Ba	0.021	0.02	0.023	0.024	0.026	0.023	0.023	0.022
Ca	1.193	1.141	1.092	0.978	0.942	0.936	1.049	1.086
Na	2.513	2.577	2.614	2.633	2.625	2.665	2.607	2.611
K	0.28	0.298	0.346	0.371	0.374	0.397	0.329	0.335
Ab	63	64.2	64.5	66.1	66.6	66.7	65.4	64.8
An	29.9	28.4	26.9	24.6	23.9	23.4	26.3	26.9
Or	7	7.4	8.5	9.3	9.5	9.9	8.3	8.3

Table A.2: Con't

	LT067-032	LT067-033	LT067-034	LT067-035	LT067-036	LT067-037	LT067-038	LT067-039
SiO_2	60.942	60.498	60.805	61.259	61.492	61.251	60.791	60.976
Al_2O_3	23.846	23.485	22.973	23.217	23.502	23.286	23.45	23.545
FeOт	0.375	0.403	0.399	0.415	0.415	0.464	0.438	0.462
MgO	0.011	0.026	0.012	0.012	0.01	0.001	0.01	0.041
BaO	0.306	0.317	0.332	0.364	0.37	0.394	0.345	0.315
SrO	0.129	0.176	0.144	0.168	0.146	0.169	0.17	0.176
CaO	5.67	5.743	5.44	5.214	5.273	5.186	5.607	5.458
Na_2O	7.389	7.517	7.617	7.481	7.526	7.601	7.349	7.279
K_2O	1.432	1.419	1.565	1.598	1.596	1.603	1.457	1.467
Total	100.1	99.58	99.29	99.73	100.33	99.96	99.62	99.72
				Oxygen = 32.000				
Si	10.911	10.908	10.992	11.011	10.987	10.995	10.946	10.956
Al	5.028	4.987	4.891	4.914	4.945	4.923	4.972	4.982
Fe	0.056	0.061	0.06	0.062	0.062	0.07	0.066	0.069
Mg	0.003	0.007	0.003	0.003	0.003	0	0.003	0.011
Ba	0.021	0.022	0.024	0.026	0.026	0.028	0.024	0.022
Ca	1.088	1.109	1.054	1.004	1.009	0.997	1.082	1.051
Na	2.565	2.628	2.67	2.607	2.607	2.646	2.566	2.536
K	0.327	0.326	0.361	0.366	0.364	0.367	0.335	0.336
Ab	64.4	64.7	65.4	65.6	65.5	66	64.4	64.6
An	27.3	27.3	25.8	25.2	25.4	24.9	27.2	26.8
Or	8.2	8	8.8	9.2	9.1	9.2	8.4	8.6

Table A.2: Con't

	LT067-040	LT067-041	LT067-042	LT067-043	LT068-001	LT068-002	LT068-003	LT068-004
SiO_2	60.819	61.447	61.852	60.069	63.932	63.814	63.696	61.401
Al_2O_3	24.016	23.171	23.311	17.887	21.332	21.302	21.33	22.75
FeOт	0.443	0.426	0.4	4.906	0.32	0.35	0.323	0.298
MgO	0.017	0.023	0.003	1.387	0.01	0.001	0	0.012
BaO	0.309	0.364	0.38	0.101	0.389	0.34	0.375	0.364
SrO	0.206	0.17	0.209	0	0	0	0	0
CaO	5.717	5.267	5.147	3.307	3.168	3.155	3.144	3.368
Na_2O	7.395	7.455	7.531	7.33	7.614	7.555	7.638	7.326
K_2O	1.414	1.568	1.67	3.985	3.559	3.671	3.518	3.493
Total	100.34	99.89	100.5	98.97	100.32	100.19	100.02	99.01
				Oxygen = 32.000				
Si	10.876	11.024	11.032	11.23	11.425	11.423	11.416	11.14
Al	5.058	4.895	4.896	3.938	4.489	4.491	4.502	4.861
Fe	0.066	0.064	0.06	0.767	0.048	0.052	0.048	0.045
Mg	0.005	0.006	0.001	0.387	0.003	0	0	0.003
Ba	0.022	0.026	0.027	0.007	0.027	0.024	0.026	0.026
Ca	1.095	1.012	0.984	0.662	0.607	0.605	0.604	0.655
Na	2.564	2.593	2.605	2.657	2.638	2.622	2.654	2.577
K	0.323	0.359	0.38	0.95	0.811	0.838	0.804	0.808
Ab	64.4	65.4	65.6	62.2	65	64.5	65.3	63.8
An	27.5	25.5	24.8	15.5	15	14.9	14.9	16.2
Or	8.1	9.1	9.6	22.3	20	20.6	19.8	20

Table A.2: Con't

	LT068-005	LT068-006	LT068-007	LT068-008	LT068-009	LT068-010	LT068-011	LT068-012
SiO_2	63.952	61.243	64.19	63.965	63.728	63.774	63.284	63.711
Al_2O_3	21.497	23.324	21.486	21.552	21.516	21.738	21.669	22.044
FeOт	0.311	0.294	0.304	0.326	0.329	0.325	0.283	0.32
MgO	0.013	0.008	0.003	0	0.006	0.008	0.012	0.006
BaO	0.371	0.33	0.323	0.32	0.295	0.35	0.38	0.392
SrO	0	0	0	0	0	0	0	0
CaO	3.199	3.042	2.974	3.091	3.071	3.186	3.225	3.237
Na_2O	7.532	7.084	7.653	7.618	7.566	7.688	7.485	7.492
K_2O	3.456	3.495	3.69	3.613	3.63	3.539	3.442	3.528
Total	100.33	98.82	100.62	100.49	100.14	100.61	99.78	100.73
				Oxygen = 32.000				
Si	11.415	11.105	11.429	11.407	11.403	11.367	11.364	11.338
Al	4.519	4.981	4.505	4.526	4.534	4.563	4.583	4.62
Fe	0.046	0.045	0.045	0.049	0.049	0.048	0.043	0.048
Mg	0.003	0.002	0.001	0	0.002	0.002	0.003	0.002
Ba	0.026	0.023	0.023	0.022	0.021	0.024	0.027	0.027
Ca	0.612	0.591	0.567	0.591	0.589	0.608	0.621	0.617
Na	2.607	2.491	2.642	2.634	2.625	2.657	2.606	2.585
K	0.787	0.809	0.838	0.822	0.829	0.805	0.789	0.801
Ab	65.1	64	65.3	65.1	64.9	65.3	64.9	64.6
An	15.3	15.2	14	14.6	14.6	14.9	15.5	15.4
Or	19.6	20.8	20.7	20.3	20.5	19.8	19.6	20

Table A.2: Con't

	LT068-016	LT068-017	LT068-018	LT068-019	LT068-020	LT068-021	LT068-022	LT068-023
SiO_2	63.407	63.914	64.259	63.76	64.215	64.092	63.916	63.664
Al_2O_3	21.3	21.315	21.326	21.36	21.472	21.301	21.334	21.134
FeOт	0.343	0.253	0.308	0.303	0.337	0.272	0.3	0.334
MgO	0.007	0.003	0	0.006	0.008	0.005	0.017	0.005
BaO	0.304	0.309	0.314	0.26	0.248	0.276	0.337	0.282
SrO	0	0	0	0	0	0	0	0
CaO	3.041	3.085	3.09	2.914	2.979	2.999	3.034	3.045
Na_2O	7.489	7.553	7.687	7.574	7.73	7.504	7.646	7.629
K_2O	3.577	3.568	3.533	3.661	3.593	3.57	3.629	3.576
Total	99.47	100	100.52	99.84	100.58	100.02	100.21	99.67
				Oxygen = 32.000				
Si	11.419	11.441	11.448	11.433	11.431	11.46	11.43	11.443
Al	4.517	4.494	4.474	4.511	4.501	4.486	4.493	4.473
Fe	0.052	0.038	0.046	0.045	0.05	0.041	0.045	0.05
Mg	0.002	0.001	0	0.002	0.002	0.001	0.005	0.001
Ba	0.021	0.022	0.022	0.018	0.017	0.019	0.024	0.02
Ca	0.587	0.592	0.59	0.56	0.568	0.575	0.581	0.586
Na	2.615	2.622	2.655	2.633	2.668	2.602	2.651	2.659
K	0.822	0.815	0.803	0.838	0.816	0.814	0.828	0.82
Ab	65	65.1	65.6	65.3	65.8	65.2	65.3	65.4
An	14.6	14.7	14.6	13.9	14	14.4	14.3	14.4
Or	20.4	20.2	19.8	20.8	20.1	20.4	20.4	20.2

Table A.2: Con't

	LT068-024	LT068-025	LT068-026	LT068-027	LT068-028	LT068-029	LT068-030	LT068-031
SiO_2	63.953	64.024	63.838	63.948	64.331	64.502	60.726	63.82
Al_2O_3	21.361	21.064	21.081	21.061	21.112	21.226	23.064	21.621
FeOT	0.302	0.3	0.33	0.333	0.328	0.316	0.295	0.304
MgO	0.005	0.002	0	0	0.006	0.007	0.005	0.003
BaO	0.271	0.27	0.378	0.276	0.278	0.272	0.265	0.255
SrO	0	0	0	0	0	0	0	0
CaO	3.056	3.012	2.945	2.842	2.747	2.766	2.972	2.654
Na_2O	7.581	7.577	7.634	7.548	7.593	7.674	7.134	7.537
K_2O	3.608	3.733	3.763	3.739	3.85	3.726	3.688	3.974
Total	100.14	99.98	99.97	99.75	100.25	100.49	98.15	100.17
				Oxygen = 32.000				
Si	11.435	11.471	11.455	11.479	11.491	11.486	11.101	11.415
Al	4.498	4.444	4.455	4.452	4.441	4.451	4.965	4.554
Fe	0.045	0.045	0.05	0.05	0.049	0.047	0.045	0.045
Mg	0.001	0.001	0	0	0.002	0.002	0.001	0.001
Ba	0.019	0.019	0.027	0.019	0.019	0.019	0.019	0.018
Ca	0.585	0.578	0.566	0.547	0.526	0.528	0.582	0.509
Na	2.628	2.632	2.656	2.627	2.63	2.65	2.529	2.614
K	0.823	0.853	0.861	0.856	0.877	0.846	0.86	0.907
Ab	65.1	64.8	65.1	65.2	65.2	65.9	63.7	64.9
An	14.5	14.2	13.9	13.6	13	13.1	14.7	12.6
Or	20.4	21	21.1	21.2	21.7	21	21.7	22.5

Table A.2: Con't

	LT068-032	LT068-033	LT068-034	LT068-035	LT068-036	LT068-037	LT068-038	LT068-039
SiO_2	64.45	64.275	64.021	64.089	64.215	64.246	63.968	64.259
Al_2O_3	21.138	21.209	21.229	21.281	21.2	21.159	21.032	21.306
FeOT	0.316	0.268	0.311	0.296	0.28	0.334	0.281	0.326
MgO	0.012	0	0.005	0.005	0.011	0.002	0	0
BaO	0.275	0.303	0.263	0.275	0.275	0.262	0.305	0.267
SrO	0	0	0	0	0	0	0	0
CaO	2.815	2.813	2.824	2.832	2.785	2.791	2.787	2.702
Na_2O	7.527	7.622	7.546	7.568	7.54	7.556	7.57	7.544
K_2O	3.994	3.924	3.94	3.896	4.038	4.029	3.918	3.944
Total	100.53	100.41	100.14	100.24	100.34	100.38	99.86	100.35
				Oxygen = 32.000				
Si	11.488	11.471	11.458	11.455	11.47	11.474	11.48	11.469
Al	4.437	4.458	4.474	4.48	4.46	4.45	4.445	4.478
Fe	0.047	0.04	0.047	0.044	0.042	0.05	0.042	0.049
Mg	0.003	0	0.001	0.001	0.003	0.001	0	0
Ba	0.019	0.021	0.018	0.019	0.019	0.018	0.021	0.019
Ca	0.538	0.538	0.541	0.542	0.533	0.534	0.536	0.517
Na	2.601	2.638	2.619	2.623	2.612	2.617	2.634	2.611
K	0.908	0.893	0.9	0.888	0.92	0.918	0.897	0.898
Ab	64.3	64.8	64.5	64.7	64.3	64.3	64.8	64.9
An	13.3	13.2	13.3	13.4	13.1	13.1	13.2	12.8
Or	22.4	21.9	22.2	21.9	22.6	22.6	22.1	22.3

Table A.2: Con't

	LT068-040	LT068-041	LT068-042	LT068-043	LT068-044	LT068-045	LT068-046	LT068-047
SiO_2	64.48	64.253	64.337	64.125	64.321	64.363	64.106	64.283
Al_2O_3	21.079	20.933	20.944	21.123	21.041	21.13	21.062	21.296
FeOT	0.276	0.319	0.347	0.284	0.313	0.306	0.321	0.293
MgO	0.014	0.012	0	0.011	0	0.006	0.008	0.016
BaO	0.273	0.223	0.24	0.249	0.265	0.273	0.234	0.277
SrO	0	0	0	0	0	0	0	0
CaO	2.785	2.808	2.737	2.697	2.77	2.712	2.692	2.788
Na_2O	7.571	7.632	7.643	7.571	7.658	7.768	7.595	7.712
K_2O	3.982	3.913	4.006	4.005	3.996	3.941	4.04	3.972
Total	100.46	100.09	100.25	100.07	100.36	100.5	100.06	100.64
				Oxygen = 32.000				
Si	11.498	11.5	11.502	11.481	11.489	11.48	11.483	11.454
Al	4.427	4.412	4.41	4.454	4.426	4.438	4.443	4.469
Fe	0.041	0.048	0.052	0.043	0.047	0.046	0.048	0.044
Mg	0.004	0.003	0	0.003	0	0.002	0.002	0.004
Ba	0.019	0.016	0.017	0.017	0.019	0.019	0.016	0.019
Ca	0.532	0.538	0.524	0.517	0.53	0.518	0.517	0.532
Na	2.618	2.649	2.65	2.628	2.652	2.687	2.638	2.664
K	0.906	0.893	0.914	0.915	0.911	0.897	0.923	0.903
Ab	64.5	64.9	64.8	64.7	64.8	65.5	64.7	65
An	13.1	13.2	12.8	12.7	12.9	12.6	12.7	13
Or	22.3	21.9	22.4	22.5	22.3	21.9	22.6	22

Table A.2: Con't

	LT068-048	LT068-050	LT068-051	LT068-052	LT068-053	LT068-054	LT068-055	LT068-056
SiO_2	64.36	64.353	63.904	64.374	63.827	64.289	64.104	63.886
Al_2O_3	21.418	21.155	20.985	21.397	21.106	21.19	21.126	21.24
FeOT	0.321	0.297	0.33	0.289	0.291	0.287	0.289	0.3
MgO	0.016	0	0.003	0	0.006	0.005	0.01	0.002
BaO	0.266	0.237	0.228	0.252	0.278	0.303	0.314	0.417
SrO	0	0	0	0	0	0	0	0
CaO	2.718	2.761	2.713	2.679	2.667	2.744	2.743	2.948
Na_2O	7.572	7.604	7.497	7.652	7.634	7.611	7.657	7.488
K_2O	3.948	4.038	3.896	3.941	3.949	3.879	3.912	3.735
Total	100.62	100.45	99.56	100.58	99.76	100.31	100.16	100.02
				Oxygen = 32.000				
Si	11.457	11.481	11.492	11.462	11.467	11.48	11.473	11.45
Al	4.49	4.445	4.444	4.487	4.466	4.456	4.453	4.483
Fe	0.048	0.044	0.05	0.043	0.044	0.043	0.043	0.045
Mg	0.004	0	0.001	0	0.002	0.001	0.003	0.001
Ba	0.019	0.017	0.016	0.018	0.02	0.021	0.022	0.029
Ca	0.518	0.528	0.523	0.511	0.513	0.525	0.526	0.566
Na	2.614	2.631	2.614	2.642	2.659	2.635	2.657	2.602
K	0.897	0.919	0.894	0.895	0.905	0.884	0.893	0.854
Ab	64.9	64.5	64.8	65.3	65.2	65.2	65.2	64.7
An	12.9	12.9	13	12.6	12.6	13	12.9	14.1
Or	22.3	22.5	22.2	22.1	22.2	21.9	21.9	21.2

Table A.2: Con't

	LT068-057	LT068-058	LT068-059	LT068-060	LT068-061	LT068-062	LT068-064	LT069-001
SiO_2	63.627	63.803	58.584	63.859	63.912	63.733	63.617	64.873
Al_2O_3	21.242	21.353	25.296	21.454	21.187	21.287	21.315	20.691
FeOT	0.322	0.33	0.247	0.325	0.329	0.329	0.34	0.293
MgO	0.005	0.009	0.021	0.01	0.001	0.003	0.019	0.014
BaO	0.431	0.414	0.419	0.43	0.375	0.407	0.305	0.209
SrO	0	0	0	0	0	0	0	0
CaO	3.023	2.966	3.262	2.968	2.984	2.978	2.941	2.346
Na_2O	7.5	7.504	6.746	7.508	7.541	7.444	7.523	7.45
K_2O	3.789	3.789	3.457	3.688	3.676	3.777	3.648	4.512
Total	99.94	100.17	98.03	100.24	100.01	99.96	99.71	100.39
				Oxygen = 32.000				
Si	11.426	11.426	10.741	11.421	11.453	11.434	11.429	11.578
Al	4.492	4.503	5.462	4.519	4.471	4.498	4.509	4.349
Fe	0.048	0.049	0.038	0.049	0.049	0.049	0.051	0.044
Mg	0.001	0.002	0.006	0.003	0	0.001	0.005	0.004
Ba	0.03	0.029	0.03	0.03	0.026	0.029	0.021	0.015
Ca	0.582	0.569	0.641	0.569	0.573	0.572	0.566	0.449
Na	2.612	2.606	2.398	2.604	2.62	2.59	2.621	2.578
K	0.868	0.866	0.809	0.841	0.84	0.864	0.836	1.027
Ab	64.3	64.5	62.3	64.9	65	64.3	65.2	63.6
An	14.3	14.1	16.7	14.2	14.2	14.2	14.1	11.1
Or	21.4	21.4	21	21	20.8	21.5	20.8	25.3

Table A.2: Con't

	LT069-002	LT069-003	LT069-004	LT069-005	LT069-006	LT069-007	LT069-008	LT069-010
SiO_2	64.484	64.566	64.765	64.73	64.949	65.252	65.286	65.384
Al_2O_3	20.722	20.74	20.806	20.583	20.297	20.598	20.693	20.52
FeOT	0.323	0.274	0.248	0.304	0.292	0.28	0.314	0.291
MgO	0.003	0.016	0.012	0	0	0	0.007	0
BaO	0.17	0.216	0.194	0.252	0.233	0.261	0.248	0.235
SrO	0	0	0	0	0	0	0	0
CaO	2.374	2.315	2.412	2.073	1.876	1.901	1.957	1.86
Na_2O	7.463	7.548	7.603	7.425	7.389	7.343	7.333	7.465
K_2O	4.412	4.517	4.452	5.033	5.304	5.26	5.099	5.144
Total	99.95	100.19	100.49	100.4	100.34	100.9	100.94	100.9
				Oxygen = 32.000				
Si	11.557	11.554	11.551	11.582	11.632	11.615	11.607	11.63
Al	4.374	4.371	4.37	4.337	4.281	4.318	4.333	4.299
Fe	0.048	0.041	0.037	0.045	0.044	0.042	0.047	0.043
Mg	0.001	0.004	0.003	0	0	0	0.002	0
Ba	0.012	0.015	0.014	0.018	0.016	0.018	0.017	0.016
Ca	0.456	0.444	0.461	0.397	0.36	0.363	0.373	0.354
Na	2.594	2.619	2.629	2.576	2.566	2.534	2.528	2.575
K	1.009	1.031	1.013	1.149	1.212	1.194	1.157	1.167
Ab	63.9	64	64.1	62.5	62	61.9	62.3	62.9
An	11.2	10.8	11.2	9.6	8.7	8.9	9.2	8.6
Or	24.9	25.2	24.7	27.9	29.3	29.2	28.5	28.5

Table A.2: Con't

	LT069-011	LT069-013	LT069-014	LT069-015	LT069-016	LT070-001	LT070-002
SiO_2	65.525	65.422	65.363	65.567	65.451	65.751	65.513
Al_2O_3	20.277	20.223	20.177	20.357	20.113	19.538	19.42
FeOT	0.278	0.287	0.274	0.281	0.301	0.246	0.261
MgO	0.002	0.002	0	0.004	0.006	0.011	0.014
BaO	0.25	0.269	0.23	0.16	0.197	0.248	0.192
SrO	0	0	0	0	0	0	0
CaO	1.586	1.545	1.58	2.029	1.938	1.305	1.317
Na_2O	7.042	7.052	7.136	7.399	7.311	6.675	6.82
K_2O	5.833	5.999	5.791	5.101	5.257	6.714	6.552
Total	100.79	100.8	100.55	100.9	100.57	100.49	100.09
				Oxygen = 32.000			
Si	11.682	11.678	11.683	11.654	11.68	11.786	11.785
Al	4.257	4.251	4.247	4.261	4.227	4.124	4.114
Fe	0.041	0.043	0.041	0.042	0.045	0.037	0.039
Mg	0.001	0.001	0	0.001	0.002	0.003	0.004
Ba	0.017	0.019	0.016	0.011	0.014	0.017	0.014
Ca	0.303	0.295	0.303	0.386	0.371	0.251	0.254
Na	2.434	2.441	2.473	2.55	2.53	2.32	2.379
K	1.327	1.366	1.321	1.157	1.197	1.535	1.504
Ab	59.9	59.5	60.4	62.3	61.7	56.5	57.5
An	7.5	7.2	7.4	9.4	9.1	6.1	6.1
Or	32.7	33.3	32.2	28.3	29.2	37.4	36.4

Table A.2: Con't

	LT070-003	LT070-004	LT070-005	LT070-006	LT070-007	LT070-008	LT070-009
SiO_2	65.451	65.475	65.197	65.464	65.425	65.249	64.668
Al_2O_3	19.502	19.475	19.766	19.666	19.548	19.297	20.226
FeOT	0.25	0.255	0.264	0.268	0.283	0.253	0.262
MgO	0	0.011	0	0	0.002	0.005	0.002
BaO	0.207	0.242	0.244	0.293	0.28	0.25	0.209
SrO	0	0	0	0	0	0	0
CaO	1.348	1.271	1.523	1.27	1.262	1.121	1.908
Na_2O	6.777	6.698	7.027	6.765	6.734	6.628	7.184
K_2O	6.532	6.778	6.107	6.792	6.834	6.816	5.355
Total	100.07	100.21	100.13	100.52	100.37	99.62	99.81
				Oxygen = 32.000			
Si	11.776	11.778	11.721	11.749	11.761	11.802	11.637
Al	4.132	4.126	4.185	4.157	4.138	4.111	4.286
Fe	0.038	0.038	0.04	0.04	0.043	0.038	0.039
Mg	0	0.003	0	0	0.001	0.001	0.001
Ba	0.015	0.017	0.017	0.021	0.02	0.018	0.015
Ca	0.26	0.245	0.293	0.244	0.243	0.217	0.368
Na	2.364	2.336	2.449	2.354	2.347	2.325	2.507
K	1.499	1.555	1.401	1.555	1.567	1.573	1.229
Ab	57.3	56.5	59.1	56.7	56.5	56.5	61.1
An	6.3	5.9	7.1	5.9	5.8	5.3	9
Or	36.4	37.6	33.8	37.4	37.7	38.2	29.9

Table A.2: Con't

	LT070-010	LT070-011	LT070-012	LT070-013	LT070-014	LT070-015	LT070-016	LT070-017
SiO_2	65.017	64.713	64.904	64.412	65.282	65.157	65.053	65.102
Al_2O_3	19.865	20.17	19.887	20.549	19.971	20.003	19.68	19.713
FeOT	0.304	0.247	0.286	0.298	0.287	0.331	0.289	0.343
MgO	0	0.009	0.016	0.01	0.007	0.002	0	0
BaO	0.221	0.218	0.252	0.205	0.182	0.226	0.231	0.158
SrO	0	0	0	0	0	0	0	0
CaO	1.477	1.838	1.332	2.262	1.686	1.703	1.485	1.663
Na_2O	6.974	7.162	6.684	7.427	7.126	7.145	6.903	7.089
K_2O	6.288	5.522	6.756	4.749	5.724	5.855	6.207	5.693
Total	100.15	99.88	100.12	99.91	100.27	100.42	99.85	99.76
				Oxygen = 32.000				
Si	11.698	11.645	11.698	11.569	11.699	11.678	11.729	11.724
Al	4.209	4.274	4.221	4.347	4.215	4.222	4.179	4.181
Fe	0.046	0.037	0.043	0.045	0.043	0.05	0.044	0.052
Mg	0	0.002	0.004	0.003	0.002	0.001	0	0
Ba	0.016	0.015	0.018	0.014	0.013	0.016	0.016	0.011
Ca	0.285	0.354	0.257	0.435	0.324	0.327	0.287	0.321
Na	2.433	2.499	2.336	2.587	2.476	2.483	2.413	2.475
K	1.443	1.268	1.553	1.088	1.309	1.339	1.428	1.308
Ab	58.5	60.6	56.3	62.9	60.3	59.8	58.5	60.3
An	6.8	8.6	6.2	10.6	7.9	7.9	7	7.8
Or	34.7	30.8	37.5	26.5	31.9	32.3	34.6	31.9

Table A.2: Con't

	LT070-018	LT070-019	LT070-020	LT070-021	LT070-022	LT070-023	LT070-024	LT070-025
SiO_2	64.909	65.134	65.071	65.286	65.459	65.275	65.154	65.399
Al_2O_3	19.904	19.568	19.561	19.855	19.703	19.784	19.85	19.863
FeOT	0.307	0.276	0.261	0.251	0.295	0.235	0.264	0.252
MgO	0.01	0.006	0	0.011	0.011	0.013	0	0.003
BaO	0.147	0.175	0.235	0.245	0.242	0.241	0.208	0.253
SrO	0	0	0	0	0	0	0	0
CaO	1.866	1.7	1.538	1.36	1.336	1.476	1.363	1.253
Na_2O	7.195	7.047	6.851	6.711	6.667	6.911	6.872	6.693
K_2O	5.328	5.701	6.19	6.74	6.672	6.273	6.458	6.613
Total	99.67	99.61	99.71	100.46	100.39	100.21	100.17	100.33
				Oxygen = 32.000				
Si	11.688	11.745	11.746	11.719	11.75	11.726	11.716	11.738
Al	4.221	4.155	4.158	4.197	4.165	4.186	4.204	4.199
Fe	0.046	0.042	0.039	0.038	0.044	0.035	0.04	0.038
Mg	0.003	0.002	0	0.003	0.003	0.003	0	0.001
Ba	0.01	0.012	0.017	0.017	0.017	0.017	0.015	0.018
Ca	0.36	0.328	0.297	0.262	0.257	0.284	0.263	0.241
Na	2.512	2.464	2.398	2.336	2.321	2.407	2.396	2.329
K	1.224	1.311	1.425	1.543	1.528	1.438	1.482	1.514
Ab	61.3	60.1	58.2	56.4	56.5	58.3	57.9	57
An	8.8	8	7.2	6.3	6.3	6.9	6.4	5.9
Or	29.9	32	34.6	37.3	37.2	34.8	35.8	37.1

Table A.3: All EMP analyses for pyroxene from DH Wall

	C001-001	C002-001	C002-002	C002-003	C002-004	C003-001	C003-002	C003-003	C003-004	C004-001
SiO_2	48.087	49.349	48.993	49.005	49.47	47.627	46.413	46.319	47.072	47.017
TiO_2	1.442	1.132	1.268	1.163	1.114	2.226	2.559	2.518	2.384	2.372
Al_2O_3	3.382	2.601	2.867	2.797	2.58	5.302	6.189	6.054	5.448	5.66
FeO_T	8.399	8.096	8.167	8.013	8.412	7.999	7.242	7.637	7.917	7.819
Cr_2O_3	0	0	0.004	0	0	0	0	0	0	
MnO	0.52	0.549	0.55	0.54	0.595	0.275	0.146	0.215	0.274	0.289
MgO	13.183	13.46	13.214	13.512	13.088	13.109	13.485	13.19	12.871	13.298
CaO	21.869	21.959	21.961	21.946	21.813	22.076	22.282	22.337	22.383	22.877
Na_2O	1.119	1.058	1.058	1.009	1.084	0.801	0.587	0.68	0.723	0.695
K_2O	0.017	0.024	0.02	0.021	0.019	0.024	0.029	0.014	0.024	0.017
Total	98.02	98.23	98.1	98.01	98.18	99.44	98.93	98.96	99.1	100.044
					Oxygen = 6.000					
Si	1.816	1.859	1.85	1.85	1.869	1.776	1.736	1.734	1.764	1.742
Al	0.15	0.115	0.127	0.124	0.115	0.233	0.272	0.267	0.24	0.247
Ti	0.041	0.032	0.036	0.033	0.032	0.062	0.072	0.071	0.067	0.066
Fe*	0.266	0.255	0.257	0.253	0.266	0.25	0.227	0.239	0.248	0.243
Cr	0	0	0	0	0	0	0	0	0	0
Mg	0.742	0.756	0.744	0.76	0.737	0.729	0.752	0.736	0.719	0.735
Mn	0.017	0.018	0.018	0.017	0.019	0.009	0.005	0.007	0.009	0.009
Ca	0.885	0.886	0.889	0.888	0.883	0.882	0.893	0.896	0.899	0.908
Na	0.082	0.077	0.077	0.074	0.079	0.058	0.043	0.049	0.053	0.05
K	0.001	0.001	0.001	0.001	0.001	0.001	0.001	0.001	0.001	0.001
WO	46	46	47	46	46	47	48	48	48	48
EN	39	39	39	40	39	39	40	39	38	39
FS	15	14	14	14	15	14	12	13	14	13

Table A.3: Con't

	C004-002	C004-003	C004-004	C004-005	C004-006	C004-007	C004-008	C004-009	C004-010	C004-011
SiO_2	45.133	47.994	45.877	46.157	46.065	44.316	44.813	44.246	45.826	46.519
TiO_2	3.051	2.073	2.662	2.814	2.612	3	3.036	3.425	2.761	2.154
Al_2O_3	7.431	4.902	6.702	6.756	6.315	7.251	7.369	8.171	6.705	5.605
FeO	7.256	7.304	7.322	7.087	7.109	7.309	7.483	7.456	7.001	7.157
Cr_2O_3				0.019					0.005	0.031
MnO	0.126	0.254	0.188	0.166	0.173	0.186	0.181	0.14	0.158	0.169
MgO	13.003	13.87	13.181	13.452	13.669	13.115	13.015	12.389	13.367	13.699
CaO	23.009	22.949	22.994	23.152	22.909	22.945	23.033	23.061	23.208	23.254
Na_2O	0.569	0.6	0.646	0.535	0.563	0.622	0.603	0.635	0.603	0.606
K_2O	0.01	0.018	0.027	0.017	0.015	0.027	0.025	0.009	0.019	0.01
Total	99.588	99.964	99.599	100.155	99.43	98.771	99.558	99.532	99.653	99.204
					Oxygen = 6.000					
Si	1.679	1.776	1.705	1.706	1.713	1.66	1.668	1.651	1.701	1.732
Al	0.326	0.214	0.293	0.294	0.276	0.32	0.323	0.359	0.293	0.246
Ti	0.085	0.058	0.074	0.078	0.073	0.085	0.085	0.096	0.077	0.06
Fe*	0.226	0.225	0.228	0.219	0.221	0.229	0.233	0.232	0.217	0.223
Cr	0	0	0	0.001	0	0	0	0	0	0.001
Mg	0.721	0.765	0.73	0.741	0.757	0.733	0.722	0.689	0.739	0.76
Mn	0.004	0.008	0.006	0.005	0.005	0.006	0.006	0.004	0.005	0.005
Ca	0.917	0.91	0.916	0.917	0.913	0.921	0.919	0.922	0.923	0.928
Na	0.041	0.043	0.047	0.038	0.041	0.045	0.044	0.046	0.043	0.044
K	0	0.001	0.001	0.001	0.001	0.001	0.001	0	0.001	0
WO	49	48	49	49	48	49	49	50	49	48
EN	39	40	39	39	40	39	38	37	39	40
FS	12	12	12	12	12	12	13	13	12	12

Table A.3: Con't

	C004-012	C005-001	C005-002	C005-003	C005-004	C005-005	C005-006	C006-002	C006-003	C006-004
SiO_2	44.502	46.532	43.666	43.885	46.483	44.662	44.767	45.194	47.003	44.973
TiO_2	2.835	2.276	3.364	3.265	2.27	3.132	3.094	3.29	2.535	3.389
Al_2O_3	6.76	6.016	8.412	8.27	5.842	7.83	7.387	8.032	6.601	8.388
FeO	7.522	6.799	7.417	7.313	6.652	7.724	6.971	7.403	7.16	7.507
Cr_2O_3	0.009	0.003	0.049		0.015	0.004			0.004	
MnO	0.179	0.183	0.128	0.121	0.094	0.123	0.148	0.096	0.171	0.164
MgO	13.158	14.076	12.471	12.782	14.072	12.922	13.249	12.728	13.529	12.632
CaO	23.102	22.962	23.33	23.447	23.49	23.118	23.217	23.117	22.995	23.112
Na_2O	0.617	0.449	0.469	0.491	0.493	0.482	0.552	0.567	0.488	0.628
K_2O	0.019	0.022	0.018	0.016	0.01	0.025	0.023	0.007	0.028	0.013
Total	98.703	99.318	99.324	99.59	99.421	100.022	99.408	100.434	100.514	100.806
					Oxygen = 6.000					
Si	1.669	1.729	1.633	1.634	1.724	1.657	1.666	1.67	1.731	1.656
Al	0.299	0.263	0.37	0.363	0.255	0.342	0.324	0.349	0.286	0.363
Ti	0.08	0.064	0.095	0.091	0.063	0.087	0.087	0.091	0.07	0.094
Fe*	0.236	0.211	0.232	0.228	0.207	0.24	0.217	0.229	0.22	0.231
Cr	0	0	0.001	0	0	0	0	0	0	0
Mg	0.736	0.78	0.696	0.709	0.778	0.715	0.735	0.701	0.743	0.693
Mn	0.006	0.006	0.004	0.004	0.003	0.004	0.005	0.003	0.005	0.005
Ca	0.928	0.914	0.935	0.935	0.934	0.919	0.926	0.915	0.907	0.912
Na	0.045	0.032	0.034	0.035	0.035	0.035	0.04	0.041	0.035	0.045
K	0.001	0.001	0.001	0.001	0	0.001	0.001	0	0.001	0.001
WO	49	48	50	50	49	49	49	50	48	50
EN	39	41	37	38	41	38	39	38	40	38
FS	13	11	13	12	11	13	12	13	12	13

Table A.3: Con't

	LTO18-001	LTO18-003	LTO18-004	LTO18-005	LTO18-006	LTO18-007	LTO18-008	LTO18-009	LTO18-010	LTO18-011
SiO_2	43.995	44.291	43.381	44.159	45.418	45.388	43.982	47.196	46.834	47.066
TiO_2	3.582	3.439	3.71	3.515	3.061	3.046	3.754	2.223	2.242	2.193
Al_2O_3	8.739	8.12	8.529	8.037	7.336	7.239	8.579	5.65	5.605	5.557
FeO	7.835	8.066	8.572	8.204	7.294	7.351	7.688	6.932	6.935	6.863
Cr_2O_3	0.01	0	0.024	0	0.012	0.016	0	0	0	0.002
MnO	0.12	0.153	0.178	0.148	0.137	0.12	0.131	0.124	0.137	0.147
MgO	12.393	12.308	11.782	12.229	13.032	12.96	12.248	14.194	14.271	14.291
CaO	22.144	22.282	21.623	21.943	22.353	22.214	22.39	22.519	22.288	22.456
Na_2O	0.597	0.616	0.687	0.68	0.574	0.556	0.539	0.467	0.482	0.451
K_2O	0.025	0.033	0.009	0.018	0.019	0.013	0	0.008	0.016	0.015
Total	99.44	99.31	98.5	98.93	99.24	98.9	99.31	99.31	98.81	99.04
					Oxygen = 6.000					
Si	1.644	1.659	1.643	1.661	1.696	1.702	1.648	1.754	1.748	1.753
Al	0.385	0.358	0.38	0.356	0.323	0.319	0.379	0.247	0.246	0.244
Ti	0.101	0.097	0.106	0.099	0.086	0.086	0.106	0.062	0.063	0.061
Fe*	0.245	0.253	0.272	0.257	0.228	0.231	0.241	0.216	0.217	0.213
Cr	0	0	0.001	0	0	0	0	0	0	0
Mg	0.69	0.687	0.665	0.686	0.726	0.724	0.684	0.783	0.776	0.782
Mn	0.004	0.005	0.006	0.005	0.004	0.004	0.004	0.004	0.004	0.005
Ca	0.887	0.894	0.877	0.884	0.894	0.892	0.899	0.897	0.891	0.896
Na	0.043	0.045	0.05	0.05	0.042	0.04	0.039	0.034	0.035	0.033
K	0.001	0.002	0	0.001	0.001	0.001	0	0	0.001	0.001
WO	49	49	48	48	48	48	49	47	47	47
EN	38	37	37	37	39	39	37	41	42	42
FS	14	14	15	14	13	13	13	12	12	11

Table A.3: Con't

	LT018-012	LT018-013	LT018-014	LT018-015	LT018-016	LT018-017	LT018-018	LT018-019	LT018-020	LT018-021
SiO_2	46.959	47.132	47.654	47.894	47.728	47.438	47.459	47.542	47.492	47.73
TiO_2	2.214	2.161	2.353	2.331	2.257	2.211	2.132	2.272	2.191	2.204
Al_2O_3	5.517	5.464	5.459	5.423	5.486	5.663	5.623	5.458	5.709	5.525
FeO	6.831	6.918	6.967	6.996	7.034	7.013	6.993	6.884	6.683	6.79
Cr_2O_3	0	0	0	0	0	0.016	0	0	0.011	0.004
MnO	0.15	0.106	0.124	0.146	0.124	0.145	0.101	0.159	0.111	0.137
MgO	14.199	14.179	14.121	14.127	14.057	13.996	14.184	14.074	14.648	14.157
CaO	22.304	22.375	22.525	22.484	22.584	22.373	22.304	22.383	21.911	22.395
Na_2O	0.434	0.445	0.458	0.476	0.457	0.503	0.461	0.452	0.492	0.511
K_2O	0.012	0.003	0	0	0.014	0.014	0.026	0.012	0.005	0.015
Total	98.62	98.78	99.66	99.88	99.74	99.37	99.28	99.24	99.25	99.47
					Oxygen = 6.000					
Si	1.757	1.761	1.767	1.773	1.769	1.764	1.764	1.77	1.762	1.771
Al	0.244	0.241	0.239	0.236	0.239	0.247	0.247	0.24	0.249	0.241
Ti	0.062	0.061	0.066	0.065	0.063	0.062	0.06	0.064	0.061	0.062
Fe*	0.214	0.215	0.216	0.217	0.218	0.218	0.217	0.214	0.207	0.211
Cr	0	0	0	0	0	0	0	0	0	0
Mg	0.788	0.79	0.781	0.779	0.777	0.776	0.786	0.781	0.788	0.783
Mn	0.005	0.003	0.004	0.005	0.004	0.005	0.003	0.005	0.003	0.004
Ca	0.894	0.896	0.895	0.892	0.897	0.891	0.888	0.893	0.871	0.89
Na	0.031	0.032	0.033	0.034	0.033	0.036	0.033	0.033	0.035	0.037
K	0.001	0	0	0	0.001	0.001	0.001	0.001	0	0.001
WO	47	47	47	47	47	47	47	47	46	47
EN	42	41	41	41	41	41	41	41	43	41
FS	11	12	12	12	12	12	12	12	11	11

Table A.3: Con't

	LT018-022	LT018-023	LT018-025	LT018-026	LT018-027	LT018-029	LT018-030	LT018-031	LT018-032	LT018-034
SiO_2	48.031	47.685	48.143	47.727	47.631	47.371	47.26	47.055	44.297	43.718
TiO_2	2.177	2.137	2.053	2.032	2.109	2.083	2.077	2.167	3.361	3.405
Al_2O_3	5.464	5.411	5.378	5.414	5.346	5.23	5.128	5.299	8.06	8.386
FeO	6.813	6.791	6.871	6.812	6.768	6.793	6.818	6.856	7.56	7.396
Cr_2O_3	0	0	0.001	0	0	0.003	0	0	0.002	0
MnO	0.181	0.125	0.139	0.141	0.139	0.17	0.113	0.12	0.085	0.088
MgO	14.25	14.257	14.353	14.241	14.235	14.199	14.127	14.25	12.661	12.347
CaO	22.026	22.123	22.069	21.831	22.303	22.419	22.447	22.4	22.302	22.276
Na_2O	0.499	0.447	0.468	0.459	0.488	0.477	0.449	0.442	0.484	0.541
K_2O	0.017	0.014	0.016	0.024	0.032	0.025	0.013	0.035	0.02	0.01
Total	99.46	98.99	99.49	98.68	99.05	98.77	98.43	98.62	98.83	98.17
					Oxygen = 6.000					
Si	1.782	1.778	1.785	1.784	1.774	1.77	1.772	1.761	1.665	1.654
Al	0.239	0.237	0.235	0.239	0.235	0.23	0.226	0.233	0.356	0.373
Ti	0.061	0.06	0.057	0.057	0.059	0.059	0.059	0.061	0.095	0.097
Fe*	0.212	0.211	0.212	0.213	0.211	0.211	0.214	0.214	0.237	0.233
Cr	0	0	0	0	0	0	0	0	0	0
Mg	0.788	0.792	0.794	0.794	0.79	0.791	0.79	0.789	0.709	0.696
Mn	0.006	0.004	0.004	0.004	0.004	0.005	0.004	0.004	0.003	0.003
Ca	0.876	0.884	0.877	0.874	0.89	0.897	0.902	0.898	0.898	0.903
Na	0.036	0.032	0.034	0.033	0.035	0.035	0.033	0.032	0.035	0.04
K	0.001	0.001	0.001	0.001	0.002	0.001	0.001	0.002	0.001	0
WO	47	47	46	46	47	47	47	47	49	49
EN	42	42	42	42	42	41	41	42	38	38
FS	12	11	12	12	11	11	11	11	13	13

Table A.3: Con't

	LTO18-035	LTO18-036	LTO18-037	LTO18-039	LTO18-040	LTO18-041	LTO18-042	LTO18-043	LTO18-044	LTO18-045
SiO_2	44.233	44.136	43.912	44.011	44.267	45.495	45.209	44.958	45.185	44.926
TiO_2	3.424	3.424	3.515	3.443	3.431	2.991	3.312	3.191	3.053	3.172
Al_2O_3	8.588	8.622	8.634	8.351	8.396	7.144	7.779	7.519	7.621	7.55
FeO	7.54	7.501	7.512	7.361	7.391	7.504	8.014	8.14	8.011	7.985
Cr_2O_3	0.022	0	0.008	0.025	0	0	0	0	0	0.002
MnO	0.131	0.136	0.107	0.119	0.141	0.163	0.188	0.161	0.133	0.164
MgO	12.416	12.459	12.366	12.373	12.31	12.895	12.452	12.305	12.402	12.357
CaO	22.256	22.333	22.292	22.264	22.407	22.18	22.13	22.217	22.212	22.194
Na_2O	0.503	0.512	0.529	0.525	0.529	0.574	0.594	0.683	0.606	0.641
K_2O	0.027	0.005	0.009	0.011	0.007	0.018	0.005	0.017	0.017	0
Total	99.14	99.13	98.88	98.48	98.88	98.96	99.68	99.19	99.24	98.99
					Oxygen = 6.000					
Si	1.658	1.654	1.65	1.66	1.664	1.706	1.688	1.686	1.693	1.688
Al	0.379	0.38	0.382	0.371	0.371	0.315	0.342	0.332	0.336	0.334
Ti	0.097	0.097	0.099	0.098	0.097	0.084	0.093	0.09	0.086	0.09
Fe*	0.236	0.235	0.236	0.232	0.212	0.235	0.25	0.256	0.251	0.251
Cr	0.001	0	0	0.001	0	0	0	0	0	0
Mg	0.694	0.696	0.693	0.696	0.69	0.721	0.693	0.688	0.693	0.692
Mn	0.004	0.004	0.003	0.004	0.004	0.005	0.006	0.005	0.004	0.005
Ca	0.894	0.897	0.897	0.9	0.902	0.891	0.885	0.893	0.892	0.893
Na	0.037	0.037	0.039	0.038	0.039	0.042	0.043	0.05	0.044	0.047
K	0.001	0	0	0.001	0	0.001	0	0.001	0.001	0
WO	49	49	49	49	49	48	48	48	48	49
EN	38	38	38	38	38	39	38	37	38	38
FS	13	13	13	13	13	13	14	14	14	14

Table A.3: Con't

	LT018-046	LT020-002	LT020-003	LT020-005	LT020-006	LT020-007	LT020-008	LT020-009	LT020-010	LT020-011
SiO_2	43.487	48.656	48.565	50.854	50.859	50.789	51.443	51.392	51.074	51.229
TiO_2	3.567	1.655	1.722	1.134	0.944	0.913	0.967	0.855	0.891	0.921
Al_2O_3	8.472	3.982	4.182	2.599	2.138	2.156	2.121	2.133	2.183	2.119
FeO	7.782	8.114	8.198	8.183	8.34	8.299	8.242	8.27	8.217	8.386
Cr_2O_3	0	0	0	0.001	0.065	0.016	0.009	0	0	0.026
MnO	0.138	0.433	0.388	0.567	0.604	0.663	0.61	0.674	0.601	0.643
MgO	12.1	13.039	13.132	13.3	13.503	13.424	13.306	13.275	13.286	13.299
CaO	22.092	21.897	21.94	22.224	22.214	22.232	22.266	22.429	22.235	22.328
Na_2O	0.598	0.928	0.921	1.082	1.089	1.104	1.1	1.033	1.072	1.106
K_2O	0.034	0.019	0.019	0.026	0.02	0.01	0.012	0.017	0.022	0.009
Total	98.27	98.72	99.07	99.97	99.78	99.61	100.08	100.08	99.58	100.07
					Oxygen = 6.000					
Si	1.646	1.828	1.818	1.886	1.889	1.89	1.907	1.906	1.902	1.899
Al	0.378	0.176	0.184	0.114	0.094	0.094	0.093	0.093	0.096	0.093
Ti	0.102	0.047	0.048	0.032	0.026	0.026	0.027	0.024	0.025	0.026
Fe*	0.246	0.255	0.256	0.255	0.259	0.259	0.256	0.257	0.257	0.259
Cr	0	0	0	0	0.002	0	0	0	0	0.001
Mg	0.683	0.73	0.733	0.735	0.748	0.745	0.735	0.734	0.737	0.735
Mn	0.004	0.014	0.012	0.018	0.019	0.021	0.019	0.021	0.019	0.02
Ca	0.896	0.881	0.88	0.883	0.884	0.886	0.884	0.891	0.887	0.887
Na	0.044	0.068	0.067	0.078	0.078	0.08	0.079	0.074	0.077	0.08
K	0.002	0.001	0.001	0.001	0.001	0	0.001	0.001	0.001	0
WO	49	47	47	47	46	46	47	47	47	47
EN	37	39	39	39	39	39	39	39	39	39
FS	14	14	14	14	15	15	14	15	14	15

Table A.3: Con't

	LT020-012	LT020-013	LT020-014	LT020-015	LT020-016	LT020-017	LT020-018	LT020-019	LT020-020	LT020-021
SiO_2	50.703	50.51	50.682	50.394	50.558	50.399	50.823	51.029	50.547	50.587
TiO_2	0.92	0.906	0.897	0.854	0.934	0.898	0.942	0.941	0.927	0.937
Al_2O_3	2.172	2.147	2.126	2.123	2.084	2.061	2.111	2.192	2.199	2.221
FeO	8.168	8.443	8.219	8.325	8.173	8.144	8.139	8.198	8.211	8.251
Cr_2O_3	0	0	0	0	0	0	0.001	0	0.016	0
MnO	0.65	0.6	0.625	0.579	0.577	0.59	0.586	0.604	0.58	0.613
MgO	13.332	13.257	13.342	13.383	13.388	13.423	13.535	13.348	13.335	13.375
CaO	22.201	22.239	22.244	22.007	22.44	22.531	22.282	22.301	22.381	22.325
Na_2O	1.1	1.051	1.09	1.015	1.051	1.029	0.943	1.056	1.045	1.1
K_2O	0.018	0.019	0.028	0.016	0.022	0.001	0.028	0.011	0.013	0.016
Total	99.26	99.17	99.25	98.7	99.23	99.08	99.39	99.68	99.25	99.43
					Oxygen = 6.000					
Si	1.893	1.889	1.892	1.893	1.888	1.885	1.896	1.898	1.888	1.885
Al	0.095	0.095	0.093	0.094	0.092	0.091	0.093	0.096	0.097	0.097
Ti	0.026	0.025	0.025	0.024	0.026	0.025	0.026	0.026	0.026	0.026
Fe*	0.255	0.265	0.256	0.262	0.255	0.254	0.254	0.256	0.257	0.256
Cr	0	0	0	0	0	0	0	0	0	0
Mg	0.742	0.739	0.743	0.749	0.745	0.748	0.753	0.74	0.742	0.743
Mn	0.021	0.019	0.02	0.018	0.018	0.019	0.019	0.019	0.018	0.019
Ca	0.888	0.891	0.89	0.886	0.898	0.903	0.89	0.889	0.896	0.891
Na	0.08	0.076	0.079	0.074	0.076	0.075	0.068	0.076	0.076	0.079
K	0.001	0.001	0.001	0.001	0.001	0	0.001	0.001	0.001	0.001
WO	47	47	47	46	47	47	46	47	47	47
EN	39	39	39	39	39	39	39	39	39	39
FS	14	15	14	15	14	14	14	14	14	14

Table A.3: Con't

	LT020-022	LT020-023	LT020-024	LT020-025	LT020-028	LT020-030	LT020-031	LT020-032	LT020-033	LT020-034
SiO_2	50.583	50.629	50.37	50.816	50.832	50.716	51.118	50.89	50.79	50.542
TiO_2	0.978	1.002	0.928	1.057	0.967	0.979	0.934	0.942	0.923	0.897
Al_2O_3	2.223	2.195	2.217	2.245	2.281	2.212	2.165	2.117	2.175	2.044
FeO	8.363	8.311	8.129	8.329	8.402	8.248	8.203	8.076	8.244	8.353
Cr_2O_3	0	0	0.008	0	0	0	0	0	0	0
MnO	0.568	0.622	0.587	0.609	0.622	0.598	0.584	0.662	0.623	0.589
MgO	13.221	13.25	13.077	13.32	13.339	13.306	13.414	13.536	13.414	13.331
CaO	22.176	22.054	22.033	22.336	22.271	22.227	22.294	22.505	22.441	22.4
Na_2O	1.136	1.063	1.034	1.087	1.068	1.042	1.028	1.018	1.053	1.013
K_2O	0.015	0.014	0.001	0.008	0.027	0.014	0.007	0.016	0.018	0.016
Total	99.26	99.14	98.38	99.81	99.81	99.31	99.75	99.76	99.68	99.19
					Oxygen = 6.000					
Si	1.889	1.894	1.899	1.888	1.889	1.893	1.9	1.89	1.889	1.89
Al	0.098	0.097	0.098	0.098	0.1	0.097	0.095	0.093	0.095	0.09
Ti	0.027	0.028	0.026	0.03	0.027	0.027	0.026	0.026	0.026	0.025
Fe*	0.262	0.26	0.256	0.259	0.261	0.257	0.255	0.25	0.256	0.261
Cr	0	0	0	0	0	0	0	0	0	0
Mg	0.736	0.739	0.735	0.738	0.739	0.74	0.743	0.75	0.744	0.743
Mn	0.018	0.02	0.019	0.019	0.02	0.019	0.018	0.021	0.02	0.019
Ca	0.887	0.884	0.89	0.889	0.887	0.889	0.888	0.896	0.894	0.897
Na	0.082	0.077	0.076	0.078	0.077	0.075	0.074	0.073	0.076	0.073
K	0.001	0.001	0	0	0.001	0.001	0	0.001	0.001	0.001
WO	47	46	47	47	47	47	47	47	47	47
EN	39	39	39	39	39	39	39	39	39	39
FS	15	15	14	15	15	15	14	14	14	15

Table A.3: Con't

	LT020-035	LT020-036	LT020-037	LT020-038	LT049-001	LT049-002	LT049-003	LT049-004	LT049-005	LT049-006
SiO_2	50.688	50.898	50.662	51.171	44.743	44.806	45.127	44.956	44.953	45.178
TiO_2	0.91	0.87	0.964	0.997	3.579	3.568	3.504	3.414	3.381	3.377
Al_2O_3	2.093	2.17	2.155	2.186	8.449	8.51	8.427	8.289	8.192	8.232
FeO	8.344	8.178	8.24	8.358	7.322	7.339	7.144	7.286	7.163	7.235
Cr_2O_3	0	0	0.003	0						0.026
MnO	0.625	0.585	0.59	0.63	0.144	0.139	0.175	0.122	0.13	0.13
MgO	13.413	13.449	13.332	13.254	12.599	12.555	12.562	12.617	12.769	12.777
CaO	22.132	22.278	22.249	22.166	23.208	23.179	23.159	23.311	23.568	23.405
Na_2O	1.084	1.04	1.027	1.097	0.519	0.509	0.58	0.525	0.55	0.579
K_2O	0.013	0	0.018	0.028	0.027	0.022	0.016	0.011	0.013	0.004
Total	99.3	99.47	99.24	99.89	100.59	100.627	100.694	100.531	100.719	100.943
					Oxygen = 6.000					
Si	1.892	1.896	1.893	1.901	1.652	1.654	1.664	1.66	1.656	1.66
Al	0.092	0.095	0.095	0.096	0.368	0.37	0.366	0.361	0.355	0.357
Ti	0.026	0.024	0.027	0.028	0.099	0.099	0.097	0.095	0.094	0.093
Fe*	0.26	0.255	0.258	0.261	0.227	0.226	0.22	0.226	0.22	0.222
Cr	0	0	0	0	0	0	0	0	0	0.001
Mg	0.746	0.747	0.743	0.734	0.694	0.691	0.69	0.695	0.701	0.7
Mn	0.02	0.018	0.019	0.02	0.005	0.004	0.005	0.004	0.004	0.004
Ca	0.885	0.889	0.891	0.882	0.918	0.917	0.915	0.922	0.93	0.922
Na	0.078	0.075	0.074	0.079	0.037	0.036	0.041	0.038	0.039	0.041
K	0.001	0	0.001	0.001	0.001	0.001	0.001	0.001	0.001	0
WO	46	47	47	47	50	50	50	50	50	50
EN	39	39	39	39	38	38	38	38	38	38
FS	15	14	14	15	13	13	12	12	12	12

Table A.3: Con't

	LT049-007	LT049-008	LT049-009	LT049-010	LT049-011	LT049-012	LT049-013	LT049-014	LT049-015	LT049-016
SiO_2	44.903	45.037	45.372	45.624	46.203	46.763	46.781	45.898	45.53	45.141
TiO_2	3.434	3.328	3.251	3.238	2.914	2.722	2.789	3.08	3.233	3.258
Al_2O_3	8.223	8.193	7.742	7.47	7.041	6.639	6.775	7.423	7.829	7.834
FeO	7.25	7.107	7.027	7.04	6.899	6.826	6.866	6.908	7.07	6.985
Cr_2O_3		0.023	0.018	0.004			0.003		0.021	0.012
MnO	0.142	0.103	0.148	0.16	0.129	0.132	0.134	0.181	0.155	0.141
MgO	12.719	12.749	12.921	13.165	13.407	13.555	13.638	13.339	12.987	12.985
CaO	23.328	23.242	23.171	23.478	23.405	23.114	23.197	23.157	23.218	23.294
Na_2O	0.51	0.5	0.541	0.59	0.501	0.448	0.543	0.499	0.497	0.515
K_2O	0.018	0.016	0.001	0.02	0.017	0.02	0.027	0.002	0.012	0.021
Total	100.527	100.298	100.192	100.789	100.516	100.219	100.753	100.487	100.552	100.186
					Oxygen = 6.000					
Si	1.658	1.666	1.679	1.677	1.701	1.727	1.717	1.691	1.679	1.67
Al	0.358	0.357	0.337	0.323	0.306	0.289	0.293	0.322	0.34	0.341
Ti	0.095	0.093	0.09	0.09	0.081	0.076	0.077	0.085	0.09	0.091
Fe*	0.224	0.22	0.218	0.217	0.212	0.21	0.211	0.212	0.219	0.216
Cr	0	0.001	0.001	0	0	0	0	0	0.001	0
Mg	0.7	0.703	0.713	0.721	0.736	0.746	0.746	0.733	0.714	0.716
Mn	0.004	0.003	0.005	0.005	0.004	0.004	0.004	0.006	0.005	0.004
Ca	0.923	0.921	0.919	0.925	0.923	0.915	0.912	0.914	0.917	0.923
Na	0.037	0.036	0.039	0.042	0.036	0.032	0.039	0.036	0.036	0.037
K	0.001	0.001	0	0.001	0.001	0.001	0.001	0	0.001	0.001
WO	50	50	50	50	49	49	49	49	49	50
EN	38	38	38	39	39	40	40	39	39	39
FS	12	12	12	12	12	11	11	12	12	12

Table A.3: Con't

	LT049-017	LT049-020	LT049-021	LT049-022	LT049-023	LT049-024	LT049-026	LT049-027	LT049-028	LT049-029
SiO_2	45.082	44.22	45.165	45.789	45.54	45.533	45.214	45.604	45.548	45.245
TiO_2	3.341	3.235	3.308	3.11	3.1	3.161	3.138	3.199	3.176	3.228
Al_2O_3	7.999	7.717	8.103	7.754	7.516	7.737	7.549	7.776	7.873	7.858
FeO	7.039	7.296	7.44	7.286	7.319	7.326	7.338	7.435	7.525	7.485
Cr_2O_3		0.015		0.011			0.017		0.002	0.004
MnO	0.157	0.158	0.12	0.158	0.148	0.14	0.133	0.144	0.172	0.142
MgO	12.925	12.582	12.789	12.813	13	12.774	12.652	12.818	12.736	12.848
CaO	23.267	23.036	23.222	23.342	23.285	23.485	22.982	23.389	23.095	23.363
Na_2O	0.566	0.504	0.542	0.594	0.502	0.536	0.579	0.567	0.559	0.602
K_2O	0.017	0.036	0.023	0.016	0.01	0.008	0.007	0.019	0.002	0.031
Total	100.393	98.799	100.712	100.873	100.42	100.7	99.609	100.951	100.688	100.806
					Oxygen = 6.000					
Si	1.664	1.662	1.664	1.684	1.682	1.678	1.685	1.677	1.68	1.665
Al	0.348	0.341	0.352	0.336	0.327	0.336	0.331	0.336	0.342	0.34
Ti	0.093	0.091	0.092	0.086	0.086	0.088	0.088	0.088	0.088	0.089
Fe*	0.216	0.229	0.23	0.223	0.226	0.225	0.229	0.228	0.232	0.23
Cr	0	0	0	0	0	0	0.001	0	0	0
Mg	0.711	0.705	0.703	0.702	0.716	0.702	0.703	0.703	0.7	0.705
Mn	0.005	0.005	0.004	0.005	0.005	0.004	0.004	0.004	0.005	0.004
Ca	0.92	0.927	0.917	0.92	0.922	0.927	0.918	0.921	0.913	0.921
Na	0.041	0.037	0.039	0.042	0.036	0.038	0.042	0.04	0.04	0.043
K	0.001	0.002	0.001	0.001	0	0	0	0.001	0	0.001
WO	50	50	49	50	49	50	50	50	49	50
EN	38	38	38	38	38	38	38	38	38	38
FS	12	13	13	12	12	12	13	13	13	13

Table A.3: Con't

	LT049-030	LT049-032	LT049-033	LT049-034	LT049-037	LT049-038	LT049-039	LT049-043	LT050-001	LT050-002
SiO_2	44.892	45.049	44.926	45.033	44.706	45.052	44.871	45.452	49.409	49.8
TiO_2	3.386	3.445	3.491	3.467	3.279	3.334	3.166	3.158	1.375	1.285
Al_2O_3	8.064	8.118	8.359	8.165	7.891	7.976	7.778	8.306	3.337	3.042
FeO	7.39	7.452	7.516	7.322	7.281	7.427	7.242	7.427	9.613	10.11
Cr_2O_3	0.024			0.024		0.009	0.014			0.006
MnO	0.127	0.142	0.105	0.142	0.126	0.115	0.15	0.131	0.591	0.645
MgO	12.696	12.518	12.608	12.587	12.666	12.599	11.909	12.929	12.993	12.761
CaO	23.189	23.175	23.189	23.232	23.193	22.812	22.855	22.967	22.559	22.325
Na_2O	0.494	0.536	0.53	0.52	0.542	0.58	0.505	0.521	0.862	0.926
K_2O	0.012	0.012	0.011	0.006	0.014	0.024	0.01	0.014	0.028	0.016
Total	100.274	100.447	100.735	100.498	99.698	99.928	98.5	100.905	100.767	100.916
					Oxygen = 6.000					
Si	1.663	1.667	1.657	1.665	1.664	1.674	1.696	1.67	1.827	1.842
Al	0.352	0.354	0.363	0.355	0.316	0.349	0.346	0.36	0.145	0.133
Ti	0.094	0.096	0.097	0.096	0.092	0.093	0.09	0.087	0.038	0.036
Fe*	0.229	0.231	0.232	0.227	0.226	0.23	0.228	0.229	0.296	0.314
Cr	0.001	0	0	0.001	0	0	0	0	0	0
Mg	0.701	0.691	0.693	0.694	0.703	0.698	0.671	0.708	0.716	0.704
Mn	0.004	0.004	0.003	0.004	0.004	0.004	0.005	0.004	0.019	0.02
Ca	0.92	0.919	0.916	0.92	0.925	0.908	0.925	0.904	0.894	0.885
Na	0.035	0.038	0.038	0.037	0.039	0.042	0.037	0.037	0.062	0.066
K	0.001	0.001	0.001	0	0.001	0.001	0	0.001	0.001	0.001
WO	50	50	50	50	50	49	51	49	46	46
EN	38	37	38	38	38	38	37	38	37	37
FS	13	13	13	13	12	13	13	13	16	17

Table A.3: Con't

	LT050-003	LT050-004	LT050-008	LT050-010	LT050-011	LT050-012	LT050-013	LT050-014	LT050-015	LT050-017
SiO_2	47.355	50.305	49.17	50.525	49.926	50.196	50.484	50.587	50.595	50.396
TiO_2	1.767	0.778	0.948	0.743	0.991	1.171	1.133	1.208	1.311	1.35
Al_2O_3	4.222	1.837	1.841	1.899	2.515	2.793	2.616	2.592	3.158	3.113
FeO	10.105	12.884	13.271	12.781	11.372	11.276	9.592	9.095	8.328	8.034
Cr_2O_3					0.014		0.021	0.042		
MnO	0.593	1.02	1.175	1.165	1.021	1.029	0.795	0.743	0.62	0.541
MgO	11.814	10.788	9.727	10.751	11.063	11.188	12.239	12.74	13.031	13.573
CaO	22.464	21.606	21.684	21.747	22.003	21.908	22.682	22.75	22.595	22.759
Na_2O	0.821	1.198	1.218	1.283	1.416	1.39	1.231	1.194	1.075	1.034
K_2O	0.025	0.026	0.032	0.02	0.011	0.017	0.016	0.023	0.008	0.016
Total	99.166	100.442	99.066	100.914	100.332	100.968	100.809	100.974	100.721	100.816
					oxygen = 6.000					
Si	1.788	1.893	1.886	1.892	1.869	1.867	1.868	1.864	1.865	1.851
Al	0.188	0.081	0.083	0.084	0.111	0.122	0.114	0.113	0.137	0.135
Ti	0.05	0.022	0.027	0.021	0.028	0.033	0.032	0.033	0.036	0.037
Fe*	0.32	0.406	0.426	0.4	0.356	0.351	0.297	0.28	0.256	0.246
Cr	0	0	0	0	0	0	0.001	0.001	0	0
Mg	0.665	0.605	0.556	0.6	0.617	0.62	0.675	0.7	0.716	0.743
Mn	0.019	0.033	0.038	0.037	0.032	0.032	0.025	0.023	0.019	0.017
Ca	0.909	0.871	0.891	0.872	0.883	0.873	0.899	0.898	0.892	0.896
Na	0.06	0.087	0.091	0.093	0.103	0.1	0.088	0.085	0.077	0.074
K	0.001	0.001	0.002	0.001	0.001	0.001	0.001	0.001	0	0.001
WO	48	46	47	46	47	47	47	47	47	47
EN	35	32	29	31	33	33	36	37	38	39
FS	18	23	24	23	21	20	17	16	15	14

Table A.3: Con't

	LT050-018	LT050-019	LT050-020	LT050-021	LT050-023	LT050-024
SiO_2	49.595	46.601	46.158	45.711	45.112	45.839
TiO_2	1.56	2.88	2.944	3.097	3.245	3.161
Al_2O_3	3.741	6.519	6.863	7.348	7.633	7.358
FeO	8.035	8.072	8.115	8.05	7.75	7.581
Cr_2O_3	0.039	0.028	0.014	0.009	0.002	
MnO	0.463	0.266	0.253	0.246	0.206	0.203
MgO	13.678	12.753	12.768	12.613	12.657	12.918
CaO	22.805	22.831	22.838	22.731	22.786	23.006
Na_2O	0.89	0.737	0.831	0.737	0.644	0.664
K_2O	0.021	0.029	0.033	0.024	0.03	0.023
Total	100.827	100.716	100.817	100.566	100.065	100.753
			Oxygen = 6.000			
Si	1.822	1.72	1.7	1.689	1.674	1.688
Al	0.162	0.283	0.298	0.32	0.334	0.319
Ti	0.043	0.08	0.082	0.086	0.091	0.088
Fe*	0.247	0.249	0.25	0.249	0.241	0.233
Cr	0.001	0.001	0	0	0	0
Mg	0.749	0.702	0.701	0.695	0.7	0.709
Mn	0.014	0.008	0.008	0.008	0.006	0.006
Ca	0.898	0.903	0.901	0.9	0.906	0.908
Na	0.063	0.053	0.059	0.053	0.016	0.047
K	0.001	0.001	0.002	0.001	0.001	0.001
WO	47	48	48	49	49	49
EN	39	38	38	38	38	38
FS	14	14	14	14	13	13

Table A.4: All EMP analysis for amphibole from Diego Hernandez Formation.

	AM001-001	AM001-002	AM001-003	AM001-004	AM001-005	AM001-006	AM001-007	AM001-008	AM001-009	AM001-010	AM002-001
SiO_2	39.215	39.376	39.147	39.134	39.051	39.557	38.683	39.498	39.336	39.156	40.042
TiO_2	6.437	6.188	6.098	6.029	5.962	5.97	6.146	6.318	5.957	6.009	6.044
Al_2O_3	12.612	12.224	12.495	11.921	12.601	11.755	12.797	12.463	12.068	12.227	11.687
FeO_T	11.649	11.784	12.043	11.766	12.197	12.248	12.002	11.509	11.913	11.857	12.347
Cr_2O_3	0.01	0.004	0.004	0	0	0.005	0	0	0.004	0	0
MnO	0.223	0.225	0.264	0.29	0.209	0.325	0.27	0.242	0.255	0.263	0.297
MgO	12.838	12.809	12.631	12.631	12.581	12.729	12.398	12.734	12.633	12.761	12.862
CaO	11.973	11.765	11.651	11.517	11.766	11.636	11.86	11.804	11.796	11.757	11.821
Na_2O	2.885	2.818	2.874	2.875	2.74	2.827	2.769	2.817	2.818	2.735	2.86
K_2O	1.106	1.118	1.227	1.199	1.185	1.268	1.132	1.102	1.189	1.148	1.225
F	0.048	0.107	0.061	0.059	0.082	0.051	0.091	0.075	0.076	0.107	0.063
Cl	0.014	0.021	0.027	0.022	0.016	0.017	0.017	0.013	0.023	0.023	0.024
Total	99	98.43	98.52	97.44	98.39	98.38	98.16	98.58	98.06	98.04	99.27
					Oxygen = 23.000						
Si	5.923	6.138	6.015	6.058	6.032	6.045	6.014	6.01	6.095	6.14	6.106
Al	2.243	2.244	2.261	2.173	2.292	2.116	2.344	2.245	2.201	2.258	2.099
Cr	0.001	0	0	0	0	0.001	0	0	0	0	0
Ti	0.731	0.726	0.705	0.702	0.693	0.686	0.719	0.727	0.694	0.709	0.693
Mg	2.891	2.976	2.893	2.915	2.897	2.9	2.874	2.903	2.918	2.983	2.924
Fe*	1.471	1.536	1.547	1.523	1.575	1.565	1.561	1.472	1.544	1.555	1.575
Mn	0.029	0.03	0.034	0.038	0.027	0.042	0.036	0.031	0.033	0.035	0.038
Ca	1.937	1.965	1.918	1.91	1.947	1.905	1.976	1.934	1.958	1.975	1.932
Na	0.845	0.852	0.856	0.863	0.821	0.838	0.835	0.835	0.847	0.832	0.846
K	0.213	0.222	0.241	0.237	0.234	0.247	0.225	0.215	0.235	0.23	0.238
Cl	0.004	0.006	0.007	0.006	0.004	0.004	0.004	0.003	0.006	0.006	0.006
F	0.023	0.053	0.03	0.029	0.04	0.025	0.015	0.036	0.037	0.053	0.03

Table A.4: Con't

	AM002-002	AM002-003	AM002-004	AM002-005	AM002-006	AM002-007	AM002-008	AM002-009	AM002-010	AM002-011	AM003-001
SiO_2	40.187	40.071	39.946	39.652	39.598	39.767	39.708	39.921	39.766	39.389	39.765
TiO_2	5.859	5.698	5.801	5.811	5.845	5.874	5.783	5.746	5.632	5.951	6.596
Al_2O_3	11.666	11.586	11.514	11.512	11.595	11.531	11.64	11.634	11.324	11.875	13.143
FeO_T	12.258	12.172	12.112	12.149	12.212	12.321	12.247	12.231	12.149	11.982	10.691
Cr_2O_3	0	0	0	0.013	0.005	0	0	0	0	0	0
MnO	0.355	0.38	0.309	0.342	0.31	0.313	0.293	0.3	0.33	0.287	0.129
MgO	12.825	12.79	12.83	12.692	12.682	12.776	12.82	12.82	12.809	12.842	13.509
CaO	11.608	11.583	11.597	11.715	11.634	11.607	11.598	11.62	11.553	11.719	12.231
Na_2O	2.935	2.852	2.748	2.78	2.913	2.741	2.872	2.957	2.837	2.941	2.681
K_2O	1.264	1.277	1.275	1.204	1.254	1.275	1.247	1.261	1.305	1.21	0.996
F	0.063	0.082	0.112	0.063	0.135	0.142	0.083	0.118	0.127	0.101	0.125
Cl	0.015	0.02	0.016	0.015	0.019	0.028	0.025	0.022	0.02	0.016	0.004
Total	99.04	98.51	98.26	97.93	98.2	98.38	98.32	98.63	97.85	98.31	99.87
						Oxygen = 23.000					
Si	6.117	6.189	6.246	6.107	6.274	6.327	6.166	6.256	6.302	6.136	6.062
Al	2.091	2.107	2.121	2.088	2.163	2.16	2.128	2.147	2.114	2.179	2.36
Cr	0	0	0	0.002	0.001	0	0	0	0	0	0
Ti	0.671	0.662	0.682	0.673	0.697	0.703	0.675	0.677	0.671	0.697	0.756
Mg	2.91	2.945	2.991	2.914	2.995	3.03	2.968	2.995	3.026	2.983	3.07
Fe*	1.561	1.572	1.583	1.565	1.618	1.639	1.591	1.603	1.61	1.561	1.363
Mn	0.046	0.05	0.041	0.045	0.042	0.042	0.039	0.04	0.044	0.038	0.017
Ca	1.893	1.917	1.943	1.933	1.975	1.979	1.93	1.951	1.961	1.956	1.997
Na	0.866	0.854	0.833	0.83	0.895	0.846	0.865	0.898	0.872	0.888	0.792
K	0.245	0.252	0.254	0.237	0.253	0.259	0.247	0.252	0.264	0.24	0.194
Cl	0.004	0.005	0.004	0.004	0.005	0.008	0.007	0.006	0.005	0.004	0.001
F	0.03	0.04	0.055	0.031	0.068	0.071	0.041	0.058	0.064	0.05	0.06

Table A.4: Con't

	AM003-002	AM003-003	AM003-004	AM003-005	AM003-006	AM003-007	AM003-008	AM003-009	AM003-010	AM003-011	AM004-001
SiO_2	39.52	39.718	39.738	39.539	39.627	39.576	39.31	39.574	39.678	39.288	39.51
TiO_2	6.531	6.511	6.564	6.684	6.547	6.589	6.616	6.669	6.653	6.495	6.047
Al_2O_3	13.14	13.159	13.188	13.006	12.901	13.191	13.256	13.034	13.075	13.111	12.363
FeO_T	10.603	10.689	10.543	10.512	10.725	10.568	10.484	10.624	10.617	10.514	13.668
Cr_2O_3	0	0	0.015	0.006	0.005	0.017	0	0.018	0.031	0	0
MnO	0.149	0.159	0.125	0.126	0.11	0.162	0.116	0.168	0.112	0.108	0.31
MgO	13.539	13.529	13.501	13.42	13.379	13.464	13.406	13.489	13.369	13.512	11.893
CaO	12.214	12.275	12.126	12.057	12.147	12.034	12.168	12.105	12.189	12.245	11.657
Na_2O	2.707	2.661	2.697	2.696	2.628	2.523	2.686	2.585	2.665	2.648	2.848
K_2O	1.009	0.973	1.037	0.973	1.059	1.025	0.999	1.004	1.015	0.996	1.182
F	0.069	0.094	0.071	0.069	0.054	0.089	0.042	0.098	0.106	0.056	0.068
Cl	0.016	0.011	0.012	0.016	0.006	0.005	0.012	0.015	0.01	0.008	0.024
Total	99.5	99.78	99.6	99.1	99.18	99.23	99.1	99.37	99.49	98.98	99.57
					Oxygen = 23.000						
Si	5.95	6.006	5.963	5.97	5.928	5.985	5.869	6.025	6.04	5.897	6.053
Al	2.33	2.343	2.331	2.312	2.273	2.349	2.331	2.336	2.344	2.318	2.23
Cr	0	0	0.002	0.001	0.001	0.002	0	0.006	0.004	0	0
Ti	0.74	0.741	0.741	0.759	0.737	0.75	0.743	0.764	0.762	0.733	0.697
Mg	3.039	3.05	3.02	3.021	2.984	3.035	2.984	3.061	3.034	3.024	2.716
Fe*	1.335	1.351	1.323	1.327	1.342	1.336	1.309	1.353	1.351	1.32	1.751
Mn	0.019	0.02	0.016	0.016	0.014	0.021	0.015	0.022	0.014	0.014	0.04
Ca	1.97	1.989	1.95	1.951	1.947	1.95	1.947	1.975	1.988	1.969	1.913
Na	0.79	0.78	0.785	0.789	0.762	0.74	0.778	0.763	0.787	0.771	0.846
K	0.194	0.188	0.199	0.187	0.202	0.198	0.19	0.195	0.197	0.191	0.231
Cl	0.004	0.003	0.003	0.004	0.002	0.001	0.003	0.004	0.003	0.002	0.006
F	0.033	0.045	0.034	0.033	0.026	0.043	0.02	0.047	0.051	0.027	0.033

Table A.4: Con't

	AM004-002	AM004-003	AM004-004	AM005-001	AM005-002	AM005-003	AM005-004	AM005-005	AM005-006	AM005-007	AM005-008
SiO_2	39.365	39.556	39.245	39.299	39.604	39.431	39.668	39.444	39.245	39.228	40.302
TiO_2	5.726	6.06	5.99	6.63	6.64	6.603	6.527	6.502	6.389	6.458	6.045
Al_2O_3	12.509	12.67	12.537	13.385	13.132	13.177	13.18	13.007	13.136	13.057	12.326
FeO_T	13.612	13.398	13.717	10.874	11.004	10.95	10.778	11.916	11.817	12.012	12.001
Cr_2O_3	0	0.006	0	0	0.002	0.01	0	0	0	0.015	0
MnO	0.287	0.268	0.321	0.116	0.131	0.164	0.175	0.199	0.233	0.199	0.278
MgO	12.055	12.137	11.639	13.201	13.218	13.242	13.426	12.606	12.637	12.446	12.926
CaO	11.62	11.57	11.722	12.251	12.047	12.215	12.085	11.89	11.955	11.902	11.645
Na_2O	2.908	2.841	2.716	2.553	2.627	2.705	2.617	2.863	2.798	2.836	2.829
K_2O	1.198	1.135	1.195	1.089	1.023	1.099	1.048	1.072	1.119	1.117	1.185
F	0.043	0.085	0.047	0.05	0.075	0.075	0.112	0.05	0.044	0.069	0.05
Cl	0.024	0.022	0.022	0.01	0.016	0.008	0.011	0.016	0.015	0.008	0.023
Total	99.35	99.74	99.15	99.46	99.52	99.67	99.63	99.57	99.39	99.33	99.61
					Oxygen = 23.000						
Si	5.986	6.069	5.987	5.87	5.979	5.935	6.051	5.929	5.896	5.941	6.066
Al	2.24	2.289	2.253	2.355	2.335	2.335	2.368	2.302	2.324	2.329	2.184
Cr	0	0.001	0	0	0	0.001	0	0	0	0.002	0
Ti	0.655	0.699	0.687	0.745	0.754	0.748	0.749	0.735	0.722	0.736	0.684
Mg	2.733	2.776	2.647	2.94	2.975	2.971	3.053	2.825	2.83	2.81	2.9
Fe*	1.731	1.719	1.75	1.359	1.39	1.378	1.375	1.498	1.484	1.522	1.51
Mn	0.037	0.035	0.041	0.015	0.017	0.021	0.023	0.025	0.03	0.026	0.035
Ca	1.894	1.901	1.916	1.961	1.949	1.97	1.975	1.914	1.924	1.932	1.877
Na	0.857	0.845	0.803	0.739	0.769	0.789	0.774	0.834	0.815	0.833	0.826
K	0.232	0.222	0.233	0.208	0.197	0.211	0.204	0.206	0.214	0.216	0.228
Cl	0.006	0.006	0.006	0.003	0.004	0.002	0.003	0.004	0.004	0.002	0.006
F	0.021	0.041	0.023	0.024	0.036	0.036	0.054	0.024	0.021	0.033	0.024

Table A.4: Con't

	AM005-009	AM006-001	AM006-002	AM006-003	AM006-004	AM006-005	AM006-006	AM006-007	AM006-008	AM006-009	AM006-010
SiO_2	39.373	39.92	39.776	39.979	40.296	40.253	39.788	39.785	39.727	39.942	39.708
TiO_2	6.5	6.432	6.439	6.366	5.987	6.224	6.265	6.465	6.423	6.42	6.132
Al_2O_3	13.015	12.701	12.693	12.738	12.276	12.385	12.781	12.8	12.72	12.716	12.634
FeO_T	11.821	10.858	11.063	10.969	11.924	11.479	10.905	11.032	11.161	10.934	12.176
Cr_2O_3	0.022	0	0	0.017	0	0	0	0	0.009	0	0
MnO	0.229	0.179	0.15	0.173	0.269	0.224	0.157	0.167	0.179	0.163	0.271
MgO	12.505	13.527	13.344	13.359	13.096	13.26	13.258	13.327	13.328	13.374	12.943
CaO	12.014	11.98	11.918	11.997	11.837	11.999	11.95	11.984	12.076	12.049	11.918
Na_2O	2.866	2.783	2.771	2.785	2.63	2.711	2.827	2.706	2.851	2.784	2.764
K_2O	1.084	1.025	1.071	1.052	1.154	1.139	1.032	1.024	1.028	1.02	1.083
F	0.04	0.05	0.048	0.065	0.069	0.075	0.063	0.042	0.102	0.083	0.07
Cl	0.019	0.011	0.014	0.013	0.017	0.014	0.017	0.014	0.017	0.015	0.018
Total	99.47	99.47	99.29	99.5	99.56	99.76	99.04	99.35	99.61	99.5	99.72
					Oxygen = 23.000						
Si	5.909	5.959	5.958	6.007	6.094	6.073	6.011	5.939	6.07	6.048	6.017
Al	2.301	2.233	2.239	2.254	2.187	2.2	2.274	2.25	2.289	2.267	2.254
Cr	0.003	0	0	0.002	0	0	0	0	0.001	0	0
Ti	0.734	0.722	0.726	0.719	0.681	0.706	0.712	0.726	0.738	0.731	0.699
Mg	2.798	3.01	2.98	2.992	2.953	2.982	2.986	2.966	3.036	3.019	2.924
Fe*	1.484	1.355	1.386	1.379	1.508	1.448	1.378	1.377	1.426	1.384	1.543
Mn	0.029	0.023	0.019	0.022	0.034	0.029	0.02	0.021	0.023	0.021	0.035
Ca	1.932	1.916	1.912	1.931	1.918	1.94	1.934	1.917	1.977	1.955	1.935
Na	0.834	0.806	0.805	0.811	0.771	0.793	0.828	0.783	0.845	0.817	0.812
K	0.208	0.195	0.205	0.202	0.223	0.219	0.199	0.195	0.2	0.197	0.209
Cl	0.005	0.003	0.004	0.003	0.004	0.004	0.004	0.004	0.004	0.004	0.005
F	0.019	0.024	0.023	0.031	0.033	0.036	0.03	0.02	0.049	0.04	0.034

Table A.4: Con't

	AM006-011	AM006-012	AM006-013	AM006-014	LT051-001	LT051-002	LT051-003	LT051-004	LT051-005	LT051-006	LT051-007
SiO_2	39.794	39.868	39.707	39.679	39.769	39.605	39.251	39.571	39.841	39.243	29.887
TiO_2	6.11	6.474	6.368	6.134	6.346	6.432	6.43	6.299	6.455	6.494	6.517
Al_2O_3	12.526	12.626	12.797	12.545	12.855	12.769	12.696	12.866	12.919	13.423	10.162
FeO_T	11.784	11.279	11.497	11.924	11.194	11.018	10.954	10.839	10.402	10.782	10.704
Cr_2O_3	0	0.023	0	0.012	0.014	0	0	0	0	0	0.001
MnO	0.219	0.202	0.168	0.255	0.192	0.154	0.142	0.165	0.149	0.16	0.09
MgO	13.029	13.364	13.112	12.935	13.479	13.393	13.153	13.29	13.485	13.392	10.281
CaO	11.768	12.025	11.89	11.792	12.083	12.043	12.025	11.981	12.029	12.26	12.132
Na_2O	2.676	2.714	2.851	2.664	2.741	2.596	2.629	2.561	2.657	2.553	1.887
K_2O	1.206	1.063	1.067	1.093	1.039	1.066	1	1.03	1.016	1.105	1.025
F	0.05	0.102	0.071	0.069	0.086	0.059	0.069	0.059	0.062	0.048	0.046
Cl	0.015	0.017	0.02	0.02	0.014	0.019	0.013	0.015	0.008	0.011	0.011
Total	99.18	99.73	99.55	99.11	99.8	99.15	98.36	98.68	99.02	99.47	82.74
					Oxygen = 23.000						
Si	5.996	6.083	6.012	6.041	6.018	5.977	5.983	5.983	5.978	5.859	5.538
Al	2.223	2.268	2.282	2.249	2.29	2.269	2.279	2.29	2.283	2.36	2.218
Cr	0	0.003	0	0.001	0.002	0	0	0	0	0	0
Ti	0.693	0.743	0.725	0.702	0.722	0.73	0.737	0.716	0.729	0.729	0
Mg	2.927	3.04	2.96	2.936	3.04	3.013	2.989	2.995	3.016	2.981	2.84
Fe*	1.485	1.439	1.456	1.518	1.416	1.391	1.397	1.371	1.305	1.347	1.659
Mn	0.028	0.026	0.022	0.033	0.025	0.02	0.018	0.021	0.019	0.02	0
Ca	1.9	1.966	1.929	1.923	1.959	1.947	1.964	1.941	1.934	1.961	1.922
Na	0.782	0.803	0.837	0.786	0.804	0.76	0.777	0.751	0.773	0.739	0.6
K	0.232	0.207	0.206	0.212	0.201	0.205	0.194	0.199	0.194	0.21	0.242
Cl	0.004	0.004	0.005	0.005	0.004	0.005	0.003	0.004	0.002	0.003	0.003
F	0.024	0.049	0.034	0.033	0.041	0.028	0.033	0.028	0.029	0.023	0.027

Table A.4: Con't

	LT051-008	LT051-009	LT051-010	LT051-011	LT051-012	LT051-013	LT051-014	LT051-015	LT051-016	LT051-017	LT051-018
SiO_2	16.031	39.457	38.953	39.055	38.972	39.477	39.279	38.87	39.501	39.144	39.071
TiO_2	6.138	6.489	6.742	6.512	6.716	6.573	6.681	6.569	6.682	6.57	6.663
Al_2O_3	5.445	13.768	13.504	13.534	13.495	13.678	13.612	13.384	13.693	13.613	13.457
FeO_T	9.285	10.191	10.443	10.274	10.253	10.213	10.309	10.21	10.181	10.279	10.225
Cr_2O_3	0.005	0	0	0.012	0.015	0	0	0	0.034	0	0
MnO	0.135	0.129	0.129	0.109	0.107	0.114	0.122	0.114	0.13	0.09	0.112
MgO	7.094	13.183	13.51	13.361	13.511	13.546	13.405	13.292	13.669	13.584	13.543
CaO	9.222	11.763	12.241	12.24	12.326	12.205	12.253	12.325	12.347	12.111	12.32
Na_2O	1.038	2.621	2.619	2.56	2.5	2.614	2.481	2.417	2.561	2.499	2.538
K_2O	0.755	0.991	1.092	1.036	1.065	1.085	1.098	1.081	1.04	1.102	1.048
F	0.033	0.081	0.054	0.086	0.06	0.069	0.083	0.088	0.06	0.052	0.104
Cl	0.008	0.014	0.015	0.012	0.009	0.007	0.006	0.011	0.012	0.016	0.016
Total	55.18	98.69	99.3	98.78	99.01	99.58	99.33	98.36	99.88	99.06	99.1
					Oxygen = 23.000						
Si	4.702	5.984	5.844	5.944	5.855	5.903	5.922	5.947	5.878	5.87	5.98
Al	1.881	2.459	2.386	2.426	2.387	2.408	2.417	2.412	2.399	2.404	2.426
Cr	0.001	0	0	0.001	0.002	0	0	0	0.004	0	0
Ti	0	0.74	0.761	0.746	0.759	0.739	0.758	0.756	0.748	0.741	0.767
Mg	3.102	2.981	3.021	3.032	3.026	3.019	3.013	3.032	3.032	3.037	3.09
Fe*	2.278	1.292	1.31	1.307	1.288	1.277	1.3	1.307	1.267	1.289	1.309
Mn	0.034	0.017	0.016	0.014	0.014	0.014	0.016	0.015	0.016	0.011	0.015
Ca	2.898	1.911	1.968	1.996	1.984	1.955	1.98	2.02	1.968	1.945	2.021
Na	0.59	0.771	0.762	0.756	0.728	0.758	0.725	0.717	0.739	0.727	0.753
K	0.283	0.192	0.209	0.201	0.204	0.207	0.211	0.211	0.197	0.211	0.205
Cl	0.004	0.004	0.004	0.003	0.002	0.002	0.002	0.003	0.003	0.004	0.004
F	0.031	0.039	0.026	0.041	0.029	0.033	0.04	0.043	0.028	0.025	0.05

Table A.4: Con't

	LT051-019	LT051-020	LT051-021	LT051-022	LT051-023	LT051-024	LT051-025	LT051-026	LT051-027	LT051-028	LT051-029
SiO_2	39.166	38.416	38.426	39.297	38.793	38.259	38.454	38.759	38.415	38.8	37.147
TiO_2	6.664	6.639	6.574	6.603	6.677	6.582	6.564	6.66	6.569	6.676	6.555
Al_2O_3	13.445	13.439	13.458	13.669	13.563	13.436	13.477	13.396	13.517	13.464	12.961
FeO_T	10.28	10.332	10.447	10.38	10.373	10.298	10.396	10.335	10.148	10.291	10.331
Cr_2O_3	0	0	0	0.001	0	0.008	0.011	0	0	0	0
MnO	0.097	0.13	0.127	0.12	0.133	0.118	0.146	0.11	0.09	0.132	0.13
MgO	13.371	13.26	13.434	13.367	13.187	12.939	13.075	12.977	13.178	13.108	12.87
CaO	12.326	12.187	12.355	12.302	12.358	12.144	12.266	12.307	12.226	12.292	12.228
Na_2O	2.51	2.504	2.476	2.474	2.485	2.461	2.432	2.496	2.478	2.577	2.445
K_2O	1.082	1.068	1.089	1.109	1.031	1.098	1.091	1.082	1.09	1.079	1.056
F	0.071	0.04	0.056	0.075	0.065	0.113	0.059	0.111	0.1	0.109	0.046
Cl	0.02	0.01	0.014	0.005	0.005	0.015	0.017	0.013	0.018	0.011	0.012
Total	99.03	98.03	98.46	99.4	98.67	97.46	97.98	98.25	97.83	98.54	95.78
					Oxygen = 23.000						
Si	5.932	5.797	5.825	5.902	5.856	5.987	5.866	6.002	5.959	5.98	5.779
Al	2.398	2.389	2.402	2.418	2.41	2.476	2.421	2.443	2.469	2.444	2.375
Cr	0	0	0	0	0	0.001	0.001	0	0	0	0
Ti	0.759	0.754	0.75	0.746	0.758	0.775	0.753	0.776	0.766	0.774	0.767
Mg	3.019	2.983	3.036	2.993	2.967	3.018	2.973	2.996	3.047	3.012	2.985
Fe*	1.302	1.304	1.324	1.304	1.309	1.348	1.327	1.338	1.316	1.327	1.344
Mn	0.012	0.017	0.016	0.015	0.017	0.016	0.019	0.014	0.012	0.017	0.017
Ca	2	1.971	2.006	1.98	1.999	2.036	2.004	2.042	2.032	2.03	2.039
Na	0.737	0.733	0.728	0.721	0.727	0.747	0.719	0.749	0.745	0.77	0.738
K	0.209	0.206	0.211	0.212	0.199	0.219	0.212	0.214	0.216	0.212	0.21
Cl	0.005	0.003	0.004	0.001	0.001	0.004	0.004	0.003	0.005	0.003	0.003
F	0.034	0.019	0.027	0.036	0.031	0.056	0.028	0.054	0.049	0.053	0.023

Table A.4: Con't

	LT051-033	LT051-034	LT051-035	LT051-036	LT051-037	LT051-038	LT051-039	LT051-040	LT051-041	LT051-042	LT051-043
SiO_2	37.173	38.677	38.926	39.01	38.514	38.979	39.013	39.246	39.253	38.65	38.246
TiO_2	6.602	6.708	6.617	6.607	6.677	6.623	6.702	6.706	6.566	6.579	6.704
Al_2O_3	13.047	13.706	13.595	13.789	13.599	13.675	13.547	13.592	13.53	13.423	13.258
FeO_T	9.831	9.994	10.019	9.97	9.976	9.931	10.085	9.923	9.922	9.84	9.895
Cr_2O_3	0	0	0.014	0	0	0.02	0.014	0	0	0.033	0.016
MnO	0.097	0.1	0.125	0.119	0.125	0.087	0.097	0.12	0.089	0.12	0.115
MgO	12.93	13.328	13.418	13.546	13.113	13.557	13.566	13.572	13.678	13.333	13.422
CaO	11.796	12.305	12.289	12.272	12.331	12.309	12.382	12.353	12.358	12.358	12.306
Na_2O	2.388	2.538	2.471	2.472	2.49	2.411	2.644	2.549	2.511	2.347	2.476
K_2O	1.034	1.055	1.065	1.075	1.062	1.118	1.083	1.099	1.052	1.105	1.052
F	0.086	0.123	0.1	0.108	0.121	0.065	0.096	0.071	0.048	0.091	0.075
Cl	0.01	0.011	0.012	0.012	0.012	0.007	0.008	0.009	0.01	0.007	0.009
Total	94.99	98.54	98.64	98.98	98.02	98.76	99.22	99.24	99.02	97.85	97.56
					Oxygen = 23.000						
Si	5.894	5.984	5.961	5.967	5.992	5.866	5.926	5.896	5.859	5.934	5.869
Al	2.436	2.497	2.451	2.484	2.492	2.423	2.424	2.405	2.378	2.427	2.396
Cr	0	0	0.002	0	0	0.002	0.002	0	0	0.004	0.002
Ti	0.787	0.781	0.762	0.76	0.781	0.75	0.766	0.758	0.737	0.76	0.774
Mg	3.056	3.074	3.063	3.089	3.041	3.041	3.072	3.04	3.043	3.052	3.07
Fe*	1.303	1.293	1.283	1.275	1.298	1.25	1.282	1.247	1.239	1.263	1.27
Mn	0.013	0.013	0.016	0.015	0.016	0.011	0.012	0.015	0.011	0.016	0.015
Ca	2.004	2.039	2.016	2.012	2.056	1.985	2.015	1.988	1.976	2.033	2.023
Na	0.734	0.761	0.734	0.733	0.751	0.703	0.779	0.743	0.727	0.699	0.737
K	0.209	0.208	0.208	0.21	0.211	0.215	0.21	0.211	0.2	0.216	0.206
Cl	0.003	0.003	0.003	0.003	0.003	0.002	0.002	0.002	0.003	0.002	0.002
F	0.043	0.06	0.048	0.052	0.06	0.031	0.046	0.034	0.023	0.044	0.036

Table A.4: Con't

	LT051-014	LT051-015	LT051-016	LT051-017	LT051-018	LT051-019
SiO_2	39.257	39.14	39.34	39.144	39.016	38.297
TiO_2	6.726	6.571	6.559	6.571	6.597	6.534
Al_2O_3	13.639	13.579	13.559	13.583	13.499	13.145
FeO_T	9.985	10.034	10.104	10.046	10.118	10.09
Cr_2O_3	0	0.015	0.012	0.011	0	0.013
MnO	0.109	0.098	0.125	0.102	0.115	0.1
MgO	13.46	13.725	13.526	13.595	13.425	13.333
CaO	12.219	12.307	12.373	12.379	12.393	12.316
Na_2O	2.457	2.451	2.576	2.465	2.391	2.428
K_2O	1.067	1.063	1.07	1.025	1.024	1.086
F	0.048	0.058	0.042	0.071	0.077	0.083
Cl	0.01	0.01	0.005	0.011	0.01	0.018
Total	98.98	99.04	99.28	98.99	98.67	97.43
			Oxygen = 23.000			
Si	5.859	5.865	5.837	5.9	5.916	5.93
Al	2.398	2.397	2.369	2.412	2.411	2.396
Cr	0	0.002	0.001	0.001	0	0.002
Ti	0.755	0.741	0.732	0.745	0.752	0.761
Mg	2.995	3.066	2.992	3.055	3.035	3.077
Fe*	1.246	1.258	1.253	1.267	1.283	1.307
Mn	0.014	0.012	0.016	0.013	0.015	0.013
Ca	1.954	1.976	1.967	1.999	2.013	2.043
Na	0.711	0.712	0.741	0.72	0.703	0.729
K	0.203	0.203	0.203	0.197	0.198	0.215
Cl	0.003	0.003	0.001	0.003	0.003	0.005
F	0.023	0.027	0.02	0.034	0.037	0.041

Table A.5: All Biotite EMP analyses from DH Wall.

	BT001-001	BT001-002	BT001-003 rim	BT001-004	BT001-005	BT001-006	BT001-007	BT001-008 core	BT001-009 rim	BT002-001 rim
SiO_2	36.012	35.947	36.313	35.8	35.866	36.181	36.008	36.023	35.943	37.15
TiO_2	8.184	8.161	8.006	8.032	8.127	7.948	8.099	8.047	8.053	4.896
Al_2O_3	14.383	14.261	14.181	14.173	14.348	14.225	14.249	14.281	14.564	13.292
Cr_2O_3	0.011	0	0	0	0	0.006	0	0.004	0	0
FeO_T	13.891	13.666	13.503	13.613	13.424	13.399	13.66	13.607	13.383	17.505
MnO	0.274	0.233	0.245	0.255	0.26	0.262	0.25	0.285	0.271	0.759
MgO	14.73	14.594	14.902	14.649	14.581	14.849	14.588	14.692	14.383	14.005
CaO	0.018	0	0	0	0.007	0.023	0.023	0.006	0.027	0.005
Na_2O	0.961	0.985	1.021	1.034	0.985	0.951	0.966	1.013	1.086	0.808
K_2O	8.708	8.852	9.013	8.787	8.714	8.943	8.885	8.945	8.686	9.648
F	0.211	0.191	0.158	0.147	0.149	0.188	0.158	0.131	0.217	0.272
Cl	0.024	0.023	0.021	0.02	0.023	0.027	0.023	0.022	0.02	0.019
Total	97.41	96.91	97.36	96.51	96.48	97	96.91	97.06	96.63	98.36
					Oxygen = 22.000					
Si	5.278	5.294	5.319	5.293	5.294	5.317	5.302	5.297	5.298	5.512
Al	2.483	2.474	2.446	2.468	2.494	2.462	2.471	2.473	2.528	2.323
Ti	0.902	0.904	0.882	0.893	0.902	0.879	0.897	0.89	0.893	0.546
Fe*	1.703	1.683	1.654	1.683	1.657	1.647	1.682	1.673	1.65	2.172
Cr	0.001	0	0	0	0	0.001	0	0	0	0
Mn	0.034	0.029	0.03	0.032	0.033	0.033	0.031	0.035	0.034	0.095
Mg	3.219	3.204	3.254	3.229	3.209	3.253	3.202	3.22	3.161	3.098
Ca	0.003	0	0	0	0.001	0.004	0.004	0.001	0.004	0.001
Na	0.273	0.281	0.29	0.296	0.282	0.271	0.276	0.289	0.31	0.232
K	1.628	1.663	1.684	1.657	1.641	1.677	1.669	1.678	1.634	1.826
F	0.196	0.178	0.146	0.137	0.139	0.175	0.147	0.122	0.202	0.255
Cl	0.012	0.011	0.01	0.01	0.012	0.013	0.011	0.011	0.01	0.01

Table A.5: Con't

	BT002-002	BT002-003	BT002-004	BT002-005	BT003-001 rim	BT003-002	BT003-003	BT003-004	BT003-005 rim
SiO_2	35.903	36.095	36.95	36.297	36.803	36.983	37.269	37.207	36.902
TiO_2	5.133	5.627	4.263	4.756	7.569	7.091	7.13	7.536	7.143
Al_2O_3	13.585	13.618	13.211	13.525	13.996	13.751	13.852	13.739	13.924
Cr_2O_3	0	0	0	0	0	0.002	0	0	0.025
FeO_T	19.31	18.289	17.451	18.097	14.09	13.884	14.125	14.195	14.027
MnO	0.749	0.751	0.744	0.714	0.324	0.316	0.328	0.321	0.325
MgO	13.243	13.071	14.4	13.684	15.129	15.293	15.239	15.141	15.209
CaO	0	0	0	0.001	0.025	0.003	0.026	0.015	0.017
Na_2O	0.815	0.776	0.809	0.82	1.012	0.977	0.92	0.903	0.939
K_2O	9.412	9.569	9.717	9.548	9.454	9.398	9.627	9.382	9.59
F	0.246	0.259	0.302	0.324	0.229	0.212	0.208	0.181	0.187
Cl	0.022	0.015	0.012	0.022	0.02	0.024	0.024	0.022	0.018
Total	98.42	98.07	97.86	97.79	98.65	97.93	98.75	98.64	98.31
					Oxygen = 22.000				
Si	5.378	5.402	5.517	5.444	5.348	5.404	5.407	5.398	5.379
Al	2.396	2.4	2.323	2.389	2.395	2.366	2.367	2.347	2.39
Ti	0.578	0.633	0.479	0.537	0.827	0.779	0.778	0.822	0.783
Fe*	2.419	2.289	2.179	2.27	1.712	1.696	1.714	1.722	1.71
Cr	0	0	0	0	0	0	0	0	0.003
Mn	0.095	0.095	0.094	0.091	0.04	0.039	0.04	0.039	0.04
Mg	2.957	2.916	3.205	3.059	3.277	3.331	3.296	3.275	3.305
Ca	0	0	0	0	0.004	0	0.004	0.002	0.003
Na	0.237	0.225	0.234	0.238	0.285	0.277	0.259	0.254	0.265
K	1.799	1.827	1.851	1.827	1.753	1.752	1.782	1.737	1.783
F	0.233	0.245	0.285	0.307	0.21	0.196	0.191	0.166	0.172
Cl	0.011	0.008	0.006	0.011	0.01	0.012	0.012	0.011	0.009

Table A.6: All EMP analyses of Nepheline.

	LT012-001	LT012-002	LT012-004	LT012-007	LT012-010	LT012-012	LT012-018
SiO_2	45.741	46.108	46.673	45.731	45.582	46.787	48.744
Al_2O_3	32.383	31.713	32.439	31.864	31.681	32.555	29.244
FeO_T	0.548	0.547	0.547	0.566	0.645	0.632	1.115
MgO	0.004	0	0.01	0.013	0.005	0.018	0.033
CaO	0.769	0.756	0.755	0.743	0.77	0.729	1.366
Na_2O	16.499	16.611	16.901	16.522	16.215	16.528	16.068
K_2O	3.868	3.781	3.572	3.838	3.808	3.52	3.112
Total	99.81	99.52	100.9	99.28	98.71	100.77	99.68
				oxygen = 32.000			
Si	8.687	8.778	8.752	8.733	8.75	8.769	9.218
Al	7.243	7.111	7.164	7.166	7.162	7.185	6.513
Mg	0.001	0	0.003	0.004	0.001	0.005	0.009
Fe*	0.087	0.087	0.086	0.09	0.104	0.099	0.176
Na	6.076	6.132	6.145	6.118	6.035	6.006	5.892
Ca	0.156	0.154	0.152	0.152	0.158	0.146	0.277
K	0.937	0.918	0.855	0.935	0.933	0.842	0.751

Table A.6: Con't

	LT012-024	LT012-025	LT012-027	LT012-028	LT012-029	LT012-030	LT012-031
SiO_2	45.311	45.535	45.591	45.92	44.966	45.786	45.294
Al_2O_3	32.239	32.246	31.796	32.069	31.792	31.938	32.111
FeO_T	0.647	0.722	0.663	0.654	0.708	0.689	0.635
MgO	0.004	0.011	0.008	0.011	0.005	0.004	0.011
CaO	0.768	0.757	0.781	0.741	0.759	0.706	0.75
Na_2O	16.466	16.33	16.453	16.59	16.39	16.421	16.434
K_2O	3.873	3.93	3.855	3.83	3.879	3.703	3.724
Total	99.31	99.53	99.15	99.82	98.5	99.25	98.96
				oxygen = 32.000			
Si	8.66	8.681	8.725	8.724	8.672	8.738	8.678
Al	7.256	7.239	7.166	7.175	7.221	7.178	7.245
Mg	0.001	0.003	0.002	0.003	0.001	0.001	0.003
Fe*	0.103	0.115	0.106	0.104	0.114	0.11	0.102
Na	6.102	6.036	6.105	6.112	6.129	6.077	6.105
Ca	0.157	0.155	0.16	0.151	0.157	0.144	0.154
K	0.944	0.956	0.941	0.928	0.954	0.902	0.91

Table A.6: Con't

	LT012-032	LT012-033	LT012-034	LT012-035	LT012-036	LT012-038	LT012-039
SiO_2	45.34	45.432	45.42	45.618	45.461	44.919	44.595
Al_2O_3	31.882	31.947	32.225	32.066	32.253	32.034	31.427
FeO_T	0.672	0.664	0.652	0.644	0.703	0.67	0.61
MgO	0.005	0.005	0.002	0	0.001	0.004	0.008
CaO	0.775	0.755	0.787	0.769	0.738	0.741	0.738
Na_2O	16.586	16.407	16.551	16.386	16.314	16.408	16.396
K_2O	3.757	3.818	3.81	3.749	3.926	3.894	3.849
Total	99.02	99.03	99.45	99.23	99.4	98.67	97.62
				oxygen = 32.000			
Si	8.691	8.702	8.667	8.711	8.677	8.647	8.679
Al	7.197	7.206	7.242	7.211	7.25	7.262	7.203
Mg	0.001	0.001	0.001	0	0	0.001	0.002
Fe*	0.108	0.106	0.104	0.103	0.112	0.108	0.099
Na	6.165	6.093	6.124	6.067	6.038	6.124	6.187
Ca	0.159	0.155	0.161	0.157	0.151	0.153	0.154
K	0.919	0.933	0.928	0.913	0.956	0.956	0.956

Table A.6: Con't

	LT012-044	LT012-045	LT012-046	LT012-047	LT012-048	LT012-049	LT012-053
SiO_2	45.953	46.06	45.756	46.089	46.17	46.229	48.238
Al_2O_3	32.1	32.015	32.222	32.062	31.684	31.628	28.805
FeO_T	0.628	0.639	0.627	0.68	0.692	0.703	0.594
MgO	0.018	0.007	0.005	0.003	0	0.006	0
CaO	0.703	0.778	0.793	0.747	0.742	0.708	0.489
Na_2O	16.673	16.574	16.388	16.453	16.562	16.684	19.813
K_2O	3.816	3.774	3.755	3.725	3.665	3.674	1.966
Total	99.89	99.85	99.55	99.76	99.52	99.63	99.91
				oxygen = 32.000			
Si	8.723	8.743	8.707	8.749	8.787	8.792	9.14
Al	7.176	7.157	7.221	7.168	7.102	7.084	6.427
Mg	0.005	0.002	0.001	0.001	0	0.002	0
Fe*	0.1	0.101	0.1	0.108	0.11	0.112	0.094
Na	6.137	6.1	6.047	6.056	6.112	6.153	7.279
Ca	0.143	0.158	0.162	0.152	0.151	0.144	0.099
K	0.924	0.914	0.912	0.902	0.89	0.891	0.475

Table A.6: Con't

	LT012-054	LT012-058	LT012-059	LT012-060	LT012-063	LT012-066	LT012-070
SiO_2	45.653	45.458	45.821	45.98	46.526	46.322	44.87
Al_2O_3	31.982	31.832	31.841	31.723	32.186	31.923	32.316
FeO_T	0.694	0.633	0.623	0.635	0.706	0.708	0.618
MgO	0.009	0.004	0.002	0.005	0.011	0.002	0
CaO	0.746	0.757	0.776	0.758	0.713	0.745	0.768
Na_2O	16.443	16.427	16.392	16.243	16.473	16.523	15.875
K_2O	3.893	3.942	3.806	3.709	3.745	3.961	4.124
Total	99.42	99.05	99.26	99.05	100.36	100.18	98.57
				oxygen = 32.000			
Si	8.713	8.711	8.748	8.783	8.774	8.769	8.637
Al	7.188	7.184	7.159	7.136	7.148	7.117	7.326
Mg	0.003	0.001	0.001	0.001	0.003	0.001	0
Fe*	0.111	0.101	0.099	0.101	0.111	0.112	0.099
Na	6.085	6.104	6.068	6.016	6.023	6.065	5.925
Ca	0.153	0.155	0.159	0.155	0.144	0.151	0.158
K	0.948	0.964	0.927	0.904	0.901	0.957	1.013

Table A.6: Con't

	LT012-071	LT012-074	LT012-075	LT012-080	LT012-081	LT012-082	LT013-001
SiO_2	44.233	45.763	45.853	45.674	45.178	45.887	45.002
Al_2O_3	33.782	31.845	32.387	32.016	31.696	32.276	32.183
FeO_T	0.592	0.526	0.567	0.534	0.583	0.587	0.606
MgO	0.011	0.002	0.021	0.015	0.012	0.014	0.005
CaO	0.797	0.804	0.706	0.786	0.764	0.764	0.808
Na_2O	15.813	16.288	16.315	15.923	15.912	16.125	16.399
K_2O	4.068	4.159	4.144	4.262	4.221	4.254	3.894
Total	99.3	99.39	99.99	99.21	98.37	99.91	98.9
				oxygen = 32.000			
Si	8.451	8.738	8.698	8.73	8.717	8.713	8.64
Al	7.601	7.161	7.235	7.206	7.202	7.218	7.277
Mg	0.003	0.001	0.006	0.004	0.003	0.004	0.001
Fe*	0.095	0.084	0.09	0.085	0.094	0.093	0.097
Na	5.858	6.031	6.001	5.901	5.953	5.937	6.105
Ca	0.163	0.164	0.143	0.161	0.158	0.155	0.166
K	0.992	1.013	1.003	1.039	1.039	1.031	0.954

Table A.6: Con't

	LT013-002	LT013-007	LT013-008	LT013-009	LT013-010	LT013-011	LT013-014
SiO_2	45.132	45.112	45.45	46.225	46.336	45.604	45.763
Al_2O_3	31.915	31.589	31.531	32.575	31.973	31.328	31.993
FeO_T	0.531	0.655	0.644	0.653	0.615	0.692	0.665
MgO	0.011	0	0.003	0.007	0	0.012	0.002
CaO	0.757	0.754	0.72	0.692	0.715	0.746	0.763
Na_2O	16.171	16.008	15.97	16.348	16.518	16.106	16.246
K_2O	4.059	3.878	3.779	3.752	3.789	3.723	3.832
Total	98.58	98	98.1	100.25	99.95	98.21	99.26
				oxygen = 32.000			
Si	8.688	8.726	8.769	8.722	8.778	8.792	8.734
Al	7.235	7.196	7.164	7.239	7.133	7.112	7.191
Mg	0.003	0	0.001	0.002	0	0.003	0.001
Fe*	0.085	0.106	0.104	0.103	0.097	0.112	0.106
Na	6.036	6.004	5.974	5.981	6.067	6.021	6.012
Ca	0.156	0.156	0.149	0.14	0.145	0.154	0.156
K	0.997	0.957	0.93	0.903	0.916	0.916	0.933

Table A.6: Con't

	LT013-015	LT013-016	LT013-017	LT013-018	LT013-019	LT013-020	LT013-022
SiO_2	46.095	45.029	45.856	46.255	45.392	45.938	45.978
Al_2O_3	32.292	31.637	32.23	32.554	31.945	32.227	32.095
FeO_T	0.661	0.665	0.644	0.626	0.654	0.694	0.625
MgO	0	0.001	0.014	0	0.021	0.015	0.007
CaO	0.742	0.792	0.739	0.734	0.808	0.751	0.712
Na_2O	16.672	16.16	16.492	16.714	16.293	16.548	16.398
K_2O	3.86	3.869	3.864	3.823	3.816	3.819	3.792
Total	100.32	98.15	99.84	100.71	98.93	99.99	99.61
				oxygen = 32.000			
Si	8.714	8.704	8.708	8.705	8.701	8.711	8.741
Al	7.19	7.202	7.208	7.215	7.211	7.197	7.186
Mg	0	0	0.004	0	0.006	0.004	0.002
Fe*	0.105	0.108	0.102	0.099	0.105	0.11	0.099
Na	6.112	6.057	6.073	6.099	6.056	6.085	6.045
Ca	0.15	0.164	0.15	0.148	0.166	0.153	0.145
K	0.931	0.954	0.936	0.918	0.933	0.924	0.92

Table A.6: Con't

	LT013-023	LT013-024	LT013-030	LT013-031	LT013-038	LT013-042	LT013-044
SiO_2	45.916	46.103	45.288	46.169	45.661	45.593	46.3
Al_2O_3	32.052	32.008	31.762	32.361	32.1	31.458	31.538
FeO_T	0.614	0.698	0.607	0.619	0.648	0.651	0.681
MgO	0.003	0.016	0	0.001	0.007	0	0.009
CaO	0.715	0.737	0.739	0.779	0.771	0.716	0.698
Na_2O	16.398	16.516	16.128	16.768	16.504	16.189	16.542
K_2O	3.812	3.744	3.784	3.821	3.849	3.771	3.554
Total	99.51	99.82	98.31	100.52	99.54	98.38	99.32
				oxygen = 32.000			
Si	8.74	8.75	8.726	8.711	8.702	8.777	8.819
Al	7.185	7.154	7.207	7.19	7.204	7.132	7.074
Mg	0.001	0.005	0	0	0.002	0	0.003
Fe*	0.098	0.111	0.098	0.098	0.103	0.105	0.108
Na	6.052	6.078	6.025	6.134	6.099	6.043	6.109
Ca	0.146	0.15	0.153	0.157	0.157	0.148	0.142
K	0.926	0.907	0.93	0.92	0.936	0.926	0.864

Table A.6: Con't

	LT013-047	LT013-048	LT013-049	LT013-050	LT014-001	LT014-002	LT014-003
SiO_2	45.843	45.834	46.536	45.905	45.54	45.816	45.758
Al_2O_3	31.918	31.973	32.298	32.261	32.286	32.28	32.23
FeO_T	0.663	0.682	0.659	0.643	0.63	0.589	0.575
MgO	0.002	0.008	0	0.004	0.007	0.008	0.009
CaO	0.722	0.732	0.72	0.736	0.819	0.81	0.785
Na_2O	16.406	16.449	16.882	16.457	16.357	16.618	16.458
K_2O	3.757	3.732	3.729	3.803	4.118	4.128	3.937
Total	99.31	99.41	100.82	99.81	99.76	100.25	99.75
				oxygen = 32.000			
Si	8.745	8.736	8.747	8.714	8.671	8.684	8.7
Al	7.17	7.176	7.149	7.212	7.239	7.205	7.216
Mg	0.001	0.002	0	0.001	0.002	0.002	0.003
Fe*	0.106	0.109	0.104	0.102	0.1	0.093	0.091
Na	6.068	6.079	6.153	6.058	6.039	6.108	6.067
Ca	0.148	0.149	0.145	0.15	0.167	0.164	0.16
K	0.914	0.907	0.894	0.921	1	0.998	0.955

Table A.6: Con't

	LT014-004	LT014-005	LT014-006	LT014-007	LT014-008	LT014-009	LT014-010
SiO_2	45.449	45.285	45.644	46.231	46.495	45.246	46.578
Al_2O_3	31.196	32.175	31.899	31.859	31.582	31.181	32.373
FeO_T	0.563	0.631	0.641	0.685	0.638	0.689	0.628
MgO	0.005	0.009	0	0.005	0.015	0	0.011
CaO	0.807	0.768	0.756	0.736	0.703	0.786	0.752
Na_2O	16.431	16.246	16.282	16.619	16.702	16.252	16.593
K_2O	4.085	3.895	3.826	3.805	3.549	3.85	3.752
Total	98.54	99.01	99.05	99.94	99.68	98	100.69
				oxygen = 32.000			
Si	8.764	8.674	8.732	8.769	8.825	8.761	8.756
Al	7.085	7.258	7.187	7.117	7.059	7.11	7.167
Mg	0.001	0.003	0	0.001	0.004	0	0.003
Fe*	0.091	0.101	0.103	0.109	0.101	0.112	0.099
Na	6.144	6.034	6.04	6.112	6.147	6.102	6.048
Ca	0.167	0.158	0.155	0.15	0.143	0.163	0.151
K	1.005	0.952	0.934	0.921	0.859	0.951	0.9

Table A.6: Con't

	LT014-013	LT014-016	LT014-017	LT014-018	LT014-019	LT014-026	LT014-027
SiO_2	46.331	45.74	45.451	45.827	45.588	45.518	46.298
Al_2O_3	32.144	32.062	32.893	31.877	32.541	32.109	32.399
FeO_T	0.635	0.673	0.644	0.653	0.673	0.659	0.625
MgO	0	0.007	0.019	0	0	0.012	0.001
CaO	0.759	0.774	0.735	0.703	0.797	0.783	0.786
Na_2O	16.876	16.355	16.266	16.368	16.357	16.361	16.587
K_2O	3.87	3.892	3.678	3.763	3.755	3.825	3.787
Total	100.62	99.5	99.69	99.19	99.71	99.27	100.48
				oxygen = 32.000			
Si	8.738	8.717	8.63	8.75	8.663	8.695	8.728
Al	7.139	7.196	7.355	7.168	7.283	7.223	7.193
Mg	0	0.002	0.005	0	0	0.003	0
Fe*	0.1	0.107	0.102	0.104	0.107	0.105	0.099
Na	6.171	6.044	5.989	6.06	6.027	6.06	6.063
Ca	0.153	0.158	0.15	0.144	0.162	0.16	0.159
K	0.931	0.946	0.891	0.917	0.91	0.932	0.911

Table A.6: Con't

	LT014-028	LT014-029	LT014-030	LT014-031	LT014-035	LT014-036	LT015-001
SiO_2	46.392	45.515	46.228	44.432	46.245	46.652	45.838
Al_2O_3	32.401	31.78	32.249	33.965	32.23	32.27	32.414
FeO_T	0.633	0.618	0.633	0.663	0.67	0.66	0.584
MgO	0.002	0	0.004	0	0.002	0.009	0.004
CaO	0.746	0.757	0.746	0.757	0.812	0.794	0.794
Na_2O	16.7	15.881	16.577	15.813	16.676	16.799	16.507
K_2O	3.714	3.691	3.791	3.803	3.824	3.801	4.052
Total	100.59	98.24	100.23	99.43	100.46	100.99	100.19
				oxygen = 32.000			
Si	8.734	8.758	8.737	8.461	8.73	8.756	8.683
Al	7.184	7.201	7.178	7.617	7.165	7.133	7.231
Mg	0.001	0	0.001	0	0.001	0.003	0.001
Fe*	0.1	0.099	0.1	0.106	0.106	0.104	0.093
Na	6.096	5.925	6.075	5.839	6.104	6.114	6.063
Ca	0.15	0.156	0.151	0.154	0.164	0.16	0.161
K	0.892	0.906	0.914	0.924	0.921	0.91	0.979

Table A.6: Con't

	LT015-002	LT015-003	LT015-004	LT015-005	LT015-006	LT015-007	LT015-008
SiO_2	45.599	45.121	45.295	45.871	45.606	45.05	45.988
Al_2O_3	32.755	32.598	32.506	32.2	32.164	32.484	30.837
FeO_T	0.573	0.56	0.573	0.584	0.587	0.696	0.65
MgO	0.006	0.008	0.015	0.007	0.012	0.002	0
CaO	0.76	0.78	0.799	0.776	0.788	0.761	0.724
Na_2O	16.326	16.273	16.211	16.569	16.327	15.985	16.469
K_2O	4.039	3.991	3.935	3.818	3.839	3.884	3.654
Total	100.06	99.33	99.33	99.83	99.32	98.86	98.32
				oxygen = 32.000			
Si	8.643	8.619	8.645	8.711	8.701	8.637	8.859
Al	7.312	7.333	7.307	7.201	7.227	7.334	6.996
Mg	0.002	0.002	0.004	0.002	0.003	0.001	0
Fe*	0.091	0.089	0.091	0.093	0.094	0.112	0.105
Na	6	6.027	6	6.101	6.04	5.942	6.151
Ca	0.154	0.16	0.163	0.158	0.161	0.156	0.149
K	0.977	0.973	0.958	0.925	0.934	0.95	0.898

Table A.6: Con't

	LT015-009	LT015-010	LT015-011	LT015-012	LT015-014	LT015-015	LT015-016
SiO_2	45.605	45.242	45.459	45.691	45.686	45.591	45.662
Al_2O_3	31.55	32.857	32.16	32.258	32.421	32.48	32.682
FeO_T	0.67	0.682	0.676	0.611	0.629	0.648	0.615
MgO	0	0	0.005	0.02	0.011	0.01	0
CaO	0.767	0.738	0.783	0.728	0.712	0.729	0.767
Na_2O	16.258	16.029	16.136	16.203	16.22	16.303	16.329
K_2O	3.801	3.792	3.799	3.798	3.72	3.775	3.762
Total	98.65	99.34	99.02	99.31	99.4	99.54	99.82
				oxygen = 32.000			
Si	8.761	8.622	8.697	8.71	8.697	8.675	8.662
Al	7.138	7.375	7.246	7.241	7.268	7.279	7.302
Mg	0	0	0.001	0.006	0.003	0.003	0
Fe*	0.108	0.109	0.108	0.097	0.1	0.103	0.098
Na	6.056	5.923	5.986	5.989	5.987	6.015	6.007
Ca	0.158	0.151	0.16	0.149	0.145	0.149	0.156
K	0.932	0.922	0.927	0.924	0.903	0.916	0.91

Table A.6: Con't

	LT015-017	LT015-018	LT015-019	LT015-020	LT015-022	LT015-023	LT015-024
SiO_2	46.026	45.502	46.032	46.425	45.542	46.079	46.101
Al_2O_3	31.119	31.615	32.428	32.677	31.604	32.282	32.148
FeO_T	0.681	0.649	0.69	0.623	0.64	0.654	0.692
MgO	0.013	0.008	0.01	0.002	0.013	0.005	0.011
CaO	0.754	0.764	0.751	0.781	0.748	0.735	0.762
Na_2O	16.451	16.115	16.614	16.608	16.083	16.517	16.458
K_2O	3.795	3.729	3.794	3.7	3.711	3.711	3.771
Total	98.84	98.38	100.32	100.82	98.34	99.98	99.94
				oxygen = 32.000			
Si	8.828	8.757	8.699	8.716	8.764	8.727	8.738
Al	7.029	7.165	7.217	7.224	7.162	7.2	7.176
Mg	0.004	0.002	0.003	0.001	0.004	0.001	0.003
Fe*	0.109	0.104	0.109	0.098	0.103	0.104	0.11
Na	6.118	6.013	6.088	6.046	6.001	6.066	6.049
Ca	0.155	0.158	0.152	0.157	0.154	0.149	0.155
K	0.929	0.916	0.915	0.886	0.911	0.897	0.912

Table A.6: Con't

	LT015-027	LT015-029	LT015-031	LT015-032	LT015-033	LT015-034	LT015-035
SiO_2	45.901	46.124	46.006	46.026	46.364	45.923	46.443
Al_2O_3	32.396	31.687	32.046	31.863	31.996	31.747	31.871
FeO_T	0.667	0.639	0.667	0.672	0.703	0.642	0.625
MgO	0.011	0.007	0	0.009	0.004	0.013	0.004
CaO	0.755	0.7	0.733	0.763	0.699	0.737	0.733
Na_2O	16.452	16.433	16.36	16.499	16.495	16.619	16.334
K_2O	3.68	3.624	3.659	3.658	3.684	3.587	3.489
Total	99.86	99.21	99.47	99.49	99.95	99.27	99.5
				oxygen = 32.000			
Si	8.703	8.795	8.752	8.761	8.78	8.761	8.814
Al	7.234	7.116	7.179	7.142	7.135	7.133	7.123
Mg	0.003	0.002	0	0.003	0.001	0.004	0.001
Fe*	0.106	0.102	0.106	0.107	0.111	0.102	0.099
Na	6.049	6.076	6.035	6.089	6.056	6.148	6.011
Ca	0.153	0.143	0.149	0.156	0.142	0.151	0.149
K	0.89	0.882	0.888	0.888	0.89	0.873	0.845

Table A.6: Con't

	LT015-036	LT015-037	LT015-038	LT015-039	LT015-040	LT015-041	LT015-042
SiO_2	46.201	46.128	45.542	45.622	45.535	45.797	45.739
Al_2O_3	30.993	32.477	32.643	32.426	32.427	31.811	32.23
FeO_T	0.603	0.627	0.629	0.7	0.651	0.662	0.598
MgO	0.007	0	0	0.014	0.001	0.008	0.008
CaO	0.712	0.75	0.81	0.775	0.776	0.762	0.729
Na_2O	16.883	16.497	16.242	16.454	16.253	16.496	16.313
K_2O	3.712	3.678	3.755	3.741	3.753	3.65	3.696
Total	99.11	100.16	99.62	99.73	99.4	99.19	99.31
				oxygen = 32.000			
Si	8.841	8.716	8.657	8.671	8.677	8.747	8.716
Al	6.985	7.227	7.308	7.258	7.277	7.155	7.233
Mg	0.002	0	0	0.004	0	0.002	0.002
Fe*	0.097	0.099	0.1	0.111	0.104	0.106	0.095
Na	6.265	6.044	5.987	6.064	6.005	6.109	6.027
Ca	0.146	0.152	0.165	0.158	0.158	0.156	0.149
K	0.906	0.887	0.911	0.907	0.912	0.889	0.898

Table A.6: Con't

	LT015-043	LT015-044	LT015-045	LT015-046	LT015-047	LT015-048	LT015-049
SiO_2	45.708	45.801	45.143	45.779	45.556	45.564	46.114
Al_2O_3	32.419	32.122	32.282	32.13	32.199	32.081	32.446
FeO_T	0.601	0.692	0.658	0.635	0.668	0.656	0.648
MgO	0.005	0.009	0.017	0.005	0.01	0	0.011
CaO	0.788	0.745	0.784	0.747	0.804	0.77	0.773
Na_2O	16.268	16.364	16.066	16.338	16.574	16.322	16.361
K_2O	3.777	3.835	3.821	3.851	3.657	3.768	3.809
Total	99.57	99.57	98.77	99.49	99.47	99.16	100.16
				oxygen = 32.000			
Si	8.692	8.719	8.661	8.719	8.683	8.707	8.717
Al	7.26	7.201	7.294	7.207	7.228	7.22	7.223
Mg	0.001	0.003	0.005	0.001	0.003	0	0.003
Fe*	0.096	0.11	0.106	0.101	0.106	0.105	0.102
Na	5.998	6.04	5.977	6.034	6.126	6.048	5.997
Ca	0.161	0.152	0.161	0.152	0.164	0.158	0.157
K	0.916	0.931	0.935	0.936	0.889	0.919	0.919

Table A.6: Con't

	LT015-050	LT015-053	LT015-054	LT015-055	LT015-056	LT015-057	LT015-058
SiO_2	46.087	45.867	45.726	45.958	46.295	45.788	45.411
Al_2O_3	31.904	32.306	32.235	32.277	32.074	32.309	32.696
FeO_T	0.701	0.624	0.616	0.619	0.672	0.709	0.637
MgO	0.002	0.027	0.006	0	0	0.007	0.013
CaO	0.739	0.758	0.758	0.768	0.745	0.794	0.795
Na_2O	16.268	16.16	16.352	16.388	16.455	16.337	16.249
K_2O	3.744	3.788	3.814	3.73	3.546	3.811	3.707
Total	99.44	99.53	99.51	99.74	99.79	99.76	99.51
				oxygen = 32.000			
Si	8.772	8.72	8.706	8.723	8.772	8.699	8.642
Al	7.151	7.233	7.228	7.215	7.157	7.229	7.327
Mg	0.001	0.008	0.002	0	0	0.002	0.004
Fe*	0.112	0.099	0.098	0.098	0.106	0.113	0.101
Na	6.004	5.957	6.037	6.031	6.046	6.018	5.996
Ca	0.151	0.154	0.155	0.156	0.151	0.162	0.162
K	0.909	0.919	0.926	0.903	0.857	0.924	0.9

Table A.6: Con't

	LT015-059	LT015-060	LT015-061	LT015-065	LT015-066
SiO_2	45.485	45.197	45.954	46.376	46.227
Al_2O_3	32.121	32.781	32.418	32.189	31.742
FeO_T	0.648	0.642	0.638	0.671	0.659
MgO	0.005	0.003	0.006	0.011	0.008
CaO	0.784	0.796	0.792	0.756	0.711
Na_2O	16.425	16.211	16.487	16.504	16.578
K_2O	3.697	3.784	3.774	3.525	3.599
Total	99.16	99.41	100.07	100.03	99.52
			Oxygen = 32.000		
Si	8.693	8.615	8.701	8.765	8.791
Al	7.229	7.358	7.228	7.165	7.109
Mg	0.001	0.001	0.002	0.003	0.002
Fe*	0.104	0.102	0.101	0.106	0.105
Na	6.087	5.991	6.053	6.048	6.113
Ca	0.161	0.163	0.161	0.153	0.145
K	0.901	0.92	0.912	0.85	0.873

Table A.7: All Oxide EMP analysis for DH Wall.

	Titanomagnetite						
	026-001	026-002	026-003	026-004	026-005	026-006	026-007
SiO_2	0.074	0.044	0.027	0.068	0.095	10.66	29.093
TiO_2	17.464	17.339	17.478	17.733	17.276	13.992	8.498
Al_2O_3	6.789	6.742	6.703	6.706	6.743	6.706	7.447
FeO_T	66.131	66.583	66.286	66.605	65.614	52.507	27.567
Cr_2O_3	0.659	0.646	0.479	0.343	0.271	0.138	0.054
MnO	0.467	0.469	0.456	0.481	0.438	0.395	0.277
MgO	7.15	7.224	7.07	7.131	7.131	8.243	10.434
NiO	0.012	0.031	0	0	0	0.015	0.027
CaO	0.003	0	0.012	0.011	0.405	6.103	15.62
Total	98.75	99.08	98.51	99.08	97.97	98.76	99.02
				Oxygen = 4.000			
Si	0.003	0.002	0.001	0.003	0.004	0.363	0.832
Al	0.303	0.3	0.3	0.298	0.303	0.269	0.251
Ti	0.498	0.493	0.5	0.504	0.496	0.358	0.183
Fe*	2.095	2.107	2.109	2.105	2.096	1.495	0.66
Cr	0.02	0.019	0.014	0.01	0.008	0.004	0.001
Mn	0.015	0.015	0.015	0.015	0.014	0.011	0.007
Mg	0.404	0.407	0.401	0.402	0.406	0.418	0.445
Ni	0	0	0	0	0	0	0
Ca	0	0	0	0	0.017	0.223	0.479

Table A.7: Con't

	Titanomagnetite						
	026-009	026-010	026-011	026-012	026-013	026-014	030-001
SiO_2	0.046	3.22	26.015	0.15	0.102	0.06	0.047
TiO_2	17.298	15.877	8.729	17.178	17.285	17.675	18.217
Al_2O_3	6.726	6.647	6.941	6.596	6.692	6.594	7.018
FeO_T	66.197	61.221	30.758	65.906	65.515	66.024	65.937
Cr_2O_3	0.31	0.158	0.085	0.219	0.126	0.376	0.029
MnO	0.448	0.463	0.326	0.447	0.424	0.438	0.448
MgO	7.224	7.306	9.467	7.121	7.124	7.23	7.486
NiO	0.028	0	0	0	0.01	0.013	0.024
CaO	0.186	2.629	14.439	0.318	0.362	0.012	0
Total	98.46	97.52	96.76	97.94	97.64	98.42	99.21
				Oxygen = 4.000			
Si	0.002	0.12	0.782	0.006	0.004	0.002	0.002
Al	0.301	0.291	0.246	0.297	0.302	0.295	0.31
Ti	0.495	0.444	0.197	0.495	0.498	0.505	0.514
Fe*	2.107	1.904	0.773	2.109	2.1	2.099	2.068
Cr	0.009	0.005	0.002	0.007	0.004	0.011	0.001
Mn	0.014	0.015	0.008	0.014	0.014	0.014	0.014
Mg	0.41	0.405	0.424	0.406	0.407	0.41	0.419
Ni	0	0	0	0	0	0	0
Ca	0.008	0.105	0.465	0.013	0.015	0	0

Table A.7: Con't

	Titanomagnetite						
	030-002	030-003	030-004	030-005	030-006	030-007	030-008
SiO_2	0.069	0.058	0.06	0.072	0.073	0.09	0.107
TiO_2	18.16	18.276	18.202	18.24	18.06	17.141	17.174
Al_2O_3	6.956	6.884	6.975	6.95	6.882	6.66	6.538
FeO_T	65.729	66.037	65.858	65.56	65.59	65.365	64.932
Cr_2O_3	0.018	0.028	0.012	0.022	0.021	0.032	0.01
MnO	0.448	0.484	0.45	0.47	0.452	0.661	0.567
MgO	7.526	7.441	7.445	7.41	7.503	7.147	7.281
NiO	0.041	0.046	0	0.054	0.054	0.081	0.062
CaO	0	0	0	0.004	0.043	0.021	0.038
Total	98.95	99.25	99	98.78	98.68	97.2	96.71
				Oxygen = 4.000			
Si	0.003	0.002	0.002	0.003	0.003	0.003	0.004
Al	0.308	0.304	0.309	0.308	0.306	0.302	0.298
Ti	0.514	0.516	0.515	0.517	0.513	0.497	0.5
Fe*	2.067	2.073	2.07	2.065	2.07	2.108	2.102
Cr	0.001	0.001	0	0.001	0.001	0.001	0
Mn	0.014	0.015	0.014	0.015	0.014	0.022	0.019
Mg	0.422	0.416	0.417	0.416	0.422	0.411	0.42
Ni	0	0	0	0	0	0	0
Ca	0	0	0	0	0.002	0.001	0.002

Table A.7: Con't

	Titanomagnetite						
	030-009	031-001	031-002	031-003	031-004	031-005	031-006
SiO_2	0.115	0.024	0.049	0.04	0.065	0.054	0.063
TiO_2	17.048	17.744	17.535	17.616	17.455	17.642	17.598
Al_2O_3	6.446	5.795	5.796	5.779	5.65	5.76	5.792
FeO_T	66.01	68.029	68.299	68.294	68.01	68.268	68.348
Cr_2O_3	0.041	0.008	0.018	0	0.015	0.033	0.037
MnO	0.692	0.504	0.528	0.495	0.555	0.508	0.517
MgO	6.982	6.659	6.607	6.533	6.61	6.606	6.59
NiO	0.057	0	0	0	0	0	0
CaO	0.072	0.012	0.012	0	0.018	0.019	0.013
Total	97.46	98.78	98.84	98.76	98.38	98.89	98.96
				Oxygen = 4.000			
Si	0.004	0.001	0.002	0.002	0.003	0.002	0.002
Al	0.293	0.262	0.262	0.262	0.257	0.26	0.262
Ti	0.495	0.512	0.506	0.509	0.507	0.509	0.508
Fe*	2.13	2.183	2.193	2.195	2.196	2.19	2.192
Cr	0.001	0	0.001	0	0	0.001	0.001
Mn	0.023	0.016	0.017	0.016	0.018	0.017	0.017
Mg	0.402	0.381	0.378	0.374	0.38	0.378	0.377
Ni	0	0	0	0	0	0	0
Ca	0.003	0	0	0	0.001	0.001	0.001

Table A.7: Con't

	Titanomagnetite						
	031-007	031-008	033-001	033-002	033-003	033-004	033-005
SiO_2	0.038	0.05	0.061	0.048	0.062	0.068	0.073
TiO_2	17.594	17.55	17.735	17.392	17.747	17.621	17.639
Al_2O_3	5.74	5.77	5.966	5.93	5.94	6.007	5.976
FeO_T	68.37	67.841	67.678	67.549	67.485	67.348	67.382
Cr_2O_3	0.035	0.051	0	0.048	0.025	0.005	0.052
MnO	0.542	0.511	0.533	0.542	0.495	0.577	0.494
MgO	6.628	6.576	6.743	6.766	6.905	6.869	6.863
NiO	0	0	0	0	0	0	0
CaO	0	0.024	0.017	0.003	0	0	0.006
Total	98.95	98.37	98.73	98.28	98.66	98.49	98.49
			Oxygen = 4.00				
Si	0.001	0.002	0.002	0.002	0.002	0.003	0.003
Al	0.259	0.262	0.269	0.269	0.268	0.271	0.27
Ti	0.508	0.509	0.511	0.504	0.511	0.508	0.509
Fe*	2.194	2.187	2.167	2.176	2.16	2.16	2.161
Cr	0.001	0.002	0	0.001	0.001	0	0.002
Mn	0.018	0.017	0.017	0.018	0.016	0.019	0.016
Mg	0.379	0.378	0.385	0.389	0.394	0.393	0.392
Ni	0	0	0	0	0	0	0
Ca	0	0.001	0.001	0	0	0	0

Table A.7: Con't

	Titanomagnetite						
	033-007	036-001	036-002	036-003	036-004	036-005	036-006
SiO_2	0.068	0.038	0.048	0.041	0.053	0.061	0.069
TiO_2	17.427	17.283	17.714	17.422	17.441	17.626	17.732
Al_2O_3	5.946	5.617	5.689	5.629	5.548	5.687	5.653
FeO_T	67.19	68.329	68.35	68.46	68.478	68.336	68.183
Cr_2O_3	0	0.062	0.043	0.067	0.05	0.048	0.033
MnO	0.521	0.534	0.578	0.566	0.55	0.561	0.546
MgO	6.954	6.517	6.504	6.545	6.568	6.535	6.659
NiO	0	0	0	0	0	0	0
CaO	0.021	0	0.005	0	0.021	0.004	0.021
Total	98.13	98.38	98.93	98.73	98.71	98.86	98.9
			Oxygen = 4.00				
Si	0.003	0.001	0.002	0.002	0.002	0.002	0.003
Al	0.27	0.256	0.257	0.255	0.252	0.257	0.255
Ti	0.505	0.503	0.511	0.505	0.506	0.509	0.512
Fe*	2.164	2.211	2.194	2.206	2.208	2.195	2.187
Cr	0	0.002	0.001	0.002	0.002	0.001	0.001
Mn	0.017	0.017	0.019	0.018	0.018	0.018	0.018
Mg	0.399	0.376	0.372	0.376	0.377	0.374	0.381
Ni	0	0	0	0	0	0	0
Ca	0.001	0	0	0	0.001	0	0.001

Table A.7: Con't

	Titanomagnetite						
	036-007	037-001	037-002	037-003	037-004	037-005	037-006
SiO_2	0.089	0.037	0.047	0.065	0.049	0.033	0.041
TiO_2	17.06	18.476	18.62	18.488	18.621	18.473	18.322
Al_2O_3	5.494	7.472	7.452	7.488	7.49	7.481	7.367
FeO_T	67.672	64.47	64.579	64.534	64.945	64.636	65.1
Cr_2O_3	0.06	0.045	0.065	0.026	0.011	0.036	0.017
MnO	0.675	0.463	0.399	0.41	0.398	0.402	0.421
MgO	6.645	8.001	7.914	7.836	7.846	7.847	7.91
NiO	0.03	0	0	0.042	0	0	0
CaO	0.063	0	0.02	0.011	0.006	0.024	0.005
Total	97.79	98.96	99.1	98.9	99.37	98.93	99.18
				Oxygen = 4.000			
Si	0.003	0.001	0.002	0.002	0.002	0.001	0.002
Al	0.252	0.328	0.326	0.329	0.328	0.329	0.323
Ti	0.499	0.518	0.521	0.519	0.52	0.518	0.514
Fe*	2.202	2.009	2.009	2.013	2.017	2.016	2.03
Cr	0.002	0.001	0.002	0.001	0	0.001	0.001
Mn	0.022	0.015	0.013	0.013	0.013	0.013	0.013
Mg	0.385	0.444	0.439	0.436	0.434	0.436	0.44
Ni	0	0	0	0	0	0	0
Ca	0.003	0	0.001	0	0	0.001	0

Table A.7: Con't

	Titanomagnetite						
	037-007	041-001	041-003	041-004	042-001	042-002	042-003
SiO_2	0.081	0.038	0.031	0.057	0.049	0.009	0.036
TiO_2	17.715	14.639	14.654	14.419	14.613	14.635	14.749
Al_2O_3	7.458	2.857	2.856	2.826	2.866	2.873	2.815
FeO_T	65.201	74.78	74.865	74.589	75.194	75.043	74.809
Cr_2O_3	0.01	0.015	0.047	0.016	0.015	0.002	0.031
MnO	0.509	1.318	1.295	1.312	1.29	1.278	1.288
MgO	7.62	3.732	3.696	3.69	3.769	3.726	3.764
NiO	0	0	0	0	0	0	0
CaO	0.066	0	0.018	0.156	0.004	0.005	0.005
Total	98.66	97.38	97.46	97.07	97.8	97.57	97.5
				Oxygen = 4.000			
Si	0.003	0.002	0.001	0.002	0.002	0	0.001
Al	0.33	0.14	0.139	0.139	0.14	0.14	0.137
Ti	0.501	0.457	0.457	0.452	0.454	0.456	0.46
Fe*	2.05	2.595	2.597	2.6	2.599	2.601	2.592
Cr	0	0	0.002	0.001	0	0	0.001
Mn	0.016	0.046	0.045	0.046	0.045	0.045	0.045
Mg	0.427	0.231	0.229	0.229	0.232	0.23	0.232
Ni	0	0	0	0	0	0	0
Ca	0.003	0	0.001	0.007	0	0	0

Table A.7: Con't

	Titanomagnetite						
	042-005	042-006	043-001	043-002	043-003	043-004	043-005
SiO_2	0.061	0.061	0.029	0.008	0.001	0.045	0.038
TiO_2	14.445	14.497	11.279	11.365	11.246	11.225	11.085
Al_2O_3	2.888	2.846	1.102	1.116	1.081	1.118	1.111
FeO_T	74.773	74.711	80.28	80.243	80.317	80.354	80.279
Cr_2O_3	0.004	0.018	0.018	0.02	0	0.025	0.016
MnO	1.335	1.305	2.69	2.616	2.716	2.72	2.692
MgO	3.814	3.742	0.947	0.985	0.971	0.946	1.004
NiO	0	0	0	0	0	0	0
CaO	0.153	0.139	0.048	0	0.011	0.001	0
Total	97.47	97.32	96.39	96.35	96.34	96.43	96.23
				Oxygen = 4.000			
Si	0.003	0.003	0.001	0	0	0.002	0.002
Al	0.141	0.139	0.058	0.058	0.057	0.059	0.058
Ti	0.45	0.453	0.378	0.38	0.377	0.376	0.372
Fe*	2.593	2.595	2.988	2.986	2.993	2.99	2.996
Cr	0	0.001	0.001	0.001	0	0.001	0.001
Mn	0.047	0.046	0.101	0.099	0.103	0.103	0.102
Mg	0.236	0.232	0.063	0.065	0.065	0.063	0.067
Ni	0	0	0	0	0	0	0
Ca	0.007	0.006	0.002	0	0.001	0	0

Table A.7: Con't

	Ilmenite						
	025-001	025-002	025-004	025-005	025-007	025-008	025-009
SiO_2	0	0	0	0	0.01	0.026	0.043
TiO_2	49.863	49.671	49.779	49.841	49.964	49.35	49.46
Al_2O_3	0.646	0.635	0.661	0.648	0.657	0.657	0.593
FeO_T	43.456	43.26	43.278	43.149	42.887	42.645	42.992
Cr_2O_3	0	0	0.005	0.039	0	0	0.001
MnO	0.594	0.6	0.63	0.545	0.61	0.586	0.675
MgO	7.278	7.134	7.194	7.385	7.385	7.379	7.314
NiO	0	0	0	0	0.004	0.015	0
CaO	0.025	0.031	0.029	0.021	0.075	0.033	0.058
Total	101.86	101.33	101.58	101.63	101.59	100.69	101.14
				Oxygen = 3.000			
Si	0	0	0	0	0	0.001	0.001
Al	0.018	0.018	0.019	0.018	0.019	0.019	0.017
Ti	0.908	0.91	0.909	0.909	0.911	0.908	0.907
Fe*	0.88	0.881	0.879	0.875	0.869	0.872	0.877
Cr	0	0	0	0.001	0	0	0
Mn	0.012	0.012	0.013	0.011	0.013	0.012	0.014
Mg	0.263	0.259	0.26	0.267	0.267	0.269	0.266
Ni	0	0	0	0	0	0	0
Ca	0.001	0.001	0.001	0.001	0.002	0.001	0.002

Table A.7: Con't

	Ilmenite						
	025-011	040-001	040-002	040-003	040-004	040-005	040-006
SiO_2	0.034	0.006	0	0	0	0	0.016
TiO_2	49.865	47.33	47.34	47.343	47.167	47.087	46.592
Al_2O_3	0.65	0.37	0.367	0.377	0.378	0.355	0.382
FeO_T	43.097	46.769	47.052	47.023	46.859	46.814	46.494
Cr_2O_3	0.024	0.028	0	0	0	0	0
MnO	0.622	1.359	1.379	1.374	1.347	1.348	1.356
MgO	7.293	4.961	4.973	4.949	4.944	4.913	4.917
NiO	0	0	0.003	0	0	0.015	0.004
CaO	0.095	0.027	0	0.01	0.028	0.044	0.378
Total	101.68	100.85	101.11	101.08	100.72	100.58	100.14
			Oxygen = 3.000				
Si	0.001	0	0	0	0	0	0
Al	0.019	0.011	0.011	0.011	0.011	0.011	0.011
Ti	0.909	0.893	0.892	0.892	0.892	0.892	0.887
Fe*	0.873	0.981	0.985	0.985	0.985	0.986	0.984
Cr	0	0.001	0	0	0	0	0
Mn	0.013	0.029	0.029	0.029	0.029	0.029	0.029
Mg	0.263	0.186	0.186	0.185	0.185	0.184	0.185
Ni	0	0	0	0	0	0	0
Ca	0.002	0.001	0	0	0.001	0.001	0.01

Table A.7: Con't

	Ilmenite	Titanite		
	040-007	044-001	044-002	044-003
SiO_2	0.02	29.576	29.841	29.696
TiO_2	46.801	34.722	35.345	35.559
Al_2O_3	0.373	0.925	0.984	1.077
FeO_T	46.541	1.994	2.259	1.992
Cr_2O_3	0	0	0	0
MnO	1.365	0.13	0.145	0.109
MgO	5.014	0.032	0.023	0.032
NiO	0	0	0.021	0
CaO	0.258	27.197	27.473	27.42
Total	100.37	94.58	96.09	95.89
	Oxygen = 3.000		Oxygen = 20.00	
Si	0.001	4.108	4.085	4.069
Al	0.011	0.151	0.159	0.174
Ti	0.888	3.628	3.64	3.665
Fe*	0.982	0.232	0.259	0.228
Cr	0	0	0	0
Mn	0.029	0.015	0.017	0.013
Mg	0.189	0.007	0.005	0.007
Ni	0	0	0	0
Ca	0.007	4.047	4.03	4.025

Appendix B

The following three tables are intended to show from where each electron microprobe analysis comes from in terms of a particular pumice type.

Table B.A: Abrigo Ignimbrite - Mixed Pumice (CS-002)

Mineral	Analyses id				
Feldspar	LT021	LT023	019	021	
	LT022	LT024	020		
Glass	G027	G029	G031	LT054	LT056
	G028	G030	G047	LT055	LT057
Pyroxene	C007				
Amphibole	AM007	AM008			

Table B.B: Abrigo Ignimbrite - Mixed Pumice (CS-015A)

Mineral	Analyses id			
Feldspar	LT025	LT027	022	024
	LT026		023	
Glass	G032	G034	G036	G038
	G033	G035	G037	

Table B.C: Abrigo Ignimbrite - Felsic Pumcie (TK-25B)

Mineral	Analyses id
Feldspar	LT062
	LT063
Glass	G049
	G050

LT - line traverse

Table B.1: All EMP analysis of glass from El Abrigo Ignimbrite.

	G027-001	G027-002	G027-003	G027-004	G027-005	G027-006	G027-007	G027-008	G027-009	G027-010	G027-011
Na_2O	8.342	8.199	7.814	4.552	8.028	8.225	7.984	8.165	7.743	7.643	7.448
Al_2O_3	19.191	19.064	18.742	18.916	19.233	19.547	19.168	19.023	18.927	19.174	19.066
SiO_2	58.644	57.646	55.314	56.408	58.007	59.328	58.947	56.453	58.683	60.269	60.64
MgO	0.632	0.748	1.297	1.346	0.897	0.531	0.675	0.799	0.65	0.384	0.379
TiO_2	0.828	1.077	1.413	1.482	1.029	0.845	0.88	1.161	0.911	0.739	0.739
K_2O	5.422	5.276	4.683	4.827	5.079	5.418	5.268	5.278	5.139	5.511	5.603
CaO	1.905	2.188	3.632	3.668	2.459	1.618	2.344	2.122	2.288	1.625	1.465
FeO	3.323	3.604	4.545	4.659	3.845	2.94	3.399	3.742	3.331	2.665	2.535
MnO	0.133	0.162	0.198	0.133	0.195	0.168	0.173	0.174	0.14	0.142	0.113
Total	98.42	97.964	97.638	95.991	98.772	98.62	98.838	96.917	97.812	98.152	97.988

Table B.1: Con't

	G027-012	G027-013	G027-014	G027-015	G027-016	G027-017	G028-001	G028-002	G029-002	G029-003	G029-004
Na_2O	8.039	7.852	8.184	8.302	8.305	8.132	8.182	6.594	7.931	8.135	8.408
Al_2O_3	18.998	19.12	19.332	19.64	19.265	18.936	19.915	18.067	19.25	19.409	19.617
SiO_2	60.477	57.685	58.835	59.118	58.968	56.988	59.599	52.451	57.379	57.338	58.197
MgO	0.404	0.812	0.625	0.418	0.559	0.972	0.333	1.598	0.839	0.628	0.734
TiO_2	0.763	0.966	0.872	0.601	0.768	1.171	0.542	2.149	1.029	0.865	0.813
K_2O	5.576	5.1	5.343	5.439	5.352	5.028	5.632	4.496	4.854	5.08	5.263
CaO	1.565	2.381	1.938	1.814	1.899	2.835	1.349	4.684	2.769	3.159	2.222
FeO	2.648	3.721	3.321	2.797	3.025	4.017	2.586	5.964	3.699	3.39	3.284
MnO	0.14	0.149	0.191	0.131	0.165	0.17	0.168	0.243	0.205	0.161	0.167
Total	98.61	97.786	98.641	98.26	98.306	98.249	98.306	96.246	97.955	98.165	98.705

Table B.1: Con't

	G029-005	G029-006	G029-007	G029-008	G029-009	G029-010	G029-011	G029-012	G029-013	G029-014	G029-015
Na_2O	8.213	8.199	8.075	8.227	7.626	7.954	7.943	7.218	7.331	7.888	7.579
Al_2O_3	19.189	19.687	19.157	19.185	19.437	19.637	19.476	18.537	18.509	19	18.61
SiO_2	56.615	58.253	57.017	56.433	57.309	57.447	57.69	54.309	54.448	55.248	54.308
MgO	0.824	0.552	1.01	1.034	0.928	0.832	0.83	1.749	1.796	1.652	1.839
TiO_2	1.031	0.848	1.167	1.108	1.01	1.059	0.89	1.77	1.773	1.613	1.885
K_2O	5.027	5.331	4.706	4.681	4.895	4.887	4.735	4.031	4.116	4.256	4.159
CaO	2.438	1.827	2.926	3.167	2.834	2.518	2.74	4.558	4.671	4.329	4.758
FeO	3.732	3.034	4.06	4.188	3.962	3.782	3.801	5.51	5.549	5.284	5.596
MnO	0.176	0.143	0.176	0.172	0.16	0.127	0.131	0.185	0.222	0.178	0.219
Total	97.245	97.874	98.294	98.198	98.191	98.243	98.236	97.867	98.415	99.448	98.953

Table B.1: Con't

	G029-016	G031-001	G031-002	G032-001	G032-002	G032-003	G032-004	G032-005	G033-001	G033-002	G034-001
Na_2O	7.063	6.042	5.617	7.233	7.668	7.496	7.402	7.441	5.921	6.351	8.349
Al_2O_3	18.213	16.789	16.567	17.88	18	18.519	18.278	18.401	17.37	16.791	18.523
SiO_2	53.396	51.698	50.206	58.196	57.935	60.454	60.011	61.541	54.358	52.999	61.658
MgO	1.643	2.312	2.882	1.135	1.204	0.8	0.751	0.674	2.114	2.395	0.445
TiO_2	1.844	2.61	2.991	1.208	1.35	0.943	0.936	0.885	1.95	2.341	0.766
K_2O	4.138	4.474	4.276	4.426	4.11	4.716	4.785	5.018	2.826	2.943	5.37
CaO	5.369	5.031	5.79	2.755	2.865	1.804	1.542	1.543	5.384	5.206	0.788
FeO	5.027	6.673	8.941	4.03	4.743	3.1	2.95	2.966	5.95	7.121	2.832
MnO	0.184	0.229	0.279	0.195	0.228	0.133	0.137	0.127	0.157	0.192	0.197
Total	96.877	95.858	97.549	97.058	98.103	97.965	96.792	98.596	96.03	96.339	98.928

Table B.1: Con't

	G034-002	G034-003	G034-004	G034-005	G034-006	G035-001	G035-002	G035-003	G035-004	G035-005	G035-006
Na_2O	7.754	8.214	7.167	7.433	8.129	6.403	7.206	7.28	7.223	7.374	6.77
Al_2O_3	18.43	18.476	18.107	18.473	18.382	16.873	17.956	18.048	17.952	18.26	17.436
SiO_2	61.205	61.695	56.933	61.594	60.369	50.89	55.217	55.382	54.441	55.678	52.657
MgO	0.694	0.439	1.344	0.584	0.439	2.7	1.634	1.662	1.603	1.677	2.296
TiO_2	0.919	0.785	1.544	0.87	0.759	2.424	1.584	1.574	1.619	1.544	2.283
K_2O	5.203	5.314	4.25	4.873	5.155	2.136	3.918	3.868	3.861	3.89	3.563
CaO	1.573	0.976	3.078	1.361	0.787	5.801	4.15	4.292	4.166	4.033	5.598
FeO	3.107	2.689	4.928	2.97	2.788	8.116	5.863	5.431	5.875	5.371	6.735
MnO	0.178	0.161	0.202	0.165	0.169	0.244	0.194	0.234	0.23	0.222	0.243
Total	99.063	98.749	97.553	98.323	96.977	95.587	97.722	97.771	96.97	98.049	97.581

Table B.1: Con't

	G035-007	G035-008	G035-009	G035-012	G036-001	G036-002	G036-003	G036-004	G036-005	G036-006	G037-001
Na_2O	6.904	7.251	7.287	7.688	7.722	7.526	7.323	7.497	7.33	7.21	7.964
Al_2O_3	17.481	17.839	18.284	18.128	17.662	17.807	17.646	17.646	17.625	17.71	18.01
SiO_2	53.424	59.121	59.404	57.865	59.62	59.494	59.7	59.794	59.714	59.172	59.589
MgO	2.239	1.187	0.575	0.964	0.39	0.422	0.429	0.421	0.407	0.426	0.503
TiO_2	2.259	1.26	0.818	1.176	0.683	0.722	0.76	0.703	0.711	0.773	0.771
K_2O	3.61	4.545	5.257	4.68	5.473	5.584	5.581	5.502	5.526	5.546	5.662
CaO	5.092	2.688	1.193	2.263	0.566	0.614	0.664	0.632	0.683	0.688	0.849
FeO	6.68	4.177	2.742	3.76	2.606	2.586	2.598	2.613	2.516	2.677	2.677
MnO	0.175	0.144	0.169	0.208	0.166	0.153	0.167	0.187	0.131	0.151	0.162
Total	97.864	98.212	95.729	96.732	94.888	94.908	94.868	94.995	94.643	94.353	96.187

Table B.1: Con't

	G037-002	G037-003	G037-004	G038-001	G038-002	G038-003	G038-004	G049-001	G049-002	G049-003	G049-006
Na_2O	9.309	8.672	8.979	7.318	7.576	7.216	8.133	5.843	5.994	5.936	5.985
Al_2O_3	19.078	18.837	18.985	18.134	18.185	17.407	18.735	19.156	19.257	19.375	19.551
SiO_2	59.172	59.664	59.28	58.681	58.749	54.69	59.54	58.746	58.694	59.439	59.991
MgO	0.331	0.362	0.323	0.768	0.783	1.964	0.613	0.367	0.383	0.386	0.406
TiO_2	0.651	0.697	0.638	0.957	0.969	1.966	0.878	0.735	0.739	0.717	0.734
K_2O	5.541	5.797	5.385	4.573	4.543	4.006	5.085	5.65	5.803	5.522	5.272
CaO	0.753	0.627	0.694	1.6	1.542	4.164	1.418	0.744	0.73	0.75	0.658
FeO	3.065	3.044	3.121	3.102	3.21	5.485	3.287	2.833	2.862	2.826	2.888
MnO	0.235	0.222	0.222	0.177	0.215	0.22	0.185	0.188	0.214	0.212	0.252
Total	98.135	97.922	97.627	95.31	95.772	97.118	97.874	94.262	94.676	95.163	95.737

Table B.1: Con't

	G049-007	G049-008	G049-009	G049-010	G049-011	G049-012	G049-013	G050-002	G050-003	G050-008	G050-010
Na_2O	6.881	6.441	5.578	5.254	6.039	6.549	5.417	6.916	7.572	5.902	5.904
Al_2O_3	19.736	19.552	19.328	19.342	19.312	19.955	19.519	20.018	19.969	19.526	19.362
SiO_2	60.573	59.676	59.397	59.596	59.115	60.433	60.119	60.928	60.518	59.533	59.105
MgO	0.372	0.369	0.385	0.408	0.389	0.412	0.394	0.389	0.392	0.37	0.359
TiO_2	0.755	0.705	0.747	0.712	0.779	0.741	0.678	0.723	0.7	0.75	0.711
K_2O	5.774	5.818	5.366	5.306	5.397	5.845	5.575	5.782	5.873	5.508	5.45
CaO	0.783	0.78	0.746	0.714	0.745	0.801	0.748	0.71	0.829	0.684	0.739
FeO	2.864	2.835	2.75	2.833	2.794	2.917	2.815	2.88	2.932	2.889	2.831
MnO	0.203	0.21	0.205	0.226	0.246	0.217	0.2	0.194	0.244	0.192	0.255
Total	97.941	96.386	94.502	94.391	94.816	97.87	95.465	98.54	99.029	95.354	94.716

Table B.1: Con't

	G050-011	G050-012	G050-013	G050 014	G050-015	G050 017	G050 019	G050 020	G050-021	G050 022	G050-023
Na_2O	6.391	6.577	7.022	6.206	6.833	5.919	5.885	6.135	5.639	5.506	6.096
Al_2O_3	19.683	19.798	19.801	19.194	19.814	19.46	19.349	19.272	19.567	19.412	19.407
SiO_2	59.925	60.231	60.717	60.716	60.533	59.832	59.937	59.951	60.411	59.933	59.713
MgO	0.394	0.38	0.39	0.393	0.399	0.387	0.394	0.398	0.404	0.364	0.393
TiO_2	0.786	0.698	0.726	0.707	0.684	0.734	0.748	0.747	0.753	0.785	0.753
K_2O	5.798	5.849	5.952	5.384	5.926	5.463	5.424	5.641	5.18	5.419	5.728
CaO	0.713	0.747	0.697	0.735	0.749	0.734	0.733	0.754	0.748	0.716	0.749
FeO	2.834	2.865	2.872	2.848	2.848	2.915	2.883	2.815	2.883	2.833	2.857
MnO	0.228	0.212	0.254	0.205	0.211	0.201	0.206	0.226	0.248	0.231	0.255
Total	96.752	97.357	98.431	96.388	97.997	95.645	95.559	95.939	95.833	95.199	95.951

Table B.1: Con't

	G050-024	G050-025	G050-026	G050-027	G050-028	G050-030	G050-031	G050-032	G050-033	G050-034	G050-035
Na_2O	6.184	5.746	6.323	5.48	6.426	6.026	6.036	6.422	5.723	5.847	6.578
Al_2O_3	19.152	19.358	19.638	19.104	19.59	19.458	19.561	19.409	19.708	19.288	19.64
SiO_2	59.171	59.872	60.03	59.579	61.708	59.804	58.995	61.417	60.237	59.715	60.173
MgO	0.389	0.385	0.374	0.418	0.396	0.354	0.394	0.404	0.385	0.416	0.38
TiO_2	0.705	0.768	0.76	0.667	0.71	0.687	0.769	0.675	0.738	0.666	0.717
K_2O	5.46	5.64	5.63	5.385	5.462	5.555	5.548	5.341	5.77	5.594	5.676
CaO	0.785	0.675	0.743	0.761	0.734	0.683	0.732	0.683	0.763	0.748	0.725
FeO	2.901	2.786	2.707	2.756	2.819	2.688	2.894	2.654	2.794	2.813	2.864
MnO	0.203	0.224	0.168	0.219	0.189	0.225	0.246	0.197	0.223	0.217	0.195
Total	94.95	95.454	96.373	94.369	98.034	95.48	95.175	97.202	96.341	95.304	96.948

Table B.1: Con't

	G050-036	G050-037	G050-038	LT054-001	LT054-002	LT054-003	LT054-004	LT054-005	LT054-006	LT054-007	LT054-008
Na_2O	6.067	5.607	6.718	7.22	7.398	6.673	6.268	7.196	7.447	7.236	7.029
Al_2O_3	19.57	19.293	19.654	18.375	18.834	18.082	17.987	18.508	18.643	18.099	18.155
SiO_2	60.072	59.661	61.039	54.909	56.092	53.776	53.749	53.951	54.178	52.574	53.681
MgO	0.395	0.373	0.378	1.743	1.57	1.592	1.781	2.106	1.972	1.713	2.019
TiO_2	0.698	0.69	0.703	1.699	1.586	1.734	1.669	1.825	1.814	1.662	1.903
K_2O	5.631	5.314	5.722	4.333	4.548	4.451	3.455	4.014	4.089	4.216	4.092
CaO	0.71	0.658	0.708	4.335	3.836	4.641	5.506	5.416	4.726	4.477	4.969
FeO	2.85	2.922	2.876	5.192	4.662	4.756	4.937	5.611	5.714	5.083	5.711
MnO	0.212	0.223	0.262	0.198	0.201	0.157	0.171	0.13	0.241	0.185	0.136
Total	96.205	94.741	98.06	98.001	98.727	95.862	95.523	98.787	98.824	95.245	97.695

Table B.1: Con't

	LT054-009	LT054-010	LT054-011	LT054-012	LT054-013	LT054-014	LT054-018	LT054-019	LT054-020	LT054-021	LT054-022
Na_2O	7.16	7.349	6.99	7.438	7.665	7.703	7.474	7.528	7.289	8.172	7.466
Al_2O_3	18.556	18.839	18.353	19.194	19.269	19.547	19.021	19.474	19.334	20.407	19.171
SiO_2	54.602	55.242	54.223	57.017	57.672	57.568	55.442	56.985	57.749	59.279	56.689
MgO	1.748	1.754	1.262	0.867	0.956	0.991	1.14	0.894	0.687	0.788	1.185
TiO_2	1.657	1.773	1.362	1.117	1.13	1.169	1.345	1.034	0.991	1.018	1.215
K_2O	4.367	4.42	4.551	4.911	4.942	5.014	4.715	5.038	3.87	3.61	4.782
CaO	4.574	4.361	5.11	3.039	2.722	2.714	2.869	2.547	3.093	3.661	3.05
FeO	5.274	4.654	4.208	3.401	3.842	3.74	5.455	3.577	2.985	2.989	3.389
MnO	0.146	0.177	0.152	0.169	0.158	0.165	0.205	0.144	0.154	0.112	0.132
Total	98.084	98.569	96.211	97.153	98.356	98.611	97.666	97.221	96.152	100.036	97.079

Table B.1: Con't

	LT054-023	LT054-0224	LT054-025	LT054-026	LT054-027	LT054-028	LT054-029	LT054-030	LT054-031	LT054-032	LT055-001
Na_2O	7.835	7.662	7.801	7.608	7.623	7.806	7.128	7.581	7.472	6.982	7.45
Al_2O_3	19.681	19.022	19.359	19.166	19.819	19.669	18.64	19.155	18.856	18.717	18.684
SiO_2	57.809	56.981	56.686	56.934	58.282	57.778	54.992	56.019	54.54	54.362	55.366
MgO	1.046	1.404	1.223	1.11	0.938	1.204	1.603	1.479	1.58	1.677	1.623
TiO_2	1.084	1.292	1.352	1.177	1.118	1.244	1.617	1.465	1.478	1.699	1.558
K_2O	4.957	4.795	4.7	4.891	5.021	4.789	4.545	4.515	4.376	4.44	4.504
CaO	2.742	3.23	3.217	3.116	2.547	3.043	4.227	3.797	4.015	4.219	4.417
FeO	4.053	4.321	4.449	4.076	3.591	3.891	4.785	4.733	4.969	5.313	4.93
MnO	0.176	0.217	0.2	0.142	0.144	0.154	0.205	0.169	0.187	0.179	0.181
Total	99.383	98.924	98.987	98.22	99.083	99.578	97.742	98.913	97.473	97.588	98.713

Table B.1: Con't

	LT055-002	LT055-003	LT055-004	LT055-005	LT055-006	LT055-007	LT055-008	LT055-009	LT055-010	LT055-011	LT055-012
Na_2O	7.152	7.752	7.459	6.23	6.231	7.418	7.362	7.43	7.507	7.63	7.141
Al_2O_3	18.534	18.826	19.053	18.072	18.086	18.615	18.687	18.516	18.713	18.938	18.266
SiO_2	54.729	55.826	55.776	52.879	51.613	54.621	54.091	53.936	54.627	55.752	53.927
MgO	1.673	1.601	1.434	2.758	2.255	1.633	1.873	1.756	1.677	1.65	1.902
TiO_2	1.494	1.675	1.439	2.084	2.06	1.772	1.712	1.675	1.508	1.59	1.738
K_2O	4.541	4.437	4.67	3.845	4.041	4.536	4.238	4.219	4.304	4.442	4.195
CaO	4.421	4.101	3.811	7.27	5.945	4.02	4.749	4.458	4.238	4.263	4.856
FeO	4.907	4.992	4.673	6.084	5.815	5.037	5.447	5.557	5.003	5.045	5.319
MnO	0.217	0.189	0.191	0.225	0.175	0.163	0.178	0.218	0.192	0.191	0.165
Total	97.668	99.399	98.506	99.447	96.221	97.815	98.337	97.765	97.769	99.501	97.509

Table B.1: Con't

	LT055-013	LT055-014	LT055-017	LT055-019	LT055-020	LT055-021	LT055-022	LT055-023	LT055-024	LT055-025	LT055-026
Na_2O	7.527	7.418	7.663	7.049	7.731	7.8	7.777	8.019	7.886	7.838	7.567
Al_2O_3	19.146	19.306	19.131	18.173	19.394	19.265	19.268	19.405	19.316	19.302	19.08
SiO_2	56.983	57.867	56.828	56.076	57.181	56.208	57.141	57.411	57.5	57.517	56.713
MgO	1.487	1.089	1.012	1.541	1.187	1.227	1.146	1.057	0.988	1.062	1.497
TiO_2	1.488	1.216	1.013	1.292	1.164	1.338	1.178	1.125	1.064	1.205	1.348
K_2O	4.749	4.949	4.856	4.844	4.898	4.695	4.793	4.891	4.899	4.98	4.656
CaO	3.655	2.956	2.716	3.122	2.957	3.447	3.228	3.116	3.025	3.072	3.52
FeO	4.187	3.683	3.925	4.118	4.04	4.373	4.268	4.008	3.925	4.111	4.372
MnO	0.157	0.146	0.176	0.191	0.207	0.193	0.168	0.166	0.156	0.219	0.21
Total	99.379	98.63	97.32	96.406	98.759	98.546	98.967	99.198	98.759	99.306	98.963

Table B.1: Con't

	LT055-027	LT055-028	LT055-029	LT056-001	LT056-002	LT056-003	LT056-004	LT056-006	LT056-007	LT056-008	LT056-009
Na_2O	7.54	7.937	7.836	7.494	7.015	7.047	7.208	5.938	6.806	7.464	7.221
Al_2O_3	19.333	19.627	19.48	19.177	18.481	18.925	18.478	18.613	18.417	18.066	18.474
SiO_2	55.906	58.6	58.648	56.158	55.081	55.171	54.395	52.82	54.359	53.634	54.634
MgO	1.11	0.819	0.723	1.418	1.574	1.744	1.821	1.573	1.552	1.405	1.553
TiO_2	1.032	1.045	0.952	1.465	1.683	1.755	1.785	1.713	1.603	1.474	1.617
K_2O	4.926	5.155	5.22	4.62	4.638	4.334	4.292	2.76	2.879	4.448	4.575
CaO	2.762	2.198	2.094	3.912	3.87	4.272	4.372	6.408	5.848	3.401	3.964
FeO	3.816	3.441	3.282	4.574	4.351	5.271	5.247	5.526	5.469	4.348	5.061
MnO	0.153	0.175	0.156	0.158	0.105	0.154	0.177	0.129	0.13	0.131	0.202
Total	96.578	98.997	98.391	99.006	96.798	98.673	97.775	95.48	97.063	94.371	97.301

Table B.1: Con't

	LT056-010	LT056-011	LT056-012	LT056-013	LT056-014	LT056-015	LT056-016	LT056-017	LT057-001	LT057-002	LT057-003
Na_2O	7.607	7.555	7.661	7.561	7.636	7.832	7.629	7.614	7.905	7.683	7.166
Al_2O_3	19.406	19.581	19.407	19.692	19.466	19.387	19.215	19.527	19.02	19.304	19.43
SiO_2	58.33	58.663	58.277	59.152	58.148	58.391	57.418	57.494	57.732	58.012	58.005
MgO	0.731	0.691	0.768	0.634	0.8	0.797	0.89	1.03	1.032	0.956	0.98
TiO_2	0.867	0.835	0.974	0.943	0.889	0.937	1.063	1.073	1.105	1.134	1.096
K_2O	4.986	5.181	5.113	5.382	5.049	5.073	4.938	4.985	4.933	5.057	4.98
CaO	2.445	2.521	2.44	2.101	2.683	2.697	2.993	2.871	2.898	2.635	2.919
FeO	3.361	3.347	3.455	3.021	3.492	3.429	3.71	3.975	3.905	3.635	3.9
MnO	0.152	0.193	0.167	0.132	0.2	0.197	0.199	0.188	0.154	0.133	0.143
Total	97.885	98.567	98.262	98.618	98.363	98.74	98.055	98.757	98.684	98.549	98.619

Table B.1: Con't

	LT057-004	LT057-005	LT057-006	LT057-008	LT057-012	LT057-013	LT057-014	LT057-017	LT057-020	LT057-021	LT057-025
Na_2O	7.637	7.043	7.515	6.944	6.729	6.223	6.947	7.073	6.882	6.839	6.811
Al_2O_3	19.083	19.405	19.121	17.899	18.223	18.034	17.564	18.44	17.996	19.261	19.368
SiO_2	57.003	58.061	56.496	53.075	53.186	52.605	51.314	50.962	52.85	59.145	59.456
MgO	1.019	0.946	1.112	2.07	2.173	2.114	2.02	2.038	1.872	0.576	0.37
TiO_2	1.134	1.08	1.203	1.914	1.934	2.006	1.968	2.113	1.996	0.847	0.674
K_2O	4.926	5.17	4.734	4.059	4.049	4.094	4.032	3.271	4.236	5.422	5.587
CaO	3.115	2.913	3.452	5.1	5.495	5.347	4.827	5.429	4.625	1.976	1.436
FeO	3.905	3.59	4.33	5.982	6.095	6.005	6.122	5.86	5.437	2.766	2.429
MnO	0.148	0.159	0.174	0.207	0.204	0.169	0.212	0.169	0.134	0.147	0.17
Total	97.97	98.367	98.137	97.25	98.088	96.597	95.006	95.355	96.028	96.979	96.301

Table B.2: All feldspar EMP analyses from El Abrigo.

	019-001	019-002	019-003	019-004	019-007	019-008	019-009
SiO_2	54.775	54.136	54.599	52.648	51.429	51.411	52.049
Al_2O_3	28.26	28.476	28.679	29.558	30.399	29.674	30.279
FeO_T	0.59	0.566	0.564	0.561	0.579	0.583	0.616
MgO	0.06	0.061	0.077	0.056	0.071	0.06	0.072
BaO	0.072	0.025	0.069	0.033	0.074	0.02	0.032
SrO	0.446	0.515	0.432	0.408	0.427	0.457	0.441
CaO	11.019	11.275	11.359	12.762	13.558	13.424	13.448
Na_2O	4.93	4.826	4.689	4.07	3.596	3.537	3.681
K_2O	0.368	0.368	0.319	0.272	0.275	0.276	0.253
Total	100.52	100.25	100.79	100.37	100.41	99.44	100.87
				Oxygen = 32.000			
Si	9.891	9.815	9.832	9.564	9.368	9.448	9.428
Al	6.01	6.08	6.082	6.323	6.521	6.422	6.459
Fe*	0.089	0.086	0.085	0.085	0.088	0.09	0.093
Mg	0.016	0.016	0.021	0.015	0.019	0.016	0.019
Ba	0.005	0.002	0.005	0.002	0.005	0.001	0.002
Ca	2.132	2.19	2.192	2.484	2.646	2.643	2.61
Na	1.726	1.697	1.637	1.434	1.27	1.26	1.293
K	0.085	0.085	0.073	0.063	0.064	0.065	0.058
Ab	43.8	42.7	42	36	31.9	31.8	32.6
An	54.1	55.1	56.2	62.4	66.5	66.6	65.9
Or	2.2	2.1	1.9	1.6	1.6	1.6	1.5

Table B.2: Con't

	019-010	019-011	019-012	019-013	020-003	020-005	020-007
SiO_2	54.715	54.985	50.949	51.86	48.896	49.656	48.797
Al_2O_3	28.387	28.249	30.598	30.482	30.848	30.622	31.668
FeO_T	0.632	0.644	0.693	0.576	0.646	0.697	0.668
MgO	0.082	0.075	0.073	0.06	0.058	0.068	0.048
BaO	0.061	0.04 -		0.04	0.009	0.033	0.045
SrO	0.395	0.437	0.366	0.431	0.457	0.454	0.508
CaO	11.388	11.119	14.129	13.617	14.681	14.32	15.072
Na_2O	4.689	4.902	3.328	3.626	2.874	2.995	2.652
K_2O	0.348	0.346	0.278	0.243	0.179	0.195	0.169
Total	100.7	100.8	100.41	100.94	98.65	99.04	99.63
				Oxygen = 32.000			
Si	9.864	9.9	9.293	9.391	9.104	9.196	9.007
Al	6.027	5.99	6.572	6.5	6.764	6.679	6.884
Fe*	0.095	0.097	0.106	0.087	0.101	0.108	0.103
Mg	0.022	0.02	0.02	0.016	0.016	0.019	0.013
Ba	0.004	0.003	0	0.003	0.001	0.002	0.003
Ca	2.2	2.145	2.761	2.642	2.929	2.841	2.981
Na	1.639	1.711	1.177	1.273	1.038	1.075	0.949
K	0.08	0.079	0.065	0.056	0.043	0.046	0.04
Ab	41.8	43.5	29.4	32.1	25.9	27.1	23.9
An	56.1	54.5	69	66.5	73	71.7	75.1
Or	2	2	1.6	1.4	1.1	1.2	1

Table B.2: Con't

	020-008	020-010	020-013	020-014	020-016	021-001	021-004
SiO_2	49.873	49.756	52.817	55.601	49.706	50.517	49.909
Al_2O_3	31.31	31.584	29.834	26.146	30.259	30.393	31.299
FeO_T	0.691	0.641	0.633	0.614	0.576	0.511	0.606
MgO	0.047	0.058	0.073	0.042	0.061	0.062	0.051
BaO	0.037	0.028	0.072	0.261	0.047	0.045	0.059
SrO	0.527	0.581	0.46	0.706	0.46	0.536	0.512
CaO	14.766	14.819	12.632	8.99	14.294	14.111	14.877
Na_2O	2.715	2.844	4.066	5.717	2.923	3.211	2.87
K_2O	0.183	0.189	0.27	0.55	0.188	0.17	0.181
Total	100.15	100.5	100.86	98.63	98.51	99.56	100.36
				Oxygen = 32.000			
Si	9.138	9.094	9.55	10.223	9.245	9.292	9.131
Al	6.756	6.798	6.353	5.661	6.628	6.584	6.744
Fe*	0.106	0.098	0.096	0.094	0.09	0.079	0.093
Mg	0.013	0.016	0.02	0.012	0.017	0.017	0.014
Ba	0.003	0.002	0.005	0.019	0.003	0.003	0.004
Ca	2.899	2.902	2.447	1.771	2.849	2.781	2.916
Na	0.965	1.008	1.426	2.038	1.054	1.145	1.018
K	0.043	0.044	0.062	0.129	0.045	0.04	0.042
Ab	24.7	25.5	36.2	51.8	26.7	28.9	25.6
An	74.2	73.4	62.2	45	72.2	70.1	73.3
Or	1.1	1.1	1.6	3.3	1.1	1	1.1

Table B.2: Con't

	022-001	022-002	022-004	022-005	022-006	023-002	023-003
SiO_2	61.829	62.135	62.713	62.219	62.24	64.998	64.455
Al_2O_3	22.21	22.643	22.673	22.616	22.961	20.97	20.82
FeO_T	0.398	0.364	0.388	0.429	0.373	0.329	0.375
MgO	0.017	0.014	0.015	0.013	0.029	0.004	0.006
BaO	1.35	1.127	1.105	1.122	1.02	0.911	0.84
SrO	0.247	0.269	0.241	0.245	0.282	0.103	0.094
CaO	3.417	3.992	4.11	4.048	4.315	2.143	2.233
Na_2O	7.793	7.762	7.968	7.793	7.864	8.197	7.881
K_2O	2.189	1.774	1.769	1.864	1.62	3.366	3.241
Total	99.45	100.08	100.98	100.35	100.7	101.02	99.95
				Oxygen = 32.000			
Si	11.205	11.16	11.168	11.156	11.109	11.545	11.553
Al	4.74	4.789	4.755	4.776	4.826	4.386	4.395
Fe*	0.06	0.055	0.058	0.064	0.056	0.049	0.056
Mg	0.005	0.004	0.004	0.003	0.008	0.001	0.002
Ba	0.096	0.079	0.077	0.079	0.071	0.063	0.059
Ca	0.663	0.768	0.784	0.778	0.825	0.408	0.429
Na	2.738	2.703	2.751	2.709	2.722	2.823	2.739
K	0.506	0.406	0.402	0.426	0.369	0.763	0.741
Ab	70.1	69.7	69.9	69.2	69.5	70.7	70.1
An	17	19.8	19.9	19.9	21.1	10.2	11
Or	13	10.5	10.2	10.9	9.4	19.1	19

Table B.2: Con't

	023-008	023-009	023-010	024-004	024-005	024-008	024-010
SiO_2	64.698	64.967	64.4	62.003	62.262	62.503	61.749
Al_2O_3	21.101	20.46	21.12	23.182	23.106	22.688	23.436
FeO_T	0.38	0.355	0.413	0.397	0.433	0.458	0.414
MgO	0.005	0.007	0.006	0.02	0.009	0.006	0.013
BaO	0.795	0.88	0.829	1.288	1.256	1.207	1.15
SrO	0.125	0.098	0.123	0.301	0.3	0.293	0.294
CaO	2.386	1.837	2.407	4.545	4.23	3.864	4.742
Na_2O	7.988	7.941	8.039	7.626	7.546	7.933	7.65
K_2O	3.242	3.708	3.212	1.524	1.6	1.77	1.467
Total	100.72	100.25	100.55	100.89	100.74	100.72	100.92
				Oxygen = 32.000			
Si	11.516	11.624	11.492	11.067	11.113	11.166	11.017
Al	4.423	4.311	4.439	4.873	4.857	4.773	4.924
Fe*	0.057	0.053	0.062	0.059	0.065	0.068	0.062
Mg	0.001	0.002	0.002	0.005	0.002	0.002	0.003
Ba	0.055	0.062	0.058	0.09	0.088	0.084	0.08
Ca	0.455	0.352	0.46	0.869	0.809	0.74	0.906
Na	2.757	2.755	2.782	2.639	2.611	2.748	2.646
K	0.736	0.846	0.731	0.347	0.364	0.403	0.334
Ab	69.8	69.7	70	68.5	69	70.6	68.1
An	11.5	8.9	11.6	22.5	21.4	19	23.3
Or	18.6	21.4	18.4	9	9.6	10.4	8.6

Table B.2: Con't

	024-011	024-013	024-014	024-013	024-016	024-017	024-018
SiO_2	62.005	61.846	62.02	61.846	61.998	61.255	61.625
Al_2O_3	23.081	23.18	23.133	23.18	22.726	22.969	23.039
FeO_T	0.424	0.412	0.37	0.412	0.411	0.397	0.402
MgO	0.019	0.016	-	0.016	0.012	0.021	0.011
BaO	1.254	1.196	1.31	1.196	1.195	1.194	1.127
SrO	0.29	0.373	0.386	0.373	0.336	0.311	0.287
CaO	4.409	4.631	4.433	4.631	4.165	4.74	4.686
Na_2O	7.768	7.74	7.666	7.74	7.892	7.454	7.754
K_2O	1.594	1.497	1.596	1.497	1.595	1.427	1.445
Total	100.84	100.89	100.91	100.89	100.33	99.77	100.38
				Oxygen = 32.000			
Si	11.076	11.047	11.076	11.047	11.125	11.052	11.053
Al	4.856	4.876	4.865	4.876	4.802	4.881	4.866
Fe*	0.063	0.062	0.055	0.062	0.062	0.06	0.06
Mg	0.005	0.004	0	0.004	0.003	0.006	0.003
Ba	0.088	0.084	0.092	0.084	0.084	0.084	0.079
Ca	0.844	0.886	0.848	0.886	0.801	0.916	0.901
Na	2.691	2.681	2.654	2.681	2.746	2.608	2.697
K	0.363	0.341	0.364	0.341	0.365	0.328	0.331
Ab	69	68.6	68.6	68.6	70.2	67.7	68.6
An	21.7	22.7	21.9	22.7	20.5	23.8	22.9
Or	9.3	8.7	9.4	8.7	9.3	8.5	8.4

Table B.2: Con't

	024-019	LT021-001	LT021-002	LT021-003	LT021-004	LT021-005	LT021-007
SiO_2	62.221	53.751	53.686	53.285	52.514	53.679	53.82
Al_2O_3	22.907	28.988	28.776	28.874	28.388	29.087	28.982
FeO_T	0.367	0.558	0.579	0.564	0.508	0.522	0.54
MgO	0.002	0.044	0.051	0.061	0.052	0.067	0.056
BaO	1.274	0.069	0.104	0.071	0.088	0.059	0.048
SrO	0.371	0.591	0.514	0.575	0.554	0.496	0.534
CaO	4.301	11.782	11.761	12.108	11.978	11.993	11.751
Na_2O	7.774	4.499	4.414	4.443	4.231	4.406	4.499
K_2O	1.64	0.346	0.325	0.329	0.36	0.337	0.296
Total	100.86	100.63	100.21	100.31	98.67	100.65	100.53
				Oxygen = 32.000			
Si	11.113	9.725	9.748	9.686	9.7	9.706	9.736
Al	4.818	6.176	6.153	6.181	6.175	6.194	6.174
Fe*	0.055	0.084	0.088	0.086	0.078	0.079	0.082
Mg	0.001	0.012	0.014	0.017	0.014	0.018	0.015
Ba	0.089	0.005	0.007	0.005	0.006	0.004	0.003
Ca	0.823	2.284	2.288	2.358	2.37	2.323	2.278
Na	2.692	1.578	1.554	1.566	1.515	1.545	1.578
K	0.374	0.08	0.075	0.076	0.085	0.078	0.068
Ab	69.2	40	39.7	39.2	38.2	39.2	40.2
An	21.2	57.9	58.4	59	59.7	58.9	58.1
Or	9.6	2	1.9	1.9	2.1	2	1.7

Table B.2: Con't

	LT021-008	LT021-009	LT021-010	LT021-011	LT021-012	LT021-013	LT021-014
SiO_2	53.618	53.345	53.616	53.037	52.904	52.709	52.35
Al_2O_3	28.844	28.91	29.184	29.284	29.353	29.588	30.05
FeO_T	0.507	0.544	0.543	0.501	0.528	0.534	0.502
MgO	0.051	0.048	0.06	0.066	0.039	0.07	0.057
BaO	0.074	0.109	0.082	0.075	0.063	0.026	0.032
SrO	0.527	0.49	0.51	0.517	0.543	0.526	0.492
CaO	11.926	12.155	12.274	12.313	12.512	12.773	13.151
Na_2O	4.424	4.196	4.404	4.165	4.102	3.968	3.779
K_2O	0.322	0.32	0.285	0.292	0.289	0.249	0.246
Total	100.29	100.12	100.96	100.25	100.33	100.44	100.66
				Oxygen = 32.000			
Si	9.73	9.701	9.676	9.637	9.612	9.567	9.489
Al	6.164	6.192	6.203	6.266	6.281	6.325	6.414
Fe*	0.077	0.083	0.082	0.076	0.08	0.081	0.076
Mg	0.014	0.013	0.016	0.018	0.011	0.019	0.015
Ba	0.005	0.008	0.006	0.005	0.004	0.002	0.002
Ca	2.319	2.368	2.373	2.397	2.436	2.484	2.554
Na	1.557	1.48	1.541	1.467	1.445	1.397	1.328
K	0.075	0.074	0.066	0.068	0.067	0.058	0.057
Ab	39.4	37.7	38.7	37.3	36.6	35.5	33.7
An	58.7	60.4	59.6	61	61.7	63.1	64.8
Or	1.9	1.9	1.7	1.7	1.7	1.5	1.4

Table B.2: Con't

	LT021-015	LT021-016	LT021-018	LT021-020	LT021-023	LT021-024	LT021-025
SiO_2	52.254	52.557	51.133	50.809	49.32	52.534	52.599
Al_2O_3	30.086	29.77	29.489	29.81	28.29	29.958	29.994
FeO_T	0.589	0.564	0.527	0.509	0.535	0.538	0.52
MgO	0.05	0.059	0.065	0.06	0.047	0.058	0.054
BaO	0.051	0.05	0.052	0.069	0.055	0.028	0.029
SrO	0.529	0.519	0.455	0.441	0.428	0.443	0.492
CaO	13.359	13.109	12.873	13.027	12.88	12.866	13.009
Na_2O	3.866	4.022	3.755	3.582	3.497	3.973	4.019
K_2O	0.233	0.255	0.255	0.255	0.279	0.269	0.271
Total	101.02	100.91	98.6	98.56	95.33	100.67	100.99
				Oxygen = 32.000			
Si	9.457	9.516	9.468	9.413	9.461	9.516	9.506
Al	6.412	6.348	6.43	6.504	6.391	6.391	6.384
Fe*	0.089	0.085	0.082	0.079	0.086	0.082	0.079
Mg	0.013	0.016	0.018	0.017	0.013	0.016	0.015
Ba	0.004	0.004	0.004	0.005	0.004	0.002	0.002
Ca	2.59	2.543	2.554	2.586	2.647	2.497	2.519
Na	1.357	1.412	1.348	1.287	1.301	1.395	1.408
K	0.054	0.059	0.06	0.06	0.068	0.062	0.062
Ab	33.9	35.2	34	32.7	32.4	35.3	35.3
An	64.7	63.4	64.5	65.8	65.9	63.2	63.1
Or	1.3	1.5	1.5	1.5	1.7	1.6	1.6

Table B.2: Con't

	LT021-028	LT021-029	LT021-030	LT021-031	LT021-032	LT021-033	LT021-035
SiO_2	52.53	52.616	52.904	52.65	52.744	52.648	52.742
Al_2O_3	29.713	29.762	29.867	29.823	29.711	29.776	29.531
FeO_T	0.577	0.535	0.496	0.527	0.462	0.512	0.53
MgO	0.051	0.056	0.056	0.052	0.053	0.063	0.061
BaO		0.035	0.023	0.039	0.034	0.049	0.062
SrO	0.449	0.425	0.469	0.426	0.435	0.481	0.501
CaO	12.93	12.869	12.765	12.826	12.792	12.723	12.68
Na_2O	4.049	4.039	4.104	4.009	4.147	4.009	4.072
K_2O	0.259	0.271	0.272	0.241	0.268	0.267	0.257
Total	100.56	100.61	100.96	100.59	100.65	100.53	100.44
				Oxygen = 32.000			
Si	9.531	9.538	9.552	9.54	9.554	9.548	9.576
Al	6.349	6.354	6.351	6.364	6.338	6.359	6.314
Fe*	0.088	0.081	0.075	0.08	0.07	0.078	0.08
Mg	0.014	0.015	0.015	0.014	0.014	0.017	0.017
Ba	0	0.002	0.002	0.003	0.002	0.003	0.004
Ca	2.514	2.499	2.469	2.49	2.483	2.472	2.467
Na	1.425	1.42	1.437	1.409	1.457	1.41	1.434
K	0.06	0.063	0.063	0.056	0.062	0.062	0.06
Ab	35.6	35.7	36.2	35.6	36.4	35.8	36.2
An	62.9	62.8	62.2	63	62	62.7	62.3
Or	1.5	1.6	1.6	1.4	1.5	1.6	1.5

Table B.2: Con't

	LT021-036	LT021-037	LT021-038	LT021-040	LT021-041	LT021-044	LT021-045
SiO_2	53.007	52.599	52.282	52.768	52.654	52.635	52.698
Al_2O_3	29.767	29.583	29.478	29.517	29.538	29.46	29.508
FeO_T	0.528	0.53	0.527	0.56	0.514	0.54	0.519
MgO	0.065	0.056	0.058	0.045	0.049	0.061	0.069
BaO	0.021	0.007	0.002	0.066	0.051	0.035	0.049
SrO	0.44	0.493	0.466	0.445	0.427	0.429	0.485
CaO	12.719	12.7	12.574	12.653	12.714	12.682	12.703
Na_2O	4.074	3.884	4.039	3.987	4.223	4.127	4.058
K_2O	0.268	0.274	0.273	0.246	0.28	0.292	0.277
Total	100.89	100.13	99.7	100.29	100.45	100.26	100.37
				Oxygen = 32.000			
Si	9.572	9.57	9.557	9.587	9.562	9.573	9.574
Al	6.331	6.339	6.346	6.316	6.317	6.31	6.314
Fe*	0.08	0.081	0.081	0.085	0.078	0.082	0.079
Mg	0.017	0.015	0.016	0.012	0.013	0.017	0.019
Ba	0.001	0	0	0.005	0.004	0.002	0.003
Ca	2.461	2.476	2.463	2.463	2.474	2.471	2.473
Na	1.427	1.37	1.432	1.405	1.487	1.455	1.43
K	0.062	0.064	0.064	0.057	0.065	0.068	0.064
Ab	36.1	35	36.2	35.8	36.9	36.4	36
An	62.3	63.3	62.2	62.8	61.5	61.9	62.3
Or	1.6	1.6	1.6	1.5	1.6	1.7	1.6

Table B.2: Con't

	LT021-046	LT021-047	LT021-048	LT021-050	LT021-051	LT021-052	LT021-053
SiO_2	52.72	52.755	52.625	52.889	52.069	52.438	53.286
Al_2O_3	29.778	29.714	29.571	29.489	29.237	29.767	28.623
FeO_T	0.488	0.513	0.492	0.505	0.518	0.492	0.509
MgO	0.062	0.045	0.053	0.056	0.064	0.053	0.062
BaO	0.051	0.049	0.047	0.034	0.02 -		0.07
SrO	0.499	0.457	0.512	0.477	0.475	0.428	0.513
CaO	12.743	12.68	12.766	12.641	12.709	12.807	11.928
Na_2O	4.043	4.11	4.061	4.099	4.045	3.852	4.54
K_2O	0.268	0.274	0.272	0.286	0.254	0.288	0.317
Total	100.65	100.6	100.4	100.48	99.39	100.13	99.85
				Oxygen = 32.000			
Si	9.55	9.56	9.561	9.593	9.557	9.54	9.721
Al	6.353	6.342	6.327	6.299	6.32	6.378	6.149
Fe*	0.074	0.078	0.075	0.077	0.08	0.075	0.078
Mg	0.017	0.012	0.014	0.015	0.018	0.014	0.017
Ba	0.004	0.003	0.003	0.002	0.001	0	0.005
Ca	2.473	2.462	2.485	2.457	2.499	2.496	2.331
Na	1.42	1.444	1.431	1.442	1.44	1.359	1.606
K	0.062	0.063	0.063	0.066	0.059	0.067	0.074
Ab	35.9	36.4	36	36.4	36	34.7	40
An	62.5	62	62.5	62	62.5	63.6	58.1
Or	1.6	1.6	1.6	1.7	1.5	1.7	1.8

Table B.2: Con't

	LT021-057	LT021-058	LT021-059	LT022-001	LT022-003	LT022-004	LT022-005
SiO_2	52.466	54.607	54.733	53.534	53.626	53.405	53.401
Al_2O_3	30.133	28.319	28.157	29.355	29.083	29.174	29.058
FeO_T	0.576	0.663	0.635	0.548	0.578	0.569	0.552
MgO	0.068	0.07	0.07	0.065	0.051	0.063	0.065
BaO	0.047	0.034	0.088	0.078	0.056	0.047	0.043
SrO	0.462	0.51	0.484	0.491	0.502	0.491	0.535
CaO	12.971	11.27	11.064	12.084	12.078	12.077	12.064
Na_2O	3.948	4.861	4.884	4.402	4.362	4.427	4.367
K_2O	0.281	0.364	0.379	0.268	0.277	0.296	0.288
Total	100.95	100.7	100.49	100.83	100.61	100.55	100.37
			Oxygen = 32.000				
Si	9.486	9.857	9.893	9.666	9.701	9.672	9.687
Al	6.416	6.02	5.994	6.242	6.196	6.222	6.207
Fe*	0.087	0.1	0.096	0.083	0.087	0.086	0.084
Mg	0.018	0.019	0.019	0.017	0.014	0.017	0.018
Ba	0.003	0.002	0.006	0.006	0.004	0.003	0.003
Ca	2.513	2.18	2.143	2.338	2.341	2.343	2.345
Na	1.384	1.701	1.712	1.541	1.53	1.555	1.536
K	0.065	0.084	0.087	0.062	0.064	0.068	0.067
Ab	34.9	42.9	43.4	39.1	38.9	39.2	38.9
An	63.4	55	54.4	59.3	59.5	59.1	59.4
Or	1.6	2.1	2.2	1.6	1.6	1.7	1.7

Table B.2: Con't

	LT022-006	LT022-007	LT022-008	LT022-009	LT022-010	LT022-011	LT022-012
SiO_2	53.552	53.541	54.197	53.701	53.751	52.353	52.969
Al_2O_3	29.137	29.017	28.959	28.96	29.041	29.544	29.288
FeO_T	0.538	0.527	0.582	0.54	0.575	0.521	0.58
MgO	0.075	0.059	0.071	0.058	0.059	0.056	0.086
BaO	0.077	0.06	0.059	0.098	0.083	0.034	0.039
SrO	0.5	0.508	0.553	0.468	0.482	0.552	0.516
CaO	12.111	12.028	11.569	11.863	11.864	12.818	12.338
Na_2O	4.428	4.363	4.58	4.439	4.416	3.909	4.195
K_2O	0.289	0.304	0.314	0.325	0.296	0.237	0.263
Total	100.71	100.41	100.88	100.45	100.57	100.02	100.27
			Oxygen = 32.000				
Si	9.684	9.704	9.767	9.726	9.722	9.547	9.625
Al	6.205	6.194	6.146	6.177	6.186	6.345	6.267
Fe*	0.081	0.08	0.088	0.082	0.087	0.079	0.088
Mg	0.02	0.016	0.019	0.016	0.016	0.015	0.023
Ba	0.005	0.004	0.004	0.007	0.006	0.002	0.003
Ca	2.346	2.336	2.234	2.302	2.299	2.504	2.402
Na	1.553	1.533	1.6	1.559	1.549	1.382	1.478
K	0.067	0.07	0.072	0.075	0.068	0.055	0.061
Ab	39.2	38.9	41	39.6	39.6	35.1	37.5
An	59.2	59.3	57.2	58.5	58.7	63.5	60.9
Or	1.7	1.8	1.8	1.9	1.7	1.4	1.5

Table B.2: Con't

	LT022-013	LT023-001	LT023-002	LT023-003	LT023-004	LT023-005	LT023-007
SiO_2	53.409	65.742	65.881	63.273	65.736	64.371	66.179
Al_2O_3	29.213	19.686	19.729	21.266	19.901	21.016	19.659
FeO_T	0.545	0.286	0.252	0.251	0.232	0.238	0.265
MgO	0.064	0.011	0.015	0.015	0.003	0.014	0.009
BaO	0.054	0.382	0.388	0.411	0.417	0.357	0.358
SrO	0.534	0.042	0.042	0.037	0.019	0.053	0.025
CaO	12.053	0.73	0.736	0.968	0.76	0.923	0.725
Na_2O	4.351	6.04	5.881	5.649	6.192	5.879	6.045
K_2O	0.284	7.42	7.623	7.126	7.608	7.272	7.656
Total	100.51	100.34	100.55	99	100.87	100.12	100.92
				Oxygen = 32.000			
Si	9.674	11.813	11.817	11.529	11.771	11.597	11.829
Al	6.231	4.166	4.167	4.563	4.197	4.459	4.138
Fe*	0.083	0.043	0.038	0.038	0.035	0.036	0.04
Mg	0.017	0.003	0.004	0.004	0.001	0.004	0.002
Ba	0.004	0.027	0.027	0.029	0.029	0.025	0.025
Ca	2.339	0.141	0.141	0.189	0.146	0.178	0.139
Na	1.528	2.104	2.045	1.996	2.15	2.054	2.095
K	0.066	1.701	1.744	1.656	1.738	1.671	1.746
Ab	38.9	53.3	52	52	53.3	52.6	52.6
An	59.5	3.6	3.6	4.9	3.6	4.6	3.5
Or	1.7	43.1	44.4	43.1	43.1	42.8	43.9

Table B.2: Con't

	LT023-009	LT023-011	LT023-013	LT023-015	LT023-016	LT023-017	LT023-018
SiO_2	65.411	62.724	64.962	64.536	62.208	65.666	63.025
Al_2O_3	19.78	22.081	20.403	20.459	21.861	20.194	21.071
FeO_T	0.279	0.283	0.274	0.294	0.244	0.283	0.263
MgO	0.017	0.031	0.008	0.017	0.017	0.008	0.016
BaO	0.376	0.378	0.398	0.318	0.308	0.423	0.441
SrO	0.022	0.032	0.029	0.045	0.026	0.055	0.036
CaO	0.763	1.178	1.141	1.42	1.823	1.341	1.271
Na_2O	6.03	6.131	6.287	6.678	6.482	6.503	5.889
K_2O	7.554	6.646	6.735	5.87	5.232	6.366	6.412
Total	100.23	99.48	100.24	99.64	98.2	100.84	98.42
				Oxygen = 32.000			
Si	11.779	11.379	11.677	11.641	11.374	11.72	11.531
Al	4.195	4.718	4.319	4.346	4.707	4.245	4.54
Fe*	0.042	0.043	0.041	0.044	0.037	0.042	0.04
Mg	0.005	0.008	0.002	0.005	0.005	0.002	0.004
Ba	0.027	0.027	0.028	0.022	0.022	0.03	0.032
Ca	0.147	0.229	0.22	0.274	0.357	0.256	0.249
Na	2.106	2.157	2.191	2.336	2.298	2.251	2.089
K	1.735	1.538	1.544	1.351	1.22	1.45	1.497
Ab	52.8	55	55.4	59	59.3	56.9	54.5
An	3.7	5.8	5.6	6.9	9.2	6.5	6.5
Or	43.5	39.2	39	34.1	31.5	36.6	39

Table B.2: Con't

	LT023-019	LT023-020	LT023-023	LT023-024	LT023-025	LT023-026	LT023-027
SiO_2	65.766	63.807	62.678	64.907	60.817	62.599	64.731
Al_2O_3	20.225	21.297	22.599	21.163	23.074	21.208	21.208
FeO_T	0.273	0.286	0.286	0.272	0.298	0.297	0.278
MgO	0.003	0.02	0.022	0.006	0.022	0.031	0.022
BaO	0.425	0.318	0.305	0.434	0.318	0.316	0.263
SrO	0.038	0.034	0.048	0.059	0.034	0.052	0.036
CaO	1.47	1.675	1.851	1.371	1.721	1.323	1.894
Na_2O	6.869	6.859	7.005	6.708	6.081	6.082	7.177
K_2O	5.838	5.569	4.953	5.882	5.631	6.244	4.812
Total	100.91	99.86	99.75	100.8	98	98.15	100.42
				Oxygen = 32.000			
Si	11.713	11.491	11.289	11.578	11.172	11.483	11.546
Al	4.242	4.517	4.793	4.446	4.992	4.582	4.455
Fe*	0.041	0.043	0.043	0.041	0.046	0.046	0.041
Mg	0.001	0.005	0.006	0.002	0.006	0.008	0.006
Ba	0.03	0.022	0.022	0.03	0.023	0.023	0.018
Ca	0.281	0.323	0.357	0.262	0.339	0.26	0.362
Na	2.372	2.395	2.446	2.32	2.166	2.163	2.482
K	1.326	1.28	1.138	1.338	1.32	1.461	1.095
Ab	59.6	59.9	62.1	59.2	56.6	55.7	63
An	7.1	8.1	9.1	6.7	8.9	6.7	9.2
Or	33.3	32	28.9	34.1	34.5	37.6	27.8

Table B.2: Con't

	LT023-028	LT023-029	LT023-030	LT023-031	LT023-034	LT023-035	LT023-036
SiO_2	65.014	66.097	64.946	65.272	64.64	63.809	61.039
Al_2O_3	21.327	20.247	21.409	20.566	20.835	21.069	23.275
FeO_T	0.283	0.296	0.272	0.31	0.283	0.26	0.238
MgO	0.004 -		0.024	0.009	0.008	0.019	0.026
BaO	0.196	0.209	0.177	0.179	0.169	0.111	0.121
SrO	0.096	0.048	0.053	0.022	0.035	0.017	0.004
CaO	1.614	1.436	1.505	1.395	1.399	1.404	1.658
Na_2O	7.091	7.137	6.893	6.96	7.017	6.689	6.298
K_2O	5.187	5.46	5.511	5.438	5.732	5.611	5.42
Total	100.81	100.93	100.79	100.15	100.12	98.99	98.08
				Oxygen = 32.000			
Si	11.556	11.731	11.551	11.67	11.594	11.553	11.17
Al	4.464	4.232	4.484	4.33	4.401	4.492	5.016
Fe*	0.042	0.044	0.04	0.046	0.042	0.039	0.036
Mg	0.001	0	0.006	0.002	0.002	0.005	0.007
Ba	0.014	0.015	0.012	0.013	0.012	0.008	0.009
Ca	0.307	0.273	0.287	0.267	0.269	0.272	0.325
Na	2.444	2.456	2.377	2.413	2.44	2.348	2.235
K	1.176	1.236	1.25	1.24	1.312	1.296	1.265
Ab	62.2	61.9	60.7	61.6	60.7	60	58.4
An	7.8	6.9	7.3	6.8	6.7	6.9	8.5
Or	29.9	31.2	31.9	31.6	32.6	33.1	33.1

Table B.2: Con't

	LT023-037	LT023-038	LT023-039	LT023-041	LT023-042	LT023-043	LT023-044
SiO_2	62.961	65.808	65.109	62.727	65.673	65.487	64.832
Al_2O_3	21.158	20.182	20.905	22.371	20.426	20.613	20.933
FeO_T	0.293	0.277	0.272	0.291	0.286	0.277	0.29
MgO	0.023	0.002	0.001	0.026	0.002	0.024	0.011
BaO	0.226	0.233	0.22	0.235	0.238	0.28	0.263
SrO	0.016	0.058	0.04	0.054	0.049	0.049	0.083
CaO	1.618	1.383	1.461	1.747	1.492	1.529	1.53
Na_2O	6.698	7.156	7.095	6.602	7.249	7.144	6.937
K_2O	5.334	5.678	5.538	5.271	5.495	5.438	5.391
Total	98.33	100.78	100.64	99.32	100.91	100.84	100.27
				Oxygen = 32.000			
Si	11.49	11.718	11.607	11.337	11.678	11.651	11.597
Al	4.547	4.232	4.389	4.762	4.277	4.319	4.41
Fe*	0.045	0.041	0.041	0.044	0.043	0.041	0.043
Mg	0.006	0.001	0	0.007	0.001	0.006	0.003
Ba	0.016	0.016	0.015	0.017	0.017	0.02	0.018
Ca	0.316	0.264	0.279	0.338	0.284	0.291	0.293
Na	2.37	2.471	2.453	2.314	2.499	2.465	2.406
K	1.242	1.29	1.26	1.215	1.247	1.234	1.23
Ab	60.3	61.4	61.4	59.8	62	61.8	61.2
An	8	6.6	7	8.7	7	7.3	7.5
Or	31.6	32	31.6	31.4	30.9	30.9	31.3

Table B.2: Con't

	LT023-045	LT023-047	LT023-049	LT023-050	LT023-051	LT023-052	LT023-053
SiO_2	64.121	64.389	65.455	65.533	65.765	65.182	63.436
Al_2O_3	21.181	20.993	20.43	20.736	20.459	20.55	21.679
FeO_T	0.281	0.29	0.271	0.283	0.297	0.3	0.291
MgO	0.021	0.014 -	-		0.003	0.02	0.005
BaO	0.25	0.336	0.295	0.228	0.242	0.247	0.236
SrO	0.025	0.056	0.011	0.053	0.013	0.044	0.056
CaO	1.521	1.605	1.506	1.526	1.406	1.418	1.649
Na_2O	7.031	6.921	7.066	6.975	7.067	7.011	6.783
K_2O	5.318	5.351	5.508	5.454	5.552	5.566	5.287
Total	99.75	99.96	100.54	100.79	100.8	100.34	99.42
				Oxygen = 32.000			
Si	11.533	11.565	11.678	11.653	11.694	11.654	11.449
Al	4.487	4.44	4.292	4.342	4.284	4.327	4.608
Fe*	0.042	0.044	0.04	0.042	0.044	0.045	0.044
Mg	0.006	0.004	0	0	0.001	0.005	0.001
Ba	0.018	0.024	0.021	0.016	0.017	0.017	0.017
Ca	0.293	0.309	0.288	0.291	0.268	0.272	0.319
Na	2.452	2.41	2.444	2.405	2.437	2.431	2.374
K	1.22	1.226	1.254	1.237	1.259	1.27	1.217
Ab	61.8	61.1	61.3	61.1	61.5	61.2	60.7
An	7.4	7.8	7.2	7.4	6.8	6.8	8.2
Or	30.8	31.1	31.5	31.5	31.8	32	31.1

Table B.3: All EMP analyses for pyroxene from El Abrigo.

	C007-001	C007-002	C007-003	C007-004	C007-005	C007-006
SiO_2	51.093	51.186	51.135	50.032	51.43	51.137
TiO_2	0.976	0.904	0.907	1.21	0.906	0.995
Al_2O_3	2.258	2.377	2.209	3.027	2.132	2.351
FeO_T	7.817	7.81	7.861	8.287	7.898	7.881
Cr_2O_3	0.007		0.016	0.014	0.018	
MnO	0.602	0.595	0.635	0.573	0.617	0.625
MgO	13.859	13.782	13.71	13.229	13.794	13.849
CaO	22.983	23.056	23.043	22.852	23.24	23.037
Na_2O	0.902	0.91	0.973	1.118	0.935	0.957
K_2O	0.017	0.017	0.021	0.018	0.013	0.013
Total	100.514	100.637	100.51	100.36	100.983	100.845
			Oxygen = 6.000			
Si	1.882	1.883	1.884	1.847	1.886	1.877
Al	0.098	0.103	0.096	0.132	0.092	0.102
Ti	0.027	0.025	0.025	0.034	0.025	0.027
Fe*	0.241	0.24	0.242	0.255	0.242	0.241
Cr	0	0	0	0	0.001	0
Mg	0.761	0.756	0.753	0.728	0.754	0.758
Mn	0.019	0.019	0.02	0.018	0.019	0.019
Ca	0.907	0.909	0.909	0.904	0.913	0.906
Na	0.064	0.065	0.07	0.08	0.066	0.068
K	0.001	0.001	0.001	0.001	0.001	0.001
WO	47.054	47.247	47.261	47.43	47.346	47.06
EN	39.48	39.297	39.125	38.204	39.101	39.364
FS	13.466	13.456	13.614	14.366	13.553	13.576

Table B.4: All EMP analyses for amphibole from El Abrigo.

	AM007-001	AM007-002	AM007-003	AM007-004	AM007-005	AM007-006	AM007-007
SiO_2	38.2	39.427	39.941	39.73	39.722	39.463	38.453
TiO_2	6.616	6.247	6.174	6.371	6.255	6.406	6.59
Al_2O_3	14.086	13.022	12.81	13.017	13.072	13.153	13.714
FeO_T	11.843	11.557	11.37	11.521	11.538	11.513	11.01
Cr_2O_3	0	0.014	0.016	0	0	0.037	0.003
MnO	0.156	0.205	0.288	0.229	0.184	0.194	0.141
MgO	12.731	13.193	13.4	13.166	13.099	13.214	13.086
CaO	12.179	12.266	11.877	12.086	12.014	12.106	12.194
Na_2O	2.696	2.735	2.764	2.714	2.79	2.798	2.589
K_2O	0.98	1.015	1.075	0.995	1.013	0.981	1.002
F	0.063	0.089	0.053	0.027	0.095	0.065	0.059
Cl	0.009	0.012	0.015	0.013	0.009	0.008	0.011
Total	99.56	99.77	99.77	99.87	99.79	99.9	98.85
				Oxygen = 23.000			
Si	5.763	5.987	5.974	5.879	6.027	5.913	5.814
Al	2.503	2.328	2.257	2.268	2.335	2.321	2.442
Cr	0	0.002	0.002	0	0	0.004	0
Ti	0.751	0.713	0.695	0.709	0.714	0.722	0.749
Mg	2.863	2.986	2.988	2.904	2.963	2.952	2.95
Fe*	1.494	1.467	1.423	1.425	1.464	1.443	1.392
Mn	0.02	0.026	0.036	0.029	0.024	0.025	0.018
Ca	1.969	1.995	1.903	1.916	1.953	1.944	1.976
Na	0.789	0.805	0.802	0.779	0.821	0.813	0.759
K	0.189	0.197	0.205	0.188	0.196	0.188	0.193
Cl	0.002	0.003	0.004	0.003	0.002	0.002	0.003
F	0.03	0.043	0.025	0.013	0.046	0.031	0.028

Table B.4: Con't

	AM007-008	AM008-001	AM008-002	AM008-003	AM008-005	AM008-006	AM008-007
SiO_2	38.948	39.59	39.819	39.499	40.458	40.226	40.322
TiO_2	6.176	4.832	5.074	5.07	4.784	5.262	5.068
Al_2O_3	12.841	12.022	12.105	12.035	11.271	11.551	11.989
FeO_T	12.337	13.994	14.357	14.153	13.87	13.517	13.659
Cr_2O_3	0	0	0	0.019	0	0	0
MnO	0.246	0.378	0.389	0.393	0.492	0.5	0.442
MgO	12.631	11.634	11.672	11.829	12.093	12.124	12.182
CaO	12.039	11.733	11.611	11.722	11.401	11.462	11.61
Na_2O	2.752	2.811	2.76	2.82	2.865	2.982	2.929
K_2O	1.075	1.294	1.304	1.252	1.391	1.4	1.224
F	0.074	0.056	0.041	0.067	0.075	0.101	0.091
Cl	0.013	0.026	0.026	0.017	0.022	0.023	0.019
Total	99.13	98.37	99.16	98.86	98.72	99.15	99.54
				Oxygen = 23.000			
Si	5.951	6.132	6.085	6.096	6.27	6.27	6.216
Al	2.311	2.193	2.178	2.188	2.057	2.12	2.177
Cr	0	0	0	0.002	0	0	0
Ti	0.71	0.563	0.583	0.589	0.558	0.617	0.588
Mg	2.877	2.686	2.659	2.722	2.794	2.817	2.8
Fe*	1.577	1.812	1.835	1.827	1.798	1.762	1.761
Mn	0.032	0.05	0.05	0.051	0.065	0.066	0.058
Ca	1.971	1.947	1.901	1.938	1.893	1.914	1.917
Na	0.815	0.844	0.818	0.844	0.861	0.901	0.876
K	0.21	0.256	0.254	0.247	0.275	0.278	0.241
Cl	0.003	0.007	0.007	0.004	0.006	0.006	0.005
F	0.036	0.027	0.02	0.033	0.037	0.05	0.044

IMAGE EVALUATION TEST TARGET (QA-3)

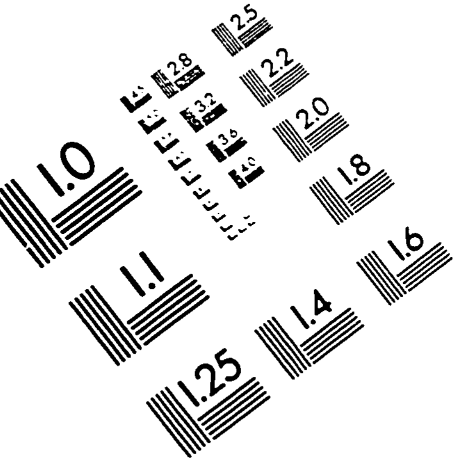
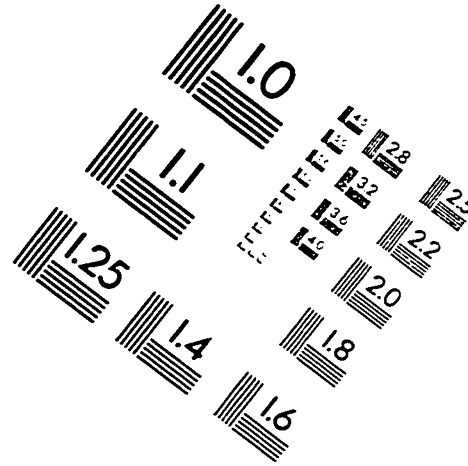
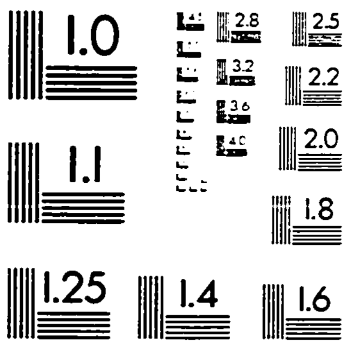
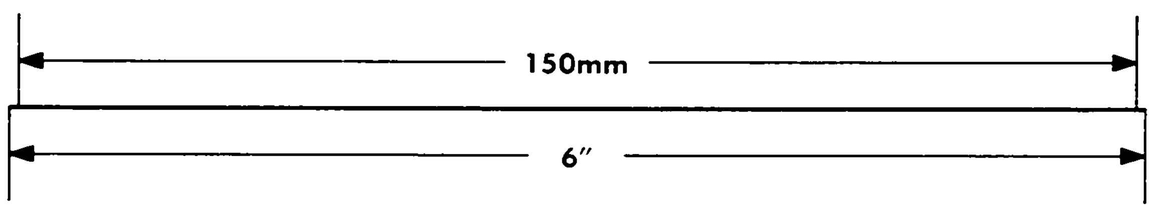
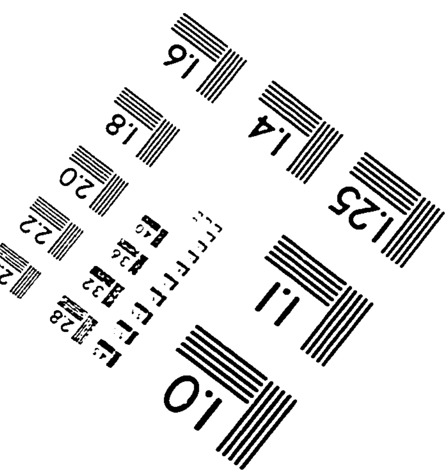
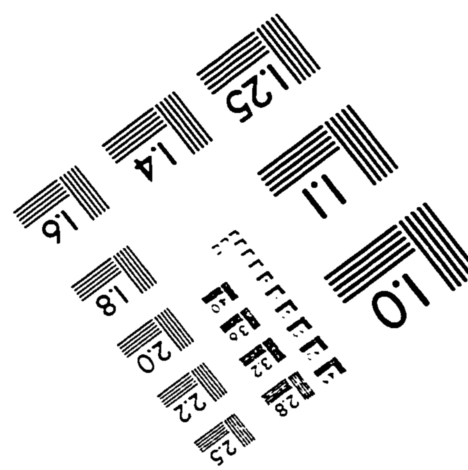


APPLIED IMAGE, Inc
1653 East Main Street
Rochester, NY 14609 USA
Phone: 716/482-0300
Fax: 716/288-5989